EARTHQUAKE ENGINEERING TO EXTREME EVENTS

ISSN 1520-295X

Real Time Control of Shake Tables for Nonlinear Hysteretic Systems

by

Ki Pung Ryu and Andrei M. Reinhorn

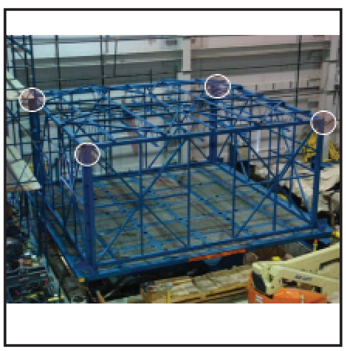

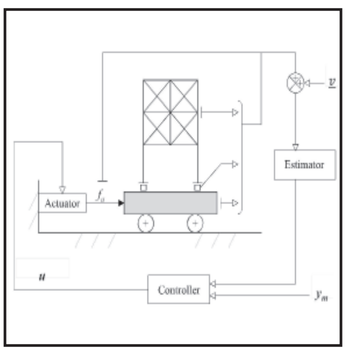

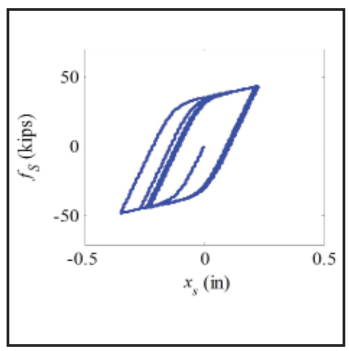

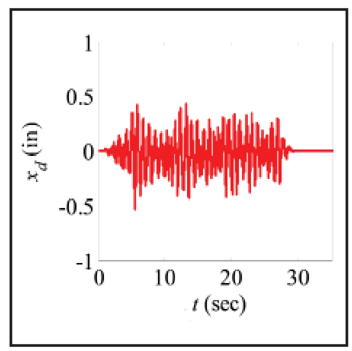

Technical Report MCEER-16-0004

October 22, 2016

This research was conducted at the University at Buffalo, State University of New York, and was supported primarily by MCEER Thrust Area 3: Innovative Technologies.

Real Time Control of Shake Tables for Nonlinear Hysteretic Systems

by

Ki Pung Ryu[1] and Andrei M. Reinhorn[2]

Publication Date: October 22, 2016
Submittal Date: January 21, 2016

Technical Report MCEER-16-0004

MCEER Thrust Area 3: Innovative Technologies

1 Postdoctoral Research Scientist, Department of Civil, Structural and Environmental Engineering, University at Buffalo, State University of New York
2 Professor Emeritus, Department of Civil, Structural and Environmental Engineering, University at Buffalo, State University of New York

MCEER
University at Buffalo, State University of New York
212 Ketter Hall, Buffalo, NY 14260
E-mail: *mceer@buffalo.edu*; Website: *http://mceer.buffalo.edu*

Preface

MCEER is a national center of excellence dedicated to the discovery and development of new knowledge, tools and technologies that equip communities to become more disaster resilient in the face of earthquakes and other extreme events. MCEER accomplishes this through a system of multidisciplinary, multi-hazard research, in tandem with complimentary education and outreach initiatives.

Headquartered at the University at Buffalo, The State University of New York, MCEER was originally established by the National Science Foundation in 1986, as the first National Center for Earthquake Engineering Research (NCEER). In 1998, it became known as the Multidisciplinary Center for Earthquake Engineering Research (MCEER), from which the current name, MCEER, evolved.

Comprising a consortium of researchers and industry partners from numerous disciplines and institutions throughout the United States, MCEER's mission has expanded from its original focus on earthquake engineering to one which addresses the technical and socio-economic impacts of a variety of hazards, both natural and man-made, on critical infrastructure, facilities, and society.

The Center derives support from several Federal agencies, including the National Science Foundation, Federal Highway Administration, Department of Energy, Nuclear Regulatory Commission, and the State of New York, foreign governments and private industry.

The research presented herein was developed to service multiple projects executed at the University at Buffalo's Structural Engineering and Earthquake Simulation Laboratory (SEESL), which required advanced testing capabilities beyond those that currently exist. Based on stringent requirements of qualification testing, the research developed tools suitable for investigative and qualification purposes. The initiatives from the Suspended Nonstructural Component Systems Consortium, the NEES Nonstructural Components Research Project and most recently the Bonneville Power Administration projects on the protection and isolation of transformers and bushings, triggered the need to improve the controls of the shake tables. These controls have much broader applications in the control of structures and critical equipment through active isolation.

ABSTRACT

Shake table testing is an important tool to challenge integrity and service behavior of structural and nonstructural specimens by imposing strong excitations at their base. High fidelity of bare shake tables can be achieved through feedback control of actuators' inner loop with fixed gains, based on table tuning procedures. When shake tables are loaded with specimens, the interaction between tables and specimens influence the system dynamics that might result in undesired performance. In order to compensate the effects of the interaction, open loop feedforward compensation methods have been satisfactorily used in the current practice of table controls, assuming that the specimens remain linear and unchanged. On the contrary, unsatisfactory signal performances during shake table testing were observed when flexible and heavy specimens experience nonlinear behavior. While lack of high fidelity might be acceptable for the purpose of research, i.e. to explore responses of specimens subject to random excitations, a high fidelity of signal reproduction is necessary for the shake table applications for qualification testing where specific target motions are required to challenge the specimens.

In this study, tracking control schemes are proposed for shake tables in order to simulate target motions at specific locations of structural test specimens. The motion applied at the shake table level would probably be different than the target motion within the test structure; however, proper design of the shake table motion would ensure the desired performance of the controlled structure. The design of such controller is dependent on the dynamics of the shake table, dynamics of the test structure and their interaction. Additionally, when the specimens change properties due to nonlinearities and yielding caused by extreme excitations, the controller must be adaptive in order to account for the changes and uncertainties in system models and to ensure the desired tracking.

Metaphorically, the procedure suggested herein would seem to help the performance of an acrobat, who tries to balance a flexible stick on his palm, ensuring that the payload at the upper end of his stick will not fall or have undesired movement. But even for the acrobat, the success will be limited by the strength of his palm and the space where he will have to maneuver. Similarly the methodology sought in this report attempts to determine the procedures and limitations for real life applications of base movements with targeted control in test structures.

"This Page Intentionally Left Blank"

ACKNOWLEDGEMENTS

The work was supported by the Multidisciplinary Center of Earthquake Engineering Research (MCEER) and the Structural Engineering and Earthquake Simulation Laboratory (SEESL) at the University at Buffalo. Financial support was provided by the MCEER Suspended Nonstructural Component Systems Consortium, by the Bonneville Power Administration and by the SEESL leadership. All support is greatly acknowledged.

"This Page Intentionally Left Blank"

TABLE OF CONTENTS

TABLE OF CONTENTS (CONT'D)

X

TABLE OF CONTENTS (CONT'D)

“This Page Intentionally Left Blank”

LIST OF ILLUSTRATIONS

LIST OF ILLUSTRATIONS (CONT'D

x

LIST OF ILLUSTRATIONS (CONT'D)

LIST OF ILLUSTRATIONS (CONT'D)

LIST OF TABLES

“This Page Intentionally Left Blank”

SECTION 1
INTRODUCTION

1.1 Seismic Testing of Nonlinear Structures

Shake table tests allow realistic earthquake motions to be reproduced in order to challenge complex specimens and provide valuable knowledge of seismic performance of structures and nonstructural systems. However, the reproduction of dynamic signals is usually imperfect due to the dynamics of the shake table and mostly due to the complexity of test specimens. When shake tables are loaded with the test specimens, the interaction between tables and such specimens affect the system dynamics and might result in undesired performance. In order to compensate for these interaction effects, open loop feedforward methods with offline and online error correction methods have been developed and widely used in practice. Even though these control methods were proved to be valuable and practical tools to challenge linear structures using shake tables, most developments assume that specimens remain linear or their nonlinear behavior is negligible.

However, when flexible and heavy specimens (compared to shake table weight) experience nonlinear behavior, the signal reproduction of the shake table can be unsatisfactory; for instance, large differences between the target motion and achieved shake table motions with a heavy nonlinear specimen were observed by Schachter and Reinhorn (2007). These phenomena might be acceptable for exploratory research of structures subjected to random excitations, where no specific forcing motions are required. Unlike such exploratory research projects, "qualification testing" designed to verify certain performance of test specimens, must have high fidelity of signal reproduction that can challenge the structures by specifically required target motions. For example, qualification tests of nonstructural ceiling systems demand the reproduction of the required motions at specific locations within specimens mounted on shake tables. This can be a challenge for currently existing control methods if specimens experience nonlinear behavior that continuously changes their behavior.

The objective of this study is to develop a controller for shake tables combined with a parameter estimator such that an output response y at a specific location in a nonlinear hysteretic test structure (e.g. the roof/floor of a specimen) will track a pre-defined desired target response motion y_m. The control target motions considered in this study include: i) any total floor acceleration history that could be expected in the specimen and ii) total floor acceleration defined by a required response spectrum, such as AC156, the standard for shake-table testing of nonstructural components (ICC, 2010). It is noted that in order to generate realistic "target floor" motions within structures for (i) above, such motion should be obtained from a numerical linear structural model subjected to simple pulse type excitations or real earthquake records. This kind of model is used herein and is referred to as the "reference model". However, any theoretical target motion, such as recorded floor motions, without the reference model, can also be used. This control concept is schematically shown in Figure 1-1 where a test specimen is represented by a single degree-of-freedom nonlinear structure whose parameters are not fully known (the table displacement with respect to the ground is defined as x_t and the relative displacement at the top of the structure with respect to the shake table is x_s, and other terms are defined in the following sections). The motion applied at the shake table level would probably be different than the target motion, y_m within the structure, but proper design of the table motion will insure the desired performance is achieved. The design of such a controller is dependent on the dynamics of the shake table, dynamics of the structure and their interactions. Additionally, when the structures change properties due to nonlinearities and yielding, the controller would have to be adaptive in order to insure the desired tracking.

If successful, development of such a controller could be further expanded and used to achieve a desired performance at control locations in real structures using a hybrid passive-active isolation system, for example. Simple buildings, utility structures such as those used in transportation systems and power distribution, or sensitive manufacturing plants can benefit from such solutions.

Metaphorically, the procedure would seem to help the work of an acrobat that tries to balance a flexible stick on his palm insuring that the payload at the upper end of his stick will not fall or have undesired movement. But even the acrobat' success will be limited by the strength of his palm and the space where he will have to maneuver. The methodology sought in this study will try to determine procedures and their limitations for real life applications.

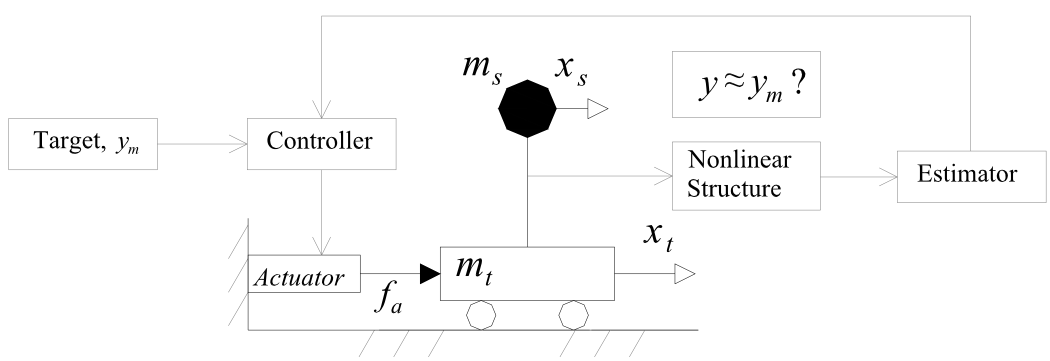

Figure 1-1 Schematic of tracking control to simulate the target motion at a test structure

More specifically, the problem can be understood from previous studies and developments. In order to simulate a target motion in a linear structure (specimen), an open-loop (feed forward) compensation method using a table-structure system transfer function was developed (Maddaloni, Ryu, and Reinhorn,

2010) and implemented at the University at Buffalo (UB – SEESL) by the authors of this report. However, when specimens experience nonlinear behavior due to high intensity excitations, the pre-computed compensation functions are not valid anymore, and the signal reproduction at the specified locations can be highly inaccurate. This can cause unreliable responses of a structure and secondary systems installed on the system. Therefore, more advanced control algorithms are needed to extend the use of shake tables to continuously changing and nonlinear specimens.

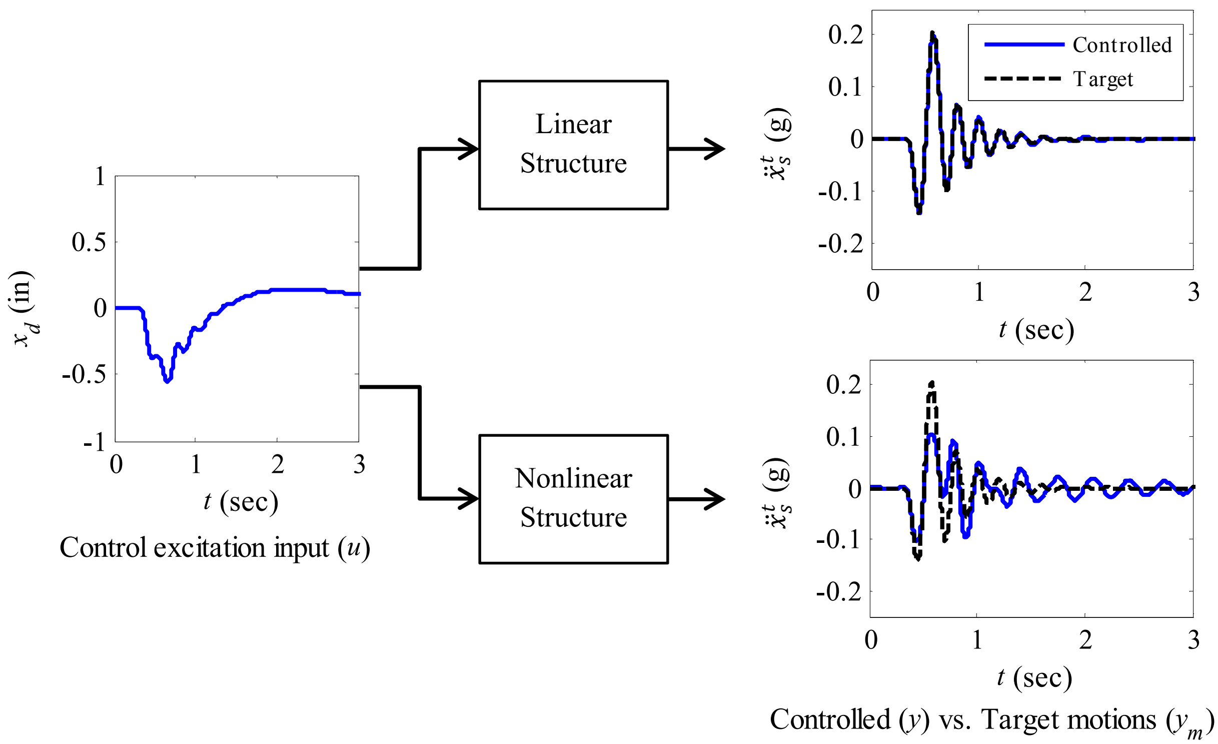

(a) Feed-forward tracking control scheme
using pre-computed excitation (left) and the responses (right)

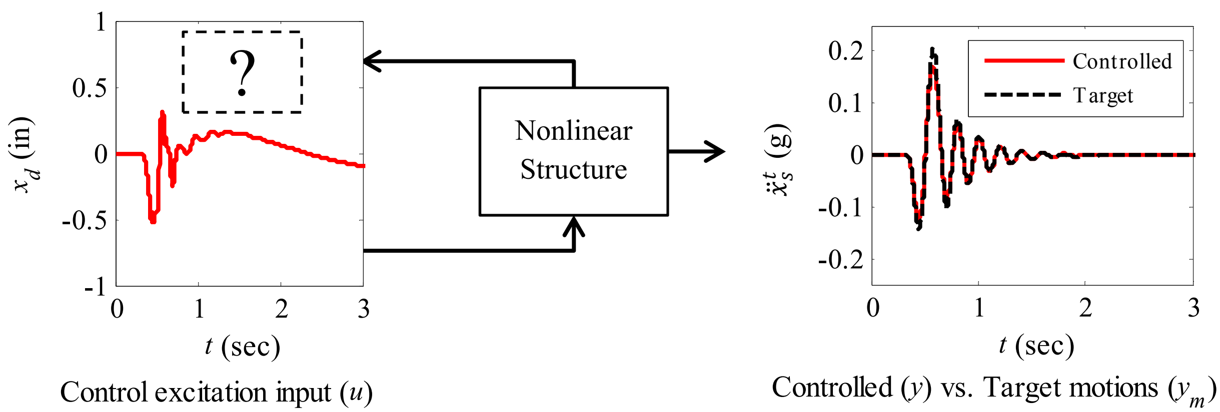

(b) Feedback tracking control scheme
using real-time computed excitation (left) and the response (right)

Figure 1-2 Schematic of closed-loop compensation procedure

This concept is schematically described in Figure 1-2. For the tracking control problem using a shake table, the control excitation input $u(t)$ might be pre-computed using the feed-forward compensation control method (described in Section 2.5). The tracking will be satisfactory if the controlled structure is linear (i.e. in this study, referring to *linear system* or *linear time invariant* system). However, if the structure experiences nonlinear behavior, the pre-computed excitation input cannot account for it and results in the tracking errors between the target motion [$y_m(t)$] and the achieved response [$y(t)$] of the controlled structure as shown in Figure 1-2 (a). If feedback tracking control methods are introduced as shown in Figure 1-2 (b), the control excitation input $u(t)$ can be computed in real time using a feedback controller combined with a parameter estimator such that the achieved response could follow a target motion. The system properties and more results of this example shown in Figure 1-2 can be found in Appendix A.1.

A feedback tracking control procedure proposed in this study to simulate target motions at nonlinear structures using shake table control is presented in Figure 1-3 with the assumption that it is possible to provide a real time control excitation input, computed through an outer loop (ex. using a *real time hybrid simulation controller* (UB-RTHSC) such as one at the University at Buffalo), to the servovalve-actuator of the shake table system (which has inner closed-loop feedback control). The control excitation input $u(t)$ can be the desired shake table displacement $x_d(t)$ (such as used in a typical shake table control), primarily driven by stability considerations. When a target motion $y_m(t)$ at a structure with its initial condition is specified, the control excitation input $u(t)$ is to be determined in real time, which will reduce the tracking error between the target motion $y_m(t)$ and the output $y(t)$ of the structure, such that $y(t)$ will follow the target $y_m(t)$. To determine the control excitation input $u(t)$, the system parameters are to be known. In order to deal with parameter uncertainties due to hysteretic behavior in nonlinear structures, a real time estimator is introduced and combined with the controller.

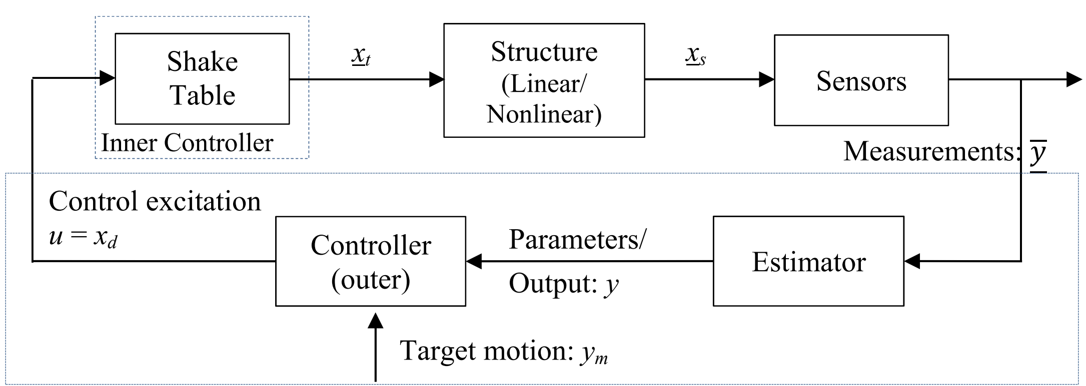

Figure 1-3 Schematic of the feedback tracking control scheme

The research problem is stated in Section 1. The current practice for shake table control is reviewed in Section 2. Tracking control methods for linear systems are introduced in Section 3, assuming that all parameters are known. In Section 4, feedback tracking control methods are extended to nonlinear hysteretic systems. Real time parameter estimation methods are introduced in Section 5 for systems with unknown parameters. The above control schemes are combined with the real time parameter estimators in Section 6 and Section 7 for linear and nonlinear systems, respectively. The developed methods are numerically applied to a realistic shake table – structure setup, using their real characteristic values, and the results are presented in Section 8. The remarks and conclusions are addressed at the end of this report.

1.2 Tracking Control in Shake Table Testing (Literature Review)

Shake table systems play a pivotal role in experimental earthquake engineering. The systems provide effective ways to subject structural components, substructures, or entire structural systems to dynamic excitations, which are similar to those induced by real earthquakes. In general, shake table systems consist of mechanical (e.g. platform), hydraulic or electromagnetic actuators (with servovalve), and electronic (controller and sensors) components (Ozcelik et al., 2008). The shake table (platform), which supports a specimen (structure), is constructed to provide high stiffness with minimum weight and is usually controlled by servo-hydraulic actuators. The controller provides the servovalve command to achieve a specific position of the actuator such that the platform will follow a pre-defined target motion. However, reproduction of a dynamic signal has many challenges involving servovalve actuator dynamics, shake table-structure interaction, nonlinear behavior such as compressibility of oil column in the actuator chamber and oil leakage through actuator seals, etc. (Ozcelik et al., 2008 and Maddaloni, Ryu and Reinhorn, 2010).

In order to provide a better understanding of the shake table system and to improve its performance, mathematical models were developed by researchers (Blondet and Esparza, 1988, Rinawi and Clough, 1991, Conte and Trombetti, 2000, Trombetti and Conte, 2002, and EFAST, 2009). The models developed for shake table systems were represented by transfer functions (in frequency domain) and validated by experimental results.

In general, as addressed above, the objective of a shake table control is to simulate the pre-defined target motion such as an earthquake history at a shake table platform; this goal might be achieved by "tuning" (i.e. by tuning the inner loop feedback control parameters of servo-actuators) for a bare shake table system (Thoen and Laplace, 2004, Luco et al., 2010, and EFAST, 2009) such that the transfer function (i.e. the frequency domain ratio) between the target motion and the output of the shake tale has a unity gain in the frequency range of interest.

However, when a structure (specimen) is mounted on a shake table, the transfer function is distorted due to the shake table-structure interaction; i.e. this interaction between shake tables and linear structures was addressed by Blondet and Esparza (1988), Rinawi and Clough (1991), and Conte and Trombetti (2000). It is noted that the linear system model in the time domain, developed by Rinawi and Clough (1991), can be extended to nonlinear system models. In order to compensate for the distortion, a feedforward compensation method using the inverse transfer function, assuming the shake table-structure system is linear, has been widely used in industry (MTS, 2004) to reduce the tracking error between the target motion and the ***shake table response*** due to simulator dynamics and servovalve nonlinearities by this method, an offline iterative approach can be adopted; a detailed review of this method can be found in Spencer and Yang (1998). Recently, the feedforward compensation methods combined with real-time feedback loops to reduce the tracking errors were introduced by Nakata (2010) and Phillips and Spencer (2012) where outer feedback loops (i.e. "outer" is used to distinguish the feedback loop from the inner feedback loop of actuators) are used to reduce the tracking errors instead of the offline iteration approach. The methods were verified by experiments showing good agreements between the target and the output.

More studies in the actuator-structure interaction in structural control applications can be found in Dyke et al. (1995) where the results with and without the interaction in control methods were presented and quantitatively showed that by considering interaction, better and more stable control methods could be established.

Unlike general shake table testing where it is required to simulate a desired target motion at the shake table level, in other applications including the experimental evaluation of architectural or nonstructural components such as suspended ceiling systems (Reinhorn et al., 2010) or the qualification testing of complex equipment (IEEE, 2006) it is often required to simulate a floor/roof motion at a specific location (such as roof corners or mid spans) of a structure mounted on a shake table. In order to simulate a target motion at the structure level (instead of the shake table platform), a feedforward compensation procedure using a shake table-structure system transfer function with possible offline iteration correction was developed (Maddaloni, Ryu, and Reinhorn, 2010); the control method was implemented and experimentally verified.

The key element, for the development of tracking control methods for shake tables discussed above, is a feedforward compensation method using the inverse transfer function. It is also noted that for a tracking control of a linear shake table-structure system, one may also use an optimal tracking control method (Kwakernaak and Sivan, 1972 and Kirk, 2004), which combines a feedforward loop with a feedback loop; the feedback loop may be more effective to reduce possible unknown errors and noise (like the methods developed by Nakata, 2010 and Phillips and Spencer, 2012). However, if a testing structure has more complex, nonlinear behavior (e.g. base-isolated systems) or a linear structure experiences yielding due to high intensity excitation, the transfer function (i.e. which can be defined for a linear time invariant system (Chen, 1999)) is not valid anymore; therefore, the feedforward compensation loop, which is conducted offline, cannot be used and real time feedback control schemes are needed (Maddaloni, Ryu and Reinhorn, 2010).

In order to reduce the effects of structure (specimen) nonlinearities, various advanced methods have been developed: For example, an adaptive control method involving the minimal control synthesis algorithm was introduced to reduce the signal distortion due to a linear model assumption (Stoten and Gomez, 2001); a disturbance observer-based control approach was developed also to compensate the unknown disturbances, caused by structure nonlinearities, in a shake table (Iwasaki et al., 2005); and hierarchical control strategy and nonlinear control techniques, utilizing the sliding mode control technique, were proposed to compensate structure nonlinearity and uncertainties in experiments (Yang et al., 2015).

While these methods aim to reproduce a target motion at a shake table platform by reducing the effects of nonlinear structures, the objective (as discussed in Section 1.1) of this study is to simulate a target motion at a specific location in a nonlinear structure mounted on a shake table. To solve this tracking control problem for a nonlinear structure using a shake table, the real time feedback control schemes including the predictive control method (Lu, 1994 and Lu, 1995) and the feedback linearization method (Ioannou and Fidan, 2006) are adopted: For the predictive tracking control scheme, first, the response (output) of a nonlinear system is predicted and a control law is developed by minimizing the predicted tracing errors between the predicted output and the target motion at every instant; for the feedback linearization method, the control law is developed in order to cancel the nonlinear terms in a system such that the system behaves as a linear or partially linear system and the output follows the target motion. These tracking methods for nonlinear systems can be extended to shake table and nonlinear structure applications by reformulating the system governing equations and by analyzing error dynamics and state responses.

Another challenge to control a nonlinear structure is that the system parameters might not be known a priori; for example, the change of structure stiffness in hysteretic behavior and/or the yielding force may not be accurately known in advance. Therefore, the real time parameter estimation, combined with the feedback controller, might be required. In structural applications of the real time (online) parameter estimation for nonlinear systems, many advanced methods including the least squares method (Smith et al., 1999 and Yang and Lin, 2004), the extended Kalman filter (Yun and Shinozuka, 1980 and Wu and Smyth, 2007) and the unscented Kalman filter (Wu and Smyth, 2007, Omrani et al., 2013, Hashemi et al., 2014, and Song and Dyke, 2014) have been successfully applied numerically and experimentally. For the least squares method, a system equation is formulated in a certain way such that the unknown parameters are linearly related to the state of the system and the estimate is updated using the measurements in real time: one can show the stability of this method in that the estimate error will be bounded (Ioannou and Sun, 2012). However, it might be difficult to apply this method to complex nonlinear systems where the nonlinear terms cannot be separated by the parameters and the state (i.e. this issue will be discussed in Section 5.1.1.3). Both the extend Kalman filter (EKF) and the unscented Kalman filter (UKF) are extensions of the Kalman filter, which is a widely used observer to estimate the state of a linear system (Song, 2011); the EKF and UKF are able to estimate the state and system parameters of nonlinear systems. For the EKF, the unknown parameters are augmented to the state vector and at each instant the nonlinear system matrix is approximated by its Jacobian matrix using the 1st order Taylor series expansion; the estimator gain is computed to minimize the length of the estimate error vector (Crassidis and Junkins, 2012). Even though the method does not have certain stability properties (unlike the least squares method) because of the unknown effects of remaining terms of the Taylor series, this method might be applicable to more complex nonlinear systems. Unlike the EKF, the UKF does not require the Jacobian matrix and can be applied to non-differentiable functions. However, the UKF typically involves more computations than the EKF (Crassidis and Junkins, 2012), which might cause difficulties in real time control applications. In this study, the Jacobian matrix of the interested nonlinear hysteretic system will be determined; therefore, the EKF is applicable. The nonlinear tracking controllers will be reformulated to be combined with the real time estimator using the EKF.

As addressed above, in this study, the real time feedback controllers using the predictive control method and the feedback linearization method are modified and combined with the extended Kalman filter as the real time state and parameter estimator in order to develop a methodology to determine the excitation of a shake table, such that the response of a nonlinear hysteretic structure will follow a pre-defined target motion.

Furthermore, if successful, the proposed methods could be expanded to control real structures using base motion controls (although this is not a scope of this study). Similar structural control concepts, known as *active base isolation* that consists of a passive isolation system combined with control actuators (Chang and Spencer, 2010), have been developed by many researchers, including Reinhorn et al. (1987), Kelly et al. (1987), Inaudi et al. (1992), Nagarajaiah et al. (1992), Yang et al. (1996), Luo et al. (2000), Pozo et al. (2006), Chang and Spencer (2010), and Suresh et al. (2012). These linear control methods, nonlinear control methods, and nonlinear adaptive control methods (Pozo et al., 2006, and Suresh et al., 2012) have provided excellent active base isolation control design. Especially, the developed methods of Nagarajaiah et al. (1992), Yang et al. (1996), and Chang and Spencer (2010) were experimentally verified. While the most methods focus on stabilizing (making zeros of) the system responses, the proposed control method in this study could be also used to control system responses to track desired target motions like the controllers by Pozo et al. (2006), providing another possible and flexible control scheme to the design engineers.

1.3 Notation

All symbols used are defined where they first appear in the report, and are also summarized here. The principal meanings of the commonly used notations for the tracking control methods are provided below.

Symbols	Description	Index (Section)
$\underline{x}$	True state of controlled (shake table-structure) system; State vector $\underline{x}$ contains the state variables such as the displacement and velocity responses, etc.	2.2, 3
$\hat{\underline{x}}$	Predicted (estimated) values of the true state $\underline{x}$	5.2
$\tilde{\underline{x}}$	Estimated error of the true state; i.e. $\tilde{\underline{x}}(t) = \hat{\underline{x}}(t) - \underline{x}(t)$	5.2
$\underline{x}_m$	State of a reference model	3
u	Control excitation input	2.2, 3
r	Excitation input of a reference model	3
y	Response output of a controlled system, which is the selected response to track the target motion, and is the combination of the state variables; i.e. $y(t) = C\underline{x}(t)$ where C is defined in the context	2.2, 3
$\hat{y}$	Predicted (estimated) response output of the true system y	3.3
$\overline{y}$	Measured output (state variables) of controlled system; i.e. $\overline{y}(t) = H\underline{x}(t) + \underline{v}(t)$ where H and $v(t)$ are defined in the context	5.2
y_m	Target motion, which can be the output of a reference model subjected to the reference input $r(t)$	3
e	Tracking error of target ; i.e. $e(t) = y(t) - y_m(t)$	3.3
$\tilde{\underline{\theta}}$	Error vector of estimated parameters; i.e. $\tilde{\underline{\theta}}(t) = \hat{\underline{\theta}}(t) - \underline{\theta}^*$; $\underline{\theta}^*$ is the true parameter and $\hat{\underline{\theta}}(t)$ is the predicted (estimated) parameter vectors	5.2

“This Page Intentionally Left Blank”

SECTION 2
CURRENT PRACTICE FOR SHAKE TABLE CONTROL

A shake table-structure system consists of a platform supported by bearings driven by servo controlled actuators with a structure (specimen) mounted rigidly on its surface. The simplified schematic of the assembly of a shake table–structure system is shown in Figure 2-1 where actuators' forces and internal stress resultants acting on the system are also presented (i.e. $f_{s,I}$, f_D, f_S are the structure inertia, damping, and resisting forces; $f_{t,I}$ is the table inertia force; f_a is the actuator force).

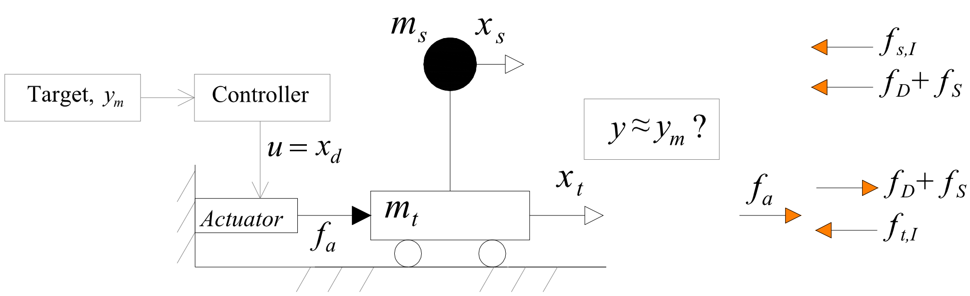

Figure 2-1 Schematic of a shake table-structure system

In order to move the structure sitting on the platform to match a target response, a controlled excitation should be applied at its base. The objective of the control system of the shake table–structure is to determine the desired excitation input $x_d(t)$ such that the response output $y(t)$ of the shake table, or the mounted structure will follow the pre-defined target motion $y_m(t)$. In order to achieve this goal, a mathematical model of the system is used; in this section, the mathematical model for a linear system is introduced based on the developments by Rinawi and Clough (1991) and Conte et al. (2000), which will be used in the following sections for the development of the tracking control method, for both linear and nonlinear systems.

2.1 Servovalve – Actuator Shake Table System

Figure 2-2 shows a schematic of a typical shake table-actuator system. It consists of a rigid platform (table) driven by horizontal actuators that are controlled by servovalves.

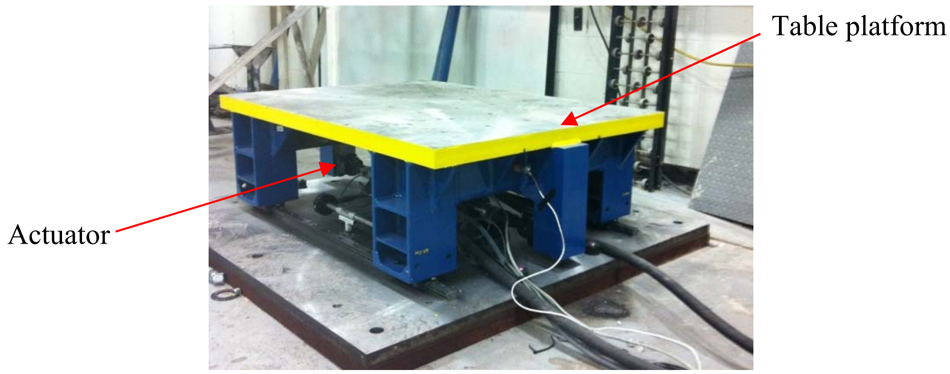

Figure 2-2 Typical unidirectional shake table-actuator system (after Stefanakis and Sivaselvan, 2015)

In this study, for simplicity a unidirectional shake table movement using uniaxial horizontal actuators is considered. Actuators' motions are controlled by servovalves usually mounted on actuators (see Figure 2-3 (left)) that establish the direction of movement and the amount of fluid flow to actuators' chambers. Figure 2-3 (right) schematically shows a three stage servovalve.

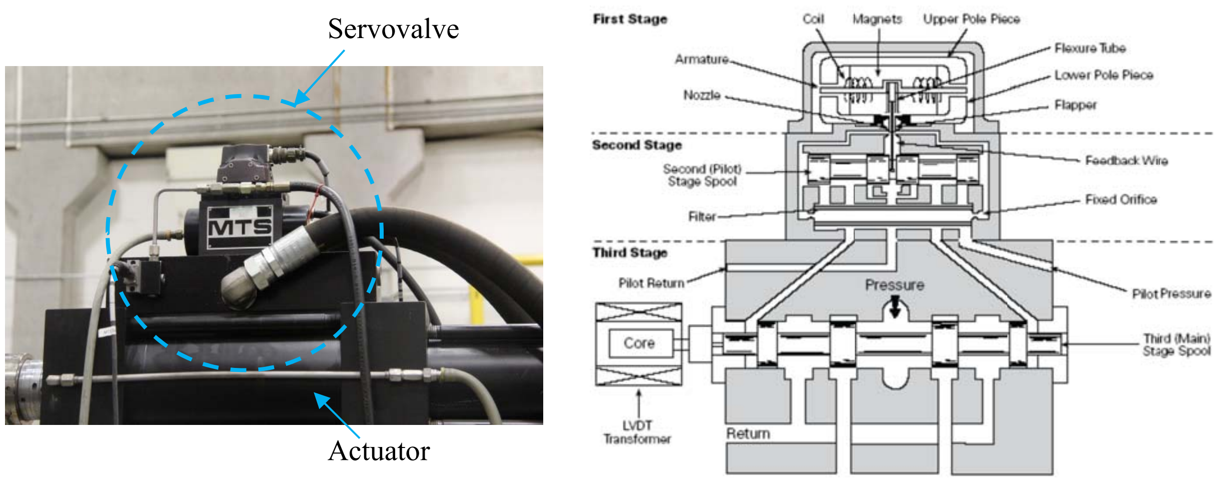

Figure 2-3 Servovalve mounted on an actuator (left) and schematic of a three stage servovalve (right - reproduced from Maddaloni et. al, 2008)

The simplified functional diagram of a servovalve-actuator shake table system is presented in Figure 2-4; each term shown in the schematic is described below. This schematic diagram is to represent the relation between the input, the desired shake table displacement x_d, and the output, the actual (measured) shake table displacement x_t, and includes several subsystems. The subsystem includes: i) the *Servovalve* transfer function H_V between servovalve input signal Δx_{c3} and servovalve oil flow rate q_s, ii) the *Actuator* transfer function H_A between the servovalve flow rate q_s and shake table displacement x_t, and iii) the shake table feedback *Controller* in displacement control, where the servovalve input signal Δx_{c3} is computed using the error signal between the target (= the desired shake table displacement x_d) and the actual (measured) shake table displacement x_t. Using these subsystems, the system transfer function H_T between the desired shake table displacement x_d and the actual displacement x_t is determined.

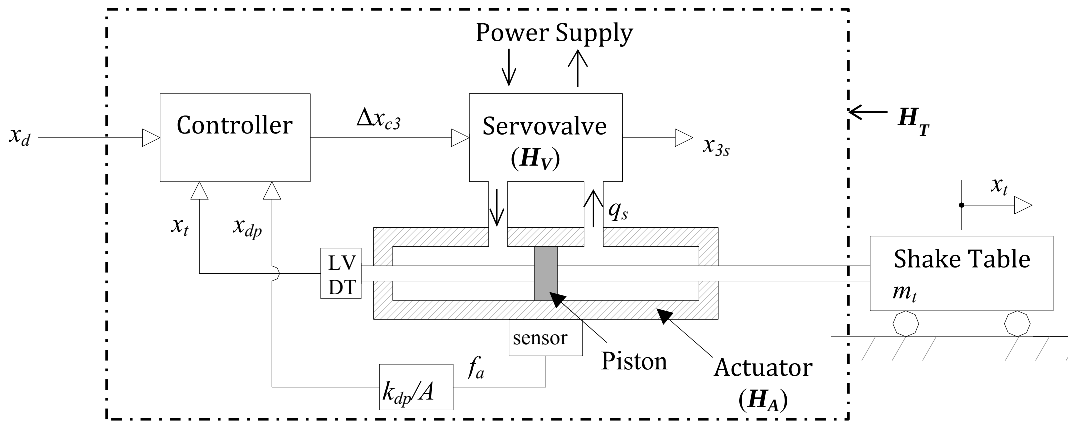

Figure 2-4 Simplified functional diagram of a servovalve-actuator shake table system

Servovalve's transfer function

The servovalve controller involves an inner loop feedback and a PID controller (see Figure 2-5). The relationship between the input signal Δx_{c3} (measured in volts), applied to the servovalve and the output servovalve' spool displacement x_{3s} can be expressed as

$$x_{3s}(s) = \frac{k_1 k_2 (k_p^i + k_d^i s)}{1 + k_{3s} k_1 k_2 (k_p^i + k_d^i s)} \Delta x_{c3}(s) \tag{2-1}$$

where "s" is a complex variable of the Laplace transform and

k_1 and k_2 are the first and second stage gains

k_p^i and k_d^i are the proportional and derivative gains

k_{3s} is the gain of the servovalve main stage spool displacement

In this study, this relationship is assumed to be linear (following the suggestions of Nachtigal, 1990, Rinawi and Clough, 1991, and Conte et al., 2000), so that Eq. (2-1) becomes:

$$x_{3s}(t) = k_{sv} \Delta x_{c3}(t) \tag{2-2}$$

where k_{sv} is the global gain of the servovalve. The servovalve' spool displacement x_{3s} (in) produces a high pressure oil flow rate q_s (in^3/s) to the actuator chamber (Blonet and Esparza, 1987), which is also assumed to be linearly related:

$$q_s(t) = k_{xq} x_{3s}(t) \tag{2-3}$$

where k_{xq} is the global flow-gain. From Eq. (2-2) and Eq. (2-3) one has the servovalve transfer function $H_V(s)$ between the input signal Δx_{c3} (volts) and the output servovalve flow rate q_s (in^3/s)

$$H_V(s) = \frac{q_s(s)}{\Delta x_{c3}(s)} = k_{xq}k_{sv} \tag{2-4}$$

Figure 2-5 also schematically represents this relationship in a block diagram form (i.e. the outer box represents the servovalve transfer function $H_V(s)$, shown in Figure 2-4), which is the dynamic response of the servovalve system, as described by Eq. (2-1) through Eq. (2-4).

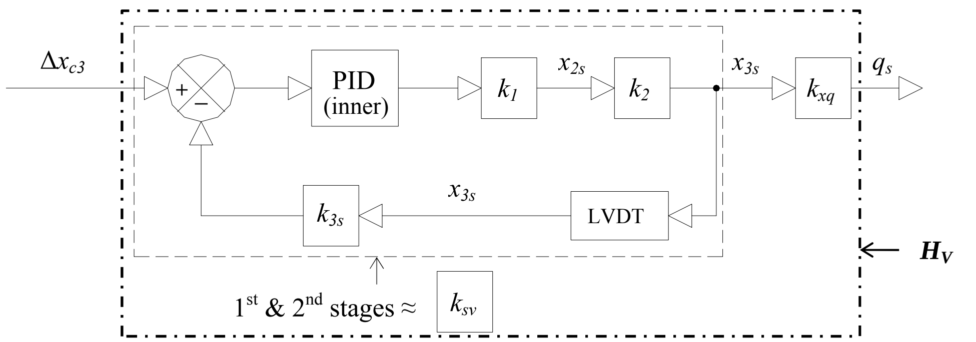

Figure 2-5 Block diagram of servovalve system

Actuator's transfer function

The total oil flow rate q_t (in^3/s) applied to the actuator's chamber is a nonlinear function of the servovalve' spool displacement x_{3s} (in) and the actuator force f_a (lbs) (Blonet and Esparza, 1987, Ogata, 2010, and Rinawi and Clough, 1991); thus q_t = f(x_{3s}, f_a). This relationship can be linearized about the origin ($x_{3s} = 0, f_a = 0$):

$$q_t(t) = q_s(t) - q_L(t) = k_{xq}x_{3s}(t) - k_L f_a(t) \tag{2-5}$$

The first term on the right hand side q_s (in^3/s) represents the flow rate induced by the servovalve spool displacement, and the second term q_L (in^3/s) represents the flow rate due to leakage. The terms k_{xq} and k_L are the flow-gain and the flow-force (loss) coefficient. With the oil flow input, the governing equation of the actuator piston can be expressed as

$$q_t(t) = q_m(t) + q_c(t) = A\dot{x}_t(t) + \left(V / 4\beta A\right)\dot{f}_a(t) \tag{2-6}$$

where

q_m (in^3/s) is the useful flow rate to the chamber causing piston to move

q_c (in^3/s) is the equivalent **c**ompressibility flow rate

A (in^2) is the actuator piston area

V (in^3) is the volume of oil in the actuator

β (psi) is the bulk modulus of fluid

x_t (in) is the shake table displacement

f_a (lbs) is the actuator force applied to the shake table

From Eq. (2-5) and Eq. (2-6) it is obtained

$$q_s(t) = q_m(t) + q_L(t) + q_c(t) = A\dot{x}_t(t) + (V/4\beta A)\dot{f}_a(t) + k_L f_a(t) \tag{2-7}$$

Simply the total flow (q_s) is a sum of the flow moving the piston (q_m), the flow going to losses (q_L), and the flow that go to the compression of the fluid (q_c). Through this equation one can obtain the actuator transfer function $H_A(s)$ between the servovalve flow rate q_s (in^3/s) and the table displacement x_t (in) considering losses and fluid compression:

$$H_A(s) = \frac{x_t(s)}{q_s(s)} = \frac{1}{As + (V/4\beta A)sf_a(s)/x_t(s) + k_L f_a(s)/x_t(s)} \tag{2-8}$$

Figure 2-6 also schematically represents this relationship in a block diagram form (i.e. the outer box represents the actuator transfer function $H_A(s)$, shown in Figure 2-4), which is the dynamic response of the actuator system, as described by Eq. (2-7) and Eq. (2-8). The potential interaction due to a mounted structure is indicated in the figure by a dot line – this issue is addressed further in Section 2.2.

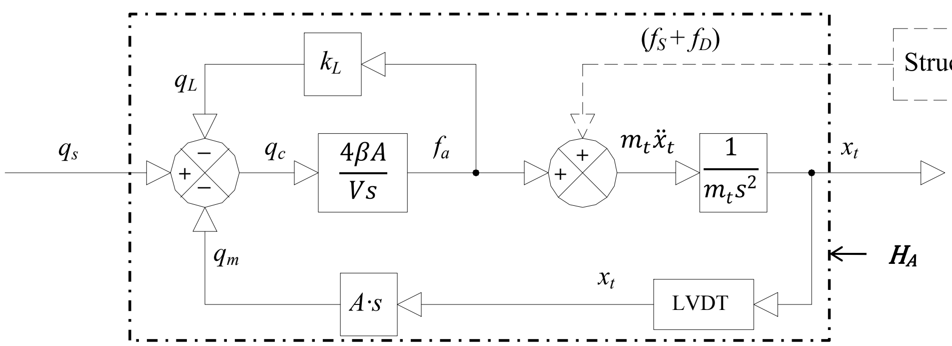

Figure 2-6 Block diagram of actuator system

From Eq. (2-4) and Eq. (2-8), the transfer function $H_{VA}(s)$ between the input signal Δx_{c3} (volts) and the output table displacement x_t[1] (in) for the servovalve-actuator system is

$$H_{VA}(s) = H_V(s)H_A(s) = \frac{x_t(s)}{\Delta x_{c3}(s)} = k_{xq}k_{sv}\frac{1}{As + (V/4\beta A)sf_a(s)/x_t(s) + k_L f_a(s)/x_t(s)} \tag{2-9}$$

[1] In this section, for simplicity, for the x_d and x_t the conversion factors from their physical dimensions (in) to the corresponding electrical signals (volts) are assumed to be lumped to the gain constants.

Servovalve to Shake Table System Transfer Function

The servovalve input signal Δx_{c3} (volts) can be computed as described in Conte et al. (2000):

$$\Delta x_{c3}(t) = \Delta x_{c2}(t) + x_{ff}(t) - x_{dp}(t) \tag{2-10}$$

or in more detail:

$$\Delta x_{c2}(s) = \underbrace{\left[k_p^o + (1/s)k_i^o + k_d^o s\right]}_{H_{PID}^o}\Delta x_c(s) = H_{PID}^o(s)\left(x_d(s) - x_t(s)\right) \tag{2-11}$$

where Δx_c (volts) is the table error signal ($\Delta x_c = x_d - x_t$) between the shake table displacement x_t (volts) and the target (desired) command signal x_d (volts). H_{PID}^o is therefore described as the transfer function of the actuator controller (PID - proportional-integral-derivative) in which k_p^o, k_i^o, k_d^o are the proportional, the integral, the derivative control gains, respectively. The second term x_{ff} (volts) in Eq. (2-10) is the feed forward component:

$$x_{ff}(s) = k_{ff} s x_d(s) \tag{2-12}$$

in which k_{ff} is the feed forward control gain. The last term x_{dp} (volts) in Eq. (2-10) is the differential pressure component

$$x_{dp}(s) = k_{dp}\Delta P(s) = k_{dp}\left(f_a(s)/A\right) \tag{2-13}$$

where k_{dp} is the delta pressure control gain, and ΔP (psi), the differential pressure across the actuator piston, is expressed as $\Delta P = f_a/A$. Substituting Eq. (2-11) though Eq. (2-13) into Eq. (2-10), the servovalve input signal is therefore:

$$\Delta x_{c3}(t) = H_{PID}^o(s)\left(x_d(s) - x_t(s)\right) + k_{ff} s x_d(s) - k_{dp}\left(f_a(s)/A\right) \tag{2-14}$$

The transfer function between the target displacement x_d (in) and the shake table displacement x_t (in) is obtained from Eq. (2-9) and Eq. (2-14):

$$\begin{aligned} H_T(s) &= \frac{\Delta x_{c3}(s)}{x_d(s)} \cdot \frac{x_t(s)}{\Delta x_{c3}(s)} = \frac{\Delta x_{c3}(s)}{x_d(s)} H_{VA}(s) \quad \text{or} \\ H_T(s) &= \frac{H_{VA}(s)\left(H_{PID}^o(s) + k_{ff}s\right)}{1 + H_{VA}(s)\left[H_{PID}^o(s) + \left(k_{dp}/A\right)\left(f_a(s)/x_t(s)\right)\right]} \end{aligned} \tag{2-15}$$

Figure 2-7 also schematically represents this relationship in a block diagram form; i.e. the outer box represents the system transfer function $H_T(s)$, which is the dynamic response of the servovalve-actuator shake table system (or “shake table system” for brevity).

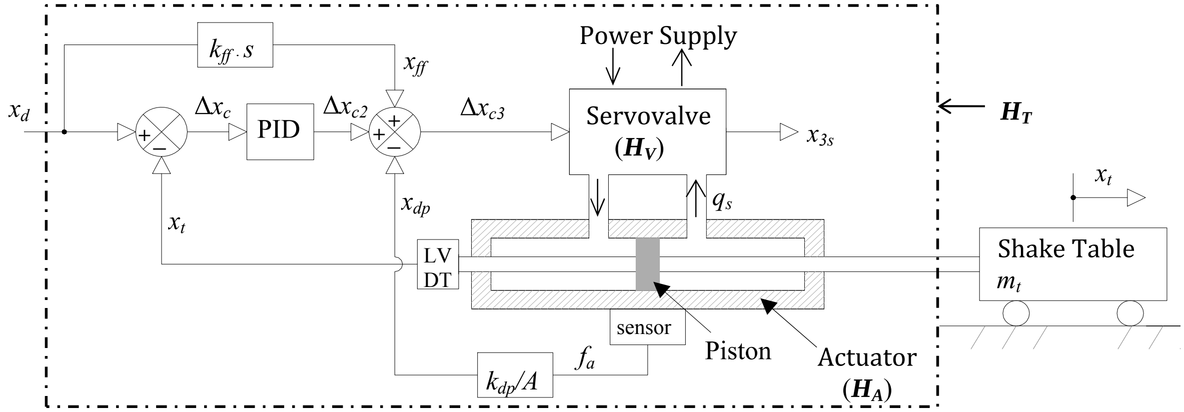

Figure 2-7 Schematic diagram of a servovalve-actuator shake table system

The transfer function in Eq. (2-15) is presented in the Laplace (complex frequency) domain. For the real time control development, the time domain solution is needed, and first the same relationship (shown in Eq.(2-15)) between the input target displacement x_d and the output shake table displacement x_t is expressed as:

$$\begin{aligned}&\left(\frac{k_{xq}k_{sv}k_d^o s + k_{xq}k_{sv}k_p^o}{k_{xq}k_{sv}k_i^o s}\right)x_d(s) = \\ &\frac{Vm_t}{4\beta A}\frac{\dot{f}_a(s)}{m_t} + \left(k_L + \frac{k_{xq}k_{sv}k_{dp}}{A}\right)m_t\frac{f_a(s)}{m_t} + \left(A + k_{xq}k_{sv}k_d^o\right)\dot{x}_t(s) + k_{xq}k_{sv}k_p^o x_t(s) + k_{xq}k_{sv}k_i^o\frac{x_t(s)}{s}\end{aligned} \quad (2\text{-}16)$$

It is noted that due to the actuator PID controller H_{PID}^o and the feed forward component x_{ff}, filtering to x_t and x_d are applied. These filtering effects might be important in real system applications and need to be monitored from actual experimental setups; however, in this study, it is assumed that the gains are chosen as $H_{PID}^o = k_P^o$ and $k_{ff} = 0$ ($x_{ff} = 0$); therefore, Eq. (2-16) can be expressed in the time domain:

$$\begin{aligned}&k_{xq}k_{sv}k_p^o x_d(t) = \frac{Vm_t}{4\beta A}\frac{\dot{f}_a(t)}{m_t} + \left(k_L + \frac{k_{xq}k_{sv}k_{dp}}{A}\right)m_t\frac{f_a(t)}{m_t} + A\dot{x}_t(t) + k_{xq}k_{sv}k_p^o x_t(t) \quad or \\ &k_a x_d(t) = \frac{1}{\omega_a^2}\frac{\dot{f}_a(t)}{m_t} + \frac{2\xi_a}{\omega_a}\frac{f_a(t)}{m_t} + \dot{x}_t(t) + k_a x_t(t)\end{aligned} \quad (2\text{-}17)$$

where

$\omega_a{}^2 = 4\beta A^2/Vm_t$; ω_a (s^{-1}) is the natural frequency of the shake table system (i.e. $f_{n,a}$ (Hz) = ω_a / 2π), which is also known as oil column frequency (Conte et al., 2000).

$\xi_a = \frac{\omega_a m_t}{2}\left(\frac{Ak_L + k_{xq}k_{sv}k_{dp}}{A^2}\right)$; ξ_a (dimensionless) is the equivalent damping ratio of the shake system

$k_a = k_{xq}k_{sv}k_P^o/A$; k_a (s^{-1}) is the control gain of the shake table system

In the state space form, this equation can be written (Blondet et al.,1988 and Rinawi and Clough, 1991)

$$\underline{\dot{x}}(t) = A\underline{x}(t) + Bu(t) \qquad or$$
$$\frac{d}{dt}\begin{bmatrix} x_t(t) \\ \dot{x}_t(t) \\ f_a(t)/m_t \end{bmatrix} = \begin{bmatrix} 0 & 1 & 0 \\ 0 & 0 & 1 \\ -k_a\omega_a^2 & -\omega_a^2 & -2\xi_a\omega_a \end{bmatrix}\begin{bmatrix} x_t(t) \\ \dot{x}_t(t) \\ f_a(t)/m_t \end{bmatrix} + \begin{bmatrix} 0 \\ 0 \\ k_a\omega_a^2 \end{bmatrix} x_d(t), \qquad \underline{x}(0) = \underline{x}_0 \tag{2-18}$$

The equation can be solved using the 4th order Runge-Kutta method for actual implementations.

2.2 Shake Table – Structure System (2DOF System Model)

When the structure is mounted on the shake table which is mounted on a reaction mass, the dynamics of the system is changed and the transfer functions have to be adjusted. Figure 2-8 shows a schematic of a structure mounted on a shake table including the base reaction mass (see also Conte et al., 2000); the shaded area represents the effects of movement of the reaction mass (m_b), which are assumed to be minor in this study as discussed below.

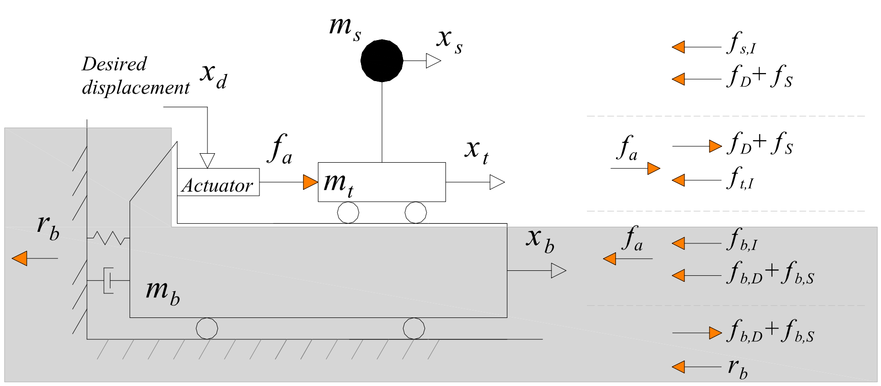

Figure 2-8 Schematic of a shake table-structure system with the reaction mass

The governing equations of motion of the system can be expressed as:

$$\begin{aligned}
&m_s\ddot{x}_s(t) + c_s\dot{x}_s(t) + k_s x_s(t) = -m_s\left(\ddot{x}_t(t) + \ddot{x}_b(t)\right) && or && f_{s,I}(t) + f_D(t) + f_S(t) = 0 \\
&m_t\ddot{x}_t(t) - \{c_s\dot{x}_s(t) + k_s x_s(t)\} = f_a(t) - m_t\ddot{x}_b(t) && or && f_{t,I}(t) - \{f_D(t) + f_S(t)\} = f_a(t) \\
&m_b\ddot{x}_b(t) + c_b\dot{x}_b(t) + k_b x_b(t) = -f_a(t) && or && f_{b,I}(t) + f_{b,D}(t) + f_{b,S}(t) = -f_a(t) \\
&\frac{1}{\omega_a^2}\frac{\dot{f}_a(t)}{m_t} + \frac{2\xi_a}{\omega_a}\frac{f_a(t)}{m_t} + \frac{dx_t(t)}{dt} + k_a x_t(t) = k_a x_d(t)
\end{aligned} \tag{2-19}$$

Where x_s, $\dot{x}_s$, $\ddot{x}_s$ are the relative displacement, velocity and acceleration of the structure with respect to the shake table; m_s, c_s, k_s are the mass, damping coefficient, stiffness of the structure, respectively; x_b, $\dot{x}_b$, $\ddot{x}_b$ are the displacement, velocity and acceleration of the reaction mass with respect to the laboratory floor; m_b, c_b, k_b are the mass, damping coefficient, the effective stiffness of the reaction mass, respectively. All other terms are explained in the previous section. It is clearly shown from the equations that the actuator force $f_a(t)$ is coupled with the structure and the reaction mass responses. This shake table – structure & reaction mass interaction can be also shown by the Laplace domain equation of the actuator force $f_a(s)$ (see also Conte et al., 2000):

$$f_a(s) = m_t s^2 x_t(s)\left[1 + H_B(s)\right]\left[1 + (m_s/m_t)H_S(s)\right] \tag{2-20}$$

where

$$H_B(s) = \frac{x_b(s)}{x_t(s)} = \frac{-s^2\left[m_t/(m_s+m_t)\right]\left\{1+\left[m_s/(m_s+m_t)H_S(s)\right]\right\}}{s^2\left\{1+\left[m_s/(m_s+m_t)H_S(s)\right]\right\} + s2\xi_b\omega_b + \omega_b^2} \tag{2-21}$$

$$H_S(s) = \frac{x_s(s)+x_t(s)+x_b(s)}{x_t(s)+x_b(s)} = \frac{2s\xi_s\omega_s + \omega_s^2}{s^2 + 2\xi_s\omega_s s + \omega_s^2} \tag{2-22}$$

where $\omega_b = \sqrt{k_b/m_b}$; $\xi_b = c_b / 2\omega_b m_b$ and $\omega_s = \sqrt{k_s/m_s}$ (the natural frequency of the structure); $\xi_s = c_s / 2\omega_s m_s$ (the damping ratio of the structure). Substituting the actuator force f_a in Eq. (2-20) to Eq. (2-15), the system transfer function between the target displacement x_d and the shake table displacement x_t can be computed considering the effects of the structure and the reaction mass. It is assumed for simplicity in this study that the reaction mass movement is not significant (as considered also by Rinawi and Clough, 1991); therefore, $x_b = 0$ and $H_B = 0$, and the actuator force f_a becomes:

$$f_a(s) = m_t s^2 x_t(s)\left[1 + (m_s/m_t)H_S(s)\right] \tag{2-23}$$

Without the reaction mass movement, the governing equations of the shake table-structure system in Eq. (2-19) can be rewritten in the state space form as

$$\dot{\underline{x}}(t) = A\underline{x}(t) + Bu(t), \qquad \underline{x}(0) = \underline{x}_0 \qquad or$$

$$\frac{d}{dt}\begin{bmatrix} x_s(t) \\ \dot{x}_s(t) \\ x_t(t) \\ \dot{x}_t(t) \\ f_a(t)/m_t \end{bmatrix} = \begin{bmatrix} 0 & 1 & 0 & 0 & 0 \\ -\left(m_s^{-1}+m_t^{-1}\right)k_s & -\left(m_s^{-1}+m_t^{-1}\right)c_s & 0 & 0 & -1 \\ 0 & 0 & 0 & 1 & 0 \\ m_t^{-1}k_s & m_t^{-1}c_s & 0 & 0 & 1 \\ 0 & 0 & -k_a\omega_a^2 & -\omega_a^2 & -2\xi_a\omega_a \end{bmatrix}\begin{bmatrix} x_s(t) \\ \dot{x}_s(t) \\ x_t(t) \\ \dot{x}_t(t) \\ f_a(t)/m_t \end{bmatrix} + \begin{bmatrix} 0 \\ 0 \\ 0 \\ 0 \\ k_a\omega_a^2 \end{bmatrix} x_d(t) \tag{2-24}$$

The output $y(t)$, defined here as the total structure acceleration response $\ddot{x}_s^{\,t}(t)$, can be expressed by the "output equation":

$$\begin{aligned} y(t) &= C\underline{x}(t), \qquad or \\ y(t) &= \begin{bmatrix} -m_s^{-1}k_s & -m_s^{-1}c_s & 0 & 0 & 0 \end{bmatrix}\underline{x}(t) \end{aligned} \tag{2-25}$$

The equations can be solved using the 4th order Runge-Kutta method.

The shake table with a simple structure, mounted on it as expressed by Eq. (2-24), can be considered as a *2DOF shake table-structure system model*; i.e. the *degree-of-freedoms* (DOF) include the lateral displacement $x_s(t)$ of the structure (defined here also as the test specimen) with respect to the shake table and the lateral displacement $x_t(t)$ of the shake table with respect to the laboratory ground, as shown in Figure 2-1. The control excitation of the shake table is defined as $u(t)$. If the position of the shake table is controlled, then the control excitation $u(t)$ is specified as the desired shake table displacement $x_d(t)$, which should be computed in real time for the displacement control if the controlled system experiences nonlinear behavior (as discussed in SECTION 4).

In order to facilitate the development of a tracking control method, first, it is considered that only an SDOF structure system (denoted as an *SDOF system model*) is controlled in the next section, assuming that the dynamics of the shake table can be ignored. With this simplified model, a new control excitation input $u(t)$ is considered as the excitation force $-m_s\ddot{x}_t(t)$ due to the shake table acceleration $\ddot{x}_t(t)$ (instead of the actual control excitation input $x_d(t)$) as shown in Figure 2-9. In such case, the governing equation of a structure shown in the first equation of Eq. (2-19) can be rewritten as:

$$m_s\ddot{x}_s(t)+c_s\dot{x}_s(t)+k_sx_s(t)=-m_s\ddot{x}_t(t) \quad or \quad =u(t) \tag{2-26}$$

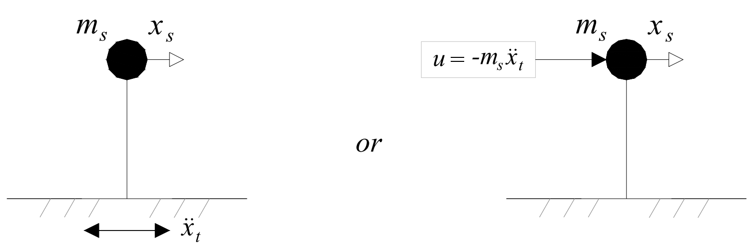

Figure 2-9 Schematic of a simplified SDOF system model with a new control excitation

Then, the developed tracking control method using the simplified SDOF system model will be extended to the 2DOF system model (shown in Figure 2-1), where the shake table dynamics and the table-structure interaction are included. Using the 2DOF system model, the actual control excitation input $u(t)$, which is the desired shake table displacement $x_d(t)$, will be determined in real time, such that the output of a controlled structure will follow a specified target motion.

2.3 Shake Table - Structure Interaction

As shown in the previous section, the relationship (i.e. the transfer function) between the target motion x_d and the shake table displacement x_t changes due to the shake table-structure interaction (Rinawi and Clough, 1991, Dyke et al., 1995, and Conte et al., 2000). Two major reasons of the interaction can be expressed as following;

(1) The actuator force f_a applied to the shake table is coupled with the structure response as clearly shown in Eq. (2-23) and Eq. (2-24).

(2) The servovalve systems have nonlinear behavior (Maddaloni, Ryu and Reinhorn, 2010). The shake table parameters; ω_a, ξ_a and k_a, (which are assumed to be constant) might vary depending on structure characteristics (Rinawi and Clough, 1991 and Trombetti et al., 2002). For example, in general shake table system parameters, obtained from a bare table, are different with the ones estimated after a structure is mounted.

The table-structure interaction caused by the first reason (1) above is mainly considered in this study, and it is assumed that the estimated shake table parameters in preliminary experiments will remain the same in the operating range of interest. This might be acceptable since shake table system parameters, as shown from experiments by Trombetti et al. (2002), were similar in a wide range of the natural frequencies for different structures.

The table-structure interaction can be compensated using the transfer function and its inverse transfer function, if the structure is linear; this method is presented in Section 2.6. When the structure experiences nonlinear behavior due to possibly high intensity excitation, the inverse transfer function compensation is not satisfactory and real time control is necessary; this method is presented in SECTION 4.

2.4 Shake Table Actuator Inner Loop Feedback (PID) Control

The mathematical model of a servovalve-shake table actuator system (a bare table without a mounted structure) was described in Section 2.1. The relation between the excitation input $u(t) = x_d(t)$ (the desired shake table displacement) and the output $y(t) = x_t(t)$ (the achieved shake table displacement) can be expressed as the transfer function H_T in the frequency domain as shown in Eq. (2-15). By choosing the target motion $y_m(t) = x_d(t)$, the control objective of the table-actuator system is to adjust the transfer function through the inner-loop feedback control, such that the output $y(t)$ will follow the target motion $y_m(t)$, which becomes the excitation input $u(t)$ in this case; thus, the desired transfer function is to have unity magnitude and a linear phase (i.e. a simple time delay). The block diagram of the shake table-actuator system is presented in Figure 2-10 (for simplicity the effect of x_{dp}, the differential pressure component, is not included; but see Figure 2-4 for the schematic of the system in detail); note that the terminology was introduced in Section 2.1.

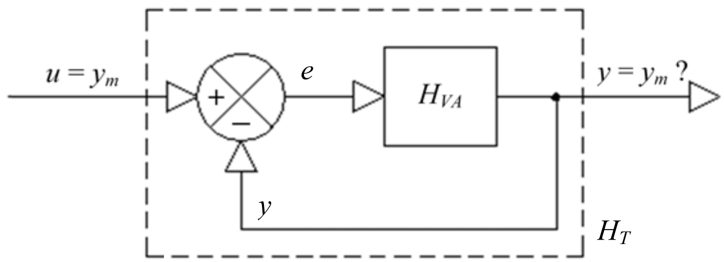

Figure 2-10 Block diagram of shake table-actuator system

For example, the magnitude and the phase angle of the transfer function of a bare shake table-actuator system having selected properties as $f_{n,a}$ = 30.0 Hz, ξ_a = 0.707, and k_a = 70, obtained from Eq. (2-18) are presented in Figure 2-11.

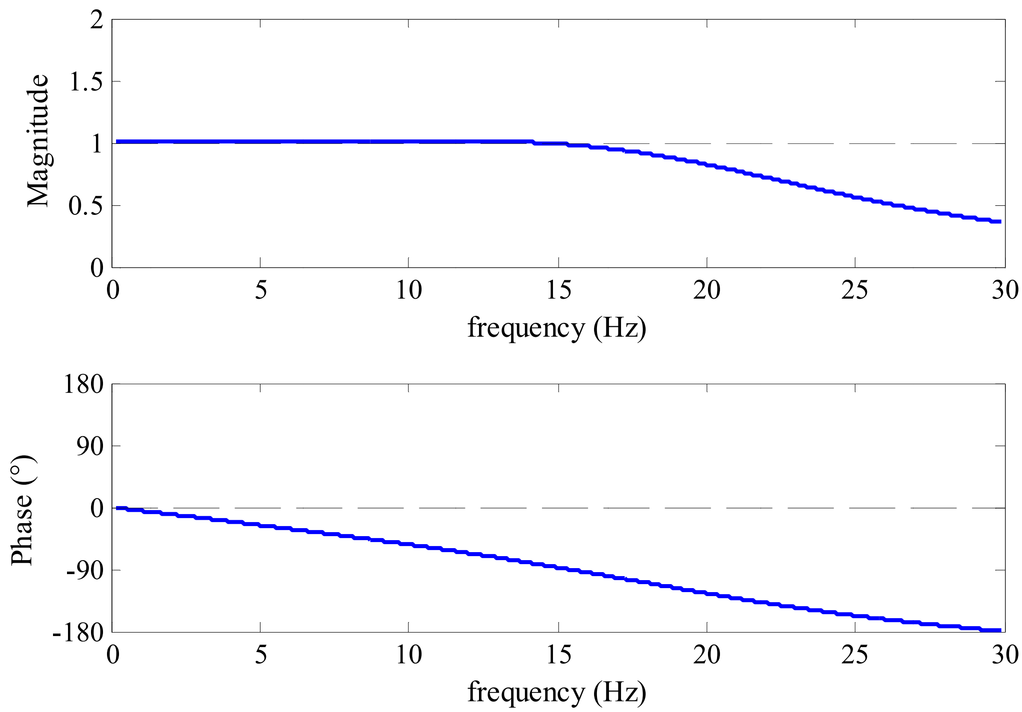

Figure 2-11 Transfer function response of a bare shake table actuator system

The results show that the unity magnitude of the transfer function is obtained up to about 15 Hz, and the phase angle is almost linear in the 0-30Hz range; therefore, the results indicate that the shake table has the operating frequency range of 0-15 Hz with a constant time lag (i.e. delay due to the control dynamics), which satisfies the objective. The time lag can be computed by dividing the phase by the frequency (Chung, Soong, and Reinhorn, 1989 and Phillips et al., 2012); in this example, the time lag is about -16 msec.

However, when a structure is mounted on a shake table, the transfer function is affected by the shake table-structure interaction, as discussed in Section 2.3. The effects vary depending on the properties of the table and the structure. In order to demonstrate the effect of this interaction, the transfer function response of a shake table (the same as presented in Figure 2-11) with a structure is presented in Figure 2-12: the selected properties for this example are: m_s = 1 kips·sec^2/in., k_s = 987 kips/in., and c_s = 1.89 kips·sec/in., (f_n = 5.0 Hz, ξ_n = 0.03), $\mu = m_s / m_t = 1.5$, $f_{n,a}$ = 30.0 Hz, ξ_a = 0.707, and k_a = 70 in Eq. (2-24). The results clearly show the effects of the shake table-structure interaction, with both variable amplification and phase shift around the resonant frequency of the structure.

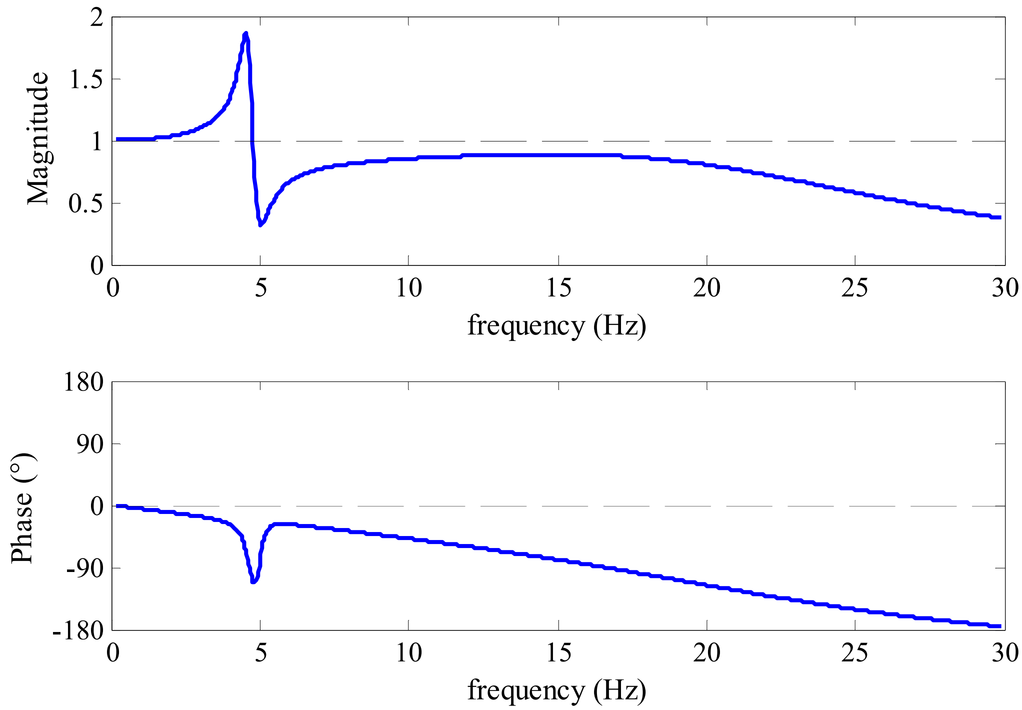

Figure 2-12 Transfer function response of a shake table – structure system

This example indicates that a more advanced control procedure is needed in order to simulate the desired motion at the shake table, or structure, by overcoming the table-structure interaction. Feed-forward compensation procedure is a well-known shake table control method, which is widely used by the most shake table manufacturers (Maddaloni, Ryu and Reinhorn, 2010).

2.5 Feed-Forward Compensation using Inverse Transfer Functions

The inverse transfer function method (ITF), which is the feed-forward method, can be used for a tracking control for a target motion at a shake table (Clark et al, 1970, and Reinhorn, 1985 (class notes), Spencer et al, 1998). The same scheme can be extended to simulate a target motion in a linear structure mounted on a shake table; this method was developed at the University at Buffalo including the authors of this report (see Ryu, 2009, and Maddaloni, Ryu, and Reinhorn, 2010). The method has been implemented by the authors for real applications at the UB-SEESL. The procedure (Ryu, 2009) is explained again in this report for the sake of completion, since the method provides an important base for understanding further developments of a tracking control for nonlinear systems.

2.5.1 Shake Table System

As indicated above, the primary use of a shake table is to simulate the base motion. However, the reproduction of a dynamic signal, due to several factors (e.g. servovalve's dynamic response, compressibility of the actuator fluid, oil leakage through the actuator seals, influence of the test specimen) can be imperfect (Conte et al., 2000). High fidelity responses can be obtained using compensated motions as described in (MTS, 2004) and summarized here for practical implementations.

Assuming that the shake table system is linear, the analytical model represents mathematically the input-output relationship between the excitation $u(t)$ and the output $y(t)$. For shake table testing in displacement control mode, a typical target motion $y_m(t)$ for the shake table is derived from an earthquake acceleration while the excitation input $u(t)$ is the desired table displacement $x_d(t)$. This can be obtained from double integral of the target motion $y_m(t)$ (Spencer and Yang, 1998); i.e. it is noted that in order to avoid a large drift of a shake table, the target motion is to be high-pass filtered (Phillips and Spencer, 2012) to remove a very low frequency depending on the target and the displacement capacity of the shake table). The output $y(t)$ is the measured (achieved) shake table acceleration response $\ddot{x}_t(t)$. While the analytical model is presented for a uni-axial system, the same procedure can be used for multi-axial systems, where matrices of uni-axial models and cross-coupling components would replace the single mathematical model (see Eq. (2-33))

For a shake table system, the transfer function $H_t(\omega)$ between the excitation input $u(t) = x_d(t)$ and the output $y(t) = \ddot{x}_t(t)$ can be expressed in the frequency domain as:

$$H_t(\omega) = \frac{y(\omega)}{u(\omega)} = \frac{\ddot{x}_t(\omega)}{x_d(\omega)} \tag{2-27}$$

where $y(\omega)$ and $u(\omega)$ are the Fourier transforms[2] of $y(t)$ and $u(t)$, respectively. It is also noted that if a built-in shake table controller, such as STEX at the University Buffalo, will generate the excitation input

[2] Fourier Transform is an operation that converts one function of a real variable into a complex function. The new function, often called the *frequency domain representation* of the original function, describes which frequencies are included in the original function; $\omega = 2\pi f$ is the circular frequency (in rad/s) and f is the cyclic frequency (in Hz); $i = \sqrt{-1}$

$u(t)$ by doubly integrating the target (table acceleration) motion $y_m(t)$ (i.e. $u(t) = y_m(t) / (i\omega)^2$), the transfer function $H_t^*(\omega)$ from the relation between the target motion $y_m(t)$ (i.e. which is the user excitation input to STEX) and output $y(t) = \ddot{x}_t(t)$ can also be expressed in the frequency domain as:

$$H_t^*(\omega) = \frac{y(\omega)}{y_m(\omega)} \tag{2-28}$$

and it is noted that the same transfer function can be obtained from Eq. (2-15) by replacing s by $i\omega$.

The transfer function $H_t(\omega)$ (or $H_t^*(\omega)$) represents the steady state response, which would represent the total response with the zero initial conditions (Rinawi and Clough, 1991), and can be interpreted as the degree of "distortion" in signal reproduction of the target motion $y_m(t)$ due to the mechanical and servo-hydraulic system. In order to obtain the best fidelity of the achieved output $y(t)$, a compensated excitation $u_c(t)$ can be applied.

Figure 2-13 presents the schematic diagram of this concept. The target motion y_m represents the start point of the compensation while the achieved output y is the end point. The compensated excitation input applied to the table for the shaking is indicated as u_c.

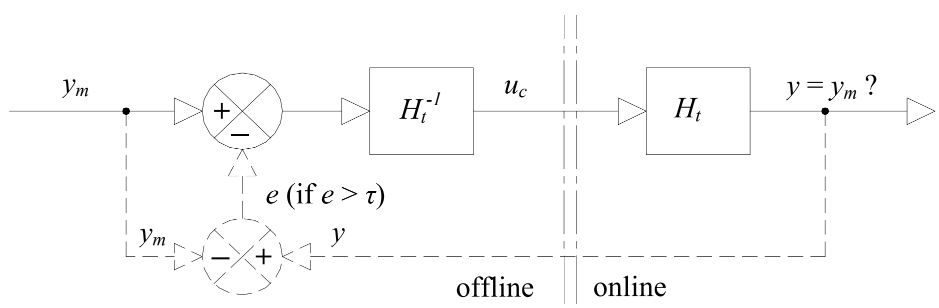

Figure 2-13 Schematic diagram of shake table simulation of an earthquake record (dashed line indicates possible off-line iterations)

According to this scheme and Eq. (2-27), a compensated excitation input $u_c(t)$ should be applied in order to achieve the output $y(t)$, which will track then the target motion $y_m(t)$ as shown in the following equation:

$$\begin{aligned} &if\ u_c(\omega) = H_t(\omega)^{-1} y_m(\omega);\ then \\ &\quad y = H_t(\omega) u_c(\omega) = H_t(\omega) H_t(\omega)^{-1} y_m(\omega) \cong y_m(\omega) \end{aligned} \tag{2-29}$$

where $H_t(\omega)$ and $H_t(\omega)^{-1}$ are the transfer and the inverse transfer functions of the shake table system respectively. Therefore, the excitation input $u_c(\omega)$ is calculated multiplying the target motion $y_m(\omega)$ by the inverse transfer function of the shake table. In practical applications using the compensated excitation input $u_c(t)$ for the shake table, the achieved motion $y(t)$ could not match perfectly the target motion $y_m(t)$

due to non-linearities of the servo-hydraulic system. As shown in Figure 2-13, an error $e(t) = y(t) - y_m(t)$ is calculated and an offline iteration procedure (dashed line) can be used to improve the compensation. The block diagram shows that the iterations are stopped when the error is smaller than a predefined tolerance ($\|e\| < \tau$): it means that this is an acceptable reproduction of the desired motion. In order to reduce the tracking error $e(t)$ of the shake table control, Nakata (2010) and Phillips and Spencer (2012) also introduced outer feedback compensation loops instead of the offline iteration.

The method presented above is a well-known feed-forward compensation procedure used by most shake table manufacturers (Spencer and Yang, 1998 and Maddaloni, Ryu and Reinhorn, 2010). However, when the target is to simulate a desired/target motion at the top of a testing structure mounted on a shake table, the procedure should be modified, as described below.

2.5.2 Shake Table-Structure System Control

In the experimental evaluation of architectural or non-structural components (Reinhorn et al., 2010) or in the qualification testing of complex equipment (IEEE, 2006), it is often necessary to produce the target motion at a specified position of a structure such as a floor/roof of a structure. The previous compensation approach can be generalized for a multi-degree of freedom (MDOF) system (Conte et al., 2000 and Maddaloni, Ryu and Reinhorn, 2010), which represents the specimen in a shake table test. For simplicity, the MDOF structure is represented in this development as a simple plane frame as shown in Figure 2-14.

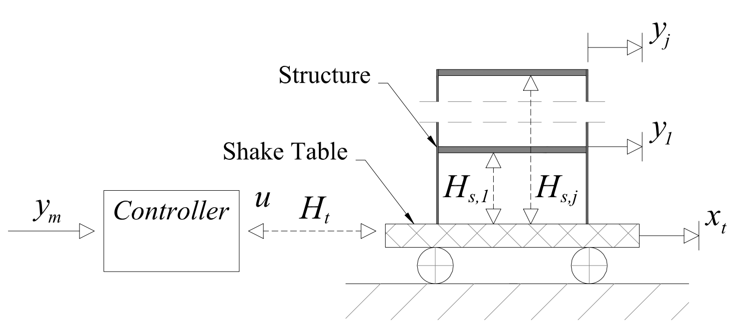

Figure 2-14 Schematic representation of the transfer functions for the shake table (H_t) and structure (H_s)

The acceleration transfer function defined by the ratio of the output structural total acceleration response $y(t) = \ddot{x}_s^t(t)$ to a shake table motion in the frequency domain can be obtained from the procedure described in Maddaloni, Ryu and Reinhorn, (2010); for an SDOF structure, the structure transfer function $H_s(\omega)$ is expressed as:

$$H_s(\omega) = \frac{\ddot{x}_s^t(\omega)}{\ddot{x}_t(\omega)} = \frac{2i\omega\xi_s\omega_s + \omega_s^2}{-\omega^2 + 2i\omega\xi_s\omega_s + \omega_s^2} \tag{2-30}$$

which is the same equation to Eq. (2-22) after substituting $s = i\omega$, and indicates the degree of amplification of the base motion due to the dynamic characteristics of the structure.

The input-output relationship between the shake table excitation input $u(t)$ and achieved (measured) motion $y(t)$ at the specified location of a structure in the uniaxial direction, assuming that the system is linear and remains linear during excitation, can be represented using the system transfer function, which can be computed by multiplying two transfer functions $H_t(\omega)$ and $H_s(\omega)$ shown in Eq. (2-27) and Eq. (2-30):

$$H(\omega) = H_s(\omega) \times H_t(\omega) = \frac{y(\omega)}{u(\omega)} = \frac{\ddot{x}_s^t(\omega)}{x_d(\omega)} \tag{2-31}$$

In a similar fashion described previously, the concept of signal compensation can be applied in order to match the output of a structure to a target motion. Figure 2-15 presents the schematic diagram of this concept. The target motion y_m represents the start point of the compensation while the achieved output y is the end point. The compensated excitation input applied to the table for the shaking is indicated as u_c.

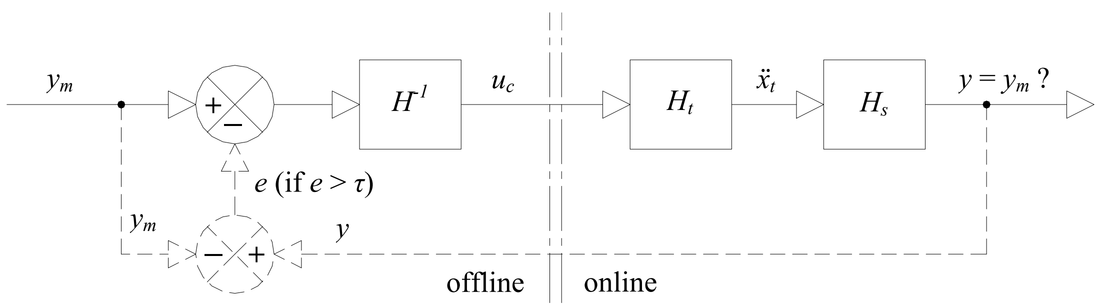

Figure 2-15 Schematic diagram of 'open-loop' compensation procedure (dashed line indicates possible off-line iterations)

According to this scheme and Eq.(2-31), a compensated excitation input $u_c(t)$ should be applied in order to achieve the output $y(t)$ at a structure, which equals to the target motion $y_m(t)$ as shown in the following equation:

$$\begin{aligned} &if\ u_c(\omega) = H(\omega)^{-1} y_m(\omega);\ then \\ &\quad y = H(\omega) u_c(\omega) = H(\omega) H(\omega)^{-1} y_m(\omega) \cong y_m(\omega) \end{aligned} \tag{2-32}$$

where $H(\omega)$ and $H(\omega)^{-1}$ are the transfer and the inverse transfer function of the shake table-structure system, respectively.

In practical applications, the system transfer function is determined from identification with associated uncertainties due to non-linearity in the structure and the shake table and imperfections in identification process. Therefore, the achieved output $y(t)$ cannot perfectly match the target motion $y_m(t)$. In this case, as shown in Figure 2-15, an off-line iteration (dashed line) can be performed to improve the compensation.

2.5.3 Experimental Verification

The compensation procedure developed above was implemented experimentally for a 20ft. × 20ft. test frame, constructed for suspended ceiling system dynamic testing, mounted on a shake table at the University at Buffalo-Structural Engineering and Earthquake Laboratory (UB-SEESL) as shown in Figure 2-16. The objective was to simulate tri-axial target motions in the longitudinal x, transverse y, and vertical z directions at the top corners of the test frame. The target motions were generated to match the AC156-RRS of S_S = 1.0g in each direction. It is noted that the target motions for the three rotational axes (roll r, pitch p, and yaw w) are all zeros.

For a 6 DOF shake table system like the UB-SEESL shake table system, the system transfer function can be expressed as a 6 × 6 matrix and each element of the transfer function matrix at each frequency is determined as:

$$H_{ij}(\omega) = y_{ij}(\omega) / u_j(\omega) \tag{2-33}$$

which is the ratio between the i axis output and the j axis excitation input. Each column of $H(\omega)$ can be established from each uni-axial test in the longitudinal x, transverse y, vertical z, roll r, pitch p, and yaw w axes, respectively. If the system is not coupled, the matrix becomes diagonal and each transfer function is explained as a single mathematical model (i.e. which is the same as the transfer function of a uni-axial system). If the responses in all different directions are coupled, cross-coupling components have to be added and the transfer function matrix $H(\omega)$ becomes a full matrix.

For this application, an uncoupled system in each excitation axis (x, y, and z) was assumed; therefore, the 6 × 6 transfer function matrix in Eq. (2-33) was reduced to a 3 × 3 diagonal matrix and each diagonal element was determined from the input (the target motion) and output (the uncompensated achieved output at the structure, which were computed as the average of the response histories obtained from the accelerometers installed at the 4 top corners of the structure as shown in Figure 2-16) in the x, y, and z axes respectively.

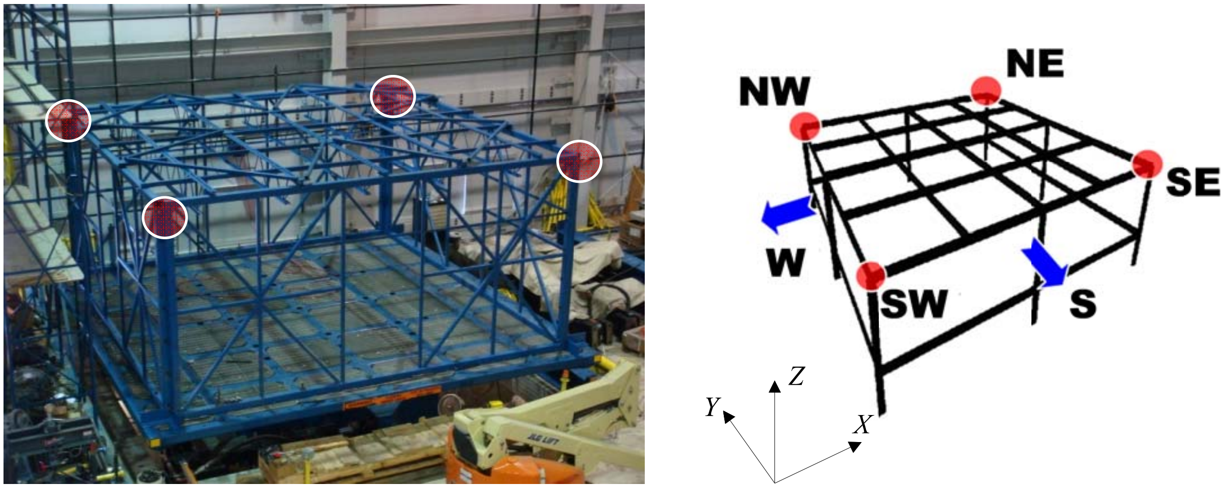

Figure 2-16 Experimental implementation: 20ft. × 20ft. test frame on a shake table at the UB-SEESL (structure responses at frame top corners)

Using the 3×1compensated desired motion vector, the achieved compensated motions are obtained and the results in the longitudinal and vertical directions (i.e. the ones in the transverse direction are very similar with the ones in the longitudinal direction) are presented in Figure 2-17, which shows in each direction, the required response spectrum (RRS) per AC156 (ICC 2010); the response spectrum of the desired target motion y_m ("Desired target"); the response spectrum of the uncompensated achieved output (Y_U), the response spectrum of the compensated target motion $y_{m,c}$ (Target$_C$) (i.e. $y_{m,c}(\omega)$ is obtained by the first equation of Eq. (2-32), where $H(\omega)$ is replaced by $H^*(\omega) = y(\omega)/y_m(\omega)$, which was more straightforward for the UB shake table controller application as discussed for Eq. (2-28), and the response spectrum of the compensated achieved output (Y_C) at the south-west (SW) frame top corner. The achieved compensated output (Y_C) shows good agreement to the target motion in the horizontal direction (Figure 2-17 (a)), while there are relatively large differences between the achieved and the target in the vertical direction (Figure 2-17 (b)).

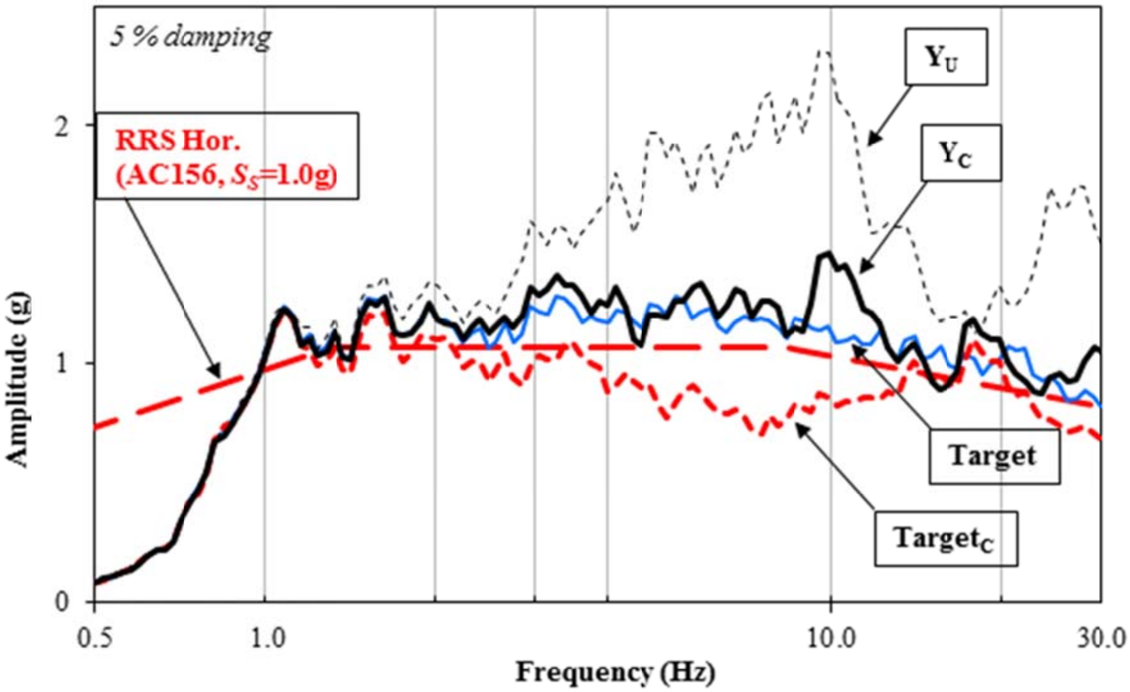

(a) longitudinal

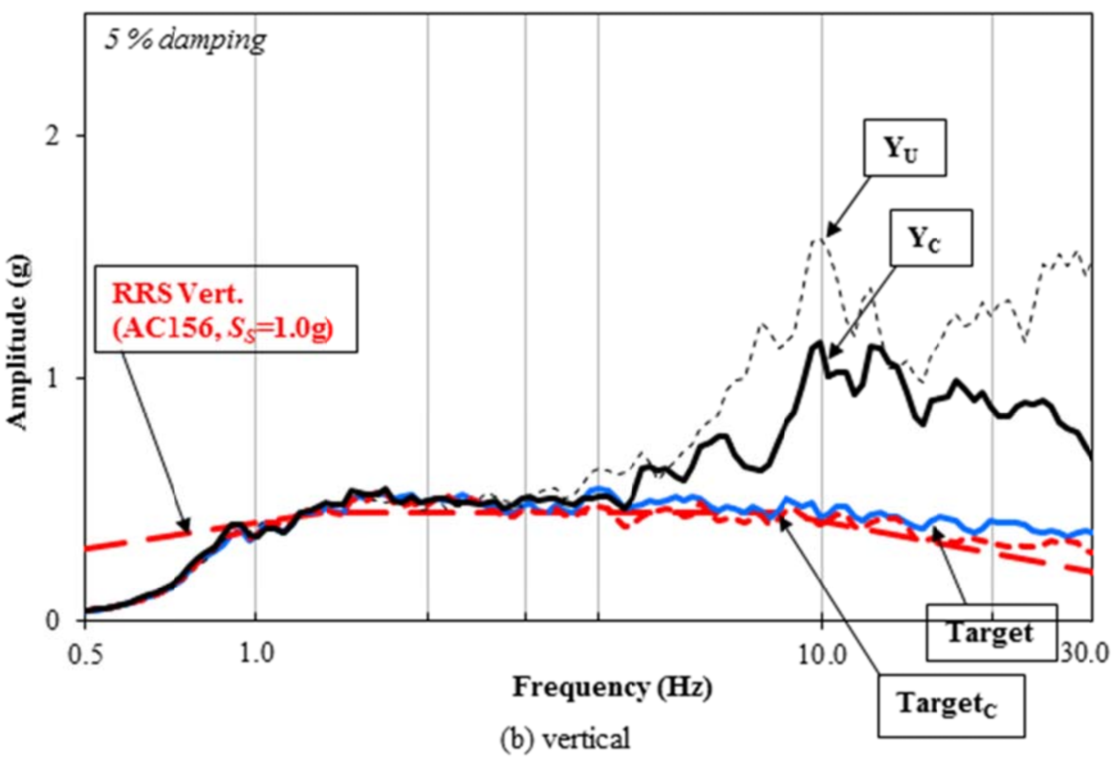

(b) vertical

Figure 2-17 Compensation results (Target vs. achieved motions at SW frame top corner)

The degrees of distortion between the RRS and the response spectrum (RS) of the achieved structure output in signal reproduction can be evaluated by the index:

$$\delta = \sqrt{\frac{1}{N}\sum_{i=1}^{N}\left[\frac{RRS(f_i)-RS(f_i)}{RRS(f_i)}\right]^2} \tag{2-34}$$

The degrees of distortion of the achieved structure outputs in the range of 1 to 30 Hz (with 20 frequencies per octave) are shown in Table 2-1. For purpose of comparison, the degrees of distortion in the target motions (due to their initial generation) are also presented. The distortions are small (<0.15) in the horizontal directions, however, although showing improvement, are large (>0.80) in the vertical.

Table 2-1 Degrees of distortion in signal reproduction (at SW frame top corner)

δ (1)	Target (2)	Uncompensated achieved output (3)	Compensated achieved output (4)
Longitudinal	0.08	0.40	0.12
Lateral	0.09	0.41	0.11
Vertical	0.17	1.46	0.84
Average	0.11	0.75	0.35

The errors in the vertical direction are mainly caused by the coupling between the horizontal and rotational motions. The coupling between responses is evident from non-zero responses in the vertical direction at the top north-west (NW) and north-east (NE) corners, measured from a longitudinal uniaxial excitation input test (with the peak longitudinal acceleration of 0.55g measured at the shake table), as shown in Figure 2-18. Without coupling, the vertical responses of the corners are supposed to be zero. The coupling between the longitudinal-rotational motions at the top of the frame occurred due to the flexibility of the cantilevers of the shake table extension (shown in Figure 2-19).

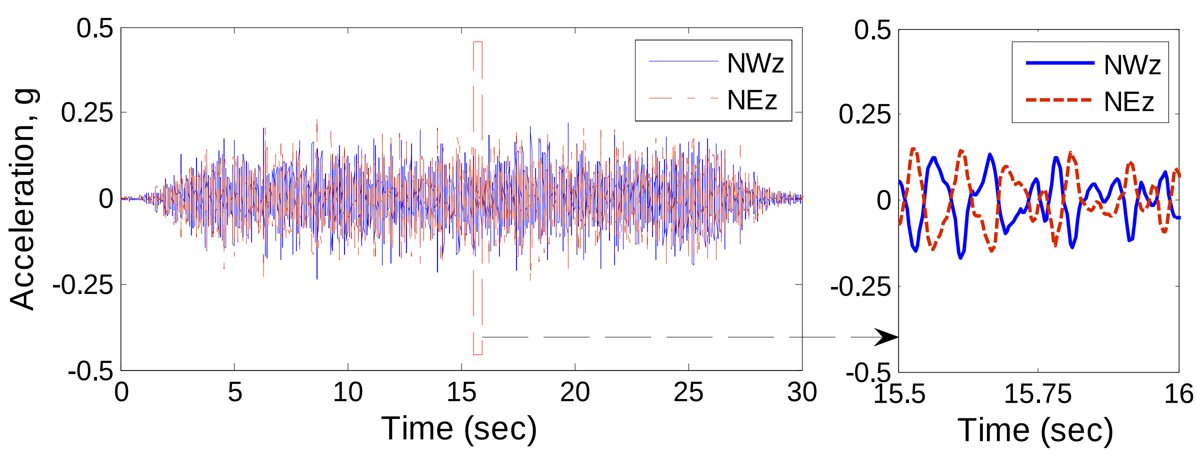

Figure 2-18 Undesired corner vertical motions at NW and NE frame top corners

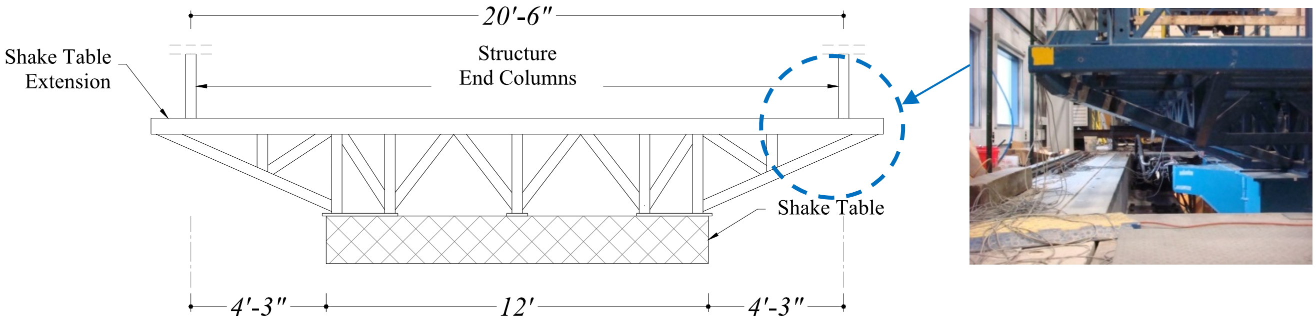

Figure 2-19 Shake table and extension at UB-SEESL, Front elevation

The vertical motions in the corners caused by the coupling of the horizontal-rotational motions might be compensated using the coupled transfer function matrix as described in the previous section; the compensation procedure was numerically implemented and the results were presented in Ryu et al (2013): A simplified analytical model showed that the coupling effects could be compensated using the developed transfer function matrix. The experimental study was also performed at the UB-SEESL and the results did not show much improvement due to the capacity limits of the rotational DOFs (roll r, pitch p, and yaw w) of the shake table: the results indicate that the compensation procedure may produce reasonable target motions only in the shake table operating frequency bandwidth.

In this section, the current practices for shake table control are reviewed. The feedforward compensation method using the system transfer function in the frequency domain can be applied to linear systems in order to reproduce a required target motion at any specific location of a specimen; however, the method is limited to the linear system applications. The mathematical model of a shake table and the governing equation of a shake table and linear structure system are presented. This linear system model will be used in the development of the tracking control schemes in the following sections and will be revised to be applied to nonlinear system control applications.

SECTION 3
TRACKING CONTROL FOR LINEAR SYSTEMS WITH KNOWN PARAMETERS

When the shake table and the test specimens, which need to be challenged by a controlled motion, are behaving linearly (such as elastic systems) with known system properties, the control can be derived from a classical control theory. As addressed in Section 1.1, the control problem considered in this study is a *tracking control* problem, whose objective is to minimize the errors $e(t) = y(t) - y_m(t)$ between the target (desired) motion $y_m(t)$ and the achieved output (response) $y(t)$ of the controlled system. This can be expressed in the following equations:

Behavior of the true system that has to be controlled

$$\begin{aligned} &\dot{\underline{x}}(t) = A\underline{x}(t) + Bu(t), \qquad \underline{x}(0) = \underline{x}_0 \\ &y(t) = C\underline{x}(t) \end{aligned} \tag{3-1}$$

Behavior of a reference model that provides a realistic target:

$$\begin{aligned} &\dot{\underline{x}}_m(t) = A_m\underline{x}_m(t) + B_m r(t), \qquad \underline{x}_m(0) = \underline{x}_{m,0} \\ &y_m(t) = C_m\underline{x}_m(t) \end{aligned} \tag{3-2}$$

Our task (the control objective) is to compute the control excitation input $u(t)$ to drive the table with a specific motion in order to simulate the target motion $y_m(t)$ at a specific location of a test structure mounted on the shake table. For the linear system, various methods can be used in the frequency domain or in the time domain. In this section, four well known tracking control methods, which are the foundation of this study, are introduced.

3.1 Feed-forward Control (Inverse Transfer Function Methods)

The inverse transfer function method (ITF), which is the feed-forward method, can be used for a tracking control as was discussed previously in Section 2.5. The concept is briefly reviewed and reformulated as follows.

The relationship between the control input $u(s)$ and the structure response $y(s)$ for the true system in Eq. (3-1) can be represented in the Laplace domain (complex frequency domain) using the transfer functions $H(s)$, and the relationship between the reference input $r(s)$ and the reference model response $y_m(s)$ in Eq. (3-2) can be represented using the transfer functions $H_m(s)$:

$$H(s) = \frac{y(s)}{u(s)} = k_t \frac{Z_t(s)}{R_t(s)} \tag{3-3}$$

where $Z_t(s)$ and $R_t(s)$ are polynomials (e.g. $s^n + a_1 s^{n-1} + \cdots + a_{n-1}s + a_n$) and k_t is a constant, and

$$H_m(s) = \frac{y_m(s)}{r(s)} = k_m \frac{Z_m(s)}{R_m(s)} \tag{3-4}$$

where $Z_m(s)$ and $R_m(s)$ are polynomials and k_m is a constant. According to the inverse transfer function method introduced in Section 2.5, the control input $u(s)$ is computed by pre-multiplying the target motion $y_m(s)$ with $H^{-1}(s)$:

Control Law

$$u(s) = H^{-1}(s)\, y_m(s) = \left[\frac{1}{k_t}\frac{R_t(s)}{Z_t(s)}\right]\left[k_m \frac{Z_m(s)}{R_m(s)} r(s)\right] \tag{3-5}$$

The control input $u(t)$ in the time domain from that of Eq. (3-5) can simply be computed using the inverse Fourier transform. By substituting this control input into the system equation in Eq. (3-1) the achieved motion $y(t)$ will be the target motion $y_m(t)$, or in the Laplace domain the expected achieved response can be expressed:

Expected Achieved Response

$$y(s) = H(s)\, u(s) = H(s)\cdot H^{-1}(s)\, y_m(s) = \left[k_t \frac{Z_t(s)}{R_t(s)}\right]\left[\frac{1}{k_t}\frac{R_t(s)}{Z_t(s)}\right] y_m(s) \cong y_m(s) \tag{3-6}$$

The main advantages of this method are: (1) the information about the testing system parameters such as the mass, the stiffness, and the damping of a structure and the shake table is normally not required (Maddaloni, Ryu, and Reinhorn, 2010); i.e. the transfer function involving the system properties can easily be obtained by experiments although it can also be computed through the curve fitting method (Nakata, 2010), and (2) the feed-forward (open loop) control scheme can be used so that feedback (closed) loop is not required. However, as previously addressed, this frequency domain method using the system transfer function is limited to linear systems since the pre-computed transfer function is not valid anymore if the system parameters change. It is also known that the feed-forward (open loop) control suffers from the usual drawbacks of deterioration of performance due to small parameter changes and of inexact zero-pole cancellation (Ioannou et al., 2012), which might cause the controlled system to become unstable if the original system is unstable.

3.2 Feed-back + Feed-forward Control (Optimal Tracking Control)

The *optimal tracking control* (OTC) method, which is the feed-back and feed-forward control as explained below, can be also used to solve a tracking problem. As expected, this method like the feed-forward method can only be applied to linear systems. However, the computed control input and the tracking results give valuable information in this study in order to compare the optimal results with other alternative methods; therefore, it is introduced here. It is noted that the *optimal tracking control* problem is a special case of the *linear quadratic regulation* (LQR) problem (Kwakernaak and Sivan, 1972). The control law is obtained using the augmented state equations and the *linear quadratic regulation* (LQR) formulation (Soong, 1990). The thorough derivation in detail can be found in Kwakernaak and Sivan (1972).

The performance index of an optimal tracking control problem can be expressed

$$J = \frac{1}{2}\int_{t_o}^{t_f} \left\{ \left[y(t) - y_m(t) \right]^T Q \left[y(t) - y_m(t) \right] + u^T(t) R u(t) \right\} dt \tag{3-7}$$

where Q is a positive semi-definite weighting matrix and R is a positive definite weighting matrix. This criterion expresses that the controlled achieved response $y(t)$ is to track the target motion $y_m(t)$ while the control input amplitude is restricted. This augmented system of equations from Eq. (3-1) and Eq. (3-2) can be written as:

$$\begin{aligned} \dot{\underline{x}}_a(t) &= \begin{bmatrix} A & 0 \\ 0 & A_m \end{bmatrix} \begin{bmatrix} \underline{x}(t) \\ \underline{x}_m(t) \end{bmatrix} + \begin{bmatrix} B \\ 0 \end{bmatrix} u(t) + \begin{bmatrix} 0 \\ B_m \end{bmatrix} r(t) = A_a \underline{x}_a(t) + B_a u(t) + B_{m,a} r(t), \qquad \underline{x}_a(0) = \begin{bmatrix} \underline{x}(0) \\ \underline{x}_m(0) \end{bmatrix} = \underline{x}_{a,0} \\ y_a(t) &= y(t) - y_m(t) = \begin{bmatrix} C & -C_m \end{bmatrix} \begin{bmatrix} \underline{x}(t) \\ \underline{x}_m(t) \end{bmatrix} = C_a \underline{x}_a(t) \end{aligned} \tag{3-8}$$

The performance index subject to the constraint represented by Eq. (3-8) can be re-written

$$J = \int_{t_o}^{t_f} \left\{ \frac{1}{2} \left[\underline{x}_a^T(t) Q_a \underline{x}_a(t) + u^T(t) R u(t) \right] + \underline{\lambda}^T(t) \left[A_a \underline{x}_a(t) + B_a u(t) + B_{m,a} r(t) - \dot{\underline{x}}_a(t) \right] \right\} dt + \frac{1}{2} \underline{x}_a^T(t_f) S \underline{x}_a(t_f) \tag{3-9}$$

where

$$Q_a = \begin{bmatrix} C^T \\ -C_m^T \end{bmatrix} Q \begin{bmatrix} C & -C_m \end{bmatrix} = \begin{bmatrix} C^T Q C & -C^T Q C_m \\ -C_m^T Q C & C_m^T Q C_m \end{bmatrix}$$

The Hamiltonian can be written as:

$$\mathbf{H}(t) = \frac{1}{2} \left[\underline{x}_a^T(t) Q_a \underline{x}_a(t) + u^T(t) R u(t) \right] + \underline{\lambda}^T(t) \left[A_a \underline{x}_a(t) + B_a u(t) + B_{m,a} r(t) \right] \tag{3-10}$$

The necessary conditions for the control input $u(t)$ to minimize the cost function J are:

$$\dot{\underline{\lambda}}(t) = -\frac{\partial \mathbf{H}(t)}{\partial \underline{x}_a(t)} = -Q_a \underline{x}_a(t) - A_a^T \underline{\lambda}(t) \tag{3-11}$$

$$\dot{\underline{x}}_a(t) = \frac{\partial \mathbf{H}(t)}{\partial \underline{\lambda}(t)} = A_a \underline{x}_a(t) + B_a u(t) + B_{m,a} r(t) \tag{3-12}$$

$$\frac{\partial \mathbf{H}(t)}{\partial u(t)} = 0 = Ru(t) + B_a^{\ T}\underline{\lambda}(t) \ \Rightarrow \ u(t) = -R^{-1}B_a^{\ T}\underline{\lambda}(t) \tag{3-13}$$

For the boundary condition,

$$\left[\partial\left\{\frac{1}{2}\underline{x}_a^{\ T}(t_f)S\underline{x}_a(t_f)\right\} / \partial\underline{x}_a(t) - \underline{\lambda}_a(t)\right]_{t_f} = 0 \qquad \Rightarrow \qquad S\underline{x}_a(t_f) = \underline{\lambda}_a(t_f) \tag{3-14}$$

where t_f is the terminal time. When the control input is generated by the augmented state vector, one has

$$\underline{\lambda}(t) = P(t)\underline{x}_a(t) = \begin{bmatrix} P_{11}(t) & P_{12}(t) \\ P_{21}(t) & P_{22}(t) \end{bmatrix}\begin{bmatrix} \underline{x}(t) \\ \underline{x}_m(t) \end{bmatrix}, \quad P(t_f) = S \tag{3-15}$$

Using Eq. (3-11) to Eq.(3-12), one has the Riccati equation

$$\dot{P}(t) = -Q_a + P(t)B_aR^{-1}B_a^{\ T}P(t) - P(t)A_a - A_a^{\ T}P(t) \tag{3-16}$$

By the partitioning this Riccati equation according to the augmented state vector as shown in Eq. (3-15), it can be found that $P_{11}(t)$ and $P_{12}(t)$, which are needed to compute the control input in Eq. (3-13), are the solution of the matrix differential equations

$$\dot{P}_{11}(t) = -C^TQC + P_{11}(t)BR^{-1}B^TP_{11}(t) - P_{11}(t)A - A^TP_{11}(t), \quad P_{11}(t_f) = 0 \tag{3-17}$$

$$\dot{P}_{12}(t) = C^TQC_m + P_{11}(t)BR^{-1}B^TP_{12}(t) - P_{12}(t)A_m - A^TP_{12}(t), \quad P_{12}(t_f) = 0 \tag{3-18}$$

These partitioned matrix differential equations are solved backwards in time since they are specified at t_f, and produces the optimal solution (Soong, 1990 and Kwakernnak and Sivan, 1972). Substituting these expressions, the control input in Eq. (3-13) can be expressed:

Control Law

$$u(t) = -R^{-1}B_a^{\ T}\underline{\lambda}(t) = -R^{-1}\begin{bmatrix} B \\ 0 \end{bmatrix}^T\begin{bmatrix} P_{11}(t) & P_{12}(t) \\ P_{21}(t) & P_{22}(t) \end{bmatrix}\begin{bmatrix} \underline{x}(t) \\ \underline{x}_m(t) \end{bmatrix} = \begin{bmatrix} K_{fb}(t) & K_{ff}(t) \end{bmatrix}\begin{bmatrix} \underline{x}(t) \\ \underline{x}_m(t) \end{bmatrix} \tag{3-19}$$

where the feedback gain matrix $K_{fb}(t)$ and the feedforward gain matrix $K_{ff}(t)$ are

$$\begin{aligned} K_{fb}(t) &= -R^{-1}B^TP_{11}(t) \\ K_{ff}(t) &= -R^{-1}B^TP_{12}(t) \end{aligned} \tag{3-20}$$

It is noted that in structural engineering applications $P_{11}(t)$ typically remains a constant positive semi-definite solution (Soong, 1990) and the Riccati equation in Eq. (3-17) becomes the algebraic Riccati equation (known also as ARE):

$$-C^TQC + P_{11}BR^{-1}B^TP_{11} - P_{11}A - A^TP_{11} = 0 \tag{3-21}$$

Thus, Eq. (3-20) provides a constant gain ($K_{fb} = -R^{-1}B^TP_{11}$) feedback control, which can be implemented in real time (Crassidis and Junkins, 2012).

Figure 3-1 presents a schematic of an *optimal tracking control*. It clearly shows that the feedback link is independent of the properties of the reference model while, as expected, the feedforward link is affected by both the properties of the reference model and by the true system (controlled).

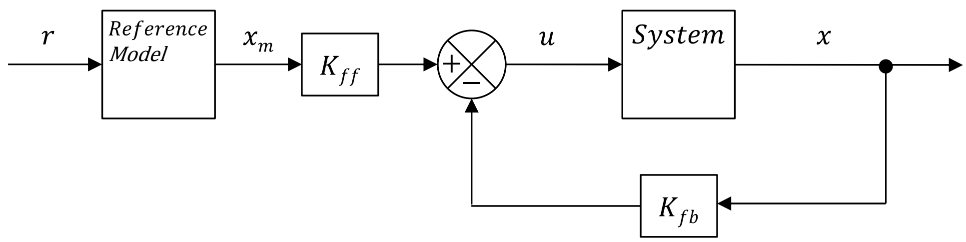

Figure 3-1 Schematic diagram of an optimal tracking control method

By substituting the control excitation input $u(t)$ into the system equation in Eq. (3-1), the expected achieved output $y(t)$ of the controlled structure can be expressed:

<u>Expected Achieved Responses</u>

$$\begin{aligned} &\dot{\underline{x}}(t) = \left[A + BK_{fb}\right]\underline{x}(t) + BK_{ff}(t)\underline{x}_m(t), \qquad \underline{x}(0) = \underline{x}_0 \\ &y(t) = C\underline{x}(t) \end{aligned} \tag{3-22}$$

where the feedback gain matrix $K_{fb}(t)$ and the feedforward gain matrix $K_{ff}(t)$ are shown in Eq. (3-20) and repeated here:

$$\begin{aligned} &K_{fb}(t) = -R^{-1}B^T P_{11}(t) \\ &K_{ff}(t) = -R^{-1}B^T P_{12}(t) \end{aligned} \tag{3-23}$$

Because these gain matrices are derived from the index function J in Eq. (3-7) that is to minimize the difference between the achieved output $y(t)$ and the target motion $y_m(t)$, it is expected that the output $y(t)$ will follow $y_m(t)$ to fulfill the control objective.

<u>Stability of control</u>

The tracking controller must meet the design criteria such that all responses (output) in the closed-loop system are bounded and the controlled achieved output $y(t)$ tracks the target motion $y_m(t)$ as close as possible (Ioannou et al., 2012).

The bounded output stability of the linear systems can be checked using the *Bounded-Input-Bounded-Output* (BIBO) stability (Crassidis et al., 2012). A system with a relaxed condition[3]; i.e. $\underline{x}_0 = \underline{0}$, is said to

[3] Stability for the zero-input response; i.e. non zero-state response can be also examined using the eigenvalues of the closed loop system matrix (Chen, 1999).

be BIBO stable if the output is bounded for any bounded input. An excitation input $u(t)$ is said to be *bounded* if $u(t)$ does not grow to positive or negative infinity (Chen, 1999) such that:

$$\left|u(t)\right| \leq u_m < \infty \tag{3-24}$$

where u_m is a positive constant. Assuming the input is bounded, the responses $\underline{x}(t)$ (therefore, the output $y(t)$) of the *linear time invariant* (LTI) system in Eq. (3-1) is bounded if all eigenvalues of the system matrix have negative real parts (Chen, 1999).

For the *optimal tracking control* (OTC), it is expected that the tracking error $e(t) = y(t) - y_m(t)$ will be minimized by the computed excitation input $u(t)$, fulfilling one of the tracking objectives. The other objective, the bounded response, can be ensured if the eigenvalues of the closed loop system matrix $A_{CL} = [A+BK_{fb}]$ in Eq. (3-22) have negative real parts and the feedforward input $BK_{ff}(t)\underline{x}_m(t)$ is bounded, assuming the feedback gain matrix K_{fb} is a constant matrix (Soong, 1990),.

First, assuming the feedforward input is bounded, it is desired to show that the eigenvalues of the closed loop system matrix A_{CL} are stable (i.e. every eigenvalue has no positive real part), however, it is not straightforward to examine the eigenvalues of A_{CL} due to the complex of the solution for P_{11} from the algebraic Riccati equation in Eq.(3-21).

Instead, the *Lyapunov's direct method*[4] (Crassidis and Junkins, 2012) can be used to show the stability of the OTC system. The close loop dynamics of the OTC in Eq. (3-22), after substituting the feedback gain $K_{fb} = -R^{-1}B^TP_{11}$, is

$$\underline{\dot{x}}(t) = \left[A - BR^{-1}BP_{11}\right]\underline{x}(t), \qquad \underline{x}(0) = \underline{x}_0 \tag{3-25}$$

which is the same equation as the *linear quadratic regulator* (LQR) and the stability of the LQR controller is shown using the *Lyapunov's direct method* in Crassidis and Junkins (2012). For the introduction of the Lyapunov's direct method, the procedure is presented below. The following candidate Lyapunov function is considered

$$V\left[\underline{x}(t)\right] = \underline{x}(t)^T P_{11}\underline{x}(t) \tag{3-26}$$

The time derivative of Eq. (3-26) yields

$$\dot{V}\left[\underline{x}(t)\right] = \underline{\dot{x}}(t)^T P_{11}\underline{x}(t) + \underline{x}(t)^T P_{11}\underline{\dot{x}}(t) \tag{3-27}$$

Substituting Eq. (3-25) into Eq. (3-27) leads to

---

[4] *Lyapunov's direct method* (Crassidis and Junkins, 2012): Lyapunov stability is given if a chosen scalar function $V(\underline{x})$, which is closely related to the energy of a system, satisfies the following conditions: i. $V(\underline{x}_e) = 0$ where $\underline{x}_e$ = an equilibrium point (i.e. $\underline{\dot{x}}(t) = 0$); ii. $V(\underline{x}) > 0$ for $\underline{x} \neq \underline{x}_e$; iii. $\dot{V}(\underline{x}) \leq 0$; then, the equilibrium point $\underline{x}_e$ is stable. Furthermore, if $\dot{V}(\underline{x}) < 0$ for $x \neq x_e$; then, the equilibrium point $\underline{x}_e$ is asymptotically stable.

$$\dot{V}\left[\underline{x}(t)\right]=\underline{x}(t)^T\left[A^TP_{11}+P_{11}A-2P_{11}BR^{-1}B^TP_{11}\right]\underline{x}(t) \tag{3-28}$$

By substituting $[A^TP_{11}+P_{11}A] = [-C^TQC + P_{11}BR^{-1}B^TP_{11}]$ from Eq. (3-21), it is obtained

$$\dot{V}\left[\underline{x}(t)\right]=-\underline{x}(t)^T\left[C^TQC+P_{11}BR^{-1}B^TP_{11}\right]\underline{x}(t) \tag{3-29}$$

Clearly, if R and C^TQC are positive definite matrices, then the Lyapunov condition; i.e. $\dot{V}[\underline{x}(t)] < 0$, is satisfied and the close loop dynamics is asymptotically stable, which indicates that all eigenvalues of A_{CL} have negative real parts. Also, if C^TQC is only a positive semi-definite matrix, $\dot{V}[\underline{x}(t)] \leq 0$ and the close loop dynamics are marginally stable.

Secondly, to show the stability of the OTC controller it is required to prove that the feedforward input $BK_{ff}(t)\underline{x}_m(t)$ is also bounded. The target state $\underline{x}_m(t)$ is known and chosen to be bounded; however, it is difficult to show if $K_{ff}(t)$ is bounded due to the complex of the solution for P_{11} and P_{12} from the Riccati equation in Eq.(3-16). Therefore, the performance of $K_{ff}(t)$ is examined using a simple scalar system example where the system equations in Eq. (3-1) and Eq. (3-2) with C and $C_m = 1$ can be expressed

$$\begin{aligned}\dot{x}(t)&=ax(t)+bu(t), \qquad x(0)=x_0\\ \dot{x}_m(t)&=-a_mx_m(t)+b_mr(t), \qquad x_m(0)=x_{m,0}\end{aligned} \tag{3-30}$$

where $a_m > 0$ for a stable system target response. The value for $p_{11} = P_{11}$ in the algebraic Riccati equation, Eq. (3-21) can be found using the property $p_{11} \geq 0$ (Crassidis and Junkins, 2012);

$$p_{11}=rb^{-2}\left(a+\sqrt{a^2+b^2\,q/r}\right) \tag{3-31}$$

where $r = R$ and $q = Q$ are positive constant. Substituting p_{11} into the differential equation for $p_{12}(t) = P_{12}(t)$ in Eq. (3-18) yields

$$\dot{p}_{12}(t)=\left[a_m+\sqrt{a^2+b^2\,q/r}\right]p_{12}(t)+q, \quad p_{12}(t_f)=0 \tag{3-32}$$

which must be integrated backward in time. To express this equation more conveniently, set $\tau = t_f - t$ (i.e. $t = t_f - \tau$). Since $d\tau = -dt$, writing Eq. (3-32) in terms of τ gives

$$-\frac{d}{d\tau}p_{12}(t_f-\tau)=\left[a_m+\sqrt{a^2+b^2\,q/r}\right]p_{12}(t_f-\tau)+q, \quad p_{12}(\tau_0)=0 \tag{3-33}$$

Clearly, it is shown that the equation is asymptotically stable since $[-a_m - \sqrt{a^2+b^2q/r}] < 0$; therefore, $p_{12}(t)$ is bounded as well as $k_{ff}(t) = -r^{-1}bp_{11}$ is bounded; the feedforward input $bk_{ff}(t)\underline{x}_m(t)$ is also bounded. This simple scalar example demonstrates the stability of the OTC controller.

3.3 Feedback Control

Two tracking control methods using the feedback control scheme are presented. These methods can be used for nonlinear systems by computing the control input in real time with available information at every instant. The similarity and/or the differences of the two methods are discussed in this section.

3.3.1 Predictive Tracking Control (PTC)

The discrete predictive control strategy for linear systems was developed and presented by Rodellar et al. (1987), where the control objective was mainly to reduce the response of structures under dynamic excitations. This method can be used for a target tracking control.

A general performance index for the prediction horizon [$k\Delta t$, $(k+n)\Delta t$] is expressed

$$\begin{aligned} J = &\frac{1}{2}\sum_{j=0}^{n}\left\{\left[\hat{y}(k+j\,|\,k)-y_m(k+j\,|\,k)\right]^T Q(j)\left[\hat{y}(k+j\,|\,k)-y_m(k+j\,|\,k)\right]\right\} \\ &+\frac{1}{2}\sum_{j=0}^{n-1}\left\{\hat{u}(k+j\,|\,k)^T R(j)\hat{u}(k+j\,|\,k)\right\} \end{aligned} \tag{3-34}$$

where $\hat{y}(k+j|k)$ is the predicted output of the controlled system and $y_m(k+j|k)$ is the target motion at instant $k\Delta t$ for instant $(k+j)\Delta t$, and $\hat{u}(k+j|k)$ is the corresponding control sequence. $Q(j)$ is a positive semi-definite weighting matrix and $R(j)$ is a positive definite weighting matrix. It is noted that if in Eq. (3-34) one makes $k = 0$ and $n = N$ where N is the final instant of the control action, this equation is the discrete counterpart of the performance index of the continuous optimal tracking control shown in Eq. (3-9) where $\underline{x}_a(t_f) = \underline{0}$ chosen. To make the problem simpler and to achieve fast tracking, n is chosen as 1 (one) with $Q(0) = 0$ in this study; i.e. a smaller value of n results in a smaller tracking error while it demands lager control inputs, as discussed by Soong (1990). The chosen instantaneous performance index J (i.e. based on Rodellar et al., 1987) is

$$J = \frac{1}{2}\left[\hat{y}_{k+1}-y_{m,k+1}\right]^T Q\left[\hat{y}_{k+1}-y_{m,k+1}\right]+\frac{1}{2}u_k^{\,T} R u_k \tag{3-35}$$

where Q and R are the positive definite and positive semi-definite weighting matrices, respectively, and subscript k+1 indicates 'computed at instant $k\Delta t$ for instant $(k+1)\Delta t$' like '$(k+j)|k$' in Eq. (3-34) and $\hat{u}(k|k) = u_k$, the control input at instant $k\Delta t$. The predicted output $\hat{y}_{k+1}$ and the target motion $y_{m,k+1}$ can be computed using a discrete time state-space models, which are the counterpart of the continuous system equations in Eq. (3-1) and Eq. (3-2)

$$\begin{aligned} &\underline{\hat{x}}_{k+1} = A_D\underline{\hat{x}}_k + B_D u_k, \qquad \underline{x}(0) = \underline{x}_0 \\ &\hat{y}_{k+1} = C_D\underline{\hat{x}}_{k+1} \end{aligned} \tag{3-36}$$

where $\hat{\underline{x}}_k$ is the estimate of the true state vector $\underline{x}_k$ at instant $k\Delta t$; i.e. $\hat{\underline{x}}_k = \underline{x}_k$ for the systems with known parameters and no measurement noise considered; therefore, the predicted output is equal to the true one $\hat{y}_{k+1} = y_{,k+1}$, and

$$\begin{aligned} &\underline{x}_{m,k+1} = A_{m,D}\underline{x}_{m,k} + B_{m,D}r_k, \qquad \underline{x}_m(0) = \underline{x}_{m,0} \\ &y_{m,k+1} = C_{m,D}\underline{x}_{m,k+1} \end{aligned} \tag{3-37}$$

For the linear time-invariant system, the solutions of discrete-time system matrices A_D and B_D ($A_{m,D}$ and $B_{m,D}$) can be computed, assuming the input u_k (r_k) is piecewise constant in a digital controller (Chen, 1999),

$$\begin{aligned} &A_D = e^{A\Delta t} = I + A\Delta t + \frac{1}{2!}(A\Delta t)^2 + \frac{1}{3!}(A\Delta t)^3 + \ldots \quad and \\ &B_D = \int_0^{\Delta t} e^{A\tau} d\tau B = \Delta t(I + \frac{1}{2!}A\Delta t + \frac{1}{3!}(A\Delta t)^2 + \ldots)B = \left(\sum_{n=1}^{\infty} \frac{\Delta t}{n!}(A\Delta t)^{n-1}\right)B \\ &\qquad\qquad\qquad\qquad\qquad\qquad\qquad\qquad or\ A^{-1}(A_D - I)\underline{B}\ \text{(if } A \text{ is nonsingular)} \end{aligned} \tag{3-38}$$

and C_D is the same as C ($C_{m,D} = C_m$).

The control input u_k, which minimizes the performance index J in Eq. (3-35), can be computed by imposing the condition $\partial J/\partial u_k = 0$;

Control Law

$$u_k = \left[B_D^{*T} Q B_D^* + R\right]^{-1} B_D^{*T} Q\left[y_{m,k+1} - A_D^* \hat{\underline{x}}_k\right] = \Gamma\left[y_{m,k+1} - A_D^* \hat{\underline{x}}_k\right] \tag{3-39}$$

where $A_D^* = C_D A_D$ and $B_D^* = C_D B_D$ and $\Gamma = [B_D^{*T} Q B_D^* + R]^{-1} B_D^{*T} Q$. The predicted response using this calculated control input u_k can be obtained by substituting Eq. (3-39) into Eq. (3-36)

Expected Achieved Responses

$$\hat{y}_{k+1} = C_D \hat{\underline{x}}_{k+1} = C_D\left[A_D \hat{\underline{x}}_k + B_D \Gamma\left\{y_{m,k+1} - A_D^* \hat{\underline{x}}_k\right\}\right] = C_D\left\{\left(A_D - B_D \Gamma A_D^*\right)\hat{\underline{x}}_k + B_D \Gamma y_{m,k+1}\right\} \tag{3-40}$$

If $B_D^* = C_D B_D$ is an invertible matrix and $R = 0$ chosen (i.e. indicating no limit for the control input), then Eq. (3-40) becomes

$$\hat{y}_{k+1} = C_D \hat{\underline{x}}_{k+1} = A_D^* \hat{\underline{x}}_k + \left(B_D^* B_D^{*-1}\right) Q^{-1}\left(B_D^{*-T} B_D^{*T}\right) Q\left\{y_{m,k+1} - A_D^* \hat{\underline{x}}_k\right\} = y_{m,k+1} \tag{3-41}$$

and the predicted tracking error $e_{k+1} = \hat{y}_{k+1} - y_{m,k+1}$ becomes 0 (zero) as desired.

Stability

As discussed, the tracking objectives are to minimize the tracking error and to have the state responses in the closed-loop system be bounded. It is shown that the predicted tracking error becomes zero; i.e. $e_{k+1} \rightarrow 0$. In order to check if the responses of the state (e.g. the displacements $\underline{x}$ and velocities $\dot{\underline{x}}$), of the controlled system are bounded, one can check the closed loop stability (as discussed in Section 3.2). The closed loop equation can be expressed by substituting the control input u_k into the system equation of Eq. (3-36):

$$\begin{aligned}\underline{\hat{x}}_{k+1} &= A_D\underline{\hat{x}}_k + B_D\Gamma\left[y_{m,k+1} - A_D^*\underline{\hat{x}}_k\right] \\ &= \underbrace{\left[A_D - B_D\Gamma A_D^*\right]}_{A_{CL,D}}\underline{\hat{x}}_k + B_D\Gamma y_{m,k+1}\end{aligned} \tag{3-42}$$

The state responses will be bounded if every eigenvalues of $A_{CL,D}$ has a magnitude less than 1 (Chen, 1999). This procedure is applied for an example in Ch 3.3.2 where the feedback linearization method is used.

Limitation of 2DOF Shake Table-Structure Systems

When the product $C \times B$, of the output and input matrices in the system equations in Eq. (3-1) and Eq. (3-2), is singular, it is required to change the procedure in order to establish a valid control law; for example, $C \times B = 0$ for the shake table-structure 2DOF model shown in Equations (2-24) and (2-25) with the output $y(t)$ of the total acceleration response $\ddot{x}_s^t(t)$ at the structure.

In order to force the control input u_k to appear in the output equation, a higher order differentiation of the output $\hat{y}_{k+1}$ in discrete time or $\hat{y}(t+h)$ in continuous time is needed. Even though the equivalent control law can be developed in both time formats, the continuous time form $\hat{y}(t+h)$ is preferred in that the predicted time interval h is not restricted to be the same as Δt, the sampling time step. Thus, h can be chosen by the design engineer as a controller parameter (as discussed in Lu, 1995). The procedure to formulate the predictive tracking control law for nonlinear continuous systems was presented by Lu (1994). One possible way to predict (estimate) the output is to use the Taylor series expansion (Sauer, 2006):

$$\hat{y}(t+h) = y(t) + h\dot{y}(t) + \left(h^2/2\right)\ddot{y}(t) + \ldots + \left(h^n/n!\right)y^{(n)}(t) + \ldots \tag{3-43}$$

For our shake table-structure 2DOF model, the output needs up to three terms; thus, the approximated predicted output $\hat{y}^*(t+h)$ and target motion $y_m^*(t+h)$ are defined

$$\begin{aligned}\hat{y}^*(t+h) &= y(t) + h\dot{y}(t) + \left(h^2/2\right)\ddot{y}(t) \\ y_m^*(t+h) &= y_m(t) + h\dot{y}_m(t) + \left(h^2/2\right)\ddot{y}_m(t)\end{aligned} \tag{3-44}$$

where $\dot{y}(t)$ and $\ddot{y}(t)$ in the first equation can be expressed using Equations (2-24) and (2-25)

$$\begin{aligned}\dot{y}(t) &= C\dot{\underline{\hat{x}}}(t) = C\left[A\underline{\hat{x}}(t) + Bu(t)\right] = CA\underline{\hat{x}}(t) \\ \ddot{y}(t) &= C\ddot{\underline{\hat{x}}}(t) = CA\dot{\underline{\hat{x}}}(t) = CA\left[A\underline{\hat{x}}(t) + Bu(t)\right] = CA^2\underline{\hat{x}}(t) + CABu(t)\end{aligned} \tag{3-45}$$

It is noted that the control input does not appear in the right side of first equation due to $CB = 0$ (i.e. scalar for this *single input single output* system) and does appear in the second equation because $CAB \neq 0$.

The control excitation input $u(t)$ can be obtained by minimizing the performance index J in Eq. (3-35) by replacing the output $\hat{y}(t+h)$ and the target $y_m(t+h)$ to their approximations $\hat{y}^*(t+h)$ and $y_m^*(t+h)$ after substituting Eq. (3-45) in Eq. (3-44);

Control Law

$$u(t) = \left[B^{*T} Q B^* + R\right]^{-1} B^{*T} Q \left[y_m^*(t+h) - A^* \underline{\hat{x}}(t)\right] \tag{3-46}$$

where $A^* = [C + hCA + (h^2/2)CA^2]$ and $B^* = (h^2/2)CAB$. By substituting Eq. (3-46) into the second equation of Eq. (3-45), one can establish the error dynamics. For a system having B^* is a non-zero scalar (i.e. an invertible matrix, size 1×1), and $R = 0$ chosen, $\ddot{y}(t)$ becomes

Expected Achieved Responses

$$\begin{aligned} \ddot{y}(t) &= CA^2 \underline{\hat{x}}(t) + CAB\left[B^*\right]^{-1}\left[y_m^*(t+h) - A^* \underline{\hat{x}}(t)\right] \\ &= \ddot{y}_m(t) - \left(2/h^2\right)\left[\left(y(t) - y_m(t)\right) + h\left(\dot{y}(t) - \dot{y}_m(t)\right)\right] \end{aligned} \tag{3-47}$$

which can be rewritten by introducing the tracking error ($e(t) = y(t) - y_{m,}(t)$) to show its dynamics

$$\ddot{e}(t) + (2/h)\dot{e}(t) + \left(2/h^2\right)e(t) = 0 \tag{3-48}$$

This equation clearly shows the tracking error $e(t) \to 0$ as $t \to \infty$ since $h > 0$. As addressed above, h is a tracking error design parameter and can be selected by the design engineer. The equation indicates that the faster tracking can be achieved with smaller h, but it requires larger control efforts.

To ensure the stability of the control scheme, one needs to check not only the output but also the state responses of the controlled system. This can be done by looking at the closed loop stability; this procedure is presented in Ch 3.3.2 where the feedback linearization method is presented.

3.3.2 Feedback Linearization Tracking Control (FTC)

Another possible tracking control scheme is *Feedback Linearization Tracking Control* (FTC) (Ioannou et al., 2006). FTC can be used also for the nonlinear system control (see Section 4.3); however, in this section, the method is applied to linear systems, which are the special cases of nonlinear systems. The target motion $y_m(t)$ can be chosen to be bounded and differentiable; i.e. a more realistic target motion at a structure can be generated by using the reference model, which has desired dynamic characteristics and is driven by a reference input (as discussed in Section 1.1). The controller can be designed such that, by replacing the true system parameters with the desired ones, the output $y(t)$ of the controlled system will follow the target motion.

In a scalar case; i.e. $\underline{x}(t) = x(t)$, the equations of the true system and the reference model in Eq. (3-1) and Eq. (3-2) can be rewritten:

True System Behavior

$$\begin{aligned} \dot{x}(t) &= ax(t) + bu(t), \qquad x(0) = x_0 \\ y(t) &= cx(t) \end{aligned} \tag{3-49}$$

Reference Model Governing Equations

$$\begin{aligned} \dot{x}_m(t) &= -a_m x_m(t) + b_m r(t), \qquad x_m(0) = x_{m0} \\ y_m(t) &= c_m x_m(t) \end{aligned} \tag{3-50}$$

where all coefficients are positive constants. The system output $y(t)$ is to be differentiated until the control excitation input $u(t)$ appears in the expression of the differentiated output

$$\dot{y}(t) = c\dot{x}(t) = cax(t) + cbu(t) \tag{3-51}$$

The main objective of the tracking control is by using the control excitation input $u(t)$ to reduce the tracking error signal $e(t) = y(t) - y_m(t)$, which is defined as the difference between the system output $y(t)$ and the target motion $y_m(t)$. The desired tracking error dynamics can be defined as

$$\dot{e}(t) + k_1^* e(t) = 0 \tag{3-52}$$

where k_1^* is a design error coefficient, chosen by the engineer, and a positive constant; thus, the tracking error $e(t)$ goes to zero as time goes to infinity; $e(t) \rightarrow 0$ as $t \rightarrow \infty$. Eq. (3-52) can be rewritten using the expression $e(t) = y(t) - y_m(t)$ as

$$\left[\dot{y}(t) - \dot{y}_m(t)\right] + k_1^*\left[y(t) - y_m(t)\right] = 0 \tag{3-53}$$

Moving all terms in Eq. (3-53) to the right-hand side except $\dot{y}(t)$ gives

$$\dot{y}(t) = \dot{y}_m(t) - k_1^*\left[y(t) - y_m(t)\right] \quad or \quad v(t) \tag{3-54}$$

where a new term $v(t) = \dot{y}_m(t) - k_1^*[y(t) - y_m(t)]$ is introduced for brevity. Equating this equation to the right-hand side of Eq. (3-51) yields

$$cax(t) + cbu(t) = v(t) \tag{3-55}$$

By solving this equation for the control excitation input $u(t)$, the feedback tracking control law is obtained as following:

Control Law

$$u(t) = \frac{1}{cb}\left[-cax(t) + v(t)\right] \quad or \quad \frac{1}{cb}\left[-cax(t) + \left\{\dot{y}_m(t) - k_1^*\left[y(t) - y_m(t)\right]\right\}\right] \tag{3-56}$$

where the first term in the right hand side -$cax(t)$ will cancel the original system dynamics (the first term $cax(t)$ in Eq. (3-51)), and the new input $v(t)$, the second term in the right hand side, can be chosen such that the tracking objective will be accomplished (as described above).

Expected Achieved Responses

By using the determined control excitation input $u(t)$ from Eq. (3-56), it is expected that the tracking error $e(t) \rightarrow 0$ as $t \rightarrow \infty$ as shown in Eq. (3-52). It is also expected that when the error coefficient k_1^* in the tracking error equation increases, the error will rapidly diminish, but it will require larger control efforts (thus, larger actuator forces).

Stability

To fulfill the tracking objectives, it is shown that the tracking error goes to zero, $e(t) \rightarrow 0$. It is also required to check if all the responses of the controlled system are bounded. This can be checked from the closed loop system by substituting the control excitation input $u(t)$ from Eq. (3-56) into the true system equation (3-49):

$$\begin{aligned}\dot{x}(t) &= ax(t) + c^{-1}\left[-cax(t) + \dot{y}_m(t) - k_1^*\left\{y(t) - y_m(t)\right\}\right] \\ &= c^{-1}\left[-k_1^* cx(t) + \dot{y}_m(t) + k_1^* y_m(t)\right] \\ &= -k_1^* x(t) + c^{-1}\left[\dot{y}_m(t) + k_1^* y_m(t)\right]\end{aligned} \tag{3-57}$$

Cleary, the responses $x(t)$ and $\dot{x}(t)$ will be bounded since $-k_1^* < 0$ and the input part $c^{-1}[\dot{y}_m(t) + k_1^* y_m(t)]$ is bounded (i.e. the target motion $y_m(t)$ is bounded) according to the *Bounded-Input-Bounded-Output* (BIBO) stability (Crassidis and Junkins, 2012), discussed in Section 3.2. It is noted that this stability analysis for a first order system is not applicable to higher order systems. However, the stability can be checked from the closed loop systems using the same analysis scheme.

Application to SDOF Linear Structures

The feedback linearization tracking control method is applied to a linear structure (an SDOF system model) previously shown in Eq. (2-26) with the output $y(t)$ of the total acceleration response $\ddot{x}_s^t(t)$ at the structure.

Using the same procedure described above, the control law can be obtained (see detailed Derivation 3.1 in Appendix 3.1)

Control Law

$$u(t) = \left(-c_s m_s^{-2}\right)^{-1}\left[-\dot{y}^*(t) + v(t)\right] \tag{3-58}$$

where $\dot{y}^*(t)$ is defined as

$$\dot{y}^*(t) = m_s^{-2} c_s\left[c_s \dot{x}_s(t) + k_s x_s(t)\right] - m_s^{-1} k_s \dot{x}_s(t) \tag{3-59}$$

Substituting $u(t)$ from Eq. (3-58) into the equation of the differentiated output $\dot{y}(t)$ (Eq. (B-3) in Appendix 3.1) leads to

$$\dot{y}(t) = v(t) \tag{3-60}$$

This new input $v(t)$ can be chosen as following, to reduce the tracking error signal $e(t) = y(t) - y_m(t)$,

$$v(t) = \dot{y}_m(t) - k_1^* e(t) \tag{3-61}$$

that leads to the following tracking error dynamics (as discussed in the previous derivation):

Expected Achieved Responses

$$\dot{e}(t) + k_1^* e(t) = 0 \tag{3-62}$$

where the tracking error signal $e(t) \to 0$ as $t \to \infty$ by selecting $k_1^* > 0$.

Stability

It is shown that the tracking error goes to zero, $e(t) \to 0$, indicating that $y_m(t) = \ddot{x}_s^t(t) = (\ddot{x}_s(t) - m_s^{-1}u(t))$ is bounded; however, checking is needed to find if the responses $\underline{x}(t)$ of the closed loop system are bounded. By substituting the control input $u(t)$ of Eq. (3-58) into the true system equation (2-26):

$$\begin{aligned} \ddot{x}_s(t) &= -m_s^{-1}c_s\dot{x}(t) - m_s^{-1}k_s x_s(t) + m_s^{-1}\left[\left(c_s\dot{x}_s(t) + k_s x_s(t)\right) - c_s^{-1}m_s^{2}v(t)\right] \\ &= -c_s^{-1}m_s v(t) \\ &= k_1^* c_s^{-1} m_s y(t) - \underbrace{c_s^{-1}m_s\left[\dot{y}_m(t) + k_1^* y_m(t)\right]}_{u_m(t)} \end{aligned} \tag{3-63}$$

Introducing the last known term $c_s^{-1}m_s[\dot{y}_m(t) + k_1^* y_m(t)]$ from the target motion as the new input $u_m(t)$ and substituting $y(t)$ in Eq. (3-63) lead to the closed loop system equation

$$\ddot{x}_s(t) = -k_1^*\dot{x}_s(t) - k_1^* c_s^{-1} k_s x_s(t) - u_m(t) \tag{3-64}$$

which can be written in the matrix form with the state vector $\underline{x}(t) = [x_s(t)\ \ \dot{x}_s(t)]^T$

$$\frac{d}{dt}\begin{bmatrix} x_s(t) \\ \dot{x}_s(t) \end{bmatrix} = \begin{bmatrix} 0 & 1 \\ -k_1^* c_s^{-1} k_s & -k_1^* \end{bmatrix}\begin{bmatrix} x_s(t) \\ \dot{x}_s(t) \end{bmatrix} + \begin{bmatrix} 0 \\ -1 \end{bmatrix} u_m(t) \tag{3-65}$$

The system matrix has all negative real part eigenvalues if $k_1^* c_s^{-1} k_s > 0$ (i.e. the damping coefficient and stiffness of a structure are normally positive and $k_1^* > 0$ selected) and the input part $u_m(t) = c_s^{-1}m_s[\dot{y}_m(t) + k_1^* y_m(t)]$ is bounded (i.e. the target motion $y_m(t)$ is bounded); therefore, the responses $x_s(t)$ and $\dot{x}_s(t)$ are bounded according to the *Bounded-Input-Bounded-Output* (BIBO) stability (Crassidis et al., 2012), discussed in Section 3.2.

Application to 2DOF Shake Table-Linear Structure Systems

The same feedback linearization tracking control method is applied to a linear structure mounted on a shake table (a 2DOF system model) described in Equations (2-24) and (2-25) with the output $y(t)$ of the total acceleration response $\ddot{x}_s^t(t)$ at the structure.

Using the same procedure described above, the control law can be obtained (see Derivation 3.2 in Appendix B.2) as

Control Law

$$u^*(t) = a^{-1}\left[-\ddot{y}^*(t) + v(t)\right] \tag{3-66}$$

where $u^*(t) = (\omega_a^2 k_a)^{-1} u(t)$; $u(t) = x_d(t)$; and $\ddot{y}^*(t)$ is defined as

$$\ddot{y}^*(t) = \left[a(a+c) - b\right]\ddot{x}_s(t) + a(b+d)\dot{x}_s(t) + (-ae)f_a^*(t) + (-af)\dot{x}_t(t) + (-ag)x_t(t) \tag{3-67}$$

in which new notations are introduced for simplification:

$$\begin{aligned} &a = m_s^{-1}c_s; \quad b = m_s^{-1}k_s; \quad c = m_t^{-1}c_s; \\ &e = 2\xi_a\omega_a; \quad f = \omega_a^2; \quad g = \omega_a^2 k_a; \\ &f_a^*(t) = f_a(t)/m_t; \quad u^*(t) = \omega_a^2 k_a x_d(t), \quad u(t) = x_d(t) \end{aligned} \tag{3-68}$$

Substituting $u^*(t)$ into the equation of the differentiated output $\ddot{y}(t)$, shown from Eq. (B-14) in Appendix B.2, leads to

$$\ddot{y}(t) = v(t) \tag{3-69}$$

To reduce the tracking error signal $e(t) = y(t) - y_m(t)$, the new input $v(t)$ can be obtained as:

$$v(t) = \ddot{y}_m(t) - k_1^*\dot{e}(t) - k_2^* e(t) \tag{3-70}$$

where k_1^* and k_2^* are the tracking error design coefficients, which are constant and positive; these lead to the tracking error dynamics

Expected Achieved Responses

$$\ddot{e}(t) + k_1^*\dot{e}(t) + k_2^* e(t) = 0 \tag{3-71}$$

in which the error signal $e(t)$ goes to zero as time goes to infinity; $e(t) \rightarrow 0$ as $t \rightarrow \infty$.

Stability

It is shown in Eq. (3-71) that the tracking error goes to zero, $e(t) \rightarrow 0$; this indicates that $y_m(t) = \ddot{x}_s^t(t)$ is bounded; however, checking is needed to find if the responses $\underline{x}(t)$ of the closed loop system are bounded. By substituting the control input $u(t)$ from Eq. (3-66) into the true system equation (2-24) and using the notations defined in Eq. (3-68), it is obtained

$$
\begin{aligned}
\dot{f}_a^*(t) &= -ef_a^*(t) - f\dot{x}_t(t) - gx_t(t) + a^{-1}\left[-\ddot{y}^*(t) + v(t)\right] \\
&= -\left[(a+c) - a^{-1}b\right]\ddot{x}_s(t) - (b+d)\dot{x}_s(t) + a^{-1}v(t) \\
&= \underbrace{\left\{-\left[(a+c) - a^{-1}b - k_1^*\right]\right\}}_{\bar{h}}\ddot{x}_s(t) + \underbrace{\left\{-\left[(b+d) - k_1^* a^{-1}b - k_2^*\right]\right\}}_{i}\dot{x}_s(t) + \underbrace{k_2^* a^{-1}b}_{j}x_s(t) \\
&\quad + \underbrace{a^{-1}\left[\ddot{y}_m(t) + k_1^*\dot{y}_m(t) + k_2^* y_m(t)\right]}_{u_m(t)}
\end{aligned}
\tag{3-72}
$$

By substituting $\ddot{x}_s(t)$ of Eq. (2-24) and by introducing additional notations for simplification:

$$
\bar{h} = -\left[(a+c) - a^{-1}b - k_1^*\right]; \qquad i = -\left[(b+d) - k_1^* a^{-1}b - k_2^*\right]; \qquad j = k_2^* a^{-1}b;
\tag{3-73}
$$

and also introducing the last known term $a^{-1}[\ddot{y}_m(t) + k_1^*\dot{y}_m(t) + k_1^* y_m(t)]$ from the target motion as a new input $u_m(t)$, Eq. (3-72) can be rewritten

$$
\begin{aligned}
\dot{f}_a^*(t) &= +\bar{h}\ddot{x}_s(t) + i\dot{x}_s(t) + jx_s(t) + u_m(t) \\
&= -\bar{h}f_a^*(t) + \left[-\bar{h}(a+c) + i\right]\dot{x}_s(t) + \left[-\bar{h}(b+d) + j\right]x_s(t) + u_m(t)
\end{aligned}
\tag{3-74}
$$

From this equation and the equations from Eq. (2-24), one has the closed loop system equation, which can be written in the matrix form with the state vector $\underline{x}(t) = [x_s(t)\ \ \dot{x}_s(t)\ \ f_a^*(t)]^T$

$$
\frac{d}{dt}\begin{bmatrix} x_s(t) \\ \dot{x}_s(t) \\ f_a^*(t) \end{bmatrix} = \begin{bmatrix} 0 & 1 & 0 \\ -(b+d) & -(a+c) & -1 \\ -\bar{h}(b+d) + j & -\bar{h}(a+c) + i & -\bar{h} \end{bmatrix}\begin{bmatrix} x_s(t) \\ \dot{x}_s(t) \\ f_a^*(t) \end{bmatrix} + \begin{bmatrix} 0 \\ 0 \\ 1 \end{bmatrix}u_m(t)
\tag{3-75}
$$

One can show that the state vector $\underline{x}(t) = [x_s(t)\ \ \dot{x}_s(t)\ \ f_a^*(t)]^T$ will be bounded by showing that the 3×3 closed loop system matrix has all negative real part eigenvalues with given parameters. To show if the remaining two state variables: $x_t(t)$ and $\dot{x}_t(t)$; will be bounded, one can use the fact that $y_m(t) \approx \ddot{x}_s^t(t)$ (i.e. $e(t) \to 0$ as shown in Eq. (3-71)). This indicates that the total displacement $x_s^t(t) = x_s(t) + x_t(t)$ and the total velocity $\dot{x}_s^t(t) = \dot{x}_s(t) + \dot{x}_t(t)$ tend to be the integrations of the target motion (i.e. $y_m(t) = \ddot{x}_s^t(t) = \ddot{x}_s(t) + \ddot{x}_t(t)$), assuming the initial conditions are zeros:

$$
\begin{aligned}
\dot{x}_s^t(t) &= \dot{x}_s^t(0) + \int_0^t y_m(\tau)d\tau \\
x_s^t(t) &= x_s^t(0) + \dot{x}_s^t(0)t + \int_0^t\int_0^\tau y_m(\zeta)d\zeta d\tau
\end{aligned}
\tag{3-76}
$$

Therefore, choosing the target motion $y_m(t)$ and its integration and double integration to be bounded leads to $x_s^t(t)$ and $\dot{x}_s^t(t)$ are bounded. Since $x_s(t)$ and $\dot{x}_s(t)$ are bounded, $x_t(t)$ and $\dot{x}_t(t)$ are also bounded. It is noted that the boundedness of $x_t(t)$, the shake table displacement, might suffer from small tracking errors: $e(t) = \ddot{x}_s^t(t) - y_m(t)$; as shown in the second equation of Eq. (3-76). This might be acceptable for the shake table control applications in this study where the total control time is relatively short. However, this issue might be more critical for applications where much longer control time is required. For these applications, one can reformulate the tracking control law by modifying the original target motion: the total structure acceleration; to the total structure displacement through double integrations of the original target motion; then, the stability of the controlled system can be examined using the same procedure described above.

3.3.3 Comparisons of Feedback Tracking Control Methods

It is very interesting to see the similarity and/or differences between the two feedback control methods introduced in this section. To compare the two methods, the control law of the feedback linearization control method is reformulated in the matrix form using the system equations shown in Eq. (3-1) and Eq. (3-2).

The system output $y(t) = C\underline{x}(t)$ is differentiated until the control input $u(t)$ appears in the expression of the differentiated output

$$\dot{y}(t) = C\dot{\underline{x}}(t) = CA\underline{x}(t) + CBu(t) \tag{3-77}$$

Assuming the product matrix CB is invertible (i.e. for the SDOF expressed in Eq. (2-26) with the output $y(t)$ of the total acceleration response $\ddot{x}_s^t(t)$ at the structure, CB is invertible), the feedback control is

$$u(t) = -(CB)^{-1}\left[CA\underline{x}(t) - v(t)\right] \tag{3-78}$$

where the new input $v(t) = \dot{y}_m(t) - k_1^* e(t)$; i.e. $e(t) = y(t) - y_m(t)$, is chosen to meet the tracing objective, and introducing $A^* = CA$ and $B^* = CB$ the control law of the feedback linearization becomes

$$u(t) = B^{*-1}\left[\dot{y}_m(t) - k_1^* e(t) - A^*\underline{x}(t)\right] \tag{3-79}$$

Substituting this control input into Eq. (3-77) leads to

$$\dot{y}(t) = \dot{y}_m(t) - k_1^* e(t) \tag{3-80}$$

which can be rewritten to show the tracking error dynamics

$$\dot{e}(t) + k_1^* e(t) = 0 \tag{3-81}$$

that clearly shows the tracking error $e(t) \to 0$ as $t \to \infty$ if $k_1^* > 0$.

It is noted that the control law in Eq. (3-79) is very similar with the control law of the predictive tracking control shown in Eq. (3-39), which can be rewritten, assuming $R = 0$ and $B_D^* = C_D B_D$ is invertible as $B^* = CB$ is invertible,

$$u_k = \left[B_D^{*T} Q B_D^* + R\right]^{-1} B_D^{*T} Q\left[y_{m,k+1} - A_D^*\hat{\underline{x}}_k\right] = B_D^{*-1}\left[y_{m,k+1} - A_D^*\hat{\underline{x}}_k\right] \tag{3-82}$$

For the linear systems, these two equations (3-79) and (3-82) are equivalent by choosing $k_1^* = 1/\Delta t$ where Δt is the discrete time interval, and the equations can be seen as the continuous – discrete time counterparts of the feedback control inputs.

Equivalency of Methods for 2DOF Shake Table-Structure Systems

One can also show that the two methods are equivalent for the shake table-structure system (where $C \times B$ is singular) under certain conditions. For example, the predictive tracking control law shown in Eq. (3-46) becomes the same as the control law (see Eq. (3-66)) of the feedback linearization tracking control method (i.e. see Derivation 3.3 in Appendix B.3), if the controlled system has $B(\underline{x})^*$ that is a non-zero scalar (i.e. an invertible matrix, size 1 × 1), and $R = 0$ chosen; by selecting the tracking error coefficients in Eq. (3-48) as $k_1^* = 2 / h = 2\xi_e\omega_e$ and $k_2^* = 2 / h^2 = \omega_e^2$; therefore, $\xi_e = \sqrt{2} / 2 \approx 0.707$ and $h = \sqrt{2} / \omega_e$.

3.4 Numerical Examples and Comparisons of Tracking Control Methods

Simple tracking control examples are analyzed in order to examine the performance of the four tracking control methods for linear systems introduced in this section. For all examples, the target motion is the total acceleration of a structure (specimen) mounted on the shake table although any response; i.e. a displacement or velocity response, can be selected as the target motion.

3.4.1 Examples of Linear Structures (SDOF System Model)

As discussed in Section 2.2, in order to facilitate the development of the tracking control method, first, a simplified SDOF system model is used instead of a 2DOF system model for the shake table with an SDOF structure system. In this simplified system model (shown in Figure 3-2), the excitation force $-m_s\ddot{x}_t(t)$ due to the shake table acceleration $\ddot{x}_t(t)$ is considered as a new control excitation input $u(t)$. However, the actual control excitation input $u(t)$ for the 2DOF system model is the desired displacement $x_d(t)$ of the shake table, and $u(t)$ shall be computed including the shake table dynamics and the shake table-structure interaction (as discussed in Section 2.2) as formulated in the following section (Section 3.4.2).

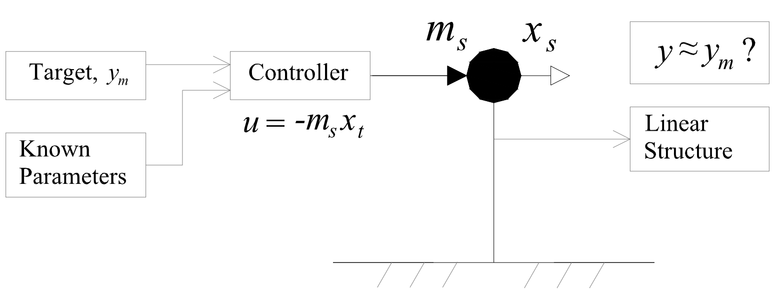

Figure 3-2 Tracking control of an SDOF system with known parameters

The governing equation of an SDOF linear structure subjected to the shake table excitation is shown in Eq. (2-26). The tracking control task for this simplified system is to compute the control excitation input

$u(t)$ = $-m_s\ddot{x}_t(t)$ so that the system output $y(t) = \ddot{x}_s^t(t)$ (the total acceleration of the structure) follows the target motion $y_m(t) = \ddot{x}_m^t(t)$ (the total acceleration of the reference model), and all responses of the controlled system are bounded. The initial condition $\underline{x}(0) = 0$; i.e. the state of a system (shake table and structure) initial condition in this study is always zeros: $x(0) = 0$, unless otherwise stated.

Example 3.1* : *An SDOF Linear System with Known Parameters

The properties of the example system are selected: m_s = 1 kips·sec^2/in., k_s = 355 kips/in., and c_s = 1.13 kips·sec/in., (f_n = 3.0 Hz, ξ_n = 0.03). Figure 3-3 (a – Target) shows the target motion. The target motion is the total acceleration output generated from a reference linear system, subjected to one-cycle sine input, whose frequency = 1.0 Hz. The reference input is high-pass-filtered at 0.2 Hz cutoff frequency to remove a large drift demand in the target motion. The properties of the reference system are: m_m = 1 kips·sec^2/in.; k_m = 987 kips/in.; and c_m = 6.28 kips·sec/in. (f_m = 5.0 Hz, ξ_m = 0.1). The reference input and the responses of the reference model are presented in Appendix A.2. The time step Δt of 0.002 sec is used for the simulation.

Tracking control results are presented in Figure 3-3. The controlled outputs, $y(t) = \ddot{x}_s^t(t)$ the total acceleration of the structure, are shown in Figure 3-3(a) that shows very good agreement with the target motion $y_m(t)$ [Target]. For comparison purposes, the results of four linear tracking control schemes: optimal tracking control [OTC]; inverse transfer function control [ITF]; predictive tracking control [PTC]; and feedback linearization tracking control [FTC]; are presented together and show the similarity of their performance. Note that for the OTC, a much smaller time step (Δt = 0.00001), which is impractical, is used as a benchmark solution; i.e. for other methods Δt = 0.002 sec. The performance can be quantitatively measured using the *normalized root-mean-square error* (E_{NRMS}), which is expressed as (Fienup, 1997):

$$E_{NRMS} = \sqrt{\sum_{i=1}^{N} \left(y_{m,i} - y_i\right)^2 \Big/ \sum_{i=1}^{N} \left(y_{m,i}\right)^2} \tag{3-83}$$

where y_m is the target motion and y is the output of the controlled system as addressed. The error of each method is computed and shown in Table 3-1; this shows that the performance of the feedback control methods (PTC and FTC), which will be used for nonlinear system control, are as good as the feed-forward method (ITF and OTC). It is noted that the performance of every method is highly affected by the control gain, which may have physical limitation in real applications.

The computed control excitations, $u(t) = -m_s\ddot{x}_t(t)$, for all four control methods using the control laws (i.e. Eq. (3-5) for the ITF method, Eq. (3-19) for the OTC method, Eq. (3-39) for the PTC method, and Eq. (3-58) for the FTC method) are shown in Figure 3-3(b) (for comparison purposes with other examples, $\ddot{x}_t(t)$ the shake table acceleration is presented). The achieved displacement and velocity responses of the controlled structure $x_s(t)$, $\dot{x}_s(t)$ are also presented in Figure 3-3 (c) and (d); it is noted that unlike the total acceleration (which was the target of the control design), the displacement and velocity responses are different from the ones of the reference because the system properties of the controlled system and ones of the reference system are different (the responses of the reference model are presented in Appendix A.2). Note that since the responses are very similar to each other, only the responses of the PTC method are presented. The relation between the structure resisting force $f_S(t)$ and displacement $x_s(t)$ is also presented in Figure 3-3 (e). As expected, all responses of the controlled system are bounded, satisfying the control objectives.

Table 3-1 Comparison of the performance of linear tracking controllers for an SDOF linear system

	OTC	ITF	PTC	FTC
E_{NRMS}	0.0002	0.0000	0.0000	0.0000

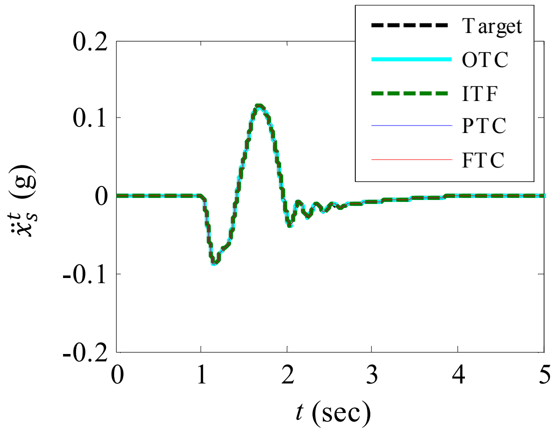

(a) Controlled (y) vs. Target motions (y_m)

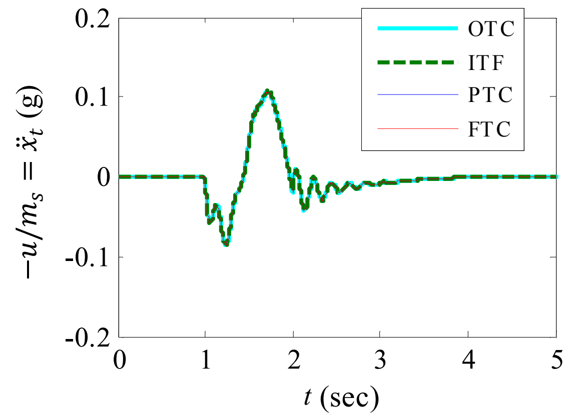

(b) Control excitation input (u)

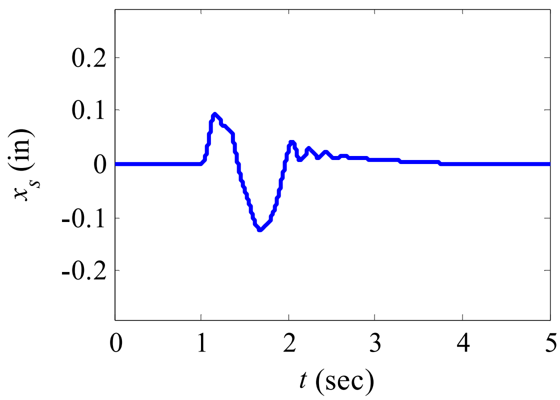

(c) Response of structure (x_s)

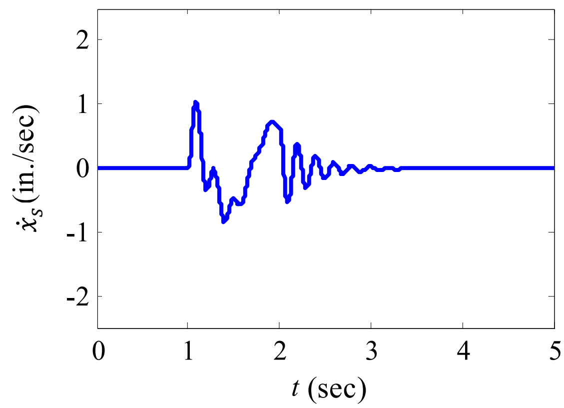

(d) Response of structure ($\dot{x}_s$)

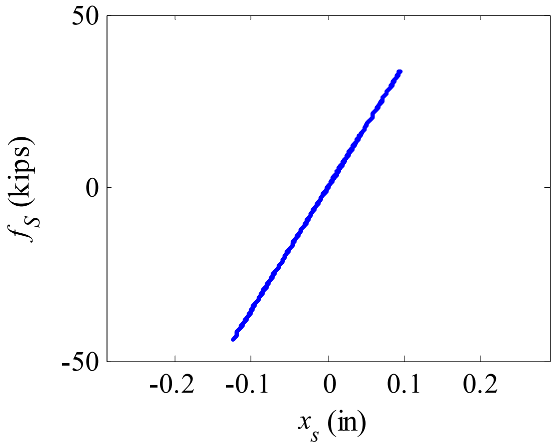

(e) Response of structure (f_S vs. x_s)

Figure 3-3 Tracking control results of an SDOF linear system

3.4.2 Examples of Shake Table-Linear Structures (2DOF System Model)

As discussed in Section 2.2, the shake table dynamics affect the performance of the control system and the interaction between the shake table and the mounted structure is to be considered. The same tracking control example above is resolved for the 2DOF linear system, expressed in Eq. (2-24) and Eq. (2-25), and schematically shown in Figure 3-4.

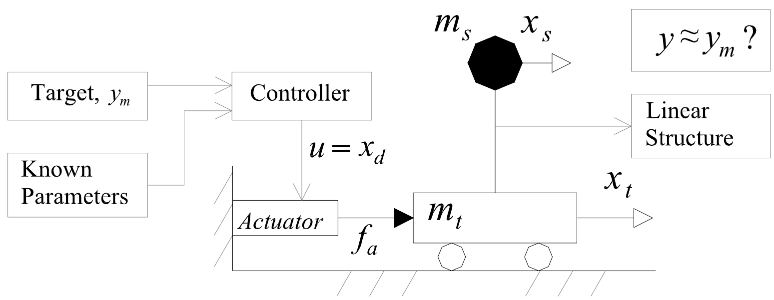

Figure 3-4 Tracking control of the shake table- structure 2DOF system with known parameters

When the target motion at a structure is specified, the required control input $u(t) = x_d(t)$, the desired shake table displacement, is determined such that the output of the system ($y(t) = \ddot{x}_s^t(t)$, the total acceleration of the structure), follows the target motion $y_m(t)$, and all responses of the controlled system are bounded. It is noted that the target motion might be required to be high-pass-filtered for the shake table applications, as discussed in Section 2.5.1 in order to avoid large drift of the shake table, by removing the DC error in the target. The 2nd order Butterworth high-pass filter (Chu, 2005) is used in the examples.

Example 3.2* : *A 2DOF Linear System with Known Parameters

Like in example 3.1, the properties of the system are selected as: m_s = 1 kips·sec^2/in., k_s = 355 kips/in., and c_s = 1.13 kips·sec/in., (f_n = 3.0 Hz, ξ_n = 0.03), $\mu = m_s / m_t = 0.1$, $f_{n,a}$ = 30.0 Hz, ξ_a = 0.5, and k_a = 25. The target motion is shown in Figure 3-5 (a) [Target]; i.e. the target motion is the total acceleration output generated from the same reference linear system (f_m = 5.0 Hz, ξ_m = 0.1) used for Example 3.1. in Section 3.4.1 (the reference excitation input and the responses of the reference model are presented in Appendix A.2). A time step of 0.002 sec is used for the simulation.

Tracking control results are presented in Figure 3-5 and Figure 3-6. The controlled outputs, $y(t) = \ddot{x}_s^t(t)$ the total accelerations of the structure, are shown in Figure 3-5 (a), showin a very good agreement with the target motion $y_m(t)$ [Target]. For comparison purposes, the results of four linear tracking control schemes: optimal tracking control [OTC]; inverse transfer function control [ITF]; predictive tracking control [PTC]; and feedback linearization tracking control [FTC]; are presented together; All show very good agreement to each other. Note that the OTC requires a much smaller time step (Δt = 0.00001), which is impractical; for all other methods the required time step is Δt = 0.002 sec. The error of each method is computed using the *normalized root-mean-square error* (E_{NRMS}), expressed in Eq. (3-83), and shown in Table 3-2. The results show that the performance of the feedback control methods (PTC and FTC), which will be used also for nonlinear system control, are as good as the feedforward method (ITF and OTC). It is noted again that the performance of every method is highly affected by the control gain, which may have physical limitation in real applications.

The computed control excitation inputs, $u(t) = x_d(t)$, for all four control methods using the control laws (i.e. Eq. (3-5) for the ITF method, Eq. (3-19) for the OTC method, Eq. (3-46) for the PTC method, and Eq. (3-66) for the FTC method) are shown in Figure 3-5 (b). The achieved displacement and velocity responses, $x_s(t)$, $\dot{x}_s(t)$, of the controlled structure are also presented in Figure 3-5 (b) and (c); it is noted that unlike the total acceleration (which was the target of the control design), the displacement and velocity responses are different from the ones of the reference because the system properties of the controlled system and ones of the reference system are different (the responses of the reference model are presented in Appendix A.2). The relation between the structure resisting force $f_S(t)$ and displacement $x_s(t)$ is also presented in Figure 3-5 (e). Note that since the responses are very similar to each other, only the responses of the PTC method are presented. Figure 3-6 presents the responses of the shake table, the achieved shake table actuator force $f_a(t)$, shake table acceleration $\ddot{x}_t(t)$, displacement $x_t(t)$ and velocity $\dot{x}_t(t)$.

It is also noted that the achieved shake table acceleration $\ddot{x}_t(t)$ (Figure 3-6 (b)) might be compared with the Example 3-1 table acceleration $\ddot{x}_t(t)$ (previously presented in Figure 3-3 (b)). It can be shown that the difference is very small. However, the simplified SDOF linear system cannot be used for the real applications because the actual control input, $u(t) = x_d(t)$ (the desired displacement of the shake table), cannot be directly computed from the shake table acceleration $\ddot{x}_t(t)$. The actual control input $u(t) = x_d(t)$ should be computed using the coupled system equation (Eq. (2-24)) including the shake table dynamics and the shake table-structure interaction, as in this example. As expected, all responses of the controlled system are bounded, satisfying the control objectives.

Table 3-2 Comparison of the performance of linear tracking controllers for a 2DOF system

	OTC	ITF	PTC	FTC
E_{NRMS}	0.0057	0.0102	0.0070	0.0070

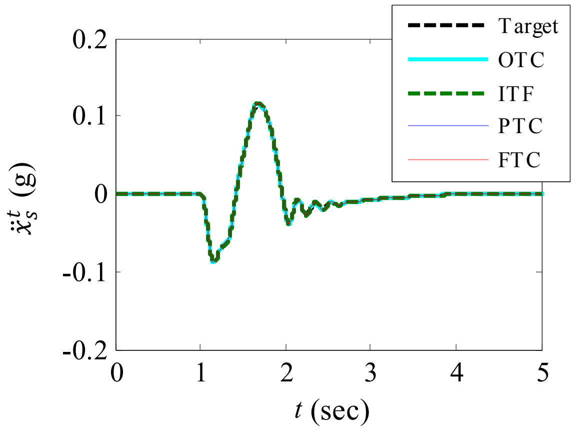

(a) Controlled (y) vs. Target motions (y_m)

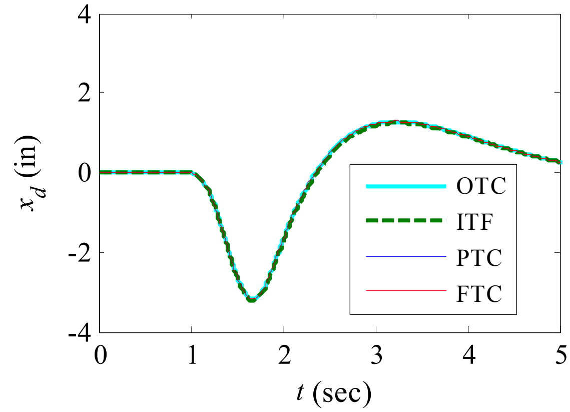

(b) Control excitation input (u)

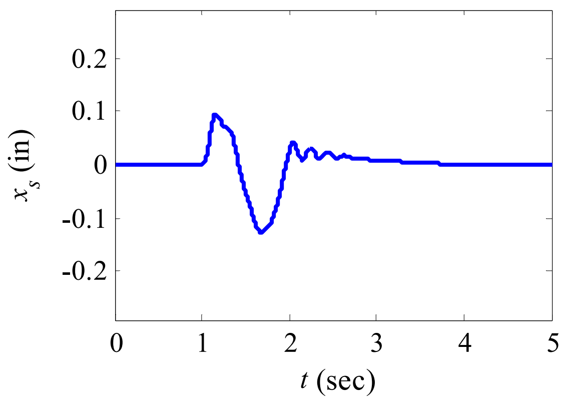

(c) Response of structure (x_s)

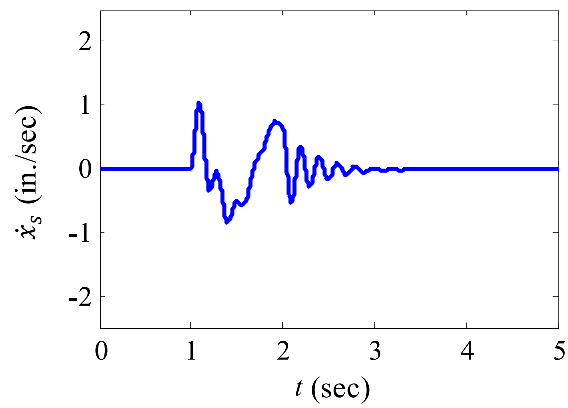

(d) Response of structure ($\dot{x}_s$)

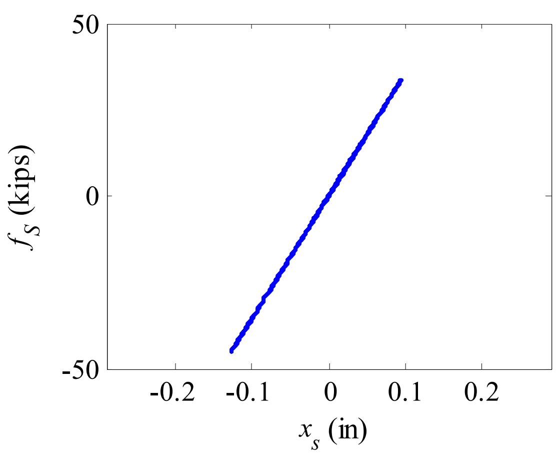

(e) Response of structure (f_S vs. x_s)

Figure 3-5 Tracking control structure responses of a 2DOF linear system

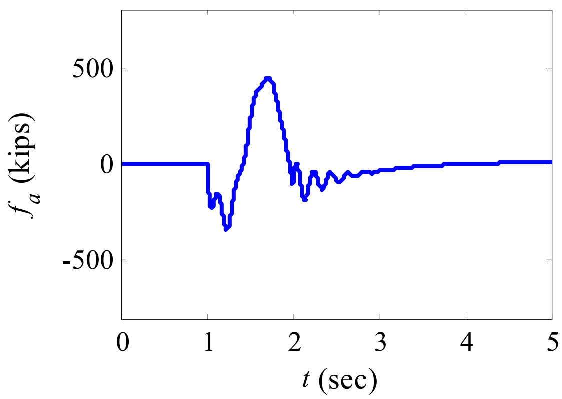

(a) Response of table (f_a)

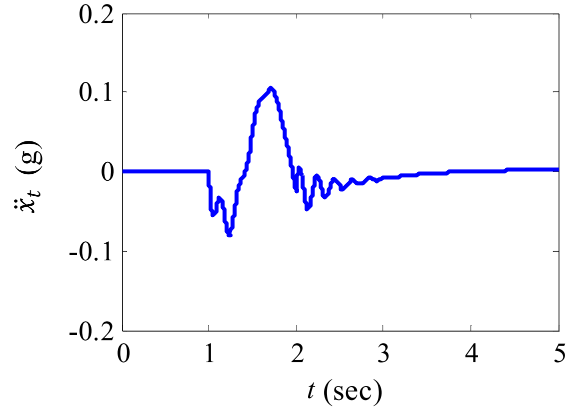

(b) Response of table ($\ddot{x}_t$)

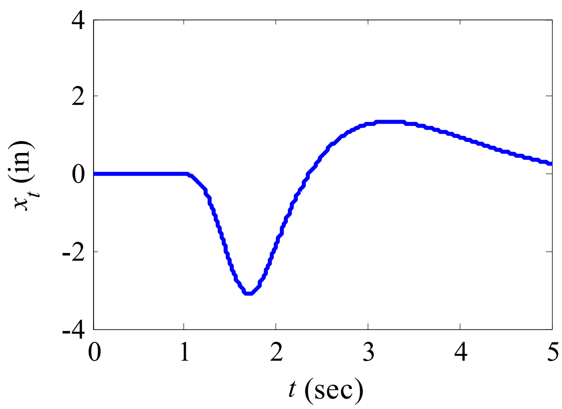

(c) Response of table (x_t)

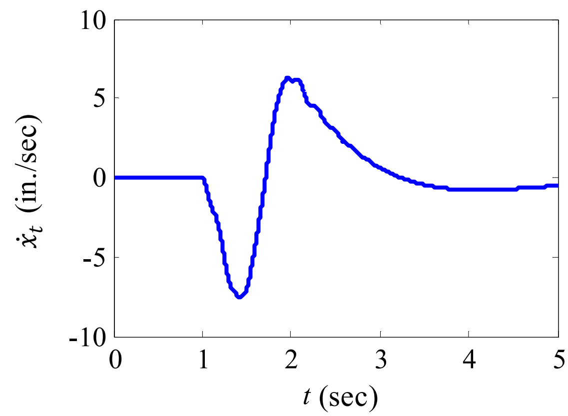

(d) Response of table ($\dot{x}_t$)

Figure 3-6 Tracking control shake table responses of a 2DOF linear system

In this section, the well-known tracking control methods including the feedforward, feedforward+feedback, and feedback control methods are reformulated in order to establish control laws for shake table and linear structure control applications. The performance of each tracking scheme is analytically examined from its expected achieved responses for the feedforward method and closed loop system responses for the feedback control methods. The performances of all control methods are also quantitatively compared using the numerical simulations. The results show very good and similar tracking performances. Especially, the performances of the feedback control methods (PTC and FTC), which will be used for nonlinear system controls, are as good as the feed-forward methods (ITF and OTC). It is also noted that the performance of every method is highly affected by the control gain, which may have physical limitation in real applications.

“This Page Intentionally Left Blank”

SECTION 4
TRACKING CONTROL FOR NONLINEAR SYSTEMS WITH KNOWN PARAMETERS

Structures (specimens) subjected to strong excitation can experience nonlinear hysteretic behavior due to yielding, or due to the nature of the seismically protected structure, such as a base isolated system. A class of smooth hysteretic models was originally proposed by Bouc (1967) and modified by several others (Wen, Y. K., 1976, Reinhorn et al., 1995, Sivaselvan and Reinhorn, 2000). In this model the restoring force $f_S(\underline{x})$ is modeled as a combination of elastic and hysteretic components as shown in Figure 4-1 (left). Even though the model is versatile and capable to simulate stiffness degradation, strength degradation, and pinching (Sivaselvan and Reinhorn, 2000), this study focuses only on a simple, bilinear type hysteretic behavior in order to facilitate the development of a real time controller; this restriction can be removed but it will require a much more elaborated explanation. For this hysteretic system, the model parameters include: k_s, the elastic stiffness; d_y, the yielding displacement (i.e. the yielding force $f_y = k_s d_y$); α the post-yielding stiffness ratio to the elastic stiffness; and N, the power controlling the smoothness of the transition from elastic to inelastic range. For the controller development, it is necessary to know these parameters; however, in real applications, only initial approximations of the true parameters might be available from static tests; in particular, for d_y and α, the hysteretic parameters, a real time estimator might be necessary. The hysteretic parameter, N, is also unknown (i.e which can be also estimated in real time

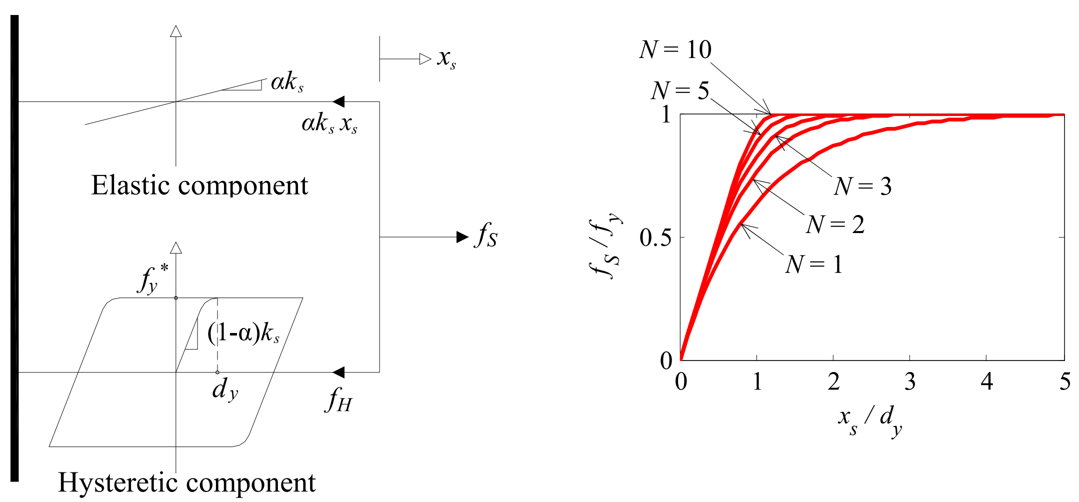

Figure 4-1 Nonlinear system model: Restoring force model[5] and effects of smoothness of transition[6]

---

[5] (Simeonov et al., 2000); all terms are explained in the following section;
[6] (Constantinou, 2008); only the response in one positive direction is presented

as shown in Wu and Smyth, 2008); in this study, it is assumed as a fixed value, $N = 3$, considering that the influence of the smooth transition changes on the entire hysteretic behavior is not significant. Figure 4-1 (right) shows different transitions due to various N of the hysteretic components. It is also noted that there are parameters (η_1, η_2 in Eq. (4-2)), which control the shape of the hysteretic loop; in this study, $\eta_1 = \eta_2 = 0.5$ are chosen also for simplicity. Feedback controllers are proposed first, in this section, assuming all parameters are known a priori. In later sections, real time estimators are introduced to be combined with the controllers.

Four tracking control methods, including (i) a feed-forward control method, (ii) a combined feed-forward feed-back control method, (iii) a predictive tracking control method and (iv) a feedback linearization tracking control method for linear systems, were introduced in the previous section. The two feedback control methods, the predictive tracking control and the feedback linearization tracking control, can be extended to nonlinear hysteretic systems. In this section, the nonlinear hysteretic model is presented first. The formulation of each control method is provided and numerical examples of an SDOF nonlinear structure and a 2DOF shake table with a nonlinear structure mounted on it are presented. The performances of these methods are compared.

4.1 Nonlinear Hysteretic Structure Model

Considering a nonlinear hysteretic SDOF system, the equation of motion can be written as (adapted from Sivaselvan and Reinhorn, 1999):

$$m_s\ddot{x}_s(t) + c_s\dot{x}_s(t) + f_S(\underline{x}) = -m_s\ddot{x}_t(t) \;\; or \;\; u(t) \tag{4-1}$$

where $f_S(\underline{x})$ is a nonlinear restoring force and the governing equation is

$$\dot{f}_S(\underline{x}) = k_T(\underline{x})\dot{x}_s(t) = \left[\alpha k_s + (1-\alpha)k_H(\underline{x})\right]\dot{x}_s(t) \tag{4-2}$$

in which $k_T(\underline{x})$ indicates the instantaneous tangent stiffness; k_s is the elastic stiffness; $k_H(\underline{x})$ is the hysteretic stiffness; and α the post-yielding stiffness ratio to the elastic stiffness. In this parallel-spring representation, the stiffness of the hysteretic spring $k_H(\underline{x})$ is expressed as

$$k_H(\underline{x}) = k_s\left\{1 - \left[\eta_2 + \eta_1 \operatorname{sgn}\left(f_H(\underline{x})\dot{x}_s(t)\right)\right]\left(\frac{\left|f_H(\underline{x})\right|}{f_y^*}\right)^N\right\} \tag{4-3}$$

where the hysteretic force $f_H(\underline{x}) = f_S(\underline{x}) - \alpha k_s x(t)$; the hysteretic yielding force $f_y^* = (1-\alpha)\, f_y$ with the yielding force $f_y = k_s d_y$ where d_y is the yielding displacement; N is the power controlling the smoothness of the transition from elastic to inelastic range (see Figure 4-1(b)); and η_1, η_2 are parameters controlling the shape of the hysteretic loop, which must satisfy $\eta_1 + \eta_1 = 1$ (Constantinou and Adane, 1987) i.e. in this study, $\eta_1 = \eta_2 = 0.5$ are chosen for simplicity. Equations (4-1) and(4-2), can be rewritten in the state space form as

$$\underline{\dot{x}}(t) = \underline{\mathrm{f}}\left(\underline{x}(t), u(t)\right) \qquad or$$

$$\frac{d}{dt}\begin{bmatrix} x_s(t) \\ \dot{x}_s(t) \\ f_S(\underline{x}) \end{bmatrix} = \begin{bmatrix} \dot{x}_s(t) \\ -m_s^{-1}\left\{c_s\dot{x}_s(t) + f_S(\underline{x})\right\} - m_s^{-1}u(t) \\ k_T(\underline{x})\dot{x}_s(t) \end{bmatrix}, \qquad \underline{x}(0) = \underline{x}_0 \tag{4-4}$$

In the matrix form, this is

$$\underline{\dot{x}}(t) = A\left(\underline{x}(t)\right)\underline{x}(t) + Bu(t) \qquad or$$

$$\frac{d}{dt}\begin{bmatrix} x_s(t) \\ \dot{x}_s(t) \\ f_S(\underline{x}) \end{bmatrix} = \begin{bmatrix} 0 & 1 & 0 \\ 0 & -m_s^{-1}c_s & -m_s^{-1} \\ 0 & k_T(\underline{x}) & 0 \end{bmatrix}\begin{bmatrix} x_s(t) \\ \dot{x}_s(t) \\ f_S(t) \end{bmatrix} + \begin{bmatrix} 0 \\ m_s^{-1} \\ 0 \end{bmatrix}u(t), \qquad \underline{x}(0) = \underline{x}_0 \tag{4-5}$$

Considering the structure mounted on the shake table shown in Figure 2-1 is a nonlinear hysteretic SDOF system, the equations of motion of the table-structure system can be expressed as

$$\begin{aligned}
&m_s\ddot{x}_s(t) + c_s\dot{x}_s(t) + f_S(\underline{x}) = -m_s\ddot{x}_t(t) \quad or \quad f_{I,s}(t) + f_D(t) + f_S(\underline{x}) = -m_s\ddot{x}_t(t) \\
&m_t\ddot{x}_t(t) - \left\{c_s\dot{x}_s(t) + f_S(\underline{x})\right\} = f_a(t) \quad or \quad f_{I,t}(t) - \left\{f_D(t) + f_S(\underline{x})\right\} = f_a(t) \\
&\dot{f}_S(\underline{x}) = k_T(\underline{x})\dot{x}_s(t) = \underbrace{\left[\alpha k_s + (1-\alpha)k_s\left\{1 - \frac{1+\operatorname{sgn}\left(f_H(\underline{x})\dot{x}_s(t)\right)}{2}\left(\frac{\left|f_H(\underline{x})\right|}{f_y^*}\right)^N\right\}\right]}_{k_T(\underline{x})}\dot{x}_s(t) \\
&\frac{1}{\omega_a^2}\frac{\dot{f}_a(t)}{m_t} + \frac{2\xi_a}{\omega_a}\frac{f_a(t)}{m_t} + \frac{dx_t(t)}{dt} + k_a x_t(t) = k_a x_d(t)
\end{aligned} \tag{4-6}$$

where ω_a (i.e. $f_{n,a}$ (Hz) = ω_a / 2π), ξ_a, and k_a are the natural frequency, the equivalent damping ratio, and the control gain of the shake table system as defined in Eq. (2-17). All parameters are previously defined. Eq. (4-6) can be written in the state space form as

$$\underline{\dot{x}}(t) = \underline{\mathrm{f}}\left(\underline{x}(t), u(t)\right) \qquad or$$

$$\frac{d}{dt}\begin{bmatrix} x_s(t) \\ \dot{x}_s(t) \\ f_S(\underline{x}) \\ x_t(t) \\ \dot{x}_t(t) \\ f_a(t)/m_t \end{bmatrix} = \begin{bmatrix} \dot{x}_s(t) \\ -\left(m_s^{-1} + m_t^{-1}\right)\left\{c_s\dot{x}_s(t) + f_S(\underline{x})\right\} - m_t^{-1}f_a(t) \\ k_T(\underline{x})\dot{x}_s(t) \\ \dot{x}_t(t) \\ m_t^{-1}\left\{c_s\dot{x}_s(t) + f_S(\underline{x})\right\} + f_a(t)/m_t \\ -k_a\omega_a^2 x_t(t) - \omega_a^2\dot{x}_t(t) - 2\xi_a\omega_a f_a(t)/m_t + k_a\omega_a^2 x_d(t) \end{bmatrix} \tag{4-7}$$

In the matrix form, this is

$$\underline{\dot{x}}(t) = A(\underline{x})\underline{x}(t) + Bu(t), \qquad \underline{x}(0) = \underline{x}_0 \qquad or$$

$$\frac{d}{dt}\begin{bmatrix} x_s(t) \\ \dot{x}_s(t) \\ f_S(\underline{x}) \\ x_t(t) \\ \dot{x}_t(t) \\ f_a(t)/m_t \end{bmatrix} = \begin{bmatrix} 0 & 1 & 0 & 0 & 0 & 0 \\ 0 & -\left(m_s^{-1}+m_t^{-1}\right)c_s & -\left(m_s^{-1}+m_t^{-1}\right) & 0 & 0 & -1 \\ 0 & k_T(\underline{x}) & 0 & 0 & 0 & 0 \\ 0 & 0 & 0 & 0 & 1 & 0 \\ 0 & m_t^{-1}c_s & m_t^{-1} & 0 & 0 & 1 \\ 0 & 0 & 0 & -k_a\omega_a^2 & -\omega_a^2 & -2\xi_a\omega_a \end{bmatrix}\begin{bmatrix} x_s(t) \\ \dot{x}_s(t) \\ f_S(t) \\ x_t(t) \\ \dot{x}_t(t) \\ f_a(t)/m_t \end{bmatrix} + \begin{bmatrix} 0 \\ 0 \\ 0 \\ 0 \\ 0 \\ k_a\omega_a^2 \end{bmatrix} x_d(t) \tag{4-8}$$

and for the output $y(t)$ of the total acceleration response $\ddot{x}_s^t(t)$ at the structure, the output equation is

$$\begin{aligned} y &= C\underline{x}(t), \qquad or \\ y &= \begin{bmatrix} 0 & -m_s^{-1}c_s & -m_s^{-1} & 0 & 0 & 0 \end{bmatrix}\underline{x}(t) \end{aligned} \tag{4-9}$$

The equations can be solved using the 4th order Runge-Kutta method.

4.2 Predictive Tracking Control (PTC)

For a tracking control of a nonlinear system, the predictive feedback control method introduced in Section 3.3.1 for a linear system can be applied. While the procedure is similar, for nonlinear systems it is required to update the system matrices in every instant, because of system variations.

Assuming that the instant stiffness $k_T(\underline{x})$ in Eq. (4-2) is piecewise constant at every instant, the equation can be rewritten between two consecutive instants $k\Delta t$ and $(k+1)\Delta t$ as

$$\underline{\dot{x}}(\tau) \approx A_k\underline{x}(\tau) + Bu(\tau), \qquad k\Delta t \le \tau < (k+1)\Delta t \tag{4-10}$$

Also, assuming that the control input $u(t)$ is piecewise constant at every instant, the equation can be expressed in the discrete-time domain as

$$\underline{x}_{k+1} = A_{D,k}\underline{x}_k + B_{D,k}u_k \tag{4-11}$$

where $A_{D,k}$ and $B_{D,k}$ are computed from Eq. (3-38) by replacing A_D with $A_{D,k}$. The predicted output response $\hat{y}_{k+1}$ at instant $k\Delta t$ can be expressed

$$\begin{aligned} \underline{\hat{x}}_{k+1} &= A_{D,k}\underline{\hat{x}}_k + B_{D,k}u_k \\ \hat{y}_{k+1} &= C_D\underline{\hat{x}}_{k+1} = \left(C_D A_{D,k}\right)\underline{\hat{x}}_k + \left(C_D B_{D,k}\right)u_k = A_{D,k}^*\underline{\hat{x}}_k + B_{D,k}^*u_k \end{aligned} \tag{4-12}$$

where $\underline{\hat{x}}_k$ is the estimate of the true state vector $\underline{x}_k$ at instant $k\Delta t$; i.e. $\underline{\hat{x}}_k \approx \underline{x}_k$ for the systems with known parameters and no measurement noise considered as Δt is sufficiently small such that the error due to the piecewise constant assumption of the nonlinear restoring force is negligible; therefore, the predicted output response is close to the true one $\hat{y}_{k+1} \approx y_{k+1}$. Given a target y_m, the control force u_k to minimize the instantaneous performance index J in Eq. (3-35) (i.e. $\partial J/\partial u_k = 0$) can be defined based on Eq. 3-38 as follows:

Control Law

$$u_k = \left[B_{D,k}^{*\ T} Q B_{D,k}^{*} + R\right]^{-1} B_{D,k}^{*\ T} Q\left[y_{m,k+1} - A_{D,k}^{*}\hat{\underline{x}}_k\right] = \Gamma_k\left[y_{m,k+1} - A_{D,k}^{*}\hat{\underline{x}}_k\right] \tag{4-13}$$

where $A_{D,k}^* = C_D A_{D,k}$ and $B_{D,k}^* = C_D B_{D,k}$. and $\Gamma_k = [B_{D,k}^{*T} Q B_{D,k}^* + R]^{-1} B_{D,k}^{*T} Q$. The true system responses will be measured at every instant $k\Delta t$ by sensors in real experiments: the measurement responses are expressed as $\underline{\bar{y}}_k = H\underline{x}_k + \underline{v}_k$ (the true responses $\underline{x}_k$ with measurement noise $\underline{v}_k$ - see Eq. (5-51)). For numerical simulations, the true responses without noise (i.e. measurement noise will be present from SECTION 5 trough SECTION 8) can be computed by substituting the control input u_k from Eq. (4-13) into the true system equation in Eq. (4-4) and using the following equation;

$$\begin{aligned} \underline{x}_{k+1} &= \underline{x}_k + \int_{t_k}^{t_{k+1}} \underline{\mathrm{f}}\left(\underline{x}(\tau), u_k\right) d\tau \\ y_{k+1} &= C_D \underline{x}_{k+1} \end{aligned} \tag{4-14}$$

where $\underline{x}_{k+1}$ and y_{k+1} are the true state vector and output at instant time $(k+1)\Delta t$, and $\underline{\mathrm{f}}(\underline{x}, u_k)$ is the system differential equation defined in Eq. (4-4). For the numerical integration, the 4th order Runge-Kutta method (Sauer, 2006) with very small time step is used assuming that the control excitation input u_k is piecewise constant.

However, in order to check the effectiveness of the proposed control scheme analytically, it is assumed that the instant stiffness $k_T(\underline{x})$ in Eq. (4-2) is piecewise constant at every instant. With this assumption, the error dynamics with the control scheme can be shown as following. Substitution of the control input u_k from Eq. (4-13) into the approximated system equation shown in Eq. (4-12) leads to

Expected Achieved Responses

$$\hat{y}_{k+1} = C_D\hat{\underline{x}}_{k+1} = C_D\left[A_{D,k}\hat{\underline{x}}_k + B_{D,k}\Gamma_k\left\{y_{m,k+1} - A_{D,k}^{*}\hat{\underline{x}}_k\right\}\right] = C_D\left\{\left(A_{D,k} - B_{D,k}\Gamma_k A_{D,k}^{*}\right)\hat{\underline{x}}_k + B_{D,k}\Gamma_k y_{m,k+1}\right\} \tag{4-15}$$

If $B_{D,k}^* = C_D B_{D,k}$ is an invertible matrix and $R = 0$ chosen (i.e. indicating no limit for the control input), then Eq. (4-15) becomes

$$\hat{y}_{k+1} = C_D\hat{\underline{x}}_{k+1} = A_D^{*}\hat{\underline{x}}_k + \left(B_{D,k}^{*} B_{D,k}^{*\ -1}\right) Q^{-1}\left(B_{D,k}^{*\ -T} B_{D,k}^{*\ T}\right) Q\left\{y_{m,k+1} - A_{D,k}^{*}\hat{\underline{x}}_k\right\} = y_{m,k+1} \tag{4-16}$$

and the predicted tracking error $e_{k+1} = \hat{y}_{k+1} - y_{m,k+1}$ becomes zero as desired.

To ensure the stability of the control scheme, one needs to check not only the output, but also the state responses of the controlled system. This can be done by tracing the closed loop stability. Note that the study of the closed loop stability of a feedback tracking control for a nonlinear structure is presented in Ch 4.3 where the feedback linearization method is used.

Limitation of 2DOF Shake Table-Structure Systems

As discussed in Section 3.3.1, if the product of the output and input matrices $C \times B$, in the equations Eq. (3-1) and Eq. (3-2), is singular, it is required to change the procedure in order to establish a valid control law. In order to force the control input u_k to appear in the output equation, a higher order differentiation of the output $\hat{y}_{k+1}$ in discrete time or $\hat{y}(t+h)$ in continuous time is needed. As discussed in Section 3.3.1, it is preferred to formulate the control law in continuous time format. The procedure to formulate the predictive tracking control law for nonlinear continuous systems was presented by Lu (1994). For the shake table-structure 2DOF model, the output needs up to three terms. The approximated predicted output $\hat{y}^*(t+h)$ and target motion $y_m^*(t+h)$ are presented in Equation (3-44) where $\dot{y}(t)$ and $\ddot{y}(t)$ in the first equation can be expressed using Equations (4-8) and (4-9) for the nonlinear hysteretic system as:

$$\begin{aligned} \dot{y}(t) &= C\dot{\hat{\underline{x}}}(t) = C\left[A(\underline{x})\hat{\underline{x}}(t) + Bu(t)\right] = CA(\underline{x})\hat{\underline{x}}(t) \\ \ddot{y}(t) &= C\ddot{\hat{\underline{x}}}(t) = C\frac{d}{dt}A(\underline{x})\hat{\underline{x}}(t) + CA(\underline{x})\dot{\hat{\underline{x}}}(t) = C\left[\frac{d}{dt}A(\underline{x}) + A^2(\underline{x})\right]\hat{\underline{x}}(t) + CA(\underline{x})Bu(t) \end{aligned} \tag{4-17}$$

It is noted that the control excitation input *u(t)* appears in the second equation because $CA(\underline{x})B \neq 0$.

The control excitation input $u(t)$ can be obtained by minimizing the performance index J in Eq. (3-35) by replacing the output $\hat{y}(t+h)$ and the target $y_m(t+h)$ to their approximations $\hat{y}^*(t+h)$ and $y_m^*(t+h)$ after substituting Eq. (4-17) for $\hat{y}^*(t+h)$ as follows:

Control Law

$$u(t) = \left[B^*(\underline{x})^T QB^*(\underline{x}) + R\right]^{-1} B^*(\underline{x})^T Q\left[y_m^*(t+h) - A^*(\underline{x})\hat{\underline{x}}(t)\right] \tag{4-18}$$

where $A^*(\underline{x}) = [C + hCA(\underline{x}) + (h^2/2)C\{d/dtA(\underline{x}) + A(\underline{x})^2\}]$ and $B^*(\underline{x}) = (h^2/2)CA(\underline{x})B$.

By substituting Eq. (4-18) into the second equation of Eq.(4-17), one can establish the error dynamics. For a system having $B^*(\underline{x})$ is a non-zero scalar (i.e. an invertible matrix, size 1 × 1), and $R = 0$ chosen, $\ddot{y}(t)$ becomes:

Expected Achieved Responses

$$\begin{aligned} \ddot{y}(t) &= C\left[\frac{d}{dt}A(\underline{x}) + A^2(\underline{x})\right]\hat{\underline{x}}(t) + CA(\underline{x})B\left[B^*(\underline{x})\right]^{-1}\left[y_m^*(t+h) - A^*(\underline{x})\hat{\underline{x}}(t)\right] \\ &= \ddot{y}_m(t) - (2/h^2)\left[\left(y(t) - y_m(t)\right) + h\left(\dot{y}(t) - \dot{y}_m(t)\right)\right] \end{aligned} \tag{4-19}$$

which can be rewritten by introducing the tracking error ($e(t) = y(t) - y_m(t)$) to show its dynamics as

$$\ddot{e}(t) + (2/h)\dot{e}(t) + (2/h^2)e(t) = 0 \tag{4-20}$$

This equation clearly shows the tracking error $e(t) \to 0$ as $t \to \infty$ since $h > 0$, where h, the predicted time interval, is not restricted to be the same as Δt, the sampling time step. Thus, h can be chosen by the design engineer as a controller parameter (as discussed in Section 3.3.1). It is noted that this is the same tracking error dynamics achieved for the linear system shown in Eq. (3-48); this indicates that the control excitation input cancels the system nonlinearity and drives the system to fit the target motion.

To ensure the stability of the control scheme, one needs to check not only the output, but also the state responses of the controlled system. This can be done by looking at the closed loop stability; this procedure is presented in Ch 4.3 where the feedback linearization method is used.

4.3 Feedback Linearization Tracking Control (FTC)

As discussed in Section 3.3.2, the controller can be designed such that the true system properties involving the nonlinear behavior are replaced to new ones that will lead to the desired linear behavior, and the output response of the controlled system will follow the target motion.

Application when the Target Motion is the Structure Displacement Response

This method is developed and applied to a nonlinear hysteretic system expressed in Eq. (4-1) using the structure displacement response $x_s(t)$ as the target motion; i.e. although feasible the formulation becomes more complex when the target motion is the total structure acceleration $\ddot{x}_s^t(t)$; therefore, for simplicity, the displacement response is considered first.

Equations for the True System

$$\begin{aligned} &\ddot{x}_s(t) = -m_s^{-1} c_s \dot{x}_s(t) - m_s^{-1} f_S(\underline{x}) + m_s^{-1} u(t), \qquad \underline{x}(0) = \underline{x}_0 \\ &y(t) = x_s(t) \end{aligned} \tag{4-21}$$

Equations for the Reference Model

$$\begin{aligned} &\ddot{x}_m(t) = -m_m^{-1} c_m \dot{x}_m(t) - m_m^{-1} k_m x_m(t) + m_m^{-1} r(t), \qquad \underline{x}_m(0) = \underline{x}_{m,0} \\ &y_m(t) = x_m(t) \end{aligned} \tag{4-22}$$

The system output $y(t)$ is to be differentiated until the control input $u(t)$ appears in the expression of the differentiated output

$$\begin{aligned} &\dot{y}(t) = \dot{x}_s(t) \\ &\ddot{y}(t) = \ddot{x}_s(t) = -m_s^{-1} c_s \dot{x}_s(t) - m_s^{-1} f_S(\underline{x}) + m_s^{-1} u(t) \end{aligned} \tag{4-23}$$

In order to achieve the desired response, the feedback control law can be defined as:

<u>Control Law</u>

$$u(t) = m_s \left[m_s^{-1} c_s \dot{x}_s(t) - m_s^{-1} f_S(\underline{x}) + v(t) \right] \tag{4-24}$$

that leads to:

$$\ddot{y}(t) = v(t) \tag{4-25}$$

To reduce the tracking error signal $e(t) = y(t) - y_m(t)$, the new input $v(t)$ can be described as:

$$v(t) = \ddot{y}_m(t) - k_1^* \dot{e}(t) - k_2^* e(t) \tag{4-26}$$

where k_1^* and k_2^* are the tracking error design coefficients, which are constant and positive; these lead to the tracking error dynamics as follows:

Expected Achieved Responses

$$\ddot{e}(t) + k_1^* \dot{e}(t) + k_2^* e(t) = 0 \tag{4-27}$$

in which the error signal $e(t)$ goes to zero as time goes to infinity; $e(t) \to 0$ as $t \to \infty$. In this second order error differential equation, the error coefficients k_1^* and k_2^* can be considered as $k_1^* = 2\xi_e\omega_e$ and $k_2^* = \omega_e^2$. In general when the coefficients increase, the error will be rapidly reduced while it will require larger control inputs (therefore, larger actuator forces).

Stability

It is shown in Eq. (4-27) that the tracking error goes to zero, $e(t) \to 0$. This indicates that the responses $\underline{x}(t)$ of the closed loop system are bounded since the target motion is $y(t) = x(t)$.

Application when the Target Motion is the Structure's Total Acceleration Response

If the target motion is the total structure acceleration $\ddot{x}_s^t(t)$, although the procedure is the same as above, more computations are involved to construct the control law. The procedure is as follows; the system output in Eq. (4-21) and the target motion in Eq. (4-22) become:

$$y(t) = \ddot{x}_s^t(t) = -m_s^{-1} c_s \dot{x}_s(t) - m_s^{-1} f_S(\underline{x}) \tag{4-28}$$

$$y_m(t) = \ddot{x}_m^t(t) = -m_m^{-1} c_m \dot{x}_m(t) - m_m^{-1} k_m x_m(t) \tag{4-29}$$

The system output function $y(t)$ is to be differentiated until the control excitation input $u(t)$ appears in the expression of the differentiated output

$$\begin{aligned} \dot{y}(t) &= -m_s^{-1} c_s \ddot{x}_s(t) - m_s^{-1} \dot{f}_S(\underline{x}) \\ &= \left[m_s^{-2} c_s \left(c_s \dot{x}_s(t) + f_S(\underline{x}) \right) - m_s^{-1} k_T(\underline{x}) \dot{x}_s(t) \right] - c_s m_s^{-2} u(t) \end{aligned} \tag{4-30}$$

which leads to the feedback control law:

Control Law

$$u(t) = c_s^{-1} m_s^2 \left[m_s^{-2} c_s \left(c_s \dot{x}_s(t) + f_S(\underline{x}) \right) - m_s^{-1} k_T(\underline{x}) \dot{x}_s(t) - v(t) \right] \tag{4-31}$$

By substituting this control excitation input $u(t)$ into Eq. (4-30), it is obtained that

$$\dot{y}(t) = v(t) \tag{4-32}$$

The new input $v(t)$ can be selected such that the error signal $e(t) = y(t) - y_m(t)$ will be reduced as shown in the previous example (see Eq. (3-61)). Again, the tracking error dynamics can be written:

Expected Achieved Responses

$$\dot{e}(t)+k_1^* e(t)=0 \tag{4-33}$$

in which the tracking error signal $e(t) \to 0$ as $t \to \infty$ by selecting $k_1^* > 0$.

Stability

It is shown in Eq. (4-33) that the tracking error goes to zero, $\underline{e}(t) \to 0$. This indicates that the output $y_m(t) = \ddot{x}_s^t(t)$ is bounded; however, one still needs to check if the state responses $\underline{x}(t)$ of the closed loop system are bounded.

By substituting the control input $u(t)$ from Eq. (4-31) into the true system equation (4-21) the total acceleration is:

$$\begin{aligned}\ddot{x}_s(t) &= -m_s^{-1}c_s\dot{x}(t) - m_s^{-1}f_S(\underline{x}) + m_s^{-1}\left[\left(c_s\dot{x}_s(t)+f_S(\underline{x})\right) - c_s^{-1}m_s k_T(\underline{x})\dot{x}_s(t) - c_s^{-1}m_s^2 v(t)\right] \\ &= -c_s^{-1}k_T(\underline{x})\dot{x}_s(t) - c_s^{-1}m_s v(t) \\ &= -c_s^{-1}k_T(\underline{x})\dot{x}_s(t) + k_1^* c_s^{-1}m_s y(t) - \underbrace{c_s^{-1}m_s\left[\dot{y}_m(t)+k_1^* y_m(t)\right]}_{u_m(t)}\end{aligned} \tag{4-34}$$

By introducing the last known term $c_s^{-1}m_s[\dot{y}_m(t) + k_1^* y_m(t)]$ from the target motion $y_m(t)$ as a new input $u_m(t)$ and substituting $y(t)$ from Eq. (4-28), it leads to the closed loop system equation:

$$\ddot{x}_s(t) = -\left[c_s^{-1}k_T(\underline{x}) + k_1^*\right]\dot{x}_s(t) - c_s^{-1}k_1^* f_S(\underline{x}) - u_m(t) \tag{4-35}$$

which is a nonlinear equation due to the variation of $k_T(\underline{x})$. The eigenvalue test of the system matrix is not applicable. The input-output stability of this nonlinear system can be checked using the L_p norm definition (Ioannou and Sun, 2012). This procedure is presented for the *Application to 2DOF Shake Table-Nonlinear Structure Systems* shown below.

For a special case, a stabilization problem, where the target motion $y_m = 0$; i.e. the structure should have nil output (i.e. thus, $u_m(t) = 0$), the stability of this nonlinear equation can be shown by using the *Lyapunov's indirect method*[7] (Crassidis et al., 2012), assuming the nonlinear hysteretic terms involving the instantaneous stiffness $k_T(\underline{x})$ is differentiable. The procedure is presented in the work of the author (Ryu, 2015). However, since the input-output stability analysis shows the desired bounded responses of the controlled closed loop system, the approximated method using the *Lyapunov's indirect method* is not included in this report.

---

[7] The *Lyapunov's indirect method* (Crassidis et al., 2012) gives the following stability condition: The equilibrium point of the actual nonlinear system is asymptotically stable if the linearized system has all eigenvalues of negative real parts.

Application to 2DOF Shake Table-Nonlinear Structure Systems

The same tracking control method (feedback linearization method) can be applied to a nonlinear hysteretic structure mounted on a shake table (2DOF system model), expressed in Eq. (4-8) and Eq. (4-9) with the output $y(t)$ of the total acceleration response $\ddot{x}_s^t(t)$ at the structure and the equations are repeated here for convenience.

Equations of the True System

$$\begin{cases} m_s\ddot{x}_s(t)+c_s\dot{x}_s(t)+f_S(\underline{x})=-m_s\ddot{x}_t(t) \\ m_t\ddot{x}_t(t)-\{c_s\dot{x}_s(t)+f_S(\underline{x})\}=f_a(t) \\ \dot{f}_S(\underline{x})=k_T(\underline{x})\dot{x}_s(t) & , \qquad \underline{x}(0)=\underline{x}_0 \\ \dfrac{1}{\omega_a^2}\dfrac{\dot{f}_a(t)}{m_t}+\dfrac{2\xi_a}{\omega_a}\dfrac{f_a(t)}{m_t}+\dfrac{dx_t(t)}{dt}+k_a x_t(t)=k_a x_d(t) \end{cases}$$
$$y(t)=\ddot{x}_s^t(t)=-m_s^{-1}c_s\dot{x}_s(t)-m_s^{-1}f_S(\underline{x}) \tag{4-36}$$

Equations of a Reference Model

$$\begin{aligned} &\ddot{x}_m(t)=-m_m^{-1}c_m\dot{x}_m(t)-m_m^{-1}k_m x_m(t)+m_m^{-1}r(t), \qquad \underline{x}_m(0)=\underline{x}_{m,0} \\ &y_m(t)=\ddot{x}_m^t(t)=-m_m^{-1}c_m\dot{x}_m(t)-m_m^{-1}k_m x_m(t) \end{aligned} \tag{4-37}$$

Using the same procedure described above, the control law can be obtained (see Derivation 4.1 in Appendix B.4) as following:

Control Law

$$u^*(t)=a^{-1}\left[-\ddot{y}^*(t)+v(t)\right] \tag{4-38}$$

where $u^*(t)=(\omega_a^2k_a)^{-1}u(t)$; $u(t)=x_d(t)$; and $\ddot{y}^*(t)$ is defined as

$$\begin{aligned} \ddot{y}^*(t)=&\left[a(a+c)-m_s^{-1}k_T(\underline{x})\right]\ddot{x}_s(t)+\left[-m_s^{-1}\dot{k}_T(\underline{x})+a\left(m_s^{-1}+m_t^{-1}\right)k_T(\underline{x})\right]\dot{x}_s(t) \\ &+(-ae)f_a^*(t)+(-af)\dot{x}_t(t)+(-ag)x_t(t) \end{aligned} \tag{4-39}$$

in which notations are introduced for simplification:

$$\begin{aligned} &a=m_s^{-1}c_s; \qquad c=m_t^{-1}c_s; \\ &e=2\xi_a\omega_a; \qquad f=\omega_a^2; \qquad g=\omega_a^2k_a; \\ &f_a^*(t)=f_a(t)/m_t; \qquad u^*(t)=\omega_a^2k_a x_d(t), \quad u(t)=x_d(t) \end{aligned} \tag{4-40}$$

Substituting $u^*(t)$ into the equation of the differentiated output $\ddot{y}(t)$ shown in Eq. (B-35) in Appendix B.4 leads to

$$\ddot{y}(t)=v(t) \tag{4-41}$$

To reduce the tracking error signal $e(t) = y(t) - y_m(t)$, the new input $v(t)$ can be

$$v(t)=\ddot{y}_m(t)-k_1^*\dot{e}(t)-k_2^*e(t) \tag{4-42}$$

where k_1^* and k_2^* are the tracking error design coefficients, which are constant and positive, these lead to the tracking error dynamics:

<u>Expected Achieved Responses</u>

$$\ddot{e}(t)+k_1^*\dot{e}(t)+k_2^*e(t)=0 \tag{4-43}$$

in which the error signal $e(t)$ goes to zero as time goes to infinity; $e(t) \rightarrow 0$ as $t \rightarrow \infty$.

<u>Stability</u>

It is shown in Eq. (4-43) that the tracking error goes to zero, $\underline{e}(t) \rightarrow 0$. And this indicates that $y(t) = \ddot{x}_s^t(t) \approx y_m(t)$ is bounded; however, one still needs to check if the state responses $\underline{x}(t)$ of the closed loop system are bounded. By substituting the control excitation input $u(t)$ from Eq. (4-38) into the true system equation (4-36) and using the notations defined in Eq. (4-40), one has

$$\begin{aligned}
\dot{f}_a^*(t) &= -ef_a^*(t)-f\dot{x}_t(t)-gx_t(t)+a^{-1}\left[-\dddot{y}^*(t)+v(t)\right] \\
&= -\left[(a+c)-a^{-1}m_s^{-1}k_T(\underline{x})\right]\ddot{x}_s(t)-\left[-a^{-1}m_s^{-1}\dot{k}_T(\underline{x})+\left(m_s^{-1}+m_t^{-1}\right)k_T(\underline{x})\right]\dot{x}_s(t)+a^{-1}v(t) \\
&= \underbrace{\left\{-\left[(a+c)-a^{-1}m_s^{-1}k_T(\underline{x})-k_1^*\right]\right\}}_{\bar{h}(\underline{x})}\ddot{x}_s(t)+\underbrace{\left\{-\left[-a^{-1}m_s^{-1}\dot{k}_T(\underline{x})+\left(m_s^{-1}+m_t^{-1}\right)k_T(\underline{x})-k_1^*a^{-1}m_s^{-1}k_T(\underline{x})-k_2^*\right]\right\}}_{i(\underline{x})}\dot{x}_s(t) \\
&\quad +\underbrace{k_2^*a^{-1}m_s^{-1}}_{j}f_S(\underline{x})+\underbrace{a^{-1}\left[\dddot{y}_m(t)+k_1^*\ddot{y}_m(t)+k_2^*\dot{y}_m(t)\right]}_{u_m(t)}
\end{aligned} \tag{4-44}$$

By substituting $\ddot{x}_s^t(t)$ from Eq. (4-36) and by introducing additional notations for simplification:

$$\bar{h}(\underline{x})=-\left[(a+c)-a^{-1}m_s^{-1}k_T(\underline{x})-k_1^*\right];$$

$$i(\underline{x})=-\left[-a^{-1}m_s^{-1}\dot{k}_T(\underline{x})+\left(m_s^{-1}+m_t^{-1}\right)k_T(\underline{x})-k_1^*a^{-1}m_s^{-1}k_T(\underline{x})-k_2^*\right]; \qquad j=k_2^*a^{-1}m_s^{-1};$$

and also introducing the last known term $a^{-1}[\dddot{y}_m(t)+k_1^*\ddot{y}_m(t)+k_1^*\dot{y}_m(t)]$ from the target motion as a new input $u_m(t)$, Eq. (4-44) can be rewritten

$$\begin{aligned}
\dot{f}_a^*(t) &= +\bar{h}(\underline{x})\ddot{x}_s(t)+i(\underline{x})\dot{x}_s(t)+jx_s(t)+u_m(t) \\
&= -\bar{h}(\underline{x})f_a^*(t)+\left[-\bar{h}(\underline{x})(a+c)+i(\underline{x})\right]\dot{x}_s(t)+\left[-\bar{h}(\underline{x})\left(m_s^{-1}+m_t^{-1}\right)+j\right]f_S(\underline{x})+u_m(t)
\end{aligned} \tag{4-45}$$

which is a nonlinear equation due to $k_T(\underline{x})$; therefore, the eigenvalue test of the system matrix is not applicable. The input-output stability of this nonlinear system can be checked as following.

The tracking error equation in Eq. (4-43) can be rewritten

$$\dot{\underline{e}}(t)=\begin{bmatrix} 0 & 1 \\ -k_2^* & -k_1^* \end{bmatrix}\begin{bmatrix} e(t) \\ \dot{e}(t) \end{bmatrix} \quad or \quad A_e\underline{e}(t) \tag{4-46}$$

where A_e is a constant 2 × 2 matrix, whose real part eigenvalues are all negative with k_1^*, k_2^* >0; i.e. a constant matrix having all negative real part eigenvalues is called a *stable* matrix. Using the *Lyapunov's* *direct method* introduced in Section 3.2, one can show that the tracking error $e(t)$ is bounded (i.e. $e \in L_\infty$; L_p norm[8] definition is adopted from Ioannou and Sun, 2012). Furthermore, it can be shown that $e \in L_2$; therefore, $e \in L_\infty \cap L_2$ (see Derivation 4.3 in Appendix B.6). Now, by choosing the target motion $y_m(t) \in L_\infty \cap L_2$ and from the tracking error equation $e(t) = y(t) - y_m(t)$, it can be shown that $y(t) \in L_\infty \cap L_2$.

It is noted that $y(t) = \ddot{x}_s^t(t)$, the total acceleration of the structure, which can be considered as the input to the structure. The first system equation in Eq. (4-36) can be rewritten using the notations in Eq. (4-40)

$$a\dot{x}_s(t) + m_s^{-1} f_S(\underline{x}) = -\left[\ddot{x}_t(t) + \ddot{x}_s(t)\right] \quad or \quad -y(t) \tag{4-47}$$

and multiplying the instantaneous stiffness $k_T(\underline{x})$ leads to

$$\begin{aligned} &ak_T(\underline{x})\dot{x}_s(t) + m_s^{-1}k_T(\underline{x}) f_S(\underline{x}) = -k_T(\underline{x}) y(t) \qquad or \\ &k_T(\underline{x})\dot{x}_s(t) + a^{-1}m_s^{-1}k_T(\underline{x}) f_S(\underline{x}) = -a^{-1}k_T(\underline{x}) y(t) \end{aligned} \tag{4-48}$$

where $k_T(\underline{x})\, \dot{x}_s(t) = \dot{f}_s(\underline{x})$ as shown in the third system equation in Eq. (4-36), and it gives

$$\dot{f}_S(\underline{x}) + a^{-1}m_s^{-1}k_T(\underline{x}) f_S(\underline{x}) = -a^{-1}k_T(\underline{x}) y(t) \tag{4-49}$$

where the instantaneous stiffness $k_T(\underline{x})$ is a positive bounded function (i.e. $k_T(\underline{x}) \in L_\infty$) as

$$\alpha k_s \le k_T(\underline{x}) \le k_s \tag{4-50}$$

where the post-yielding stiffness ratio to the elastic stiffness, α, considered in this study has the following property: $0 < \alpha < 1$. It is noted that $k_T(\underline{x})$ shown in Eq. (4-6) can be expressed in two parts: the initial elastic stiffness k_s and the inelastic part $k_{in}(\underline{x})$

$$k_T(\underline{x}) = k_s - \underbrace{(1-\alpha)k_s \frac{1+\operatorname{sgn}\left(f_H(\underline{x})\dot{x}_s(t)\right)}{2}\left(\frac{\left|f_H(\underline{x})\right|}{f_y^*}\right)^N}_{k_{in}(\underline{x})} \tag{4-51}$$

where $k_{in}(\underline{x})$ is a bounded function (i.e. $k_T(\underline{x}) \in L_\infty$), having

$$0 \le k_{in}(\underline{x}) \le (1-\alpha)k_s \tag{4-52}$$

Using Eq. (4-51), Eq. (4-49) can be rewritten as

$$\dot{f}_S(\underline{x}) + a^{-1}m_s^{-1}\left[k_s + k_{in}(\underline{x})\right] f_S(\underline{x}) = -a^{-1}k_T(\underline{x}) y(t) \tag{4-53}$$

---

[8] For functions of time, the L_p norm is defined as (Ioannou and Sun, 2012)

$$\|x\|_p \equiv \left(\int_0^\infty |x(\tau)|^p \, d\tau\right)^{1/p}$$

for $p \in [1, \infty)$ and it is said that $x \in L_p$ when $\|x\|_p$ is finite. The L_∞ norm is defined as

$$\|x\|_\infty \equiv \sup_{t \ge 0} |x(t)|$$

and it is said that $x \in L_\infty$ when $\|x\|_\infty$ is finite. Note that $x(t)$ can be a scalar or a vector function, and $|x(t)|$ denotes the absolute value if x is a scalar function, and $|\underline{x}(t)|$ denotes the vector norm in R^n (i.e n = the vector size) at each time t .

where a^{-1}, m_s^{-1} are positive constant scalars (i.e. a^{-1}, $m_s^{-1} > 0$), and since $k_T(\underline{x}) \in L_\infty$ and $y(t) \in L_\infty \cap L_2$, one can simplify the right-hand-side of the equation as following: $-a^{-1}k_T(\underline{x})y(t) = \bar{u}(t)$ where the new input term $\bar{u}(t) \in L_\infty \cap L_2$. Thus, Eq. (4-53) becomes

$$\dot{f}_S(\underline{x}) + a^{-1}m_s^{-1}k_s f_S(\underline{x}) + a^{-1}m_s^{-1}k_{in}(\underline{x}) f_S(\underline{x}) = \bar{u}(t) \tag{4-54}$$

Now, from this equation one can show that $f_S(\underline{x}) \in L_\infty \cap L_2$ and $\dot{f}_S(\underline{x}) \in L_\infty \cap L_2$ (see Derivation 4.4 in Appendix B.7); therefore, $f_S(\underline{x}) \to 0$ as $t \to \infty$ (refer to Lemma 3.2.5[9] in Ioannou and Sun, 2012), if the following condition is satisfied

$$k_s > k_{in}(\underline{x}) \tag{4-55}$$

and in fact this condition is always met since the maximum value of $k_{in}(\underline{x}) = (1-\alpha)k_s < k_s$ with $0 < \alpha < 1$ in this study (see Eq. (4-52)). Since the restoring force $f_S(\underline{x}) \in L_\infty$ and $f_S(\underline{x}) \to 0$ as $t \to \infty$, it is known from the restoring force and structure displacement relationship (shown in Figure 4-1) that the structure displacement $x_s(t)$ is bounded (i.e. $x_s(t) \in L_\infty$) and $x_s(t) \to$ *a constant value* as $t \to \infty$

Also, from Eq. (4-47), it can be shown that $\dot{x}_s(t) \in L_\infty \cap L_2$ since $f_S(\underline{x})$, $y(t) \in L_\infty \cap L_2$. Furthermore, the boundedness of the actuator force $f_a^*(t)$ can be checked as follows. Using that $\dot{x}_s(t)$, $f_S(\underline{x}) \in L_\infty \cap L_2$, and choosing the new input $u_m(t) = a^{-1}[\ddot{y}_m(t) + k_1^*\dot{y}_m(t) + k_1^* y_m(t)] \in L_\infty \cap L_2$, Eq. (4-45) can be expressed

$$\dot{f}_a^*(t) + \bar{h}(\underline{x}) f_a^*(t) = \underbrace{-\left[-\bar{h}(\underline{x})(a+c) + i(\underline{x})\right]\dot{x}_s(t) - \left[-\bar{h}(\underline{x})\left(m_s^{-1} + m_t^{-1}\right) + j\right] f_S(\underline{x}) + u_m(t)}_{\bar{u}_m(t)} \tag{4-56}$$

where in the right-hand-side the new input term $\bar{u}_m(t)$ is introduced for simplicity and $\bar{u}_m(t) \in L_\infty \cap L_2$ since $\bar{h}(\underline{x})$, $i(\underline{x})$ are bounded functions (i.e. $\bar{h}(\underline{x})$, $i(\underline{x}) \in L_\infty$). From this equation one can show that $f_a^*(t) \in L_\infty \cap L_2$ and $\dot{f}_a^*(t) \in L_\infty \cap L_2$ (see Derivation 4.5 in Appendix B.8); therefore, $f_a^*(t) \to 0$ as $t \to \infty$ (refer to Lemma 3.2.5 in Ioannou and Sun, 2012), if the following condition is satisfied

$$k_1^* + a^{-1}m_s^{-1}k_T \alpha k_s > a + c \tag{4-57}$$

and this condition can be easily met by choosing the design coefficient k_1^* in Eq. (4-42) to be larger than $(a + c)$.

From this stability analysis for the closed loop state responses, it has been shown that with the bounded target and output response (i.e. $y_m(t)$, $y(t) \in L_\infty \cap L_2$), the state variables $x_s(t)$, $\dot{x}_s(t)$, $f_S(\underline{x})$, $f_a^*(t)$ are bounded and $\dot{x}_s(t)$, $f_S(\underline{x})$, $f_a^*(t) \to 0$ as $t \to \infty$. From this results and the second system equation in Eq. (4-36), one can also show that the shake table acceleration $\ddot{x}_t(t)$ is bounded and $\ddot{x}_t(t) \to 0$ as $t \to \infty$. However, in order to show the boundedness of the shake table displacement $x_t(t)$ and velocity $\dot{x}_t(t)$, one

[9] Lemma 3.2.5 (Ioannou and Sun, 2012): if f, $\dot{f} \in L_\infty$ and $f \in L_p$ for some $p \in [1, \infty)$, then $f(t) \to 0$ as $t \to \infty$.

needs to modify the tracking control law (Eq. (4-42)), and one possible way is to add the following extra term to Eq. (4-42)

$$-k_3^*\left(\dot{x}_s^t(t)-\int_0^t y_m(\tau)d\tau\right)-k_4^*\left(x_s^t(t)-\int_0^t\int_0^\tau y_m(\zeta)d\zeta\, d\tau\right) \tag{4-58}$$

where k_3^* and k_4^* are the positive constant tracking error design coefficients, the total displacement $x_S^t(t)$ = $x_s(t)$ + $x_t(t)$ and the total velocity $\dot{x}_S^t(t)$ = $\dot{x}_s(t)$ + $\dot{x}_t(t)$, and the integration and double integration of the target motion $y_m(t)$ are also chosen to belong to $L_\infty \cap L_2$ and their initial values are zeros. With the modified control excitation input, $x_S^t(t)$ and $\dot{x}_S^t(t)$ are bounded, and also $x_s(t)$ and $\dot{x}_s(t)$ are bounded as shown above; therefore, $x_t(t)$ and $\dot{x}_t(t)$ are bounded. In this study, this additional term in Eq. (4-58) is not included for simplicity. This might be acceptable for the shake table control applications in this study where the total control time is relatively short. However, this issue might be more critical for applications where much longer control time is required. For these applications, one is to consider the extra term shown in Eq. (4-58); it is noted that the new control law with the extra term is equivalent to the control law that is obtained by modifying the original target motion (= the total structure acceleration) to the total structure displacement through double integrations of the original target motion.

4.4 Comparisons of Feedback Tracking Control Methods

As discussed in Section 3.3.3, it is very interesting to see the similarity and/or differences between the two feedback control methods introduced in this section.

One can show that the two methods are equivalent for the controller of a structure having nonlinear hysteretic behavior, under certain conditions. For example, for the shake table-structure system the predictive tracking control (PTC) law shown in Eq. (4-18) becomes the same as the control law (see Eq. (4-38)) of the feedback linearization tracking control (FTC) method (i.e. see Derivation 4.2 in Appendix B.5) if the controlled system has $B^*(\underline{x})$ = a non-zero scalar (i.e. an invertible matrix, size 1 × 1), and $R = 0$ chosen, and by selecting the tracking error coefficients in Eq. (4-20) as $k_1^* = 2 / h = 2\xi_e\omega_e$ and $k_2^* = 2 / h^2 = \omega_e^2$; therefore, $\xi_e = \sqrt{2} / 2 \approx 0.707$ and $h = \sqrt{2} / \omega_e$. Here h is a tracking error design parameter and can be selected by the design engineer, not restricted to be the same as the sampling time step.

4.5 Numerical Examples and Comparisons of Tracking Control Methods

Simple tracking control examples (like the linear system cases) are analyzed in order to examine the performance of the two feedback tracking control methods introduced for nonlinear systems. The results obtained from the numerical simulations are presented. For all examples, the target motion is the total acceleration of a structure (specimen) mounted on the shake table although any response; i.e. a displacement or velocity response, can be selected as the target motion.

4.5.1 SDOF Nonlinear Hysteretic Structures

As discussed in Section 2.2 and in the previous section, to facilitate the development of the tracking control method, first, a simplified SDOF system model is used instead of a 2DOF system model for the shake table with the SDOF structure system. In this simplified system model (shown in Figure 4-2), the excitation force $m_s\ddot{x}_t(t)$ due to the shake table acceleration $\ddot{x}_t(t)$ is considered as a new control input $u(t)$ (instead of the actual control input $u(t) = x_d(t)$, the desired shake table displacement, for the 2DOF system model). The governing equation of an SDOF nonlinear structure subjected to the shake table excitation is shown in the first equation of Eq. (4-1).

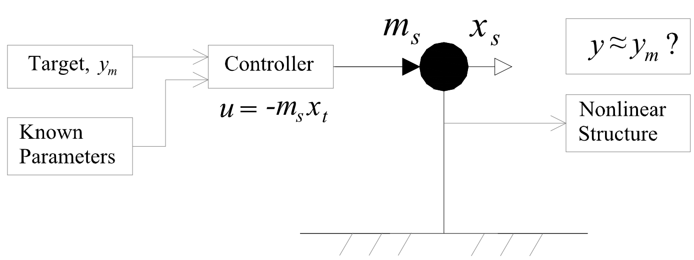

Figure 4-2 Tracking control of an SDOF nonlinear system with known parameters

For this simplified system, the tracking control task is to compute the control input $u(t) = -m_s\ddot{x}_t(t)$ so that the system output $y(t) = \ddot{x}_s^t(t)$ (the total acceleration of the structure) follows the target motion $y_m(t) = \ddot{x}_m^t(t)$ (the total acceleration of the reference model). For the shake table-structure system, however, the actual control input is the desired displacement $x_d(t)$ of the shake table and $u(t)$ shall be computed including the shake table dynamics and the shake table-structure interaction (as discussed in Section 2.2), and will be reconsidered in the following section (Section 4.5.2).

Example 4.1* : *An SDOF Nonlinear System with Known Parameters

The properties of a given system are: m_s = 1 kips·sec^2/in., k_s = 355 kips/in., and c_s = 1.13 kips·sec/in., (f_n = 3.0 Hz, ξ_n = 0.03 before yielding). N = 3, d_y = 0.11 in. (f_y = 39 kips), and α = 0.1; i.e. all terms are explained in Eq. (4-2) and Eq. (4-3). The target motion is shown in Figure 4-3 (a) [Target]: i.e. the target motion is the total acceleration output generated from the same reference linear system (f_m = 5.0 Hz, ξ_m = 0.1) used for Example 3.1. in Section 3.4.1 (the reference excitation input and the responses of the reference model are presented in Appendix A.2). The time step used for the simulation is 0.002 sec.

Tracking control results using the *predictive tracking control* (PTC) method are presented in Figure 4-3. The selected control parameters for the PTC in this example are R = 0 and Δt = 0.002. The controlled output, $\ddot{x}_s^t(t)$ the total acceleration of the structure, is shown in Figure 4-3 (a) [Controlled] and shows very good agreement with the target motion. The computed control excitation input, $u(t) = -m_s\ddot{x}_t(t)$, using the control law in Eq. (4-13) is shown in Figure 4-3 (b). $x_s(t)$, $\dot{x}_s(t)$ the achieved displacement and velocity responses of the controlled structure are also presented in Figure 4-3 (c) and (d); it is noted that unlike the total acceleration, the displacement and velocity responses are different from ones of the reference because the system properties of the controlled system and ones of the reference system are different (the responses of the reference model are presented in Appendix A.2). The relation between the structure resisting force $f_S(t)$ having hysteretic behavior and displacement $x_s(t)$ is also presented in Figure 4-3 (e). As desired, all responses of the controlled system are bounded.

The tracking control results using the *feedback linearization tracking control* (FTC) method are presented in Figure 4-4. The controlled output $\ddot{x}_s^t(t)$ is shown in Figure 4-4 (a) [Controlled] and shows very good agreement with the target motion. The computed control excitation input, $u(t) = -m_s\ddot{x}_t(t)$, using the control law in Eq. (4-31) is shown in Figure 4-4 (b). The selected control parameter in this example for the FTC is $k_1^* = 1/\Delta t$. It is noted that by choosing the control parameters carefully to satisfy the tracking objective, the control excitation inputs of the two methods (PTC and FTC) are very similar; therefore, as expected, the control results of two methods are also very similar as shown in Figure 4-3 and Figure 4-4.

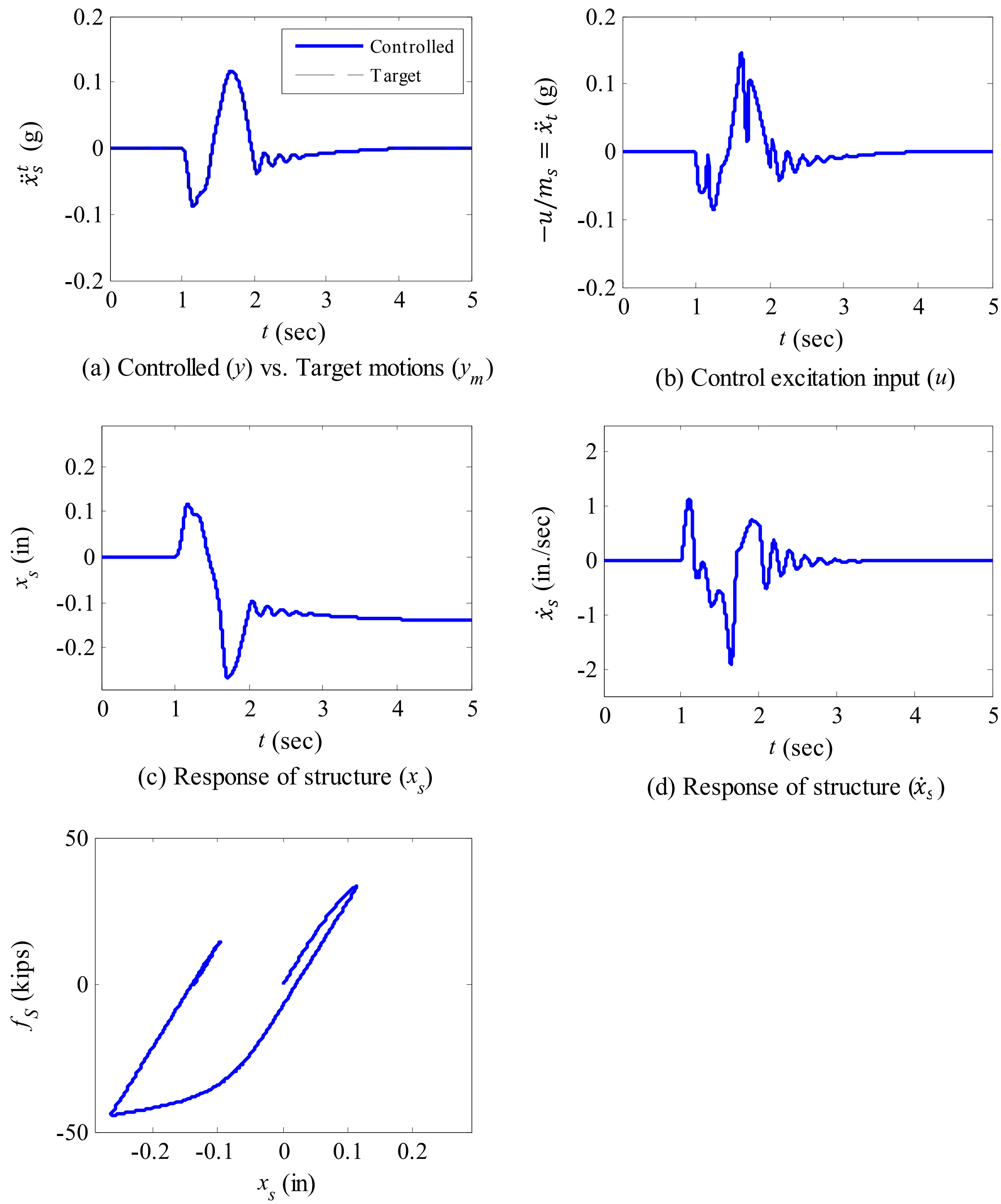

(a) Controlled (y) vs. Target motions (y_m)

(b) Control excitation input (u)

(c) Response of structure (x_s)

(d) Response of structure ($\dot{x}_s$)

(e) Response of structure (f_S vs. x_s)

Figure 4-3 Predictive tracking control results of an SDOF nonlinear system

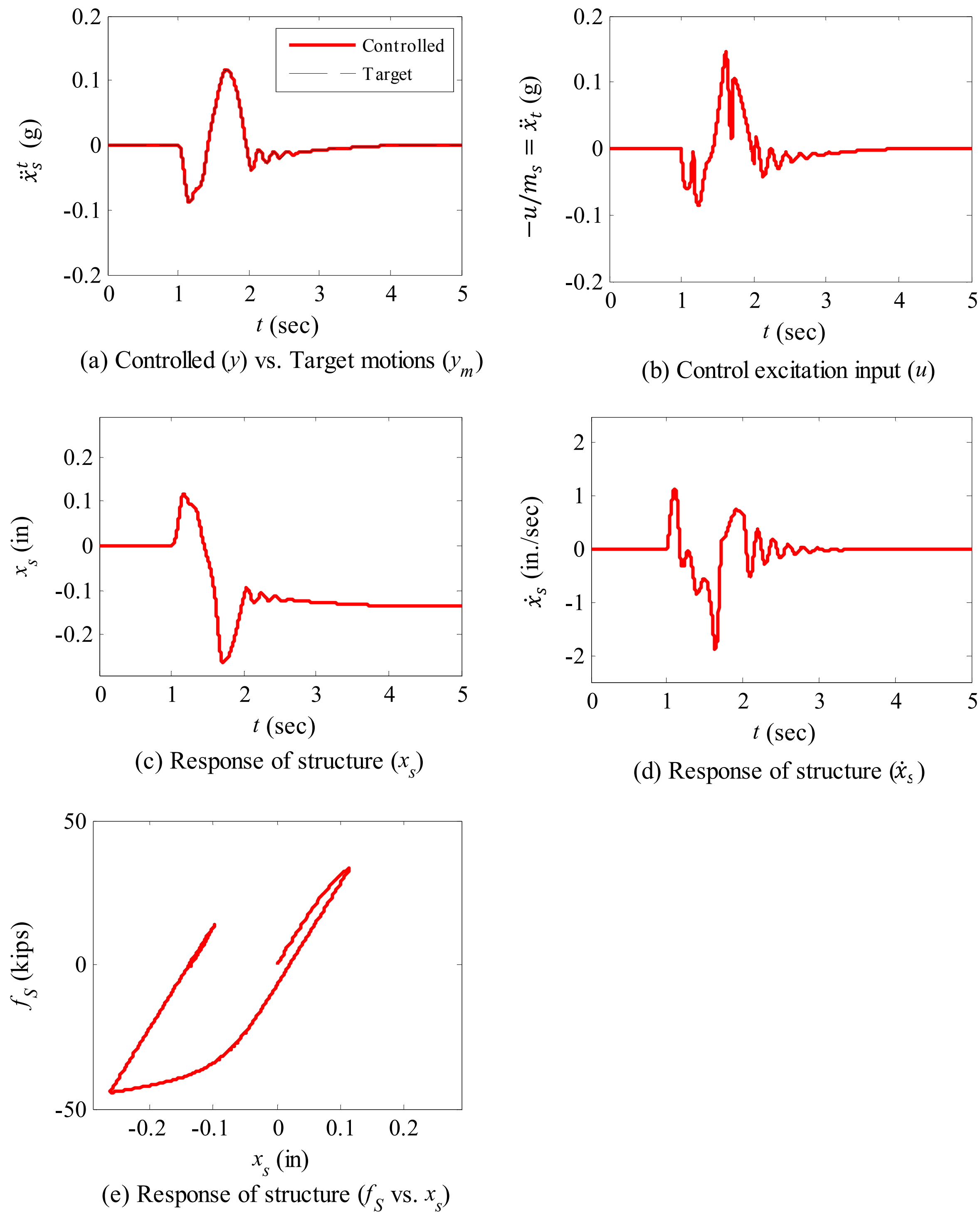

(a) Controlled (y) vs. Target motions (y_m)

(b) Control excitation input (u)

(c) Response of structure (x_s)

(d) Response of structure ($\dot{x}_s$)

(e) Response of structure (f_S vs. x_s)

Figure 4-4 Feedback linearization tracking control results of an SDOF nonlinear system

4.5.2 2DOF Shake Table - Nonlinear Hysteretic Structure Systems

As discussed in Section 2.2, the shake table dynamics affect the performance of the control system and the interaction between the shake table and the mounted structure is to be considered. The same tracking control example above is resolved for the 2DOF nonlinear system, expressed in Eq. (4-8) and Eq. (4-9), and schematically shown in Figure 4-5.

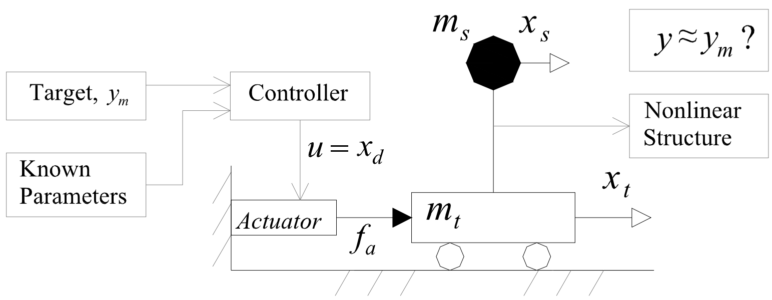

Figure 4-5 Tracking control of the shake table- structure 2DOF nonlinear system with known parameters

When a target motion at a structure is specified, the required control input $u(t) = x_d(t)$, the desired shake table displacement, is determined in order that the output of the system ($y(t) = \ddot{x}_s^t(t)$ the total acceleration of the structure) follows the target motion $y_m(t)$.

Example 4.2* : *A 2DOF Nonlinear System with Known Parameters

The properties of a given system are: m_s = 1 kips·sec^2/in., k_s = 355 kips/in., and c_s = 1.13 kips·sec/in., (f_n = 3.0 Hz, ξ_n = 0.03 before yielding); N = 3, d_y = 0.11 in. (f_y = 39 kips), and α = 0.1 for the hysteretic system (i.e. all terms are explained in Eq. (4-2) and Eq. (4-3)); and $\mu = m_s / m_t = 0.1$, $f_{n,a}$ = 30.0 Hz, ξ_a = 0.5 and k_a = 25 for the shake table. Figure 4-6 (a) [Target] shows the target motion, which is the total acceleration generated from the same reference linear system (f_m = 5.0 Hz, ξ_m = 0.1) used for Example 3.1. in Section 3.4.1. The reference input and the responses of the reference model are presented in Appendix A.2. The time step of 0.002 sec is used for the simulation.

Tracking control results using the *predictive tracking control* (PTC) method are presented in Figure 4-6 and Figure 4-7. The selected control parameters in this example R = 0 and $h = \sqrt{2} / \omega_e$ where ω_e = 100. The controlled output, $\ddot{x}_s^t(t)$ the total acceleration of the structure, is shown in Figure 4-6 (a) [Controlled] and shows very good agreement with the target motion. The control excitation input $u(t)$ = the desired table displacement $x_d(t)$, computed using the control law in Eq. (4-18) is shown in Figure 4-6 (b). The shake table acceleration $\ddot{x}_t(t)$ due to the control excitation input $u(t)$ is presented in Figure 4-7 (b); $x_s(t)$, $\dot{x}_s(t)$ the achieved displacement and velocity responses of the controlled structure are also presented in Figure 4-6 (c) and (d); it is noted that unlike the total acceleration (which was the target of the control design), the displacement and velocity responses are different from ones of the reference because the system properties of the controlled system and ones of the reference system are different. The relation between the structure resisting force $f_S(t)$ having hysteretic behavior and displacement $x_s(t)$ is also presented in Figure 4-6 (e). Figure 4-7 presents the responses of the shake table; the achieved shake table actuator force $f_a(t)$, shake table acceleration $\ddot{x}_t(t)$, displacement $x_t(t)$ and velocity $\dot{x}_t(t)$. These shake table responses are presented to show the feasibility and the stability of the control scheme; for example, in real applications, the capacity of actuators' force, displacement, and velocity are limited. This capacity limit of a shake table is examined in Ch 8 for a realistic application. As desired, all responses of the controlled system are bounded.

The tracking control results using the *feedback linearization tracking control* (FTC) method are also presented in Figure 4-8 and Figure 4-9. The controlled output $\ddot{x}_s^t(t)$ is shown in Figure 4-8 (a) [Controlled] and shows very good agreement with the target motion. The computed control excitation input, $u(t)$ = $x_d(t)$, using the control law in Eq. (4-38) is shown in Figure 4-9 (b). As discussed in Section 4.4, the control excitation inputs of the two methods (PTC and FTC) are the same if one chooses the tracking error coefficients as $k_1^* = 2 / h = 2\xi_e\omega_e$ and $k_2^* = 2 / h^2 = \omega_e^2$; therefore, $\xi_e = \sqrt{2} / 2 \approx 0.707$ and $h = \sqrt{2} / \omega_e$; (in this example, $\omega_e = 100$, $\xi_e = 0.707$ for the both methods); note that here h is a tracking error design parameter as discussed in Section 3.3.1 and it can be selected by the design engineer. As expected, the control results of the two methods are equivalent as shown in Figure 4-6 through Figure 4-9.

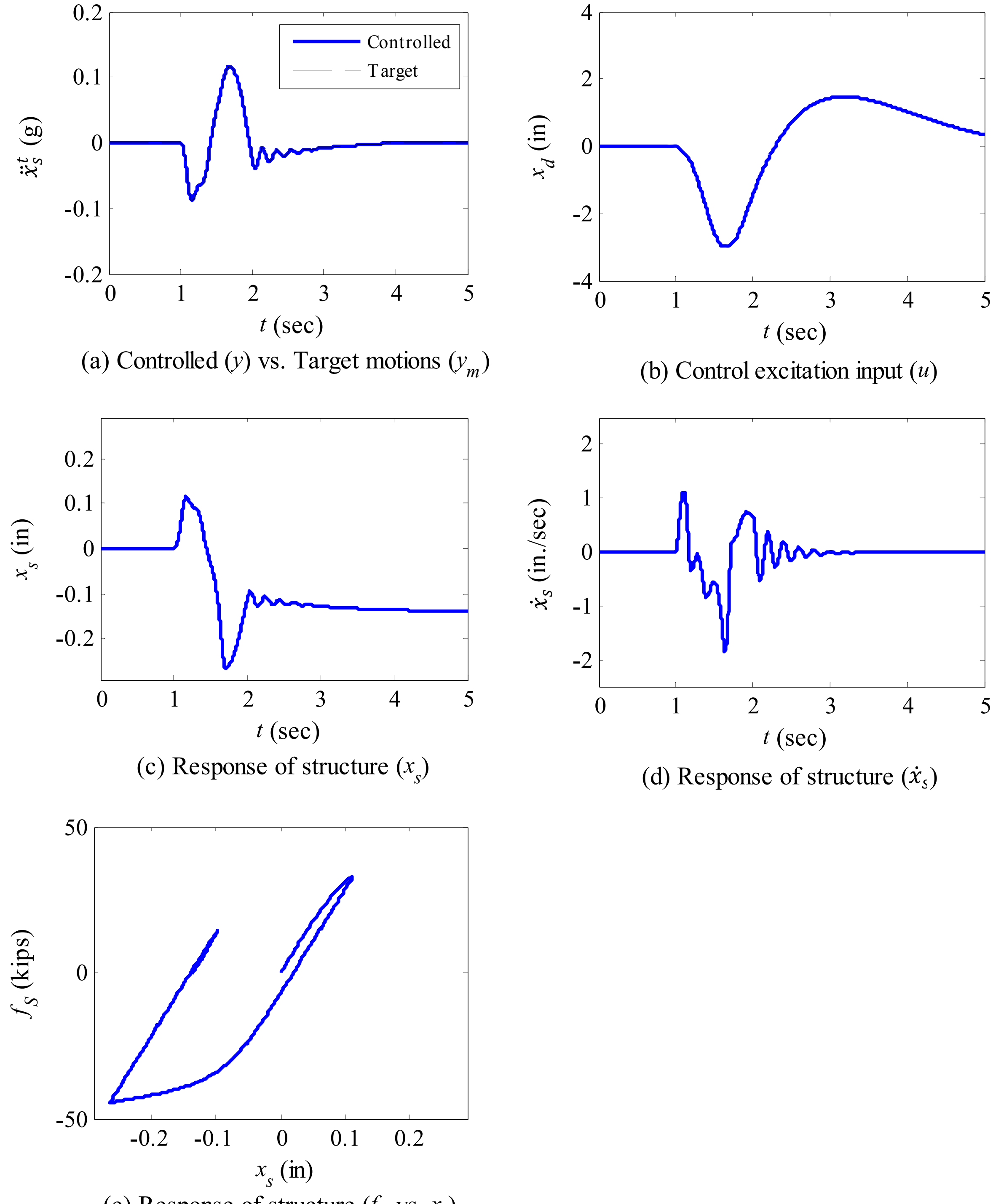

(a) Controlled (y) vs. Target motions (y_m)

(b) Control excitation input (u)

(c) Response of structure (x_s)

(d) Response of structure ($\dot{x}_s$)

(e) Response of structure (f_S vs. x_s)

Figure 4-6 Predictive tracking control structure responses of a 2DOF nonlinear system

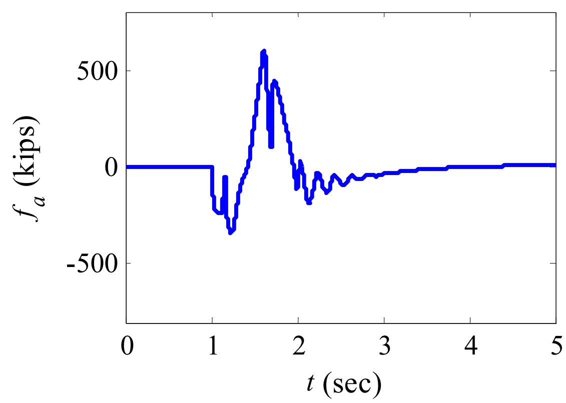

(a) Response of table (f_a)

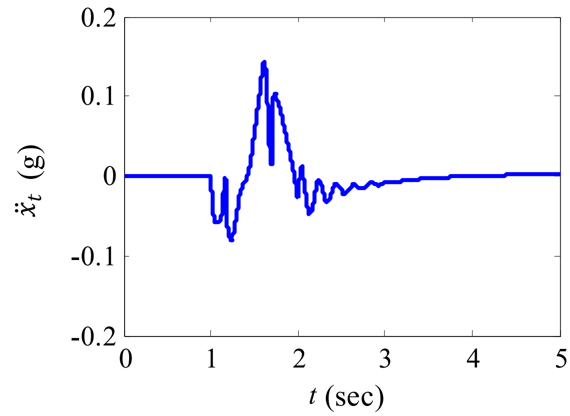

(b) Response of table ($\ddot{x}_t$)

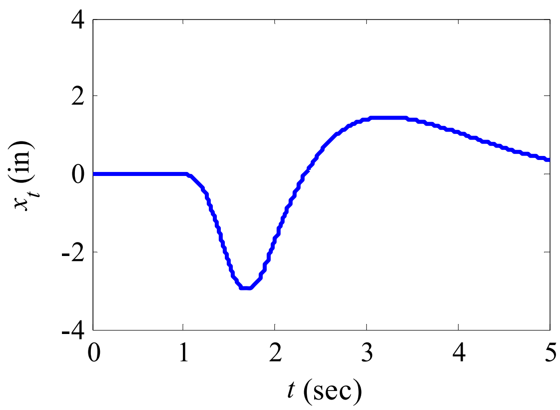

(c) Response of table (x_t)

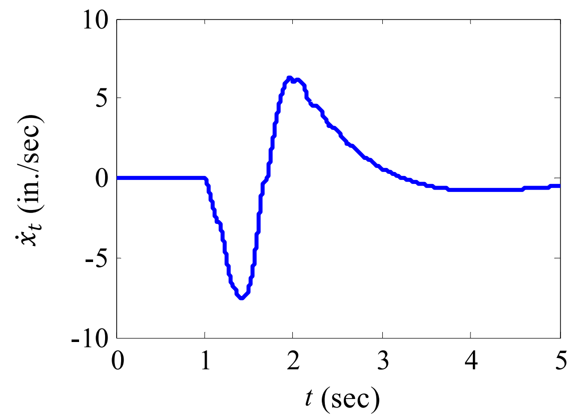

(d) Response of table ($\dot{x}_t$)

Figure 4-7 Predictive tracking control shake table responses of a 2DOF nonlinear system

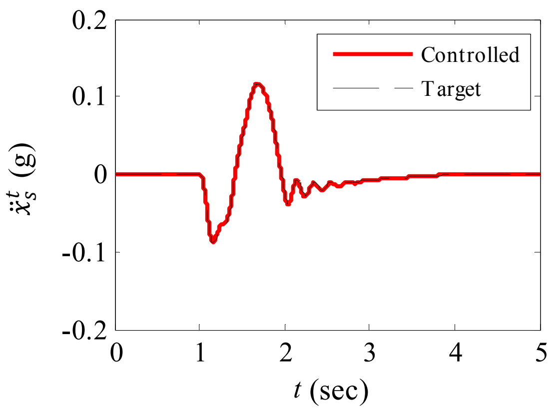

(a) Controlled (y) vs. Target motions (y_m)

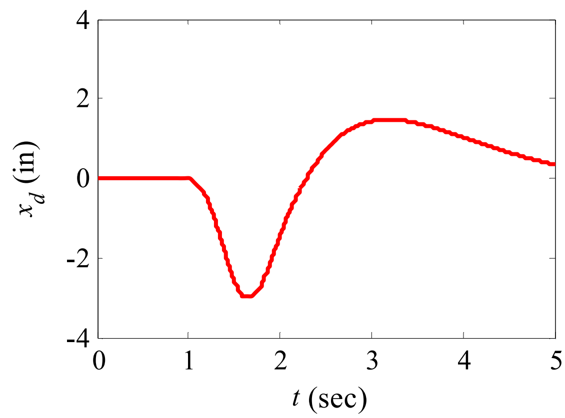

(b) Control excitation input (u)

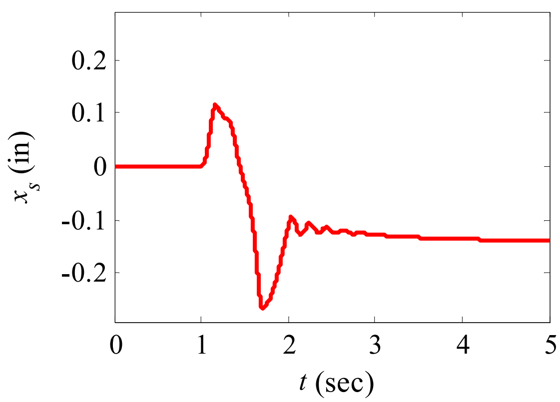

(c) Response of structure (x_s)

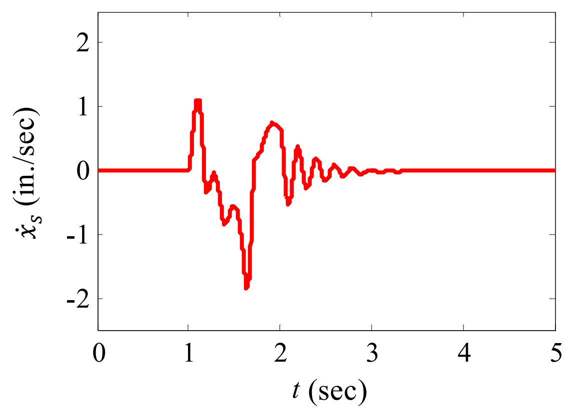

(d) Response of structure ($\dot{x}_s$)

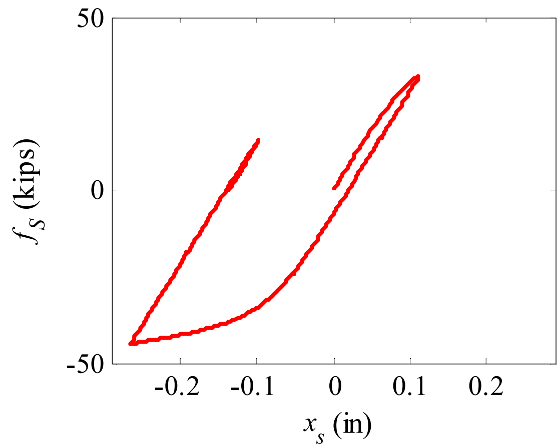

(e) Response of structure (f_S vs. x_s)

Figure 4-8 Feedback linearization tracking control structure responses of a 2DOF nonlinear system

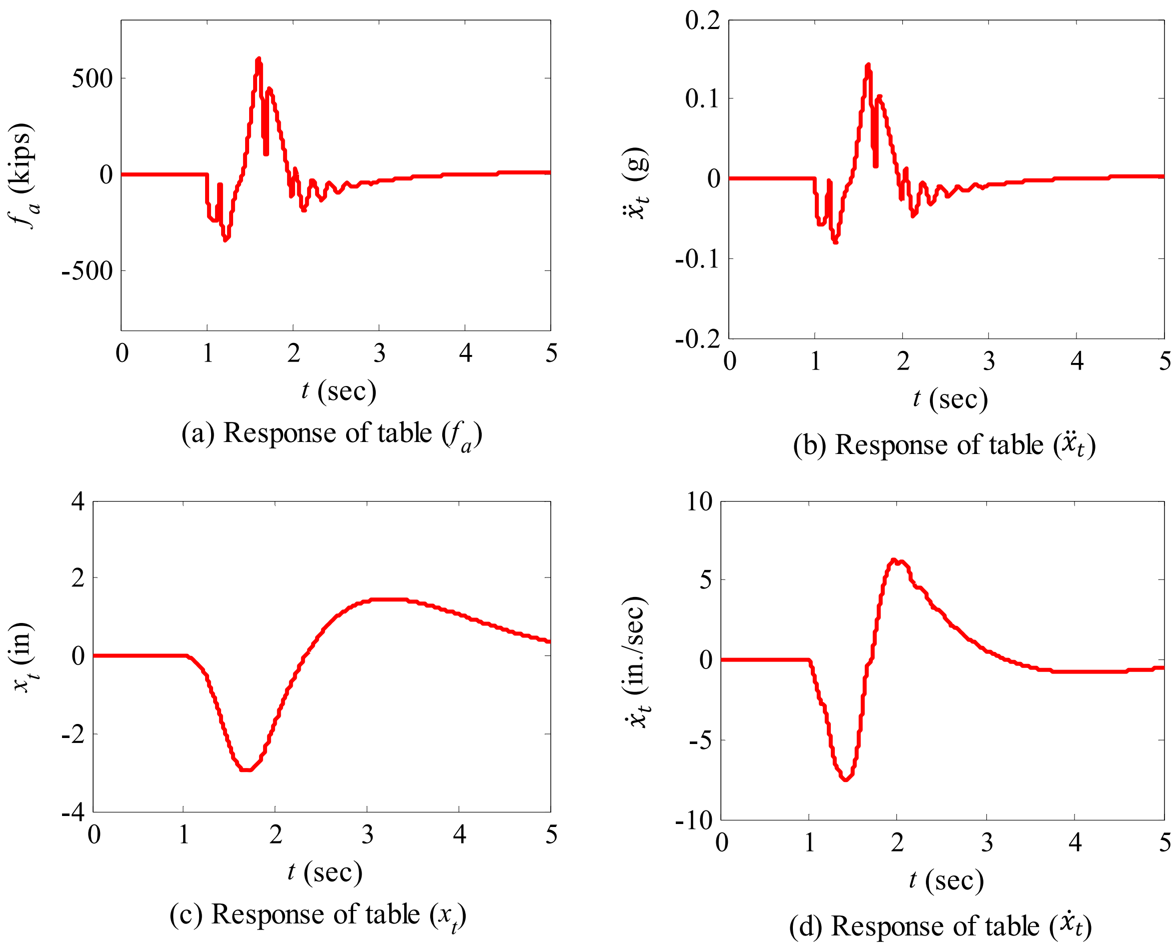

(a) Response of table (f_a)

(b) Response of table ($\ddot{x}_t$)

(c) Response of table (x_t)

(d) Response of table ($\dot{x}_t$)

Figure 4-9 Feedback linearization tracking control shake table responses of a 2DOF nonlinear system

In this section, the two tracking control algorithms: the predictive tracking control (PTC) and the feedback linearization tracking control (FTC); are reformulated in order to apply the methods to nonlinear hysteretic systems using shake table control. With assumption that all parameters are known, the performances of the controllers are analytically analyzed using their tracking error dynamics and closed loop system responses, and the boundedness of the state responses are shown by the input-output stability analyses. The performances of the tracking control methods are also examined using numerical simulations for examples where the target motion is a specific floor motion at the top of a nonlinear specimen. Very good tracking results are achieved.

SECTION 5
PARAMETER IDENTIFICATION METHODS FOR TRACKING CONTROL

When system properties are not fully known, it is essential to identify and quantify these system parameters for the tracking control problem. Two well-known online parameter identification methods (i.e. which are also called "parameter adaptive methods") are reviewed here: the *least squares* method (LS) and the *Extended Kalman filter* (EKF). The effects of the selection of the initial guess of parameters and of covariance matrices are examined. The least squares method has been used for the online system identification of nonlinear hysteretic systems without hardening (Smyth et al., 1999); in this study this method is extended to nonlinear hysteretic systems with hardening. The two methods are compared in this section and the EKF scheme is adopted for further development of the tracking control method with unknown parameters in the following sections.

5.1 Identification of a Linear Parametric Model using the Least Squares Method

The *least-squares* method is to fit a mathematical model to a sequence of observed data by minimizing the sum of the squares of the difference between the observed and computed data. The method has been used in parameter estimation for the structural applications (Smyth et al., 1999 and Yang et al., 2004). The method is simple to apply if the model parameters appear in a linear form (Ioannou et al., 2012):

$$z\left(t\right)=\underline{\theta}^{*T}\underline{\phi}\left(t\right) \tag{5-1}$$

where $z(t)$ (scalar) and $\underline{\phi}(t)$ (vector) are the signals available for measurement (i.e. such as the state variables x, $\dot{x}$, $\ddot{x}$ and the excitation input u, and their filtered values), and $\underline{\theta}^{*}$ is the vector with all unknown parameters. Eq. (5-1) is known as the linear parametric model, which can represent a linear or nonlinear dynamic system. The linear or nonlinear dynamics in the original system are hidden in the selected signals z and $\underline{\phi}$, which include the measurements and their filtered values.

The estimate error $\varepsilon(t)$ is defined as the difference between the true signal $z(t)$, obtained from the measurements, and an estimated signal $\hat{z}(t)$, computed using the least-squares method:

$$\varepsilon\left(t\right)=z\left(t\right)-\hat{z}\left(t\right) \tag{5-2}$$

One can establish that the least-squares method guarantees that the estimation error $\varepsilon(t)$ goes to zero when time goes to infinity; i.e. $\varepsilon(t) \to 0$ as $t \to \infty$ (Ioannou et. al, 2012 and Smyth et al., 1999), which is a very important and desired stability property of an online parameter identification method.

Unfortunately, it will be shown that the nonlinear hysteretic system cannot be modeled in the form of the linear parametric model, if there is hardening after yielding ($\alpha > 0$).

5.1.1 Formulation

5.1.1.1 Estimate of Linear Structures with Unknown Parameters

A linear SDOF system expressed in Eq. (2-26) can be rewritten with two unknown constant parameters for the stiffness k_s and the damping c_s, by placing the parameters to the right side of the equation (Ioannou et al., 2012)

$$m\ddot{x}(t)-u(t)=\begin{bmatrix}k_s & c_s\end{bmatrix}\begin{bmatrix}-x(t) & -\dot{x}(t)\end{bmatrix}^T \tag{5-3}$$

where the unknown parameters [k_s c_s] appear linearly to the known signal vector. It is assumed that in this section the excitation input $u(t)$ is known and bounded and a system is stable; thus, the responses are bounded (i.e. this assumption is relaxed in the following sections where the excitation input $u(t)$ is not known a priori). It is also assumed that the displacement $x(t)$ and velocity $\dot{x}(t)$ can be measured; however, the acceleration response $\ddot{x}(t)$ is not available for measurement. In this case, in order to express Eq. (5-3) in the form of the linear parametric model (Eq. (5-1)), each side of Eq. (5-3) is divided by a first order stable filter $1/\Lambda(s)$ = $(s+\lambda)^{-1}$, in which λ is the first order filter parameter (i.e. in a case, if only the displacement $x(t)$ is measurable, a second order stable filter $1/\Lambda(s)$ $(s+\lambda)^{-2}$ could be used to establish the linear parametric model for this problem); thus, Eq. (5-3) is expressed in the Laplace domain as

$$\frac{s}{s+\lambda}m\dot{x}(s)+\frac{1}{s+\lambda}\left(-u(s)\right)=\begin{bmatrix}k_s & c_s\end{bmatrix}^T\frac{1}{s+\lambda}\begin{bmatrix}-x(s) & -\dot{x}(s)\end{bmatrix} \tag{5-4}$$

where "*s*" is a complex variable of the Laplace transform. Using Eq. (5-4), the unknown parameters [k_s c_s] can be expressed in the form of Eq. (5-1) (repeated) in time domain and the Laplace domain as follows:

$$z(t)=\underline{\theta}^{*T}\underline{\phi}(t) \quad or \quad z(s)=\underline{\theta}^{*T}\underline{\phi}(s) \tag{5-5}$$

in which

$$z(s)=\frac{s}{s+\lambda}m\dot{x}(s)+\frac{1}{s+\lambda}\left(-u(s)\right) \quad or \quad z(t)=\varphi_1(t)+\varphi_2(t),$$

$$\underline{\theta}^{*}=\begin{bmatrix}k_s & c_s\end{bmatrix}^T,$$

$$\underline{\phi}(s)=\begin{bmatrix}\frac{1}{s+\lambda}\left(-x(s)\right), & \frac{1}{s+\lambda}\left(-\dot{x}(s)\right)\end{bmatrix}^T \quad or \quad \underline{\phi}(t)=\begin{bmatrix}\phi_1(t), & \phi_2(t)\end{bmatrix}^T.$$

In order to estimate the unknown parameters in real time, each term in Eq. (5-4) is needed to be determined in every instant. Therefore, it is desired to represent Eq. (5-4) in a state-space form. The state-space representation of Eq. (5-4) can be expressed by introducing augmented vectors $\underline{\phi}_a(t)$ = [$\varphi_1(t)$ $\varphi_2(t)$ $\phi_1(t)$ $\phi_2(t)$]^T and $\underline{u}_a(t)$ = [$m\dot{x}(t)$ $-u(t)$ $-x(t)$ $-\dot{x}(t)$]^T:

$$\begin{aligned}\dot{\overline{\underline{\phi}}}_a(t)&=A_\lambda\overline{\underline{\phi}}_a(t)+B_\lambda\underline{u}_a(t), \qquad \overline{\underline{\phi}}_a(0)=\underline{0}\\ \underline{\phi}_a(t)&=C_\lambda\overline{\underline{\phi}}_a(t)+D_\lambda\underline{u}_a(t)\end{aligned} \tag{5-6}$$

where the additional state vector $\overline{\underline{\phi}}_a(t)$, which is different with $\underline{\phi}_a(t)$, is introduced for this formulation and

$$A_\lambda = -\lambda I_{4\times4},\quad B_\lambda = I_{4\times4},\quad C_\lambda = diag\left(\begin{bmatrix}-\lambda & 1 & 1 & 1\end{bmatrix}\right),\quad D_\lambda = diag\left(\begin{bmatrix}1 & 0 & 0 & 0\end{bmatrix}\right),$$

$$\underline{\bar{\phi}}_a(t) = \begin{bmatrix}\bar{\phi}_1(t) & \bar{\phi}_2(t) & \bar{\phi}_3(t) & \bar{\phi}_4(t)\end{bmatrix}^T.$$

Eq. (5-6) can be solved using any integration method such as the 4th order Runge-Kutta method with the known signals $\underline{u}_a(t)$ from measurements at every instant and the signals $\underline{\phi}_a(t)$ can be obtained. Using the signals $\underline{\phi}_a(t)$, $z(t)$ and $\underline{\phi}(t)$ in Eq. (5-5) can be computed.

The estimate $\hat{z}(t)$ of $z(t)$ at time t can also be generated by modifying Eq.(5-5) as

$$\hat{z}(t) = \begin{bmatrix}\hat{k}_s(t) & \hat{c}_s(t)\end{bmatrix}\begin{bmatrix}\phi_1(t) & \phi_2(t)\end{bmatrix}^T = \underline{\hat{\theta}}^T(t)\underline{\phi}(t) \tag{5-7}$$

where $\underline{\hat{\theta}}(t)$ is the estimate of $\underline{\theta}^*$ at time t. The estimation error $\varepsilon(t)$ as in Eq. (5-2) is defined

$$\varepsilon(t) = z(t) - \hat{z}(t) = z(t) - \underline{\hat{\theta}}^T(t)\underline{\phi}(t) \tag{5-8}$$

A performance index function $J(\underline{\hat{\theta}})$ in order to reduce the estimate error $\varepsilon(t)$ in Eq. (5-8) is defined as

$$J\left(\underline{\hat{\theta}}\right) = \frac{1}{2}\int_0^t e^{-\beta(t-\tau)}\left[z(\tau) - \underline{\hat{\theta}}^T(t)\underline{\phi}(\tau)\right]^2 d\tau + \frac{1}{2}e^{-\beta t}\left[\underline{\hat{\theta}}(t) - \underline{\hat{\theta}}_0\right]^T Q_{E,0}\left[\underline{\hat{\theta}}(t) - \underline{\hat{\theta}}_0\right] \tag{5-9}$$

where $\beta \geq 0$ is the selected forgetting factor (i.e. as time t increases the effect of the old signals at time $\tau < t$ is reduced), and a penalty on the initial estimate $\underline{\hat{\theta}}_0$ of $\underline{\theta}^*$. The index $J(\underline{\hat{\theta}})$ is a convex function of $\underline{\hat{\theta}}$ since $\partial^2 J / \partial\underline{\hat{\theta}}^2 > 0$. The estimated parameter vector $\underline{\hat{\theta}}(t)$ to minimize the index $J(\underline{\hat{\theta}})$ with respect to $\underline{\hat{\theta}}$ satisfies the following condition

$$\frac{\partial J}{\partial \underline{\hat{\theta}}} = e^{-\beta t}Q_{E,0}\left[\underline{\hat{\theta}}(t) - \underline{\hat{\theta}}_0\right] + \int_0^t e^{-\beta(t-\tau)}\left[z(\tau) - \underline{\hat{\theta}}^T(t)\underline{\phi}(\tau)\right]\left(-\underline{\phi}(\tau)\right)d\tau = 0 \tag{5-10}$$

which leads to the following equation known as the *continuous-time non-recursive least squares* algorithm

$$\underline{\hat{\theta}}(t) = P(t)\left[e^{-\beta t}Q_{E,0}\underline{\hat{\theta}}_0 + \int_0^t e^{-\beta(t-\tau)}\left[z(\tau)\underline{\phi}^T(\tau)\right]d\tau\right] \tag{5-11}$$

where

$$P(t) = \left[e^{-\beta t}Q_{E,0} + \int_0^t e^{-\beta(t-\tau)}\left[\underline{\phi}(\tau)\underline{\phi}^T(\tau)\right]d\tau\right]^{-1} \tag{5-12}$$

which is also known as the *covariance matrix* and can be rewritten in a recursive form, in which the calculation of the inverse in this equation can be avoided. The *continuous-time recursive least squares algorithm with forgetting factor* can be derived from Eq. (5-11) and Eq. (5-12) (see Derivation 5.1 in Appendix B.9) with the definition of the estimation error $\varepsilon(t)$ in Eq. (5-8) and expressed

$$\dot{\underline{\hat{\theta}}}(t) = P(t)\varepsilon(t)\underline{\phi}(t)$$
$$\dot{P}(t) = \beta P(t) - P(t)\underline{\phi}(t)\underline{\phi}^T(t)P(t) \tag{5-13}$$

where the covariance matrix $P(t)$ and the parameter estimate $\underline{\hat{\theta}}(t)$ are obtained by solving the differential equations with the initial guess of $\underline{\hat{\theta}}(0) = \underline{\hat{\theta}}_0$ and $P(0) = P_0 = Q_{E,0}^{-1}$. For implementation, the algorithm in Eq. (5-13) is developed in discrete time, known as the *discrete-time recursive least squares algorithm with forgetting factor* (Ioannou et al., 2006):

$$\underline{\hat{\theta}}_{k+1} = \underline{\hat{\theta}}_k + P_{k+1}\varepsilon_k\underline{\phi}_k$$
$$P_{k+1} = \frac{1}{\beta_d}\left(P_k - \frac{P_k\underline{\phi}_k\underline{\phi}_k^T P_k}{\beta_d + \underline{\phi}_k^T P_k \underline{\phi}_k}\right) \tag{5-14}$$

where β_d is the forgetting factor $0 < \beta_d \leqslant 1$ in the discrete time form. This algorithm with the initial guess of $\underline{\hat{\theta}}(0) = \underline{\hat{\theta}}_0$ and $P(0) = P_0$ is used in the following applications. It is shown in Ioannou et al. (2012) using the Lyapunov's method that the stability properties of the *least squares* method include the estimation error $\varepsilon(t) \to 0$ as $t \to \infty$ and the rate of parameter estimation $\dot{\underline{\hat{\theta}}}(t) \to 0$ as $t \to \infty$. It is noted that the parameter estimate $\underline{\hat{\theta}}(t)$ might not approach the true values $\underline{\theta}^*$. However, without requiring the parameters to converge to their true values, the least squares method for unknown parameter estimation combined with the tracking control method, such as the feedback linearization method described in Section 3.3.2, can achieve the tracking control objective making the tracking error $e(t) \to 0$ as $t \to \infty$. This is very important and powerful property of the least squares method; however, the method is limited to the system which has constant parameters $\underline{\theta}^*$ as appear in a linear form shown in Eq. (5-1).

Example 5.1 **: Parameter estimation for an SDOF linear system**

In order to examine the performance of the least-squares (LS) method, the system identification to estimate unknown parameters of an SDOF linear system (shown in Figure 5-1) is numerically performed. It is noted that unlike the feedback tracking control methods, the control excitation input $u(t) = -m_s\ddot{x}_t(t)$ is pre-defined and not updated in real time

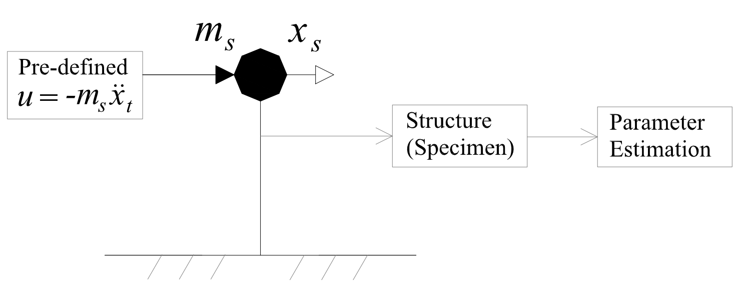

Figure 5-1 Parameter estimation of an SDOF system

The properties of the system are the same as the ones in Example 3.1; m_s = 1 kips·sec^2/in., k_s = 355 kips/in., and c_s = 1.13 kips·sec/in., (f_n = 3.0 Hz, ξ_n = 0.03). Two unknown parameters: c_s the damping coefficient and k_s the elastic stiffness; are selected and estimated in real time. The selected excitation input $u(t)$ to the system is the sinusoidal motion (the forcing frequency f_f = 1.0 Hz) and presented in Figure 5-2 (a) (for comparison purposes with other examples, $\ddot{x}_t(t) = -u(t)/m_s$, the shake table acceleration is presented). For the parameter estimation, it is chosen that the filter factor λ = 0.01; the forgetting factor β_d = 1; the initial parameter estimate $\underline{\hat{\theta}}_0 = 0.5 \times \underline{\theta}^*$; and the initial covariance matrix $P_0 = \mathrm{diag}(\underline{\hat{\theta}}_0{}^2)$. The time step = 0.002 sec. The relation between the structure resisting force $f_S(t)$ and displacement $x_s(t)$ is also presented in Figure 5-2 (b).

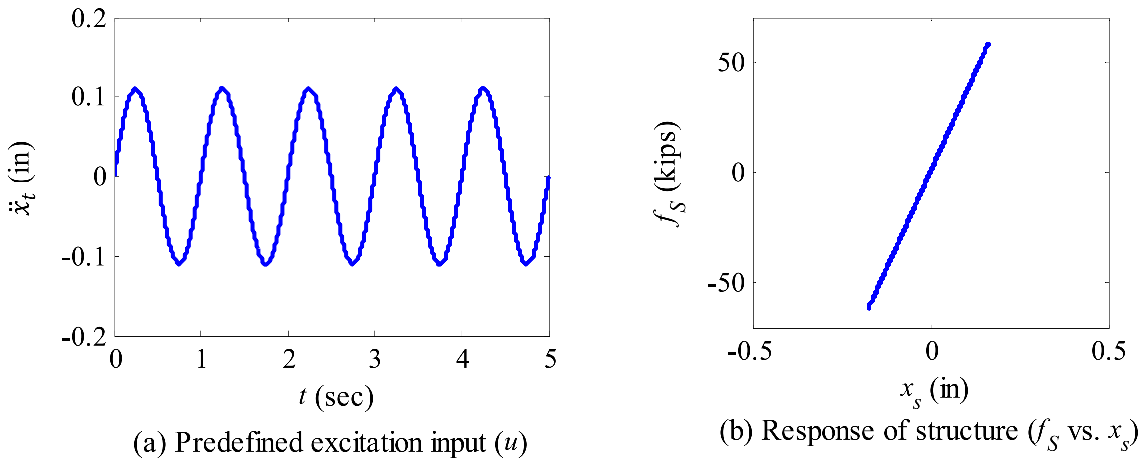

Figure 5-2 Excitation and structure response: Real time parameter estimation using the LS

The estimated parameters are updated using Eq. (5-14). The comparisons between the true parameters: k_s the elastic stiffness and c_s the damping coefficient; and the estimated parameters are shown in Figure 5-3 and the results show that the agreements are reasonably good. The errors in the estimation might be attributed to the assumption that the augmented vector $\underline{u}_a(t)$ in Eq. (5-6) is piecewise constant between $k\Delta t$ and $(k+1)\Delta t$ for the numerical implementation; i.e. as the time step becomes smaller, the estimated error between the true and the estimated parameters becomes smaller. It is also noted that the estimation performance is affected by various conditions that are discussed in Section 5.1.2.

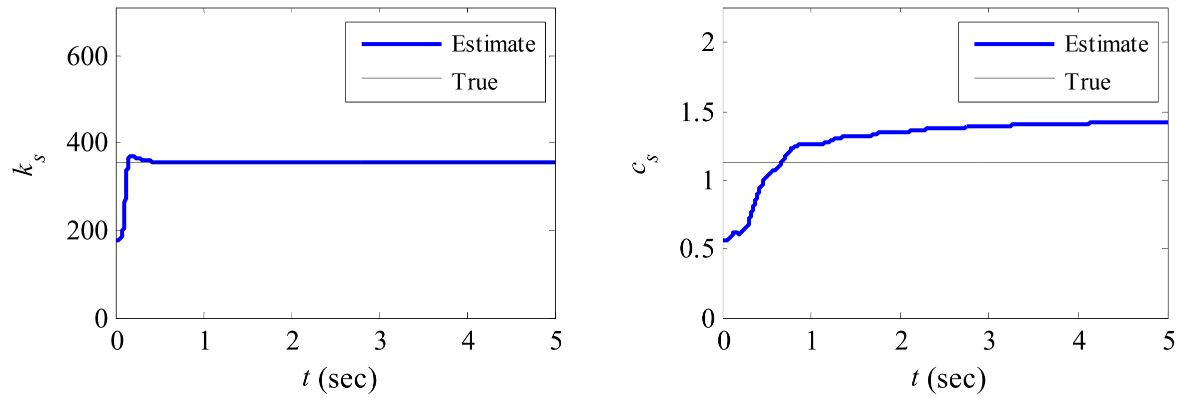

(a) Estimated parameter k_s (b) Estimated parameter c_s

Figure 5-3 Real time parameter estimation results using the LS for an SDOF linear system

5.1.1.2 Estimate of Nonlinear Hysteretic Structures with Unknown Parameters

For a nonlinear hysteretic SDOF system expressed in Eq. (4-1), four unknown constant parameters have to be estimated, i.e. the stiffness k_s, the damping c_s, the yielding displacement d_y and the post-yielding stiffness ratio α to the elastic stiffness. Unfortunately, the method is appropriate only for a linear equation in the parameter vector $\underline{\theta}^*$ from Eq. (4-1), only when $\alpha = 0$ (no hardening). This is due to the function involving $\mathrm{sgn}(f_H(\underline{x})\dot{x}_s(t))$ where the hysteretic force $f_H(\underline{x}) = f_S(\underline{x}) - \alpha k_s x_s(t)$ is unknown and it is impossible to separate the unknown parameters α, k_s from the known functions of $x_s(t)$ and $f_S(t)$, which are to be measured. Only for a system without hardening after yielding, where $\alpha = 0$ (i.e. elastic-ideal plastic system), $f_H(\underline{x})$ is the same as $f_S(\underline{x})$, which is measurable, and the governing equation of the restoring force in Eq. (4-2) can be rewritten (Smyth et al., 1999) as:

$$\dot{f}_S(\underline{x}) = \left[k_s \quad k_s/(f_S)^N\right]\left[\dot{x}_s(t) \quad -0.5\{1+\mathrm{sgn}(f_S(\underline{x})\dot{x}_s(t))\}|f_S(\underline{x})|^N \dot{x}_s(t)\right]^T \tag{5-15}$$

A nonlinear hysteretic SDOF system in Eq. (4-1) to estimate three unknown parameters of the stiffness k_s, the damping coefficient c_s and the yielding displacement d_y can be expressed by placing the parameters to the right-hand side of the equation in the Laplace domain:

$$\begin{aligned} sm\ddot{x}_s(s) - su(s) &= -sc_s\dot{x}_s(s) - \dot{f}_S(\underline{x}) \\ &= \underbrace{\left[c_s \quad k_s \quad k_s/(f_y)^N\right]}_{\underline{\theta}^{*T}}\underbrace{\left[-s\dot{x}_s(s) \quad -\dot{x}_s(s) \quad 0.5\{1+\mathrm{sgn}(f_S(\underline{x})\dot{x}_s(s))\}|f_S(\underline{x})|^N \dot{x}_s(s)\right]^T}_{\underline{x}_a(s)} \end{aligned} \tag{5-16}$$

which is linear in $\underline{\theta}^* = [c_s \;\; k_s \;\; k_s/(f_y)^N]^T$ and it is assumed that the relative displacement $x_s(t)$, velocity $\dot{x}_s(t)$, acceleration $\ddot{x}_s(t)$ and the restoring force $f_S(\underline{x})$ are measurable. Dividing each side of Eq. (5-16) by a first order stable filter $1/\Lambda(s) = (s+\lambda)^{-1}$, Eq. (5-16) can be expressed as

$$\frac{s}{s+\lambda}\left\{m\ddot{x}_s(s)-u(s)\right\}=\underline{\theta}^{*T}\frac{1}{s+\lambda}\underline{x}_a(s) \tag{5-17}$$

and this equation can be expressed in the form of Eq. (5-1) (repeated) as following

$$z(t)=\underline{\theta}^{*T}\underline{\phi}(t) \quad or \quad z(s)=\underline{\theta}^{*T}\underline{\phi}(s) \tag{5-18}$$

where

$$\begin{aligned}
&z(s)=\frac{s}{s+\lambda}\left\{m\ddot{x}_s(s)-u(s)\right\} \; or \quad z(t)=\varphi_1(t),\\
&\underline{\theta}^*=\left[c_s \quad k_s \quad k_s\big/\left(f_y\right)^N\right]^T,\\
&\underline{\phi}(s)=\left[\frac{1}{s+\lambda}\left(-s\dot{x}_s(s)\right) \quad \frac{1}{s+\lambda}\left(-\dot{x}_s(s)\right) \quad \frac{1}{s+\lambda}\left(0.5\left\{1+\mathrm{sgn}\left(f_S(\underline{x})\dot{x}_s(s)\right)\right\}\left|f_S(\underline{x})\right|^N\dot{x}_s(s)\right)\right]^T\\
&\qquad or \;\; \underline{\phi}(t)=\left[\phi_1(t) \quad \phi_2(t) \quad \phi_3(t)\right]^T.
\end{aligned} \tag{5-19}$$

A state-space representation of Eq. (5-19) by introducing augmented vectors $\underline{\phi}_a(t)$ = [$\varphi_1(t)$ $\phi_1(t)$ $\phi_2(t)$ $\phi_3(t)$]^T and $\underline{u}_a(t)$ = [($m\ddot{x}_s(t)$-$u(t)$) $\underline{x}_a(t)^T$]^T is obtained

$$\begin{aligned}
&\dot{\underline{\bar{\phi}}}_a(t)=A_\lambda\underline{\bar{\phi}}_a(t)+B_\lambda\underline{u}_a(t), \qquad \underline{\bar{\phi}}_a(0)=\underline{0}\\
&\underline{\phi}_a(t)=C_\lambda\underline{\bar{\phi}}_a(t)+D_\lambda\underline{u}_a(t)
\end{aligned} \tag{5-20}$$

where the additional state vector $\underline{\bar{\phi}}_a(t)$, which is different with $\underline{\phi}_a(t)$, is introduced for this formulation and

$$\begin{aligned}
&A_\lambda=-\lambda I_{4\times4}, \quad B_\lambda=I_{4\times4}, \quad C_\lambda=diag\left(\left[-\lambda \quad -\lambda \quad 1 \quad 1\right]\right), \quad D_\lambda=diag\left(\left[1 \quad 1 \quad 0 \quad 0\right]\right)\\
&\underline{\bar{\phi}}_a(t)=\left[\bar{\phi}_1(t) \quad \bar{\phi}_2(t) \quad \bar{\phi}_3(t) \quad \bar{\phi}_4(t)\right]^T.
\end{aligned}$$

By solving Eq. (5-20), the signals $\underline{\phi}_a(t)$ can be obtained at every instant. Using the signals $\underline{\phi}_a(t)$, $z(t)$ and $\underline{\phi}(t)$ in Eq. (5-19) can be computed. The unknown parameters $\underline{\theta}^*$ can be estimated in real time using the *discrete-time recursive least squares algorithm* shown in Eq. (5-14).

Example 5.2 **: Parameter estimation for an SDOF nonlinear hysteretic system**

The LS method is used for the system identification to estimate unknown parameters of an SDOF nonlinear hysteretic system (see Figure 5-1); in this example the structure experiences nonlinear behavior due to yielding. It is noted that unlike the feedback tracking control methods, the control excitation input $u(t) = -m_s\ddot{x}_t(t)$ is pre-defined and not updated in real time.

The properties of the system are the same as the ones in Example 4.1 (except the post-yielding stiffness ratio to the elastic stiffness α = 0); m_s = 1 kips·sec^2/in.; k_s = 355 kips/in.; and c_s = 1.13 kips·sec/in.; (f_n = 3.0 Hz, ξ_n = 0.03 before yielding); N = 3 and d_y = 0.11 in. (f_y = 39 kips). Three unknown parameters: c_s the damping coefficient; k_s the elastic stiffness; and d_y the yielding displacement; are selected and estimated in real time. The selected excitation input $u(t)$ to the system is the sinusoidal motion (the forcing frequency f_f = 1.0 Hz) and presented in Figure 5-4 (a) (for comparison purposes with other examples, $\ddot{x}_t(t) = -u(t)/m_s$, the shake table acceleration is presented). For the parameter estimation, it is chosen that the filter factor λ = 0.01; the forgetting factor β_d = 1; the initial parameter estimate $\underline{\hat{\theta}}_0 = 0.5 \times \underline{\theta}^*$; and the initial covariance matrix $P_0 = \mathrm{diag}(\underline{\hat{\theta}}_0{}^2)$. The time step = 0.002 sec. The relation between the structure resisting force $f_S(t)$ and displacement $x_s(t)$ is also presented in Figure 5-4 (b).

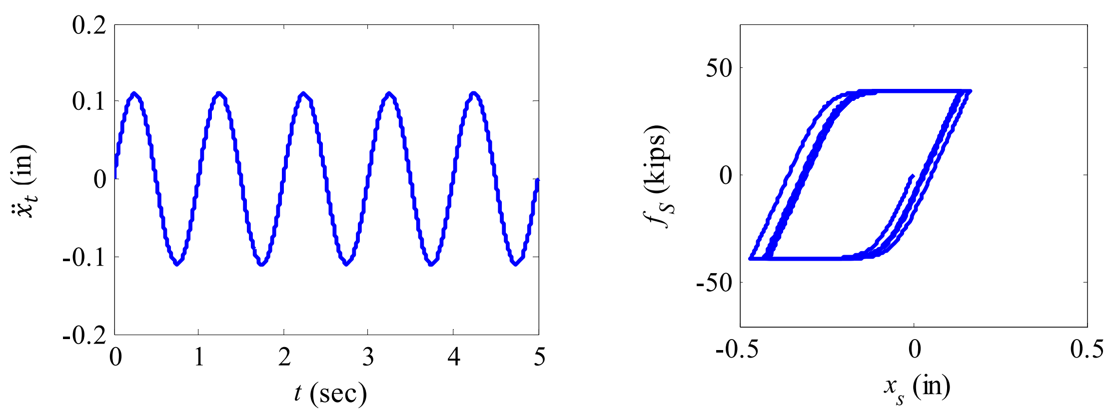

(a) Predefined excitation input (u)

(b) Response of structure (f_S vs. x_s)

Figure 5-4 Excitation and structure responses: Real time parameter estimation using the LS

The estimated parameters are updated using Eq. (5-14). The comparisons between the true parameters: $k_T(\underline{x})$ the instantaneous stiffness (i.e. the estimate of $k_T(\underline{x})$ is computed using the estimates of k_s and d_y); c_s the damping coefficient; k_s the elastic stiffness; and d_y the yielding displacement; and the estimated parameters are shown in Figure 5-5; the agreements are reasonably good although there are large errors in the beginning of the estimation procedure, which might become challenges to the tracking control.

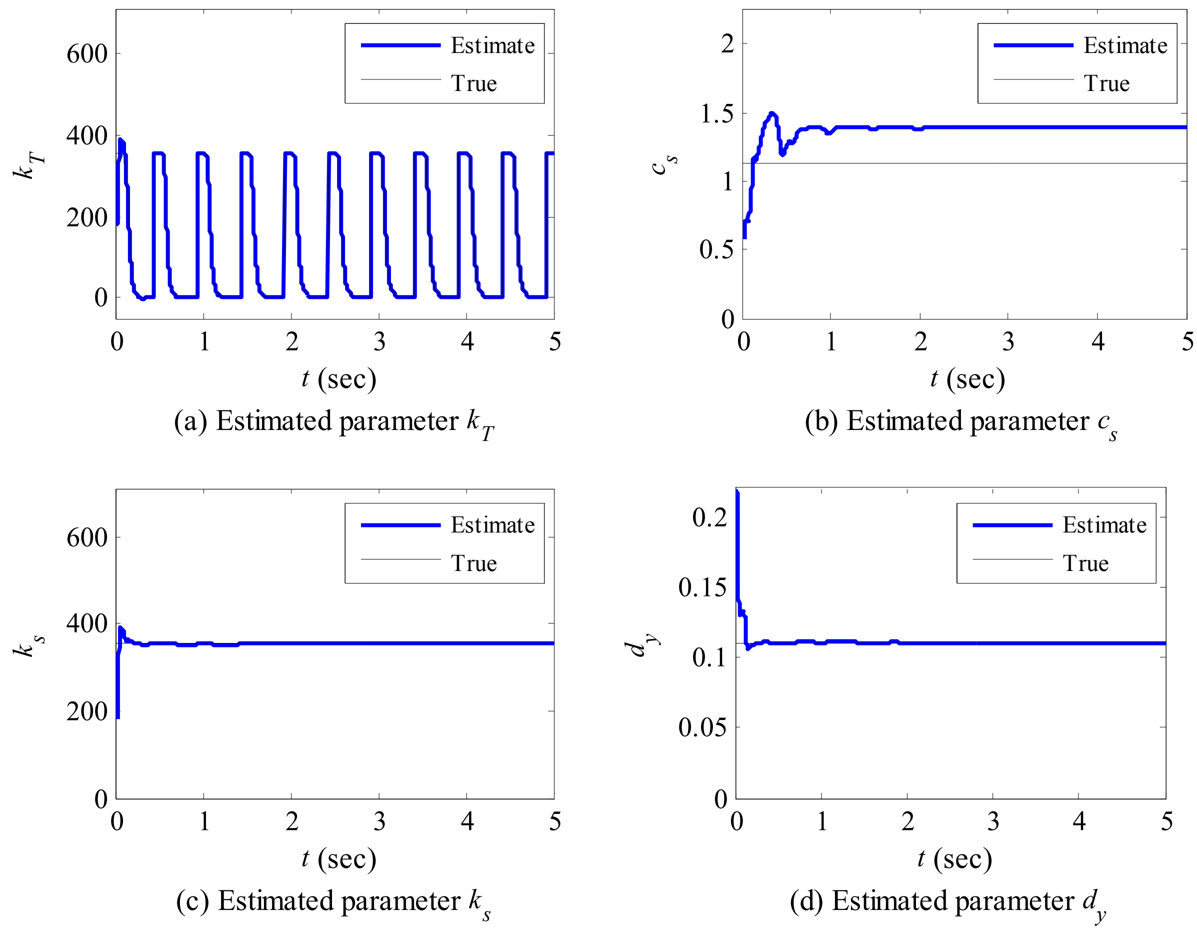

(a) Estimated parameter k_T (b) Estimated parameter c_s

(c) Estimated parameter k_s (d) Estimated parameter d_y

Figure 5-5 Real time parameter estimation results using the LS for an SDOF nonlinear system

5.1.1.3 Estimate of Nonlinear Hysteresis Structures with Hardening

As mentioned above, it is not possible to directly formulate a linear equation in the constant parameter vector $\underline{\theta}^*$ from Eq. (4-2), which is the governing equation of the restoring force in nonlinear hysteresis systems. However, by introducing the following approximation in the governing equation, a linear parametric model for hysteretic systems can be obtained (i.e. the effects of this approximation on the responses are discussed below – see Eq. (5-30)):

$$\frac{1+\operatorname{sgn}\left(f_H\left(\underline{x}\right)\dot{x}_s\left(t\right)\right)}{2}\left(\frac{\left|f_H\left(\underline{x}\right)\right|}{f_y^*}\right)^N=\frac{\operatorname{sgn}\left(f_H\left(\underline{x}\right)\right)+\operatorname{sgn}\left(\dot{x}_s\left(t\right)\right)}{2}\left(\frac{f_H\left(\underline{x}\right)}{f_y^*}\right)^N\approx\operatorname{sgn}\left(\dot{x}_s\left(t\right)\right)\left(\frac{f_H\left(\underline{x}\right)}{f_y^*}\right)^N,\ N=odd \tag{5-21}$$

which leads to the approximated governing equation of the restoring force, which is linear in the constant parameters (i.e. a very similar form of this approximate equation can be found in Constantinou, 2008)

$$\begin{aligned}\dot{f}_S\left(\underline{x}\right)&=\alpha k_s\dot{x}_s\left(t\right)+\left(1-\alpha\right)k_s\left\{1-\frac{1+\operatorname{sgn}\left(f_H\left(\underline{x}\right)\dot{x}_s\left(t\right)\right)}{2}\left(\frac{\left|f_H\left(\underline{x}\right)\right|}{f_y^*}\right)^N\right\}\dot{x}_s\left(t\right)\\&\approx\alpha k_s\dot{x}_s\left(t\right)+\left(1-\alpha\right)k_s\left\{1-\operatorname{sgn}\left(\dot{x}_s\left(t\right)\right)\left(\frac{f_H\left(\underline{x}\right)}{f_y^*}\right)^N\right\}\dot{x}_s\left(t\right)\\&=\begin{bmatrix}k_s & p_0 & p_0p_1^3 & 3p_0p_1 & 3p_0p_1^2\end{bmatrix}\cdot\Big[\dot{x}_s\left(t\right)\quad\operatorname{sgn}\left(\dot{x}_s\left(t\right)\right)\dot{x}_s\left(t\right)f_S\left(\underline{x}\right)^3\quad\operatorname{sgn}\left(\dot{x}_s\left(t\right)\right)\dot{x}_s\left(t\right)x_s\left(t\right)^3\\&\qquad\operatorname{sgn}\left(\dot{x}_s\left(t\right)\right)\dot{x}_s\left(t\right)f_S\left(\underline{x}\right)^2x\left(t\right)\quad\operatorname{sgn}\left(\dot{x}_s\left(t\right)\right)\dot{x}_s\left(t\right)f_S\left(\underline{x}\right)x_s\left(t\right)^2\Big]^T\end{aligned} \tag{5-22}$$

where N = 3 (i.e. chosen for this study), $p_0 = -1 / \{(1-\alpha)^2k_s^2(d_y)^3\}$ and $p_1 = -\alpha k_s$. Thus, a nonlinear hysteretic SDOF system in Eq. (4-1) to estimate four unknown parameters of the stiffness k_s, the damping c_s, the yielding displacement d_y and the post-yielding stiffness ratio α to the elastic stiffness can be expressed by placing the parameters to the right-hand side of the equation in the Laplace domain

$$\begin{aligned}&sm\ddot{x}_s\left(s\right)-su\left(s\right)=-sc_s\dot{x}_s\left(s\right)-\dot{f}_S\left(\underline{x}\right)\\&=-\begin{bmatrix}c_s & k_s & p_0 & p_0p_1^3 & 3p_0p_1 & 3p_0p_1^2\end{bmatrix}\cdot\Big[s\dot{x}_s\left(s\right)\quad\dot{x}_s\left(s\right)\quad\operatorname{sgn}\left(\dot{x}_s\left(s\right)\right)\dot{x}_s\left(s\right)f_S\left(\underline{x}\right)^3\quad\operatorname{sgn}\left(\dot{x}_s\left(s\right)\right)\dot{x}_s\left(s\right)x_s\left(s\right)^3\\&\qquad\operatorname{sgn}\left(\dot{x}_s\left(s\right)\right)\dot{x}_s\left(s\right)f_S\left(\underline{x}\right)^2x_s\left(s\right)\quad\operatorname{sgn}\left(\dot{x}_s\left(s\right)\right)\dot{x}_s\left(s\right)f_S\left(\underline{x}\right)x_s\left(s\right)^2\Big]^T\\&or\quad\underline{\theta}^{*T}\underline{x}_a\left(s\right)\end{aligned} \tag{5-23}$$

which is linear in $\underline{\theta}^* = [c_s\ \ k_s\ \ p_0\ \ p_0p_1^3\ \ 3p_0p_1\ \ 3p_0p_1^2]^T$ and it is assumed that the relative displacement $x_s(t)$, velocity $\dot{x}_s(t)$, acceleration $\ddot{x}_s(t)$ and the restoring force $f_S(\underline{x})$ are measurable. Dividing each side of Eq. (5-23) by a first order stable filter $1/\Lambda(s) = (s+\lambda)^{-1}$, Eq. (5-23) is expressed as

$$\frac{s}{s+\lambda}\left\{m\ddot{x}_s(s)-u(s)\right\}=\underline{\theta}^{*T}\frac{1}{s+\lambda}\underline{x}_a(s) \tag{5-24}$$

and this equation can be expressed in the form of Eq. (5-1) (repeated) as following

$$z(t) = \underline{\theta}^{*T}\underline{\phi}(t) \quad or \quad z(s) = \underline{\theta}^{*T}\underline{\phi}(s) \tag{5-25}$$

where

$$z(s) = \frac{s}{s+\lambda}\{m\ddot{x}_s(s) - u(s)\} \; or \quad z(t) = \varphi_1(t),$$
$$\underline{\theta}^* = \begin{bmatrix} c_s & k_s & p_0 & p_0 p_1^3 & 3p_0 p_1 & 3p_0 p_1^2 \end{bmatrix}^T,$$
$$\underline{\phi}(s) = \frac{1}{s+\lambda}\underline{x}_a(s) \;\; or \;\; \underline{\phi}(t) = [\phi_1(t) \quad \phi_2(t) \quad \phi_3(t) \quad \phi_4(t) \quad \phi_5(t) \quad \phi_6(t)]^T.$$

in which $p_0 = -1 / \{(1-\alpha)^2 k_s^2 (d_y)^3\}$ and $p_1 = -\alpha k_s$ and $x_a(s)$ are defined in Eq. (5-23).

A state-space representation of Eq. (5-25) by introducing augmented vectors $\underline{\phi}_a(t) = [\varphi_1(t) \;\; \phi_1(t) \;\; \phi_2(t) \;\; \phi_3(t) \;\; \phi_4(t) \;\; \phi_5(t) \;\; \phi_6(t)]^T$ and $\underline{u}_a(t) = [(m\ddot{x}_s(t)\text{-}u(t)) \;\; \underline{x}_a(t)^T]^T$ is

$$\begin{aligned} \dot{\underline{\bar{\phi}}}_a(t) &= A_\lambda \underline{\bar{\phi}}_a(t) + B_\lambda \underline{u}_a(t), \qquad \underline{\bar{\phi}}_a(0) = \underline{0} \\ \underline{\phi}_a(t) &= C_\lambda \underline{\bar{\phi}}_a(t) + D_\lambda \underline{u}_a(t) \end{aligned} \tag{5-26}$$

where

$$A_\lambda = -\lambda I_{7\times7}, \quad B_\lambda = I_{7\times7}, \quad C_\lambda = diag([-\lambda \quad -\lambda \quad 1 \quad 1 \quad 1 \quad 1 \quad 1]), \quad D_\lambda = diag([1 \quad 1 \quad 0 \quad 0 \quad 0 \quad 0 \quad 0])$$

The signals $\underline{\phi}_a(t)$ can be obtained at every instant by solving Eq.(5-26). Using these signals $\underline{\phi}_a(t)$, $z(t)$ and $\underline{\phi}(t)$ in Eq. (5-25) can be computed. The unknown parameters $\underline{\theta}^*$ can be estimated in real time using the *discrete-time recursive least squares algorithm* expressed in Eq. (5-14).

Errors in the approximated model

The approximate model of hysteretic systems with hardening after yielding ($\alpha > 0$) in order to formulate a linear parametric model for the least squares system identification introduces errors. The effects are examined by comparing the response of the *original model* (the model introduced by Sivaselvan and Reinhorn, 1999) and that of the *approximate model*. In the original model the rate form of the plasticity relation of the restoring force $f_S(\underline{x})$ is shown in Eq. (4-2) and the elastic-ideal plastic force $f_H(\underline{x})$ (hysteretic force) in the equation involves two Heaviside step functions $H_1(\underline{x})$ and $H_2(\underline{x})$ as (Sivaselvan and Reinhorn, 1999)

$$\dot{f}_H(\underline{x}) = (1-\alpha)k_s\{1 - H_2(\underline{x})H_1(\underline{x})\}\dot{x}_s(t) \tag{5-27}$$

where $H_1(\underline{x})$ signifies yielding and $H_2(\underline{x})$ signifies unloading from the yield surface

$$\begin{aligned} H_1(\underline{x}) &= \text{Heaviside}\left[|f_H(\underline{x})| - f_y^*\right] \approx \left[|f_H(\underline{x})| / f_y^*\right]^N, \qquad f_y^* = (1-\alpha)f_y \\ H_2(\underline{x}) &= \{1 + \text{sgn}(f_H(\underline{x})\dot{x}_s(t))\}/2 \end{aligned} \tag{5-28}$$

In order to separate unknown parameters (α, k_s, d_y) from the measured signals ($x_s(t)$, $\dot{x}_s(t)$, $f_s(\underline{x})$) in (5-27), it is necessary to introduce an alternate form of $\text{sgn}(f_H(\underline{x}))$; and $\text{sgn}(f_H(\underline{x}))$ might be approximated as $\text{sgn}(\dot{x}_s(t))$ if N = odd. The effects can be seen in three regions of the hysteresis behavior (see in Figure 5-6)

$$\begin{aligned} &i. \ \ \text{sgn}\left(f_H\left(\underline{x}\right)\right)=\text{sgn}\left(\dot{x}_s\left(t\right)\right), \quad \left|f_H\left(\underline{x}\right)\right|=f_y^* \\ &ii. \ \ \text{sgn}\left(f_H\left(\underline{x}\right)\right)=\text{sgn}\left(\dot{x}_s\left(t\right)\right), \ \textit{loading} \\ &iii. \ \ \text{sgn}\left(f_H\left(\underline{x}\right)\right)\neq\text{sgn}\left(\dot{x}_s\left(t\right)\right), \ \textit{unloading} \end{aligned} \Bigg\} \left|f_H\left(\underline{x}\right)\right|<f_y^* \qquad (5\text{-}29)$$

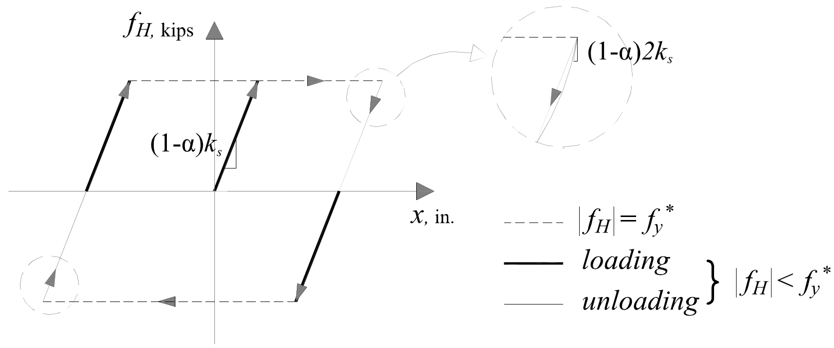

Figure 5-6 Schematic of a hysteresis behavior (elastic-ideal plastic) of $f_H(\underline{x})$

The difference (error) is introduced in the region *iii* where $\text{sgn}(f_H(\underline{x})) \neq \text{sgn}(\dot{x}_s(t))$ and at which unloading occurs as shown in Figure 5-6 in dot circles: i.e. at the transition $f_H(\underline{x}) \approx f_y^*$, the instant stiffness $k_T(\underline{x})$ of the original system and $k_T^*(\underline{x})$ of the approximate system can be expressed

$$\begin{aligned} k_T\left(\underline{x}\right) &= \alpha k_s + \left(1-\alpha\right)k_s\left\{1-\frac{\text{sgn}\left(f_H\left(\underline{x}\right)\right)+\text{sgn}\left(\dot{x}_s\left(t\right)\right)}{2}\left(\frac{f_H\left(\underline{x}\right)}{f_y^*}\right)^N\right\} = \alpha k_s + \left(1-\alpha\right)k_s = k_s \\ k_T^*\left(\underline{x}\right) &= \alpha k_s + \left(1-\alpha\right)k_s\left\{1-\text{sgn}\left(\dot{x}_s\right)\left(\frac{f_H\left(\underline{x}(t)\right)}{f_y^*}\right)^N\right\} = \alpha k_s + \left(1-\alpha\right)k_s\left\{2\right\} = \left(2-\alpha\right)k_s \end{aligned} \qquad (5\text{-}30)$$

The maximum error is $k_T^*(\underline{x})$ - $k_T(\underline{x})$ = (1 - α) k_s at the transition where unloading starts and the error rapidly decreases as $(f_H(\underline{x}) / f_y^*)^N$ goes to zero. Also noted that if $N \approx \infty$, the error becomes zero since $(f_H(\underline{x}) / f_y^*)^N \approx 0$ ($f_H(\underline{x}) \neq f_y^*$).

***Example 5.3* : Parameter estimation for an SDOF nonlinear hysteresis system with hardening**

The LS method is used for the system identification to estimate unknown parameters of an SDOF nonlinear hysteretic structure like the previous example (Example 5.2); however, in this example the hysteretic resisting force of the structure experiences hardening after yielding. It is noted that unlike the feedback tracking control methods, the control excitation input $u(t) = -m_s\ddot{x}_t(t)$ is pre-defined and not updated in real time

The properties of the system are the same as the ones in Example 4.1; m_s = 1 kips·sec^2/in.; k_s = 355 kips/in.; and c_s = 1.13 kips·sec/in.; (f_n = 3.0 Hz, ξ_n = 0.03 before yielding). N = 3; d_y = 0.11 in. (f_y = 39 kips); and α = 0.1; i.e. all terms are explained in Eq. (4-2). Four unknown parameters: c_s the damping coefficient; k_s the elastic stiffness; d_y the yielding displacement; and α the post-yielding stiffness ratio to the elastic stiffness; are selected and estimated in real time. The selected excitation input $u(t)$ to the system is the sinusoidal motion (the forcing frequency f_f = 1.0 Hz) and presented in Figure 5-7 (a) (for comparison purposes with other examples, $\ddot{x}_t(t) = -u(t)/m_s$, the shake table acceleration is presented). For the parameter estimation, it is chosen that the filter factor λ = 0.01; the forgetting factor β_d = 1; the initial parameter estimate $\hat{\underline{\theta}}_0 = 0.5 \times \underline{\theta}^*$ (50% error in the initial guess); and the initial covariance matrix P_0 = diag($\hat{\underline{\theta}}_0{}^2$) × $I_{6\times6}$. The time step = 0.002 sec. The relation between the structure resisting force $f_S(t)$ and displacement $x_s(t)$ is also presented in Figure 5-7 (b).

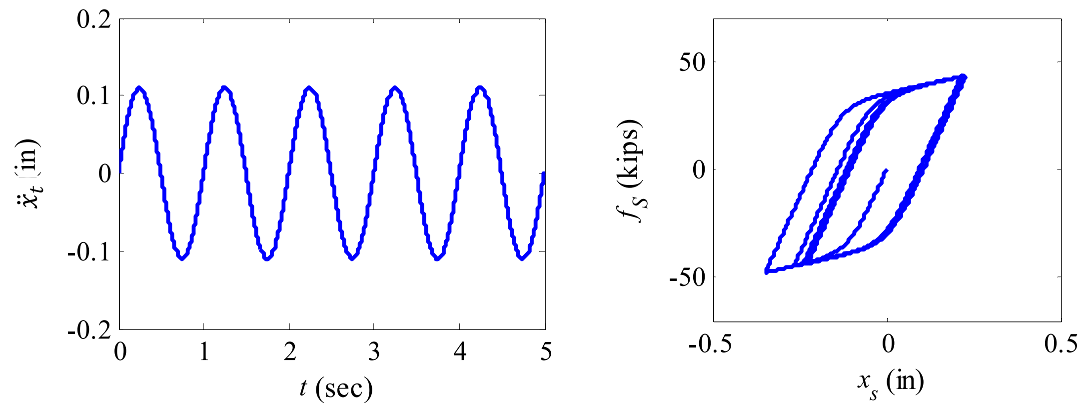

(a) Predefined excitation input (u)

(b) Response of structure (f_S vs. x_s)

Figure 5-7 Excitation and structure responses: Real time parameter estimation using the LS

The estimated parameters are updated using Eq. (5-14). The comparisons between the true parameters: $k_T(\underline{x})$ the instantaneous stiffness (i.e. the estimate of $k_T(\underline{x})$ is computed using the estimates of k_s and d_y); c_s the damping coefficient; k_s the elastic stiffness; d_y the yielding displacement; and α the post-yielding stiffness ratio to the elastic stiffness; and the estimated parameters are shown in Figure 5-8. The errors in estimation of $k_T(\underline{x})$ at the transition in Figure 5-8 (a) are attributed to the approximated model as discussed in this section; and the errors in the model seems to affect the estimation of other parameters such as c_s as shown in Figure 5-8 (b). Although the damping error is large in Figure 5-8 (b), since this damping represents the inherent damping, which is very small in hysteretic systems less important than the hysteretic energy dissipation, such error should not affect the tracking problem. However, these above errors in the parameter estimation might become challenges to the tracking control implementation as discussed in Section 5.3.

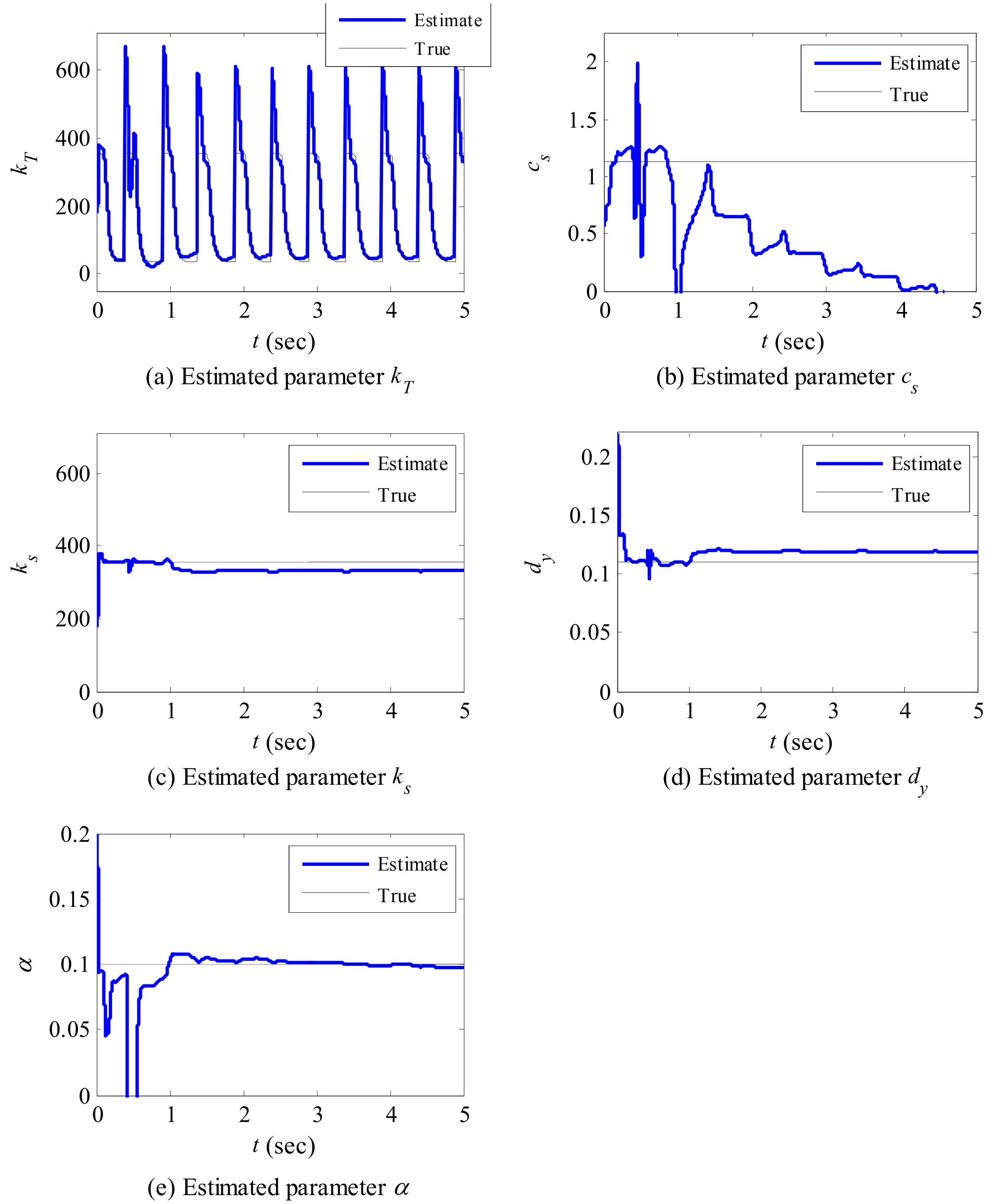

(a) Estimated parameter k_T

(b) Estimated parameter c_s

(c) Estimated parameter k_s

(d) Estimated parameter d_y

(e) Estimated parameter α

Figure 5-8 Real time parameter estimation results using the LS for an SDOF nonlinear system

5.1.2 Effects of Initial Guesses of Unknown Parameters and Covariance Matrices

The performance of the parameter estimation might be influenced by various conditions including the initial guess of the unknown parameters and by the covariance matrices, measurement noise, model errors, etc. The effects of the initial guesses of the unknown parameters and covariance matrices are numerically investigated below. The same SDOF linear model described in Example 5-1 is used where two parameters $\underline{\theta}^* = [k_s \;\; c_s]^T$: k_s the elastic stiffness and c_s the damping coefficient; are selected and estimated in real time. The excitation input $u(t)$ to the system is the same sinusoidal motion (the forcing frequency $f_f = 1.0$ Hz), shown in Figure 5-2 (a). The time step = 0.002 sec.

Example 5.4 **: Effects of initial guess of unknown parameters on the LS estimator performance**

The effects of the initial guess of the unknown parameters are investigated numerically. Three different initial guesses $\underline{\hat{\theta}}_0$ are made as the 10%, 50% and 200% of the true parameters; $\underline{\hat{\theta}}_0 = 0.1 \times \underline{\theta}^*$; $\underline{\hat{\theta}}_0 = 0.5 \times \underline{\theta}^*$; $\underline{\hat{\theta}}_0 = 2.0 \times \underline{\theta}^*$. The initial covariance matrix $P_0 = \mathrm{diag}([0.5 \times \underline{\theta}^*]^2)$ for all cases. The comparisons between the true parameters: k_s the elastic stiffness and c_s the damping coefficient; and the estimated parameters are shown in Figure 5-9 (the initial guess factors: 0.1, 0.5, 2.0; are shown in the figure); the results show that the overall agreements are reasonably good while the speed of convergence might be affected by the initial guess. As discussed in Example 5-1, the estimate error between the true and the estimated parameters becomes smaller as the time step becomes smaller.

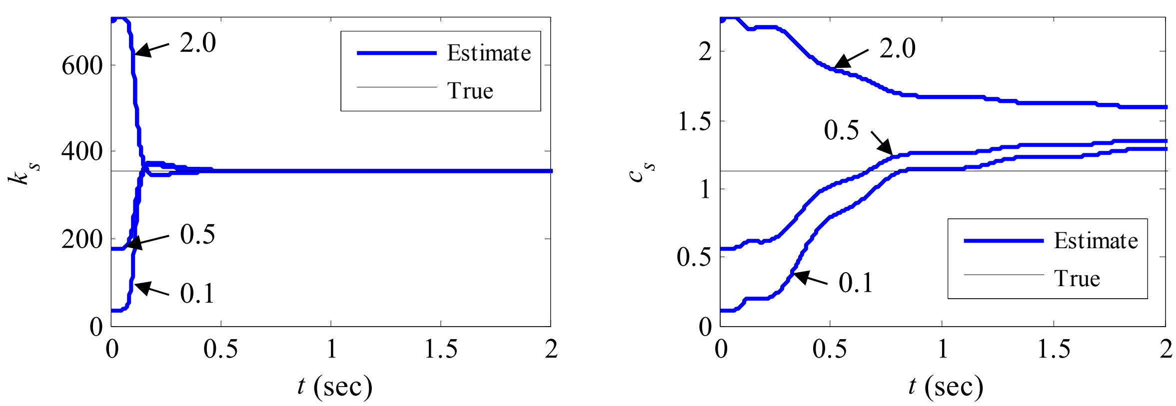

(a) Estimated parameter k_s (b) Estimated parameter c_s

Figure 5-9 Real time parameter estimation results using the LS for an SDOF linear system

Example 5.5 **: Effects of selection of the covariance matrices on the LS estimator performance**

The effects of the selection of the covariance matrices are investigated numerically. Three different initial covariance matrices P_0 are selected as the diagonal matrix whose elements are the square of the

10%, 50% and 200% of the true parameters; $P_0 = \text{diag}([0.1 \times \underline{\theta}^*]^2)$; $P_0 = \text{diag}([0.5 \times \underline{\theta}^*]^2)$; $P_0 = \text{diag}([2.0 \times \underline{\theta}^*]^2)$. The initial guesses of the unknown parameters $\underline{\hat{\theta}}_0 = 0.5 \times \underline{\theta}^*$ for all cases. The comparisons between the true parameters: k_s the elastic stiffness and c_s the damping coefficient; and the estimate of the true parameters are shown in Figure 5-10 (the selected initial covariance matrix factors: 0.1, 0.5, 2.0; are shown in the figure); the results show that the lager covariance matrix might leads faster estimation, but might occur larger overshooting at the beginning of estimation while the overall agreements are reasonably good. As discussed in Example 5-1, the estimate error between the true and the estimated parameters becomes smaller as the time step becomes smaller.

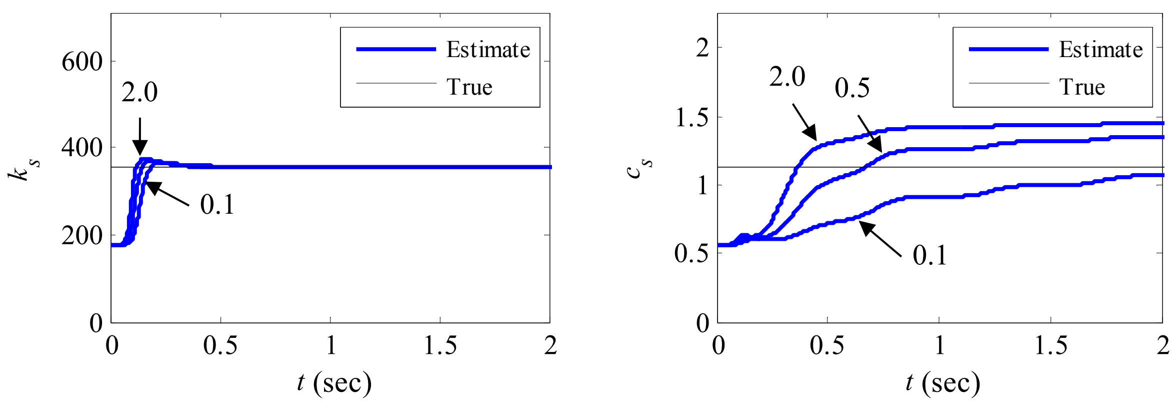

(a) Estimated parameter k_s (b) Estimated parameter c_s

Figure 5-10 Real time parameter estimation results using the LS for an SDOF linear system

5.2 Identification of System Parameters using the Extended Kalman Filter (EKF)

Another well-known system identification method, which has been used in the structural applications for numerical studies (Yun and Shinozuka, 1980, and Wu and Smyth, 2007), is the *extended Kalman filter* (EKF). It is known that the EKF can be used as the online parameter estimation for linear and nonlinear systems including the systems having hysteretic behavior (Wu and Smyth, 2007). The main concept of the EKF assumes that the true state is sufficiently close to the estimated state; therefore, the error dynamics can be represented fairly accurately by a linearized first-order Taylor series expansion (Crassidis and Junkin, 2012). Because the effects of the remaining terms in the series expansion are difficult to determine, it is very difficult to show a certain stability property of the EKF. Even so, Crassidis and Junkin (2012) addressed that the performance of the EKF method can be verified through simulation and this method has been successfully and widely used in practice, and they presented the application to the real time aircraft parameter estimation.

First, the general formulation of the extended Kalman filter is reviewed. The method is applied to the online parameter estimations for nonlinear hysteretic structures mounted on the shake table. The effects of the initial guess of the parameters and the selection of the covariance matrices are examined.

5.2.1 Formulation

5.2.1.1 KF and EKF review

The extended Kalman filter (EKF) method is the extension of the Kalman filter (KF), which is well known state estimator for linear systems. Unlike the KF, the EKF can be used to estimate state variables of nonlinear systems and also unknown parameters of linear and nonlinear systems.

The KF (Crassidis and Junkin, 2012) is a "sequential state estimator", which is used to not only reconstruct state variables $\underline{x}$ (size $n \times 1$) from limited measurements $\underline{\overline{y}}$ (size $m \times 1$, where $m \leq n$), but also "filter" noisy measurement processes. Assuming that the errors in measurements and in system models are a zero-mean Gaussian noise process[10], the KF determines the 'optimal' estimate gain with the information of the covariance matrices of the measurement noise and process noise, such that the KF provides the 'optimal' estimation of true state variables.

Before presenting the applications; first, the KF method and the EKF formulation using a linearized 1st order Taylor series expansion are briefly described as following; i.e. the thorough mathematical derivation of the methods in detail can be found in elsewhere, such as Crassidis and Junkin (2012).

[10] Gaussian noise process (Crassidis and Junkin, 2012) is the noise process having the normal distribution, which is defined by mean and variance. A zero-mean Gaussian noise process has its mean = 0.

Brief Review of the Kalman Filter

The truth model of a linear system in continuous time is expressed

$$\dot{\underline{x}}(t) = A\underline{x}(t) + B\underline{u}(t) + G\underline{w}(t) \tag{5-31}$$

$$\underline{\bar{y}}(t) = H\underline{x}(t) + \underline{v}(t) \tag{5-32}$$

where A and B are the system matrices and G is the matrix, defined based on processing noise $\underline{w}(t)$, indicating possible errors in the model, and H is the measurement matrix. $\underline{x}(t)$ is the $n \times 1$ state vector, $\underline{u}(t)$ is a control excitation input, $\underline{\bar{y}}(t)$ is the $m \times 1$ measurement output vector, and $\underline{v}(t)$ is measurement noise and $\underline{w}(t)$ is process noise (or errors in the model). The KF structure for the state estimate $\underline{\hat{x}}(t)$ and output estimate $\underline{\hat{\bar{y}}}(t)$ is expressed

$$\dot{\underline{\hat{x}}}(t) = A\underline{\hat{x}}(t) + B\underline{u}(t) + K(t)\left[\underline{\bar{y}}(t) - \underline{\hat{\bar{y}}}(t)\right] \tag{5-33}$$

$$\underline{\hat{\bar{y}}}(t) = H\underline{\hat{x}}(t) \tag{5-34}$$

where $K(t)$ is the Kalman gain matrix (size $n \times m$), indicating that if $K(t)$ is large, the estimator relies on measurements and if $K(t)$ decreases, the estimator relies more on the model. By defining the state error $\underline{\tilde{x}}(t) = \underline{\hat{x}}(t) - \underline{x}(t)$ (i.e. the estimate state - the true state) and using Equations (5-31) through (5-34), the estimate state error dynamics are given by

$$\dot{\underline{\tilde{x}}}(t) = \left[A - K(t)H\right]\underline{\tilde{x}}(t) - G\underline{w}(t) + K(t)\underline{v}(t) \tag{5-35}$$

By selecting the 'best' gain $K(t)$, the error $\underline{\tilde{x}}(t)$ will diminish and the estimator will be stable. Thus, $\underline{\hat{x}}(t)$ will be close to $\underline{x}(t)$. This concept can be expanded for parameter estimation by augmenting unknown parameter vector $\underline{\theta}$ to the state vector; i.e. $\underline{x}_a(t) = [\underline{x}^T(t) \;\; \underline{\theta}^T]^T$, which will be discussed later in the subject of the EKF.

For practical applications, the further development of the KF is described in discrete time form. The truth model (shown in Eq. (5-31) and Eq. (5-32) in continuous time) is rewritten in discrete time

$$\underline{x}_{k+1} = A_D\underline{x}_k + B_D\underline{u}_k + G_D\underline{w}_k \tag{5-36}$$

$$\underline{\bar{y}}_k = H\underline{x}_k + \underline{v}_k \tag{5-37}$$

where A_D and B_D are the system matrices and G_D is the processing noise matrix, and H is the measurement matrix (i.e. H is the same as that in continuous time form). $\underline{v}_k$ and $\underline{w}_k$ are measurement and process noise (or errors in the model), respectively, and they are assumed to be zero-mean Gaussian white-noise processes; i.e. *white-noise* means that the errors are not correlated forward or backward in time, so that

$$E\left\{\underline{v}_k \underline{v}_j^T\right\} = \begin{cases} 0, & k \neq j \\ R_{E,k}, & k = j \end{cases}$$
and
$$E\left\{\underline{w}_k \underline{w}_j^T\right\} = \begin{cases} 0, & k \neq j \\ Q_{E,k}, & k = j \end{cases} \tag{5-38}$$

where $E\{\cdot\}$ is the *expected value*[11] or "average value" of a given function. It is further assumed that $\underline{v}_k$ and $\underline{w}_k$ are *uncorrelated* so that $E\{\underline{v}_k \underline{w}_k^T\} = 0$ for all k. In this study, both noise covariance matrices $R_{E,k}$ and $Q_{E,k}$ are assumed to be constant at all time; thus $R_{E,k} = R_E$ and $Q_{E,k} = Q_E$. The measurement noise covariance matrix R_E (size $m \times m$) is usually well known, derived from the properties of the instruments; but, the processing noise covariance Q_E (size $n \times n$) is usually not well known and is often derived from experience by the design engineer based on the knowledge of the particular system (Crassidis and Junkin, 2012).

The estimator structure shown in Eq. (5-33) in continuous time can be expressed in two stages equations in discrete time as

$$\hat{\underline{x}}_{k+1}^- = A_D \hat{\underline{x}}_k^+ + B_D \underline{u}_k \tag{5-39}$$

$$\hat{\underline{x}}_k^+ = \hat{\underline{x}}_k^- + K_k \left[\underline{\bar{y}}_k - H \hat{\underline{x}}_k^- \right] \tag{5-40}$$

where K_k is the estimator gain (size $n \times m$) and Eq. (5-39) with sign '-' is known as the *prediction* equation, and Eq. (5-40) with sign '+' is known as the *update* equation. The estimate error covariance matrices are defined as

$$P_{k+1}^- = E\left\{\tilde{\underline{x}}_{k+1}^- \tilde{\underline{x}}_{k+1}^{-\,T}\right\} \tag{5-41}$$

$$P_k^+ = E\left\{\tilde{\underline{x}}_k^+ \tilde{\underline{x}}_k^{+\,T}\right\} \tag{5-42}$$

where the estimate state errors are $\tilde{\underline{x}}_{k+1}^- \equiv \hat{\underline{x}}_{k+1}^- - \underline{x}_{k+1}$ and $\tilde{\underline{x}}_k^+ \equiv \hat{\underline{x}}_k^+ - \underline{x}_k$ (i.e. the current estimate state - the true state). Substitutions of Equations (5-39) and (5-36) in $\tilde{\underline{x}}_{k+1}^- \equiv \hat{\underline{x}}_{k+1}^- - \underline{x}_{k+1}$ give

$$\tilde{\underline{x}}_{k+1}^- = A_D \tilde{\underline{x}}_k^+ - G_D \underline{w}_k \tag{5-43}$$

Then, P_{k+1}^- is defined by substituting this equation into Eq. (5-41) and using that $E\{\underline{w}_k \tilde{\underline{x}}_k^{+\,T}\} = 0$:

---

[11] The *expected value* of a function $f(x)$ of a discrete random variable x is expressed (Crassidis and Junkin, 2012)

$$E\{f(x)\} = \sum_j f(x(j))\, p(x(j))$$

where $p(x(j))$ is a probability mass function $0 \le p(x(j)) \le 1$ and $\sum p(x(j)) = 1$. For example, the expected values of x and $(x - \mu)^2$ are the mean (μ) and variance (σ^2) of x:

$$E\{x\} = \sum_j x(j)\, p(x(j)) = \mu$$

$$E\left\{(x-\mu)^2\right\} = \sum_j (x(j) - \mu)^2\, p(x(j)) = \sigma^2$$

$$P_{k+1}^{-} = A_D P_k^{+} A_D{}^T + G_D Q_E G_D{}^T \tag{5-44}$$

For the update stage, substitution of Eq. (5-40) with Eq. (5-37) for $\underline{\hat{x}}_k^+$ in $\underline{\tilde{x}}_k^+ \equiv \underline{\hat{x}}_k^+ - \underline{x}_k$ gives

$$\underline{\tilde{x}}_k^{+} = \left(I - K_k H\right)\underline{\tilde{x}}_k^{-} + K_k \underline{v}_k \tag{5-45}$$

Then, P_k^+ is defined by substituting this equation into Eq. (5-42) and using that $E\{\underline{v}_k \underline{\tilde{x}}_k^{-T}\} = 0$:

$$P_k^{+} = \left[I - K_k H\right] P_k^{-} \left[I - K_k H\right]^T + K_k R_E K_k{}^T \tag{5-46}$$

The optimal estimator gain K_k is determined by minimizing the trace of $P_k{}^+$, which is equivalent to minimize the length of the estimation error vector. The index function is expressed as:

$$J\left(K_k\right) = \mathrm{Tr}\left(P_k^{+}\right) \tag{5-47}$$

By taking the partial derivative with respect to the gain: $\partial J/\partial K_k = 0$, and solving this equation for K_k, it results in:

$$K_k = P_k^{-} H^T \left[H P_k^{-} H^T + R_E\right]^{-1} \tag{5-48}$$

Substitution of Eq. (5-48) in Eq. (5-46) leads to

$$P_k^{+} = \left[I - K_k H\right] P_k^{-} \tag{5-49}$$

Therefore, with the initial guess of the state $\underline{\hat{x}}_0^-$ and the error covariance matrix P_0^-, the Kalman filter update stage defined in Eq. (5-40) and Eq. (5-49) and the prediction stage defined in Eq. (5-39) and Eq. (5-44) can be implemented using instant measurements. This optimal estimator for linear systems can be expanded for nonlinear systems not only to estimate the state variables, but also unknown parameters.

Expansion to the Extended Kalman Filter

The truth model of a nonlinear system in continuous time is expressed

$$\underline{\dot{x}}(t) = \underline{\mathrm{f}}\left(\underline{x}(t), \underline{u}(t), t\right) + G(t)\underline{w}(t) \tag{5-50}$$

$$\underline{\bar{y}}(t) = \underline{\mathrm{h}}\left(\underline{x}(t), t\right) + \underline{v}(t) \tag{5-51}$$

where $\underline{\mathrm{f}}(\underline{x}(t),u(t),t)$ is a nonlinear system differential equation, such as one shown in Eq. (4-4), and G is the matrix, defined based on processing noise $\underline{w}(t)$, indicating possible errors in the model, and $\underline{\mathrm{h}}(\underline{x}(t),t)$ is a nonlinear equation for measurements $\underline{\bar{y}}(t)$, and other terms are previously defined in the KF model shown in Eq. (5-31) and Eq. (5-32). In the EKF, it is assumed that the true state $\underline{x}(t)$ is sufficiently close to the estimated state $\underline{\hat{x}}(t)$; therefore, the error dynamics can be represented fairly accurately by a linearized first-order Taylor series expansion (Crassidis and Junkin, 2012). Using the Taylor series expansion about the current estimate $\underline{\hat{x}}(t)$ (i.e. assuming that the true state $\underline{x}(t)$ is sufficiently close to the estimated state $\underline{\hat{x}}(t)$, which is used for the nominal state), the $\underline{\mathrm{f}}(\underline{x}(t),u(t),t)$ can be written as:

$$\underline{\mathrm{f}}\left(\underline{x}(t),\underline{u}(t),t\right)\approx\underline{\mathrm{f}}\left(\underline{\hat{x}}(t),\underline{u}(t),t\right)+\left.\frac{\partial\underline{\mathrm{f}}}{\partial\underline{x}}\right|_{\underline{\hat{x}}(t),\underline{u}(t)}\underbrace{\left(\underline{x}(t)-\underline{\hat{x}}(t)\right)}_{\underline{\tilde{x}}(t)} \tag{5-52}$$

Also, the measurement function in Eq. (5-51) can also be approximated as

$$\underline{\mathrm{h}}\left(\underline{x}(t),t\right)=\underline{\mathrm{h}}\left(\underline{\hat{x}}(t),t\right)+\left.\frac{\partial\underline{\mathrm{h}}}{\partial\underline{x}}\right|_{\underline{\hat{x}}(t)}\underbrace{\left(\underline{x}(t)-\underline{\hat{x}}(t)\right)}_{\underline{\tilde{x}}(t)} \tag{5-53}$$

The EKF structure for the state estimate $\underline{\hat{x}}(t)$ and output estimate $\hat{\underline{\bar{y}}}(t)$ is expressed

$$\dot{\underline{\hat{x}}}(t)=\underline{\mathrm{f}}\left(\underline{\hat{x}}(t),\underline{u}(t),t\right)+K(t)\left[\underline{\bar{y}}(t)-\hat{\underline{\bar{y}}}(t)\right] \tag{5-54}$$

$$\hat{\underline{\bar{y}}}(t)=\underline{\mathrm{h}}\left(\underline{\hat{x}}(t),t\right) \tag{5-55}$$

From the definition of the estimate state error $\underline{\tilde{x}}(t)$ = $\underline{\hat{x}}(t)$ - $\underline{x}(t)$, its derivative is $\dot{\underline{\tilde{x}}}(t)$ = $\dot{\underline{\hat{x}}}(t)$ - $\dot{\underline{x}}(t)$. The estimate state error dynamics can be expressed by substituting $\dot{\underline{\hat{x}}}(t)$ from Eq. (5-54) with Equations (5-53), (5-51), and Eq. (5-55), and substituting $\dot{\underline{x}}(t)$ from Eq. (5-50) with Eq. (5-52) as:

$$\dot{\underline{\tilde{x}}}(t)=\left[F(t)-K(t)H(t)\right]\underline{\tilde{x}}(t)-G(t)\underline{w}(t)+K(t)\underline{v}(t) \tag{5-56}$$

where $F(t)$ and $H(t)$ are introduced for the Jacobian matrices, shown in Eq. (5-52) and Eq. (5-53), for brevity

$$F(t)\equiv\left.\frac{\partial\underline{\mathrm{f}}}{\partial\underline{x}}\right|_{\underline{\hat{x}}(t),\underline{u}(t)},\quad H(t)\equiv\left.\frac{\partial\underline{\mathrm{h}}}{\partial\underline{x}}\right|_{\underline{\hat{x}}(t)} \tag{5-57}$$

The estimate state error dynamics in Eq. (5-56) of the EKF (i.e. the linearized error equation at instants using the Jacobian matrices in Eq. (5-57)) has the same structure as that of Eq. (5-35) of the KF. Therefore, through the same procedure presented above for the KF, the EKF update equations for $\underline{\hat{x}}_k^+$ and P_k^+ and the EKF prediction equations for $\underline{\hat{x}}_{k+1}^-$ and P_{k+1}^- can be obtained (see Derivation 5.2 in Appendix B.10). The *extended Kalman filter* in discrete time form is expressed as following (which can be also found in other references such as Yun et al., 1980).

In the update state, the estimate state $\underline{\hat{x}}_k^+$ and its error covariance matrix P_k^+ are computed as:

$$\underline{\hat{x}}_k^+=\underline{\hat{x}}_k^-+K_k\left[\underline{\bar{y}}_k-\mathrm{h}\left(\underline{\hat{x}}_k^-\right)\right] \tag{5-58}$$

$$P_k^+=E\left\{\underline{\tilde{x}}_k^+\underline{\tilde{x}}_k^{+T}\right\}=\left[I-K_kH_k\right]P_k^- \tag{5-59}$$

The optimal gain K_k is determined by minimizing the trace of $P_k{}^+$, which is equivalent to minimize the length of the estimation error vector:

$$K_k=P_k^-H_k{}^T\left[H_kP_k^-H_k{}^T+R_E\right]^{-1} \tag{5-60}$$

where H_k (size $m \times n$) is obtained from the linearization of the Kalman filter using the first-order Taylor series expansion about the selected nominal state, which is the current estimate $\underline{\hat{x}}_k^-$, (i.e. as mentioned, the EKF assumes that the true state $\underline{x}(t)$ is sufficiently close to the estimated state $\underline{\hat{x}}(t)$; thus the current estimate $\underline{\hat{x}}_k^-$ is used for the nominal state estimate) of the output in Eq. (5-55) and is expressed as:

$$H_k = \left.\frac{\partial \mathrm{h}(\underline{x}_k)}{\partial \underline{x}_k}\right|_{\underline{\hat{x}}_k^-} \tag{5-61}$$

In the predicted state, the estimate state $\underline{\hat{x}}_{k+1}^-$ and its error covariance matrix P_{k+1}^- can be approximated as:

$$\underline{\hat{x}}_{k+1}^- = \underline{\hat{x}}_k^+ + \int_{t_k}^{t_{k+1}} \mathrm{f}\left(\underline{\hat{x}}(t), \underline{u}(t), t\right) dt \tag{5-62}$$

$$P_{k+1}^- = E\left\{\underline{\tilde{x}}_{k+1}^- \underline{\tilde{x}}_{k+1}^{-\,T}\right\} = \Phi_k P_k^+ \Phi_k^T + \Upsilon_k Q_E \Upsilon_k^{\,T} \tag{5-63}$$

where Φ_k (size $n \times n$) the state transition matrix and Υ_k (size $n \times n$) can be approximated as:

$$\Phi_k = I + \Delta t \left.\frac{\partial \underline{\mathrm{f}}\left(\underline{x}(t), \underline{u}(t), t\right)}{\partial \underline{x}(t)}\right|_{\underline{\hat{x}}_k^+} \quad or \quad I + \Delta t F_k(\underline{\hat{x}}_k^+) \tag{5-64}$$

$$\Upsilon_k = \Delta t G(t) \tag{5-65}$$

where the matrix $\partial \underline{\mathrm{f}} / \partial \underline{x} = F_k(\underline{\hat{x}}_k^+)$ is obtained from the linearization of the Kalman filter using the first-order Taylor series expansion about the current estimate $\underline{\hat{x}}_k^+$. The predicted state in Eq. (5-62) is evaluated using the Runge-Kutta 4th order method in this study. With the initial guess of the state $\underline{\hat{x}}_0^-$ and the error covariance matrix P_0^- and instant measurements $\underline{\overline{y}}_k$, the EKF update and prediction stages defined above can be implemented.

5.2.1.2 Estimate of Nonlinear Hysteresis Structures using the EKF

The nonlinear *extended Kalman filter* (EKF) method is used in order to estimate the state and the system parameters of the nonlinear hysteretic system, described in Section 4.1 (see Eq. (4-4)).

System State Estimation

First, it is desired to estimate the true state $\underline{x}(t) = [x_s(t) \quad \dot{x}_s(t) \quad f_S(\underline{x})]^T$ from the discrete state measurements $\underline{\overline{y}}_k = [\overline{x}_{s,k} \quad \dot{\overline{x}}_{s,k} \quad \overline{f}_{S,k}]^T$, obtained from instruments, in which measurement noise $\underline{v}_k$ are added as shown in Eq. (5-51). The 3×3 measurement noise covariance matrix R_E is chosen as a diagonal matrix assuming measurements are not correlated to each other. The 3×3 process noise covariance matrix Q_E is chosen as a matrix whose all elements are zeroes, assuming there is negligible error in the system model.

The Jacobian matrix (shown in Eq. (5-57)) of the system equations is required for the EKF method. The 3 × 3 Jacobian matrix $F(t)$ can be expressed by defining the state $[x_s(t)\ \ \dot{x}_s(t)\ \ f_S(\underline{x})]^T \equiv [x_1\ \ x_2\ \ x_3]^T$:

$$F(t) = \frac{\partial \mathrm{f}}{\partial \underline{x}} = \begin{bmatrix} 0 & 1 & 0 \\ 0 & -c_s m^{-1} & -m^{-1} \\ \partial \mathrm{f}_3/\partial x_1 & k_T(\underline{x}) & \partial \mathrm{f}_3/\partial x_3 \end{bmatrix} \tag{5-66}$$

where

$$k_T(\underline{x}) = k_s - (1-\alpha)k_s \frac{1+\mathrm{sgn}\left(f_H(\underline{x})x_2\right)}{2}\left(\frac{|f_H(\underline{x})|}{f_y^*}\right)^N \quad or \quad k_s + \bar{\alpha}\cdot\bar{\beta}(\underline{x})\cdot\bar{\gamma}(\underline{x})$$

$$\bar{\alpha} = -0.5(1-\alpha)k_s\left(f_y^*\right)^{-N}; \qquad \bar{\beta}(\underline{x}) = 1+\mathrm{sgn}\left(f_H(\underline{x})\dot{x}_s\right); \qquad \bar{\gamma}(\underline{x}) = |f_H(\underline{x})|^N \tag{5-67}$$

in which $f_H(\underline{x}) = f_S(\underline{x}) - \alpha k_s x_s(t)$, $f_y^* = (1-\alpha)\, f_y$ with $f_y = k_s d_y$ as defined earlier, and by defining that $\delta(x(t)) \times x(t) \equiv 0$ (i.e. that is indeterminate if $x(t) = 0$ since $\delta(x(t)) \times x(t) = \infty \times 0$; in this study the relation $\delta(x) \times x = 0$ (Dannon, 2012) (i.e. $\delta(x)$ is the *Dirac delta function*) is used)

$$\frac{\partial \mathrm{f}_3}{\partial x_1} = \left\{\frac{\partial k_T(\underline{x})}{\partial x_1}\right\}x_2 = \left\{\frac{\partial \bar{\gamma}(\underline{x})}{\partial x_1}\bar{\alpha}\bar{\beta}(\underline{x})\right\}x_2; \qquad \frac{\partial \bar{\gamma}(\underline{x})}{\partial x_1} = N\,|f_H(\underline{x})|^{N-1}\,\mathrm{sgn}\left(f_H(\underline{x})\right)\left(-\alpha k_s\right) \tag{5-68}$$

$$\frac{\partial \mathrm{f}_3}{\partial x_3} = \left\{\frac{\partial k_T(\underline{x})}{\partial x_3}\right\}x_2 = \left\{\frac{\partial \bar{\gamma}(\underline{x})}{\partial x_3}\bar{\alpha}\bar{\beta}(\underline{x})\right\}x_2; \qquad \frac{\partial \bar{\gamma}(\underline{x})}{\partial x_3} = N\,|f_H(\underline{x})|^{N-1}\,\mathrm{sgn}\left(f_H(\underline{x})\right)(1) \tag{5-69}$$

$$\frac{\partial \mathrm{f}_3}{\partial x_2} = \left\{\frac{\partial k_T(\underline{x})}{\partial x_2}\right\}x_2 + k_T(\underline{x}) = \left\{\frac{\partial \bar{\beta}(\underline{x})}{\partial x_2}\bar{\alpha}\bar{\gamma}(\underline{x})\right\}x_2 + k_T(\underline{x}) = k_T(\underline{x}); \qquad \frac{\partial \bar{\beta}(\underline{x})}{\partial x_2} = 2\delta(x_2)\,\mathrm{sgn}\left(f_H(\underline{x})\right) \tag{5-70}$$

It is noted that the $\delta(x_2)$ in the last equation indicates that the function $k_T(\underline{x})$ has a jump at the unloading instant (where $x_2 = 0$) from the hardening stiffness to the initial stiffness as shown in the hysteretic loop (Figure 4-1 (left)).

For the selected measurements $\underline{\bar{y}}_k = [\bar{x}_{s,k}\ \ \dot{\bar{x}}_{s,k}\ \ \bar{f}_{S,k}]^T$, the output vector $\underline{h}(\underline{x}_k)$ and the linearized matrix H_k in Eq. (5-61) are expressed as:

$$\mathrm{h}(\underline{x}_k) = \begin{bmatrix} x_{s,k} \\ \dot{x}_{s,k} \\ f_{S,k} \end{bmatrix} = \underline{x}_k \quad \text{and} \quad H_k = \left.\frac{\partial \mathrm{h}(\underline{x}_k)}{\partial \underline{x}_k}\right|_{\hat{\underline{x}}_k^-} = I_{3\times 3} \tag{5-71}$$

State and Parameter Estimation

In addition to the true state estimation, one can estimate the system parameters using the EKF. In order to estimate the parameters, new states are augmented to the state vector. The covariance matrix Q_E in Eq. (5-63) is selected to consider the errors in these states as well as the errors in the model due to the system uncertainty. In order to identify four parameters c_s, k_s, α, and d_y shown in Eq. (4-6), the 7 × 1 augmented state vector and the 7 × 7 matrix Q_E (i.e. Q_E is chosen as a diagonal matrix assuming each state is not correlated, and its first three elements are chosen as zeroes assuming the system model has no errors) are defined as:

$$\underline{x}(t) = \begin{bmatrix} x_s(t) & \dot{x}_s(t) & f_S(t) & c_s & k_s & \alpha & d_y \end{bmatrix}^T \quad or \quad \begin{bmatrix} x_1 & x_2 & x_3 & x_4 & x_5 & x_6 & x_7 \end{bmatrix}^T \tag{5-72}$$

$$Q_E = \begin{bmatrix} 0 & 0 & 0 & Q_{44} & Q_{55} & Q_{66} & Q_{77} \end{bmatrix}^T \tag{5-73}$$

The augmented deferential equations of the system is

$$\dot{\underline{x}}(t) = \underline{\mathrm{f}}\left(\underline{x}(t), u(t)\right) \qquad or$$

$$\frac{d}{dt}\begin{bmatrix} x_s(t) \\ \dot{x}_s(t) \\ f_S(t) \\ c_s \\ k_s \\ \alpha \\ d_y \end{bmatrix} = \begin{bmatrix} \dot{x}_s(t) \\ -m^{-1}\left\{c_s\dot{x}_s(t) + f_S(t)\right\} - m^{-1}u(t) \\ k_T\left(\underline{x}\right)\dot{x}_s(t) \\ 0 \\ 0 \\ 0 \\ 0 \end{bmatrix}, \qquad \underline{x}(0) = \underline{x}_0 \tag{5-74}$$

where the last four state derivatives are zeros since the unknown parameters are constant. The 7 × 7 Jacobian matrix $F(t)$ shown in Eq. (5-57) can be expressed as:

$$F(t) = \frac{\partial \underline{\mathrm{f}}}{\partial \underline{x}} = \begin{bmatrix} 0 & 1 & 0 & 0 & 0 & 0 & 0 \\ 0 & -m^{-1}x_4 & -m^{-1} & -m^{-1}x_2 & 0 & 0 & 0 \\ \partial \mathrm{f}_3/\partial x_1 & k_T(\underline{x}) & \partial \mathrm{f}_3/\partial x_3 & 0 & \partial \mathrm{f}_3/\partial x_5 & \partial \mathrm{f}_3/\partial x_6 & \partial \mathrm{f}_3/\partial x_7 \\ \left[0\right]_{4\times 7} & & & & & & \end{bmatrix} \tag{5-75}$$

where $k_T(\underline{x})$ is the instantaneous stiffness and expressed in Eq. (5-67), repeated here for convenience,

$$k_T(\underline{x}) = k_s - (1-\alpha)k_s \frac{1+\mathrm{sgn}\left(f_H(\underline{x})\dot{x}_s\right)}{2}\left(\frac{\left|f_H(\underline{x})\right|}{f_y^*}\right)^N = x_5 - \left(1-x_6\right)x_5 \frac{1+\mathrm{sgn}\left\{\left(x_3 - x_6x_5x_1\right)x_2\right\}}{2}\left(\frac{\left|x_3 - x_6x_5x_1\right|}{\left(1-x_6\right)x_5x_7}\right)^N$$

$$or \quad x_5 + \overline{\alpha}(\underline{x})\cdot\overline{\beta}(\underline{x})\cdot\overline{\gamma}(\underline{x})$$

$$\overline{\alpha}(\underline{x}) = -0.5\frac{1}{\left(1-x_6\right)^{N-1}x_5^{\,N-1}x_7^{\,N}}; \qquad \overline{\beta}(\underline{x}) = 1 + \mathrm{sgn}\left\{\left(x_3 - x_6x_5x_1\right)x_2\right\}; \qquad \overline{\gamma}(\underline{x}) = \left|x_3 - x_6x_5x_1\right|^N \tag{5-76}$$

and by defining that $\delta(x(t)) \times x(t) \equiv 0$ (i.e. that is indeterminate if $x(t) = 0$ since $\delta(x(t)) \times x(t) = \infty \times 0$)

$$\frac{\partial \mathrm{f}_3}{\partial x_1} = \left\{\frac{\partial k_T(\underline{x})}{\partial x_1}\right\}x_2 = \left\{\frac{\partial \overline{\gamma}(\underline{x})}{\partial x_1}\overline{\alpha}\overline{\beta}(\underline{x})\right\}x_2; \qquad \frac{\partial \overline{\gamma}(\underline{x})}{\partial x_1} = N\left|x_3 - x_6x_5x_1\right|^{N-1}\mathrm{sgn}\left(x_3 - x_6x_5x_1\right)\left(-x_6x_5\right) \tag{5-77}$$

$$\frac{\partial \mathrm{f}_3}{\partial x_3} = \left\{\frac{\partial k_T(\underline{x})}{\partial x_3}\right\}x_2 = \left\{\frac{\partial \overline{\gamma}(\underline{x})}{\partial x_3}\overline{\alpha}\overline{\beta}(\underline{x})\right\}x_2; \qquad \frac{\partial \overline{\gamma}(\underline{x})}{\partial x_3} = N\left|x_3 - x_6x_5x_1\right|^{N-1}\mathrm{sgn}\left(x_3 - x_6x_5x_1\right)(1) \tag{5-78}$$

$$\frac{\partial f_3}{\partial x_5} = \left\{\frac{\partial k_T(\underline{x})}{\partial x_5}\right\} x_2 = \left\{1 + \left(\frac{\partial \bar{\alpha}(\underline{x})}{\partial x_5}\bar{\beta}(\underline{x})\bar{\gamma}(\underline{x}) + \frac{\partial \bar{\beta}(\underline{x})}{\partial x_5}\bar{\alpha}(\underline{x})\bar{\gamma}(\underline{x}) + \frac{\partial \bar{\gamma}(\underline{x})}{\partial x_5}\bar{\alpha}(\underline{x})\bar{\beta}(\underline{x})\right)\right\} x_2;$$

$$\frac{\partial \bar{\alpha}(\underline{x})}{\partial x_5} = \frac{0.5(N-1)}{(1-x_6)^{N-1} x_7{}^N x_5{}^N}; \quad \frac{\partial \bar{\beta}(\underline{x})}{\partial x_5} = 0; \quad \frac{\partial \bar{\gamma}(\underline{x})}{\partial x_5} = N\left|x_3 - x_6 x_5 x_1\right|^{N-1}\left\{(-x_6 x_1)\operatorname{sgn}(x_3 - x_6 x_5 x_1)\right\} \tag{5-79}$$

$$\frac{\partial f_3}{\partial x_6} = \left\{\frac{\partial k_T(\underline{x})}{\partial x_6}\right\} x_2 = \left\{\frac{\partial \bar{\alpha}(\underline{x})}{\partial x_6}\bar{\beta}(\underline{x})\bar{\gamma}(\underline{x}) + \frac{\partial \bar{\beta}(\underline{x})}{\partial x_6}\bar{\alpha}(\underline{x})\bar{\gamma}(\underline{x}) + \frac{\partial \bar{\gamma}(\underline{x})}{\partial x_6}\bar{\alpha}(\underline{x})\bar{\beta}(\underline{x})\right\} x_2;$$

$$\frac{\partial \bar{\alpha}(\underline{x})}{\partial x_6} = \frac{-0.5(N-1)}{x_5{}^{N-1} x_7{}^N (1-x_6)^N}; \quad \frac{\partial \bar{\beta}(\underline{x})}{\partial x_6} = 0; \quad \frac{\partial \bar{\gamma}(\underline{x})}{\partial x_6} = N\left|x_3 - x_6 x_5 x_1\right|^{N-1}\left\{(-x_5 x_1)\operatorname{sgn}(x_3 - x_6 x_5 x_1)\right\} \tag{5-80}$$

$$\frac{\partial f_3}{\partial x_7} = \left\{\frac{\partial k_T(\underline{x})}{\partial x_7}\right\} x_2 = \left\{\frac{\partial \bar{\alpha}(\underline{x})}{\partial x_7}\bar{\beta}(\underline{x})\bar{\gamma}(\underline{x}) + \frac{\partial \bar{\beta}(\underline{x})}{\partial x_7}\bar{\alpha}(\underline{x})\bar{\gamma}(\underline{x}) + \frac{\partial \bar{\gamma}(\underline{x})}{\partial x_7}\bar{\alpha}(\underline{x})\bar{\beta}(\underline{x})\right\} x_2;$$

$$\frac{\partial \bar{\alpha}(\underline{x})}{\partial x_7} = \frac{0.5N}{x_5{}^{N-1}(1-x_6)^{N-1} x_7{}^{N+1}}; \quad \frac{\partial \bar{\beta}(\underline{x})}{\partial x_7} = 0; \quad \frac{\partial \bar{\gamma}(\underline{x})}{\partial x_7} = 0 \tag{5-81}$$

For the selected measurements $\underline{\tilde{y}}_k = [\bar{x}_k \;\; \dot{\bar{x}}_k \;\; \bar{f}_{S,k}]^T$, the output vector $\underline{h}(\underline{x}_k)$ and the linearized matrix H_k in Eq. (5-61) are expressed as:

$$\mathrm{h}(\underline{x}_k) = \begin{bmatrix} x_{s,k} \\ \dot{x}_{s,k} \\ f_{S,k} \end{bmatrix} = \underline{x}_k \qquad \text{and} \qquad H_k = \left.\frac{\partial \mathrm{h}(\underline{x}_k)}{\partial \underline{x}_k}\right|_{\hat{\underline{x}}_k^-} = \begin{bmatrix} I_{3\times3} & [0]_{3\times4} \end{bmatrix} \tag{5-82}$$

Example 5.6 **: Parameter estimation for an SDOF linear system**

The EKF[12] method is used for the system identification to estimate unknown parameters of an SDOF linear system (as shown in Figure 5-1). It is noted that the formulation unlike the feedback tracking control methods, the control excitation input $u(t) = -m_s\ddot{x}_t(t)$ is pre-defined and not updated in real time.

The properties of the system are the same as the ones in Example 3.1; m_s = 1 kips·sec^2/in., k_s = 355 kips/in., and c_s = 1.13 kips·sec/in., (f_n = 3.0 Hz, ξ_n = 0.03). The measurement noise, a zero-mean Gaussian white-noise process of 1% RMS noise-to-signal, are added to the measurements $\underline{\bar{y}}_k = [\bar{x}_{s,k} \;\; \dot{\bar{x}}_{s,k}]^T$. Two unknown parameters: c_s the damping coefficient and k_s the elastic stiffness; are selected and estimated in real time. The selected excitation input $u(t)$ to the system is the sinusoidal motion (the forcing frequency f_f = 1.0 Hz) and presented in Figure 5-11 (a) (for comparison purposes with other examples, $\ddot{x}_t(t) = -u(t)/m_s$, the shake table acceleration is presented). For the parameter estimation, the initial parameter estimate $\underline{\hat{\theta}}_0$

---

[12] Although the only EKF formulation for nonlinear systems is presented above, the formulation for linear systems is very similar. Only analysis results are presented in this example for comparison purposes to the LS in Example 5.1.).

= 0.5 × $\underline{\theta}^*$; and the initial covariance matrix is chosen as P_0 = diag([0 0 $\hat{k}_{s,o}{}^2$ $\hat{c}_{s,o}{}^2]^T$ × 0.001). The covariance matrices Q_E and R_E are chosen as follows: $Q_E = 0 \times I_{4\times4}$ (all zeroes) and the R_E = diagonal matrix, whose elements; i.e. noise variance = 1% × corresponding signal variance (noise variances are assumed to be known from the instruments information). The time step = 0.002 sec. The relation between the structure resisting force $f_S(t)$ and displacement $x_s(t)$ is also presented in Figure 5-11 (b).

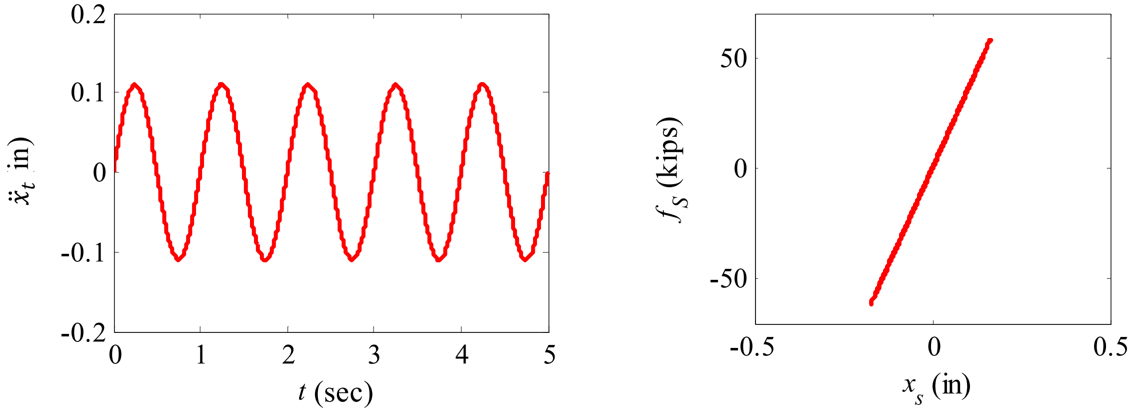

(a) Predefined excitation input (u)

(b) Response of structure (f_S vs. x_s)

Figure 5-11 Excitation and structure responses: Real time parameter estimation using the EKF

The estimated parameters are updated using Eq. (5-58) and Eq. (5-62). The comparisons between the true parameters: k_s the elastic stiffness and c_s the damping coefficient; and the estimated parameters are shown in Figure 5-12 and the results show that the agreements are very good. It is noted that the estimation performance is affected by various conditions and will be discussed in Section 5.2.2.

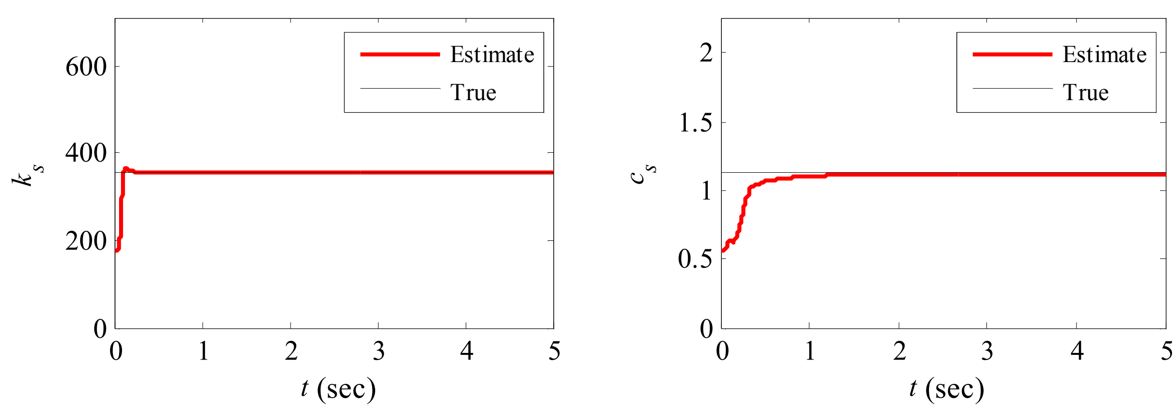

(a) Estimated parameter k_s

(b) Estimated parameter c_s

Figure 5-12 Real time parameter estimation results using the EKF for an SDOF linear system

***Example 5.7* : Parameter estimation for an SDOF nonlinear hysteresis system with hardening**

The EKF method is used for the system identification to estimate unknown parameters and the state of an SDOF nonlinear hysteretic structure (as shown in Figure 5-1; but, in this example the structure experiences nonlinear behavior due to yielding). It is noted that unlike the feedback tracking control methods, the control excitation input $u(t) = -m_s\ddot{x}_t(t)$ is pre-defined and not updated in real time .

The properties of the system are the same as the ones in Example 4.1; m_s = 1 kips·sec^2/in.; k_s = 355 kips/in.; and c_s = 1.13 kips·sec/in.; (f_n = 3.0 Hz, ξ_n = 0.03 before yielding). N = 3; d_y = 0.11 in. (f_y = 39 kips); and α = 0.1; i.e. all terms are explained in Eq. (4-2). The measurement noise, a zero-mean Gaussian white-noise process of 10% RMS noise-to-signal, are added to the measurements $\underline{y}_k = [\overline{x}_{s,k} \;\; \dot{\overline{x}}_{s,k} \;\; \overline{f}_{S,k}]^T$. Four unknown parameters: c_s the damping coefficient; k_s the elastic stiffness; d_y the yielding displacement; and α the post-yielding stiffness ratio to the elastic stiffness; are selected and estimated in real time. The selected excitation input $u(t)$ to the system is the sinusoidal motion (the forcing frequency f_f = 1.0 Hz) and presented in Figure 5-13 (a) (for comparison purposes with other examples, $\ddot{x}_t(t) = -u(t)/m_s$, the shake table acceleration is presented). For the parameter estimation, it is chosen that the initial parameter estimate $\hat{\underline{\theta}}_0 = 0.5 \times \underline{\theta}^*$ (50% error in the initial guess); and the initial covariance matrix P_0 = diag([0 0 0 $\hat{c}_{s,o}{}^2$ $\hat{k}_{s,o}{}^2$ $\hat{\alpha}_o{}^2$ $\hat{d}_{y,o}{}^2$]^T × 1). The covariance matrices Q_E and R_E are chosen as follows: Q_E = 0 × $I_{7\times7}$ (all zeroes) and the R_E = diagonal matrix, whose elements; i.e. noise variance = 10% × corresponding signal variance (noise variances are assumed to be known from the instruments information). The time step = 0.002 sec. The relation between the structure resisting force $f_S(t)$ and displacement $x_s(t)$ is also presented in Figure 5-13 (b).

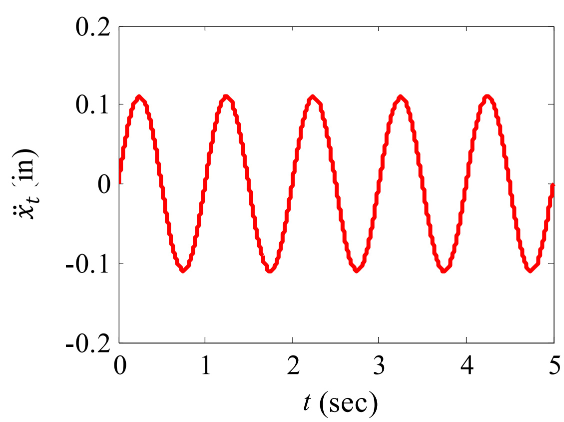

(a) Predefined excitation input (u)

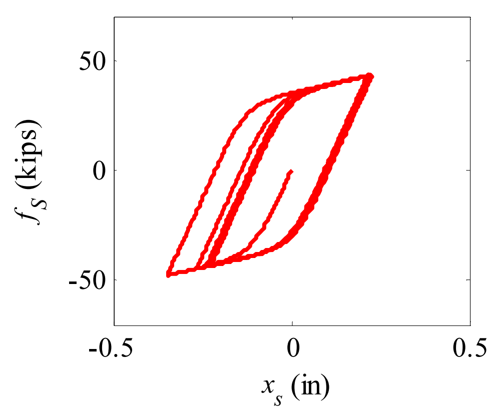

(b) Response of structure (f_S vs. x_s)

Figure 5-13 Excitation and structure responses: Real time parameter estimation using the LS

The estimated parameters are updated using Eq. (5-58) and Eq. (5-62). The comparisons between the true parameters: $k_T(\underline{x})$ the instantaneous stiffness (i.e. the estimate of $k_T(\underline{x})$ is computed using the estimates of k_s, d_y and α); c_s the damping coefficient; k_s the elastic stiffness; d_y the yielding displacement; and α the post-yielding stiffness ratio to the elastic stiffness; and the estimated parameters are shown in Figure 5-14: the results show very good agreements. In addition to the parameter estimation, the EKF is used to estimate the state responses; i.e. the state $\underline{x}$ = $[x_s(t) \quad \dot{x}_s(t) \quad f_S(\underline{x})]^T$ is estimated from the selected measurements $\underline{\overline{y}}_k$ = $[\overline{x}_{s,k} \quad \dot{\overline{x}}_{s,k} \quad \overline{f}_{S,k}]^T$, which are contaminated by measurement noise as explained in Eq. (5-51). Figure 5-15 shows the results of the state estimation; the comparisons between the measured and the truth and between the estimated and the truth are presented for the state $\underline{x}$: the structure displacement $x_s(t)$, velocity $\dot{x}_s(t)$, and the resisting force $f_S(\underline{x})$; the estimated state show very good agreements to the true state. However, it is noted that the estimation performance can be sensitive to various conditions involving the selected parameters and measurement noise; the effects will be discussed in Section 5.2.2.

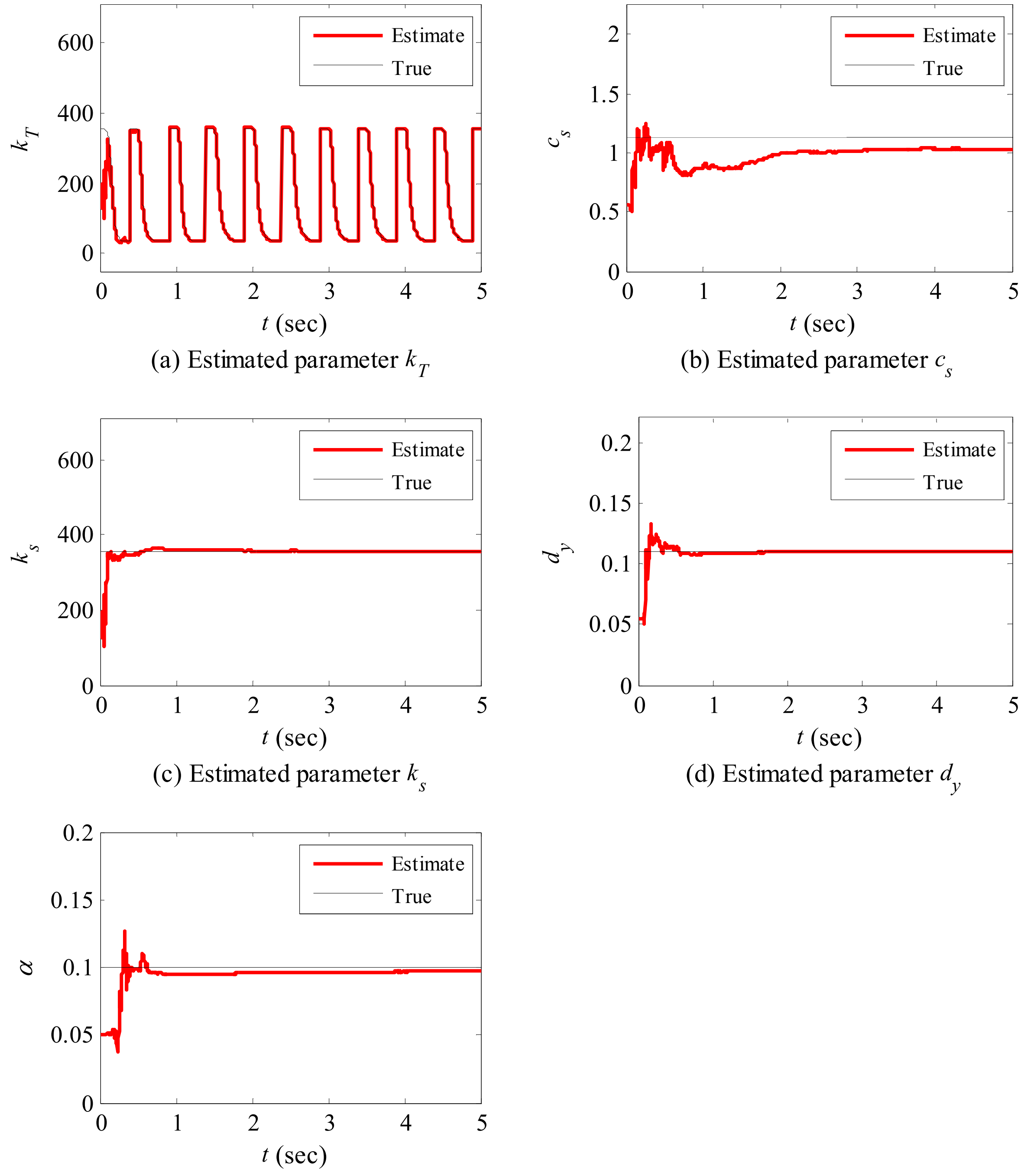

(a) Estimated parameter k_T

(b) Estimated parameter c_s

(c) Estimated parameter k_s

(d) Estimated parameter d_y

(e) Estimated parameter α

Figure 5-14 Real time parameter estimation results using the EKF for an SDOF nonlinear system

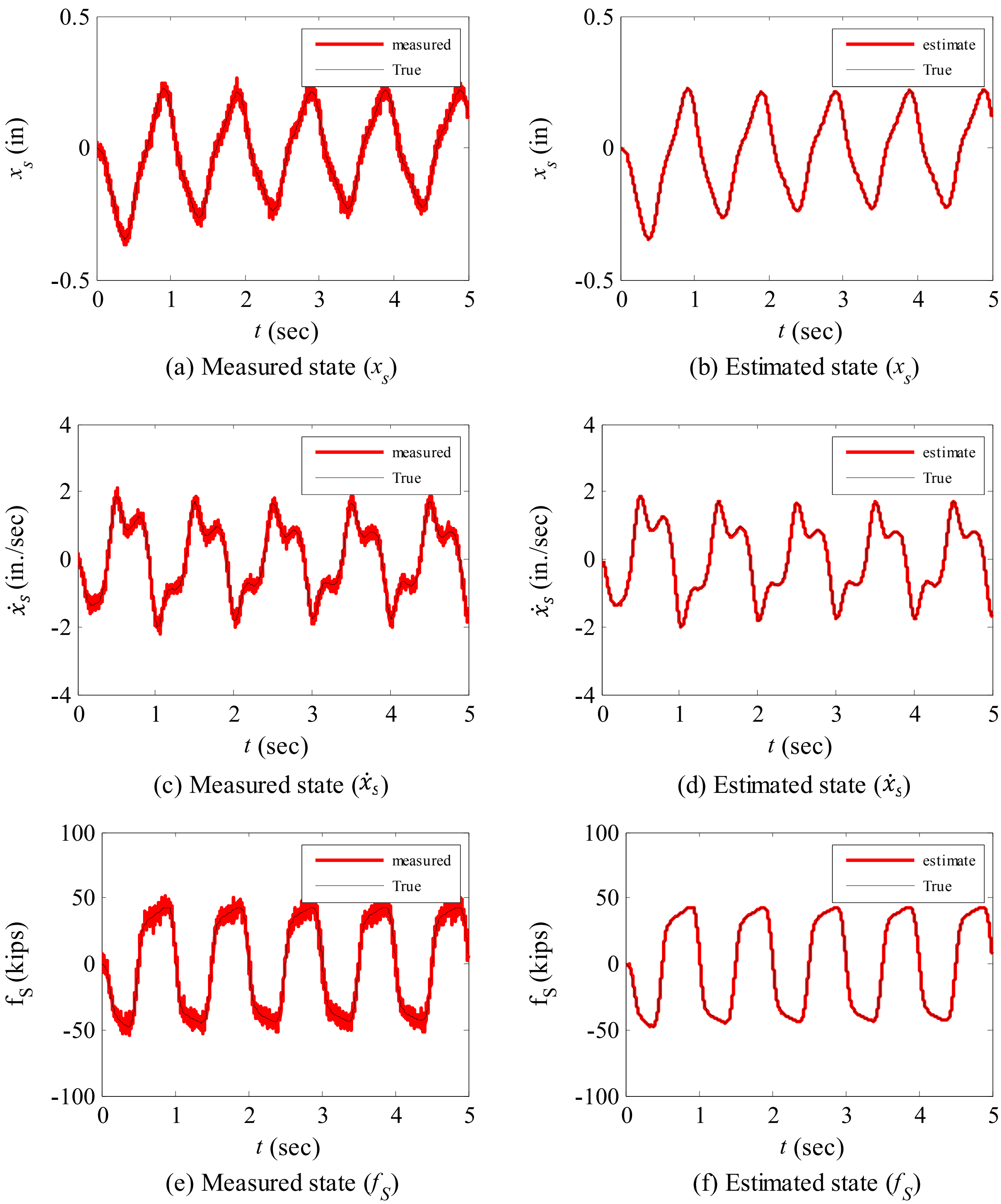

(a) Measured state (x_s) (b) Estimated state (x_s)

(c) Measured state ($\dot{x}_s$) (d) Estimated state ($\dot{x}_s$)

(e) Measured state (f_S) (f) Estimated state (f_S)

Figure 5-15 Real time state estimation results using the EKF for an SDOF nonlinear system

5.2.1.3 Estimate of Nonlinear Hysteresis Structures on Shake Tables

The nonlinear *extended Kalman filter* (EKF) method is now applied to the shake table-structure system considering their interaction, which are modeled as the 2DOF system, described in Section 4.1 (see Eq. (4-6)) in order to estimate the state and the unknown system parameters in real time.

State Estimation

First, it is desired to estimate the true state $\underline{x}(t) = [x_s(t)\ \ \dot{x}_s(t)\ \ f_S(\underline{x})\ \ x_t(t)\ \ \dot{x}_t(t)\ \ f_a(t)/m_t]^T$ from the discrete state measurements $\underline{\overline{y}}_k = [\overline{x}_{s,k}\ \ \dot{\overline{x}}_{s,k}\ \ \overline{f}_{S,k}\ \ \overline{x}_{t,k}\ \ \dot{\overline{x}}_{t,k}\ \ \overline{f}_{a,k}/m_t]^T$, obtained from instruments, where noise are added. The 6×6 covariance matrix R is chosen as a diagonal matrix assuming measurements are not correlated to each other and the 6×6 covariance matrix Q_E is chosen as a matrix whose all elements are zeroes, assuming there is no error in the system model.

The 6×6 Jacobian matrix of the system equations is, by defining the state vector $[x_s(t)\ \ \dot{x}_s(t)\ \ f_S(\underline{x})\ \ x_t(t)\ \ \dot{x}_t(t)\ \ f_a(t)/m_t] \equiv [x_1\ \ x_2\ \ x_3\ \ x_4\ \ x_5\ \ x_6]^T$:

$$F(t) = \frac{\partial \mathrm{f}}{\partial \underline{x}} = \begin{bmatrix} 0 & 1 & 0 & 0 & 0 & 0 \\ 0 & -\left(m_s^{-1}+m_t^{-1}\right)c_s & -\left(m_s^{-1}+m_t^{-1}\right) & 0 & 0 & -1 \\ \partial \mathrm{f}_3/\partial x_1 & k_T\left(\underline{x}\right) & \partial \mathrm{f}_3/\partial x_3 & 0 & 0 & 0 \\ 0 & 0 & 0 & 0 & 1 & 0 \\ 0 & m_t^{-1}c_s & m_t^{-1} & 0 & 0 & 1 \\ 0 & 0 & 0 & -k_a\omega_a^2 & -\omega_a^2 & -2\xi_a\omega_a \end{bmatrix} \tag{5-83}$$

where $k_T(\underline{x})$, $\partial \mathrm{f}_3/\partial x_1$, and $\partial \mathrm{f}_3/\partial x_3$ are expressed in Equations (5-67), (5-68), and (5-69).

For the selected measurements $\underline{\overline{y}}_k = [\overline{x}_{s,k}\ \ \dot{\overline{x}}_{s,k}\ \ \overline{f}_{S,k}\ \ \overline{x}_{t,k}\ \ \dot{\overline{x}}_{t,k}\ \ \overline{f}_{a,k}/m_t]^T$, the output vector $\underline{h}(\underline{x}_k)$ and the linearized matrix H_k in Eq. (5-61) are expressed as:

$$\mathrm{h}(\underline{x}_k) = \left[x_{s,k}\quad \dot{x}_{s,k}\quad f_{S,k}\quad x_{t,k}\quad \dot{x}_{t,k}\quad f_{a,k}/m_t\right]^T = \underline{x}_k \qquad \text{and} \qquad H_k = \left.\frac{\partial \mathrm{h}(\underline{x}_k)}{\partial \underline{x}_k}\right|_{\hat{\underline{x}}_k^-} = I_{6\times 6} \tag{5-84}$$

State and Parameter Estimation

In addition to the true state estimation, one can estimate the system parameters using the EKF. In order to estimate the parameters, new states are augmented to the state vector. The covariance matrix Q_E in Eq. (5-63) is selected to consider the errors in these states as well as the errors in the model due to the system uncertainty. It is assumed that the system parameters, ω_a, ξ_a, and k_a, of the servo-valve and actuator of the shake table system are known before the shake table tests and remain the same during the tests (as discussed in Section 2.3). In order to identify four parameters c_s, k_s, α, and d_y of the nonlinear hysteretic structure in Eq. (4-6), the 10×1 augmented state vector and the 10×10 matrix Q_E (i.e. Q_E is chosen as a diagonal matrix assuming each state is not correlated, and its first six elements are chosen as zeroes assuming the system model has no errors) are defined as:

$$\begin{aligned}\underline{x}(t) = &\left[x_s(t) \quad \dot{x}_s(t) \quad f_S(t) \quad x_t(t) \quad \dot{x}_t(t) \quad f_a(t)/m_t \quad c_s \quad k_s \quad \alpha \quad d_y \right]^T \quad or \\ &\left[x_1 \quad x_2 \quad x_3 \quad x_4 \quad x_5 \quad x_6 \quad x_7 \quad x_8 \quad x_9 \quad x_{10} \right]^T\end{aligned} \tag{5-85}$$

$$Q_E = diag(\left[0 \quad 0 \quad 0 \quad 0 \quad 0 \quad 0 \quad Q_{77} \quad Q_{88} \quad Q_{99} \quad Q_{1010} \right]) \tag{5-86}$$

The augmented deferential equations of the system is

$$\dot{\underline{x}}(t) = \underline{\mathrm{f}}\left(\underline{x}(t), u(t)\right) \qquad or$$

$$\frac{d}{dt}\begin{bmatrix} x_s(t) \\ \dot{x}_s(t) \\ f_S(t) \\ x_t(t) \\ \dot{x}_t(t) \\ f_a/m_t \\ c_s \\ k_s \\ \alpha \\ d_y \end{bmatrix} = \begin{bmatrix} \dot{x}_s(t) \\ -\left(m_s^{-1} + m_t^{-1}\right)\left\{c_s\dot{x}_s(t) + f_S(t)\right\} - m_t^{-1} f_a(t) \\ k_T\left(\underline{x}\right)\dot{x}_s(t) \\ \dot{x}_t(t) \\ m_t^{-1}\left\{c_s\dot{x}_s(t) + f_S(t)\right\} + f_a/m_t \\ -k_a\omega_a^2 x_t(t) - \omega_a^2\dot{x}_t(t) - 2\xi_a\omega_a f_a/m_t + k_a\omega_a^2 x_c(t) \\ 0 \\ 0 \\ 0 \\ 0 \end{bmatrix}, \qquad \underline{x}(0) = \underline{x}_0 \tag{5-87}$$

where the last four state derivatives are zeros since the unknown parameters are constant. The 10 × 10 Jacobian matrix $F(t)$ shown in Eq. (5-57) can be expressed as:

$$F(t) = \frac{\partial \underline{\mathrm{f}}}{\partial \underline{x}} = \begin{bmatrix} 0 & 1 & 0 & 0 & 0 & 0 & 0 & 0 & 0 & 0 \\ 0 & -\left(m_s^{-1}+m_t^{-1}\right)x_7 & -\left(m_s^{-1}+m_t^{-1}\right) & 0 & 0 & -1 & -\left(m_s^{-1}+m_t^{-1}\right)x_2 & 0 & 0 & 0 \\ \partial\mathrm{f}_3/\partial x_1 & k_T(\underline{x}) & \partial\mathrm{f}_3/\partial x_3 & 0 & 0 & 0 & 0 & \partial\mathrm{f}_3/\partial x_8 & \partial\mathrm{f}_3/\partial x_9 & \partial\mathrm{f}_3/\partial x_{10} \\ 0 & 0 & 0 & 0 & 1 & 0 & 0 & 0 & 0 & 0 \\ 0 & m_t^{-1}x_7 & m_t^{-1} & 0 & 0 & 1 & m_t^{-1}x_2 & 0 & 0 & 0 \\ 0 & 0 & 0 & -k_a\omega_a^2 & -\omega_a^2 & -2\xi_a\omega_a & 0 & 0 & 0 & 0 \\ \left[0\right]_{4\times10} & & & & & & & & & \end{bmatrix} \tag{5-88}$$

where $k_T(\underline{x})$, $\partial\mathrm{f}_3/\partial x_1$, $\partial\mathrm{f}_3/\partial x_3$, $\partial\mathrm{f}_3/\partial x_8$, $\partial\mathrm{f}_3/\partial x_9$, and $\partial\mathrm{f}_3/\partial x_{10}$ are expressed in Equations (5-76), (5-77), (5-78), (5-79), (5-80), and (5-81), respectively, by replacing the unknown state numbers from x_4, x_5, x_6, x_7 of the SDOF system to x_7, x_8, x_9, x_{10} of the 2DOF system.

For the selected measurements $\underline{\overline{y}}_k = [\overline{x}_{s,k} \ \dot{\overline{x}}_{s,k} \ \overline{f}_{S,k} \ \overline{x}_{t,k} \ \dot{\overline{x}}_{t,k} \ \overline{f}_{a,k}/m_t]^T$, the output vector $\underline{h}(\underline{x}_k)$ and the linearized matrix H_k in Eq.(5-61) are expressed as:

$$\mathrm{h}(\underline{x}_k) = \left[x_{s,k} \quad \dot{x}_{s,k} \quad f_{S,k} \quad x_{t,k} \quad \dot{x}_{t,k} \quad f_{a,k}/m_t \right]^T = \underline{x}_k \qquad \text{and} \qquad H_k = \left.\frac{\partial \mathrm{h}(\underline{x}_k)}{\partial \underline{x}_k}\right|_{\hat{\underline{x}}_k^-} = \left[I_{6\times6} \quad \left[0\right]_{6\times4} \right] \tag{5-89}$$

Example 5.8 **: Parameter estimation for a 2DOF nonlinear hysteresis system with hardening**

The EKF method is used for the system identification to estimate unknown parameters and the state of a 2DOF nonlinear hysteretic structure (as shown in Figure 5-16). It is noted that unlike the feedback tracking control methods, the control excitation input $u(t) = x_d(t)$), the desired shake table displacement, is pre-defined and not updated in real time.

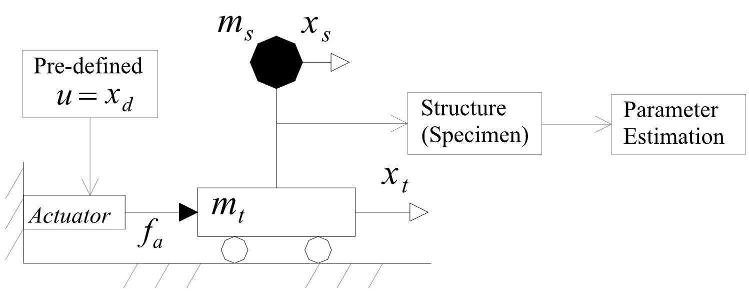

Figure 5-16 Parameter estimation of a 2DOF system

The properties of the system are the same as the ones in Example 4.2; m_s = 1 kips·sec^2/in.; k_s = 355 kips/in.; and c_s = 1.13 kips·sec/in.; (f_n = 3.0 Hz, ξ_n = 0.03 before yielding). N = 3; d_y = 0.11 in. (f_y = 39 kips); and α = 0.1; i.e. all terms are explained in Eq. (4-2), for the hysteretic system and $\mu = m_s / m_t = 0.1$, $f_{n,a}$ = 30.0 Hz, ξ_a = 0.5 and k_a = 25 for the shake table. The measurement noise, a zero-mean Gaussian white-noise process of 10% RMS noise-to-signal, are added to the measurements $\underline{\overline{y}}_k = [\overline{x}_{s,k}\ \ \dot{\overline{x}}_{s,k}\ \ \overline{f}_{S,k}\ \ \overline{x}_{t,k}\ \ \dot{\overline{x}}_{t,k}\ \ \overline{f}_{a,k}/m_t]^T$. Four unknown parameters: c_s the damping coefficient; k_s the elastic stiffness; d_y the yielding displacement; and α the post-yielding stiffness ratio to the elastic stiffness; are selected and estimated in real time. The selected excitation input $u(t) = x_d(t)$ is the sinusoidal motion (the forcing frequency f_f = 1.0 Hz) and presented in Figure 5-17 (a). For the parameter estimation, it is chosen that the initial parameter estimate $\hat{\underline{\theta}}_0 = 0.5 \times \underline{\theta}^*$ (50% error in the initial guess); and the initial covariance matrix P_0 = diag([0 0 0 0 0 0 $\hat{c}_{s,o}{}^2$ $\hat{k}_{s,o}{}^2$ $\hat{\alpha}_o{}^2$ $\hat{d}_{y,o}{}^2]^T \times 1$). The covariance matrices Q_E and R_E are chosen as follows: $Q_E = 0 \times I_{10\times10}$ (all zeroes) and the R_E = diagonal matrix, whose elements; i.e. noise variance = 10% × corresponding signal variance (noise variances are assumed to be known from the instruments information). The time step = 0.002 sec. The relation between the structure resisting force $f_S(t)$ and displacement $x_s(t)$ is also presented in Figure 5-17 (b).

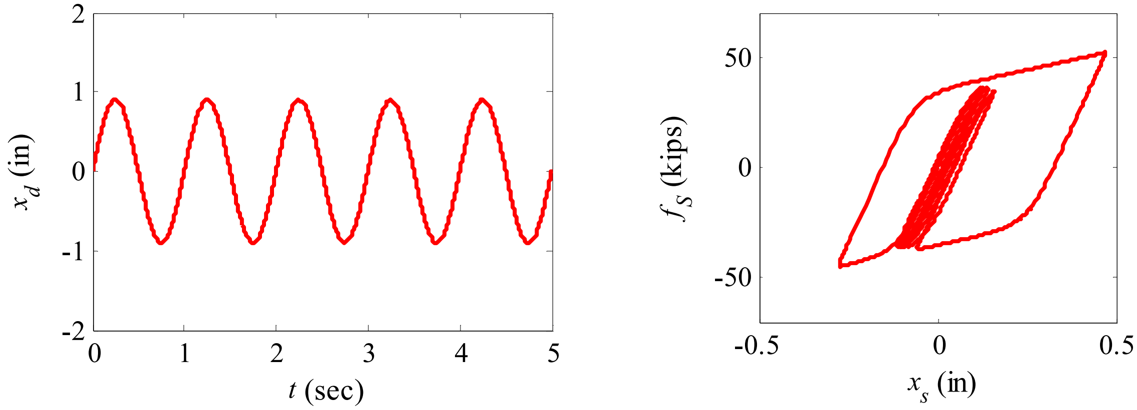

(a) Predefined excitation input (u)

(b) Response of structure (f_S vs. x_s)

Figure 5-17 Excitation and structure responses: Real time parameter estimation using the EKF

The estimated parameters are updated using Eq. (5-58) and Eq. (5-62). The comparisons between the true parameters: $k_T(\underline{x})$ the instantaneous stiffness (i.e. the estimate of $k_T(\underline{x})$ is computed using the estimates of k_s, d_y and α); c_s the damping coefficient; k_s the elastic stiffness; d_y the yielding displacement; and α the post-yielding stiffness ratio to the elastic stiffness; and the estimated parameters are shown in Figure 5-18: the results show very good agreements. In addition to the parameter estimation, the EKF is used to estimate the state responses; i.e. the state $\underline{x}(t) = [x_s(t)\ \ \dot{x}_s(t)\ \ f_S(\underline{x})\ \ x_t(t)\ \ \dot{x}_t(t)\ \ f_a(t)/m_t]^T$ is estimated from the selected measurements $\underline{\overline{y}}_k = [\overline{x}_{s,k}\ \ \dot{\overline{x}}_{s,k}\ \ \overline{f}_{S,k}\ \ \overline{x}_{t,k}\ \ \dot{\overline{x}}_{t,k}\ \ \overline{f}_{a,k}/m_t]^T$, which are contaminated by measurement noise as explained in Eq. (5-51). Figure 5-19 and Figure 5-20 show the results of the state estimation; the comparisons between the measured and the truth and between the estimated and the truth are presented for the state $\underline{x}$: the structure displacement $x_s(t)$, velocity $\dot{x}_s(t)$, and the resisting force $f_S(\underline{x})$ and the shake table displacement $x_t(t)$, velocity $\dot{x}_t(t)$, and the actuator force $f_a(\underline{x})$; the estimated state shows very good agreement to the true state. However, it is noted that the estimation performance can be sensitive to various conditions involving the selected parameters and measurement noise; the effects will be discussed in Section 5.2.2.

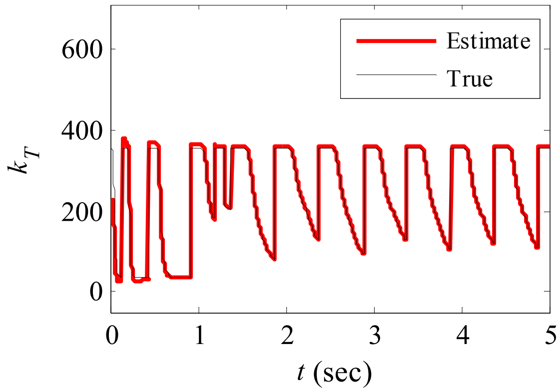

(a) Estimated parameter k_T

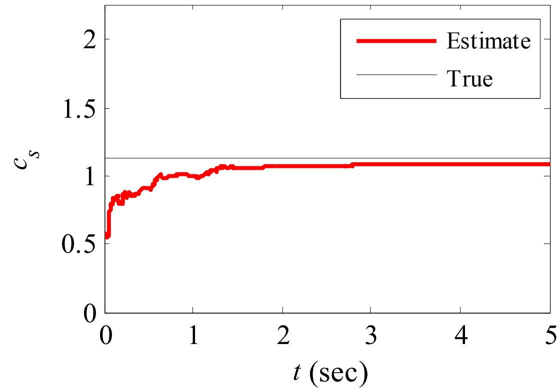

(b) Estimated parameter c_s

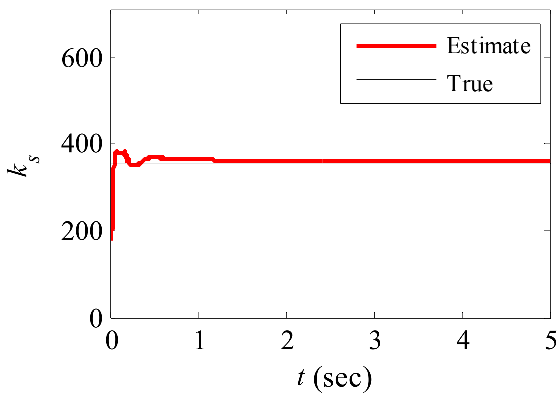

(c) Estimated parameter k_s

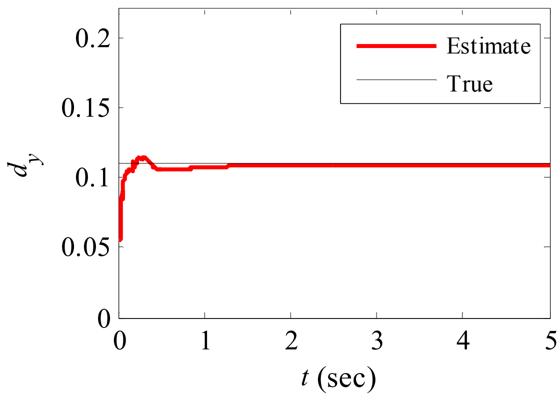

(d) Estimated parameter d_y

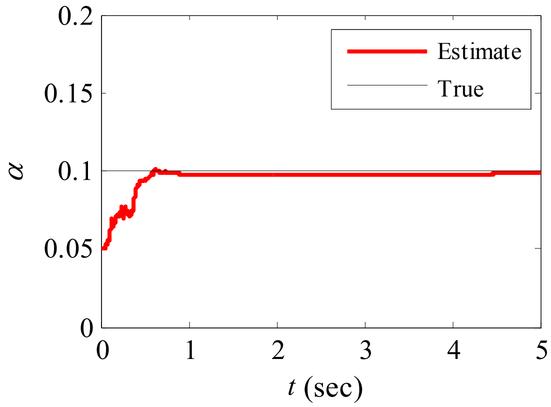

(e) Estimated parameter α

Figure 5-18 Real time parameter estimation results using the EKF for a 2DOF nonlinear system

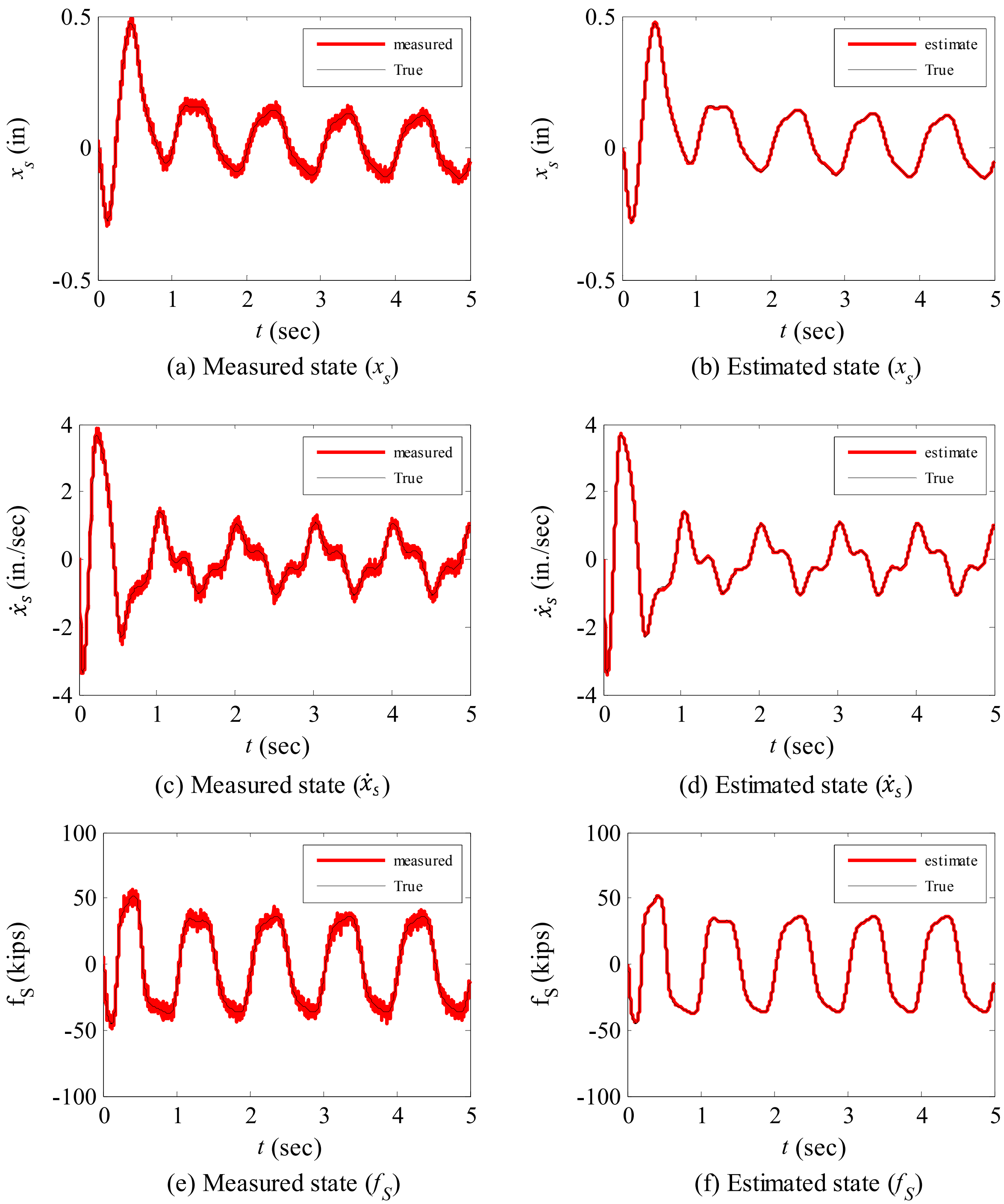

Figure 5-19 Real time state estimation (EKF) - structure responses for a 2DOF nonlinear system

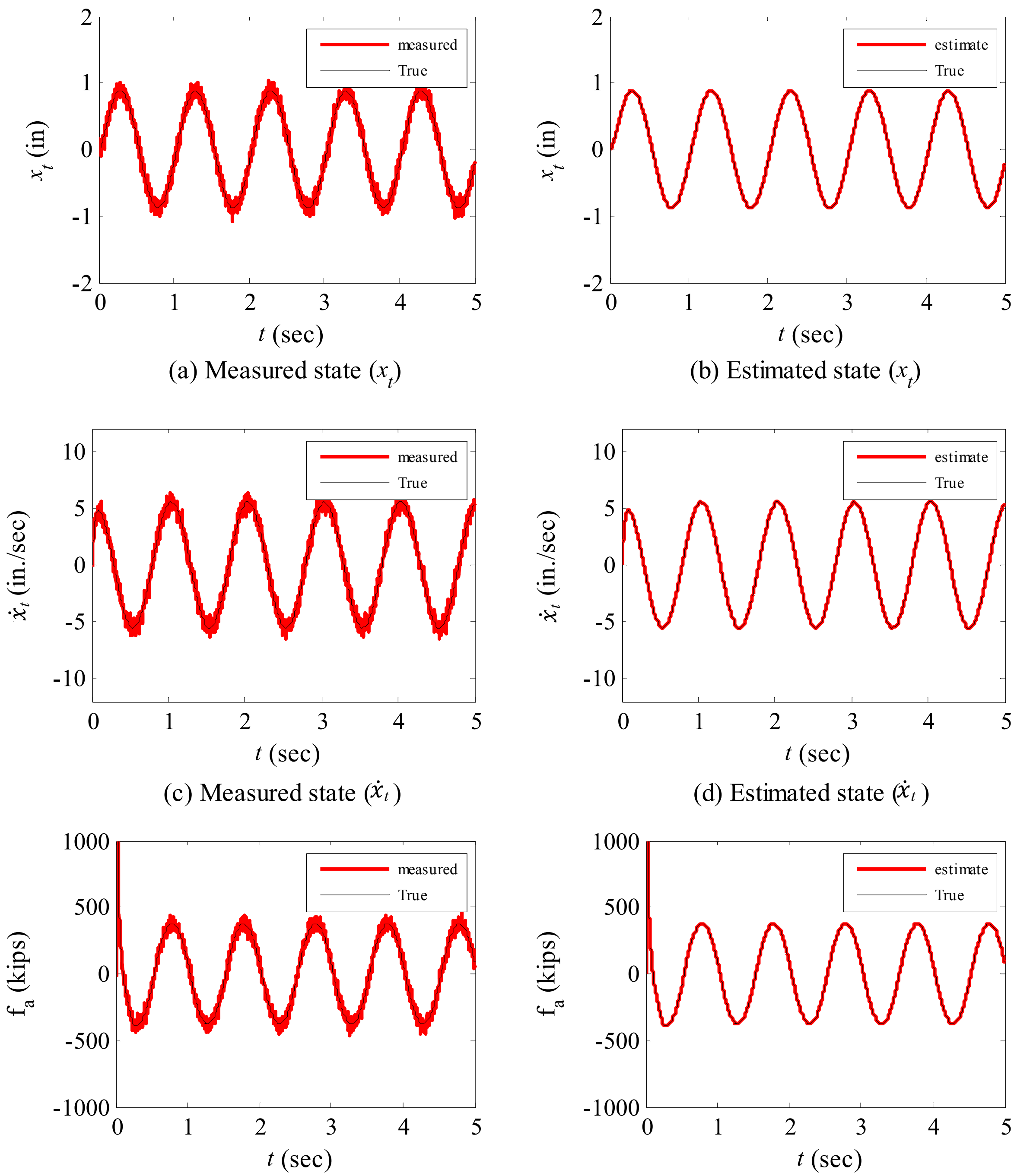

(a) Measured state (x_t)
(b) Estimated state (x_t)
(c) Measured state ($\dot{x}_t$)
(d) Estimated state ($\dot{x}_t$)
(e) Measured state (f_a)
(f) Estimated state (f_a)

Figure 5-20 Real time state estimation (EKF) – shake table responses for a 2DOF nonlinear system

5.2.2 Effects of Initial Guesses of Unknown Parameters and Covariance Matrices

As discussed in Section 5.2, it is very difficult to show a certain stability property of the EKF (Crassidis and Junkin, 2012) due to a possible error in a linearized first-order Taylor series expansion. Therefore, the robustness of the EKF is examined through numerical simulations. Two factors, which play important roles on the performance of the EKF; are considered: first, the effects of initial guess of unknown parameters; and secondly, the effects of the selection of the covariance matrices. It is noted that the estimation performance can be also affected by other conditions involving modeling errors, measurement noise, different excitation, etc. The same SDOF linear model described in Example 5.1 and Example 5.6 are used where two parameters $\underline{\theta}^* = [k_s \;\; c_s]^T$: k_s the elastic stiffness and c_s the damping coefficient; are selected and estimated in real time. The excitation input $u(t)$ to the system is the same sinusoidal motion (the forcing frequency f_f = 1.0 Hz), shown in Figure 5-11 (a). The time step = 0.002 sec.

***Example 5.9* : Effects of initial guess of unknown parameters on the EKF estimator performance**

The effects of the initial guess of the unknown parameters are investigated numerically. Three different initial guesses $\underline{\hat{\theta}}_0$ are made as the 10%, 50% and 200% of the true parameters; $\underline{\hat{\theta}}_0 = 0.1 \times \underline{\theta}^*$; $\underline{\hat{\theta}}_0 = 0.5 \times \underline{\theta}^*$; $\underline{\hat{\theta}}_0 = 2.0 \times \underline{\theta}^*$. The initial covariance matrix is chosen as $P_0 = \mathrm{diag}([0 \;\; 0 \;\; k_{s,o}^{\;2} \;\; c_{s,o}^{\;2}]^T \times 0.0005)$ for all cases. The comparisons between the true parameters: k_s the elastic stiffness and c_s the damping coefficient; and the estimated parameters are shown in Figure 5-21 (the initial guess factors: 0.1, 0.5, 2.0; are shown in the figure); the results show that the overall agreements are reasonably good while the speed of convergence might be affected by the initial guess.

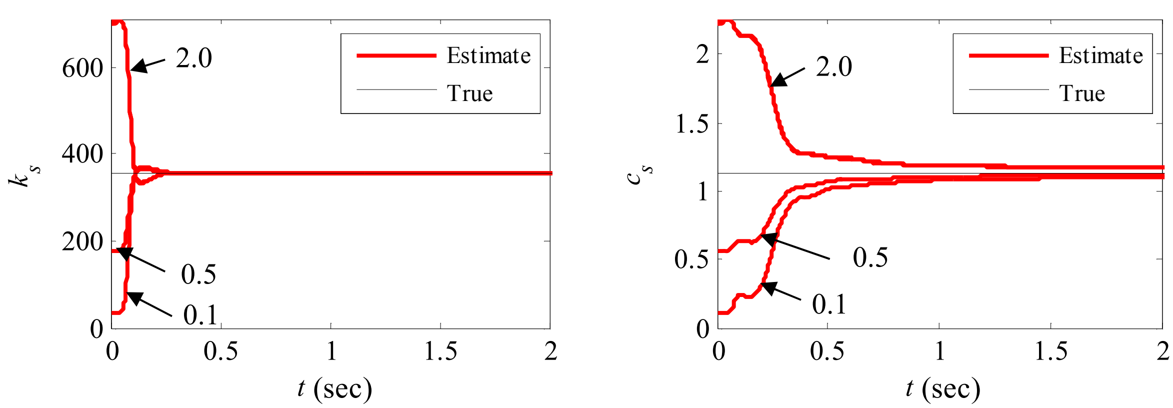

(a) Estimated parameter k_s (b) Estimated parameter c_s

Figure 5-21 Real time parameter estimation results using the EKF for an SDOF linear system

Example 5.10 **: Effects of selection of the covariance matrices on the EKF estimator performance**

The effects of the selection of the covariance matrices are investigated numerically. Three different initial covariance matrices P_0 are selected as the diagonal matrix whose elements are the square of the 0.005%, 0.05% and 50% of the true parameters; $P_0 = \mathrm{diag}([0\ \ 0\ \ k_{s,o}{}^2\ \ c_{s,o}{}^2]^T \times 0.00005$; $P_0 = \mathrm{diag}([0\ \ 0\ \ k_{s,o}{}^2\ \ c_{s,o}{}^2]^T \times 0.005$; $P_0 = \mathrm{diag}([0\ \ 0\ \ k_{s,o}{}^2\ \ c_{s,o}{}^2]^T \times 0.5)$. The initial guesses of the unknown parameters $\underline{\hat{\theta}}_0 = 0.5 \times \underline{\theta}^*$ for all cases. The comparisons between the true parameters: k_s the elastic stiffness and c_s the damping coefficient; and the estimate of the true parameters are shown in Figure 5-22 (the selected initial covariance matrix factors: 0.005%, 0.05% and 50%; are shown in the figure); the results show that the lager covariance matrix might lead faster estimation, but might occur larger overshooting at the beginning of estimation while the overall agreements are reasonably good.

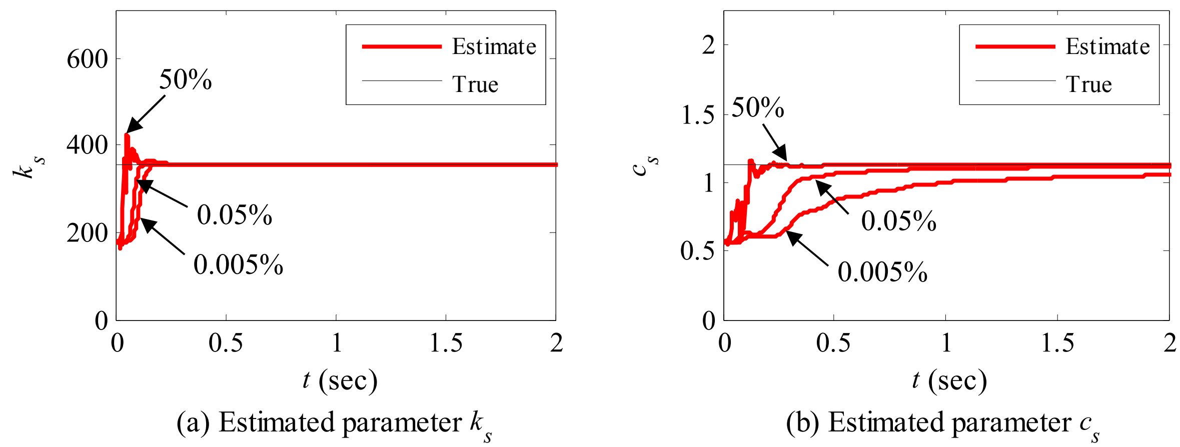

Figure 5-22 Real time parameter estimation results using the EKF for an SDOF linear system

5.3 Comparison between the Least Squares Method and Extended Kalman Filter

The *least squares* method (LS) and the *extended Kalman filter* (EKF) are introduced as real time parameter estimation methods for the tracking control of nonlinear hysteretic systems with unknown parameters. Even though both methods can be used, each one has different advantages over the other one as summarized below.

One of the most important features of the LS is that it can be shown the estimation error converges to zero $\varepsilon(t) \rightarrow 0$ as $t \rightarrow \infty$ with proper design of the estimator for systems whose unknown parameters vary linearly (Ioannou et al., 2006). However, the nonlinear hysteretic system with hardening after yielding ($\alpha > 0$) cannot be modeled in the form of the linear parametric model as shown in Section 5.1.1.3.

Unlike the LS, it is very difficult to show a certain stability property of the EKF estimator due to the approximation error in the first order Taylor expansion (Crassidis et al., 2012). Nevertheless, the EKF has important advantages; (i) the method can be applied to more complex nonlinear systems including the nonlinear hysteretic system with hardening after yielding as shown in 5.2.1.2; (ii) the EKF requires less measurements, which is more realistic and might make the EKF more practical than the LS; for example, the parameter identification can be performed using only the total accelerations (Wu and Smyth, 2007) while the LS requires more measurements, and (iii) in addition the EKF can be used not only to estimate the unknown parameters, but also to estimate the true state vector from the measurements with associated noise (as discussed in Section 5.2); i.e. both estimates of the true state vector and unknown parameters are required for the tracking control schemes.

Therefore, the EKF is adopted in this study, as the real time parameter estimator for further development of the adaptive tracking control.

SECTION 6
TRACKING CONTROL FOR LINEAR SYSTEMS WITH UNKNOWN PARAMETERS

The feedback tracking control methods and the real time parameter identification method, which were separately presented in the preceding sections, are combined herein, and new adaptive tracking control schemes are introduced. The two feedback tracking control methods; namely, the *predictive tracking control* (PTC) and the *feedback linearized tracking control* methods (FTC), combined with the *extended Kalman filter* (EKF) for the real time parameter estimation, are applied to linear systems control in this section. The methods are then extended to the nonlinear hysteretic systems in the following section.

6.1 Predictive Tracking Control with Real-time Parameter Estimation

In Section 3.3.1, the predictive control method was used to develop the control law for linear system tracking problems with known parameters. The control excitation input u_k to reduce the predicted tracking error (i.e. $e_{k+1} = \hat{y}_{k+1} - y_{k+1}$) is shown in Eq. (3-39). When there are unknown parameters in a given system to be controlled, the parameters can be estimated in real time using the system parameter estimator such as the extended Kalman filter, introduced in the previous section. The estimated parameters $\underline{\hat{\theta}}_k$ at instant $k\Delta t$ are used instead of known constant parameters $\underline{\theta}^*$. The control law equation with the estimated parameters at instants becomes

Control Law

$$u_k = \left[\hat{B}_{D,k}^{*\,T} Q \hat{B}_{D,k}^{*} + R\right]^{-1} \hat{B}_{D,k}^{*\,T} Q \left[y_{m,k+1} - \hat{A}_{D,k}^{*} \hat{\underline{x}}_k\right] = \hat{\Gamma}_k \left[y_{m,k+1} - \hat{A}_{D,k}^{*} \hat{\underline{x}}_k\right] \tag{6-1}$$

where the *hat* ^ indicates that the system matrix uses the estimated parameters $\underline{\hat{\theta}}_k$, and

$$\hat{\Gamma}_k = \left[\hat{B}_{D,k}^{*\,T} Q \hat{B}_{D,k}^{*} + R\right]^{-1} \hat{B}_{D,k}^{*\,T} Q, \quad \hat{A}_{D,k}^{*} = \hat{C}_{D,k} \hat{A}_{D,k}, \quad \hat{B}_{D,k}^{*} = \hat{C}_{D,k} \hat{B}_{D,k}, \quad \hat{A}_{D,k} = e^{\hat{A}_k \Delta t}, \quad \hat{B}_{D,k} = \int_0^{\Delta t} e^{\hat{A}_k \tau} d\tau \hat{B}_k$$

and the system matrices $\hat{A}_{D,k}$ and $\hat{B}_{D,k}$ and the output matrix $\hat{C}_{D,k}$ (i.e. $\hat{C}_{D,k} = \hat{C}_k$) are updated at every instant $k\Delta t$ with estimated parameters, $\underline{\hat{\theta}}_k = [\hat{k}_{s,k} \;\; \hat{c}_{s,k}]^T$ of the true parameters $\underline{\theta}^* = [k_s \;\; c_s]^T$; for example, the continuous-time system matrices of the linear SDOF system shown in Eq. (2-26) with estimated parameters $\underline{\hat{\theta}}_k$ are

$$\hat{A}_k = \begin{bmatrix} 0 & 1 \\ -\hat{k}_{s,k}/m & -\hat{c}_{s,k}/m \end{bmatrix}, \qquad B = \begin{bmatrix} 0 \\ 1/m \end{bmatrix}$$

and the output matrix $\hat{C}_k$ is defined according to the target motion. For example, if the target motions are the displacement and velocity $\underline{y}_m = [x_m \;\; \dot{x}_m]^T$, the matrix $\hat{C}_{D,k} = I_{2\times 2}$ that is an identity (constant) matrix, and if the target is the total acceleration $y_m = \ddot{x}_m^{\,t}$, the matrix $\hat{C}_{D,k} = [-\hat{k}_{s,k}/m \quad -\hat{c}_{s,k}/m]^T$. The control excitation input u_k can be calculated using Eq. (6-1). The predicted response can be obtained by substituting the computed control input u_k into Eq. (3-36):

Expected Achieved Responses

$$\hat{y}_{k+1} = C_D\left[\left\{A_D - B_D\hat{\Gamma}_k\hat{A}^*_{D,k}\right\}\underline{\hat{x}}_k + B_D\hat{\Gamma}_k y_{m,k+1}\right] \tag{6-2}$$

where $\hat{\Gamma}_k$ and $\hat{A}^*_{D,k}$ are defined in Eq. (6-1). If $B_D^* = C_D B_D$ is an invertible matrix, and $R = 0$ and $Q = I$ (i.e. I = identity matrix) are chosen, then Eq. (6-2) becomes

$$\hat{y}_{k+1} = \left[A_D^* - \left(B_D^*\hat{B}_{D,k}^{*\,-1}\right)\hat{A}^*_{D,k}\right]\underline{\hat{x}}_k + \left(B_D^*\hat{B}_{D,k}^{*\,-1}\right)y_{m,k+1} \tag{6-3}$$

where $A_D^* = C_D A_D$ and $B_D^* = C_D B_D$ are the true system matrices.

Stability

The predicted tracking error equation might be obtained from Eq. (6-3) by collecting the tracking error term $e_{k+1} = \hat{y}_{k+1} - y_{m,k+1}$ in the left-hand side and the estimate error terms in the right-hand side:

$$e_{k+1} = g_{k+1}\left(\underline{\tilde{\theta}}_k, \underline{\hat{x}}_k, y_{m,k+1}\right) \tag{6-4}$$

where the function g_{k+1} indicates some residual error caused by parameter estimate error $\underline{\tilde{\theta}}_k = \underline{\hat{\theta}}_k - \underline{\theta}^*$. The tracking error e_{k+1} will decrease when the estimated parameters error $\underline{\tilde{\theta}}_k$ becomes smaller. As discussed in Section 5.3, the stability of the error dynamics cannot be analyzed analytically because of the lack of knowledge of the stability properties of the *extended Kalman filter* (EKF), so the performance of the adaptive tracking control method introduced is examined using the numerical simulation in Section 6.4.

Limitations of Shake Table-Structure Systems

As discussed in Section 3.3.1, for the shake table-structure 2DOF model, the predicted output $\hat{y}_{k+1}$ in discrete time or $\hat{y}(t+h)$ in continuous time might be approximated including higher order differentiations when the product of the output and input matrices $C \times B$ is singular. Using the approximated predicted output $\hat{y}^*(t+h)$ and the target motion $y_m^*(t+h)$ (shown in Eq. (3-44)), the control law is established as shown in Eq. (3-46). When some parameters are unknown, the control input $u(t)$ can be computed using the estimated parameters $\underline{\hat{\theta}}(t)$ at instant time as following:

Control Law

$$u(t) = \left[\hat{B}^*\left(\underline{\hat{\theta}}\right)^T Q\hat{B}^*\left(\underline{\hat{\theta}}\right) + R\right]^{-1}\hat{B}^*\left(\underline{\hat{\theta}}\right)^T Q\left[y_m^*(t+h) - \hat{A}^*\left(\underline{\hat{\theta}}\right)\underline{\hat{x}}(t)\right] \tag{6-5}$$

where $\hat{A}^*(\hat{\underline{\theta}})= [\hat{C}(\hat{\underline{\theta}}) + h\hat{C}(\hat{\underline{\theta}})\hat{A}(\hat{\underline{\theta}}) + (h^2/2)\hat{C}(\hat{\underline{\theta}})\hat{A}(\hat{\underline{\theta}})^2]$ and $\hat{B}^*(\hat{\underline{\theta}})= (h^2/2)\hat{C}(\hat{\underline{\theta}})\hat{A}(\hat{\underline{\theta}})B$. By substituting Eq. (6-5) into the second equation of Eq. (3-45), one can establish the error dynamics. For a system having $\hat{B}^*(\hat{\underline{\theta}})$ as a non-zero scalar (i.e. an invertible matrix, size 1 × 1) and $R = 0$ chosen, $\ddot{y}(t)$ becomes as described below:

Expected Achieved Responses

$$\ddot{y}(t) = CA^2\underline{\hat{x}}(t) + CAB\left[\hat{B}^*\left(\hat{\underline{\theta}}\right)\right]^{-1}\left[y_m^*(t+h) - \hat{A}^*\left(\hat{\underline{\theta}}\right)\underline{\hat{x}}(t)\right] \tag{6-6}$$

which can be rewritten introducing the tracking error ($e(t) = y(t) - y_m(t)$) to show its dynamics

$$\ddot{e}(t) + (2/h)\dot{e}(t) + \left(2/h^2\right)e(t) = g\left(\underline{\tilde{\theta}}(t), \underline{\hat{x}}(t), y_m^*(t+h)\right) \tag{6-7}$$

where the function $g(\cdot)$ indicates some residual error, which are caused by the parameter estimation error $\underline{\tilde{\theta}}(t) = \underline{\hat{\theta}}(t) - \underline{\theta}^*$. The tracking error $e(t)$ will decrease when the estimated parameters error $\underline{\tilde{\theta}}(t)$ is reduced. As discussed in Section 5.3, the performance of the adaptive tracking controller is examined by means of the numerical simulations in Section 6.4.

6.2 Feedback Linearization Tracking Control with Real-time Parameter Estimation

Another possible tracking control scheme introduced in Section 3.3.2 is the *Feedback Linearization Tracking Control* (FTC) (Ioannou and Fidan, 2006). FTC can be also used for systems with unknown parameters by using the real time estimator such as the *extended Kalman filter* (EKF).

For the simplest case with a first order system as first presented in Section 3.3.2, the equations of the true system and the reference model are shown in Eq. (3-49) and (3-50). In order to achieve the tracking control objective, the tracking control law is established as shown in Eq. (3-56). With unknown parameters; for example if the parameter a in Eq. (3-49) is unknown, the possible control law is

Control Law

$$u(t) = \frac{1}{cb}\left[-c\hat{a}(t)x(t) + \left\{\dot{y}_m(t) - k_1^*e(t)\right\}\right] \tag{6-8}$$

where $\hat{a}(t)$ is the estimate of the true parameter a in real time, and the tracking error $e(t) = y(t) - y_m(t)$. By substituting this control input $u(t)$ into Eq. (3-51), it is obtained:

$$\dot{y}(t) = -c\tilde{a}(t)x(t) + \left\{\dot{y}_m(t) - k_1^*e(t)\right\} \tag{6-9}$$

where the parameter estimate error $\tilde{a}(t) = \hat{a}(t) - a$. From this equation, the tracking error dynamics can be shown below

Expected Achieved Responses

$$\dot{e}(t) + k_1^*e(t) = -c\tilde{a}(t)x(t) \tag{6-10}$$

One may establish an adaptive law for the real time parameter estimation using the Lyapunov method or the least squares method (Ioannou and Sun, 2012), such that the tracking error signal $e(t)$ goes to zero as time goes to infinity. However, this approach is not applicable to the nonlinear hysteretic system as discussed in Section 5.3. Therefore, the EKF is used as the real time estimator, and the performance of the adaptive tracking control method introduced is examined using the numerical simulation, presented in Section 6.4.

Application to SDOF Linear Structures

For a linear structure (the SDOF system model) expressed in Eq. (2-26) with the output $y(t)$ of the total acceleration response $\ddot{x}_s^t(t)$ at the structure, the tracking control law is established as shown in Eq. (3-58) for known parameters. With unknown parameters, the possible control law using the estimate $\underline{\hat{\theta}}(t) = [\hat{k}_s(t)\ \hat{c}_s(t)]^T$ of the true parameters $\underline{\theta}^* = [k_s\ \ c_s]^T$; becomes

<u>Control Law</u>

$$u(t) = \left(-\hat{c}_s(t) m_s^{-2}\right)^{-1}\left[-\dot{y}^*(t) + v(t)\right] \tag{6-11}$$

where $\dot{y}^*(t)$ is defined as

$$\dot{y}^*(t) = m_s^{-2}\hat{c}_s(t)\left[\hat{c}_s(t)\dot{x}_s(t) + \hat{k}_s(t)x_s(t)\right] - m_s^{-1}\hat{k}_s(t)\dot{x}_s(t) \tag{6-12}$$

and $v(t)$ is selected to reduce the tracking error as

$$v(t) = \dot{y}_m(t) - k_1^* e(t) \tag{6-13}$$

in which $e(t) = y(t) - y_m(t)$ and $y(t) = -m_s^{-1}[\hat{c}_s(t)\,\dot{x}_s(t) + \hat{k}_s(t)\,x_s(t)]$. Substituting $u(t)$ from Eq. (6-11) into the equation of the differentiated output $\dot{y}(t)$ (shown in Eq. (B-3) in Appendix 3.1) and collecting the tracking error terms $e(t)$ to the left-hand side and residual error terms due to estimation error to the right-hand side leads to the following tracking error dynamic equation:

<u>Expected Achieved Responses</u>

$$\dot{e}(t) + k_1^* e(t) = g\left(\underline{\tilde{\theta}}(t), \underline{x}(t), \underline{y}_m(t)\right) \tag{6-14}$$

where the function $g(\cdot)$ indicates some residual error caused by parameter estimate error $\underline{\tilde{\theta}}(t) = \underline{\hat{\theta}}(t) - \underline{\theta}^*$. The tracking error $e(t)$ will decrease when the estimated parameters error $\underline{\tilde{\theta}}(t)$ becomes smaller. The performance of this adaptive tracking controller is examined using the numerical simulation in Section 6.4.

Application to 2DOF Shake Table-Linear Structure Systems

For a linear structure mounted on a shake table (the 2DOF system model) expressed in Equations (2-24) and (2-25) with the output $y(t)$ of the total acceleration response $\ddot{x}_s^t(t)$ at the structure, the tracking control law is established as shown in Eq. (3-66) for known parameters. With unknown parameters, the possible control law using the estimate $\underline{\hat{\theta}}(t) = [\hat{k}_s(t)\ \ \hat{c}_s(t)]^T$ of the true parameters $\underline{\theta}^* = [k_s\ \ c_s]^T$ becomes

Control Law

$$u^*(t) = \hat{a}(t)^{-1}\left[-\ddot{y}^*(t) + v(t)\right] \tag{6-15}$$

where $u^*(t) = (\omega_a^2 k_a)^{-1} u(t)$; $u(t) = x_d(t)$; and $\ddot{y}^*(t)$ is defined as

$$\begin{aligned}\ddot{y}^*(t) = &\left[\hat{a}(t)\left(\hat{a}(t)+\hat{c}(t)\right)-\hat{b}(t)\right]\ddot{x}_s(t) + \hat{a}(t)\left(\hat{b}(t)+\hat{d}(t)\right)\dot{x}_s(t)\\ &+\left(-\hat{a}(t)e\right)f_a^*(t)+\left(-\hat{a}(t)f\right)\dot{x}_t(t)+\left(-\hat{a}(t)g\right)x_t(t)\end{aligned} \tag{6-16}$$

in which several functions are clustered for simplification:

$$\begin{aligned}&\hat{a}(t) = m_s^{-1}\hat{c}_s(t); \quad \hat{b}(t) = m_s^{-1}\hat{k}_s(t); \quad \hat{c}(t) = m_t^{-1}\hat{c}_s(t); \quad \hat{d}(t) = m_t^{-1}\hat{k}_s(t);\\ &e = 2\xi_a\omega_a; \quad f = \omega_a^2; \quad g = \omega_a^2 k_a;\\ &f_a^*(t) = f_a(t)/m_t; \quad u^*(t) = \omega_a^2 k_a x_d(t), \quad u(t) = x_d(t)\end{aligned} \tag{6-17}$$

$v(t)$ is selected to reduce the tracking error as

$$v(t) = \ddot{y}_m(t) - k_1^*\dot{e}(t) - k_2^* e(t) \tag{6-18}$$

in which $e(t) = y(t) - y_m(t)$ with $y(t) = -m_s^{-1}[\hat{c}_s(t)\,\dot{x}_s(t) + \hat{k}_s(t)\,x_s(t)]$; and $\dot{e}(t) = \dot{y}(t) - \dot{y}_m(t)$ with $\dot{y}(t) = -m_s^{-1}\,[\hat{c}_s(t)\,\ddot{x}_s(t) + \hat{k}_s(t)\,\dot{x}_s(t)]$. Substituting $u^*(t)$ from Eq. (6-15) into the differentiated output equation $\ddot{y}(t)$ (shown in Eq. (B-14) in Appendix B.2) and collecting the tracking error terms $e(t)$ to the left-hand side and residual error terms due to estimation error to the right-hand side gives the tracking error dynamic equation:

Expected Achieved Responses

$$\ddot{e}(t) + k_1^*\dot{e}(t) + k_2^* e(t) = g\left(\underline{\tilde{\theta}}(t), \underline{x}(t), \underline{y}_m(t)\right) \tag{6-19}$$

where the function $g(\cdot)$ indicates some residual error, which are caused by parameter estimate error $\underline{\tilde{\theta}}(t) = \underline{\hat{\theta}}(t) - \underline{\theta}^*$. The tracking error $e(t)$ will diminish when the estimated parameters error $\underline{\tilde{\theta}}(t)$ is reduced. As discussed in Section 5.3, the performance of this adaptive tracking controller using the EKF is examined by means of the numerical simulations in Section 6.4.

6.3 Comparisons of Feedback Tracking Control Methods

As discussed in Section 3.3.3, one can show that the two tracking control methods are equivalent for the shake table-structure system under certain conditions and with known parameters. For the unknown parameters, the formulations of the control laws for the two tracking control methods have not changed;

therefore, one can also show that the predictive tracking control law shown in Eq. (6-5) is the same as the control law (shown in Eq. (6-15)) of the feedback linearization tracking control method with the same conditions applied to the known parameter controllers; i.e. the controlled system has $B(\underline{x})^* =$ a non-zero scalar (i.e. an invertible matrix, size 1 × 1), and $R = 0$ chosen, and the tracking error coefficients in Eq. (4-20) are $k_1^* = 2 / h = 2\xi_e\omega_e$ and $k_2^* = 2 / h^2 = \omega_e^2$; therefore, $\xi_e = \sqrt{2} / 2 \approx 0.707$ and $h = \sqrt{2} / \omega_e$.

6.4 Numerical Examples and Comparisons of Tracking Control Methods

Simple tracking control examples (as demonstrated in Section 3.4 and Section 4.5 for the systems with known parameters) are analyzed in order to examine the performance of the introduced two feedback tracking control methods combined with the real time parameter estimation for linear systems with unknown parameters. The results are presented herein. For all examples, the target motion is the total acceleration of a structure (specimen) mounted on the shake table.

6.4.1 Examples of Linear Structures (SDOF System Model)

As discussed in Section 2.2, to facilitate the development of the tracking control method, first, a simplified SDOF system model is used instead of a 2DOF system model for a shake table with an SDOF structure system. In this simplified system model (shown in Figure 6-1), the excitation force $-m_s\ddot{x}_t(t)$ due to the shake table acceleration $\ddot{x}_t(t)$ is considered as a new control input $u(t)$. However, the actual control excitation input $u(t)$ for the 2DOF system model is the desired displacement $x_d(t)$ of the shake table, and $u(t)$ shall be computed including the shake table dynamics and the shake table-structure interaction (as discussed in Section 2.2) as formulated in the following section (Section 6.4.2).

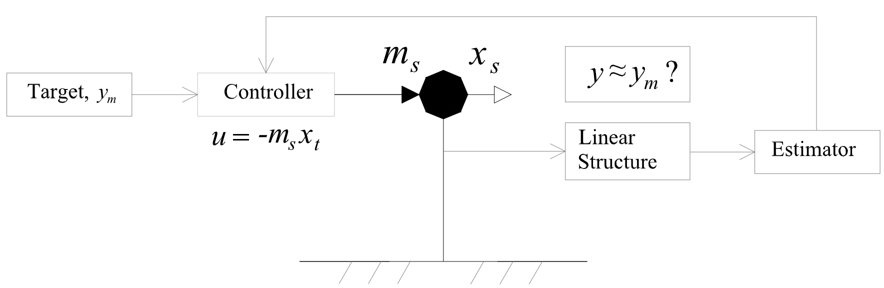

Figure 6-1 Tracking control of an SDOF nonlinear system with unknown parameters

The governing equation of an SDOF linear structure subjected to the shake table excitation is shown in Eq. (2-26). The tracking control task for this simplified system is to compute the control excitation input $u(t) = -m_s\ddot{x}_t(t)$ at every instant using the real time estimated parameters so that the system output $y(t) = \ddot{x}_s^t(t)$ (the total acceleration of the structure) follows the target motion $y_m(t) = \ddot{x}_m^t(t)$ (the total acceleration of the reference model).

Example 6.1* : *An SDOF Linear System with Unknown Parameters using PTC

The properties of the given system are: m_s = 1 kips·sec^2/in., k_s = 355 kips/in., and c_s = 1.13 kips·sec/in., (f_n = 3.0 Hz, ξ_n = 0.03), the same as the ones in Example 3.1. In order to examine the effects of measurement noise, a zero-mean Gaussian white-noise process of 3% RMS noise-to-signal are added to the measurements $\underline{\overline{y}}_k = [\overline{x}_{s,k}\ \ \dot{\overline{x}}_{s,k}\ \ \overline{f}_{S,k}]^T$, which are described in Section 5.2.1.2 (i.e. the EKF estimator is developed for a nonlinear system in Section 5.2.1.3, but, of course, this is capable for this linear system as well since a linear system is a special case of nonlinear systems having $k_T(\underline{x}) \rightarrow k_s$; thus $f_S(\underline{x}) = k_s x(t)$). Two unknown parameters: c_s the damping coefficient and k_s the elastic stiffness; are selected and estimated in real time using the extended Kalman filter.

The target motion is shown in Figure 6-3 (a) [Target]. The target motion is the total acceleration output generated from the same reference linear system (f_m = 5.0 Hz, ξ_m = 0.1), used for Example 3.1. in Section 3.4.1. The reference model is subjected to high-pass-filtered one-cycle sine input, whose frequency is 1.0 Hz. The reference excitation input and the responses of the reference model are presented in Appendix A.2. For the parameter estimation, the initial parameter estimate $\underline{\hat{\theta}}_0$ is chosen as $\underline{\hat{\theta}}_0 = 0.5 \times \underline{\theta}^*$ (50% error in the initial guess), and the initial covariance matrix is chosen as $P_0 = \mathrm{diag}([0\ \ 0\ \ 0\ \ \hat{c}_{s,o}{}^2\ \ \hat{k}_{s,o}{}^2\ \ 0\ \ 0]^T \times 0.01)$. The covariance matrices Q_E and R_E are chosen as follows: $Q_E = 0 \times I_{7\times7}$ (all zeroes) and the R_E = diagonal matrix, whose elements; i.e. noise variance = 3% × corresponding signal variance (noise variances are assumed to be known from the instruments information). The time step of 0.002 sec is used for the simulation.

The tracking control results using the *predictive tracking control* (PTC) method with the real time parameter estimations are presented in Figure 6-2 and Figure 6-3. The selected control parameters for the PTC in this example are R = 0.0003 and Δt = 0.002. Figure 6-2 shows the comparisons between the estimated parameters: k_s the elastic stiffness and c_s the damping coefficient; and the true parameters, and they show very good agreements. The controlled output, $\ddot{x}_s{}^t(t)$ the total acceleration of the structure, is shown in Figure 6-3 (a) [Controlled] and also shows very good agreement with the target motion. The computed control excitation input, $u(t) = -m_s\ddot{x}_t(t)$, using the control law in Eq. (6-5) is shown in Figure 6-3 (b). $x_s(t)$, $\dot{x}_s(t)$ the achieved displacement and velocity responses of the controlled structure are also presented in Figure 6-3 (c) and (d); it is noted that unlike the total acceleration, the displacement and velocity responses are different from ones of the reference because the system properties of the controlled system and ones of the reference system are different. The relation between the structure resisting force $f_S(t)$ having hysteretic behavior and displacement $x_s(t)$ is also presented in Figure 6-3 (e). As desired, all responses of the controlled system are bounded.

The tracking control results using the *feedback linearization tracking control* (FTC) method are presented in Figure 6-4 and Figure 6-5. Figure 6-4 presents the results of the parameter estimation in real time. The controlled output $\ddot{x}_s^t(t)$ is shown in Figure 6-5 (a) [Controlled]; it shows very good agreement with the target motion. The computed control excitation input, $u(t) = -m_s\ddot{x}_t(t)$, using the control law in Eq. (6-11) is shown in Figure 6-5 (b). The selected control parameter in this example for the FTC is $k_1^* = \frac{1}{\Delta t}/100$ (i.e. the smaller value of k_1^* than that of the system with the known parameter case in Section 3.4.1 is chosen due to the uncertainty and indicates that the tracking error will decrease slowly). It is noted that if the control parameters are carefully chosen to satisfy the tracking object, the control excitation input for the two methods (PTC and FTC) are very similar; therefore, as expected, the control results of two methods are very similar as shown in Figure 6-2 through Figure 6-5.

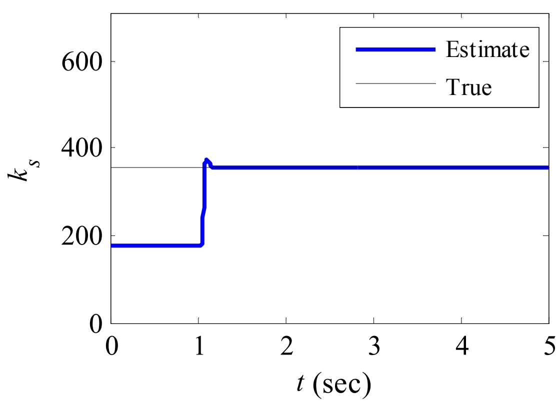

(c) Estimated parameter k_s

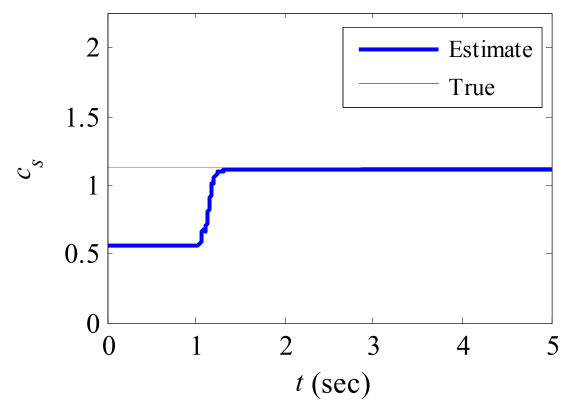

(b) Estimated parameter c_s

Figure 6-2 Real time parameter estimation results of the PTC for an SDOF linear system

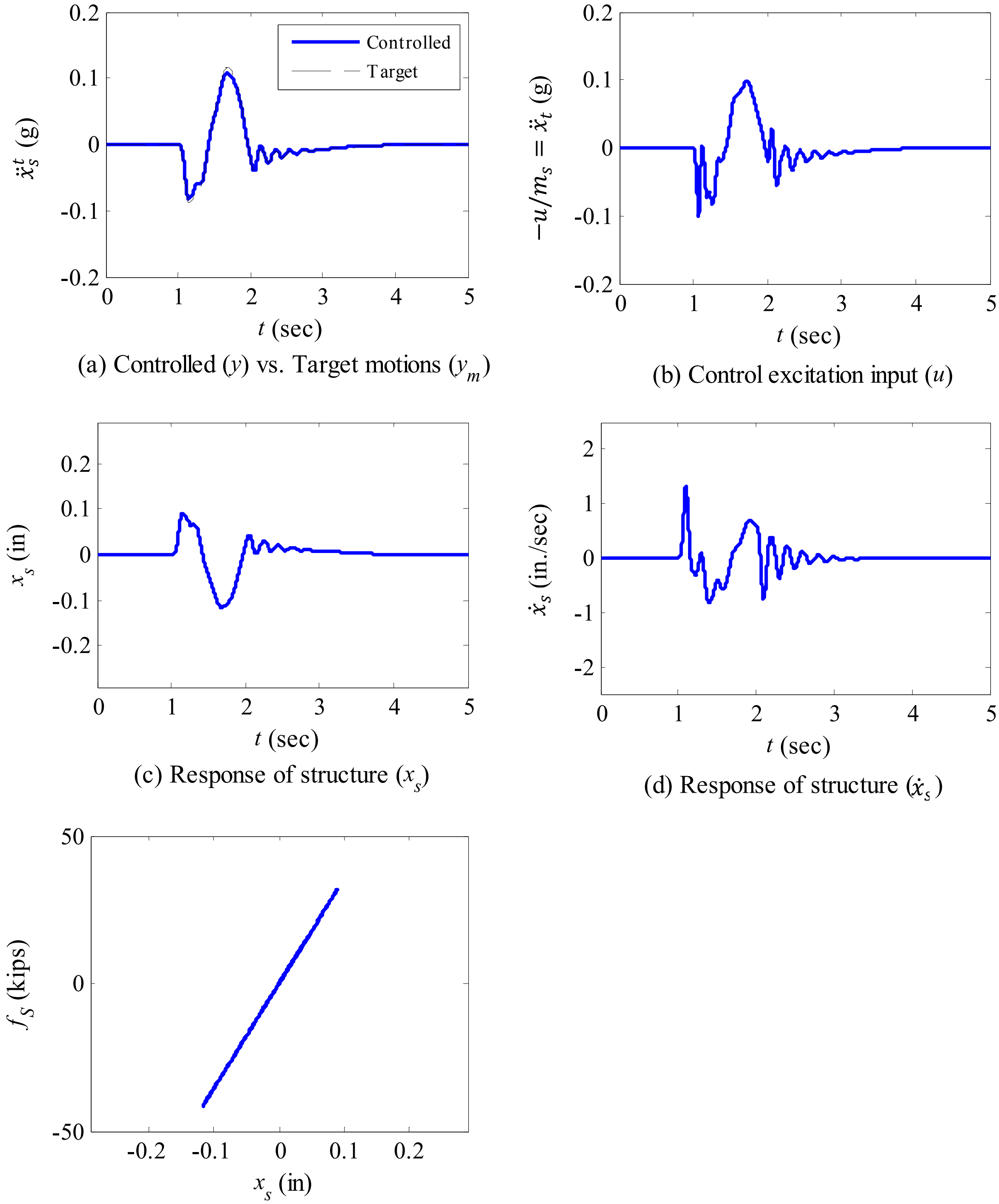

(a) Controlled (y) vs. Target motions (y_m)

(b) Control excitation input (u)

(c) Response of structure (x_s)

(d) Response of structure ($\dot{x}_s$)

(e) Response of structure (f_S vs. x_s)

Figure 6-3 PTC - structure responses for an SDOF linear system with real time estimation

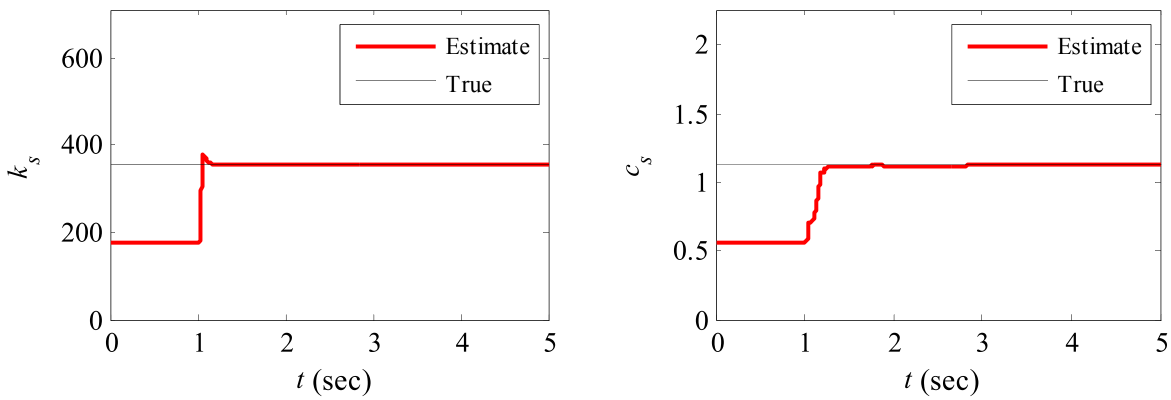

(c) Estimated parameter k_s

(b) Estimated parameter c_s

Figure 6-4 Real time parameter estimation results of the FTC for an SDOF linear system

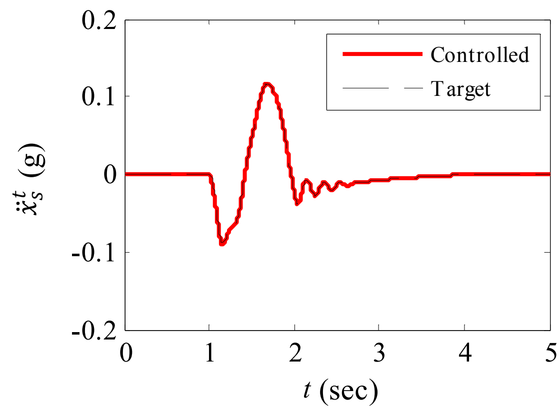

(a) Controlled (y) vs. Target motions (y_m)

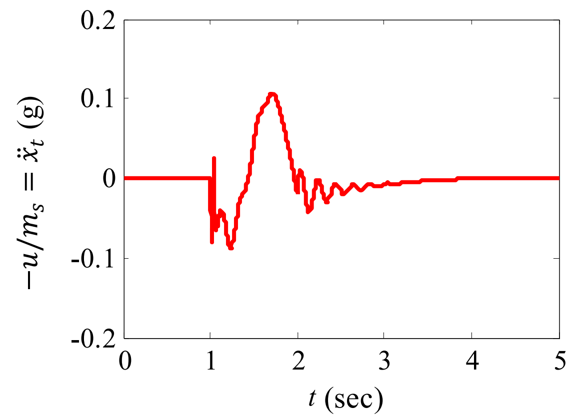

(b) Control excitation input (u)

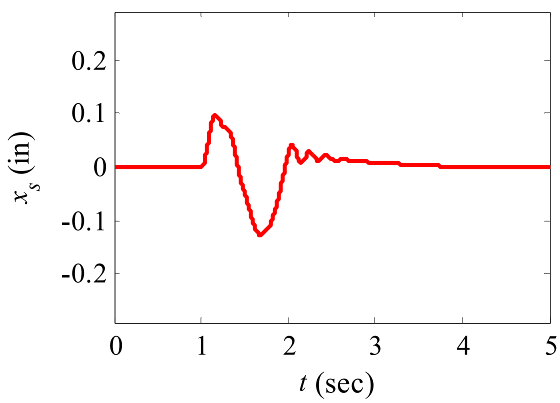

(c) Response of structure (x_s)

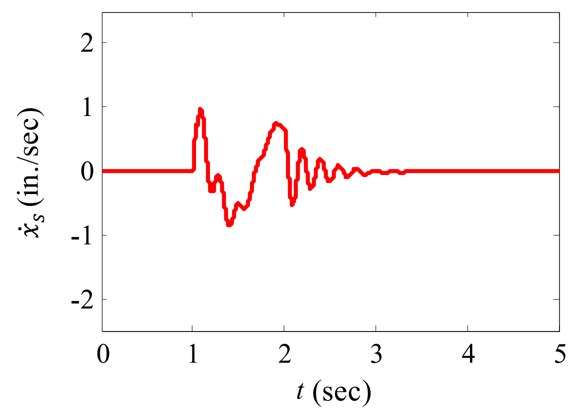

(d) Response of structure ($\dot{x}_s$)

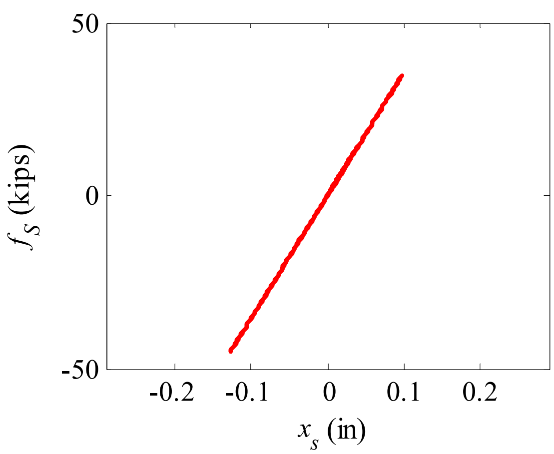

(e) Response of structure (f_S vs. x_s)

Figure 6-5 FTC - structure responses for an SDOF linear system with real time estimation

6.4.2 Examples of Shake Table - Linear Structures (2DOF System Model)

As discussed in Section 2.2, the shake table dynamics affect the performance of the control system and the interaction between the shake table and the mounted structure has to be considered. The same tracking control example (described in Section 6.4.1) is resolved for the 2DOF linear system considering the interaction, as expressed in Eq. (2-24) and Eq. (2-25), and schematically shown in Figure 6-6.

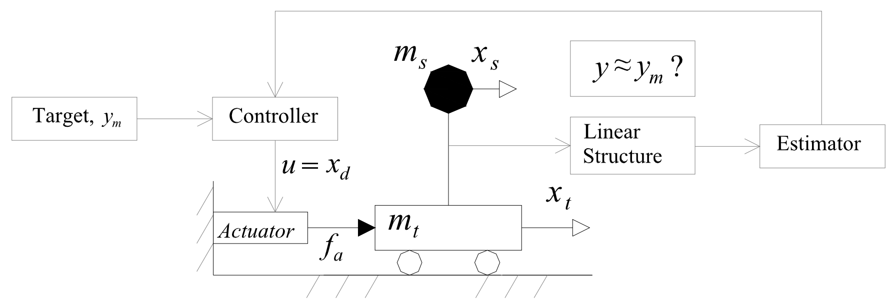

Figure 6-6 Tracking control of the shake table- structure 2DOF linear system with unknown parameters

When a target motion is specified for the specimen, the required control excitation input $u(t) = x_d(t)$, the desired shake table displacement is determined at every instant using the real time estimated parameters such that the output of the system ($y(t) = \ddot{x}_s^t(t)$, i.e. the total acceleration of the structure) follows the target motion $y_m(t)$.

Example 6.2* : *A 2DOF Linear System with Unknown Parameters

The properties of a given system are: m_s = 1 kips·sec^2/in., k_s = 355 kips/in., and c_s = 1.13 kips·sec/in., (f_n = 3.0 Hz, ξ_n = 0.03) for the mounted structure, and $\mu = m_s / m_t = 0.1$, $f_{n,a}$ = 30.0 Hz, ξ_a = 0.5 and k_a = 25 for the shake table, the same as the ones in Example 3.2. In order to examine the measurement noise effects, a zero-mean Gaussian white-noise process of 3% RMS noise-to-signal are added to the measurements $\underline{\bar{y}}_k = [\bar{x}_{s,k}\ \ \bar{\dot{x}}_{s,k}\ \ \bar{f}_{S,k}\ \ \bar{x}_{t,k}\ \ \bar{\dot{x}}_{t,k}\ \ \bar{f}_{a,k}/m_t]^T$, which are described in Section 5.2.1.3 (i.e. the EKF estimator is developed for a nonlinear system in Section 5.2.1.3, but, of course, this is capable for this linear system as well since a linear system is a special case of nonlinear systems having $k_T(\underline{x}) \rightarrow k_s$; thus $f_S(\underline{x}) = k_s x(t)$). Two unknown parameters: c_s the damping coefficient and k_s the elastic stiffness; are selected and estimated in real time using the extended Kalman filter.

The target motion is shown in Figure 6-8 (a) [Target]. The target motion is the total acceleration output generated from the same reference linear system (f_m = 5.0 Hz, ξ_m = 0.1), used for Example 6.1. in Section 6.4.1 (the reference input and the responses of the reference model are presented in Appendix A.2). For the parameter estimations, the initial parameter estimate $\underline{\hat{\theta}}_0$ is chosen as $\underline{\hat{\theta}}_0 = 0.5 \times \underline{\theta}^*$ (50%

error in the initial guess), and the initial covariance matrix is chosen as P_0 = diag([0 0 0 0 0 0 $\hat{c}_{s,o}{}^2$ $\hat{k}_{s,o}{}^2$ 0 0]^T × 0.01). The covariance matrices Q_E and R_E are chosen as follows: $Q_E = 0 \times I_{10\times10}$ (all zeroes) and the R_E = diagonal matrix, whose elements; i.e. noise variance = 3% × corresponding signal variance (noise variances are assumed to be known from the instruments information). The time step of 0.002 sec is used for the simulation.

The tracking control results using the *predictive tracking control* (PTC) method with the real time parameter estimations are presented in Figure 6-7 and Figure 6-9. The selected control parameters in this example $R = 0$ and $h = \sqrt{2} / \omega_e$ where $\omega_e = 100$. Figure 6-7 shows the comparisons between the estimated parameters: c_s the damping coefficient and k_s the elastic stiffness; and the true parameters, and they show very good agreements. The controlled output, $\ddot{x}_s{}^t(t)$ the total acceleration of the structure, is shown in Figure 6-8 (a) [Controlled] and also shows very good agreement with the target motion. The computed control excitation input, $u(t) = x_d(t)$, using the control law in. Eq. (6-5) is shown in Figure 6-8 (b). $x_s(t)$, $\dot{x}_s(t)$ the achieved displacement and velocity responses of the controlled structure are also presented in Figure 6-8 (c) and (d); it is noted that unlike the total acceleration (which was the target of the control design), the displacement and velocity responses are different from ones of the reference because the system properties of the controlled system and ones of the reference system are different. The relation between the structure resisting force $f_S(t)$ and displacement $x_s(t)$ is also presented in Figure 6-8 (e). Figure 6-9 presents the responses of the shake table; the achieved shake table actuator force $f_a(t)$, shake table acceleration $\ddot{x}_t(t)$, displacement $x_t(t)$ and velocity $\dot{x}_t(t)$. As desired, all responses of the controlled system are bounded.

The tracking control results using the *feedback linearization tracking control* (FTC) method with the real time parameter estimations are also presented in Figure 6-10 and Figure 6-12. Figure 6-10 presents the results of the parameter estimation in real time. The controlled output $\ddot{x}_s{}^t(t)$ is shown in Figure 7-11 (a) [Controlled] and shows very good agreement with the target motion. The computed control excitation input, $u(t) = x_d(t)$, using the control law in Eq. (6-15) is shown in Figure 6-11 (b). As discussed in Section 6.3, the control excitation inputs of the two methods (PTC and FTC) are the same if one chooses the tracking error coefficients as $k_1^* = 2 / h = 2\xi_e\omega_e$ and $k_2^* = 2 / h^2 = \omega_e{}^2$; therefore, $\xi_e = \sqrt{2} / 2 \approx 0.707$ and $h = \sqrt{2} / \omega_e$; (in this example, $\omega_e = 100$, $\xi_e = 0.707$ for the both methods). As expected, the control results of two methods are equivalent as shown in Figure 6-7 through Figure 6-12.

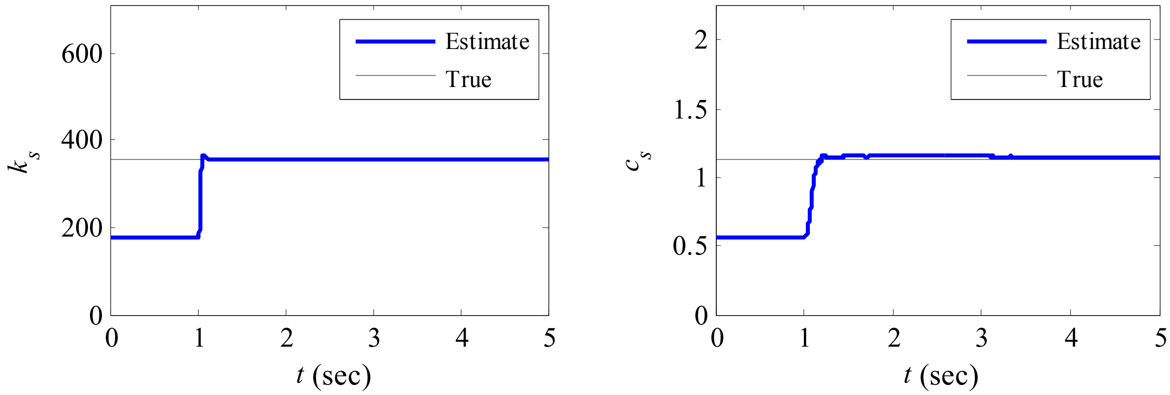

(c) Estimated parameter k_s

(b) Estimated parameter c_s

Figure 6-7 Real time parameter estimation results of the PTC for a 2DOF linear system

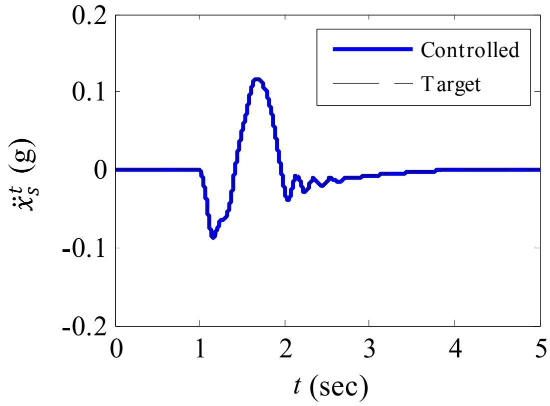

(a) Controlled (y) vs. Target motions (y_m)

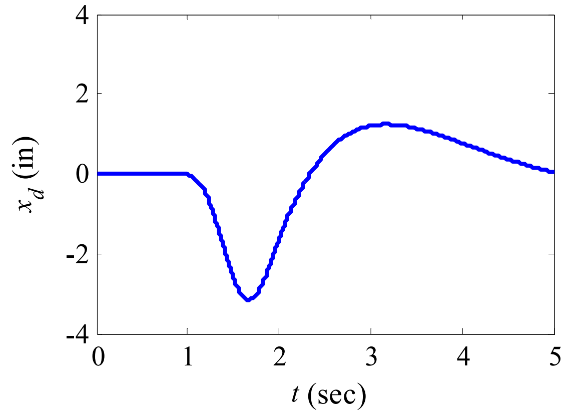

(b) Control excitation input (u)

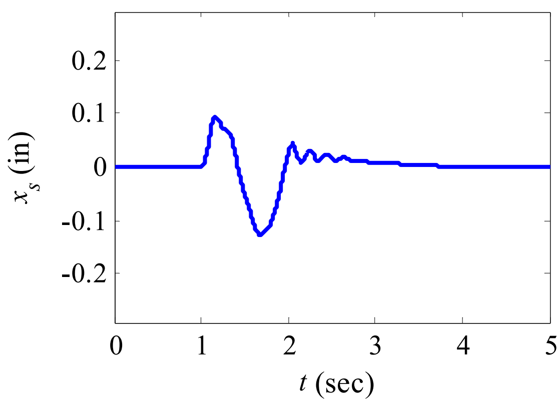

(c) Response of structure (x_s)

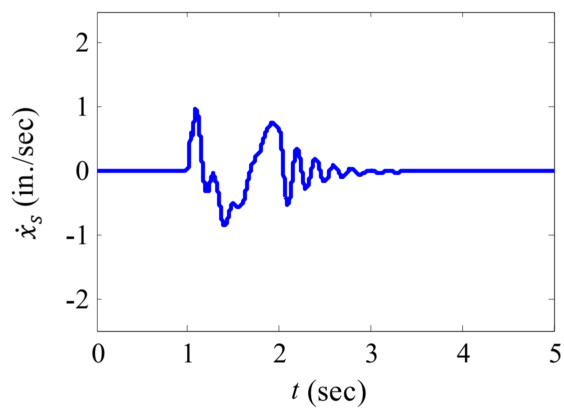

(d) Response of structure ($\dot{x}_s$)

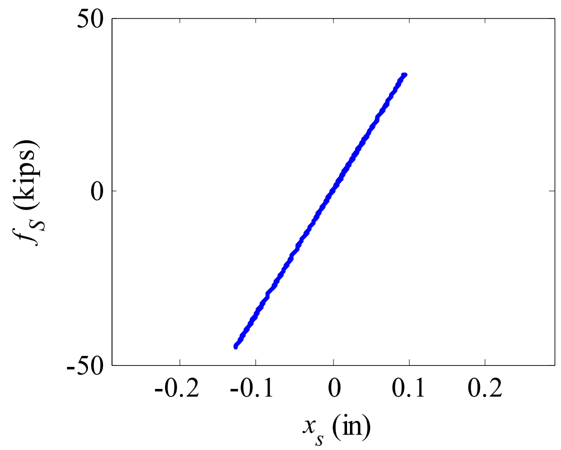

(e) Response of structure (f_S vs. x_s)

Figure 6-8 PTC - structure responses for a 2DOF linear system with real time estimation

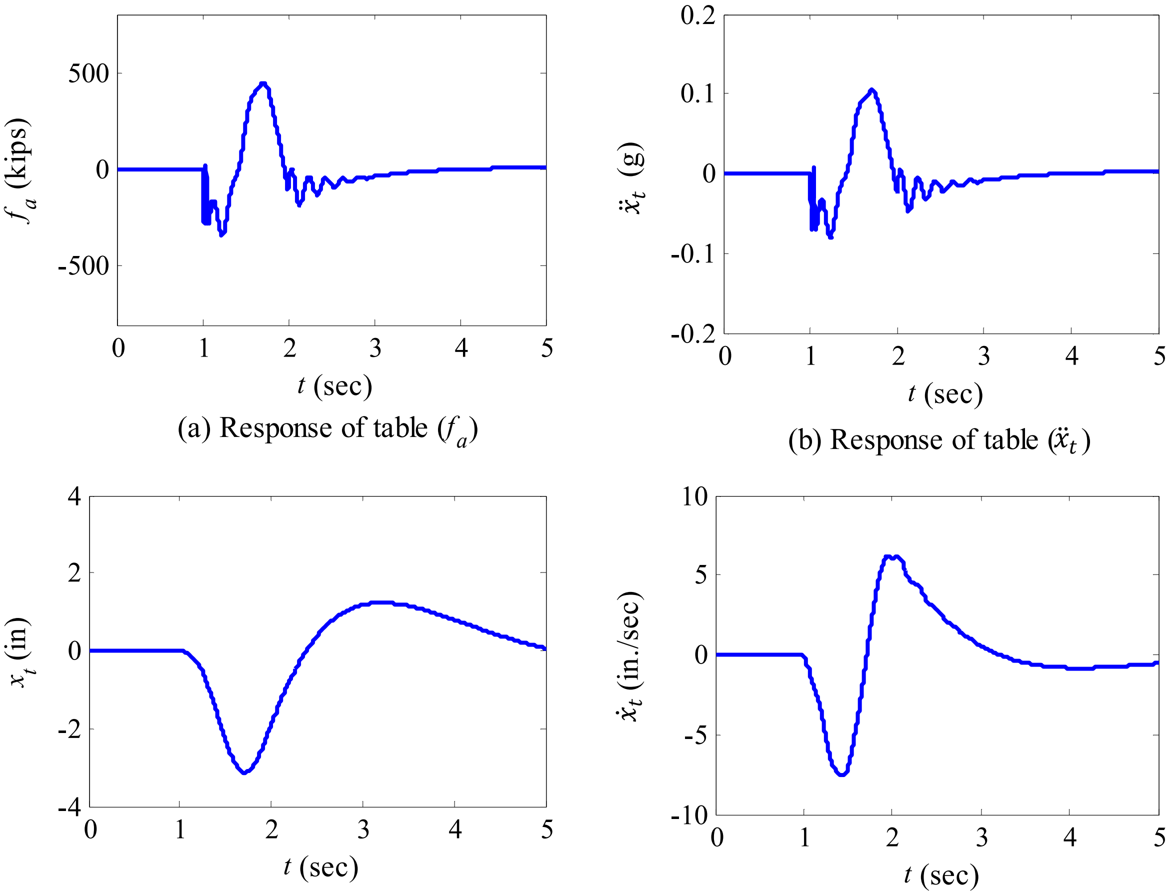

(a) Response of table (f_a)

(b) Response of table ($\ddot{x}_t$)

(c) Response of table (x_t)

(d) Response of table ($\dot{x}_t$)

Figure 6-9 PTC - shake table responses for a 2DOF linear system with real time estimation

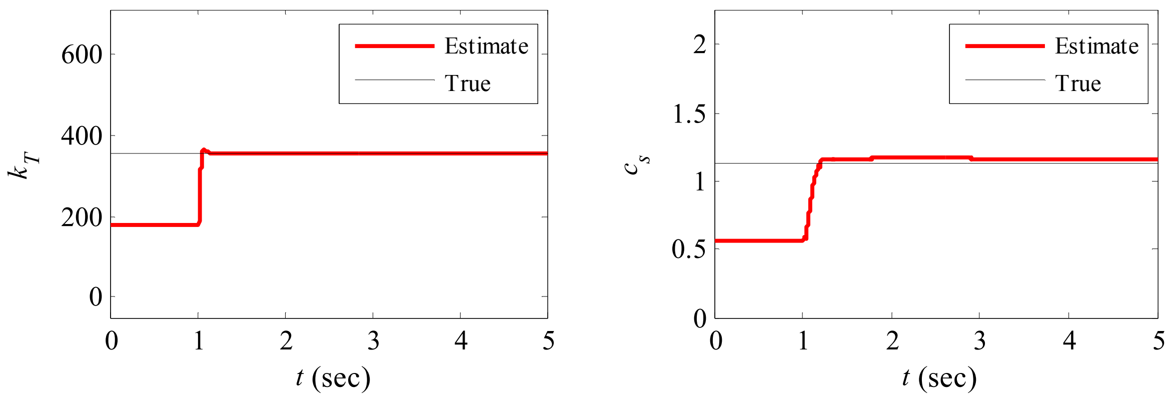

(a) Estimated parameter k_T (b) Estimated parameter c_s

Figure 6-10 Real time parameter estimation results of the FTC for a 2DOF linear system

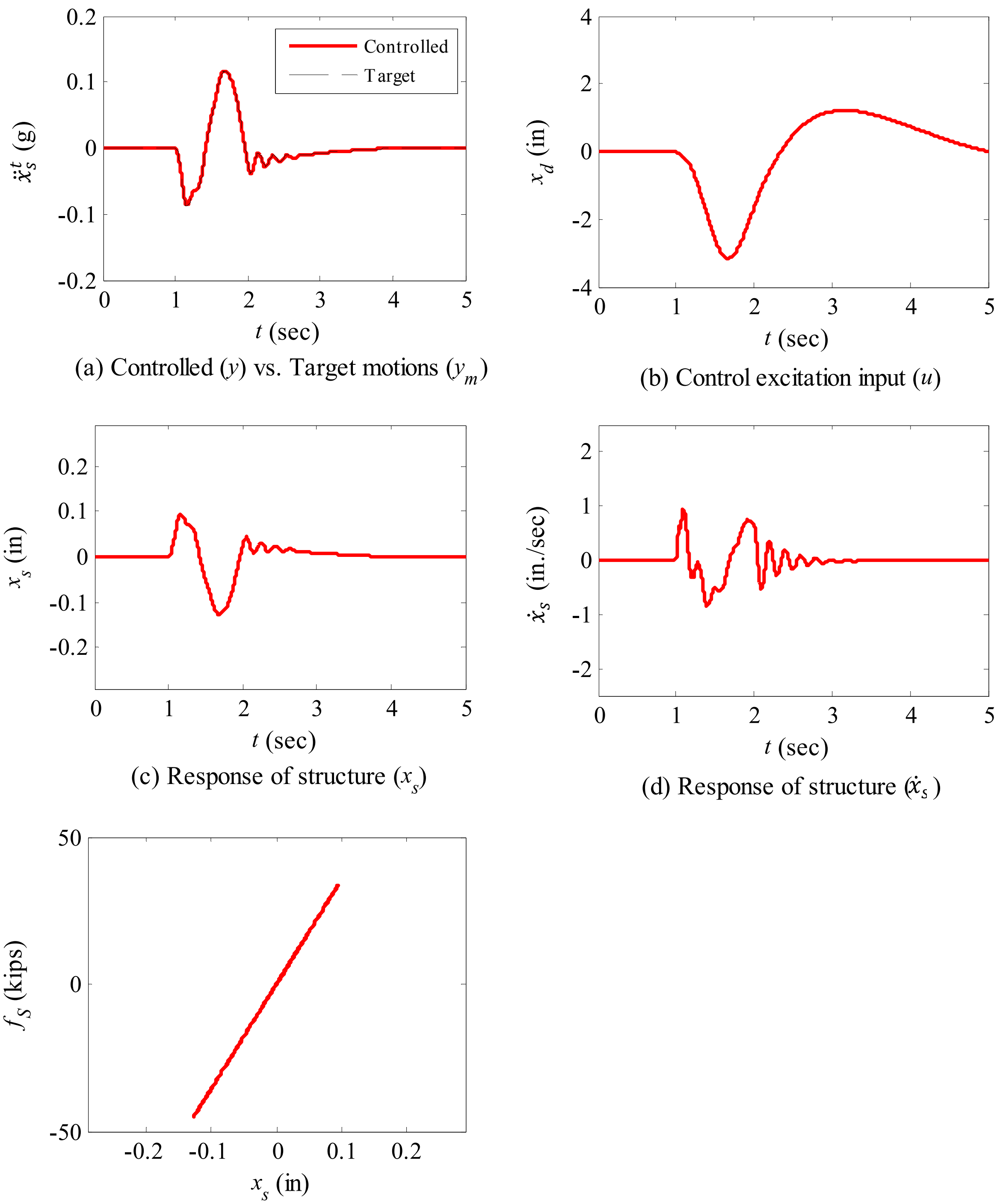

(a) Controlled (y) vs. Target motions (y_m)

(b) Control excitation input (u)

(c) Response of structure (x_s)

(d) Response of structure ($\dot{x}_s$)

(e) Response of structure (f_S vs. x_s)

Figure 6-11 FTC - structure responses for a 2DOF linear system with real time estimation

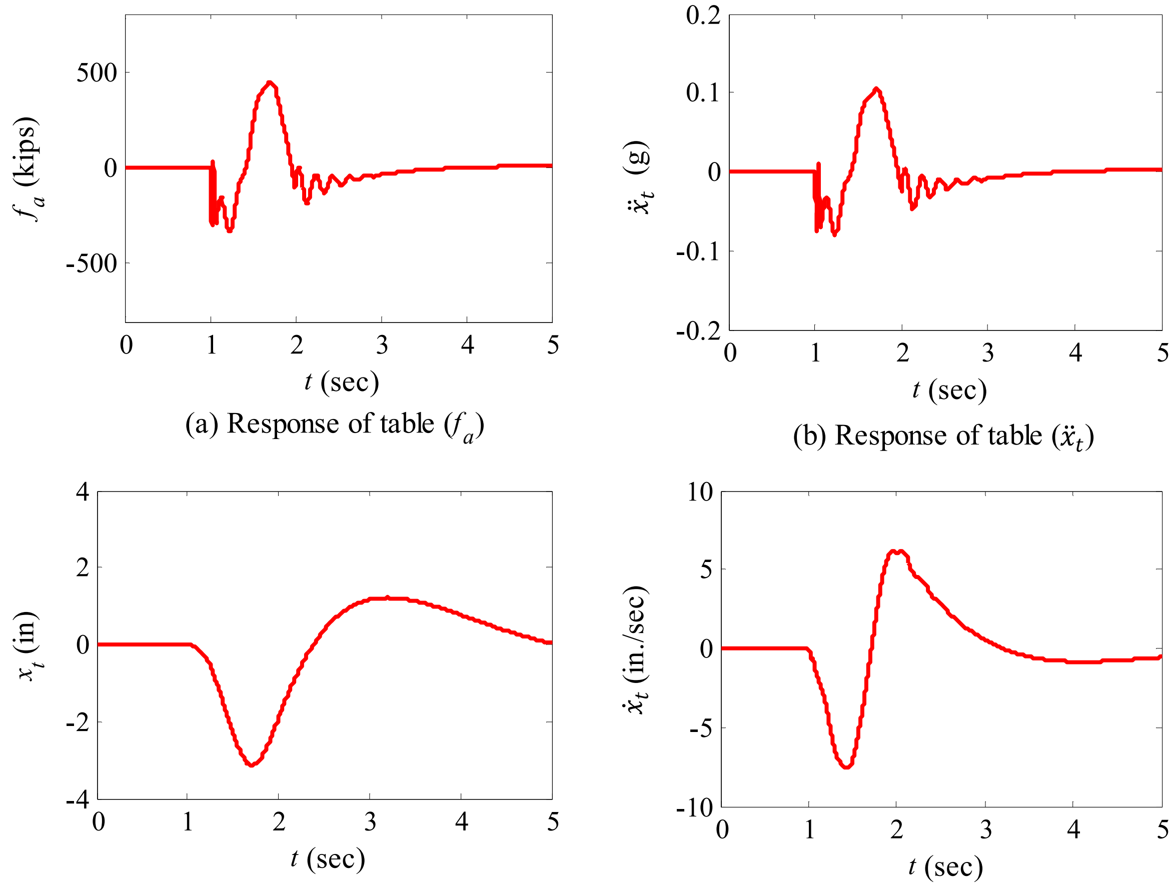

(a) Response of table (f_a)

(b) Response of table ($\ddot{x}_t$)

(c) Response of table (x_t)

(d) Response of table ($\dot{x}_t$)

Figure 6-12 FTC - shake table responses for a 2DOF linear system with real time estimation

In this section, the two feedback tracking control algorithms: the predictive tracking control (PTC) and the feedback linearization tracking control (FTC) introduced in SECTION 3; are expanded to the applications of linear systems whose parameters are not fully known a priori. In order to deal with the uncertainties in the system models, the real time estimators using the *extended Kalman filter* (EKF) introduced in SECTION 5 are combined with the tracking control methods. The tracking control laws are reformulated in order to adapt the estimated parameters. Because of the lack of the knowledge of stability properties of the EKF, the performances of tracking and the boundedness of controlled system responses are examined through numerical simulations. The results show that very good tracking performances can be obtained with fairly good initial guess of unknown parameters (i.e. 50% errors in the initial guess are used in the examples).

“This Page Intentionally Left Blank”

SECTION 7
TRACKING CONTROL FOR NONLINEAR SYSTEMS WITH UNKNOWN PARAMETERS

The adaptive tracking control schemes, which combine the *predictive tracking control* (PTC) and the *feedback linearized tracking control* methods (FTC) with the *extended Kalman filter* (EKF) for the real time parameter estimation, formulated and applied to linear systems in SECTION 6 are extended to nonlinear hysteretic systems in this section. The performance of each method is examined using the numerical simulation.

7.1 Predictive Tracking Control with Real-time Parameter Estimation

The predictive control method was used in Section 4.2 in order to develop the control law for nonlinear system tracking problems with known parameters. The control input u_k to minimize the instantaneous performance index J in Eq. (3-35) is shown in Eq. (4-13). When there are unknown parameters in a given system to be controlled, the parameters can be estimated in real time using the system parameter estimator such as the *extended Kalman filter* (EKF).

Control Law

The control excitation input can be computed using the same equation shown in Eq. (4-13) (repeated here for convenience) by using the estimated parameters $\underline{\hat{\theta}}_k = [\hat{c}_{s,k} \;\; \hat{k}_T(\underline{x}) \;]^T$ at instant $k\Delta t$ instead of the true parameters $\underline{\theta}_k^* = [c_s \;\; k_T(\underline{x})]^T$:

$$u_k = \left[\hat{B}_{D,k}^{*\,T} Q \hat{B}_{D,k}^* + R\right]^{-1} \hat{B}_{D,k}^{*\,T} Q \left[y_{m,k+1} - \hat{A}_{D,k}^* \hat{\underline{x}}_k\right] = \hat{\Gamma}_k \left[y_{m,k+1} - \hat{A}_{D,k}^* \hat{\underline{x}}_k\right] \qquad (7\text{-}1)$$

where the *hat* ^ indicates that the system matrix uses the estimated parameters $\underline{\hat{\theta}}_k$, and

$$\hat{\Gamma}_k = \left[\hat{B}_{D,k}^{*\,T} Q \hat{B}_{D,k}^* + R\right]^{-1} \hat{B}_{D,k}^{*\,T} Q, \quad \hat{A}_{D,k}^* = \hat{C}_{D,k} \hat{A}_{D,k}, \quad \hat{B}_{D,k}^* = \hat{C}_{D,k} \hat{B}_{D,k}$$

and the true system matrices in discrete-time $A_{D,k}$ and $B_{D,k}$ and the true output matrix C_D (i.e. $C_D = C$) are defined in Section 4.2 (see Eq. (4-10) to Eq. (4-12)), and their estimate matrices $\hat{A}_{D,k}$, $\hat{B}_{D,k}$, and $\hat{C}_{D,k}$ (i.e. $\hat{C}_{D,k} = \hat{C}_k$) are updated at every instant $k\Delta t$ with estimated parameters $\underline{\hat{\theta}}_k$. For numerical simulation, the true responses are computed by substituting the control excitation input u_k from Eq. (7-1) into the true system equation in Eq. (4-4) and using Eq. (4-14) for numerical integration, while in real experiments the true system responses will be measured at every instant $k\Delta t$ by sensors: the measurements using sensors are expressed as $\underline{\overline{y}}_k = H\underline{x}_k + \underline{v}_k$ (the true responses $\underline{x}_k$ with measurement noise $\underline{v}_k$ - see Eq. (5-51)).

However, as discussed in Section 4.2, it is assumed that the instant stiffness $k_T(\underline{x})$ in Eq. (4-4) is piecewise constant at every instant in order to examine the effectiveness of the proposed control scheme analytically. With this assumption, the error dynamics with the control scheme can be shown as following.

Expected Achieved Responses

Substitution of the control excitation input u_k excitation Eq. (7-1) into the approximated system in Eq. (4-12) leads to

$$\hat{y}_{k+1} = C_D\left[\left\{A_{D,k} - B_{D,k}\hat{\Gamma}_k\hat{A}^*_{D,k}\right\}\hat{\underline{x}}_k + B_{D,k}\hat{\Gamma}_k y_{m,k+1}\right] \tag{7-2}$$

where $\hat{\Gamma}_k$.and $\hat{A}^*_{D,k}$ are defined in Eq. (7-1). If $\hat{B}^*_{D,k}$= $C_D B_{D,k}$ is an invertible matrix, and R = 0 and $Q = I$ (i.e. I = identity matrix) are chosen, then Eq. (7-2) becomes

$$\hat{y}_{k+1} = \left[A^*_{D,k} - \left(B^*_{D,k}\hat{B}^{*\,-1}_{D,k}\right)\hat{A}^*_{D,k}\right]\hat{\underline{x}}_k + \left(B^*_{D,k}\hat{B}^{*\,-1}_{D,k}\right)y_{m,k+1} \tag{7-3}$$

where $A^*_{D,k}$ = $C_D A_{D,k}$ and $B^*_{D,k}$ = $C_D B_{D,k}$ are the true system matrices.

Stability

The predicted tracking error equation can be obtained from Eq. (7-3) by collecting the tracking error term $e_{k+1} = \hat{y}_{k+1} - y_{m,k+1}$ in the left-hand side and the estimate error terms in the right-hand side:

$$e_{k+1} = g_{k+1}\left(\tilde{\underline{\theta}}_k, \hat{\underline{x}}_k, y_{m,k+1}\right) \tag{7-4}$$

where the function g_{k+1} indicates some residual error due to parameter estimate error $\tilde{\underline{\theta}}_k = \hat{\underline{\theta}}_k - \underline{\theta}^*_k$. The tracking error e_{k+1} will decrease when the estimated parameters error $\tilde{\underline{\theta}}_k$ becomes smaller. As discussed in Section 5.3, because of the lack of knowledge of the stability properties of the *extended Kalman filter* (EKF), the performance of the adaptive tracking control method introduced is examined using the numerical simulation in Section 7.4.1.

Limitations of Shake Table-Structure Systems

As discussed in Section 4.2, if the product of the output and input matrices $C \times B$ is singular for the shake table-structure 2DOF model, the predicted output $\hat{y}_{k+1}$ in discrete time or $\hat{y}(t+h)$ in continuous time might be approximated including higher order differentiations. Using the approximated predicted output $\hat{y}^*(t+h)$ and target motion $y^*_m(t+h)$ (shown in Eq. (3-44)), the control law is established as shown also in Eq. (4-18). When some parameters are unknown, the control input $u(t)$ can be computed using the estimated parameters $\hat{\underline{\theta}}(t)$ of the true parameters $\underline{\theta}^*$ at instant time as following:

Control Law

$$u(t)=\left[\hat{B}^{*}\left(\underline{\hat{\theta}}\right)^{T} Q\hat{B}^{*}\left(\underline{\hat{\theta}}\right)+R\right]^{-1}\hat{B}^{*}\left(\underline{\hat{\theta}}\right)^{T} Q\left[y_{m}^{*}(t+h)-\hat{A}^{*}\left(\underline{x}\right)\underline{\hat{x}}(t)\right] \tag{7-5}$$

where $\hat{A}^{*}(\underline{x}) = [\hat{C}(\underline{\hat{\theta}}) + h\hat{C}(\underline{\hat{\theta}})\,\hat{A}(\underline{x}) + (h^{2}/2)\,\hat{C}(\underline{\hat{\theta}})\,\{d/dt\hat{A}(\underline{x}) + \hat{A}(\underline{x})^{2}\}]$ and $\hat{B}^{*}(\underline{\hat{\theta}}) = (h^{2}/2)\hat{C}(\underline{\hat{\theta}})\,\hat{A}(\underline{x})B$.

By substituting Eq. (7-5) into the second equation of Eq. (4-17), one can establish the error dynamics for the nonlinear system. For a system having $\hat{B}^{*}(\underline{\hat{\theta}})$ as a non-zero scalar (i.e. an invertible matrix, size 1 × 1) and $R = 0$ chosen, $\ddot{y}(t)$ becomes:

Expected Achieved Responses

$$\ddot{y}(t)=C\left[\frac{d}{dt}A\left(\underline{x}\right)+A^{2}\left(\underline{x}\right)\right]\underline{\hat{x}}(t)+CA\left(\underline{x}\right)B\left[\hat{B}^{*}\left(\underline{\hat{\theta}}\right)\right]^{-1}\left[y_{m}^{*}(t+h)-\hat{A}^{*}\left(\underline{x}\right)\underline{\hat{x}}(t)\right] \tag{7-6}$$

which can be rewritten by introducing the tracking error ($e(t) = y(t) - y_m(t)$) to show its dynamics are:

$$\ddot{e}(t)+(2/h)\dot{e}(t)+\left(2/h^{2}\right)e(t)=g\left(\underline{\tilde{\theta}}(t),\underline{\hat{x}}(t),y_{m}^{*}(t+h)\right) \tag{7-7}$$

where the function $g(\cdot)$ indicates some residual error, which are caused by the parameter estimate errors $\underline{\tilde{\theta}}(t) = \underline{\hat{\theta}}(t) - \underline{\theta}^{*}$. The tracking error $e(t)$ will decrease when the estimated parameter error $\underline{\tilde{\theta}}(t)$ is reduced. The performance of the adaptive tracking controller is examined using the numerical simulation in Section 7.4.2.

7.2 Feedback Linearization Tracking Control with Real-time Parameter Estimation

The *Feedback Linearization Tracking Control* (FTC) (Ioannou and Fidan, 2006) formulated in Section 4.3 can also be used for the tracking control of nonlinear hysteretic systems with unknown parameters with some modifications. The controller is designed such that the true system properties involving the nonlinear behavior are replaced to new ones that will lead to the desired linear behavior, and the output response of the controlled system will follow the target motion. For the real time parameter estimation the *extended Kalman filter* (EKF) is used.

Application to SDOF Linear Structures

The tracking control procedure for the nonlinear hysteretic structure was introduced in Section 4.3 for known parameters. The equations of the true system and the reference model are shown in Eq. (4-21) and Eq. (4-22) and for the total acceleration as the target motion the output equations are shown in Eq. (4-28) and Eq. (4-29). In order to achieve the tracking control objective, the tracking control law is established as shown in Eq. (4-31). However for unknown parameters; i.e. the structure damping c_s and the instantaneous stiffness $k_T(\underline{x})$ are unknown; the possible control law can be formulated as:

Control Law

$$u(t)=\hat{c}_s(t)^{-1}m_s^{2}\left[m_s^{-2}\hat{c}_s(t)\left(\hat{c}_s(t)\dot{x}(t)+f_S(\underline{x})\right)-m_s^{-1}\hat{k}_T(\underline{x})\dot{x}(t)-v(t)\right] \tag{7-8}$$

where a function $v(t)$ = [$\dot{y}_m$ - $k_1^*\{y(t)$ - $y_m(t)\}$] is selected to reduce the tracking error, and $\hat{c}_s(t)$ and $\hat{k}_T(\underline{x})$ are the estimates of the true parameters c_s and $k_T(\underline{x})$ respectively. It is noted that the estimate $\hat{k}_T(\underline{x})$ of the instantaneous stiffness $k_T(\underline{x})$ is computed using the estimates of constant parameters k_s, α, and d_y as shown in Section 5.2.1.2. By substituting this control input $u(t)$ into Eq. (4-30), it is obtained

$$\begin{aligned}\dot{y}(t)=&\left[m^{-2}c_s\left\{c_s\dot{x}(t)+f_S(\underline{x})\right\}-\left\{c_s\hat{c}_s(t)^{-1}\right\}m^{-2}\hat{c}_s(t)\left\{\hat{c}_s(t)\dot{x}(t)+f_S(\underline{x})\right\}\right]\\&-\left[m^{-1}k_T(\underline{x})\dot{x}(t)-\left\{c_s\hat{c}_s(t)^{-1}\right\}m^{-1}\hat{k}_T(\underline{x})\dot{x}(t)\right]+\left\{c_s\hat{c}_s(t)^{-1}\right\}\left[\dot{y}_m(t)-k_1^*\left\{y(t)-y_m(t)\right\}\right]\end{aligned} \tag{7-9}$$

From this equation, the tracking error dynamics might be determined using the defined tracking error terms: $e(t) = y(t) - y_m(t)$ and $\dot{e}(t) = \dot{y}(t) - \dot{y}_m(t)$; as presented below:

Expected Achieved Responses

$$\dot{e}(t)+k_1^*e(t)=g\left(\underline{\tilde{\theta}}(t),\underline{x}(t),y_m(t),\dot{y}_m(t)\right) \tag{7-10}$$

where the function $g(\cdot)$ indicates some residual error caused by the parameter estimate errors $\underline{\tilde{\theta}}(t)$ = $\underline{\hat{\theta}}(t) - \underline{\theta}^*(t)$, in which $\underline{\hat{\theta}}(t) = [\hat{c}_s(t)\ \ \hat{k}_T(\underline{x})]^T$ is the estimate of the true parameters $\underline{\theta}^*(t) = [c_s\ \ k_T(\underline{x})]^T$. The tracking error $e(t)$ will decrease when the estimated parameters error $\underline{\tilde{\theta}}_k = \underline{\hat{\theta}}_k - \underline{\theta}_k$ becomes smaller. As discussed in Section 5.3, the performance of the adaptive tracking controller with the *extended Kalman filter*(EKF) is examined using a numerical simulation in Section 7.4.1.

Application to 2DOF Shake Table-Nonlinear Structure Systems

For a nonlinear structure with known parameters mounted on a shake table (the 2DOF system model) expressed in Eq. (4-8) and Eq. (4-9) with the output $y(t)$ of the total acceleration response $\ddot{x}_s^t(t)$ at the structure, the tracking control law is established as shown in Eq. (4-38). However, with unknown parameters the possible control law is using the only the estimate $\underline{\hat{\theta}}(t) = [\hat{c}_s(t)\ \ \hat{k}_T(\underline{x})]^T$ of the true parameters $\underline{\theta}^*(t) = [c_s\ \ k_T(\underline{x})]^T$:

Control Law

$$u^*(t)=\hat{a}(t)^{-1}\left[-\ddot{y}^*(t)+v(t)\right] \tag{7-11}$$

where $u^*(t) = (\omega_a^2k_a)u(t)$; $u(t) = x_d(t)$; and $\ddot{y}^*(t)$ is defined as

$$\begin{aligned}\ddot{y}^*(t)=&\left[\hat{a}(t)\left(\hat{a}(t)+\hat{c}(t)\right)-m_s^{-1}\hat{k}_T(\underline{x})\right]\ddot{x}_s(t)+\left[-m_s^{-1}\dot{\hat{k}}_T(\underline{x})+\hat{a}(t)\left(m_s^{-1}+m_t^{-1}\right)\hat{k}_T(\underline{x})\right]\dot{x}_s(t)\\&+\left(-\hat{a}(t)e\right)f_a^*(t)+\left(-\hat{a}(t)f\right)\dot{x}_t(t)+\left(-\hat{a}(t)g\right)x_t(t)\end{aligned} \tag{7-12}$$

in which abbreviated parameters are introduced for simplification:

$$\begin{aligned}
&\hat{a}(t) = m_s^{-1}\hat{c}_s(t); \qquad c(t) = m_t^{-1}\hat{c}_s(t); \\
&e = 2\xi_a\omega_a; \qquad f = \omega_a^2; \qquad g = \omega_a^2 k_a; \\
&f_a^*(t) = f_a(t)/m_t; \qquad u^*(t) = \omega_a^2 k_a x_d(t), \quad u(t) = x_d(t)
\end{aligned} \tag{7-13}$$

$v(t)$ is selected to reduce the tracking error as

$$v(t) = \ddot{y}_m(t) - k_1^*\dot{e}(t) - k_2^* e(t) \tag{7-14}$$

in which $e(t) = y(t) - y_m(t)$ with $y(t) = -m_s^{-1}[\hat{c}_s(t)\,\dot{x}_s(t) + f_S(\underline{x})]$; and $\dot{e}(t) = \dot{y}(t) - \dot{y}_m(t)$ with $\dot{y}(t) = -m_s^{-1}$ $[\hat{c}_s(t)\,\ddot{x}_s(t) + \hat{k}_T(t)\,\dot{x}_s(t)]$. Substituting $u^*(t)$ from Eq. (7-11) into the differentiated output equation $\ddot{y}(t)$ (shown in Eq. (B-35) in Appendix B.4) and collecting the tracking error terms $e(t)$ to the left-hand side and residual error terms due to estimation error to the right-hand side gives the tracking error dynamic equation:

<u>Expected Achieved Responses</u>

$$\ddot{e}(t) + k_1^*\dot{e}(t) + k_2^* e(t) = g\left(\underline{\tilde{\theta}}(t), \underline{x}(t), \underline{y}_m(t)\right) \tag{7-15}$$

where the function $g(\cdot)$ indicates some residual error, which are caused by parameter estimate error $\underline{\tilde{\theta}}(t) = \underline{\hat{\theta}}(t) - \underline{\theta}^*(t)$. The tracking error $e(t)$ will diminish when the estimated parameters error $\underline{\tilde{\theta}}(t)$ becomes small. The performance of this adaptive tracking controller is examined by means of a numerical simulation in Section 7.4.2.

7.3 Comparisons of Feedback Tracking Control Methods

As discussed in Section 4.4, one can show that the two tracking control methods are equivalent for the shake table-structure system, having nonlinear hysteretic behavior, under certain conditions and with known parameters. For the unknown parameters, the formulations of the control laws for the two tracking control methods have not changed; therefore, one can also show that the predictive tracking control law shown in Eq. (7-5) is the same as the control law of the feedback linearization tracking control method shown in Eq. (7-11) with the same conditions applied to the known parameter controllers; i.e. the controlled system has $B^*(\underline{x})$ = a non-zero scalar (i.e. an invertible matrix, size 1 × 1), and $R = 0$ chosen, and the tracking error coefficients in Eq. (4-20) are $k_1^* = 2/h = 2\xi_e\omega_e$ and $k_2^* = 2/h^2 = \omega_e^2$; therefore, $\xi_e = \sqrt{2}/2 \approx 0.707$ and $h = \sqrt{2}/\omega_e$.

7.4 Numerical Examples and Comparison of Tracking Control Methods

Simple tracking control examples (as demonstrated in Section 6.4 for linear systems) are analyzed in order to examine the performance of the introduced two feedback tracking control methods combined with the real time parameter estimation for nonlinear systems with unknown parameters. The obtained results are presented. For all examples, the target motion is the total acceleration of a structure (specimen) mounted on the shake table.

7.4.1 SDOF Nonlinear Hysteretic Structure

As discussed in Section 2.2, to facilitate the development of the tracking control method, first, a simplified SDOF system model is used instead of a 2DOF system model for a shake table with an SDOF structure system. In this simplified system model (shown in Figure 7-1), the excitation force $-m_s\ddot{x}_t(t)$ due to the shake table acceleration $\ddot{x}_t(t)$ is considered as a new control input $u(t)$ However, the actual control excitation input $u(t)$ for the 2DOF system model is the desired displacement $x_d(t)$ of the shake table, and $u(t)$ shall be computed including the shake table dynamics and the shake table-structure interaction (as discussed in Section 2.2) as formulated in the following section (Section 7.4.2).

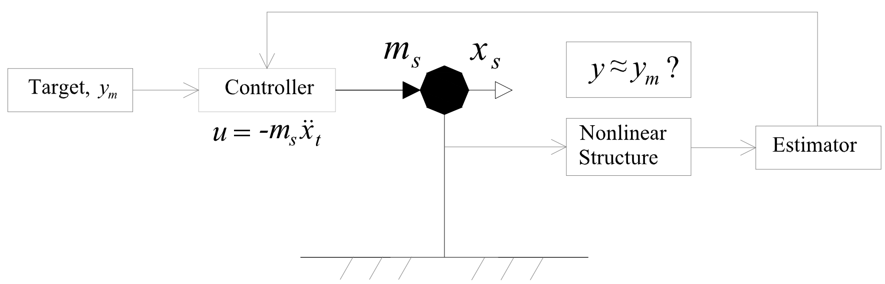

Figure 7-1 Tracking control of an SDOF nonlinear system with unknown parameters

The governing equation of an SDOF nonlinear structure subjected to the shake table excitation is shown in Eq. (4-1). The tracking control task for this simplified system is to compute the control excitation input $u(t) = -m_s\ddot{x}_t(t)$ at every instant using the real time estimated parameters so that the system output $y(t) = \ddot{x}_s^t(t)$ (the total acceleration of the structure) follows the target motion $y_m(t) = \ddot{x}_m^t(t)$ (the total acceleration of the reference model).

Example 7.1* : *Tracking A SDOF Nonlinear System with Unknown Parameters using the PTC

The properties of a given system are: m_s = 1 kips·sec^2/in., k_s = 355 kips/in., and c_s = 1.13 kips·sec/in., (f_n = 3.0 Hz, ξ_n = 0.03 before yielding). N = 3, d_y = 0.11 in. (f_y = 39 kips), and α = 0.1 (i.e. all terms are explained in Eq. (4-2) and Eq. (4-3)), the same as the ones in Example 4.1. In order to examine the measurement noise effects, a zero-mean Gaussian white-noise process of 3% RMS noise-to-signal are added to the measurements $\underline{\overline{y}}_k = [\overline{x}_{s,k}\ \ \dot{\overline{x}}_{s,k}\ \ \overline{f}_{S,k}]^T$, which are described in Section 5.2.1.2. Four unknown parameters: c_s the damping coefficient; k_s the elastic stiffness; α the post-yielding stiffness ratio to the elastic stiffness; and d_y the yielding displacement; are selected and estimated in real time using the extended Kalman filter.

The target motion is shown in Figure 7-3 (a) [Target]. The target motion is the total acceleration output generated from the same reference linear system (f_m = 5.0 Hz, ξ_m = 0.1), used for Example 6.1. in Section 6.4.1 (the reference input and the responses of the reference model are presented in Appendix A.2). For the parameter estimation, the initial parameter estimate $\underline{\hat{\theta}}_0$ is chosen as $\underline{\hat{\theta}}_0 = 0.8 \times \underline{\theta}^*$ (20% error in the initial guess), and the initial covariance matrix is chosen as $P_0 = \mathrm{diag}([0 \;\; 0 \;\; 0 \;\; \hat{c}_{s,o}{}^2 \;\; \hat{k}_{s,o}{}^2 \;\; \hat{\alpha}_o{}^2 \;\; \hat{d}_{y,o}{}^2]^T \times 0.05)$. The covariance matrices Q_E and R_E are chosen as follows: $Q_E = 0 \times I_{7\times7}$ (all zeroes) and the R_E = diagonal matrix, whose elements; i.e. noise variance = 3% × corresponding signal variance (noise variances are assumed to be known from the instruments information). A time step of 0.002 sec is used for the simulation.

The tracking control results using the *predictive tracking control* (PTC) method with the real time parameter estimations are presented in Figure 7-2 and Figure 7-3. The selected control parameters for the PTC in this example are R = 0.0001 and Δt = 0.002. Figure 7-2 shows the comparison between the true and the estimated parameters: $k_T(\underline{x})$ the instantaneous stiffness (i.e. the estimate of $k_T(\underline{x})$ is computed using the estimates of k_s, α, and d_y); c_s the damping coefficient; k_s the elastic stiffness; α the post-yielding stiffness ratio to the elastic stiffness; and d_y the yielding displacement; and they show very good agreements. The controlled output, $\ddot{x}_s^t(t)$ the total acceleration of the structure, is shown in Figure 7-3 (a) [Controlled] and also shows very good agreement with the target motion. The computed control excitation input, $u(t) = -m_s\ddot{x}_t(t)$, using the control law in Eq. (7-1) is shown in Figure 7-3 (b). $x_s(t)$, $\dot{x}_s(t)$ the achieved displacement and velocity responses of the controlled structure are also presented in Figure 7-3 (c) and (d); it is noted that unlike the total acceleration, the displacement and velocity responses are different from ones of the reference because the system properties of the controlled system and ones of the reference system are different. The relation between the structure resisting force $f_S(t)$ having hysteretic behavior and displacement $x_s(t)$ is also presented in Figure 7-3 (e). As desired, all responses of the controlled system are bounded.

The tracking control results using the *feedback linearization tracking control* (FTC) method are presented in Figure 7-4 and Figure 7-5. Figure 7-4 presents the results of the parameter estimation in real time. The controlled output $\ddot{x}_s^t(t)$ is shown in Figure 7-5 (a) [Controlled] and shows very good agreement with the target motion. The computed control excitation input, $u(t) = -m_s\ddot{x}_t(t)$, using the control law in Eq. (7-8) is shown in Figure 7-5 (b). The selected control parameter in this example for the FTC is $k_1^* = \frac{1}{\Delta t}/100$ (i.e. the smaller value of k_1^* than that of the system with the known parameter case in Section 4.5.1 is chosen due to the uncertainty and indicates that the tracking error will decrease slowly). It is noted that by choosing the control parameters carefully to satisfy the tracking object, the control excitation inputs of the two methods (PTC and FTC) are very similar; therefor, as expected, the control results of two methods are very similar as shown in Figure 7-2 through Figure 7-5.

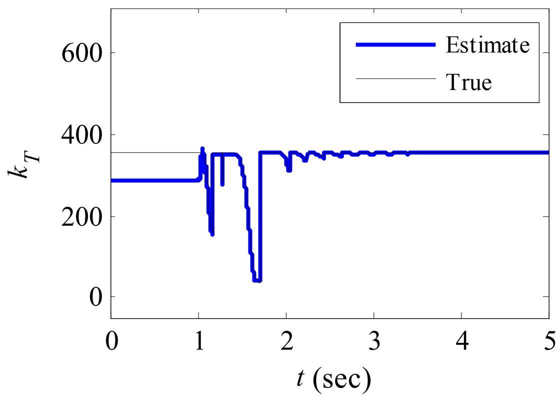

(a) Estimated parameter k_T

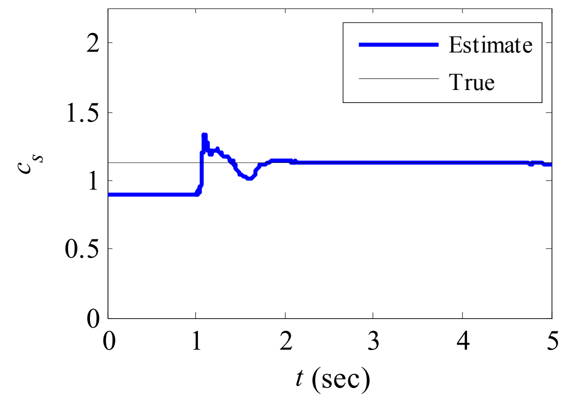

(b) Estimated parameter c_s

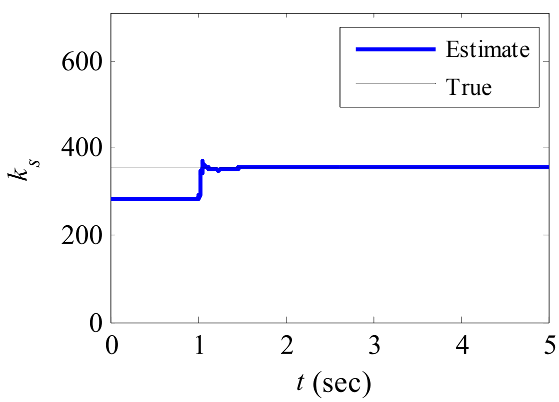

(c) Estimated parameter k_s

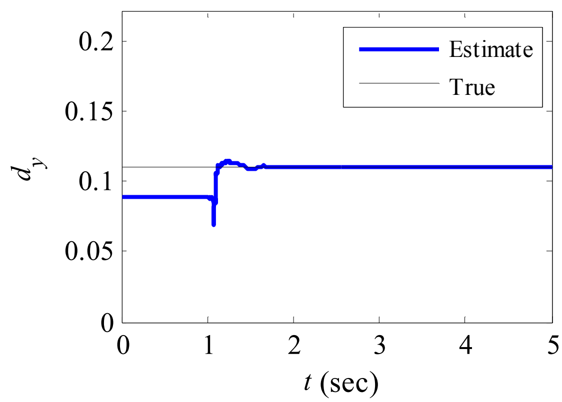

(d) Estimated parameter d_y

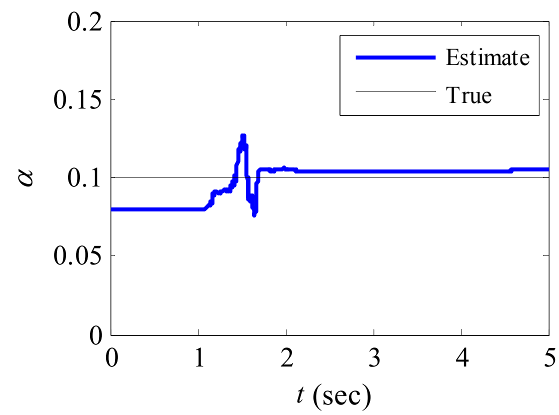

(e) Estimated parameter α

Figure 7-2 Real time parameter estimation results of the PTC for an SDOF nonlinear system

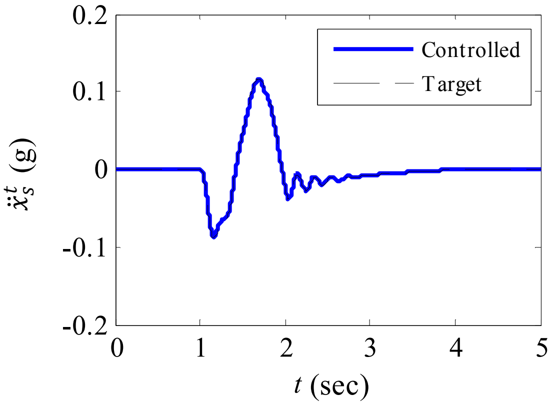

(a) Controlled (y) vs. Target motions (y_m)

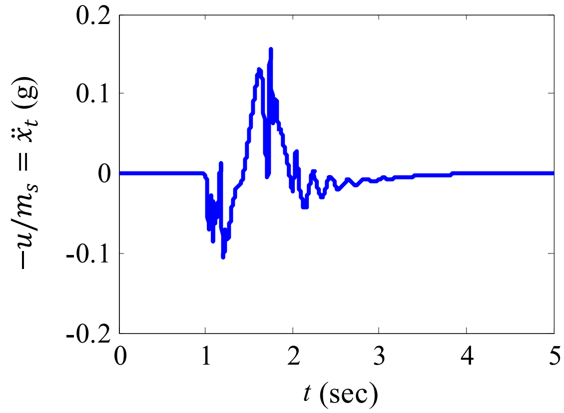

(b) Control excitation input (u)

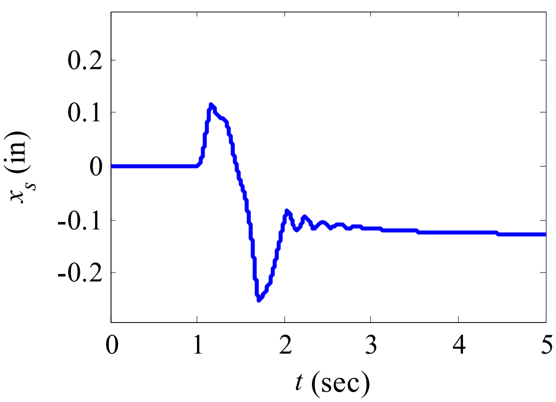

(c) Response of structure (x_s)

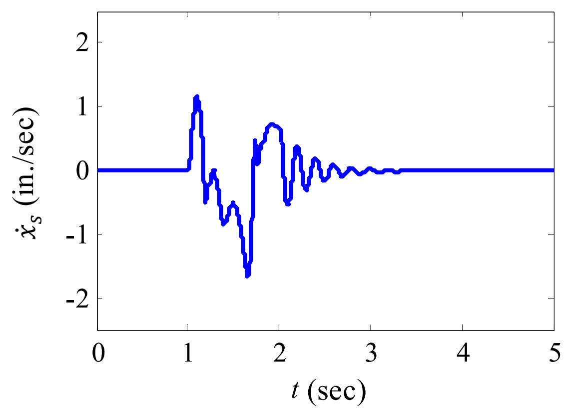

(d) Response of structure ($\dot{x}_s$)

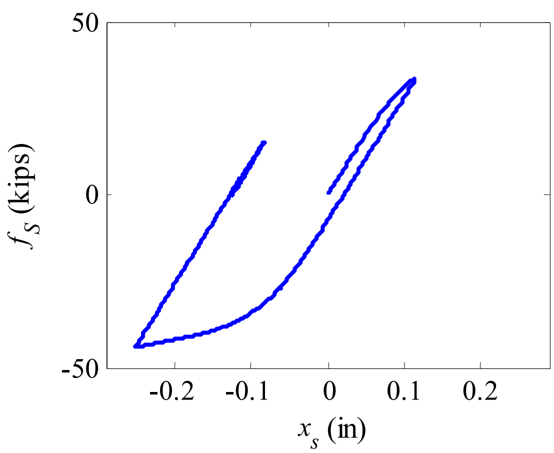

(e) Response of structure (f_S vs. x_s)

Figure 7-3 PTC - structure responses for an SDOF nonlinear system with real time estimation

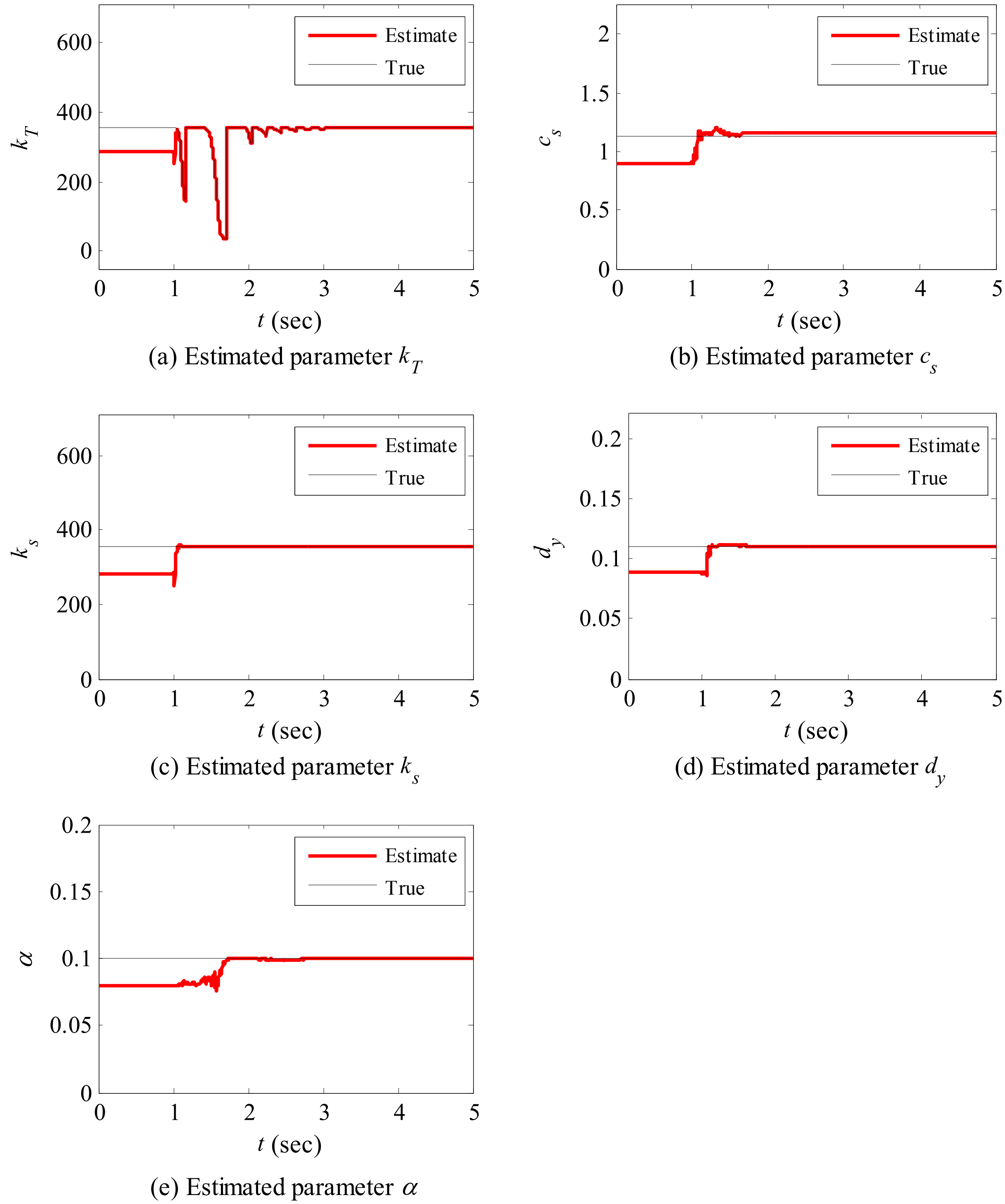

Figure 7-4 Real time parameter estimation results of the FTC for an SDOF nonlinear system

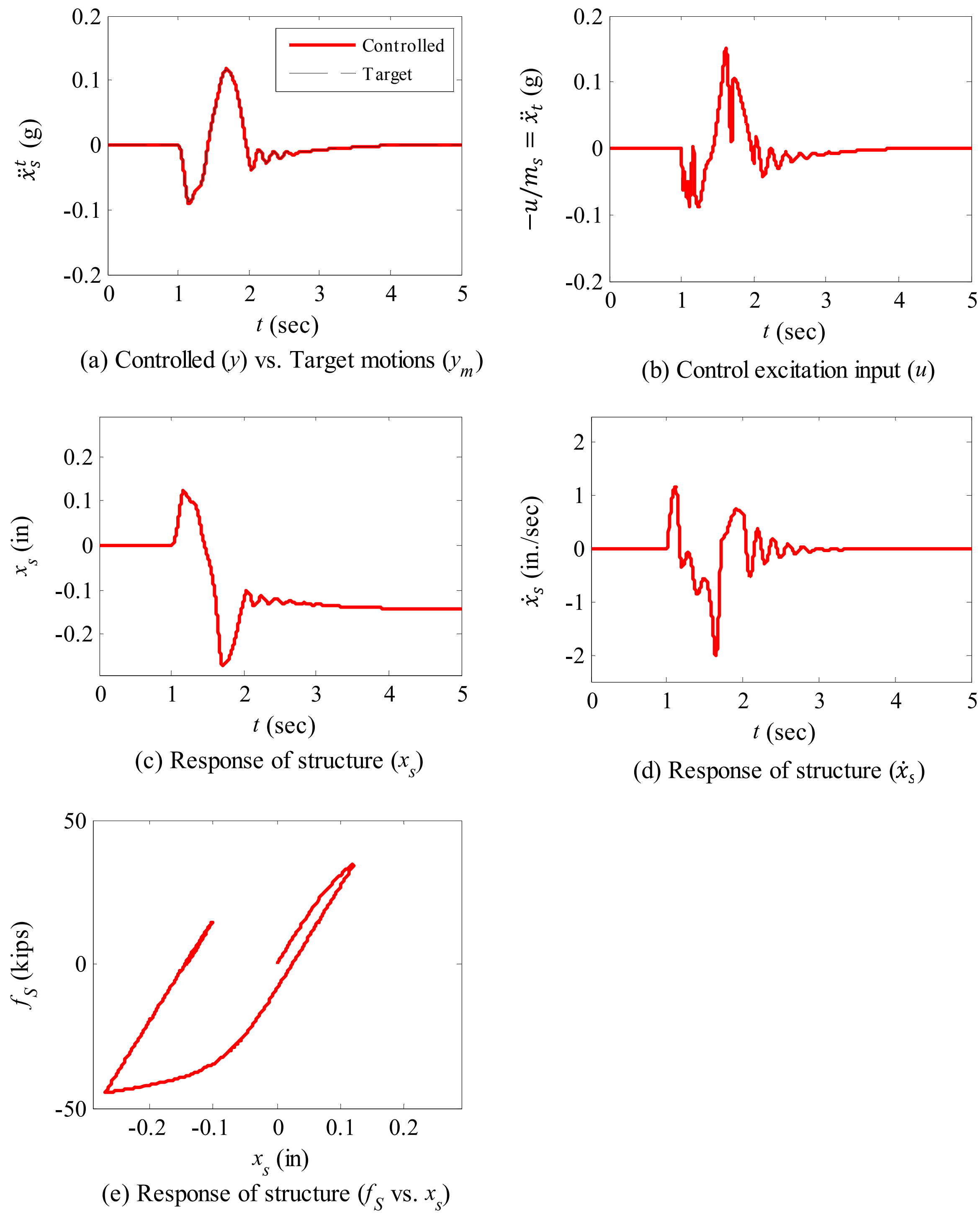

(a) Controlled (y) vs. Target motions (y_m)

(b) Control excitation input (u)

(c) Response of structure (x_s)

(d) Response of structure ($\dot{x}_s$)

(e) Response of structure (f_S vs. x_s)

Figure 7-5 FTC - structure responses for an SDOF nonlinear system with real time estimation

7.4.2 2DOF Shake Table – Nonlinear Hysteretic Structure Systems

As discussed in Section 2.2, the shake table dynamics affect the performance of the control system and the interaction between the shake table and the mounted structure is to be considered. The same tracking control example demonstrated in Section 7.4.1 is resolved for the 2DOF nonlinear system, expressed in Eq. (4-8) and Eq. (4-9), and schematically shown in Figure 7-6.

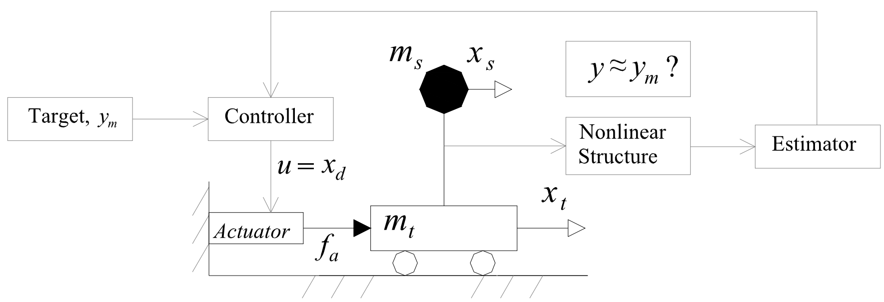

Figure 7-6 Tracking control of the shake table- structure 2DOF nonlinear system with unknown parameters

When a target motion at a structure is specified, the required control input $u(t) = x_d(t)$, the desired shake table displacement, is determined at every instant using the real time estimated parameters in order that the output of the system ($y(t) = \ddot{x}_s^t(t)$ the total acceleration of the structure) follows the target motion $y_m(t)$.

Example 7.2* : *A 2DOF Nonlinear System with Unknown Parameters

The properties of a given system are: m_s = 1 kips·sec^2/in., k_s = 355 kips/in., and c_s = 1.13 kips·sec/in., (f_n = 3.0 Hz, ξ_n = 0.03 before yielding). N = 3, d_y = 0.11 in. (f_y = 39 kips), and α = 0.1; i.e. all terms are explained in Eq. (4-2), for the hysteretic system and $\mu = m_s / m_t = 0.1$, $f_{n,a}$ = 30.0 Hz, ξ_a = 0.5 and k_a = 25 for the shake table. In order to examine the measurement noise effects, a zero-mean Gaussian white-noise process of 3% RMS noise-to-signal are added to the measurements $\underline{\overline{y}}_k = [\overline{x}_{s,k}\ \dot{\overline{x}}_{s,k}\ \overline{f}_{S,k}\ \overline{x}_{t,k}\ \dot{\overline{x}}_{t,k}\ \overline{f}_{a,k}/m_t]^T$, which are described in Section 5.2.1.3. Four unknown parameters: c_s the damping coefficient; k_s the elastic stiffness; α the post-yielding stiffness ratio to the elastic stiffness; and d_y the yielding displacement; are selected and estimated in real time using the extended Kalman filter.

The target motion is shown in Figure 7-8 (a – Target). The target motion is the total acceleration output generated from the same reference linear system (f_m = 5.0 Hz, ξ_m = 0.1), used for Example 6.1. in Section 6.4.1 (the reference input and the responses of the reference model are presented in Appendix A.2). For the parameter estimations, the initial parameter estimate $\underline{\hat{\theta}}_0$ is chosen as $\underline{\hat{\theta}}_0 = 0.8 \times \underline{\theta}^*$ (20%

error in the initial guess), and the initial covariance matrix is chosen as P_0 = diag([0 0 0 0 0 0 $\hat{c}_{s,o}{}^2$ $\hat{k}_{s,o}{}^2$ $\hat{\alpha}_o{}^2$ $\hat{d}_{y,o}{}^2]^T \times 0.01$). The covariance matrices Q_E and R_E are chosen as follows: $Q_E = 0 \times I_{10\times 10}$ (all zeroes) and the R_E = diagonal matrix, whose elements; i.e. noise variance = 3% × corresponding signal variance (noise variances are assumed to be known from the instruments information). The time step of 0.002 sec is used for the simulation.

The tracking control results using the *predictive tracking control* (PTC) method with the real time parameter estimations are presented in Figure 7-7 and Figure 7-9. The selected control parameters in this example $R = 0$ and $h = \sqrt{2} / \omega_e$ where $\omega_e = 100$. Figure 7-7 shows the comparisons between the true parameters and the estimated parameters: $k_T(\underline{x})$ the instantaneous stiffness (i.e. the estimate of $k_T(\underline{x})$ is computed using the estimates of k_s, α, and d_y); c_s the damping coefficient; k_s the elastic stiffness; α the post-yielding stiffness ratio to the elastic stiffness; and d_y the yielding displacement; and they show very good agreements. The controlled output, $\ddot{x}_s^t(t)$ the total acceleration of the structure, is shown in Figure 7-7 (a) [Controlled] and also shows very good agreement with the target motion. The computed control excitation input, $u(t) = x_d(t)$, using the control law in Eq. (7-5) is shown in Figure 7-8 (b). $x_s(t)$, $\dot{x}_s(t)$ the achieved displacement and velocity responses of the controlled structure are also presented in Figure 7-8 (c) and (d); it is noted that unlike the total acceleration (which was the target of the control design), the displacement and velocity responses are different from ones of the reference because the system properties of the controlled system and ones of the reference system are different. The relation between the structure resisting force $f_S(t)$ having hysteretic behavior and displacement $x_s(t)$ is also presented in Figure 7-8 (e). Figure 7-9 presents the responses of the shake table; the achieved shake table actuator force $f_a(t)$, shake table acceleration $\ddot{x}_t(t)$, displacement $x_t(t)$ and velocity $\dot{x}_t(t)$. As desired, all responses of the controlled system are bounded.

The tracking control results using the *feedback linearization tracking control* (FTC) method with the real time parameter estimations are also presented in Figure 7-10 and Figure 7-12. Figure 7-10 presents the results of the parameter estimation in real time. The controlled output $\ddot{x}_s^t(t)$ is shown in Figure 7-11 (a) [Controlled] and shows very good agreement with the target motion. The computed control excitation input, $u(t) = x_d(t)$, using the control law in Eq. (7-11) is shown in Figure 7-11 (b). As discussed in Section 7.3, the control excitation inputs of the two methods (PTC and FTC) are the same if one chooses the tracking error coefficients as $k_1^* = 2 / h = 2\xi_e\omega_e$ and $k_2^* = 2 / h^2 = \omega_e^2$; therefore, $\xi_e = \sqrt{2} / 2 \approx 0.707$ and $h = \sqrt{2} / \omega_e$; (in this example, $\omega_e = 100$, $\xi_e = 0.707$ for the both methods). As expected, the control results of two methods are equivalent as shown in Figure 7-7 through Figure 7-12.

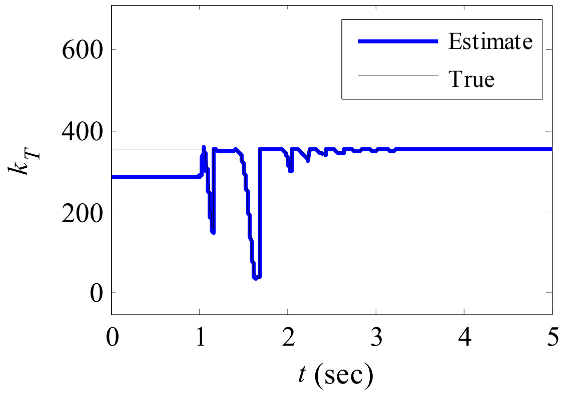

(a) Estimated parameter k_T

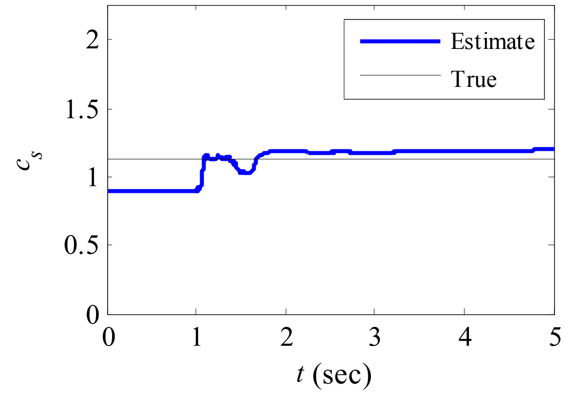

(b) Estimated parameter c_s

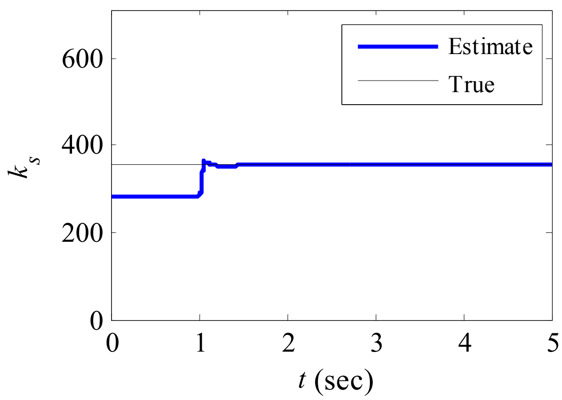

(c) Estimated parameter k_s

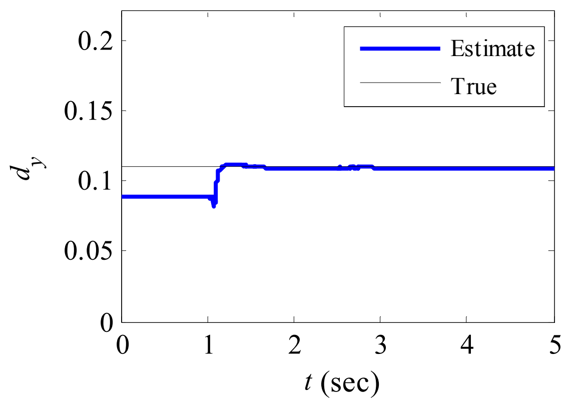

(d) Estimated parameter d_y

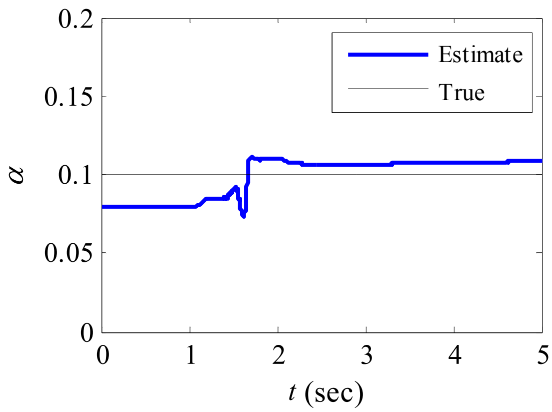

(e) Estimated parameter α

Figure 7-7 Real time parameter estimation results of the PTC for a 2DOF nonlinear system

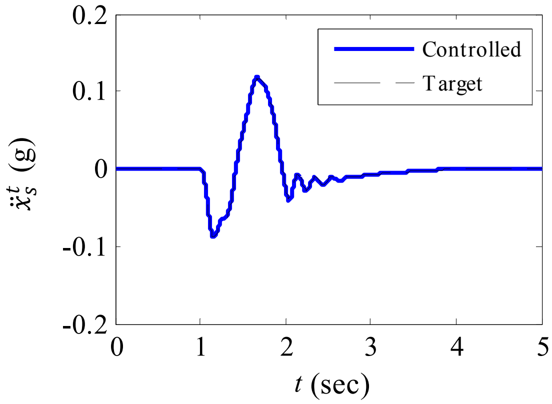

(a) Controlled (y) vs. Target motions (y_m)

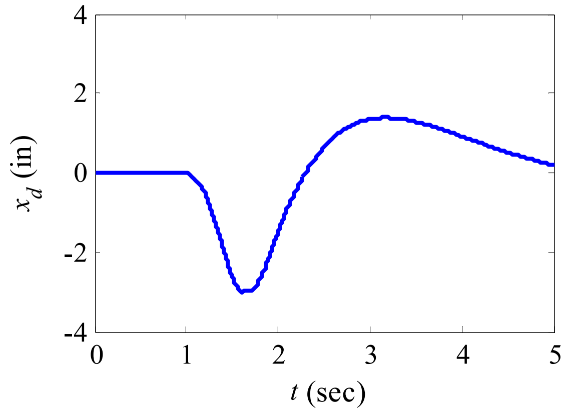

(b) Control excitation input (u)

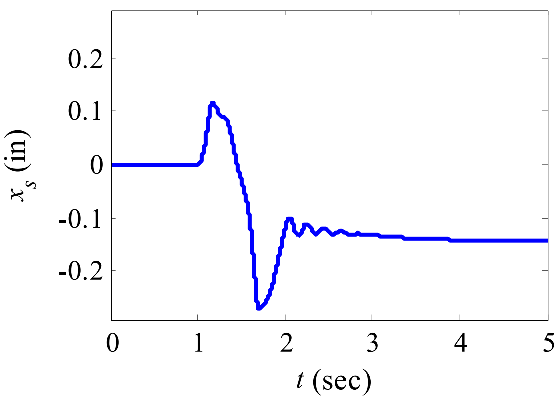

(c) Response of structure (x_s)

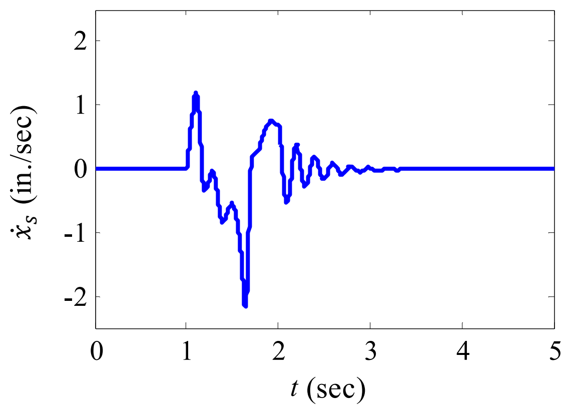

(d) Response of structure ($\dot{x}_s$)

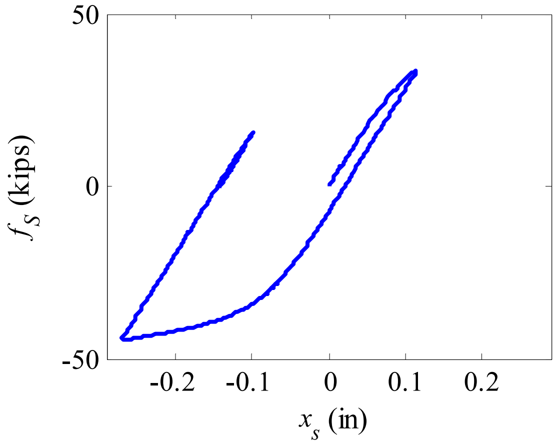

(e) Response of structure (f_S vs. x_s)

Figure 7-8 PTC - structure responses for a 2DOF nonlinear system with real time estimation

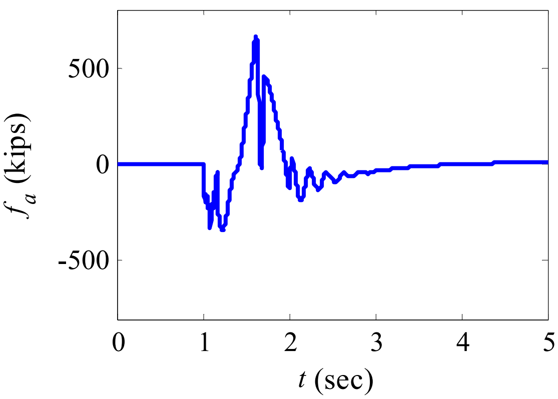

(a) Response of table (f_a)

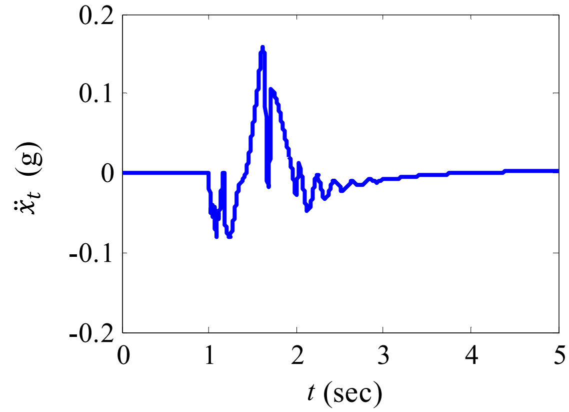

(b) Response of table ($\ddot{x}_t$)

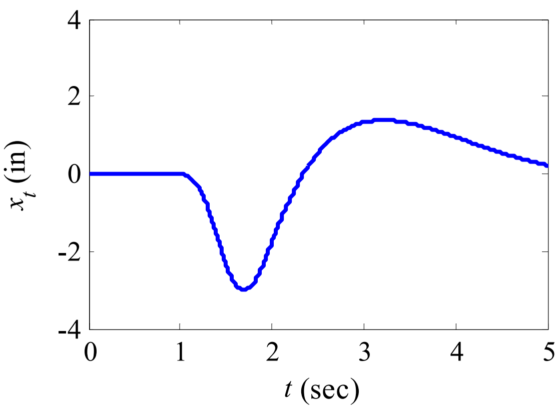

(c) Response of table (x_t)

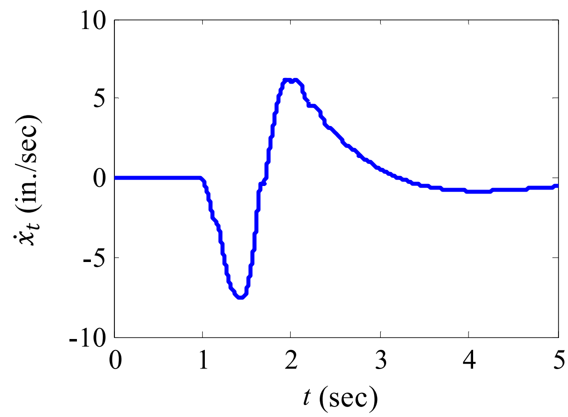

(d) Response of table ($\dot{x}_t$)

Figure 7-9 PTC - shake table responses for a 2DOF nonlinear system with real time estimation

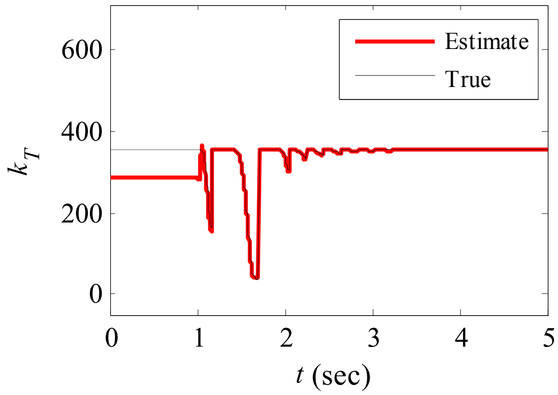

(a) Estimated parameter k_T

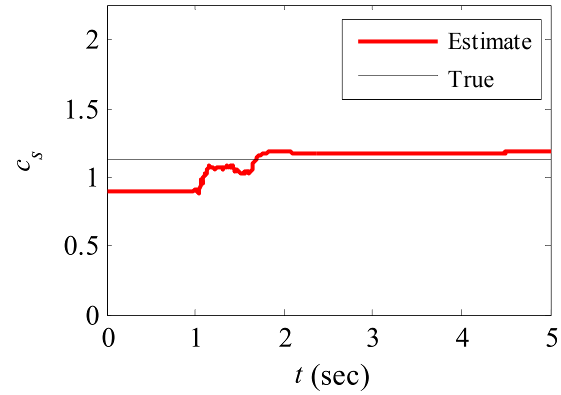

(b) Estimated parameter c_s

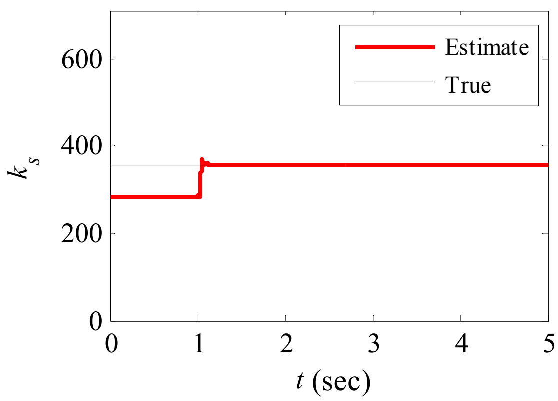

(c) Estimated parameter k_s

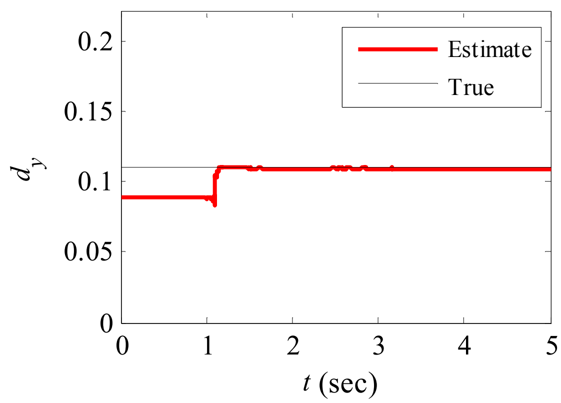

(d) Estimated parameter d_y

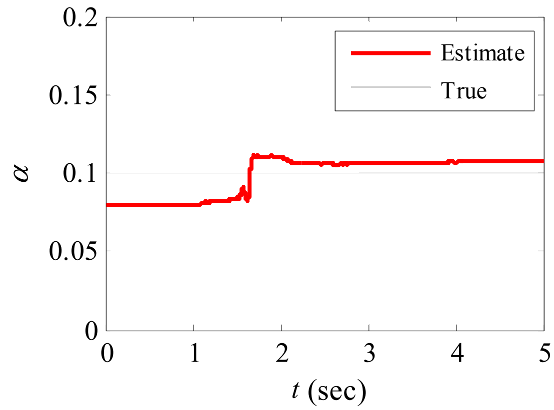

(e) Estimated parameter α

Figure 7-10 Real time parameter estimation results of the FTC for a 2DOF nonlinear system

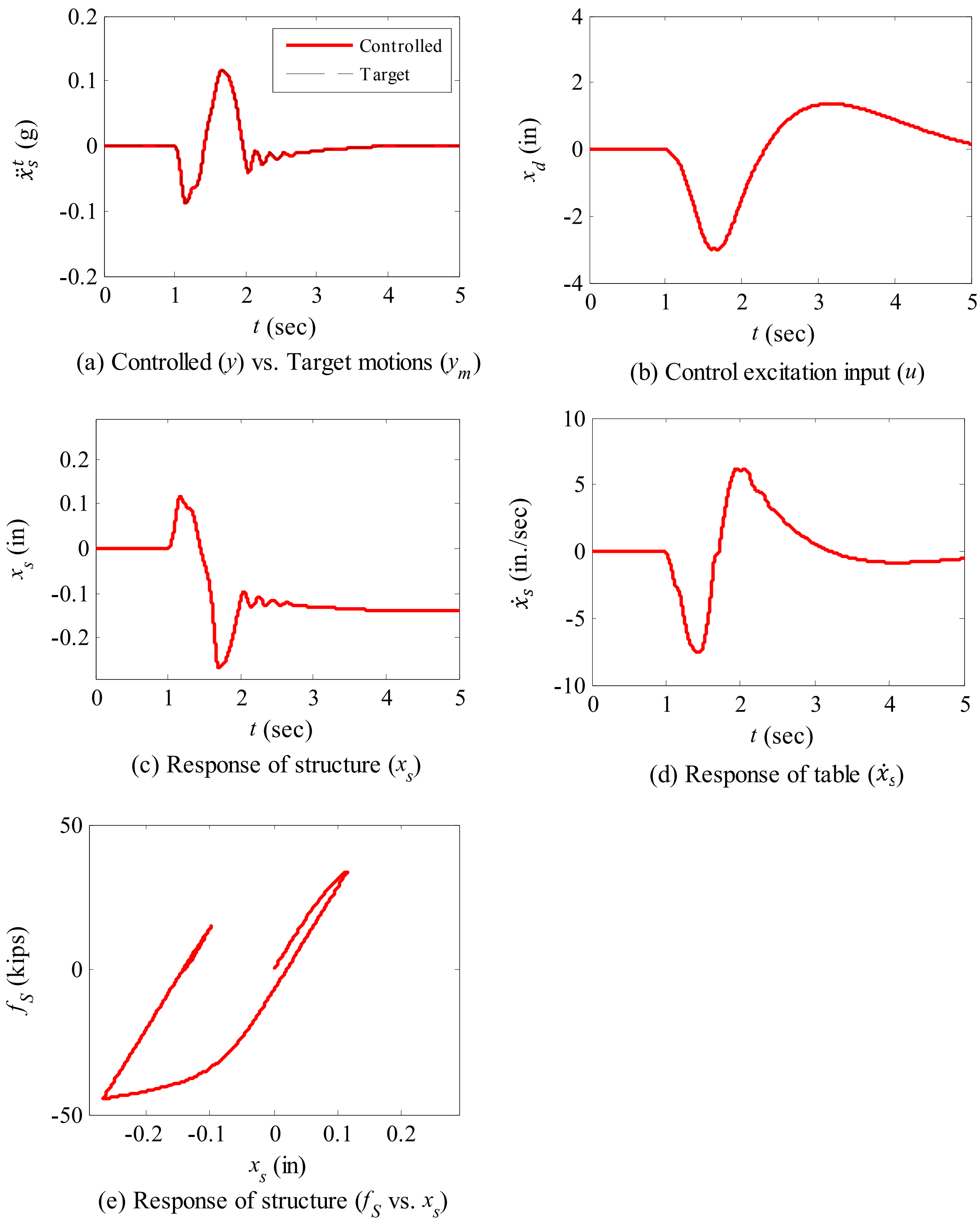

(a) Controlled (y) vs. Target motions (y_m)

(b) Control excitation input (u)

(c) Response of structure (x_s)

(d) Response of table ($\dot{x}_s$)

(e) Response of structure (f_S vs. x_s)

Figure 7-11 FTC - structure responses for a 2DOF nonlinear system with real time estimation

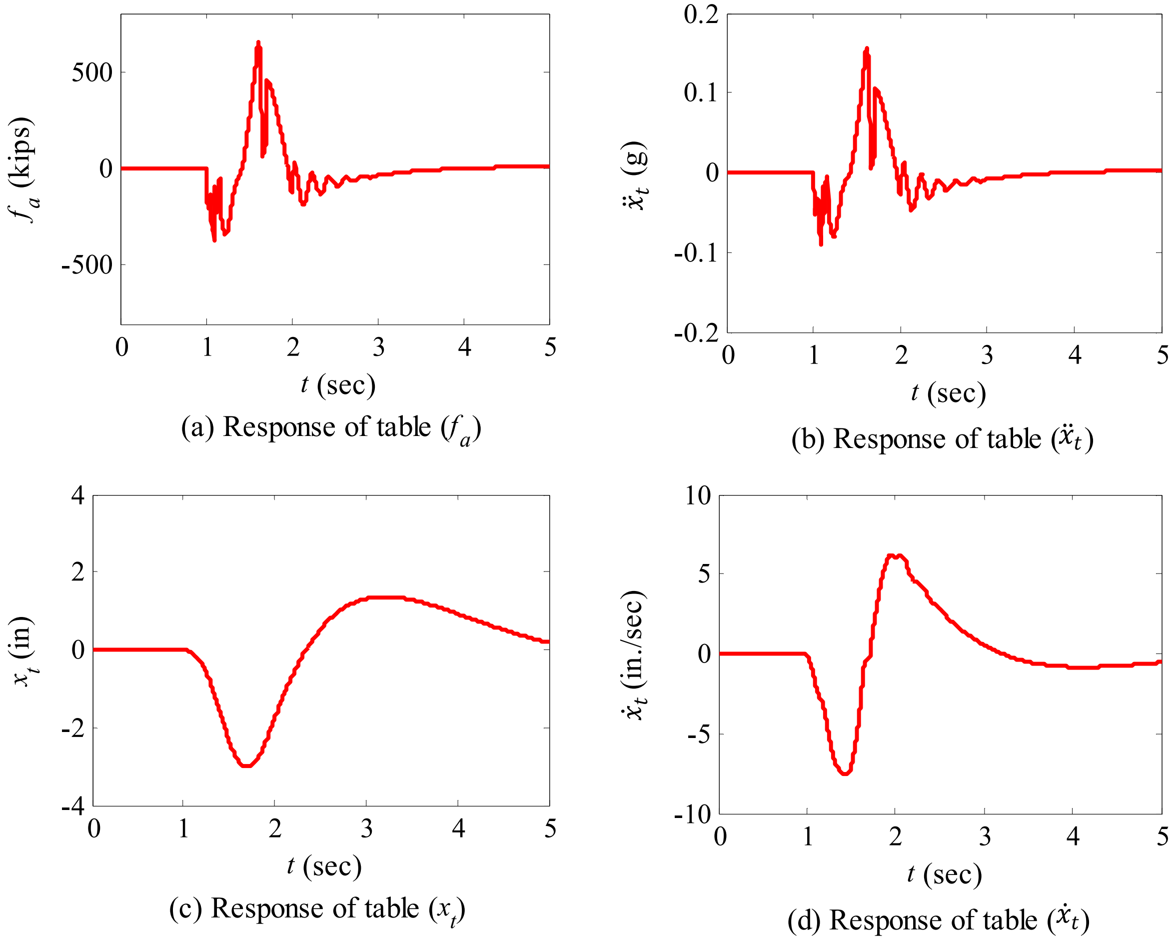

(a) Response of table (f_a)

(b) Response of table ($\ddot{x}_t$)

(c) Response of table (x_t)

(d) Response of table ($\dot{x}_t$)

Figure 7-12 FTC - shake table responses for a 2DOF nonlinear system with real time estimation

In this section, the two tracking controllers, combined with the real time estimators using the *extended Kalman filter* (EKF), proposed in the previous section are expanded to the control applications of nonlinear hysteretic specimens using the shake table motion. The tracking control laws are reformulated in order to adapt the estimated parameters. Numerical simulations are performed and the results show very good agreements between the target motion and the selected output of the controlled system. All responses of controlled systems are bounded and the estimated parameters converge to their true values with fairly good initial guess of unknown parameters (i.e. 20% errors in the initial guess are used in the examples).

"This Page Intentionally Left Blank"

SECTION 8
NUMERICAL SIMULATIONS FOR A SHAKE TABLE – STRUCTURE SYSTEM

The feedback tracking control method combined with the real time parameter estimator is applied to a realistic shake table and structure system whose characteristics are obtained from the real systems in the Structural Engineering and Earthquake Simulation Laboratory (SEESL) at the University at Buffalo (UB). Numerical simulations are performed for practical target motions generated from the selected excitation motions including real earthquake motions. The results will show the feasibility and the limitations of the proposed tracking control method in real applications.

8.1 Test Setup

The selected system for the simulation study consists of a shake table and an SDOF structure. The shake table consists of one uniaxial actuator having the maximum horizontal actuator force = 5.5 kips and 4 × 3 ft. platform as shown in Figure 8-1 (a) (Stefanakis and Sivaselvan, 2015). The structure in this simulation, shown in Figure 8-1 (b), is a three-story steel frame shear building rigidly braced in the top two floors to simulate an SDOF system (Chung, Reinhorn, and Soong, 1989). The weight of the structure is 6.4 kips. The model was previously used in multiple studies of control, either active or passive (Chung, Reinhorn, and Soong, 1989, Soong, 1990, Symans and Constantinou, 1997, Dyke et al., 1994, Stefanakis and Sivaselvan, 2015, etc.) and can be considered as a benchmark model for control studies.

(a) Uniaxial shake table
(after Stefanakis and Sivaselvan, 2015)

(b) SDOF steel frame structure
(after UB-SEESL, 2015)

Figure 8-1 UB uniaxial shake table and an SDOF structure

The properties of the shake table and the SDOF test structure are summarized in Table 8-1. It is noted that in real life experiments after mounting the structure on the shake table, the properties presented here are subject to change because of the shake table-structure interaction. Therefore it is necessary to identify them again using quasi-static (e.g. impact hammer and snap-back tests) and/or dynamic (e.g. white noise tests - the curve fitting methods using the obtained transfer functions) system identification procedures as described in Bracci et al., (1992) and Rinawi and Clough (1991). In this study, however, the properties presented in Table 8-1 are used for the numerical simulations.

Table 8-1 Properties of the UB uniaxial shake table and the SDOF structure

System	Item	Description
(1)	(2)	(3)
Shake table	Platform size	4.0 ft × 3.0 ft
	Base plate size (for structure installation)	4.5 ft × 4.5 ft
	Maximum specimen weight	33.6 kips
	Maximum overturning moment	82.0 kip-ft
	Frequency of operation	0.1~30 Hz
	Maximum actuator force; $f_{a,max}$	5.5 kips
	Stroke (X axis); $x_{t,max}$	3.0 in.
	Platform weight (with base plate); m_t × g	3.5 kips
	Fundamental frequency; $f_{n,a}$	30 Hz
	Equivalent damping ratio; ξ_a	50* %
	Control gain factor; k_a	25ǂ
SDOF structure	Weight; m_s × g	6.5 kips
	Elastic stiffness; k_s	8.0 kips/in.
	Damping coefficient; c_s	0.0091 kips·sec/in.
	Fundamental frequency; $f_{n,s}$ (before yielding)	3.47 Hz
	Inherent damping ratio; ξ_s	1.24 %
	Yielding force§; f_y	5.6 kips
	Post-yielding stiffness ratio to the elastic stiffness; α	0.1

* Equivalent damping ratio of the shake table in open-loop conditions is ξ_a = 10%; the damping ratio can be increased by feedback (Rinawi and Clough, 1991) to ξ_a = 50 %, as assumed in this numerical study.

ǂ Control gain factor can be identified from the test setup; in this study k_a = 25 assumed.

§ Different yielding forces are selected for different tests in order to demonstrate the hysteresis behavior effects on the tracking control.

Figure 8-2 shows the schematic of the tracking control test setup for the shake table-structure. The target motion $y_m(t)$ is pre-defined according to test objectives. The control excitation input $u(t) = x_d(t)$ is computed by using a tracking control method (i.e. the *predictive tracking control* (PTC) method or *feedback linearization tracking control* (FTC) method) introduced in the previous sections with the measurements from instrument sensors. In order to examine the measurement noise effects, a zero-mean Gaussian white-noise process of 3% noise-to-signal RMS are added to the measurements $\underline{\overline{y}}_k$ = [$\overline{x}_{s,k}$ $\dot{\overline{x}}_{s,k}$ $\overline{f}_{S,k}$ $\overline{x}_{t,k}$ $\dot{\overline{x}}_{t,k}$ $\overline{f}_{a,k}/m_t]^T$, which are described in Section 5.2.1.3. Four unknown parameters: c_s the damping coefficient; k_s the elastic stiffness; α the post-yielding stiffness ratio to the elastic stiffness; and d_y the yielding displacement; are selected. The *extended Kalman filter* (EKF) is used to estimate the system responses from contaminated responses with measurement noise and the unknown parameters as the procedure is described in the previous sections.

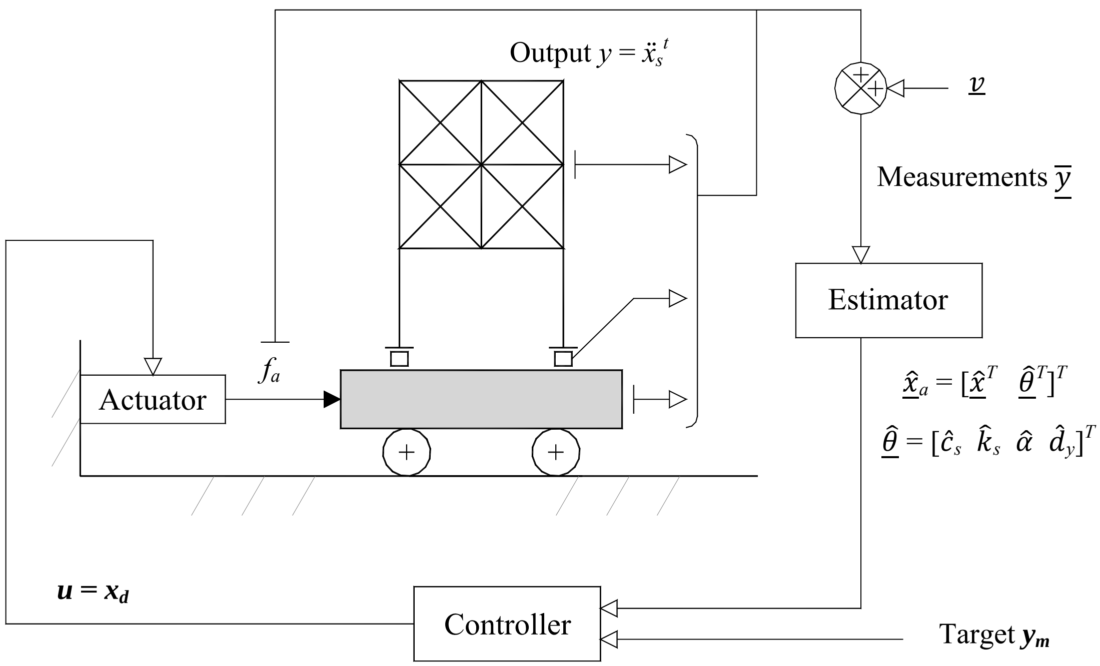

Figure 8-2 Tracking control of an SDOF nonlinear system using a shake table with unknown parameters

8.2 Test Protocol and Loading

The control objective of this study is to compute the control excitation input $u(t)$ to drive the shake table in order to simulate a target motion $y_m(t)$ at any specific location in the test structure. For this numerical simulation, the target motion is the total acceleration of a structure (specimen) mounted on the shake table although any response; i.e. displacement or velocity response, can be selected as the target motion. In this testing program, several target motions $y_m(t)$ are selected to examine the tracking control performance.

First, for Test #1 through Test #3 the target motions are the total acceleration outputs generated from a reference linear system, whose properties are: m_m = 6.5 kips/g, k_m = 16.6 kips/in., and c_m = 0.053 kips·sec/in. (f_m = 5.0 Hz, ξ_m = 0.05), subjected to one-cycle sine excitation input whose frequency = 1.0 Hz, 5.0 Hz, and 10.0 Hz and which is high-pass filtered at 0.2 Hz cutoff frequency. The purpose of these one-cycle sine motion tests where the lengths of the excitation time are relatively short is to check the feasibility of the control algorithm and to calibrate the design parameters of the tracking controller and estimator such as the tracking error dynamic coefficients k_1^* and k_2^* for controllers and the initial estimator guesses of $\underline{\hat{\theta}}_0$ and P_0 as defined in the previous sections. After ensuring that the controller can simulate these simple motions, more complex target motions are given to be tracked.

Second, for Test #4 to Test #5 the target motions are the total acceleration outputs generated from the same reference linear system, subjected to a real earthquake motion, Elcentro N-S, 1940 (Vibrationdata, 2015) 100% and 80%, which are high-pass filtered at 0.3 Hz cutoff frequency. These tests are performed to verify if the tracking controller can produce the realistic target floor motion at the top of the structure. It is expected that at the beginning the tracking error might be large due to the estimate error in unknown parameters, but the tracking error will diminish as the estimate error is reduced by the estimator.

Third, for Test #6 to Test #7 the target motions are the random floor motions generated to match the *required response spectrum* (RRS) per the ICC-ES AC156 (ICC, 2010), which are high-pass filtered at 0.2 Hz cutoff frequency and low-pass filtered at 25 Hz cutoff frequency to meet the shake table operation capacity. These tests are also performed to verify if the tracking controller can produce the realistic, general target floor motion at the top of the structure. It is noted that no reference model is used to generate the target floor motion, since the floor motion is directly defined according to the AC156. Similar performances with Test #4 and #5 are expected.

The testing program is summarized in Table 8-2.

Table 8-2 Testing program of the tracking control of the shake table-structure system

Test No.	Target motion* description
(1)	(2)
1	Reference model response subjected to one-cycle sine excitation whose freq. = 1.0 Hz
2	Reference model response subjected to one-cycle sine excitation whose freq. = 5.0 Hz
3	Reference model response subjected to one-cycle sine excitation whose freq. = 10.0 Hz
4	Reference model response subjected to Elcentro N-S 100% excitation
5	Reference model response subjected to Elcentro N-S 80% excitation
6	Floor motion to match the RRS 100% per AC156
7	Floor motion to match the RRS 30% per AC156

* All excitations are filtered as explain in the text to meet the shake table operation capacity.

8.3 Simulation Results

The tracking control results using the *feedback linearization tracking control* (FTC) method combined with the *extended Kalman filter* (EKF) estimator are obtained through numerical analyses; some of the interesting results are presented herein.

As discussed above, the purpose of Test #1 to #3 are to check the feasibility of the control algorithm and to calibrate the parameters of the controller and estimator; therefore, only the tracking performances between the target motion y_m and output y of the controlled structure are presented in Figure 8-3 (more results of Test #2 can be found in Appendix A.3). From the results of these pre-tests, it is ensured that the unknown parameters can be fairly accurately estimated at the beginning of the procedure, and the output follows the target motion very well and all responses are bounded in the interested time range, as desired.

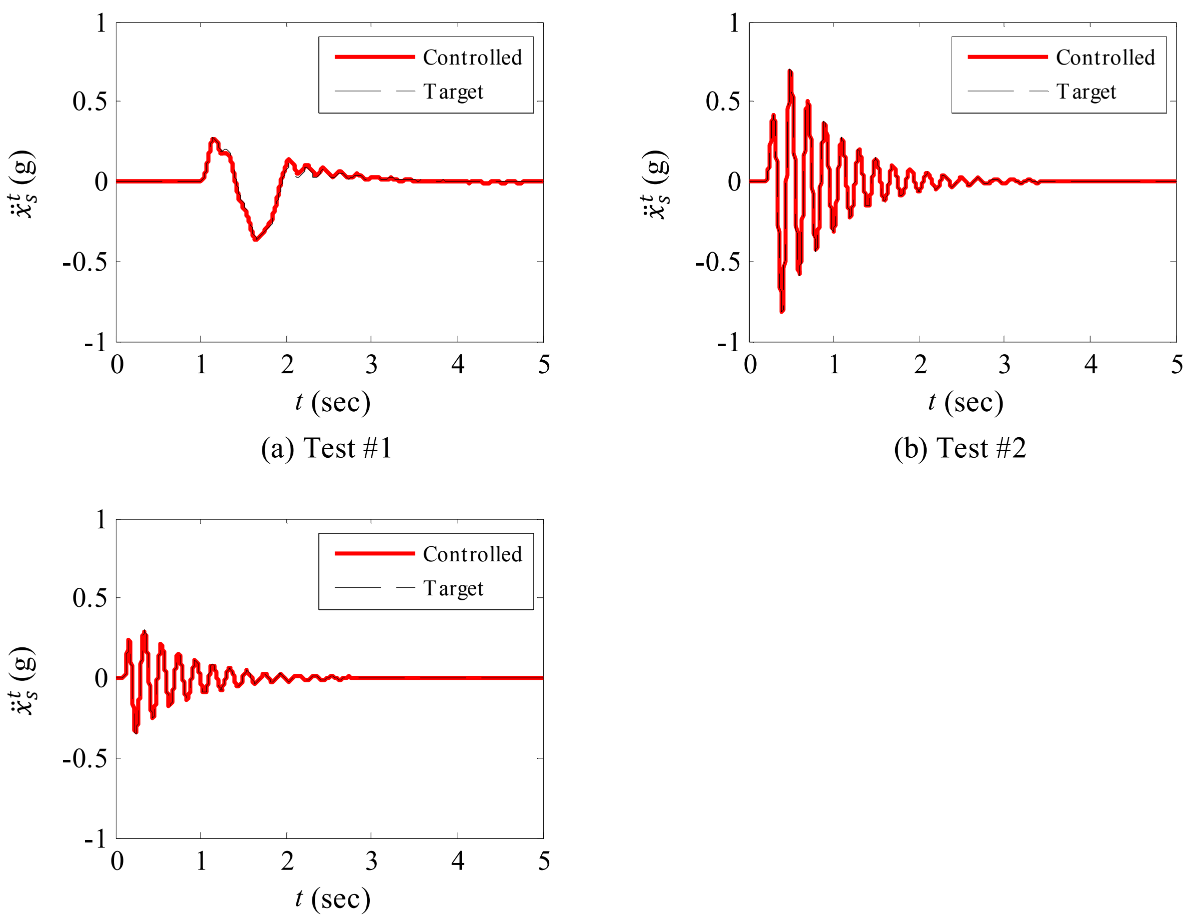

(a) Test #1

(b) Test #2

(c) Test #3

Figure 8-3 Tracking performances: Controlled (y) vs. Target motions (y_m) (Test #1 to #3)

The selected control parameters for the FTC are $k_1^* = 2\xi_e\omega_e$ and $k_2^* = \omega_e^2$ where $\omega_e = 25$, $\xi_e = 0.707$. For the parameter estimations using the EKF, the initial parameter estimate $\hat{\underline{\theta}}_0$ is chosen as $\hat{\underline{\theta}}_0 = 0.8 \times \underline{\theta}^*$ (20% error in the initial guess), and the initial covariance matrix is chosen as P_0 = diag([0 0 0 0 0 0 $\hat{c}_{s,o}{}^2$ $\hat{k}_{s,o}{}^2$ $\hat{\alpha}_o{}^2$ $\hat{d}_{y,o}{}^2]^T \times 0.01$). The error covariance matrices Q_E and R_E are chosen as follows: $Q_E = 0 \times I_{10\times 10}$ (all zeroes) and the R_E = diagonal matrix, whose elements; i.e. noise variance = 3% × corresponding signal variance (noise variances are assumed to be known from the instruments information). The time step of 0.002 sec (sampling rate = 500 sec^{-1}) is used for the simulations. The tracking control results of Test #4 and #5 are presented in Figure 8-4 through Figure 8-8. The target motion and the controlled output of Test #4 are compared in Figure 8-4 (a) and show very good agreements. Figure 8-4 (b) presents the control excitation input $u(t)$. The structure responses: the relative displacement $x_s(t)$ of the structure and the relation between the resisting force $f_S(\underline{x})$ and the relative displacement $x_s(t)$, are shown in Figure 8-4 (c) and (d), respectively. Figure 8-6 presents the parameter estimation results and show fast convergence to the true values.

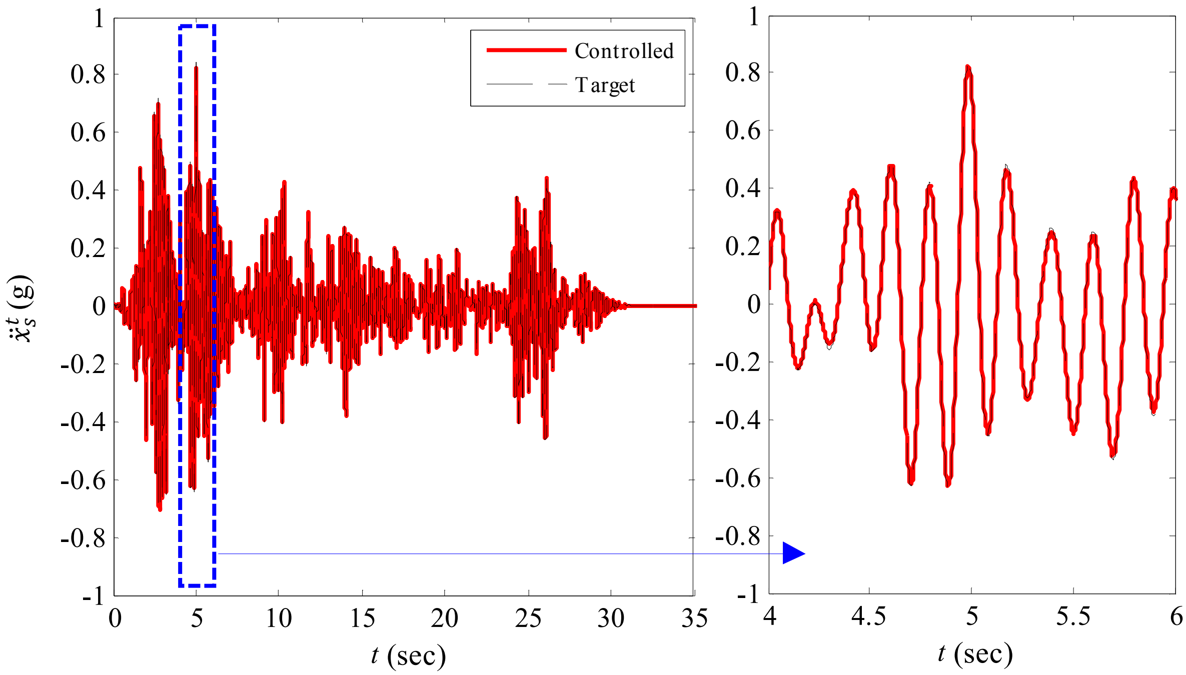

(a) Controlled (y) vs. Target motions (y_m)

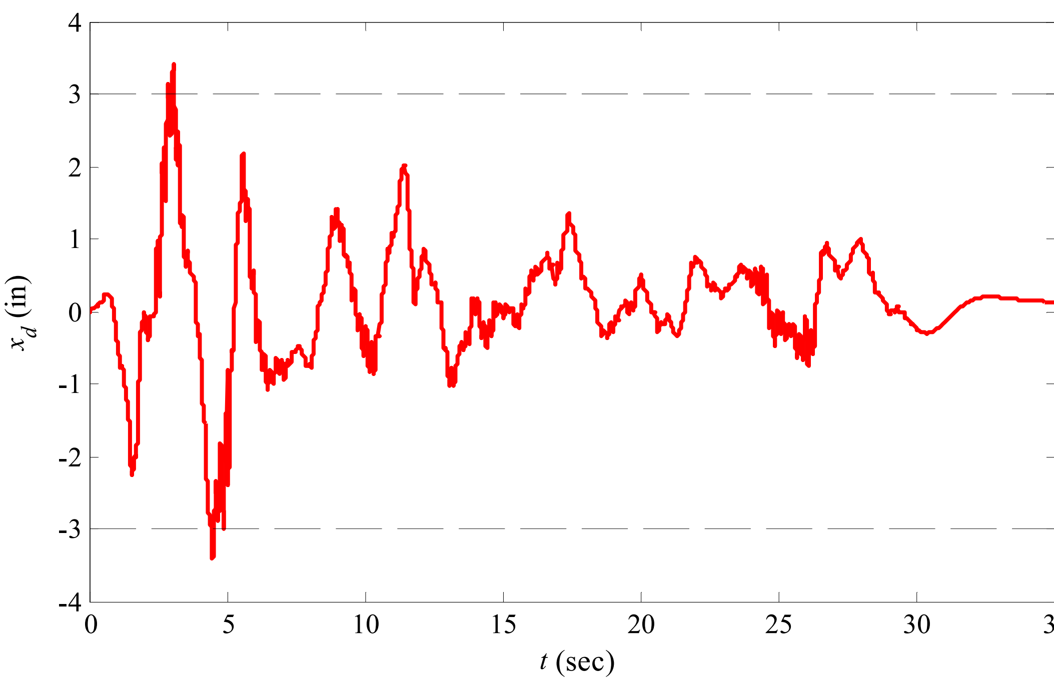

(b) Control excitation input (u)

Figure 8-4 Tracking control - structure responses (Test #4)

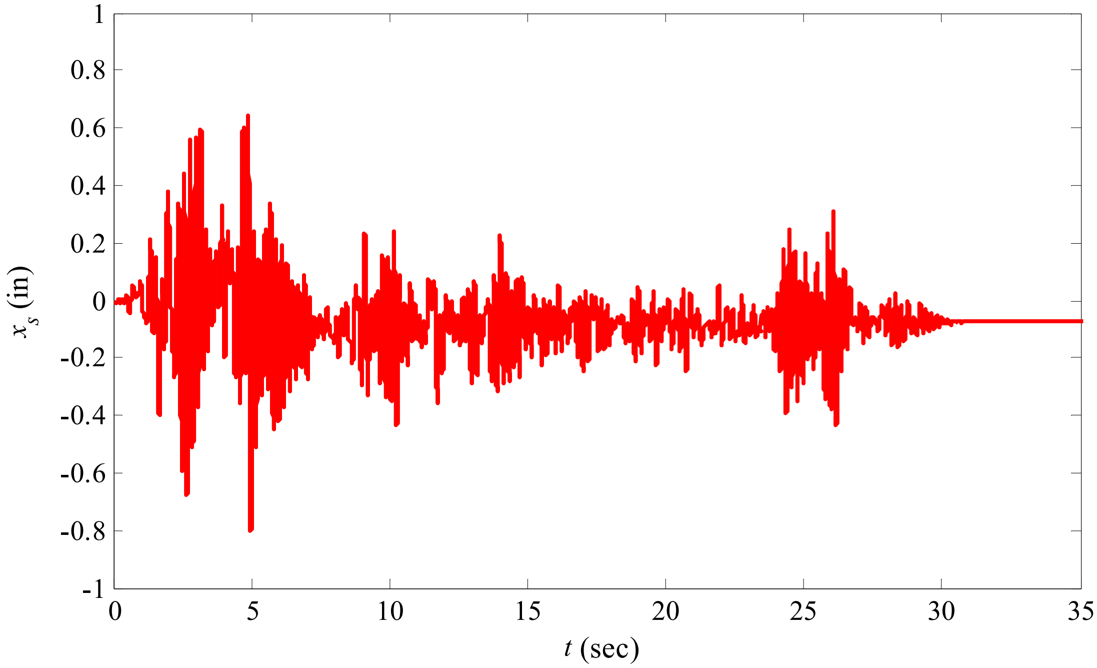

(c) Response of structure (x_s)

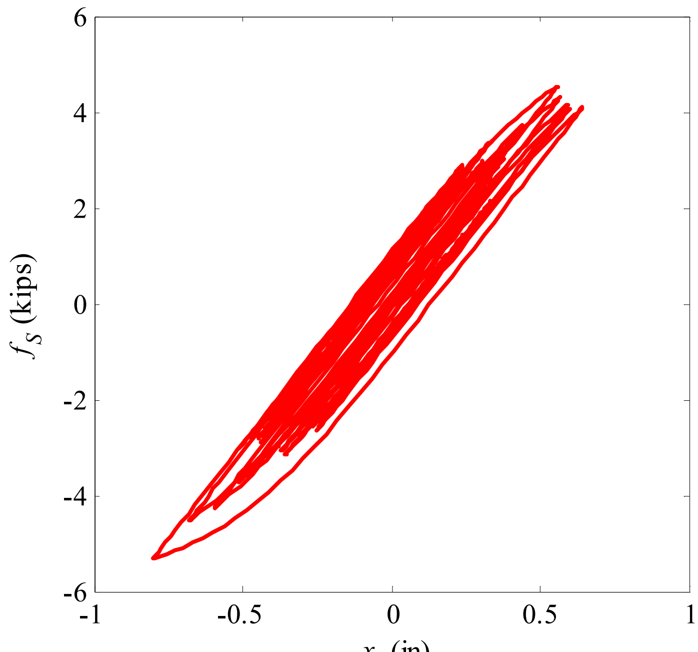

(d) Response of structure (f_S vs. x_s)

Figure 8-4 (Cont'd) Tracking control - structure responses (Test #4)

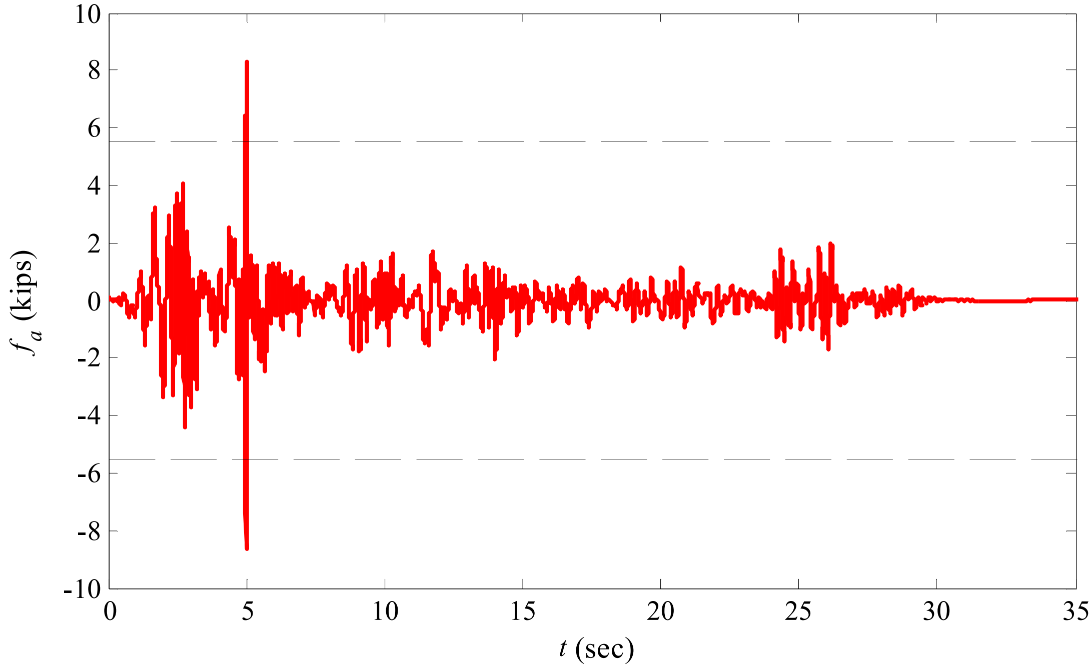

(a) Response of table (f_a)

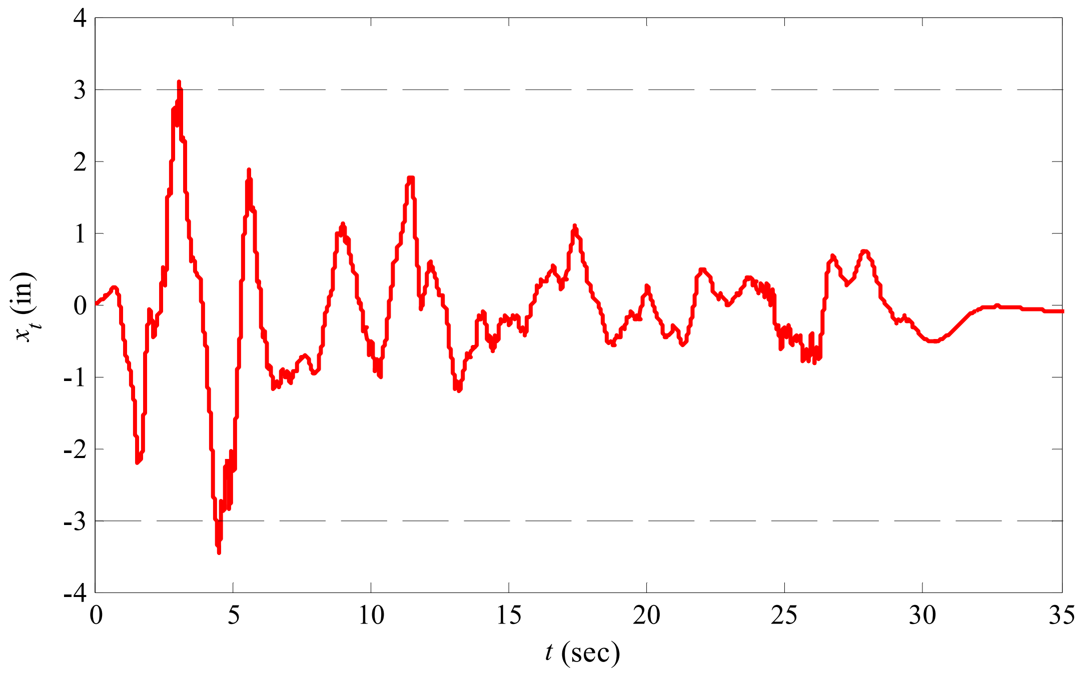

(b) Response of table (x_t)

Figure 8-5 Tracking control – shake table responses (Test #4)

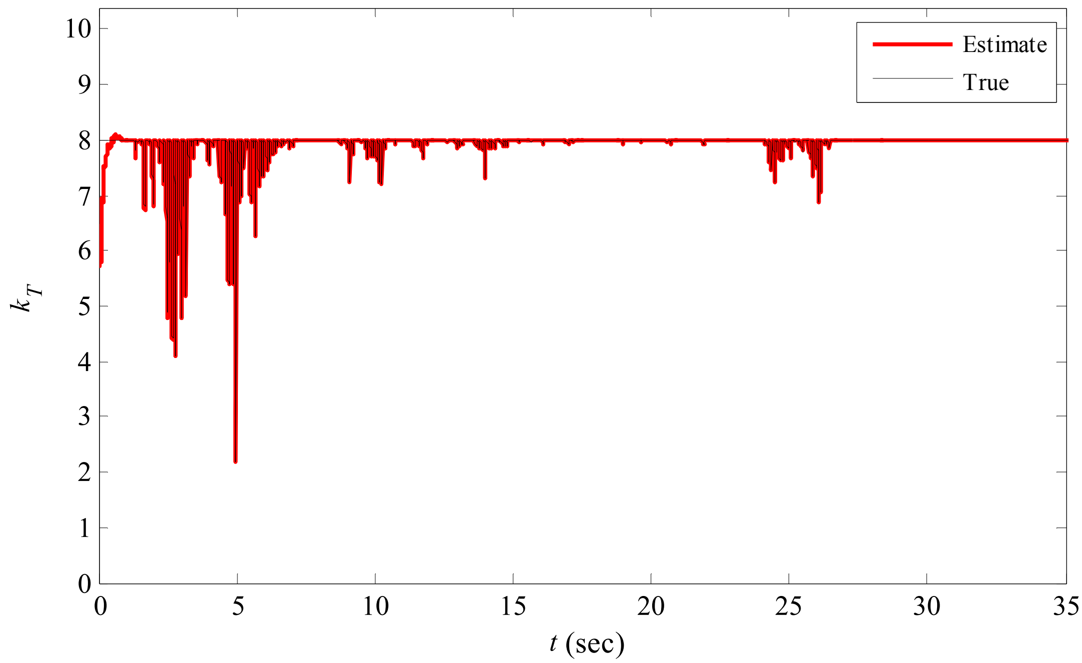

(a) Estimated parameter k_T

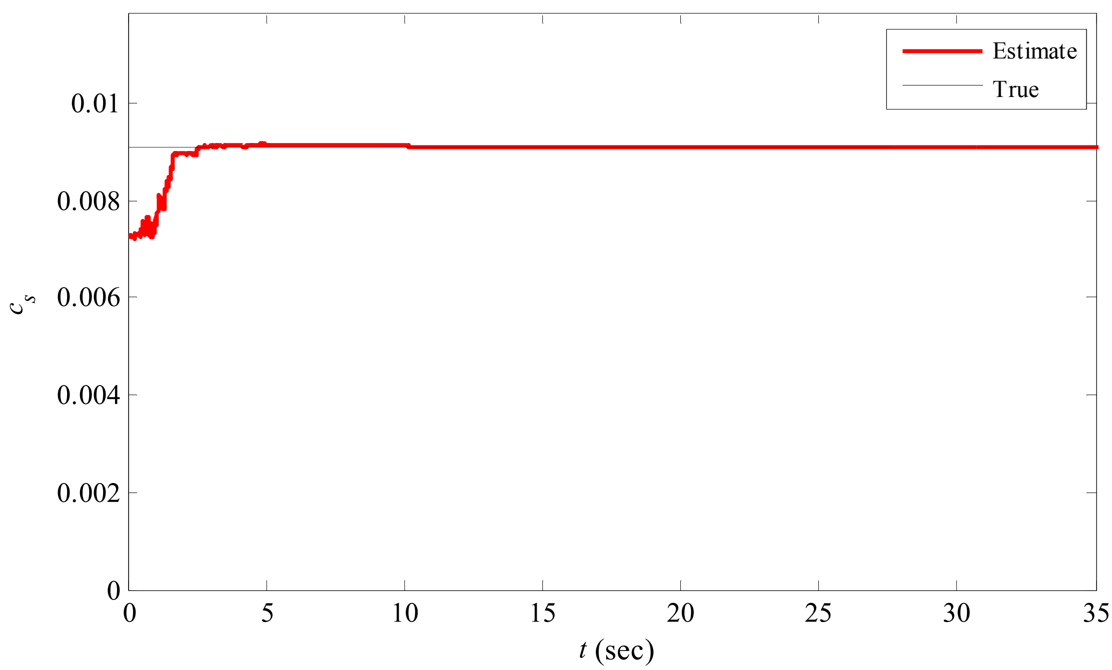

(b) Estimated parameter c_s

Figure 8-6 Real time parameter estimation results of tracking control (Test #4)

Although the tracking performance is very good and all responses of the controlled system are bounded, Figure 8-5 shows that the actuator force $f_a(t)$ and table displacement $x_t(t)$ operating capacities (shown in Table 8-1) of the shake table are exceeded. This limitation might be overcome by adjusting the target motion and/or the properties of the structure and shake table. In this study, the reference excitation is reduced by 20% (as usually done for practical purposes in laboratory when the equipment has limitations) such that the target motion is generated from the reference model subjected to Elcentro N-S 80% excitation, which is used for the target motion in Test #5.

The results of Test #5 are shown in Figure 8-7 and Figure 8-8. Figure 8-7 (a) shows the comparison between the target motion and the controlled output and show very good agreement. Figure 8-7 (b) presents the control excitation input $u(t)$. As expected, using the reduced amplitude of the target motion, the actuator force $f_a(t)$ and table displacement $x_t(t)$ responses of the shake table are within the limits as shown in Figure 8-8. It is noted that the reduced demand (the target motion) requires smaller resisting force and structural deformation as shown in Figure 8-7 (c) and (d), such that less nonlinear hysteresis behavior occurs and results in smaller responses of the shake table.

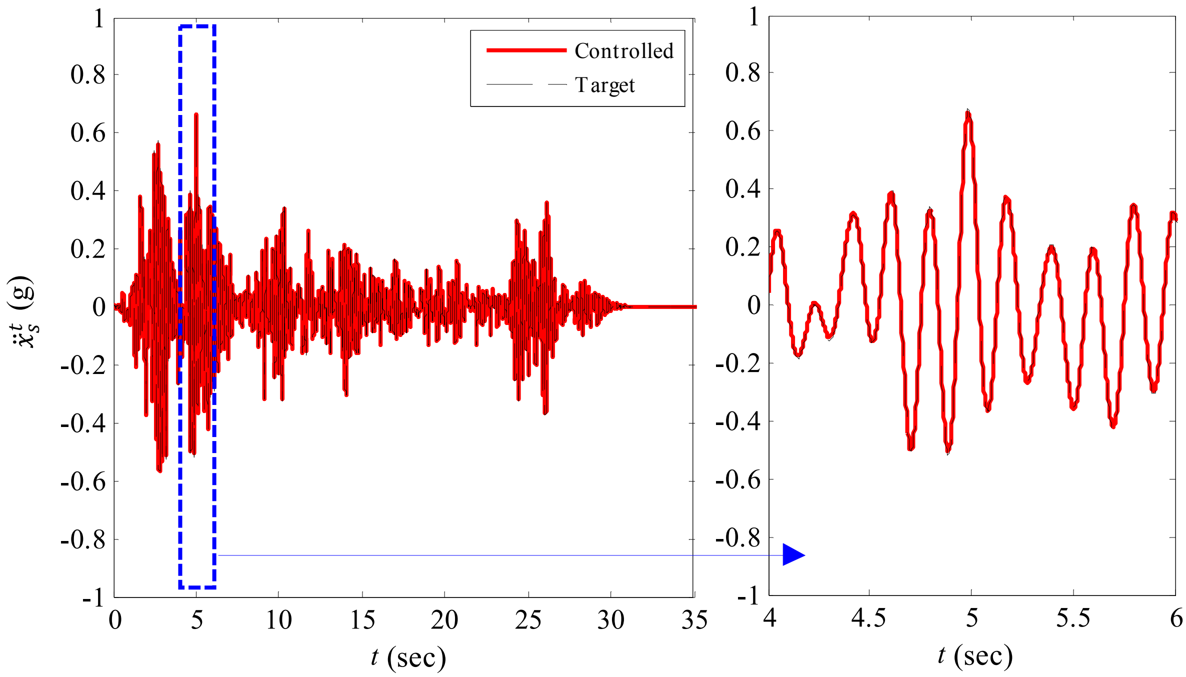

(a) Controlled (y) vs. Target motions (y_m)

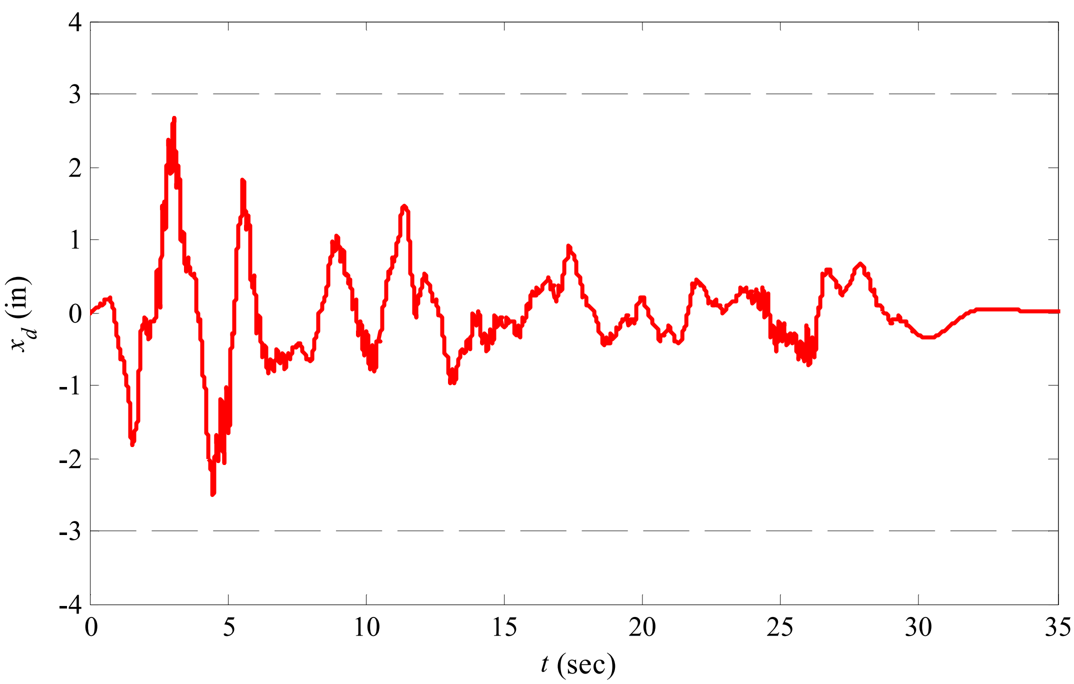

(b) Control excitation input (u)

Figure 8-7 Tracking control - structure responses (Test #5)

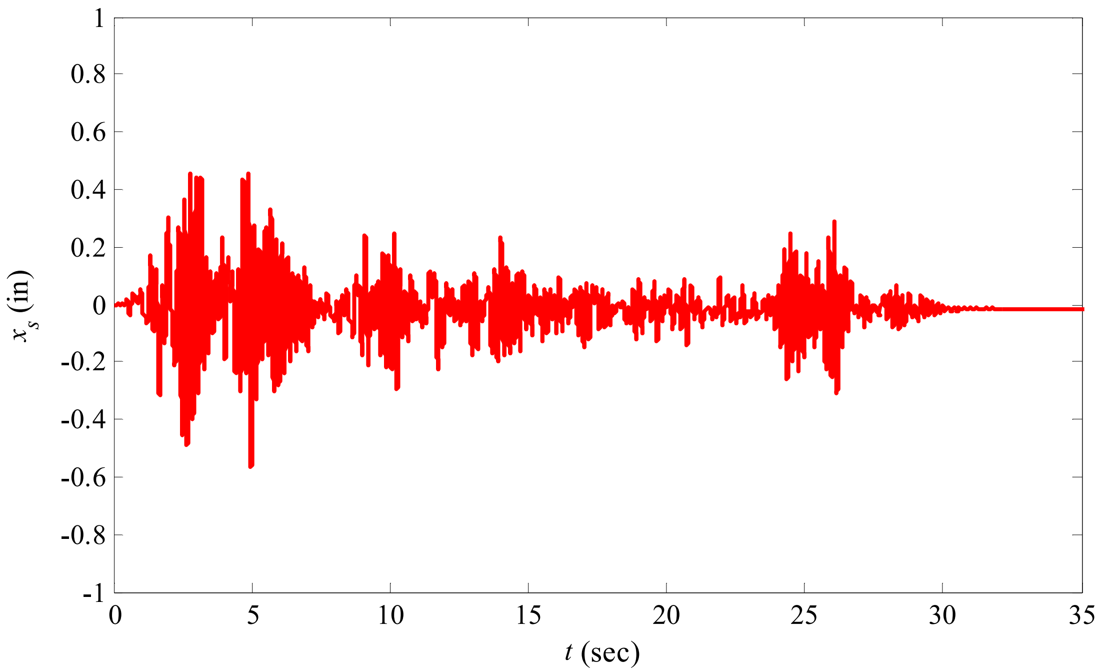

(c) Response of structure (x_s)

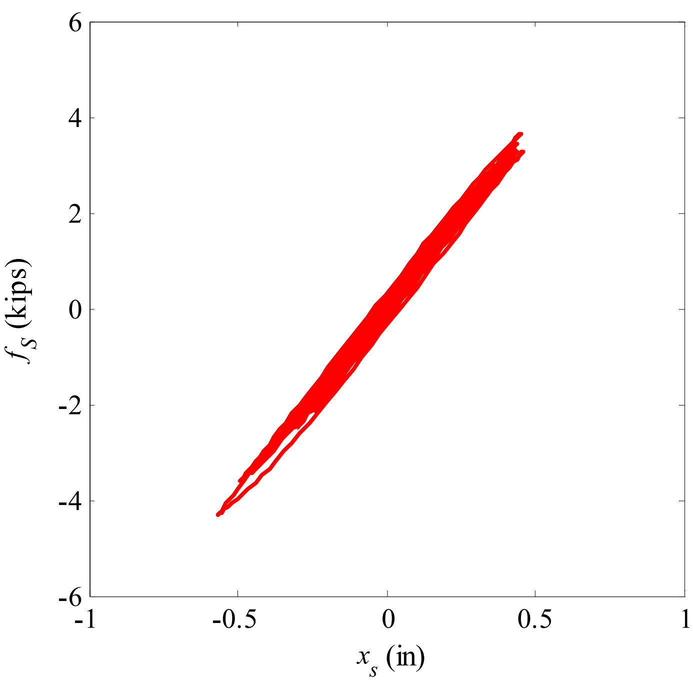

(d) Response of structure (f_S vs. x_s)

Figure 8-7 (Cont'd) Tracking control - structure responses (Test #5)

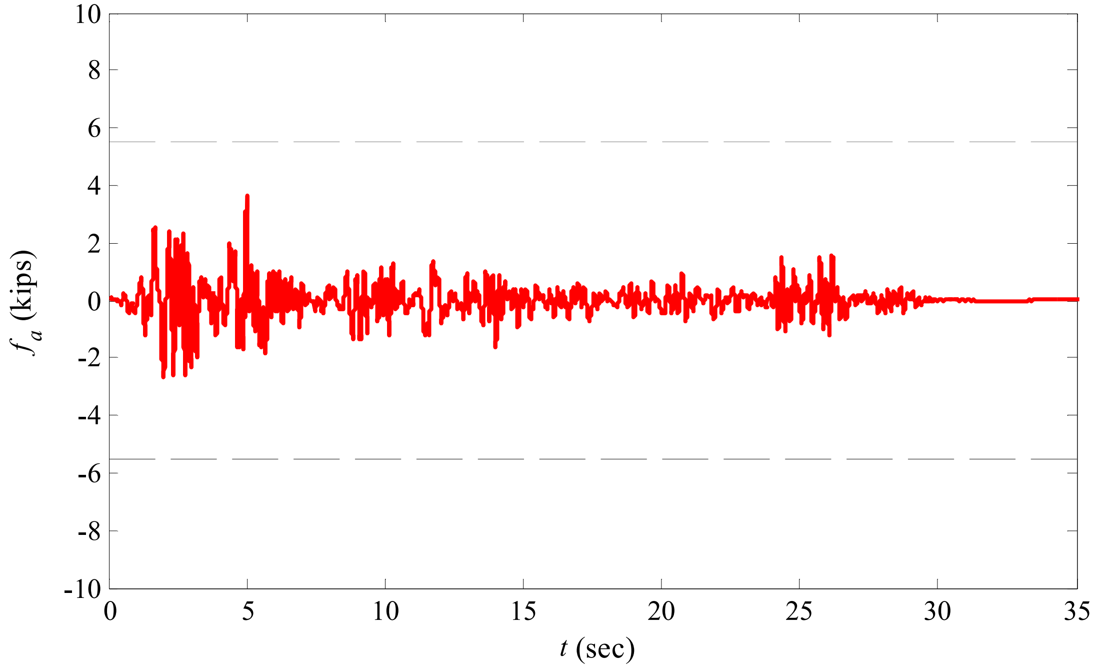

(a) Response of table (f_a)

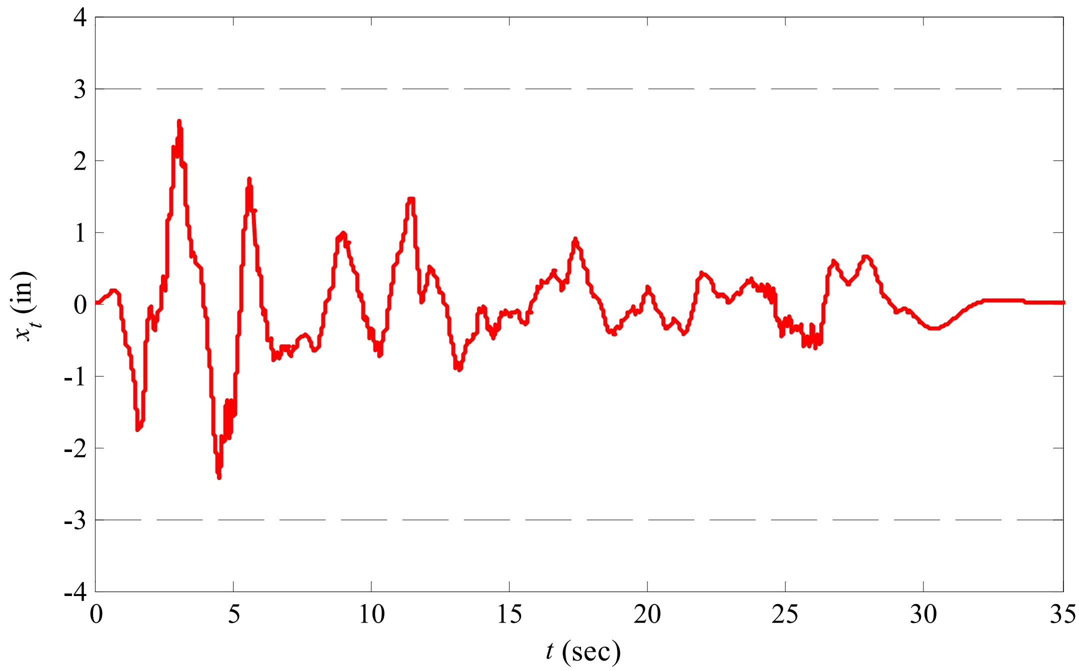

(b) Response of table (x_t)

Figure 8-8 Tracking control – shake table responses (Test #5)

The tracking control results for qualification testing obtained from Test #6 and #7 are presented in Figure 8-9 through Figure 8-13. For Test #6 and #7, the yielding force f_y = 3.4 kips used (instead of 5.6 kips in Table 8-1, but all other values in the table are the same); i.e. if the same yielding force was used, only mild hysteresis behavior would have occurred with this target motion. The decrease insured possibility to emphasize performance in a nonlinear structure. The selected control parameters for the FTC in Test #6 and #7 simulations are $k_1^* = 2\xi_e\omega_e$ and $k_2^* = \omega_e^2$ where $\omega_e = 25.6$, $\xi_e = 0.707$. The time step of 0.002 sec (sampling rate = 512 sec^{-1}) is used. The target motion and the controlled output of Test #6 are compared in Figure 8-9 (a) and show very good agreements. Figure 8-9 (b) presents the control excitation input $u(t)$. The structure responses: the relative displacement $x_s(t)$ of the structure and the relation between the resisting force $f_S(\underline{x})$ and the relative displacement $x_s(t)$, are shown in Figure 8-9 (c) and (d), respectively. Figure 8-11 presents the parameter estimation results and show fast convergence to the true values.

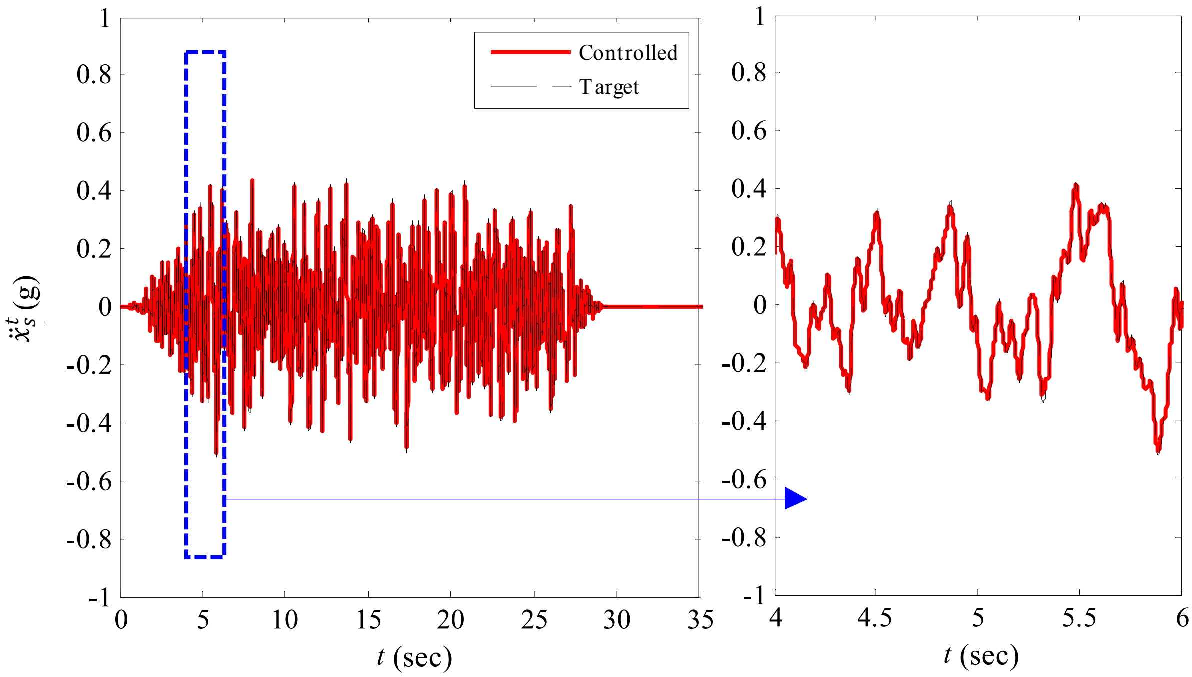

(a) Controlled (y) vs. Target motions (y_m)

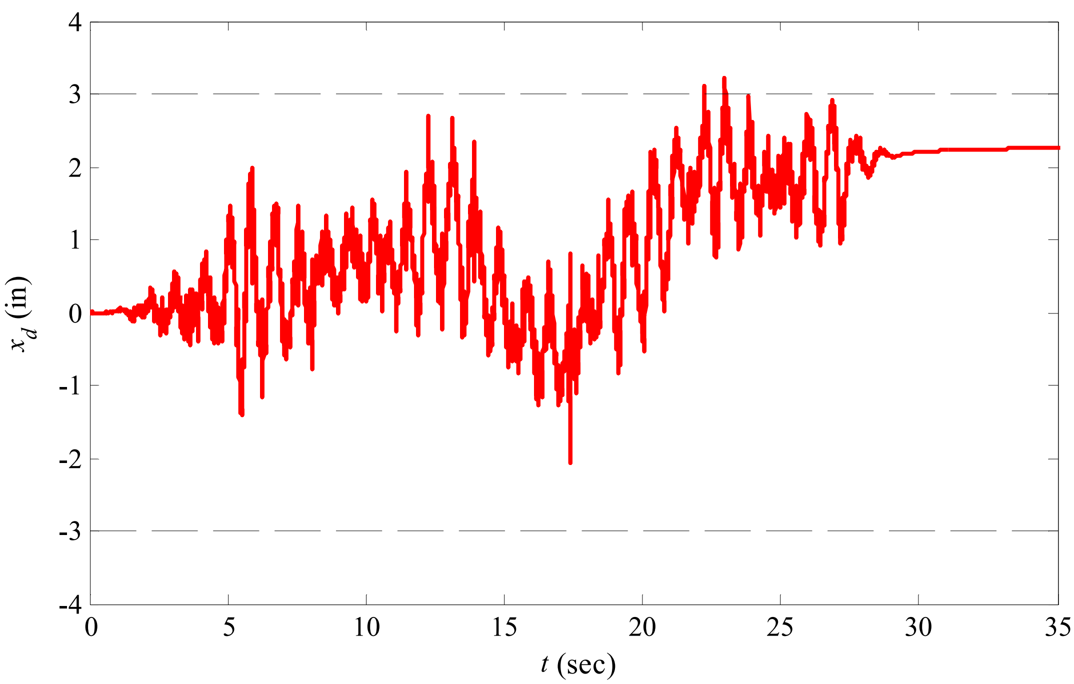

(b) Control excitation input (u)

Figure 8-9 Tracking control - structure responses (Test #6)

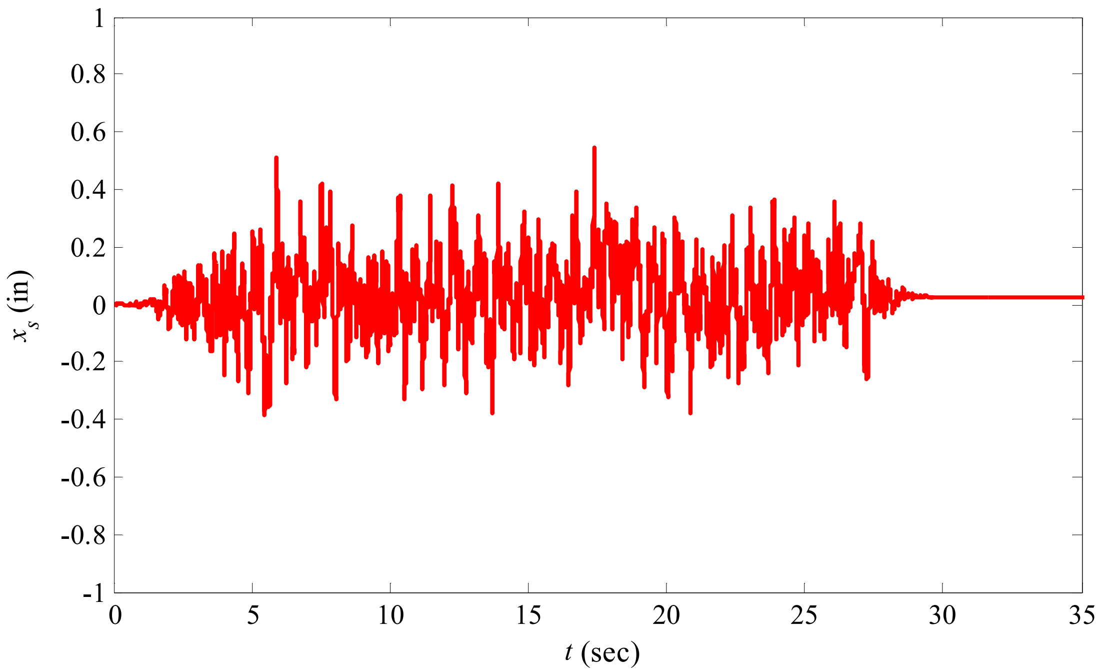

(c) Response of structure (x_s)

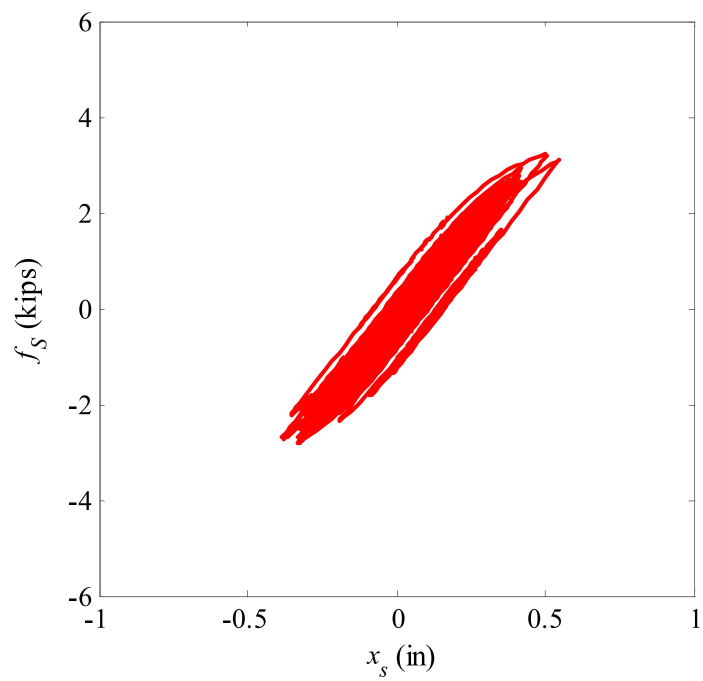

(d) Response of structure (f_S vs. x_s)

Figure 8-9 (Cont'd) Tracking control - structure responses (Test #6)

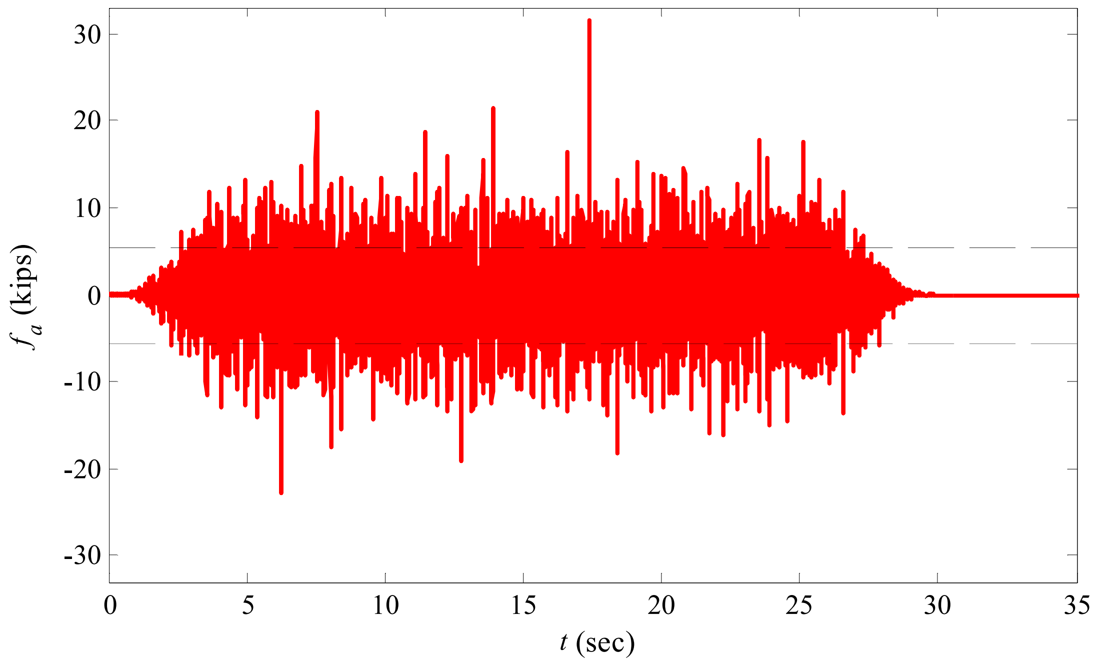

(a) Response of table (f_a)
(showing in the different scale from Figure 8-8)

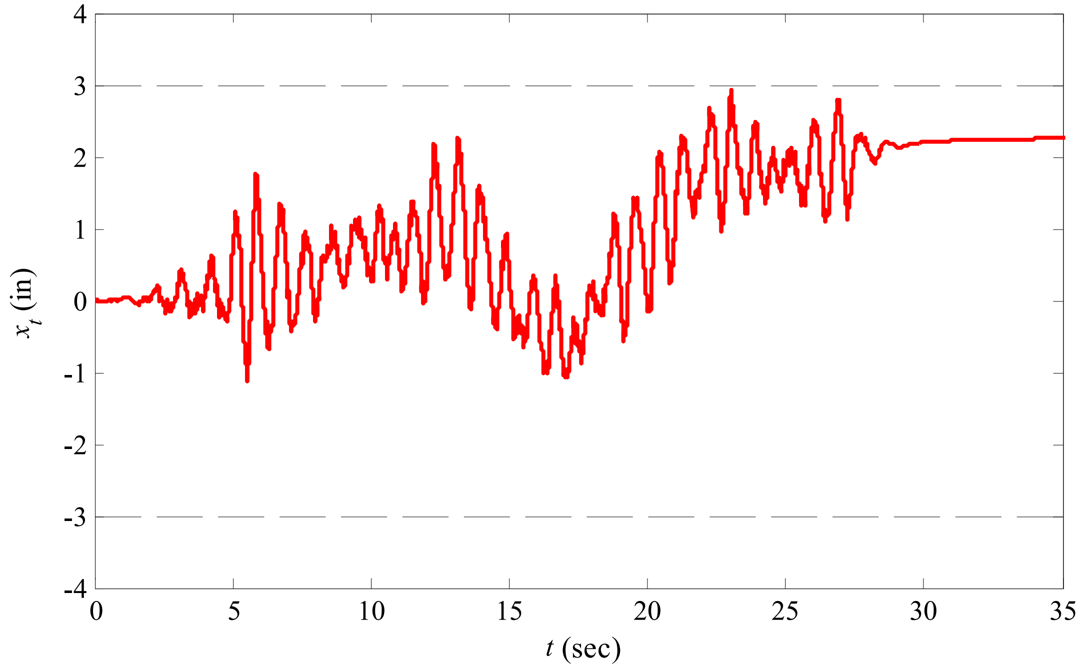

(b) Response of table (x_t)

Figure 8-10 Tracking control – shake table responses (Test #6)

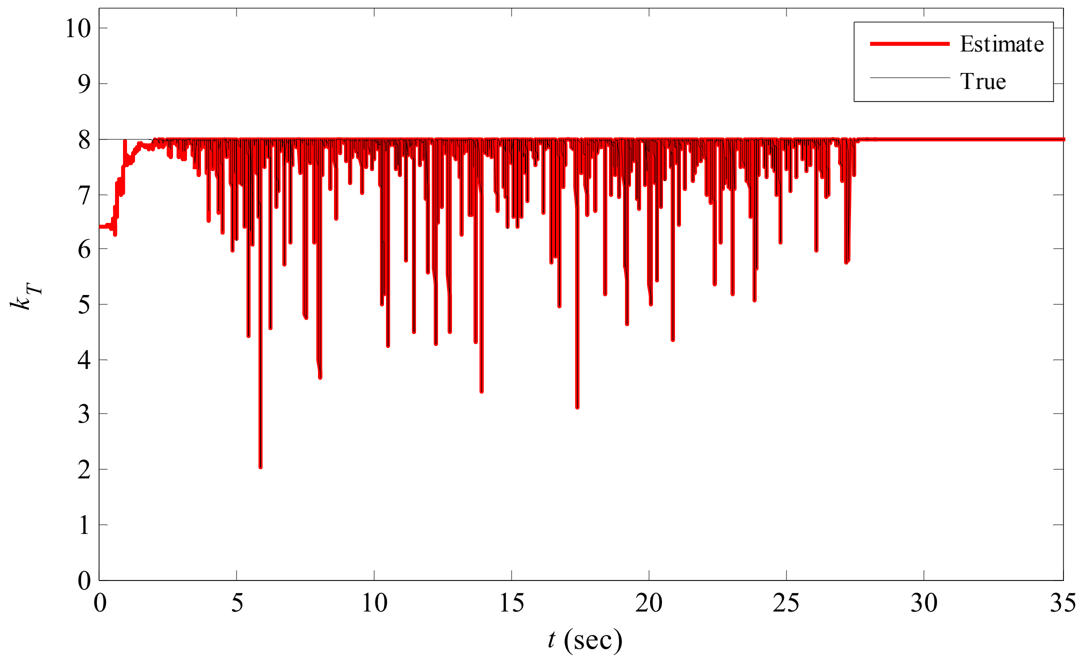

(a) Estimated parameter k_T

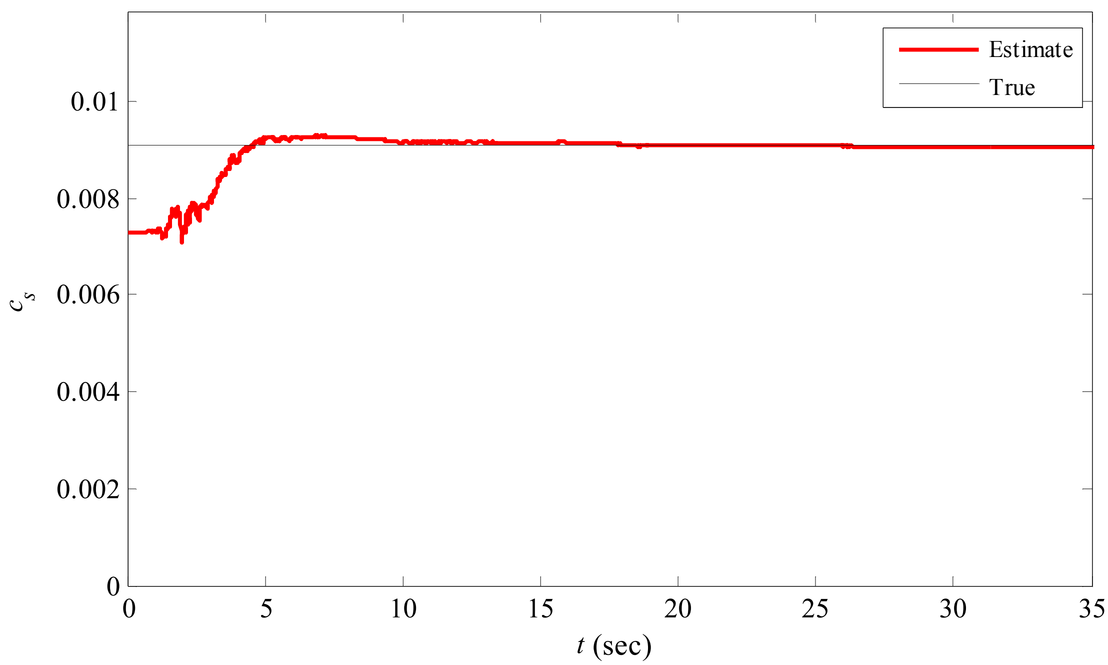

(b) Estimated parameter c_s

Figure 8-11 Real time parameter estimation results of tracking control (Test #6)

Although the tracking performance is very good and all responses of the controlled system are bounded, Figure 8-10 shows that the actuator force $f_a(t)$ and table displacement $x_t(t)$ operating capacities (shown in Table 8-1) of the shake table are exceeded. This limitation might be overcome by adjusting the target motion and/or the properties of the structure and shake table. In this study, the target motion is reduced by 70% such that the target motion is the 30% RRS matching motion, which is the target motion of Test #7.

The results of Test #7 are shown in Figure 8-12 and Figure 8-13. Figure 8-12 (a) shows the comparison between the target motion and the controlled output and shows very good agreements. Figure 8-7 (b) presents the control excitation input $u(t)$. As expected, using the reduced amplitude of the target motion, the actuator force $f_a(t)$ and table displacement $x_t(t)$ responses of the shake table are within the limits as shown in Figure 8-13. It is noted that the reduced demand (the target motion) requires smaller resisting force and structural deformation as shown in Figure 8-12 (c) and (d), such that the structure does not yield and only linear responses are observed in this test.

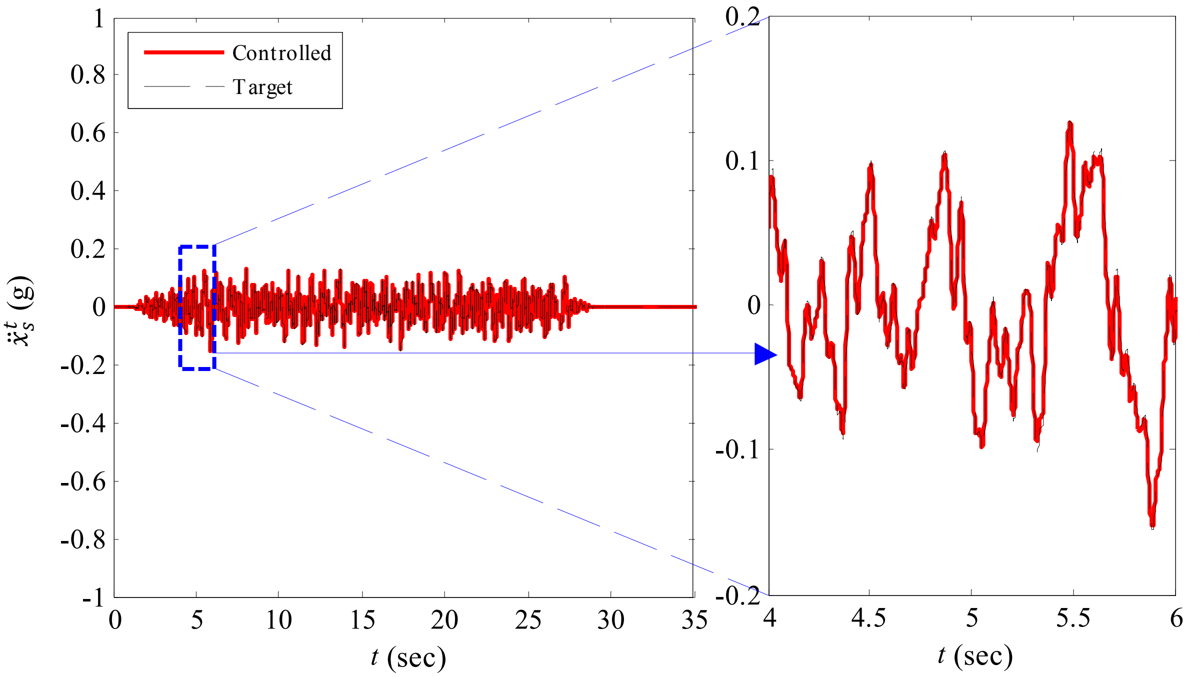

(a) Controlled (y) vs. Target motions (y_m)

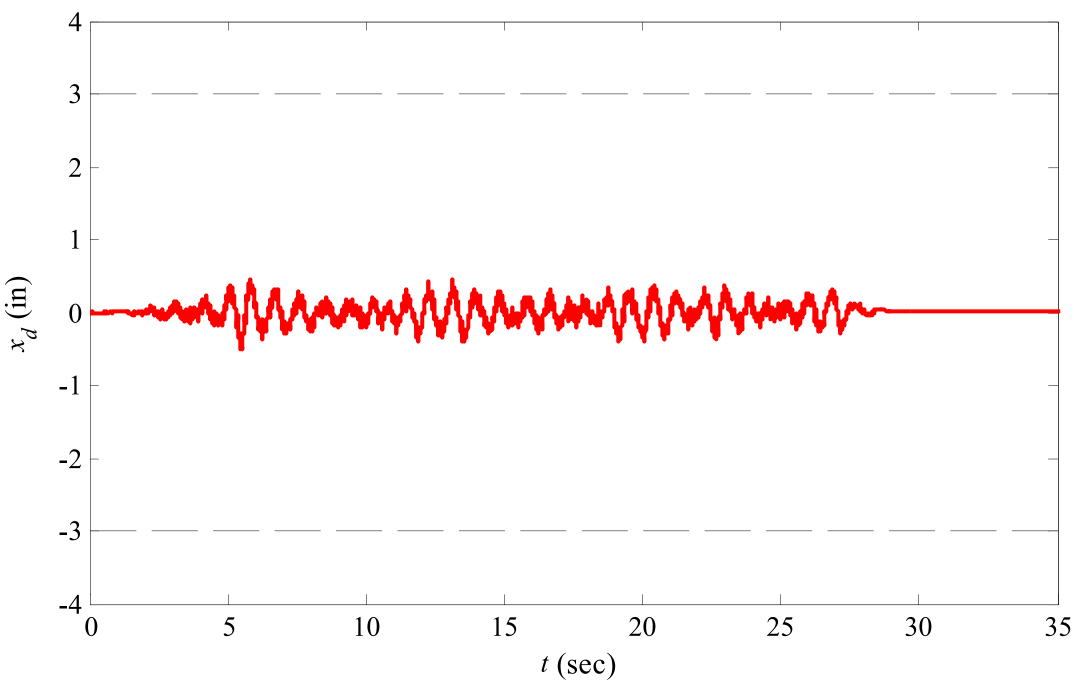

(b) Control excitation input (u)

Figure 8-12 Tracking control - structure responses (Test #7)

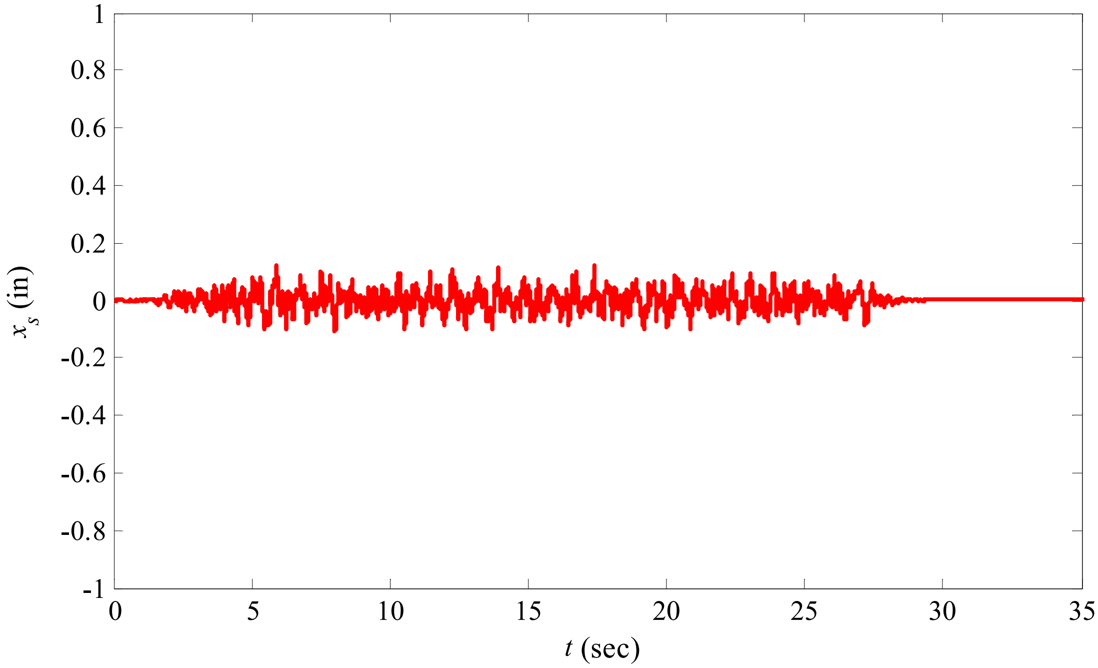

(c) Response of structure (x_s)

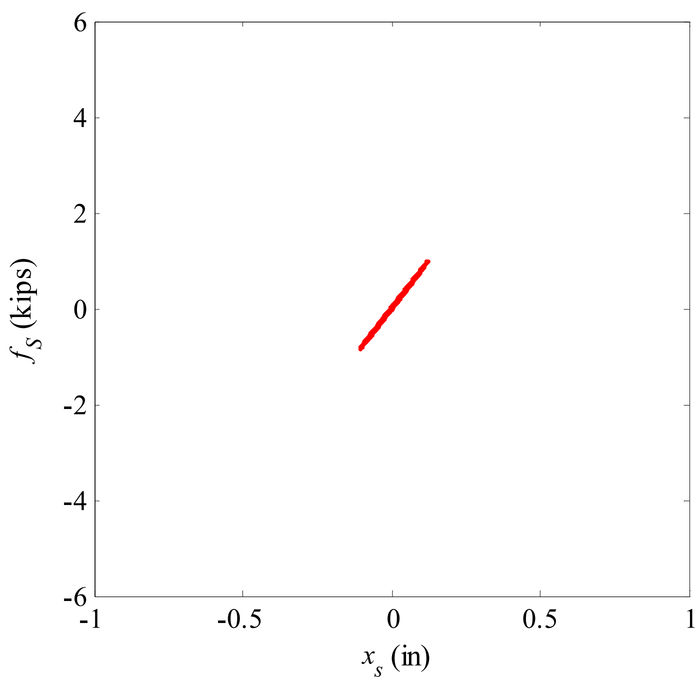

(d) Response of structure (f_S vs. x_s)

Figure 8-12 (Cont'd) Tracking control - structure responses (Test #7)

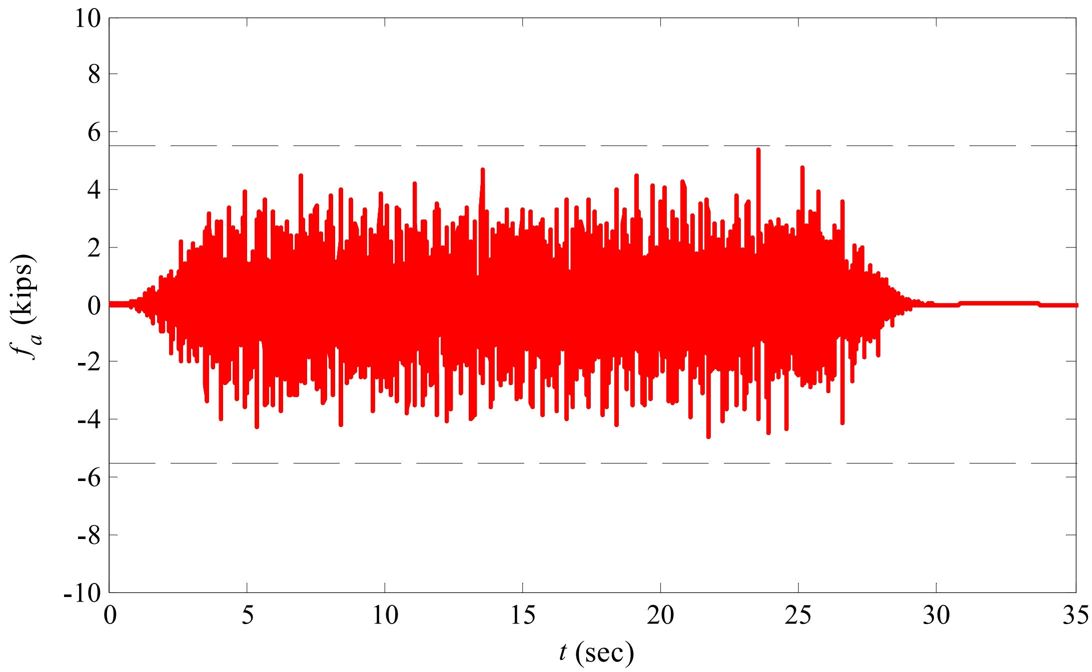

(a) Response of table (f_a)

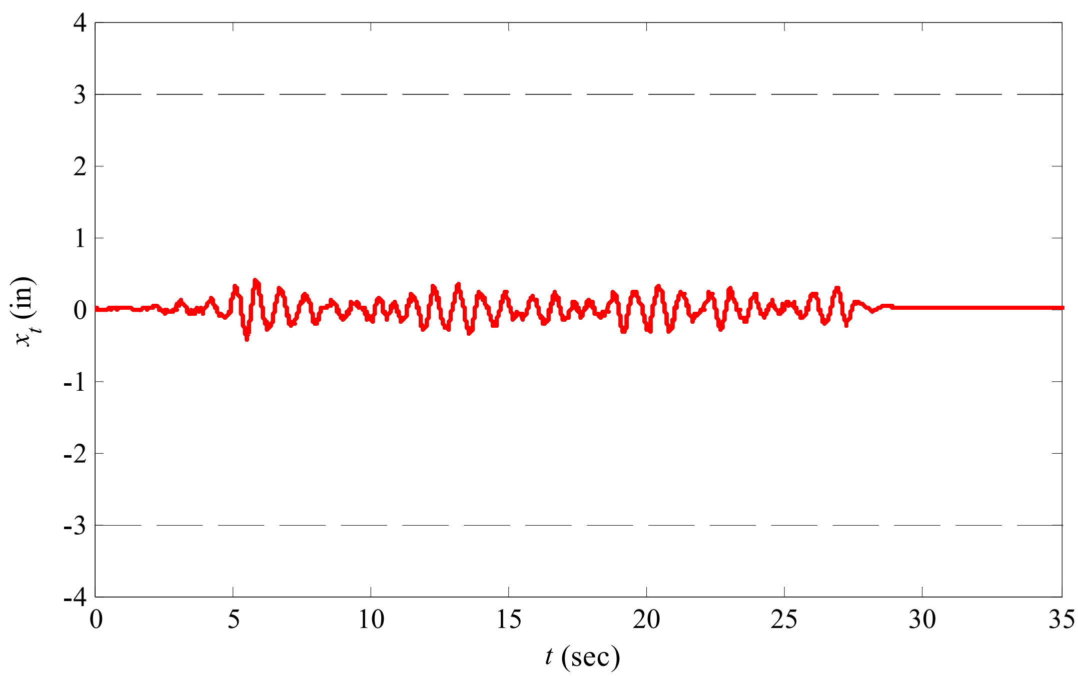

(b) Response of table (x_t)

Figure 8-13 Tracking control – shake table responses (Test #7)

The numerical simulations using the realistic test setup prove that the proposed tracking control algorithm works for nonlinear structures experiencing hysteretic behavior as shown in especially the results of Test #4 and Test #6. However, the results indicate that the performance of the tracking control depends on the capabilities of the equipment (i.e. especially, the force capacity and the stroke length of actuators). For example, if the test structure would be mounted on a larger shake table such as the UB 6DOF shake table (whose capacities are presented in Table 8-3), then test #4 and test #6 would be realistic, where the maximum forces (8.6 kips and 31.5 kips) and the maximum table displacements (3.4 in and 3.0 in) are smaller than the ones of the shake table capacities (50.7 kips and 5.9 in.).

Table 8-3 Performance data for six degrees-of-freedom (6DOF) shake table at UB (Reinhorn et al., 2011)

Item	Description
(1)	(2)
Platform size	11.8 ft × 11.8 ft
Usable testing surface	23.0 ft × 23.0 ft
Maximum specimen mass	110.2 kips/g max.; 44.1 kips/g nominal
Maximum overturning moment	332 kip-ft
Frequency of operation	0.1~50 Hz nominal; 100 Hz max.
Maximum actuators force in X axis*; $f_{a,max}$	50.7 kips
Stroke (X axis, Y axis, Z axis)	±5.9 in, ±5.9 in, ±3.0 in
Velocity (X axis, Y axis, Z axis)	±49.2 in/sec, ±49.2 in/sec, ±49.2 in/sec
Acceleration (X axis, Y axis, Z axis)	±1.2 g, ±1.2 g, ±1.2 g (with 44.1 kips specimen)

* $f_{a,max}$ is computed by 44.1 kips/g × 1.15 g ≈ 50.7 kips

In this section, the performance of the proposed tracking control scheme combined with the real time estimator is examined by means of numerical simulations of realistic shake table nonlinear system applications. The results show that not only simple target motions (in Test #1 to #3), but also realistic floor motions including that induced by an earthquake (in Test #4 to #5) and code required floor motion (in Test #6 to #7) can be reproduced using the proposed control method. The control performance is dependent on the degree of knowledge on unknown parameters (e.g. 20% errors in the initial guess are used for the simulations) for the real time estimators and the capacities of control equipment. The effects and limitations of these control parameters could be more clearly revealed through actual experimental studies.

SECTION 9
REMARKS AND CONCLUSIONS

High fidelity of bare shake table controls can be obtained through actuator control methods and table tuning. When shake tables are loaded with specimens, the interaction between shake tables and specimens influence the system dynamics and might result in undesired performance of shake tables. In order to compensate for the interaction and to simulate desired target motions using shake tables, open loop feedforward methods with offline iterative error correction have been widely used in practice (Spencer and Yang, 1998 and Maddaloni, Ryu, and Reinhorn, 2010). More recently, researchers developed more advanced methods to provide high quality of shake table motions using feedback closed loop controls, combined with the feedforward control methods (Nakata, 2010 and Phillips and Spencer, 2012). Even though these methods were verified to be valuable, practical tools to test linear structures, most developments assume that specimens remain linear or their nonlinear behavior is not significant. When flexible and heavy specimens (compared to shake table weight) experience nonlinear behavior, the signal reproduction can be unsatisfactory (e.g. large differences between the target and achieved shake table motions with a heavy nonlinear specimen were observed by Schachter and Reinhorn, 2007). These phenomena might be acceptable for the purpose of research exploring responses of structures subjected to random excitations where it is important to challenge the structures to their maximum capacity or collapse. Note that researchers have also developed several methods to compensate the nonlinear behavior of specimens, but the efforts were focused on simulating target motions at the shake table level (Stoten and Gomez, 2001, Iwasaki et al., 2005, and Yang et al., 2015), not within the tested specimens.

Unlike research projects, for qualification tests to verify certain performance of test structures or equipment, it is important to challenge the specimens by the required target motions; therefore, the fidelity of signal reproduction becomes more important. For example, qualification tests of nonstructural ceiling systems demand the reproduction of the required motions at certain levels of specimens; i.e. the required target motion is defined at the floor of a specimen (not the base) for ceiling system shake table tests per AC156 (ICC., 2010).

In this study, tracking control schemes are proposed to simulate target motions at specific locations of specimens, which experience nonlinear behavior due to possible extreme excitations. To account for the uncertainties in system parameters, real time estimators are also introduced and combined with the proposed control methods. Furthermore, the proposed methods can be expanded in order to control real structures using base motion controls. Similar structural control concepts, known as *active base isolation* that consists of a passive isolation system combined with control actuators (Chang and Spencer, 2010), have been developed by many researchers, including Reinhorn et al. (1987), Inaudi et al. (1992), Nagarajaiah et al. (1992), Yang et al. (1996), Luo et al. (2000), Pozo et al. (2006), Chang and Spencer (2010), and Suresh et al. (2012). These control methods have provided excellent active base isolation control design. While most methods focus on stabilizing (making zeros of) the system responses, the proposed control method in this study can be also used to control system responses to track desired target motions like the controllers by Pozo et al. (2006), providing another possible and flexible control scheme to the design engineers.

9.1 Concluding Remarks

The main results of this study are summarized as follows:

- Feedback tracking controllers are proposed in order to simulate target motions within nonlinear hysteretic structures mounted on shake tables. The tracking controllers can be used for nonlinear systems whose parameters are known or unknown a priori. Moreover, the controllers can be expanded to other applications to achieve desired performance during extreme seismic events.
- For shake table applications, two system models are introduced with and without the consideration of the shake table–structure interaction. In the first model, to facilitate the development of control methods, only structures are modeled, assuming that the effects of shake table dynamics can be ignored. The developed control methods are extended to the shake table–structure system models where their interactions are explicitly included in the governing equations. As discussed, since the responses of the controlled system are influenced by the shake table–structure interaction, it might be necessary to use the shake table–structure system models for real tracking control applications.
- For linear systems, four tracking control methods are introduced and the performances are qualitatively and quantitatively compared through numerical simulations. The results show that the performance of the feedback tracking control methods are as good as that of the optimal tracking control method, which involves the feedforward loop. It is also noted that the performance of any controller depends on the control gain, which is related to actuator capacities.
- When there are unknown parameters, adaptive tracking control schemes where feedback tracking controllers are combined with real time estimators are proposed. For the selection of a real time estimator, the *least squares* method (LS) and the *extended Kalman filter* (EKF) are considered. In this study, the EKF is adopted as the real time parameter estimator because of its important advantages as follows; (i) the method can be applied to the nonlinear hysteretic system with hardening after yielding; (ii) the EKF requires fewer measurements, which is more practical; and (iii) the EKF is used not only to estimate the unknown parameters, but also to estimate the true state vector from the measurements

with measurement noise; i.e. both estimates of the true state vector and unknown parameters are required for the tracking control procedure.

- Assuming all parameters are known, the stability of the controller is analytically examined and the stability properties are shown. For systems with unknown parameters and with measurement noise present, numerical simulations are conducted, and the tracking results including the differences between the target and output motions and the performances of all system responses are examined.
- The proposed tracking control scheme with the real time estimator is applied to a realistic test setup for a structural test specimen and a shake table at the University at Buffalo by means of numerical simulations. The results verify that realistic floor motions including one induced by an earthquake and a code required floor motion can be tracked using the proposed control method. The results also show that control performance depends on the capacities of shake table actuators and the degree of knowledge on unknown parameters.
- Although the developments are limited to unidirectional motions, the extension to multidirectional motions will follow the same equations with larger matrices, but with the same convergence properties.

9.2 Discussion

- The proposed methods can be expanded to control real building structures having complex nonlinear behavior such as isolated buildings (i.e. active base isolation systems) subjected to high intensity earthquakes.
- Experimental study will be very beneficial in order to solve possible implementation issues and to explore the effects of other uncertainties.
- While systems having one control excitation input in order to simulate one output target motion (i.e. Single-Input-Single-Output systems) are presented in this study, the proposed control methods can be extended to simulate more than one output target motion using one control excitation input (i.e. Single-Input-Multi-Output systems) and using several control excitation inputs (i.e. Multi-Input-Multi-Output systems). In order to deal with the excitation input and the output target vectors, a matrix format of the predictive tracking control method with weighting matrices should be used.
- For simplicity, it is assumed that all state responses are measurable with noise. Measurement output feedback through the proposed estimator using limited measurements such as total acceleration responses for measurement are to be considered for more practical applications.
- Although an approximately defined model of nonlinearity (bilinear hysteretic behavior) has been considered, the proposed control methods can be expanded to more complex nonlinear structures, formulated by more advanced models that can capture stiffness and strength degradation and/or bond-

slip effects. Additionally, modeless procedures can be developed using more complex real time identification techniques at the expense of loss of some fidelity due to intense computational effort.

SECTION 10 REFERENCES

Blondet, M. and Esparza, C. (1988). "Analysis of shaking table-structure interaction effects during seismic simulation tests", *Earthquake Engineering and Structural Dynamics*, 16(4), 473-490.

Bracci, J. M., Reinhorn, A. M., and Mander, J. B. (1992). "Seismic Resistance of Reinforced Concrete Frame Structures Designed Only for Gravity Loads - Part I: Design and Properties of a 1/3 Scale Model Structure." Tech. Rep. NCEER-92-0027, University at Buffalo, Buffalo, N.Y.

Bouc, R. (1967). "Forced Vibration of Mechanical System with Hysteresis." *Proc., 4-th Conf. on Non-Linear Oscillations*.

Chang, C. and Spencer Jr, B. F. (2010). "Active base isolation of buildings subjected to seismic excitations. " *Earthquake Engineering and Structural Dynamics*, 39, 1493–1512.

Chen, C. T. (1999). *Linear System Theory and Design*, 3rd Ed., Oxford University Press, New York.

Chu, S. Y., Soong, T. T., and Reinhorn, A. M. (2005). *Active, Hybrid and Semi-Active Structural Control: A Design and Implementation Handbook*, Wiley, England.

Chung, L. L., Lin, R. C., Soong, T. T., and Reinhorn, A. M. (1989). "Experimental study of active control for MDOF seismic structures." *J. Eng. Mech.*,115, 1609-1627.

Constantinou, M. C. (2008). "Models of viscoelastic and viscoplastic behavior." CIE519 Dynamics Class Note, State University of New York at Buffalo, Buffalo, NY.

Constantinou, M. C., and Adnane, M. A. (1987). "Dynamics of soil-base-isolated-structure systems evaluation of two models for yielding systems. " National Science Foundation.

Conte, J. P. and Trombetti, T. L. (2000). "Linear dynamic modeling of a uniaxial servo-hydraulic shaking table system." *Earthquake Engineering & Structural Dynamics*, 29(9), 1375–1404.

Crassidis, J. L. and Junkins, J. L. (2012). *Optimal Estimation of Dynamic Systems*, 2nd Ed., CRC Press, New York.

Crewe, A. J. and Severn, R. T. (2001). "The European collaborative programme on evaluating the performance of shaking tables." *Phil. Trans. Roy. Soc.* London, 359, 1671-1696.

Dannon, H. V. (2012). "The Delta Function." Gauge Institute Journal, 8(1).

Dyke, S. J., Spencer, B. F., Quast, P., Sain, M. K., Kaspari, D. C. and Soong, T. T. (1994), "Experimental Verification of Acceleration Feedback Control Strategies for an Active Tendon System." Technical Report, NCEER-94-0024, University at Buffalo, Buffalo, N.Y.

Dyke, S. J., Spencer Jr, B. F., Quast, P., and Sain, M. K. (1995). "The role of control-structure interaction in protective system design." *ASCE J. Eng. Mech.*, 121, 322-338.

EFAST. (2009). "Design Study of a European Facility for Advanced Seismic Testing." Seventh Framework Programme Capacities-Research Infrastructures

Fienup, J. R. (1997) "Invariant error metrics for image reconstruction." *Applied Optics*, 36(32), 8352-8357.

Hashemi1, M. J., Masroor, A., and Mosqueda, G. (2014). "Implementation of online model updating in hybrid simulation." *Earthquake Engng Struct. Dyn.*, 43, 395–412

ICC. (2010). *ICC-ES AC156 Acceptance criteria for the seismic certification by shake-table testing of nonstructural components*, International Code Council Evaluation Service, Whittier, CA.

IEEE Standard 693-2005. (2006). *IEEE Recommended Practice for Seismic Design of Substations*, E-ISBN: 0-7381-4845-8, Print ISBN: 0-7381-4844-X.

Inaudi, J., Lopez-Almansa, F., Kelly, J. M., and Rodellar, J. (1992). "Predictive control of base isolated structures." *Earthquake Eng. Struct. Dyn*., 21(6), 471-482.

Ioannou, P. A. and Fidan, B. (2006). *Adaptive Control Tutorial*, SIAM, Pennsylvania.

Ioannou, P. A. and Sun, J. (2012). *Robust Adaptive Control*, Dover, New York.

Iwasaki, M., Ito , K., Kawafuku, M., Hirai, H., Dozono, Y., and Kurosaki, K. (2005). "Disturbance observer-based practical control of shaking tables with nonlinear specimen." *16th IFAC World Congress*, Prague.

Kelly, J. M., Leitmann, G., and Soldatos, A. G. (1987). "Robust control of base-isolated structures under earthquake excitation." *J. Optim. Th. Appl.*, 53, 159-180.

Kirk, D. E. (2004). *Optimal Control Theory: An Introduction*, Dover, NY.

Kwakernaak, H. and Sivan, R. (1972). *Linear Optimal Control Systems*, Wiley-Interscience, New York.

Lu, P. (1994). "Nonlinear predictive controllers for continuous systems." *Journal of Guidance, Conrrol and Dynamics*, 17, 553-560.

Lu, P. (1995). "Optimal predictive control of continuous nonlinear systems." *International Journal of Control*, 62(3), 633-649.

Luco, J. E., Ozcelik, O., and Conte, J. P. (2010). "Acceleration tracking performance of the UCSD-NEES shake table." *Journal of Structural Engineering*, 136(5), 481–490.

Luo, N., Rodellar, J., Sen, DL., and Vehi, J. (2000). "Output feedback sliding mode control of base isolated structures." *Journal of the Franklin Institute*, 337, 555–577.

Maddaloni, G., Ryu, K. P. and Reinhorn, A. M. (2010). "Simulation of floor response spectra in shake table experiments." *Earthquake Engineering & Structural Dynamics*, 40(6), 591–604.

MTS System Corporation. (2004). *Real Time Hybrid Seismic Test System-User's Manual*, USA.

Nachtigal, C. L. (1990). *Instrumentation and control: fundamentals and applications*, Wiley, New York.

Nagarajaiah, S., Riley, M. A., and Reinhorn, A. M. (1993). "Hybrid control of sliding isolated bridges." *Journal of Engineering Mechanics*, 119(11), 2317-2332.

Nakata, N. (2010). “Acceleration tracking control for earthquake simulators.” *Engineering Structures*, 32(8), 2229–2236.
Omrani, R., Hudson R. E., and Taciroglu, E. (2013). “Parametric Identification of Nondegrading Hysteresis in a Laterally and Torsionally Coupled Building Using an Unscented Kalman Filter.” *Journal of Engineering Mechanics*, 139, 452-468.

Ozcelik, O., Luco, J. E., Conte, J. P., Trombetti, T. L., and Restrepo, J. I. (2008). “Experimental characterization, modeling and identification of the NEES-UCSD shake table mechanical system.” *Earthquake Engineering and Structural Dynamics*, 37(2), 243–264.

Phillips, B. M. and Spencer Jr., B. F. (2012). “Model-Based Framework for Real-Time Dynamic Structural Performance Evaluation.” NSEL Report No. NSEL-031, Urbana-Champaign, Illinois.

Pozo, F., Ikhouane, F., Pujol, G., and Rodellar, J. (2006). “Adaptive backstepping control of hysteretic base-isolated structures.” *Journal of the Vibration and Control*, 12(4), 373–394.

Reinhorn, A. M. (1985). Experimental Mechnaics (SUNY/Buffalo CIE616) Class Note, State University of New York at Buffalo, Buffalo, NY.

Reinhorn, A. M., Soong, T. T. and Wen, C. Y. (1987). "Base Isolated Structures with Active Control." Seismic Engineering: Recent Advances in Design Analysis, Testing and Qualification Methods, T.H. Lin and A. Marr (Eds.), ASME, New York, PVP 127, 413-419.

Reinhorn, A. M., Madan, A., Valles, R. E., Reichmann, Y. and Mander, J.B. (1995). “Modeling of Masonry Infill Panels for Structural Analysis.” Technical Report NCEER-95-0018, University at Buffalo, Buffalo, NY.

Reinhorn, A. M., Ryu, K. P. and Maddaloni, G. (2010). “Modeling and Seismic Evaluation of Nonstructural Components: Testing Frame for Experimental Evaluation of Suspended Ceiling Systems.” Technical Report MCEER-10-0004, Buffalo, NY.

Reinhorn, A. M., Ryu, K. P., and Pitman, M. (2011). “Shake Table Testing for Seismic Certification of Suspended Ceiling Systems: System CM1104A of Chicago Metallic Corporation.” Report No UB CSEE/SEESL-2011-08, University at Buffalo-the State University of New York, Buffalo, NY.

Rinawi, A. M. and Clough, R. W. (1991). “Shaking table–structure interaction.” EERC Report No. 91/13, Earthquake Engineering Research Center, University of California at Berkeley, CA.

Rodellar, J., Barbat, A. H., and Matin-Sanchez, J. M. (1987). “Predictive control of structures.” *Journal of Engineering Mechanics*, 113:6, 797–812.

Ryu, K. P. (2009). “Modeling and Seismic Evaluation of Nonstructural Components: Testing Frame for Experimental Evaluation of Suspended Ceiling Systems.” M.S. Thesis, University at Buffalo, NY.

Ryu, K. P. (2015). “Real Time Control of Shake Tables for Nonlinear Hysteretic Systems.” PhD Dissertation, University at Buffalo, NY.

Sauer. T. (2006). *Numerical Analysis*, Pearson, Boston.

Schachter, M. and and Reinhorn, A. M. (2007). “Three-Dimensional Modeling of Inelastic Buckling in Frame Structures.” Technical Report MCEER-07-0016, University at Buffalo, Buffalo, NY.

Simeonov, V. K., Sivaselvan, M. V. and Reinhorn, A. M. (2000). “Nonlinear Analysis of Structural Frame Systems by the State-Space Approach.” *Computer-Aided Civil and Infrastructure Engineering*, 15 (2), 76–89.

Sivaselvan, M. V. and Reinhorn, A. M. (1999). “Hysteretic models for cyclic behavior of deteriorating inelastic structures.” Technical Report MCEER-99-0018, Multidisciplinary Center for Earthquake Engineering Research, State University of New York at Buffalo, Buffalo, NY.

Sivaselvan, M. V. and Reinhorn, A. M. (2000). “Hysteretic models for deteriorating inelastic structures.” *ASCE J. Eng. Mech.*, 126 (6), 633–640.

Sivaselvan, M. V., and Reinhorn, A. M. (2004). “Nonlinear Structural Analysis Towards Collapse Simulation: A Dynamical Systems Approach.” Technical Report MCEER-04-0005, University at Buffalo, Buffalo, NY.

Smyth, A. W., Masri, S. F., and Chassiakos, A. G. (1999). “On-line parametric identification of MDOF non-linear hysteretic systems.” *ASCE J. Eng. Mech.*, 125 (2), 133–142.

Song, W. (2011). “Dynamic model updating with applications in structural and damping systems: From linear to nonlinear, from off-line to realtime.” Ph.D. Dissertation, Purdue Univ., West Lafayette, IN.

Song, W. and Dyke, S. (2014). “Real-Time Dynamic Model Updating of a Hysteretic Structural System.” *Journal of Structural Engineering*, 140(3), 04013082.DOI: 10.1061/(ASCE)ST.1943-541X.0000857.

Soong, T. T. (1990). *Active Structural Control: Theory and Practice, Longman Scientific and Technical*, Wiley, New York.

Spencer Jr., B. F. and Yang, G. (1998). "Earthquake Simulator Control By Transfer Function Iteration.” *Proceedings of the 12th ASCE Engineering Mechanics Conference*, San Diego, California, May, 1998, 776–769.

Stefanakis, K. and Sivaselvan, M. V. (2015). “Unidirectional shake table.” Personal Photograph.

Stoten, D. P. and Gomez, E. G. (2001). “Adaptive control of shaking tables using the minimal control synthesis algorithm.” *Phil Trans. Roy. Soc.*, London, 359, 1697–1723.

Suresh, S., Narasimhan, S., and Nagarajaiah, S. “Direct adaptive neural controller for the active control of earthquake-excited nonlinear base-isolated buildings.” *Struct. Control Health Monit.*, 19, 370–384.

Symans, M. D, and Constantinou, M. C. (1997). “Seismic testing of a building structure with a semi-active fluid damper control system.” *Earthquake Engineering & Structural Dynamics*, 26, 759–777.

Thoen, B. K. and Laplace, P. N. (2004). “Offline tuning of shaking tables.” *13th World Conference on Earthquake Engineering*, Paper No. 960, Vancouver, B.C., Canada.

Trombetti, T. L., and Conte, J. P. (2002). “Nonlinear shake table identification and control for near-field earthquake testing.” *Journal of Earthquake Engineering*, 6(4), 513–551.

UB-SEESL. (2015). “Lab Manual.” < http://nees.buffalo.edu/docs/labmanual/html> (April 21, 2015).

Vibrationdata. (2015). “El Centro Earthquake.” < http://www.vibrationdata.com/elcentro.htm> (April 20, 2015).

Wen, Y. K. (1976). "Methos for Random Vibration of Hysteretic Systems." *J. Engrg. Mech. Div., ASCE*, 102(2), 249-263.

Wu, M. and Smyth, A. W. (2007). “Application of the unscented Kalman filter for real-time nonlinear structural system identification.” *J. Struct Control Monitor*, 14 (7), 971–990.

Yang, J. N., Wu, J. C., Reinhorn, A. M., and Riley, M. (1996). “Control of sliding-isolated buildings using sliding-mode control.” *Journal of Structural Engineering*, 122(2), 179–186.

Yang, J. N. and Lin, S. (2004). “On-line identification of non-linear hysteretic structures using an adaptive tracking technique.” *International Journal of Non-Linear Mechanics*, 39, 1481–1491.

Yang, T. Y., Li, K., Lin, J. Y., Li, Y. and Tung, D. P. (2015). “Development of high-performance shake tables using the hierarchical control strategy and nonlinear control techniques.” *Earthquake Engineering & Structural Dynamics*, 44(11), 1717–1728. DOI: 10.1002/eqe.2551.

Yun, C. B. and Shinozuka, M. (1980). “Identification of nonlinear structural dynamic systems.” *Journal of Structural Mechanics*, 8(2), 187–203.

“This Page Intentionally Left Blank”

APPENDIX A. ADDITIONAL EXAMPLES

A.1 Shake Table - Nonlinear Hysteretic System (2DOF System Model)

The tracing control results of the example shown in Figure 1-2 are shown in this Appendix. The 2DOF shake table and a nonlinear structure system is schematically shown in Figure A-1.

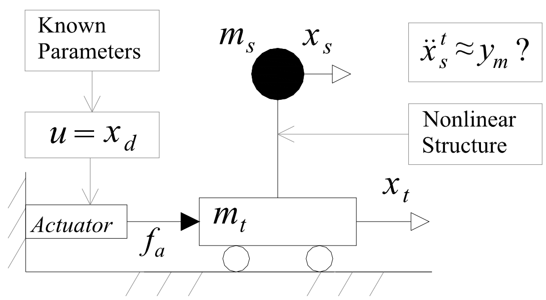

Figure A-1 Tracking control of the shake table- structure 2DOF nonlinear system with known parameters

When a target motion at a specimen is specified, the required control input $u(t) = x_d(t)$, the desired shake table displacement, is determined in order that the output of the system ($y(t) = \ddot{x}_s^t(t)$ the total acceleration of the structure) follows the target motion $y_m(t)$.

Example A-1* : *A 2DOF Nonlinear System with Known Parameters

The properties of a given system are the same as ones of Example 4-2: m_s = 1 kips·sec^2/in., k_s = 355 kips/in., and c_s = 1.13 kips·sec/in., (f_n = 3.0 Hz, ξ_n = 0.03 before yielding). N = 3, d_y = 0.11 in. (f_y = 39 kips), and α = 0.1, for the hysteretic system and $\mu = m_s / m_t = 0.1$, f_a = 30.0 Hz, ξ_a = 0.5 and k_a = 25 for the shake table. The target motion is shown in Figure A-1 (a) [Target]; i.e. the target motion is the total acceleration output generated from a reference linear system, whose properties are: m_m = 1 kips·sec^2/in., k_m = 987 kips/in., and c_m = 6.28 kips·sec/in. (f_m = 5.0 Hz, ξ_m = 0.1), subjected to one-cycle sine input whose frequency = 3.0 Hz and which is filtered at 0.2 Hz cutoff frequency (the reference input and the responses of the reference model are presented in Appendix A.2). The time step of 0.002 sec is used for the simulation.

The tracking control results using the *feedback linearization tracking control* (FTC) method are presented in Figure 4-8 and Figure 4-9 (i.e. it is noted that although the system used in this example is the same as the one of Example 4-2, the range of the responses are different due to the different excitation; thus, the scales of figures are different with the ones from Example 4-2). The controlled output $\ddot{x}_s^t(t)$ is shown in Figure 4-8 (a) [Controlled] and shows very good agreement with the target motion. The computed control excitation input, $u(t) = x_d(t)$, using the control law (i.e. Eq. (4-31)) is shown in Figure

4-8 (b). The tracking error coefficients are chosen as $k_1^* = 2 / h = 2\xi_e\omega_e$ and $k_2^* = 2 / h^2 = \omega_e^{\,2}$; therefore, $\xi_e = \sqrt{2} / 2 \approx 0.707$ and $h = \sqrt{2} / \omega_e$; (in this example, $\omega_e = 25$, $\xi_e = 0.707$ for the both methods).

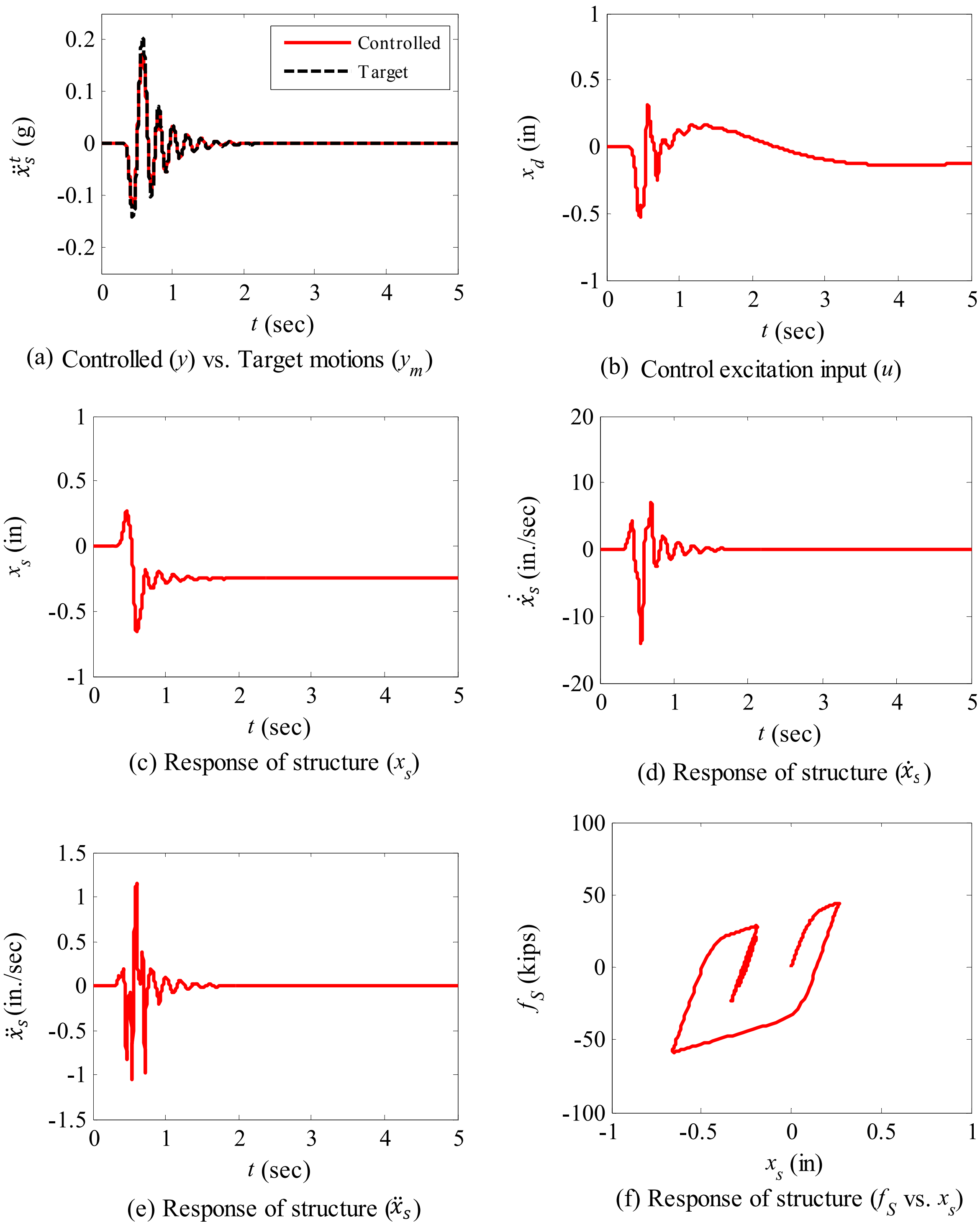

(a) Controlled (y) vs. Target motions (y_m)

(b) Control excitation input (u)

(c) Response of structure (x_s)

(d) Response of structure ($\dot{x}_s$)

(e) Response of structure ($\ddot{x}_s$)

(f) Response of structure (f_S vs. x_s)

Figure A-2 Feedback linearization tracking control structure responses of a 2DOF nonlinear system

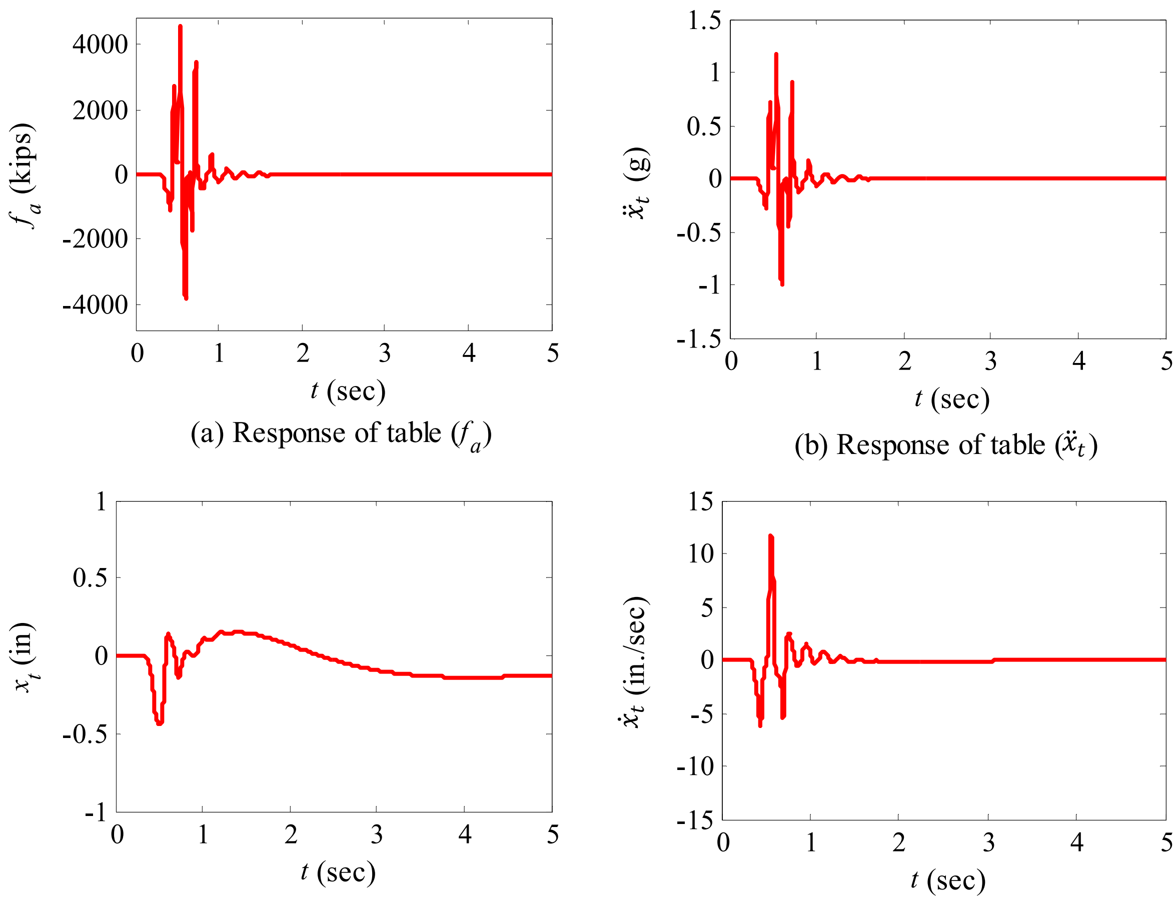

(a) Response of table (f_a)

(b) Response of table ($\ddot{x}_t$)

(c) Response of table (x_t)

(d) Response of table ($\dot{x}_t$)

Figure A-3 Feedback linearization tracking control shake table responses of a 2DOF nonlinear system

Example A-2 : A 2DOF Nonlinear System with Known Parameters

(*The control excitation input is pre-computed using the feedforward tracking control method, assuming the system remained linear without yielding*)

In order to demonstrate the limit of the feedforward tracking control method, the same nonlinear hysteretic system described above in Example A-1 is subjected to a pre-computed excitation input (see Figure A-4 (b)) using the feedforward tracking control method: i.e. the excitation input is pre-computed for the same system but assuming the system remained linear without yielding.

The results are presented in Figure A-4 and Figure A-5. Figure A-4 shows the discrepancies between the controlled output $\ddot{x}_s^t(t)$ and the target motion $y_m(t)$; the discrepancies are caused by the nonlinear hysteretic behavior in the structure, which cannot be captured by the pre-computed control excitation as discussed in SECTION 1.

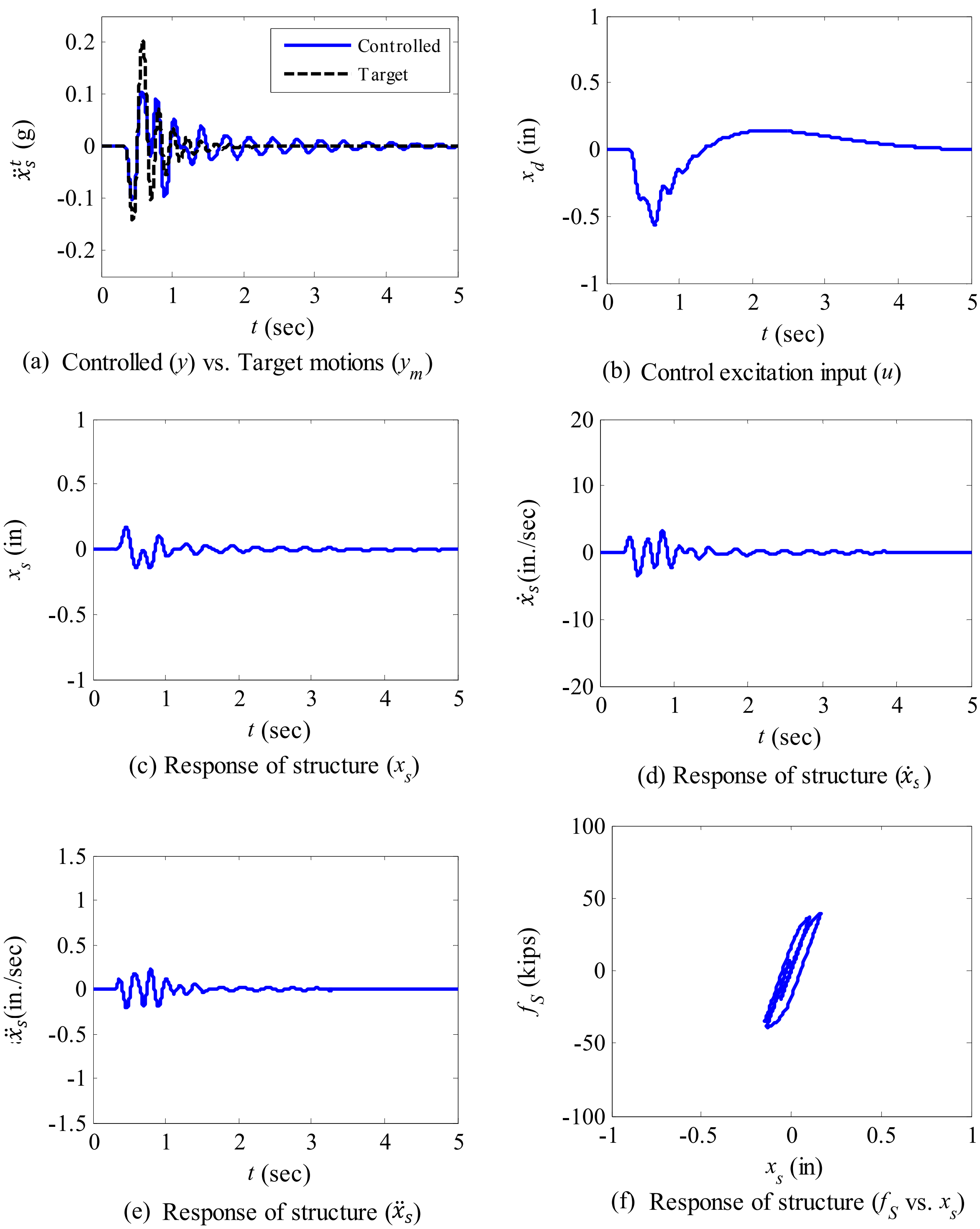

Figure A-4 Feedforward tracking control - structure responses of a 2DOF nonlinear system

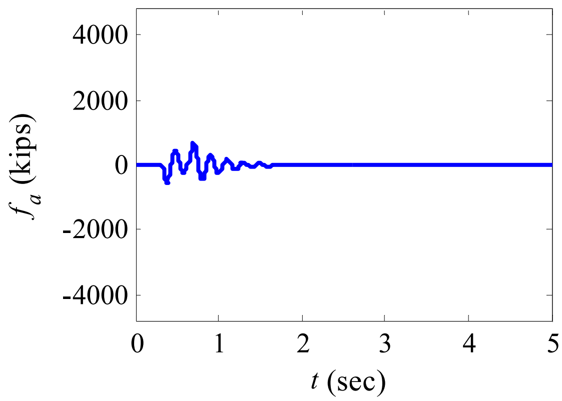

(a) Response of table (f_a)

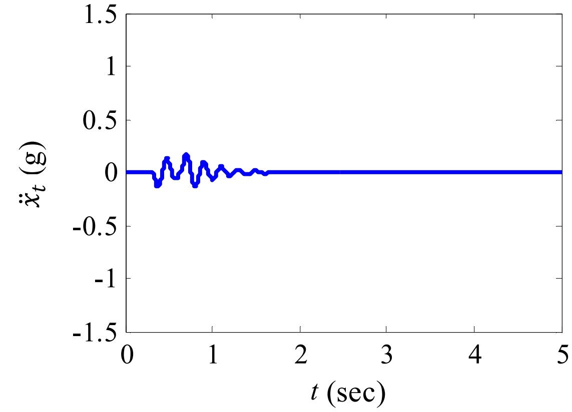

(b) Response of table ($\ddot{x}_t$)

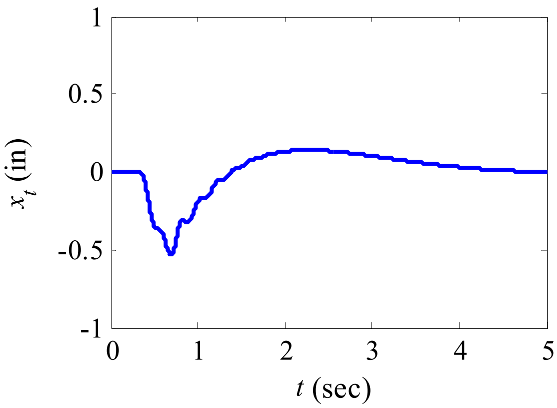

(c) Response of table (x_t)

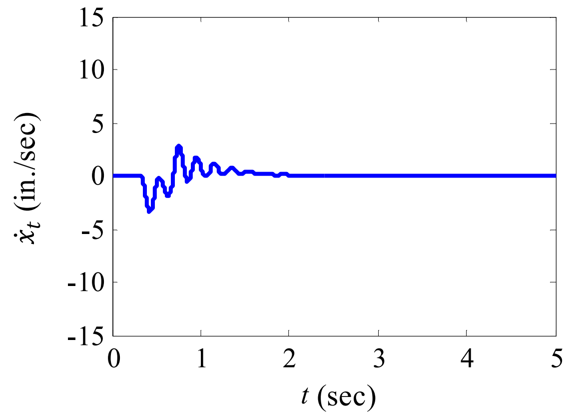

(d) Response of table ($\dot{x}_t$)

Figure A-5 Feedforward tracking control - shake table responses of a 2DOF nonlinear system

A.2 Reference Model and Its Responses (SDOF Linear System)

In order to generate a realistic target motion at a structure, an SDOF reference structure model is selected as shown in Figure A-6; the characteristics of the reference model and the reference excitation input $r(t) = -m_m\ddot{x}_g(t)$ can be selected such that the target motion can be designed as desired.

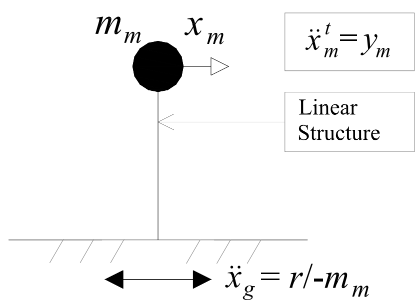

Figure A-6 Schematic of an SDOF reference model subjected to a ground excitation

The selected properties of the reference model (used in Examples 3.1, 3.2, 4.1, 4.2, 6.1, 6.2, 7.1, and 7.2) are: m_m = 1 kips·sec^2/in., k_m = 987 kips/in., and c_m = 6.28 kips·sec/in. (f_m = 5.0 Hz, ξ_m = 0.1) and subjected to one-cycle sine excitation input $r(t)$ whose frequency = 1.0 Hz and which is highpass filtered at 0.2 Hz cutoff frequency as shown in Figure A-7 (b) (for comparison purposes with other examples, $r(t)$/- m_m the ground excitation acceleration input is presented): i.e. the excitation input is highpass filtered in order to avoid large draft in the displacement and the velocity excitation, which is required for the shake table applications. The time step of 0.002 sec is used for the simulation.

The responses of the reference model are presented in Figure A-7: $\ddot{x}_m^t(t)$ the total acceleration response is shown in Figure 4-8 (a); $x_m(t)$, $\dot{x}_m(t)$ the displacement and velocity responses are presented in Figure A-7 (c) and (d). The relation between the structure resisting force $f_{S,m}(t)$ and displacement $x_m(t)$ is also presented in Figure A-7 (e).

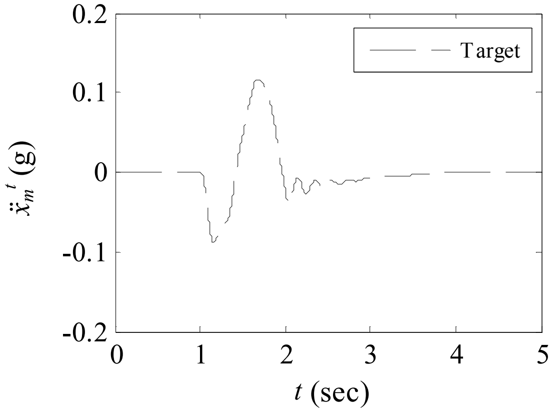

(a) Response of structure ($\ddot{x}_m{}^t$)

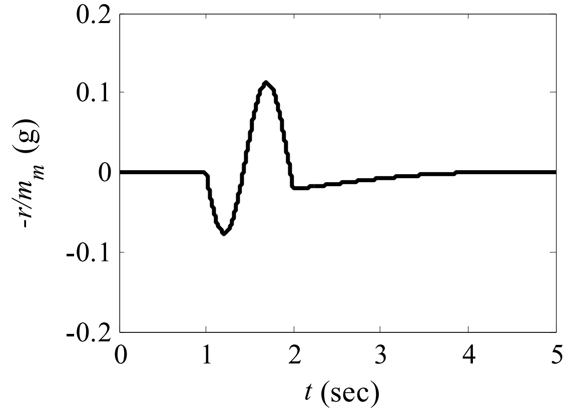

(b) Reference excitation input (r)

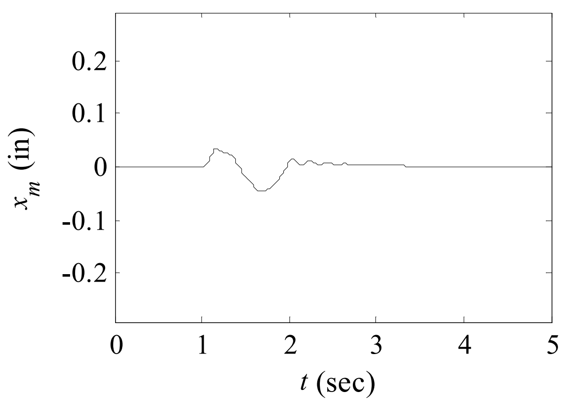

(c) Response of structure (x_m)

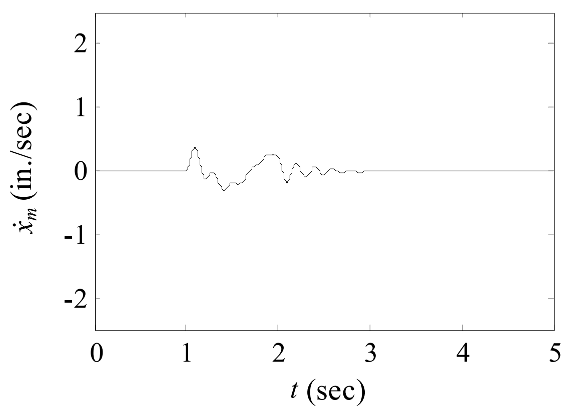

(d) Response of structure ($\dot{x}_m$)

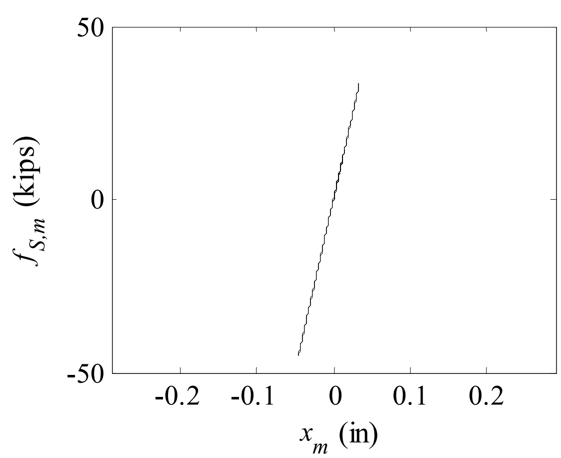

(e) Response of structure ($f_{S,m}$ vs. x_m)

Figure A-7 The responses of the SDOF linear reference model

A.3 Numerical Simulations for Shake table-Structure Systems

In SECTION 8 the developed tracking control method combined with the real time estimator was applied to a realistic shake table and an SDOF nonlinear system. The schematic of the control scheme was shown in Figure 8-2. The performance of the control method was examined through numerical simulations; the list of testing is presented in Table 8-2. In this Appendix, the results of Test #2 in which the target motion was generated from a reference model subjected to one-cycle sine excitation whose freq. = 5.0 Hz. All system parameters were explained in Section 8.2.

The tracking control results are presented in Figure A-8 through Figure A-10. The selected control and estimator parameters for the FTC (feedback tracking control) in Test #2 simulations are the same as the ones of Test #4 explained in Section 8.2.

Figure A-8 presents the parameter estimation results and show fast convergence to the true values. The target motion and the controlled output are compared in Figure A-9 (a) and show very good agreements. Figure A-9 (b) presents the control excitation input $u(t)$ = the desired shake table displacement $x_d(t)$. The structure responses: the relative displacement $x_s(t)$ and velocity $\dot{x}_s(t)$ of the structure and the relation between the resisting force $f_S(\underline{x})$ and the relative displacement $x_s(t)$, are shown in Figure A-9 (c) to (e), respectively. Although the tracking performance is very good, Figure A-10 presents the shake table responses; the achieved shake table actuator force $f_a(t)$, shake table acceleration $\ddot{x}_t(t)$, displacement $x_t(t)$ and velocity $\dot{x}_t(t)$ in order to show the feasibility and the stability of the control scheme. Although all state responses are bounded, Figure A-10 (a) shows that the actuator force $f_a(t)$ operating capacity (shown in Table 8-1) of the shake table is exceeded. This limitation might be overcome by adjusting the target motion and/or the properties of the structure and shake table as discussed in Section 8.2.

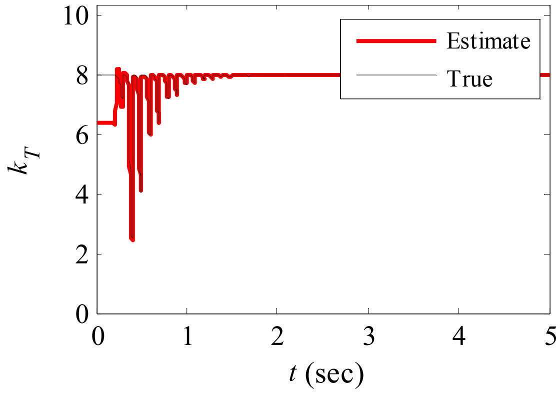

(a) Estimated parameter k_T

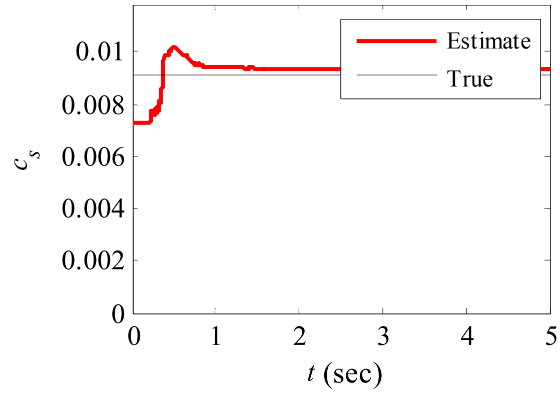

(b) Estimated parameter c_s

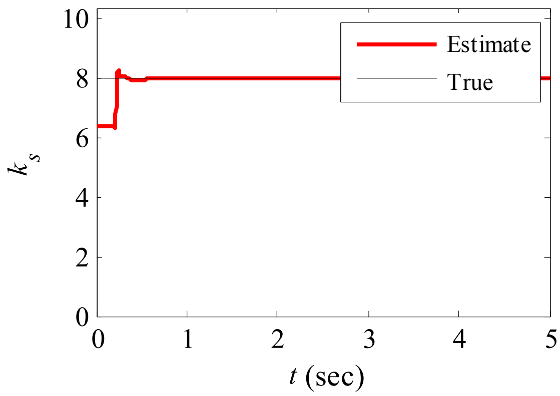

(c) Estimated parameter k_s

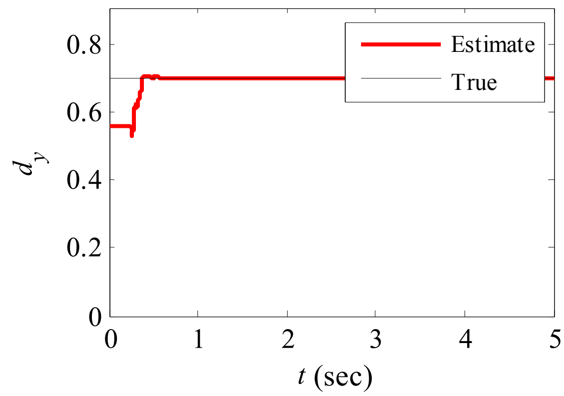

(d) Estimated parameter d_y

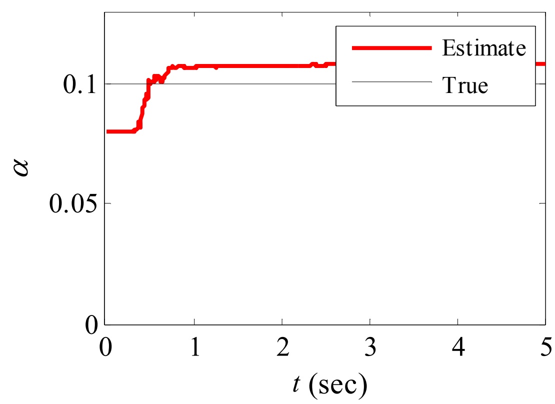

(e) Estimated parameter α

Figure A-8 Real time parameter estimation results of tracking control (Test #2)

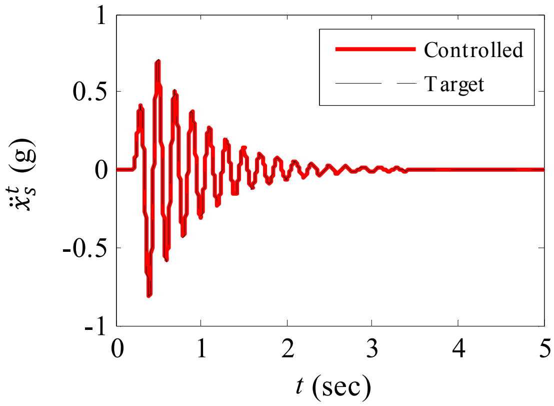

(a) Controlled (y) vs. Target motions (y_m)

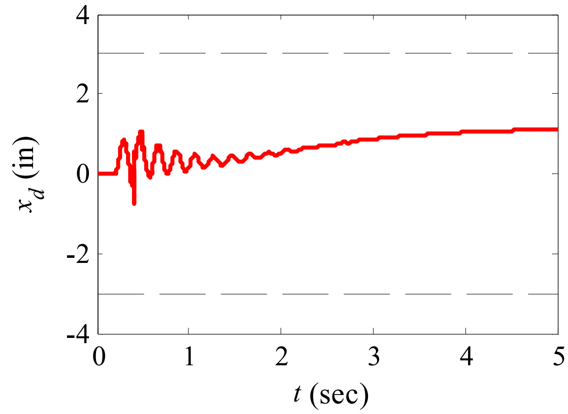

(b) Control excitation input (u)

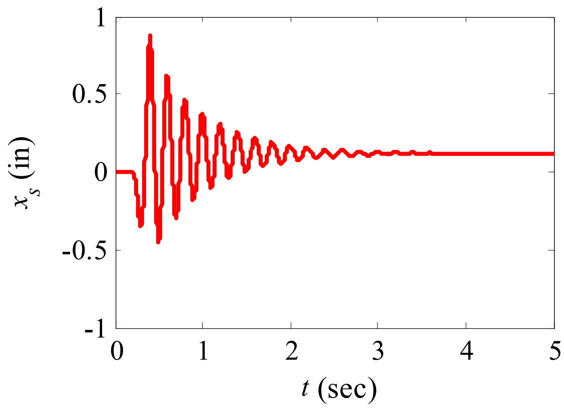

(c) Response of structure (x_s)

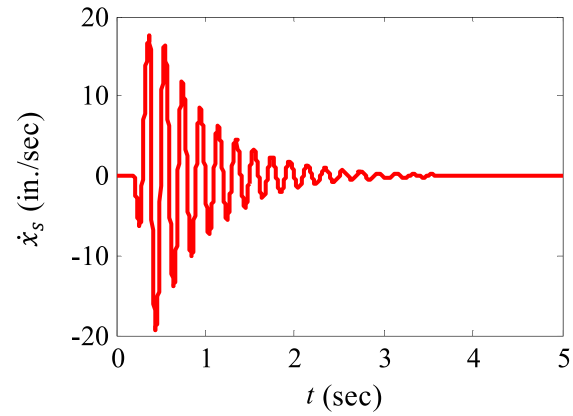

(d) Response of structure ($\dot{x}_s$)

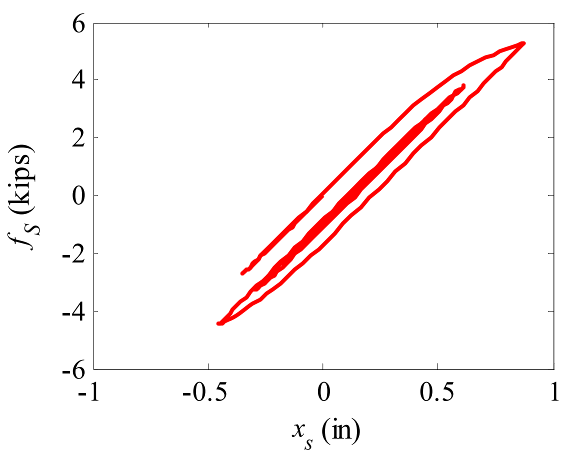

(e) Response of structure (f_S vs. x_s)

Figure A-9 Tracking control - structure responses (Test #2)

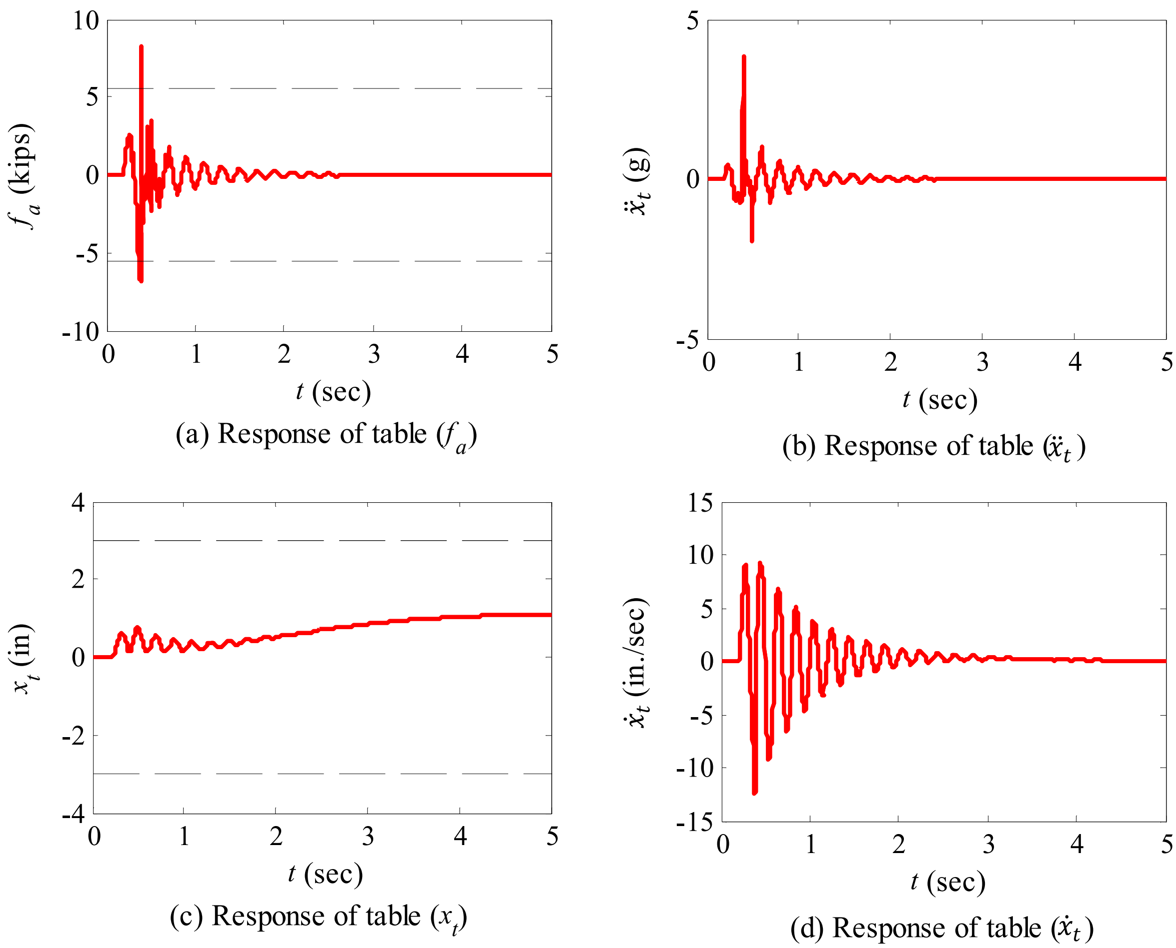

Figure A-10 Tracking control – shake table responses (Test #2)

"This Page Intentionally Left Blank"

APPENDIX B. DERIVATIONS

B.1 [Derivation 3.1]

Control law for a linear structure - SDOF system model using the FTC method

Equations for the True System

$$\begin{aligned} \ddot{x}_s(t) &= -m_s^{-1}c_s\dot{x}_s(t) - m_s^{-1}k_s x_s(t) + m_s^{-1}u(t), \qquad \underline{x}(0) = \underline{x}_0 \\ y(t) &= \ddot{x}_s^t(t) = -m_s^{-1}c_s\dot{x}_s(t) - m_s^{-1}k_s x_s(t) \end{aligned} \tag{B-1}$$

Equations for the Reference Model

$$\begin{aligned} \ddot{x}_m(t) &= -m_m^{-1}c_m\dot{x}_m(t) - m_m^{-1}k_m x_m(t) + m_m^{-1}r(t), \qquad \underline{x}_m(0) = \underline{x}_{m,0} \\ y_m(t) &= \ddot{x}_m^t(t) = -m_m^{-1}c_m\dot{x}_m(t) - m_m^{-1}k_m x_m(t) \end{aligned} \tag{B-2}$$

The system output $y(t)$ is to be differentiated until the control input $u(t)$ appears in the expression of the differentiated output

$$\begin{aligned} \dot{y}(t) &= -m_s^{-1}c_s\ddot{x}_s(t) - m_s^{-1}k_s x_s(t) \\ &= m_s^{-2}c_s\left[c_s\dot{x}_s(t) + k_s x_s(t)\right] - m_s^{-1}k_s\dot{x}_s(t) - c_s m_s^{-2}u(t) \end{aligned} \tag{B-3}$$

which leads to the feedback control law

<u>Control Law</u>

$$\boxed{u(t) = \left(-c_s m_s^{-2}\right)^{-1}\left[-\dot{y}^*(t) + v(t)\right]} \tag{B-4}$$

where $\dot{y}^*(t)$ is defined from Eq. (B-3) as

$$\dot{y}^*(t) = m_s^{-2}c_s\left[c_s\dot{x}_s(t) + k_s x_s(t)\right] - m_s^{-1}k_s\dot{x}_s(t) \tag{B-5}$$

Substituting $u^*(t)$ in Eq. (B-3) leads to

$$\dot{y}(t) = v(t) \tag{B-6}$$

To reduce the tracking error signal $e(t) = y(t) - y_m(t)$, the new input $v(t)$ can be

$$v(t) = \dot{y}_m(t) - k_1^* e(t) \tag{B-7}$$

where k_1^* is the tracking error design coefficient, which is constant and positive, which leads to the tracking error dynamics

<u>Expected Achieved Responses</u>

$$\dot{e}(t) + k_1^* e(t) = 0 \tag{B-8}$$

in which the tracking error signal $e(t) \to 0$ as $t \to \infty$ by selectin $k_1^* > 0$.

B.2 [Derivation 3.2]

Control law for a shake table – linear structure - 2DOF system model using the FTC method

Equations for the True System

$$
\begin{aligned}
& m_s\ddot{x}_s(t)+c_s\dot{x}_s(t)+k_sx_s(t)=-m_s\ddot{x}_t(t) \\
& m_t\ddot{x}_t(t)-\{c_s\dot{x}_s(t)+k_sx_s(t)\}=f_a(t) \qquad , \qquad \underline{x}(0)=\underline{x}_0 \\
& \frac{1}{\omega_a^2}\frac{\dot{f}_a(t)}{m_t}+\frac{2\xi_a}{\omega_a}\frac{f_a(t)}{m_t}+\frac{dx_t(t)}{dt}+k_ax_t(t)=k_ax_d(t) \\
& y(t)=\ddot{x}_s^t(t)=-m_s^{-1}c_s\dot{x}_s(t)-m_s^{-1}k_sx_s(t)
\end{aligned}
\tag{B-9}
$$

Equations for the Reference Model

$$
\begin{aligned}
& \ddot{x}_m(t)=-m_m^{-1}c_m\dot{x}_m(t)-m_m^{-1}k_mx_m(t)+m_m^{-1}r(t), \qquad \underline{x}_m(0)=\underline{x}_{m,0} \\
& y_m(t)=\ddot{x}_m^t(t)=-m_m^{-1}c_m\dot{x}_m(t)-m_m^{-1}k_mx_m(t)
\end{aligned}
\tag{B-10}
$$

By introducing notations for simplification:

$$
\begin{aligned}
& a=m_s^{-1}c_s; \quad b=m_s^{-1}k_s; \quad c=m_t^{-1}c_s; \quad d=m_t^{-1}k_s; \\
& e=2\xi_a\omega_a; \quad f=\omega_a^2; \quad g=\omega_a^2k_a; \\
& f_a^*(t)=f_a(t)/m_t; \quad u^*(t)=\omega_a^2k_ax_d(t), \quad u(t)=x_d(t)
\end{aligned}
\tag{B-11}
$$

Eq. (B-9) can be rewritten,

$$
\begin{aligned}
& \begin{cases}
\ddot{x}_s(t)+a\dot{x}_s(t)+bx_s(t)=-\ddot{x}_t(t) \\
\ddot{x}_t(t)-\{c\dot{x}_s(t)+dx_s(t)\}=f_a^*(t) \qquad , \qquad \underline{x}(0)=\underline{x}_0 \\
\dot{f}_a^*(t)+ef_a^*(t)+f\dot{x}_t(t)+gx_t(t)=u^*(t)
\end{cases} \\
& y(t)=-a\dot{x}_s(t)-bx_s(t)
\end{aligned}
\tag{B-12}
$$

The system output $y(t)$ is to be differentiated until the control input $u(t)$ appears in the expression of the differentiated output

$$
\begin{aligned}
\dot{y}(t)&=-a\ddot{x}_s(t)-b\dot{x}_s(t) \\
&=\left[a(a+c)-b\right]\dot{x}_s(t)+a(b+d)x_s(t)+af_a^*(t)
\end{aligned}
\tag{B-13}
$$

$$
\begin{aligned}
\ddot{y}(t)=&\left[a(a+c)-b\right]\ddot{x}_s(t)+a(b+d)\dot{x}_s(t) \\
&+(-ae)f_a^*(t)+(-af)\dot{x}_t(t)+(-ag)x_t(t)+au^*(t)
\end{aligned}
\tag{B-14}
$$

which leads to the feedback control law

<u>Control Law</u>

$$
\boxed{u^*(t)=a^{-1}\left[-\ddot{y}^*(t)+v(t)\right]}
\tag{B-15}
$$

where $u^*(t)=(\omega_a^{2}k_a)^{-1}u(t)$; $u(t)=x_d(t)$; and $\ddot{y}^*(t)$ is defined from Eq. (B-14) as

$$\dddot{y}^*(t)=\left[a(a+c)-b\right]\ddot{x}_s(t)+a(b+d)\dot{x}_s(t)+(-ae)f_a^*(t)+(-af)\dot{x}_t(t)+(-ag)x_t(t) \quad \text{(B-16)}$$

Substituting $u^*(t)$ in Eq. (B-14) leads to

$$\dddot{y}(t)=v(t) \quad \text{(B-17)}$$

To reduce the tracking error signal $e(t) = y(t) - y_m(t)$, the new input $v(t)$ can be

$$v(t)=\dddot{y}_m(t)-k_1^*\dot{e}(t)-k_2^*e(t) \quad \text{(B-18)}$$

where k_1^* and k_2^* are the tracking error design coefficients, which are constant and positive, these lead to the tracking error dynamics

Expected Achieved Responses

$$\ddot{e}(t)+k_1^*\dot{e}(t)+k_2^*e(t)=0 \quad \text{(B-19)}$$

in which the error signal $e(t)$ goes to zero as time goes to infinity; $e(t) \to 0$ as $t \to \infty$.

B.3 [Derivation 3.3]

Comparisons of Feedback Tracking Control Methods: PTC vs FTC for a 2DOF linear system

For a the shake table-structure 2DOF system, the control law of the predictive tracking control (PTC) shown in Eq. (3-46) becomes the same as the control law of the feedback linearization tracking control (FTC) method in Eq. (3-66) (or (B-15)) under certain conditions (i.e. $R = 0$ and the chosen tracking error coefficients).

For convenience, the control law of the PTC shown in Eq. (3-46) is repeated here (i.e. $\underline{\hat{x}}(t) = \underline{x}(t)$ for the systems with known parameters)

$$u(t)=\left[B^{*T}QB^*+R\right]^{-1}B^{*T}Q\left[y_m^*(t+h)-A^*\underline{x}(t)\right] \quad \text{(B-20)}$$

where $A^* = [C + hCA + (h^2/2)CA^2]$ and $B^* = (h^2/2)CAB$; i.e. here h is a time interval for prediction, which is a tracking error design parameter and can be selected by an engineer, not restricted to be equal to the sampling time step. The system matrices A, B and C in Eq. (2-24) can be expressed as, by using the notations in (B-11),

$$A=\begin{bmatrix} 0 & 1 & 0 & 0 & 0 \\ (-b-d) & (-a-c) & 0 & 0 & -1 \\ 0 & 0 & 0 & 1 & 0 \\ d & c & 0 & 0 & 1 \\ 0 & 0 & -g & -f & -e \end{bmatrix};\ B=\begin{bmatrix} 0 \\ 0 \\ 0 \\ 0 \\ 1 \end{bmatrix}k_a\omega_a^2 \quad \text{(B-21)}$$

$$C=\begin{bmatrix} -b & -a & 0 & 0 & 0 \end{bmatrix}$$

Using these matrices, $A^*\underline{x}(t)$ and B^* (size = 1 × 1) in Eq. (B-20) are computed

$$\overset{*}{A}\underline{x}(t)=[C+hCA+\left(h^2/2\right)CA^2]\underline{x}(t)=C\underline{x}(t)+hCA\underline{x}(t)+\left(h^2/2\right)CA^2\underline{x}(t) \tag{B-22}$$

which can be rewritten using $y(t) = C\underline{x}(t)$ and $\dot{y}(t) = CA\underline{x}(t)$ (see Eq. 3-44):

$$\overset{*}{A}\underline{x}(t)=y(t)+h\dot{y}(t)+\left(h^2/2\right)CA^2\underline{x}(t) \tag{B-23}$$

Substituting this equation and $y_m^*(t+h)$ in Eq. (3-43) in Eq. (B-20) leads to

$$\begin{aligned}\left[y_m^*(t+h)-\overset{*}{A}\underline{x}(t)\right]&=\left[y_m(t)+h\dot{y}_m(t)+\left(h^2/2\right)\ddot{y}_m(t)\right]-\left[y(t)+h\dot{y}(t)+\left(h^2/2\right)CA^2\underline{x}(t)\right]\\&=\left(h^2/2\right)\left[\ddot{y}_m(t)-\left(2/h\right)\dot{e}(t)-\left(2/h^2\right)e(t)-CA^2\underline{x}(t)\right]\end{aligned} \tag{B-24}$$

where $e(t) = y(t) - y_m(t)$. If one chose the tracking error coefficients: $k_1^* = 2/h$ and $k_2^* = 2/h^2$ like the ones in the FTC (see Eq. (B-18)), Eq. (B-24) becomes

$$\left[y_m^*(t+h)-\overset{*}{A}\underline{x}(t)\right]=\left(h^2/2\right)\left[v(t)-CA^2\underline{x}(t)\right] \tag{B-25}$$

in which $CA^2\underline{x}(t)$ can be expressed

$$\begin{aligned}CA^2\underline{x}(t)=\Big[&\left\{-b-a(-a-c)\right\}(-b-d) \quad -a(-b-d)+\left\{-b-a(-a-c)\right\}(-a-c)\\&-ag \quad -af \quad -\left\{-b-a(-a-c)\right\}-ae\Big]\underline{x}(t)\end{aligned} \tag{B-26}$$

One can show that this equation is the same as $\ddot{y}^*(t)$ in Eq. (B-16) by substituting $\ddot{x}_s(t)$ of Eq. (B-12):

$$\begin{aligned}\ddot{y}^*(t)=&\left\{\left[-a(-a-c)-b\right](-a-c)-a(-b-d)\right\}\dot{x}_s(t)+\left[-a(-a-c)-b\right](-b-d)x_s(t)\\&+(-af)\dot{x}_t(t)+(-ag)x_t(t)+\left\{-\left[-a(-a-c)-b\right]+(-ae)\right\}f_a^*(t)\end{aligned} \tag{B-27}$$

B^* (size = 1 × 1) in Eq. (B-20) is also computed

$$B^*=\left(h^2/2\right)CAB=\left(h^2/2\right)a\left(k_a\omega_a^2\right) \tag{B-28}$$

which is a non-zero scalar (i.e. an invertible matrix, size 1 × 1); thus $[B^{*T}QB^* + R]^{-1}B^{*T}Q = B^{*-1}$.

By substituting the equations (B-25) and (B-28) in Eq. (B-20), the control law of the PTC can be expressed

$$\boxed{u(t)=B^{*-1}\left(h^2/2\right)\left[v(t)-CA^2\underline{x}(t)\right]=a^{-1}\left(k_a\omega_a^2\right)^{-1}\left[-\ddot{y}^*(t)+v(t)\right]} \tag{B-29}$$

which is the same as the control law of the FTC shown in Eq. (B-15) (where $u^*(t) = (\omega_a^2 k_a)^{-1}u(t)$).

B.4 [Derivation 4.1]

Control law for a shake table – nonlinear structure - 2DOF system model using the FTC method

Equations for the True System

$$\begin{cases} m_s\ddot{x}_s(t)+c_s\dot{x}_s(t)+f_S(\underline{x})=-m_s\ddot{x}_t(t) \\ m_t\ddot{x}_t(t)-\{c_s\dot{x}_s(t)+f_S(\underline{x})\}=f_a(t) \\ \dot{f}_S(\underline{x})=k_T(\underline{x})\dot{x}_s(t) \\ \dfrac{1}{\omega_a^2}\dfrac{\dot{f}_a(t)}{m_t}+\dfrac{2\xi_a}{\omega_a}\dfrac{f_a(t)}{m_t}+\dfrac{dx_t(t)}{dt}+k_a x_t(t)=k_a x_d(t) \end{cases}, \qquad \underline{x}(0)=\underline{x}_0 \tag{B-30}$$
$$y(t)=\ddot{x}_s^t(t)=-m_s^{-1}c_s\dot{x}_s(t)-m_s^{-1}f_S(\underline{x})$$

Equations for the Reference Model

$$\begin{aligned} &\ddot{x}_m(t)=-m_m^{-1}c_m\dot{x}_m(t)-m_m^{-1}k_m x_m(t)+m_m^{-1}r(t), \qquad \underline{x}_m(0)=\underline{x}_{m,0} \\ &y_m(t)=\ddot{x}_m^t(t)=-m_m^{-1}c_m\dot{x}_m(t)-m_m^{-1}k_m x_m(t) \end{aligned} \tag{B-31}$$

By introducing notations for simplification:

$$\begin{aligned} &a=m_s^{-1}c_s; \quad b=m_s^{-1}k_s; \quad c=m_t^{-1}c_s; \\ &e=2\xi_a\omega_a; \quad f=\omega_a^2; \quad g=\omega_a^2 k_a; \\ &f_a^*(t)=f_a(t)/m_t; \quad u^*(t)=\omega_a^2 k_a x_d(t), \quad u(t)=x_d(t) \end{aligned} \tag{B-32}$$

Eq. (B-30) can be rewritten,

$$\begin{cases} \ddot{x}_s(t)+a\dot{x}_s(t)+m_s^{-1}f_S(\underline{x})=-\ddot{x}_t(t) \\ \ddot{x}_t(t)-\{c\dot{x}_s(t)+m_t^{-1}f_S(\underline{x})\}=f_a^*(t) \\ \dot{f}_S(\underline{x})=k_T(\underline{x})\dot{x}_s(t) \\ \dot{f}_a^*(t)+ef_a^*(t)+f\dot{x}_t(t)+gx_t(t)=u^*(t) \end{cases}, \qquad \underline{x}(0)=\underline{x}_0 \tag{B-33}$$
$$y(t)=-a\dot{x}_s(t)-m_s^{-1}f_S(\underline{x})$$

The system output $y(t)$ is to be differentiated until the control input $u(t)$ appears in the expression of the differentiated output

$$\begin{aligned} \dot{y}(t)&=-a\ddot{x}_s(t)-m_s^{-1}\dot{f}_S(\underline{x}) \\ &=\left[a(a+c)-m_s^{-1}k_T(\underline{x})\right]\dot{x}_s(t)+a(m_s^{-1}+m_t^{-1})f_S(\underline{x})+af_a^*(t) \end{aligned} \tag{B-34}$$

$$\begin{aligned} \ddot{y}(t)=&\left[a(a+c)-m_s^{-1}k_T(\underline{x})\right]\ddot{x}_s(t)+\left[-m_s^{-1}\dot{k}_T(\underline{x})+a\left(m_s^{-1}+m_t^{-1}\right)k_T(\underline{x})\right]\dot{x}_s(t) \\ &+(-ae)f_a^*(t)+(-af)\dot{x}_t(t)+(-ag)x_t(t)+au^*(t) \end{aligned} \tag{B-35}$$

where $\dot{k}_T(\underline{x})$ is expressed as, by defining the state $[x_s(t)\ \ \dot{x}_s(t)\ \ f_S(\underline{x})]^T \equiv [x_1\ \ x_2\ \ x_3]^T$:

$$\dot{k}_T(\underline{x})=\frac{dk_T(\underline{x})}{dt}=\frac{\partial k_T(\underline{x})}{\partial x_1}\dot{x}_1+\frac{\partial k_T(\underline{x})}{\partial x_2}\dot{x}_2+\frac{\partial k_T(\underline{x})}{\partial x_3}\dot{x}_3 \tag{B-36}$$

where each term is defined in Section 5.2.1.2 (i.e. Eq. (5-68) through Eq. (5-70)) and repeated here for convenience:

$$\frac{\partial k_T(\underline{x})}{\partial x_1} = \frac{\partial \overline{\gamma}(\underline{x})}{\partial x_1}\overline{\alpha}\overline{\beta}(\underline{x}); \qquad \frac{\partial \overline{\gamma}(\underline{x})}{\partial x_1} = N\left|f_H(\underline{x})\right|^{N-1}\operatorname{sgn}\left(f_H(\underline{x})\right)\left(-\alpha k_s\right) \tag{B-37}$$

$$\frac{\partial k_T(\underline{x})}{\partial x_3} = \frac{\partial \overline{\gamma}(\underline{x})}{\partial x_3}\overline{\alpha}\overline{\beta}(\underline{x}); \qquad \frac{\partial \overline{\gamma}(\underline{x})}{\partial x_3} = N\left|f_H(\underline{x})\right|^{N-1}\operatorname{sgn}\left(f_H(\underline{x})\right)(1) \tag{B-38}$$

$$\frac{\partial k_T(\underline{x})}{\partial x_2} = \frac{\partial \overline{\beta}(\underline{x})}{\partial x_2}\overline{\alpha}\overline{\gamma}(\underline{x}); \qquad \frac{\partial \overline{\beta}(\underline{x})}{\partial x_2} = 2\delta(x_2)\operatorname{sgn}\left(f_H(\underline{x})\right). \tag{B-39}$$

where the relation $\delta(x) \times x = 0$ (Dannon, 2012) (i.e. $\delta(x)$ is the *Dirac delta function*) is used, and the $\delta(x_2)$ in the last equation indicates that the function $k_T(\underline{x})$ has a jump at the unloading instant (where $x_2 = 0$) from the hardening stiffness to the initial stiffness as shown in the hysteretic loop (Figure 4-1 (left)). This $\delta(x_2)$ in $\dot{k}_T(\underline{x})$ is multiplied by x_2 as $\dot{k}_T(\underline{x}) \times x_2$ in Eq. (B-41); thus, it does not affect the control law in Eq. (B-40).

The differentiated output equation in Eq. (B-35) leads to the feedback control law

Control Law

$$\boxed{u^*(t) = a^{-1}\left[-\ddot{y}^*(t) + v(t)\right]} \tag{B-40}$$

where $u^*(t) = (\omega_a^2 k_a)^{-1} u(t)$; $u(t) = x_d(t)$; and $\ddot{y}^*(t)$ is defined from Eq. (B-35) as

$$\begin{aligned}\ddot{y}^*(t) = &\left[a(a+c) - m_s^{-1}k_T(\underline{x})\right]\ddot{x}_s(t) + \left[-m_s^{-1}\dot{k}_T(\underline{x}) + a\left(m_s^{-1} + m_t^{-1}\right)k_T(\underline{x})\right]\dot{x}_s(t) \\ &+ (-ae)f_a^*(t) + (-af)\dot{x}_t(t) + (-ag)x_t(t)\end{aligned} \tag{B-41}$$

Substituting $u^*(t)$ in Eq. (B-35) leads to

$$\ddot{y}(t) = v(t) \tag{B-42}$$

To reduce the tracking error signal $e(t) = y(t) - y_m(t)$, the new input $v(t)$ can be

$$v(t) = \ddot{y}_m(t) - k_1^*\dot{e}(t) - k_2^*e(t) \tag{B-43}$$

where k_1^* and k_2^* are the tracking error design coefficients, which are constant and positive, these lead to the tracking error dynamics

Expected Achieved Responses

$$\ddot{e}(t) + k_1^*\dot{e}(t) + k_2^*e(t) = 0 \tag{B-44}$$

in which the error signal $e(t)$ goes to zero as time goes to infinity; $e(t) \to 0$ as $t \to \infty$.

B.5 [Derivation 4.2]

Comparisons of Feedback Tracking Control Methods: PTC vs FTC for a 2DOF nonlinear system

As shown for a the shake table-structure 2DOF linear system, for a 2DOF nonlinear system one can also show that the control law of the predictive tracking control (PTC), shown in Eq. (4-18), becomes the same as the control law of the feedback linearization tracking control (FTC) method in Eq. (4-38) with certain conditions (i.e. $R = 0$ and the chosen tracking error coefficients).

For convenience, the control law of the PTC shown in Eq. (4-18) is repeated here (i.e. $\hat{\underline{x}}(t) = \underline{x}(t)$ for the systems with known parameters)

$$u(t)=\left[B(\underline{x})^{*T} QB(\underline{x})^{*}+R\right]^{-1} B(\underline{x})^{*T} Q\left[y_m^*(t+h)-A(\underline{x})^{*} \underline{x}(t)\right] \tag{B-45}$$

where $A(\underline{x})^* = [C + hCA(\underline{x}) + (h^2/2)C\{d/dtA(\underline{x}) + A(\underline{x})^2\}]$ and $B(\underline{x})^* = (h^2/2)CA(\underline{x})B$; i.e. here h is a time interval for prediction, which is a tracking error design parameter and can be selected by an engineer, not restricted to be equal to the time step of the controller or estimator. The system matrices $A(\underline{x})$, B and C in Eq. (4-8) and Eq. (4-9) can be expressed as, by using the notations in (B-32),

$$A=\begin{bmatrix} 0 & 1 & 0 & 0 & 0 & 0 \\ 0 & (-a-c) & -\left(m_s^{-1}+m_t^{-1}\right) & 0 & 0 & -1 \\ 0 & k_T(\underline{x}) & 0 & 0 & 0 & 0 \\ 0 & 0 & 0 & 0 & 1 & 0 \\ 0 & c & m_t^{-1} & 0 & 0 & 1 \\ 0 & 0 & 0 & -g & -f & -e \end{bmatrix};\; B=\begin{bmatrix} 0 \\ 0 \\ 0 \\ 0 \\ 0 \\ 1 \end{bmatrix} k_a\omega_a^2 \tag{B-46}$$

$$C=\begin{bmatrix} 0 & -a & m_s^{-1} & 0 & 0 & 0 \end{bmatrix}$$

Using these matrices, $A(\underline{x})^*\underline{x}(t)$ and $B(\underline{x})^*$ in Eq. (B-45) are computed

$$A(\underline{x})^{*} \underline{x}(t)=[C+hCA(\underline{x})+\left(h^2/2\right)C\left\{d/dtA(\underline{x})+A(\underline{x})^2\right\}]\underline{x}(t) \tag{B-47}$$

which can be rewritten using $y(t) = C\underline{x}(t)$ and $\dot{y}(t) = CA(\underline{x})\underline{x}(t)$ (see Eq. (4-17)):

$$A^{*}\underline{x}(t)=y(t)+h\dot{y}(t)+\left(h^2/2\right)C\left\{d/dtA(\underline{x})+A(\underline{x})^2\right\}]\underline{x}(t) \tag{B-48}$$

Substituting this equation and $y_m^*(t+h)$ of Eq. (3-44) in Eq. (B-45) leads to

$$\left[y_m^*(t+h)-A(\underline{x})^{*} \underline{x}(t)\right]=\left(h^2/2\right)\left[\ddot{y}_m(t)-(2/h)\dot{e}(t)-\left(2/h^2\right)e(t)-C\left\{d/dtA(\underline{x})+A(\underline{x})^2\right\}\underline{x}(t)\right] \tag{B-49}$$

where $e(t) = y(t) - y_m(t)$. If one chose the tracking error coefficients: $k_1^* = 2/h$ and $k_2^* = 2/h^2$ like the ones in the FTC (see Eq.(B-43)), Eq. (B-49)becomes

$$\left[y_m^*(t+h)-A^{*}\underline{x}(t)\right]=\left(h^2/2\right)\left[v(t)-C\left\{d/dtA(\underline{x})+A(\underline{x})^2\right\}\underline{x}(t)\right] \tag{B-50}$$

in which $C\{d/dtA(\underline{x}) + A(\underline{x})^2\}\underline{x}(t)$ can be expressed

$$C\left\{d/dtA(\underline{x})+A(\underline{x})^2\right\}\underline{x}(t)=\left[0 \quad -m_s^{-1}\dot{k}_T(\underline{x})-a\left(-m_s^{-1}-m_t^{-1}\right)k_T(\underline{x})+\left\{-a(-a-c)-m_s^{-1}k_T(\underline{x})\right\}(-a-c)\right.$$
$$\left.\left\{-a(-a-c)-m_s^{-1}k_T(\underline{x})\right\}\left(-m_s^{-1}-m_t^{-1}\right) \quad -ag \quad -af \quad -\left\{-a(-a-c)-m_s^{-1}k_T(\underline{x})\right\}-ae\right]\underline{x}(t) \tag{B-51}$$

One can show that this equation is the same as $\ddot{y}^*(t)$ in Eq. (B-41) by substituting $\ddot{x}_s(t)$ of Eq. (B-33):

$$\begin{aligned}\ddot{y}^*(t)=&\left\{\left[a(a+c)-m_s^{-1}k_T(\underline{x})\right](-a-c)+\left[-m_s^{-1}\dot{k}_T(\underline{x})+a\left(m_s^{-1}+m_t^{-1}\right)k_T(\underline{x})\right]\right\}\dot{x}_s(t)\\&+\left[a(a+c)-m_s^{-1}k_T(\underline{x})\right]\left(-m_s^{-1}-m_t^{-1}\right)f_S(\underline{x})+(-af)\dot{x}_t(t)\\&+(-ag)x_t(t)+\left\{-\left[a(a+c)-m_s^{-1}k_T(\underline{x})\right]+(-ae)\right\}f_a^*(t)\end{aligned} \tag{B-52}$$

$B(\underline{x})^*$ in Eq.(B-45) is also computed

$$B(\underline{x})^*=\left(h^2/2\right)CA(\underline{x})B=\left(h^2/2\right)a\left(k_a\omega_a^2\right) \tag{B-53}$$

which is a non-zero scalar (i.e. an invertible matrix, size 1 × 1); thus $[B(x)^{*T}QB(x)^*+R]^{-1}B(x)^{*T}Q = B(x)^{*-1}$.

By substituting the equations (B-50) and (B-53) in Eq.(B-45), the control law of the PTC can be expressed

$$\boxed{u(t)=B(\underline{x})^{*-1}\left(h^2/2\right)\left[v(t)-C\left\{d/dtA(\underline{x})+A(\underline{x})^2\right\}\right]=a^{-1}\left(k_a\omega_a^2\right)^{-1}\left[-\ddot{y}^*(t)+v(t)\right]} \tag{B-54}$$

which is the same as the control law of the FTC shown in Eq. (4-38) (where $u^*(t) = (\omega_a^2 k_a)^{-1}u(t)$).

B.6 [Derivation 4.3]

L_p property of the state with a stable matrix

For a following LTI (linear time invariant) system with a $n \times n$ stable matrix A,

$$\dot{\underline{x}}(t) = A\underline{x}(t) \tag{B-55}$$

it can be shown that a $n \times 1$ state vector $\underline{x}$ belongs to L_2 as well as L_∞ (i.e. $\underline{x} \in L_\infty \cap L_2$) as following. Since A is a stable matrix, the following Lyapunov function (i.e. a chosen scalar function $V(\underline{x}) > 0$ for $\underline{x} \neq \underline{x}_e$) can be found (i.e. refer to the *Lyapunov direct method* introduced in Section 3.2)

$$V = \underline{x}^{\mathrm{T}}(t)P\underline{x}(t) \tag{B-56}$$

where P is a $n \times n$ positive definite matrix ($P > 0$) and a unique solution of the following Lyapunov matrix equation

$$A^{\mathrm{T}}P + PA = -Q \tag{B-57}$$

where Q is a $n \times n$ positive definite matrix ($Q > 0$). The time derivative of Eq. (B-56) yields

$$\dot{V} = -\underline{x}(t)^T Q\underline{x}(t) < 0 \quad \text{(B-58)}$$

(for $\underline{x} \neq \underline{x}_e$). Therefore, the equilibrium point $\underline{x}_e = \underline{0}$ is asymptotically stable. From Eq. (B-56) and Eq. (B-58) we also know that $\underline{x}$ is bounded (i.e. $\underline{x} \in L_\infty$) (refer to Theorem 3.4.3 in Ioannou and Sun, 2012), and $V(t)$ is bounded from below ($V(t) \geq 0$) and is nonincreasing with time ($\dot{V}(t) \leq 0$), which indicates that $\lim_{t\to\infty} V(t) = V_\infty$ (finite). In addition, since $Q > 0$, we have

$$\lambda_{\min}(Q)|\underline{x}|^2 \leq \underline{x}(t)^T Q\underline{x}(t) \leq \lambda_{\max}(Q)|\underline{x}|^2 \quad \text{(B-59)}$$

It is noted that in this study the following notation is adopted unless stated otherwise: $|\underline{x}| \equiv |\underline{x}(t)|_2$ and $\|A\| \equiv \|A\|_2$, representing the Euclidean norm and the induced Euclidean norm respectively. Substituting Eq. (B-59) into Eq. (B-58) leads

$$\dot{V} = \underline{x}(t)^T Q\underline{x}(t) \leq -\lambda_{\min}(Q)|\underline{x}|^2 \quad \text{(B-60)}$$

Now one can show that

$$\int_0^\infty |\underline{x}|^2 d\tau \leq -\left(\lambda_{\min}(Q)\right)^{-1} \int_0^\infty \dot{V}(\tau)\, d\tau = -\left(\lambda_{\min}(Q)\right)^{-1}\left[V(\infty) - V(0)\right] \quad \text{(B-61)}$$

which is finite (i.e. $\underline{x} \in L_2$). Therefore, it is shown that $\underline{x} \in L_\infty \cap L_2$ for the LTI system with a stable matrix A shown in Eq. (B-55).

B.7 [Derivation 4.4]

L_p property of the restoring force of the nonlinear hysteretic system

The nonlinear hysteretic system shown in Eq. (4-54) is repeated here for convenience

$$\dot{f}_S(\underline{x}) + a^{-1}m_s^{-1}k_s f_S(\underline{x}) + a^{-1}m_s^{-1}k_{in}(\underline{x}) f_S(\underline{x}) = \overline{u}(t) \quad \text{(B-62)}$$

where a^{-1}, m_s^{-1}, k_s are positive constant scalars (i.e. a^{-1}, m_s^{-1}, $k_s > 0$), the inelastic part $k_{in}(\underline{x})$ is bounded as $0 \leq k_{in}(\underline{x}) \leq (1-\alpha)k_s < k_s$ with $0 < \alpha < 1$ in this study (see Eq. (4-52)), and the input term $\overline{u}(t) \in L_\infty \cap L_2$. From this equation, one can show that $f_S(\underline{x}) \in L_\infty \cap L_2$ and $\dot{f}_S(\underline{x}) \in L_\infty \cap L_2$ as following.

For simplicity, introducing new notations: $f_S(\underline{x}) \equiv x(t)$; $a^{-1}m_s^{-1}k_s \equiv \overline{k}_s$; and $a^{-1}m_s^{-1}k_{in}(\underline{x}) \equiv \overline{k}_{in}(t)$; Eq. (B-62) becomes

$$\dot{x}(t) + \overline{k}_s x(t) + \overline{k}_{in}(t)x(t) = \overline{u}(t) \quad \text{(B-63)}$$

The solution of this equation can be expressed

$$\begin{aligned} x(t) &= e^{-\overline{k}_s(t-t_0)}x_0 + \int_{t_0}^t e^{-\overline{k}_s(t-\tau)}\overline{k}_{in}(\tau)x(\tau)\,d\tau + \int_{t_0}^t e^{-\overline{k}_s(t-\tau)}\overline{u}(\tau)\,d\tau \\ &= e^{-\overline{k}_s t}e^{\overline{k}_s t_0}x_0 + e^{-\overline{k}_s t}\int_{t_0}^t e^{\overline{k}_s \tau}\overline{k}_{in}(\tau)x(\tau)\,d\tau + e^{-\overline{k}_s t}\int_{t_0}^t e^{\overline{k}_s \tau}\overline{u}(\tau)\,d\tau \end{aligned} \quad \text{(B-64)}$$

where $x_0 = x(t_0)$ and by multiplying each side by $exp(\overline{k}_s t)$ one has

$$e^{\overline{k}_s t}x(t) = e^{\overline{k}_s t_0}x_0 + \int_{t_0}^t e^{\overline{k}_s \tau}\overline{k}_{in}(\tau)x(\tau)\,d\tau + \int_{t_0}^t e^{\overline{k}_s \tau}\overline{u}(\tau)\,d\tau \quad \text{(B-65)}$$

Hence, the following inequality can be expressed

$$e^{\bar{k}_s t}\left|x(t)\right| \le e^{\bar{k}_s t_0}x_0 + \int_{t_0}^{t} e^{\bar{k}_s \tau}\bar{k}_{in}(\tau)\left|x(\tau)\right|d\tau + \int_{t_0}^{t} e^{\bar{k}_s \tau}\left|\bar{u}(\tau)\right|d\tau \tag{B-66}$$

which can be rewritten as

$$\left|\bar{x}(t)\right| \le \lambda(t) + \int_{t_0}^{t}\bar{k}_{in}(\tau)\left|\bar{x}(\tau)\right|d\tau \tag{B-67}$$

where

$$\left|\bar{x}(t)\right| \equiv e^{\bar{k}_s t}\left|x(t)\right|, \quad \lambda(t) \equiv e^{\bar{k}_s t_0}x_0 + \int_{t_0}^{t} e^{\bar{k}_s \tau}\left|\bar{u}(\tau)\right|d\tau.$$

Applying the *Bellman-Gronwall* Lemma II (refer to Lemma 3.3.8[13] in Ioannou and Sun, 2012) with $k(t) = \bar{k}_{in}(t)$, one has

$$\left|\bar{x}(t)\right| \le \lambda(t_0)e^{\int_{t_0}^{t}\bar{k}_{in}(s)ds} + \int_{t_0}^{t}\dot{\lambda}(s)e^{\int_{s}^{t}\bar{k}_{in}(\tau)d\tau}ds \tag{B-68}$$

where

$$\lambda(t_0) = x_0 e^{\bar{k}_s t_0}, \quad \dot{\lambda}(s) = e^{\bar{k}_s s}\left|\bar{u}(s)\right|.$$

Therefore, using that the maximum of $k_{in}(\underline{x}) \equiv k_{in,m} = (1-\alpha)k_s$ with $0 < \alpha < 1$,

$$\begin{aligned}\left|\bar{x}(t)\right| &\le x_0 e^{\bar{k}_s t_0}e^{\int_{t_0}^{t}\bar{k}_{in}(s)ds} + \int_{t_0}^{t} e^{\bar{k}_s s}\left|\bar{u}(s)\right|e^{\int_{s}^{t}\bar{k}_{in}(\tau)d\tau}ds \\ &\le x_0 e^{\bar{k}_s t_0}e^{\bar{k}_{in,m}(t-t_0)} + \int_{t_0}^{t} e^{\bar{k}_s}e^{\bar{k}_{in,m}(t-s)}\left|\bar{u}(s)\right|ds\end{aligned} \tag{B-69}$$

By multiplying each side by $exp(-\bar{k}_s t)$, one has

$$\begin{aligned}\left|x(t)\right| &\le x_0 e^{-\bar{k}_s(t-t_0)}e^{\bar{k}_{in,m}(t-t_0)} + \int_{t_0}^{t} e^{-\bar{k}_s(t-s)}e^{\bar{k}_{in,m}(t-s)}\left|\bar{u}(s)\right|ds \\ &= x_0 e^{-(\bar{k}_s-\bar{k}_{in,m})(t-t_0)} + \int_{t_0}^{t} e^{-(\bar{k}_s-\bar{k}_{in,m})(t-s)}\left|\bar{u}(s)\right|ds\end{aligned} \tag{B-70}$$

where the right-hand-side is bounded if $(\bar{k}_s - \bar{k}_{in,m}) > 0$, and it is always satisfied in this study since $0 < \alpha < 1$; thus, $(\bar{k}_s - \bar{k}_{in,m}) = \alpha\bar{k}_s = c_1\alpha k_s > 0$. Furthermore, the right-hand-side belongs to L_2 because the first term belongs to L_2 (i.e. the L_2 norm is finite) and the second term also belongs to L_2 according to Theorem

---

[13] Lemma 3.3.8 (Ioannou and Sun, 2012): Let $\lambda(t)$, $k(t)$ be nonnegative piecewise continuous function of time t and let $\lambda(t)$ be differentiable. If the function $y(t)$ satisfies the inequality

$$y(t) \le \lambda(t) + \int_{t_0}^{t} k(\tau)y(\tau)d\tau, \quad \forall t \ge t_0 \ge 0$$

then

$$y(t) \le \lambda(t_0)e^{\int_{t_0}^{t}k(s)ds} + \int_{t_0}^{t}\dot{\lambda}(s)e^{\int_{s}^{t}k(\tau)d\tau}ds, \quad \forall t \ge t_0 \ge 0.$$

3.3.2[14] (refer to Ioannou and Sun, 2012) where $h(t-\tau) = exp[-(\overline{k}_s - \overline{k}_{in,m})(t-\tau)]$, which belongs to L_1 since $(\overline{k}_s - \overline{k}_{in,m}) > 0$, and $u(t) \in L_\infty \cap L_2$. Therefore, it is shown that $x(t) \in L_\infty \cap L_2$ since the right-hand-side of Eq. (B-70) belongs to $L_\infty \cap L_2$.

B.8 [Derivation 4.5]

***L_p* property of the actuator force of the nonlinear hysteretic system**

The nonlinear system equation of the actuator force shown in Eq. (4-56) is repeated here for convenience

$$\dot{f}_a^*(t) + \overline{h}(\underline{x}) f_a^*(t) = \underbrace{-\left[-\overline{h}(\underline{x})(a+c) + i(\underline{x})\right]\dot{x}_s(t) - \left[-\overline{h}(\underline{x})\left(m_s^{-1} + m_t^{-1}\right) + j\right] f_S(\underline{x}) + u_m(t)}_{\overline{u}_m(t)} \quad \text{(B-71)}$$

where in the right-hand-side the new input term $\overline{u}_m(t)$ is introduced for simplicity, and $\overline{u}_m(t) \in L_\infty \cap L_2$ since $\dot{x}_s(t)$, $f_S(\underline{x})$, $u_m(t) \in L_\infty \cap L_2$ (as discussed for (4-56) in Section 4.3). Also, $\overline{h}(\underline{x})$, $i(\underline{x})$ are bounded functions (i.e. $\overline{h}(\underline{x})$, $i(\underline{x}) \in L_\infty$) as shown in Eq. (4-44):

$$\overline{h}(\underline{x}) = -\left[(a+c) - a^{-1}m_s^{-1}k_T(\underline{x}) - k_1^*\right];$$

$$i(\underline{x}) = -\left[-a^{-1}m_s^{-1}\dot{k}_T(\underline{x}) + \left(m_s^{-1} + m_t^{-1}\right)k_T(\underline{x}) - k_1^* a^{-1}m_s^{-1}k_T(\underline{x}) - k_2^*\right];$$

where all terms are positive constants except $k_T(\underline{x})$ and $\dot{k}_T(\underline{x})$, and $k_T(\underline{x}) \in L_\infty$ (as shown in (4-51)). $\dot{k}_T(\underline{x})$ is expressed, by defining the state $[x_s(t) \;\; \dot{x}_s(t) \;\; f_S(\underline{x})]^T \equiv [x_1 \;\; x_2 \;\; x_3]^T$, in Eq. (B-36): as repeated here for convenience

$$\dot{k}_T(\underline{x}) = \frac{dk_T(\underline{x})}{dt} = \frac{\partial k_T(\underline{x})}{\partial x_1}\dot{x}_1 + \frac{\partial k_T(\underline{x})}{\partial x_2}\dot{x}_2 + \frac{\partial k_T(\underline{x})}{\partial x_3}\dot{x}_3 \quad \text{(B-72)}$$

where each term is defined in Section 5.2.1.2 (i.e. Eq. (5-68) through Eq. (5-70)) and all terms are bounded except the following term

$$\frac{\partial k_T(\underline{x})}{\partial x_2} = \frac{\partial \overline{\beta}(\underline{x})}{\partial x_2}\overline{\alpha\gamma}(\underline{x}); \qquad \frac{\partial \overline{\beta}(\underline{x})}{\partial x_2} = 2\delta(x_2)\,\mathrm{sgn}\left(f_H(\underline{x})\right)$$

---

[14] Theorem 3.3.1 (Ioannou and Sun, 2012):

The reference considers an LTI (linear time invariant) system described by the convolution of two functions u, $h : R^+ \to R$ (i.e. $t \geq 0$) defined as

$$y(t) = u * h \equiv \int_0^t h(t-\tau)u(\tau)\,d\tau$$

where $h(t)$ is the impulse response of the system.

The reference says that the following results hold for the system above. If $u \in L_p$ and $h \in L_1$ then

$$\|y\|_p \leq \|h\|_1 \|u\|_p$$

where $p \in [1, \infty]$.

where the relation $\delta(x) \times x = 0$ (Dannon, 2012) (i.e. $\delta(x)$ is the *Dirac delta function*) is used, and the $\delta(x_2)$ in the last equation indicates that the function $k_T(\underline{x})$ has a jump at the unloading instant (where $x_2 = 0$) from the hardening stiffness to the initial stiffness as shown in the hysteretic loop (Figure 4-1 (left)). This $\delta(x_2)$ in $\dot{k}_T(\underline{x})$ is multiplied by x_2 as $\dot{k}_T(\underline{x}) \times x_2$ in Eq. (B-71); thus, it does not affect the stability of the system and it concludes that $\dot{\imath}(\underline{x}) \in L_\infty$.

Now, from Eq. (B-71) one can show that $f_a^*(t) \in L_\infty \cap L_2$ and $\dot{f}_a^*(t) \in L_\infty \cap L_2$ using the same procedure shown in Derivation 4.4 in Appendix B.7. The function $\bar{h}(\underline{x})$ in the left-hand-side of Eq. (B-71) can be expressed in two parts: an elastic part $\bar{k}$ and inelastic part $\bar{k}_{in}$;

$$\bar{h}(\underline{x}) = -\left[(a+c) - a^{-1}m_s^{-1}k_T(\underline{x}) - k_1^*\right] = \underbrace{\left[a^{-1}m_s^{-1}k_s + k_1^* - (a+c)\right]}_{\bar{k}} + \underbrace{\left[a^{-1}m_s^{-1}k_{in}(\underline{x})\right]}_{\bar{k}_{in}(t)} \tag{B-73}$$

Thus, Eq. (B-71) can be rewritten as

$$\dot{f}_a^*(t) + \bar{k}f_a^*(t) + \bar{k}_{in}(t)f_a^*(t) = \bar{u}_m(t) \tag{B-74}$$

which is the same form as Eq. (B-63); therefore, it can be shown that $f_a^*(t) \in L_\infty \cap L_2$ if $(\bar{k} - \bar{k}_{in,m}) > 0$ where

$$\bar{k} - \bar{k}_{in,m} = \left[a^{-1}m_s^{-1}k_s + k_1^* - (a+c)\right] - \left[a^{-1}m_s^{-1}(1-\alpha)k_s\right] = a^{-1}m_s^{-1}\alpha k_s + k_1^* - (a+c) \tag{B-75}$$

and this condition can be easily met by choosing the design coefficient k_1^* in Eq. (4-42) to be larger than $(a + c)$. Since $\bar{h}(\underline{x}) \in L_\infty$ and $f_a^*(t)$, $u_m(t) \in L_\infty \cap L_2$, from Eq. (B-71) $\dot{f}_a^*(t) \in L_\infty \cap L_2$.

B.9 [Derivation 5.1]

Derivation of the recursive least squares algorithm with forgetting factor

The *continuous-time non-recursive least squares* algorithm is given in Eq. (5-11) and Eq. (5-12), which are repeated for convenience:

$$\underline{\hat{\theta}}(t) = P(t)\left[e^{-\beta t}Q_{E,0}\underline{\hat{\theta}}_0 + \int_0^t e^{-\beta(t-\tau)}\left[z(\tau)\underline{\phi}^T(\tau)\right]d\tau\right] \tag{B-76}$$

where

$$P(t) = \left[e^{-\beta t}Q_{E,0} + \int_0^t e^{-\beta(t-\tau)}\left[\underline{\phi}(\tau)\underline{\phi}^T(\tau)\right]d\tau\right]^{-1} \tag{B-77}$$

Since $Q_{E,0} > 0$ (selected) and $\underline{\phi}(t)\underline{\phi}^T(t) \geq 0$, $P(t)$ is a positive definite matrix and invertible. Using the identity,

$$\frac{d}{dt}\left[P(t)P^{-1}(t)\right] = \dot{P}(t)P^{-1}(t) + P(t)\dot{P}^{-1}(t) = 0 \tag{B-78}$$

$\dot{P}(t)$ is expressed

$$\dot{P}(t) = -P(t)\dot{P}^{-1}(t)P(t) \tag{B-79}$$

where $\dot{P}^{-1}(t)$ can be obtained by taking inverse of $P(t)$ in Eq.(B-77), then differentiating it with respect to t

$$\begin{aligned}\dot{P}^{-1}(t) &= -\beta e^{-\beta t} Q_{E,0} + \left\{ \underline{\phi}(t)\underline{\phi}^T(t) - \beta \int_0^t e^{-\beta(t-\tau)} \left[\underline{\phi}(\tau)\underline{\phi}^T(\tau) \right] d\tau \right\} \\ &= \underline{\phi}(t)\underline{\phi}^T(t) - \beta P^{-1}(t)\end{aligned} \tag{B-80}$$

Substitution of this equation into Eq. (B-79) gives

$$\dot{P}(t) = \beta P(t) - P(t)\underline{\phi}(t)\underline{\phi}^T(t)P(t) \tag{B-81}$$

with $P(0) = P_0 = Q_{E,0}^{-1}$. Similarly, by differentiating $\underline{\hat{\theta}}(t)$ in Eq. (B-76) with respect to t, one has

$$\begin{aligned}\frac{d}{dt}\underline{\hat{\theta}}(t) &= \dot{P}(t)\left[e^{-\beta t} Q_{E,0}\underline{\hat{\theta}}_0 + \int_0^t e^{-\beta(t-\tau)} \left[z(\tau)\underline{\phi}^T(\tau) \right] d\tau \right] \\ &\quad + P(t)\left[z(t)\underline{\phi}(t) - \beta \left[e^{-\beta t} Q_{E,0}\underline{\hat{\theta}}_0 + \int_0^t e^{-\beta(t-\tau)} \left[z(\tau)\underline{\phi}^T(\tau) \right] d\tau \right] \right]\end{aligned} \tag{B-82}$$

which can be simplified using Eq. (B-81) and Eq. (B-76)

$$\begin{aligned}\frac{d}{dt}\underline{\hat{\theta}}(t) &= -P(t)\underline{\phi}(t)\underline{\phi}^T(t)\underbrace{P(t)\left[e^{-\beta t} Q_{E,0}\underline{\hat{\theta}}_0 + \int_0^t e^{-\beta(t-\tau)} \left[z(\tau)\underline{\phi}^T(\tau) \right] d\tau \right]}_{\underline{\hat{\theta}}(t)} + P(t)z(t)\underline{\phi}(t) \\ &= P(t)\left[z(t) - \underline{\phi}^T(t)\underline{\hat{\theta}}(t) \right]\underline{\phi}(t)\end{aligned} \tag{B-83}$$

which can be further simplified using the definition of the estimation error $\varepsilon(t)$ in Eq. (5-8)

$$\dot{\underline{\hat{\theta}}}(t) = P(t)\varepsilon(t)\underline{\phi}(t) \tag{B-84}$$

This equation with Eq. (B-81) is known as the *continuous-time recursive least squares algorithm with forgetting factor*, which are the same as Eq. (5-13).

B.10 [Derivation 5.2]

Derivation of the EKF in discrete time for implementation

The truth model of a nonlinear system (shown in Eq. (5-50) and Eq. (5-51) in continuous time) is rewritten in discrete time

$$\underline{x}_{k+1} = \underline{x}_k + \int_{t_k}^{t_{k+1}} \mathrm{f}\left(\underline{x}(t), \underline{u}(t), t\right) + G\underline{w}(t)\, dt \tag{B-85}$$

$$\underline{\bar{y}}_k = \underline{\mathrm{h}}\left(\underline{x}_k\right) + \underline{v}_k \tag{B-86}$$

where all terms are explained in Section 5.2.1.1. $\underline{v}_k$ and $\underline{w}_k$ are measurement and process noise (or errors in model), respectively, and they are assumed to be zero-mean Gaussian white-noise processes. In this study, both noise covariance matrices $R_{E,k}$ and $Q_{E,k}$ are assumed to be constant at all time; thus $R_{E,k} = R_E$ and $Q_{E,k} = Q_E$.

The estimator structure shown in Eq. (5-54) in continuous time can be expressed in two stages equations in discrete time as

$$\boxed{\underline{\hat{x}}_{k+1}^{-} = \underline{\hat{x}}_{k}^{+} + \int_{t_k}^{t_{k+1}} \underline{\mathrm{f}}\left(\underline{\hat{x}}(t), \underline{u}(t), t\right) dt} \tag{B-87}$$

$$\boxed{\underline{\hat{x}}_{k}^{+} = \underline{\hat{x}}_{k}^{-} + K_k \left[\underline{y}_k - \underline{\mathrm{h}}\left(\underline{\hat{x}}_{k}^{-}\right) \right]} \tag{B-88}$$

where K_k is the estimator gain and Eq. (B-87) with sign '-' is known as the *prediction* equation, and Eq. (B-88) with sign '+' is known as the *update* equation. The estimate error covariance matrices are defined as

$$P_{k+1}^{-} = E\left\{ \underline{\tilde{x}}_{k+1}^{-} \underline{\tilde{x}}_{k+1}^{-T} \right\} \tag{B-89}$$

$$P_{k}^{+} = E\left\{ \underline{\tilde{x}}_{k}^{+} \underline{\tilde{x}}_{k}^{+T} \right\} \tag{B-90}$$

where the estimate state errors are $\underline{\tilde{x}}_{k+1}^{-} \equiv \underline{\hat{x}}_{k+1}^{-} - \underline{x}_{k+1}$ and $\underline{\tilde{x}}_{k}^{+} \equiv \underline{\hat{x}}_{k}^{+} - \underline{x}_{k}$. Using the Taylor series expansion about the current estimate $\underline{\hat{x}}(t)$ (i.e. assuming that the true state $\underline{x}(t)$ is sufficiently close to the estimated state $\underline{\hat{x}}(t)$, which is used for the nominal state), the $\underline{\mathrm{f}}(\underline{x}(t),u(t),t)$ and $\underline{\mathrm{h}}(\underline{x}(t),t)$ were expressed in Eq. (5-52) and Eq. (5-53) and repeated here:

$$\underline{\mathrm{f}}\left(\underline{x}(t), \underline{u}(t), t\right) \approx \underline{\mathrm{f}}\left(\underline{\hat{x}}(t), \underline{u}(t), t\right) + \left. \frac{\partial \underline{\mathrm{f}}}{\partial \underline{x}} \right|_{\underline{\hat{x}}(t), \underline{u}(t)} \underbrace{\left(\underline{x}(t) - \underline{\hat{x}}(t) \right)}_{-\underline{\tilde{x}}(t)} \tag{B-91}$$

$$\underline{\mathrm{h}}\left(\underline{x}(t), t\right) \approx \underline{\mathrm{h}}\left(\underline{\hat{x}}(t), t\right) + \left. \frac{\partial \underline{\mathrm{h}}}{\partial \underline{x}} \right|_{\underline{\hat{x}}(t)} \underbrace{\left(\underline{x}(t) - \underline{\hat{x}}(t) \right)}_{-\underline{\tilde{x}}(t)} \tag{B-92}$$

The estimate state errors are $\underline{\tilde{x}}_{k+1}^{-} \equiv \underline{\hat{x}}_{k+1}^{-} - \underline{x}_{k+1}$ is given by using Eq. (B-87) for $\underline{\hat{x}}_{k+1}^{-}$ and Eq. (B-85) for $\underline{x}_{k+1}$, after substituting Eq. (B-91) for $\underline{\mathrm{f}}(\underline{x}(t),u(t),t)$:

$$\underline{\tilde{x}}_{k+1}^{-} = \underline{\tilde{x}}_{k}^{+} + \int_{t_k}^{t_{k+1}} F(t) \underline{\tilde{x}}(t) - G(t) \underline{w}(t) dt \tag{B-93}$$

where $F(t)$ is introduced for the Jacobian matrix of $\underline{\mathrm{f}}(\underline{x}(t),u(t),t)$ as shown in Eq. (5-57), evaluated at the current estimate $\underline{\hat{x}}(t)$. Using the first order approximation of the integral part, Eq. (B-93) can be rewritten as

$$\boxed{\begin{aligned} \underline{\tilde{x}}_{k+1}^{-} &= \underline{\tilde{x}}_{k}^{+} + \Delta t F_k\left(\underline{\hat{x}}_{k}^{+}\right) \underline{\tilde{x}}_{k}^{+} - \Delta t G_k \underline{w}_k \\ &= \underbrace{\left\{ I + \Delta t F_k\left(\underline{\hat{x}}_{k}^{+}\right) \right\}}_{\Phi_k} \underline{\tilde{x}}_{k}^{+} - \underbrace{\Delta t G_k}_{\Upsilon_k} \underline{w}_k = \Phi_k \underline{\tilde{x}}_{k}^{+} - \Upsilon_k \underline{w}_k \end{aligned}} \tag{B-94}$$

where $F_k(\underline{\hat{x}}_{k}^{+})$ is the same Jacobian matrix of $\underline{\mathrm{f}}(\underline{x}(t),u(t),t)$, evaluated at the current estimate $\underline{\hat{x}}_{k}^{+}$. It is noted that Eq. (B-94) is the same structure of the estimate state error $\underline{\tilde{x}}_{k+1}^{-}$ equation of the KF, shown in Eq. (5-43). Then, P_{k+1}^{-} is defined by substituting Eq. (B-94) into Eq. (B-89) and using that $E\{\underline{w}_k \underline{\tilde{x}}_{k}^{+T}\} = 0$:

$$\boxed{P_{k+1}^- = \Phi_k P_k^+ \Phi_k^T + \Upsilon_k Q_E \Upsilon_k^T} \tag{B-95}$$

For the update stage, substitution of Eq. (B-88) with Eq. (B-92) for $\underline{\hat{x}}_k^+$ in $\underline{\tilde{x}}_k^+ \equiv \underline{\hat{x}}_k^+ - \underline{x}_k$ gives

$$\begin{aligned} \underline{\tilde{x}}_k^+ &= \underline{\tilde{x}}_k^- + K_k \left[-H_k \left(\underline{\hat{x}}_k^- \right) \underline{\tilde{x}}_k^- + \underline{v}_k \right] \\ &= \left(I - K_k H_k \right) \underline{\tilde{x}}_k^- + K_k \underline{v}_k \end{aligned} \tag{B-96}$$

where $H_k(\underline{\hat{x}}_k^-)$ (or H_k for brevity) is introduced for the Jacobian matrix of $\underline{h}(\underline{x}(t),t)$ as shown in Eq. (5-57), evaluated at the current estimate $\underline{\hat{x}}_k^-$. Then, P_k^+ is defined by substituting Eq. (B-96) into Eq. (B-90) and using that $E\{\underline{v}_k \underline{\tilde{x}}_k^{-T}\} = 0$:

$$P_k^+ = \left[I - K_k H_k \right] P_k^- \left[I - K_k H_k \right]^T + K_k R_E K_k^T \tag{B-97}$$

The optimal estimator gain K_k is determined by minimizing the trace of P_k^+, which is equivalent to minimize the length of the estimation error vector. The index function, the same as that of the KF shown in Eq. (5-47), is repeated here:

$$J\left(K_k \right) = \mathrm{Tr}\left(P_k^+ \right) \tag{B-98}$$

By solving $\partial J / \partial K_k = 0$ for K_k, it results in:

$$\boxed{K_k = P_k^- H_k^T \left[H_k P_k^- H_k^T + R_E \right]^{-1}} \tag{B-99}$$

Substitution of Eq. (B-99) in Eq. (B-97) leads to

$$\boxed{P_k^+ = \left[I - K_k H_k \right] P_k^-} \tag{B-100}$$

The EKF update stage defined in Eq. (B-88) and Eq. (B-100) with the optimal gain K_k in Eq. (B-99) and the EKF prediction stage defined in Eq. (B-87) and Eq. (B-95) are presented in Section 5.2.1.1.

"This Page Intentionally Left Blank"

MCEER Technical Reports

MCEER publishes technical reports on a variety of subjects written by authors funded through MCEER. These reports are available from both MCEER Publications and the National Technical Information Service (NTIS). Requests for reports should be directed to MCEER Publications, MCEER, University at Buffalo, State University of New York, 133A Ketter Hall, Buffalo, New York 14260. Reports can also be requested through NTIS, P.O. Box 1425, Springfield, Virginia 22151. NTIS accession numbers are shown in parenthesis, if available.

NCEER-87-0001 "First-Year Program in Research, Education and Technology Transfer," 3/5/87, (PB88-134275, A04, MF-A01).

NCEER-87-0002 "Experimental Evaluation of Instantaneous Optimal Algorithms for Structural Control," by R.C. Lin, T.T. Soong and A.M. Reinhorn, 4/20/87, (PB88-134341, A04, MF-A01).

NCEER-87-0003 "Experimentation Using the Earthquake Simulation Facilities at University at Buffalo," by A.M. Reinhorn and R.L. Ketter, not available.

NCEER-87-0004 "The System Characteristics and Performance of a Shaking Table," by J.S. Hwang, K.C. Chang and G.C. Lee, 6/1/87, (PB88-134259, A03, MF-A01). This report is available only through NTIS (see address given above).

NCEER-87-0005 "A Finite Element Formulation for Nonlinear Viscoplastic Material Using a Q Model," by O. Gyebi and G. Dasgupta, 11/2/87, (PB88-213764, A08, MF-A01).

NCEER-87-0006 "Symbolic Manipulation Program (SMP) - Algebraic Codes for Two and Three Dimensional Finite Element Formulations," by X. Lee and G. Dasgupta, 11/9/87, (PB88-218522, A05, MF-A01).

NCEER-87-0007 "Instantaneous Optimal Control Laws for Tall Buildings Under Seismic Excitations," by J.N. Yang, A. Akbarpour and P. Ghaemmaghami, 6/10/87, (PB88-134333, A06, MF-A01). This report is only available through NTIS (see address given above).

NCEER-87-0008 "IDARC: Inelastic Damage Analysis of Reinforced Concrete Frame - Shear-Wall Structures," by Y.J. Park, A.M. Reinhorn and S.K. Kunnath, 7/20/87, (PB88-134325, A09, MF-A01). This report is only available through NTIS (see address given above).

NCEER-87-0009 "Liquefaction Potential for New York State: A Preliminary Report on Sites in Manhattan and Buffalo," by M. Budhu, V. Vijayakumar, R.F. Giese and L. Baumgras, 8/31/87, (PB88-163704, A03, MF-A01). This report is available only through NTIS (see address given above).

NCEER-87-0010 "Vertical and Torsional Vibration of Foundations in Inhomogeneous Media," by A.S. Veletsos and K.W. Dotson, 6/1/87, (PB88-134291, A03, MF-A01). This report is only available through NTIS (see address given above).

NCEER-87-0011 "Seismic Probabilistic Risk Assessment and Seismic Margins Studies for Nuclear Power Plants," by Howard H.M. Hwang, 6/15/87, (PB88-134267, A03, MF-A01). This report is only available through NTIS (see address given above).

NCEER-87-0012 "Parametric Studies of Frequency Response of Secondary Systems Under Ground-Acceleration Excitations," by Y. Yong and Y.K. Lin, 6/10/87, (PB88-134309, A03, MF-A01). This report is only available through NTIS (see address given above).

NCEER-87-0013 "Frequency Response of Secondary Systems Under Seismic Excitation," by J.A. HoLung, J. Cai and Y.K. Lin, 7/31/87, (PB88-134317, A05, MF-A01). This report is only available through NTIS (see address given above).

NCEER-87-0014 "Modelling Earthquake Ground Motions in Seismically Active Regions Using Parametric Time Series Methods," by G.W. Ellis and A.S. Cakmak, 8/25/87, (PB88-134283, A08, MF-A01). This report is only available through NTIS (see address given above).

NCEER-87-0015 "Detection and Assessment of Seismic Structural Damage," by E. DiPasquale and A.S. Cakmak, 8/25/87, (PB88-163712, A05, MF-A01). This report is only available through NTIS (see address given above).

NCEER-87-0016 "Pipeline Experiment at Parkfield, California," by J. Isenberg and E. Richardson, 9/15/87, (PB88-163720, A03, MF-A01). This report is available only through NTIS (see address given above).

NCEER-87-0017 "Digital Simulation of Seismic Ground Motion," by M. Shinozuka, G. Deodatis and T. Harada, 8/31/87, (PB88-155197, A04, MF-A01). This report is available only through NTIS (see address given above).

NCEER-87-0018 "Practical Considerations for Structural Control: System Uncertainty, System Time Delay and Truncation of Small Control Forces," J.N. Yang and A. Akbarpour, 8/10/87, (PB88-163738, A08, MF-A01). This report is only available through NTIS (see address given above).

NCEER-87-0019 "Modal Analysis of Nonclassically Damped Structural Systems Using Canonical Transformation," by J.N. Yang, S. Sarkani and F.X. Long, 9/27/87, (PB88-187851, A04, MF-A01).

NCEER-87-0020 "A Nonstationary Solution in Random Vibration Theory," by J.R. Red-Horse and P.D. Spanos, 11/3/87, (PB88-163746, A03, MF-A01).

NCEER-87-0021 "Horizontal Impedances for Radially Inhomogeneous Viscoelastic Soil Layers," by A.S. Veletsos and K.W. Dotson, 10/15/87, (PB88-150859, A04, MF-A01).

NCEER-87-0022 "Seismic Damage Assessment of Reinforced Concrete Members," by Y.S. Chung, C. Meyer and M. Shinozuka, 10/9/87, (PB88-150867, A05, MF-A01). This report is available only through NTIS (see address given above).

NCEER-87-0023 "Active Structural Control in Civil Engineering," by T.T. Soong, 11/11/87, (PB88-187778, A03, MF-A01).

NCEER-87-0024 "Vertical and Torsional Impedances for Radially Inhomogeneous Viscoelastic Soil Layers," by K.W. Dotson and A.S. Veletsos, 12/87, (PB88-187786, A03, MF-A01).

NCEER-87-0025 "Proceedings from the Symposium on Seismic Hazards, Ground Motions, Soil-Liquefaction and Engineering Practice in Eastern North America," October 20-22, 1987, edited by K.H. Jacob, 12/87, (PB88-188115, A23, MF-A01). This report is available only through NTIS (see address given above).

NCEER-87-0026 "Report on the Whittier-Narrows, California, Earthquake of October 1, 1987," by J. Pantelic and A. Reinhorn, 11/87, (PB88-187752, A03, MF-A01). This report is available only through NTIS (see address given above).

NCEER-87-0027 "Design of a Modular Program for Transient Nonlinear Analysis of Large 3-D Building Structures," by S. Srivastav and J.F. Abel, 12/30/87, (PB88-187950, A05, MF-A01). This report is only available through NTIS (see address given above).

NCEER-87-0028 "Second-Year Program in Research, Education and Technology Transfer," 3/8/88, (PB88-219480, A04, MF-A01).

NCEER-88-0001 "Workshop on Seismic Computer Analysis and Design of Buildings With Interactive Graphics," by W. McGuire, J.F. Abel and C.H. Conley, 1/18/88, (PB88-187760, A03, MF-A01). This report is only available through NTIS (see address given above).

NCEER-88-0002 "Optimal Control of Nonlinear Flexible Structures," by J.N. Yang, F.X. Long and D. Wong, 1/22/88, (PB88-213772, A06, MF-A01).

NCEER-88-0003 "Substructuring Techniques in the Time Domain for Primary-Secondary Structural Systems," by G.D. Manolis and G. Juhn, 2/10/88, (PB88-213780, A04, MF-A01).

NCEER-88-0004 "Iterative Seismic Analysis of Primary-Secondary Systems," by A. Singhal, L.D. Lutes and P.D. Spanos, 2/23/88, (PB88-213798, A04, MF-A01).

NCEER-88-0005 "Stochastic Finite Element Expansion for Random Media," by P.D. Spanos and R. Ghanem, 3/14/88, (PB88-213806, A03, MF-A01).

NCEER-88-0006 "Combining Structural Optimization and Structural Control," by F.Y. Cheng and C.P. Pantelides, 1/10/88, (PB88-213814, A05, MF-A01).

NCEER-88-0007 "Seismic Performance Assessment of Code-Designed Structures," by H.H-M. Hwang, J-W. Jaw and H-J. Shau, 3/20/88, (PB88-219423, A04, MF-A01). This report is only available through NTIS (see address given above).

NCEER-88-0008 "Reliability Analysis of Code-Designed Structures Under Natural Hazards," by H.H-M. Hwang, H. Ushiba and M. Shinozuka, 2/29/88, (PB88-229471, A07, MF-A01). This report is only available through NTIS (see address given above).

NCEER-88-0009 "Seismic Fragility Analysis of Shear Wall Structures," by J-W Jaw and H.H-M. Hwang, 4/30/88, (PB89-102867, A04, MF-A01).

NCEER-88-0010 "Base Isolation of a Multi-Story Building Under a Harmonic Ground Motion - A Comparison of Performances of Various Systems," by F-G Fan, G. Ahmadi and I.G. Tadjbakhsh, 5/18/88, (PB89-122238, A06, MF-A01). This report is only available through NTIS (see address given above).

NCEER-88-0011 "Seismic Floor Response Spectra for a Combined System by Green's Functions," by F.M. Lavelle, L.A. Bergman and P.D. Spanos, 5/1/88, (PB89-102875, A03, MF-A01).

NCEER-88-0012 "A New Solution Technique for Randomly Excited Hysteretic Structures," by G.Q. Cai and Y.K. Lin, 5/16/88, (PB89-102883, A03, MF-A01).

NCEER-88-0013 "A Study of Radiation Damping and Soil-Structure Interaction Effects in the Centrifuge," by K. Weissman, supervised by J.H. Prevost, 5/24/88, (PB89-144703, A06, MF-A01).

NCEER-88-0014 "Parameter Identification and Implementation of a Kinematic Plasticity Model for Frictional Soils," by J.H. Prevost and D.V. Griffiths, not available.

NCEER-88-0015 "Two- and Three- Dimensional Dynamic Finite Element Analyses of the Long Valley Dam," by D.V. Griffiths and J.H. Prevost, 6/17/88, (PB89-144711, A04, MF-A01).

NCEER-88-0016 "Damage Assessment of Reinforced Concrete Structures in Eastern United States," by A.M. Reinhorn, M.J. Seidel, S.K. Kunnath and Y.J. Park, 6/15/88, (PB89-122220, A04, MF-A01). This report is only available through NTIS (see address given above).

NCEER-88-0017 "Dynamic Compliance of Vertically Loaded Strip Foundations in Multilayered Viscoelastic Soils," by S. Ahmad and A.S.M. Israil, 6/17/88, (PB89-102891, A04, MF-A01).

NCEER-88-0018 "An Experimental Study of Seismic Structural Response With Added Viscoelastic Dampers," by R.C. Lin, Z. Liang, T.T. Soong and R.H. Zhang, 6/30/88, (PB89-122212, A05, MF-A01). This report is available only through NTIS (see address given above).

NCEER-88-0019 "Experimental Investigation of Primary - Secondary System Interaction," by G.D. Manolis, G. Juhn and A.M. Reinhorn, 5/27/88, (PB89-122204, A04, MF-A01).

NCEER-88-0020 "A Response Spectrum Approach For Analysis of Nonclassically Damped Structures," by J.N. Yang, S. Sarkani and F.X. Long, 4/22/88, (PB89-102909, A04, MF-A01).

NCEER-88-0021 "Seismic Interaction of Structures and Soils: Stochastic Approach," by A.S. Veletsos and A.M. Prasad, 7/21/88, (PB89-122196, A04, MF-A01). This report is only available through NTIS (see address given above).

NCEER-88-0022 "Identification of the Serviceability Limit State and Detection of Seismic Structural Damage," by E. DiPasquale and A.S. Cakmak, 6/15/88, (PB89-122188, A05, MF-A01). This report is available only through NTIS (see address given above).

NCEER-88-0023 "Multi-Hazard Risk Analysis: Case of a Simple Offshore Structure," by B.K. Bhartia and E.H. Vanmarcke, 7/21/88, (PB89-145213, A05, MF-A01).

NCEER-88-0024 "Automated Seismic Design of Reinforced Concrete Buildings," by Y.S. Chung, C. Meyer and M. Shinozuka, 7/5/88, (PB89-122170, A06, MF-A01). This report is available only through NTIS (see address given above).

NCEER-88-0025 "Experimental Study of Active Control of MDOF Structures Under Seismic Excitations," by L.L. Chung, R.C. Lin, T.T. Soong and A.M. Reinhorn, 7/10/88, (PB89-122600, A04, MF-A01).

NCEER-88-0026 "Earthquake Simulation Tests of a Low-Rise Metal Structure," by J.S. Hwang, K.C. Chang, G.C. Lee and R.L. Ketter, 8/1/88, (PB89-102917, A04, MF-A01).

NCEER-88-0027 "Systems Study of Urban Response and Reconstruction Due to Catastrophic Earthquakes," by F. Kozin and H.K. Zhou, 9/22/88, (PB90-162348, A04, MF-A01).

NCEER-88-0028 "Seismic Fragility Analysis of Plane Frame Structures," by H.H-M. Hwang and Y.K. Low, 7/31/88, (PB89-131445, A06, MF-A01).

NCEER-88-0029 "Response Analysis of Stochastic Structures," by A. Kardara, C. Bucher and M. Shinozuka, 9/22/88, (PB89-174429, A04, MF-A01).

NCEER-88-0030 "Nonnormal Accelerations Due to Yielding in a Primary Structure," by D.C.K. Chen and L.D. Lutes, 9/19/88, (PB89-131437, A04, MF-A01).

NCEER-88-0031 "Design Approaches for Soil-Structure Interaction," by A.S. Veletsos, A.M. Prasad and Y. Tang, 12/30/88, (PB89-174437, A03, MF-A01). This report is available only through NTIS (see address given above).

NCEER-88-0032 "A Re-evaluation of Design Spectra for Seismic Damage Control," by C.J. Turkstra and A.G. Tallin, 11/7/88, (PB89-145221, A05, MF-A01).

NCEER-88-0033 "The Behavior and Design of Noncontact Lap Splices Subjected to Repeated Inelastic Tensile Loading," by V.E. Sagan, P. Gergely and R.N. White, 12/8/88, (PB89-163737, A08, MF-A01).

NCEER-88-0034 "Seismic Response of Pile Foundations," by S.M. Mamoon, P.K. Banerjee and S. Ahmad, 11/1/88, (PB89-145239, A04, MF-A01).

NCEER-88-0035 "Modeling of R/C Building Structures With Flexible Floor Diaphragms (IDARC2)," by A.M. Reinhorn, S.K. Kunnath and N. Panahshahi, 9/7/88, (PB89-207153, A07, MF-A01).

NCEER-88-0036 "Solution of the Dam-Reservoir Interaction Problem Using a Combination of FEM, BEM with Particular Integrals, Modal Analysis, and Substructuring," by C-S. Tsai, G.C. Lee and R.L. Ketter, 12/31/88, (PB89-207146, A04, MF-A01).

NCEER-88-0037 "Optimal Placement of Actuators for Structural Control," by F.Y. Cheng and C.P. Pantelides, 8/15/88, (PB89-162846, A05, MF-A01).

NCEER-88-0038 "Teflon Bearings in Aseismic Base Isolation: Experimental Studies and Mathematical Modeling," by A. Mokha, M.C. Constantinou and A.M. Reinhorn, 12/5/88, (PB89-218457, A10, MF-A01). This report is available only through NTIS (see address given above).

NCEER-88-0039 "Seismic Behavior of Flat Slab High-Rise Buildings in the New York City Area," by P. Weidlinger and M. Ettouney, 10/15/88, (PB90-145681, A04, MF-A01).

NCEER-88-0040 "Evaluation of the Earthquake Resistance of Existing Buildings in New York City," by P. Weidlinger and M. Ettouney, 10/15/88, not available.

NCEER-88-0041 "Small-Scale Modeling Techniques for Reinforced Concrete Structures Subjected to Seismic Loads," by W. Kim, A. El-Attar and R.N. White, 11/22/88, (PB89-189625, A05, MF-A01).

NCEER-88-0042 "Modeling Strong Ground Motion from Multiple Event Earthquakes," by G.W. Ellis and A.S. Cakmak, 10/15/88, (PB89-174445, A03, MF-A01).

NCEER-88-0043 "Nonstationary Models of Seismic Ground Acceleration," by M. Grigoriu, S.E. Ruiz and E. Rosenblueth, 7/15/88, (PB89-189617, A04, MF-A01).

NCEER-88-0044 "SARCF User's Guide: Seismic Analysis of Reinforced Concrete Frames," by Y.S. Chung, C. Meyer and M. Shinozuka, 11/9/88, (PB89-174452, A08, MF-A01).

NCEER-88-0045 "First Expert Panel Meeting on Disaster Research and Planning," edited by J. Pantelic and J. Stoyle, 9/15/88, (PB89-174460, A05, MF-A01).

NCEER-88-0046 "Preliminary Studies of the Effect of Degrading Infill Walls on the Nonlinear Seismic Response of Steel Frames," by C.Z. Chrysostomou, P. Gergely and J.F. Abel, 12/19/88, (PB89-208383, A05, MF-A01).

NCEER-88-0047 "Reinforced Concrete Frame Component Testing Facility - Design, Construction, Instrumentation and Operation," by S.P. Pessiki, C. Conley, T. Bond, P. Gergely and R.N. White, 12/16/88, (PB89-174478, A04, MF-A01).

NCEER-89-0001 "Effects of Protective Cushion and Soil Compliancy on the Response of Equipment Within a Seismically Excited Building," by J.A. HoLung, 2/16/89, (PB89-207179, A04, MF-A01).

NCEER-89-0002 "Statistical Evaluation of Response Modification Factors for Reinforced Concrete Structures," by H.H-M. Hwang and J-W. Jaw, 2/17/89, (PB89-207187, A05, MF-A01).

NCEER-89-0003 "Hysteretic Columns Under Random Excitation," by G-Q. Cai and Y.K. Lin, 1/9/89, (PB89-196513, A03, MF-A01).

NCEER-89-0004 "Experimental Study of `Elephant Foot Bulge' Instability of Thin-Walled Metal Tanks," by Z-H. Jia and R.L. Ketter, 2/22/89, (PB89-207195, A03, MF-A01).

NCEER-89-0005 "Experiment on Performance of Buried Pipelines Across San Andreas Fault," by J. Isenberg, E. Richardson and T.D. O'Rourke, 3/10/89, (PB89-218440, A04, MF-A01). This report is available only through NTIS (see address given above).

NCEER-89-0006 "A Knowledge-Based Approach to Structural Design of Earthquake-Resistant Buildings," by M. Subramani, P. Gergely, C.H. Conley, J.F. Abel and A.H. Zaghw, 1/15/89, (PB89-218465, A06, MF-A01).

NCEER-89-0007 "Liquefaction Hazards and Their Effects on Buried Pipelines," by T.D. O'Rourke and P.A. Lane, 2/1/89, (PB89-218481, A09, MF-A01).

NCEER-89-0008 "Fundamentals of System Identification in Structural Dynamics," by H. Imai, C-B. Yun, O. Maruyama and M. Shinozuka, 1/26/89, (PB89-207211, A04, MF-A01).

NCEER-89-0009 "Effects of the 1985 Michoacan Earthquake on Water Systems and Other Buried Lifelines in Mexico," by A.G. Ayala and M.J. O'Rourke, 3/8/89, (PB89-207229, A06, MF-A01).

NCEER-89-R010 "NCEER Bibliography of Earthquake Education Materials," by K.E.K. Ross, Second Revision, 9/1/89, (PB90-125352, A05, MF-A01). This report is replaced by NCEER-92-0018.

NCEER-89-0011 "Inelastic Three-Dimensional Response Analysis of Reinforced Concrete Building Structures (IDARC-3D), Part I - Modeling," by S.K. Kunnath and A.M. Reinhorn, 4/17/89, (PB90-114612, A07, MF-A01). This report is available only through NTIS (see address given above).

NCEER-89-0012 "Recommended Modifications to ATC-14," by C.D. Poland and J.O. Malley, 4/12/89, (PB90-108648, A15, MF-A01).

NCEER-89-0013 "Repair and Strengthening of Beam-to-Column Connections Subjected to Earthquake Loading," by M. Corazao and A.J. Durrani, 2/28/89, (PB90-109885, A06, MF-A01).

NCEER-89-0014 "Program EXKAL2 for Identification of Structural Dynamic Systems," by O. Maruyama, C-B. Yun, M. Hoshiya and M. Shinozuka, 5/19/89, (PB90-109877, A09, MF-A01).

NCEER-89-0015 "Response of Frames With Bolted Semi-Rigid Connections, Part I - Experimental Study and Analytical Predictions," by P.J. DiCorso, A.M. Reinhorn, J.R. Dickerson, J.B. Radziminski and W.L. Harper, 6/1/89, not available.

NCEER-89-0016 "ARMA Monte Carlo Simulation in Probabilistic Structural Analysis," by P.D. Spanos and M.P. Mignolet, 7/10/89, (PB90-109893, A03, MF-A01).

NCEER-89-P017 "Preliminary Proceedings from the Conference on Disaster Preparedness - The Place of Earthquake Education in Our Schools," Edited by K.E.K. Ross, 6/23/89, (PB90-108606, A03, MF-A01).

NCEER-89-0017 "Proceedings from the Conference on Disaster Preparedness - The Place of Earthquake Education in Our Schools," Edited by K.E.K. Ross, 12/31/89, (PB90-207895, A012, MF-A02). This report is available only through NTIS (see address given above).

NCEER-89-0018 "Multidimensional Models of Hysteretic Material Behavior for Vibration Analysis of Shape Memory Energy Absorbing Devices, by E.J. Graesser and F.A. Cozzarelli, 6/7/89, (PB90-164146, A04, MF-A01).

NCEER-89-0019 "Nonlinear Dynamic Analysis of Three-Dimensional Base Isolated Structures (3D-BASIS)," by S. Nagarajaiah, A.M. Reinhorn and M.C. Constantinou, 8/3/89, (PB90-161936, A06, MF-A01). This report has been replaced by NCEER-93-0011.

NCEER-89-0020 "Structural Control Considering Time-Rate of Control Forces and Control Rate Constraints," by F.Y. Cheng and C.P. Pantelides, 8/3/89, (PB90-120445, A04, MF-A01).

NCEER-89-0021 "Subsurface Conditions of Memphis and Shelby County," by K.W. Ng, T-S. Chang and H-H.M. Hwang, 7/26/89, (PB90-120437, A03, MF-A01).

NCEER-89-0022 "Seismic Wave Propagation Effects on Straight Jointed Buried Pipelines," by K. Elhmadi and M.J. O'Rourke, 8/24/89, (PB90-162322, A10, MF-A02).

NCEER-89-0023 "Workshop on Serviceability Analysis of Water Delivery Systems," edited by M. Grigoriu, 3/6/89, (PB90-127424, A03, MF-A01).

NCEER-89-0024 "Shaking Table Study of a 1/5 Scale Steel Frame Composed of Tapered Members," by K.C. Chang, J.S. Hwang and G.C. Lee, 9/18/89, (PB90-160169, A04, MF-A01).

NCEER-89-0025 "DYNA1D: A Computer Program for Nonlinear Seismic Site Response Analysis - Technical Documentation," by Jean H. Prevost, 9/14/89, (PB90-161944, A07, MF-A01). This report is available only through NTIS (see address given above).

NCEER-89-0026 "1:4 Scale Model Studies of Active Tendon Systems and Active Mass Dampers for Aseismic Protection," by A.M. Reinhorn, T.T. Soong, R.C. Lin, Y.P. Yang, Y. Fukao, H. Abe and M. Nakai, 9/15/89, (PB90-173246, A10, MF-A02). This report is available only through NTIS (see address given above).

NCEER-89-0027 "Scattering of Waves by Inclusions in a Nonhomogeneous Elastic Half Space Solved by Boundary Element Methods," by P.K. Hadley, A. Askar and A.S. Cakmak, 6/15/89, (PB90-145699, A07, MF-A01).

NCEER-89-0028 "Statistical Evaluation of Deflection Amplification Factors for Reinforced Concrete Structures," by H.H.M. Hwang, J-W. Jaw and A.L. Ch'ng, 8/31/89, (PB90-164633, A05, MF-A01).

NCEER-89-0029 "Bedrock Accelerations in Memphis Area Due to Large New Madrid Earthquakes," by H.H.M. Hwang, C.H.S. Chen and G. Yu, 11/7/89, (PB90-162330, A04, MF-A01).

NCEER-89-0030 "Seismic Behavior and Response Sensitivity of Secondary Structural Systems," by Y.Q. Chen and T.T. Soong, 10/23/89, (PB90-164658, A08, MF-A01).

NCEER-89-0031 "Random Vibration and Reliability Analysis of Primary-Secondary Structural Systems," by Y. Ibrahim, M. Grigoriu and T.T. Soong, 11/10/89, (PB90-161951, A04, MF-A01).

NCEER-89-0032 "Proceedings from the Second U.S. - Japan Workshop on Liquefaction, Large Ground Deformation and Their Effects on Lifelines, September 26-29, 1989," Edited by T.D. O'Rourke and M. Hamada, 12/1/89, (PB90-209388, A22, MF-A03).

NCEER-89-0033 "Deterministic Model for Seismic Damage Evaluation of Reinforced Concrete Structures," by J.M. Bracci, A.M. Reinhorn, J.B. Mander and S.K. Kunnath, 9/27/89, (PB91-108803, A06, MF-A01).

NCEER-89-0034 "On the Relation Between Local and Global Damage Indices," by E. DiPasquale and A.S. Cakmak, 8/15/89, (PB90-173865, A05, MF-A01).

NCEER-89-0035 "Cyclic Undrained Behavior of Nonplastic and Low Plasticity Silts," by A.J. Walker and H.E. Stewart, 7/26/89, (PB90-183518, A10, MF-A01).

NCEER-89-0036 "Liquefaction Potential of Surficial Deposits in the City of Buffalo, New York," by M. Budhu, R. Giese and L. Baumgrass, 1/17/89, (PB90-208455, A04, MF-A01).

NCEER-89-0037 "A Deterministic Assessment of Effects of Ground Motion Incoherence," by A.S. Veletsos and Y. Tang, 7/15/89, (PB90-164294, A03, MF-A01).

NCEER-89-0038 "Workshop on Ground Motion Parameters for Seismic Hazard Mapping," July 17-18, 1989, edited by R.V. Whitman, 12/1/89, (PB90-173923, A04, MF-A01).

NCEER-89-0039 "Seismic Effects on Elevated Transit Lines of the New York City Transit Authority," by C.J. Costantino, C.A. Miller and E. Heymsfield, 12/26/89, (PB90-207887, A06, MF-A01).

NCEER-89-0040 "Centrifugal Modeling of Dynamic Soil-Structure Interaction," by K. Weissman, Supervised by J.H. Prevost, 5/10/89, (PB90-207879, A07, MF-A01).

NCEER-89-0041 "Linearized Identification of Buildings With Cores for Seismic Vulnerability Assessment," by I-K. Ho and A.E. Aktan, 11/1/89, (PB90-251943, A07, MF-A01).

NCEER-90-0001 "Geotechnical and Lifeline Aspects of the October 17, 1989 Loma Prieta Earthquake in San Francisco," by T.D. O'Rourke, H.E. Stewart, F.T. Blackburn and T.S. Dickerman, 1/90, (PB90-208596, A05, MF-A01).

NCEER-90-0002 "Nonnormal Secondary Response Due to Yielding in a Primary Structure," by D.C.K. Chen and L.D. Lutes, 2/28/90, (PB90-251976, A07, MF-A01).

NCEER-90-0003 "Earthquake Education Materials for Grades K-12," by K.E.K. Ross, 4/16/90, (PB91-251984, A05, MF-A05). This report has been replaced by NCEER-92-0018.

NCEER-90-0004 "Catalog of Strong Motion Stations in Eastern North America," by R.W. Busby, 4/3/90, (PB90-251984, A05, MF-A01).

NCEER-90-0005 "NCEER Strong-Motion Data Base: A User Manual for the GeoBase Release (Version 1.0 for the Sun3)," by P. Friberg and K. Jacob, 3/31/90 (PB90-258062, A04, MF-A01).

NCEER-90-0006 "Seismic Hazard Along a Crude Oil Pipeline in the Event of an 1811-1812 Type New Madrid Earthquake," by H.H.M. Hwang and C-H.S. Chen, 4/16/90, (PB90-258054, A04, MF-A01).

NCEER-90-0007 "Site-Specific Response Spectra for Memphis Sheahan Pumping Station," by H.H.M. Hwang and C.S. Lee, 5/15/90, (PB91-108811, A05, MF-A01).

NCEER-90-0008 "Pilot Study on Seismic Vulnerability of Crude Oil Transmission Systems," by T. Ariman, R. Dobry, M. Grigoriu, F. Kozin, M. O'Rourke, T. O'Rourke and M. Shinozuka, 5/25/90, (PB91-108837, A06, MF-A01).

NCEER-90-0009 "A Program to Generate Site Dependent Time Histories: EQGEN," by G.W. Ellis, M. Srinivasan and A.S. Cakmak, 1/30/90, (PB91-108829, A04, MF-A01).

NCEER-90-0010 "Active Isolation for Seismic Protection of Operating Rooms," by M.E. Talbott, Supervised by M. Shinozuka, 6/8/9, (PB91-110205, A05, MF-A01).

NCEER-90-0011 "Program LINEARID for Identification of Linear Structural Dynamic Systems," by C-B. Yun and M. Shinozuka, 6/25/90, (PB91-110312, A08, MF-A01).

NCEER-90-0012 "Two-Dimensional Two-Phase Elasto-Plastic Seismic Response of Earth Dams," by A.N. Yiagos, Supervised by J.H. Prevost, 6/20/90, (PB91-110197, A13, MF-A02).

NCEER-90-0013 "Secondary Systems in Base-Isolated Structures: Experimental Investigation, Stochastic Response and Stochastic Sensitivity," by G.D. Manolis, G. Juhn, M.C. Constantinou and A.M. Reinhorn, 7/1/90, (PB91-110320, A08, MF-A01).

NCEER-90-0014 "Seismic Behavior of Lightly-Reinforced Concrete Column and Beam-Column Joint Details," by S.P. Pessiki, C.H. Conley, P. Gergely and R.N. White, 8/22/90, (PB91-108795, A11, MF-A02).

NCEER-90-0015 "Two Hybrid Control Systems for Building Structures Under Strong Earthquakes," by J.N. Yang and A. Danielians, 6/29/90, (PB91-125393, A04, MF-A01).

NCEER-90-0016 "Instantaneous Optimal Control with Acceleration and Velocity Feedback," by J.N. Yang and Z. Li, 6/29/90, (PB91-125401, A03, MF-A01).

NCEER-90-0017 "Reconnaissance Report on the Northern Iran Earthquake of June 21, 1990," by M. Mehrain, 10/4/90, (PB91-125377, A03, MF-A01).

NCEER-90-0018 "Evaluation of Liquefaction Potential in Memphis and Shelby County," by T.S. Chang, P.S. Tang, C.S. Lee and H. Hwang, 8/10/90, (PB91-125427, A09, MF-A01).

NCEER-90-0019 "Experimental and Analytical Study of a Combined Sliding Disc Bearing and Helical Steel Spring Isolation System," by M.C. Constantinou, A.S. Mokha and A.M. Reinhorn, 10/4/90, (PB91-125385, A06, MF-A01). This report is available only through NTIS (see address given above).

NCEER-90-0020 "Experimental Study and Analytical Prediction of Earthquake Response of a Sliding Isolation System with a Spherical Surface," by A.S. Mokha, M.C. Constantinou and A.M. Reinhorn, 10/11/90, (PB91-125419, A05, MF-A01).

NCEER-90-0021 "Dynamic Interaction Factors for Floating Pile Groups," by G. Gazetas, K. Fan, A. Kaynia and E. Kausel, 9/10/90, (PB91-170381, A05, MF-A01).

NCEER-90-0022 "Evaluation of Seismic Damage Indices for Reinforced Concrete Structures," by S. Rodriguez-Gomez and A.S. Cakmak, 9/30/90, PB91-171322, A06, MF-A01).

NCEER-90-0023 "Study of Site Response at a Selected Memphis Site," by H. Desai, S. Ahmad, E.S. Gazetas and M.R. Oh, 10/11/90, (PB91-196857, A03, MF-A01).

NCEER-90-0024 "A User's Guide to Strongmo: Version 1.0 of NCEER's Strong-Motion Data Access Tool for PCs and Terminals," by P.A. Friberg and C.A.T. Susch, 11/15/90, (PB91-171272, A03, MF-A01).

NCEER-90-0025 "A Three-Dimensional Analytical Study of Spatial Variability of Seismic Ground Motions," by L-L. Hong and A.H.-S. Ang, 10/30/90, (PB91-170399, A09, MF-A01).

NCEER-90-0026 "MUMOID User's Guide - A Program for the Identification of Modal Parameters," by S. Rodriguez-Gomez and E. DiPasquale, 9/30/90, (PB91-171298, A04, MF-A01).

NCEER-90-0027 "SARCF-II User's Guide - Seismic Analysis of Reinforced Concrete Frames," by S. Rodriguez-Gomez, Y.S. Chung and C. Meyer, 9/30/90, (PB91-171280, A05, MF-A01).

NCEER-90-0028 "Viscous Dampers: Testing, Modeling and Application in Vibration and Seismic Isolation," by N. Makris and M.C. Constantinou, 12/20/90 (PB91-190561, A06, MF-A01).

NCEER-90-0029 "Soil Effects on Earthquake Ground Motions in the Memphis Area," by H. Hwang, C.S. Lee, K.W. Ng and T.S. Chang, 8/2/90, (PB91-190751, A05, MF-A01).

NCEER-91-0001 "Proceedings from the Third Japan-U.S. Workshop on Earthquake Resistant Design of Lifeline Facilities and Countermeasures for Soil Liquefaction, December 17-19, 1990," edited by T.D. O'Rourke and M. Hamada, 2/1/91, (PB91-179259, A99, MF-A04).

NCEER-91-0002 "Physical Space Solutions of Non-Proportionally Damped Systems," by M. Tong, Z. Liang and G.C. Lee, 1/15/91, (PB91-179242, A04, MF-A01).

NCEER-91-0003 "Seismic Response of Single Piles and Pile Groups," by K. Fan and G. Gazetas, 1/10/91, (PB92-174994, A04, MF-A01).

NCEER-91-0004 "Damping of Structures: Part 1 - Theory of Complex Damping," by Z. Liang and G. Lee, 10/10/91, (PB92-197235, A12, MF-A03).

NCEER-91-0005 "3D-BASIS - Nonlinear Dynamic Analysis of Three Dimensional Base Isolated Structures: Part II," by S. Nagarajaiah, A.M. Reinhorn and M.C. Constantinou, 2/28/91, (PB91-190553, A07, MF-A01). This report has been replaced by NCEER-93-0011.

NCEER-91-0006 "A Multidimensional Hysteretic Model for Plasticity Deforming Metals in Energy Absorbing Devices," by E.J. Graesser and F.A. Cozzarelli, 4/9/91, (PB92-108364, A04, MF-A01).

NCEER-91-0007 "A Framework for Customizable Knowledge-Based Expert Systems with an Application to a KBES for Evaluating the Seismic Resistance of Existing Buildings," by E.G. Ibarra-Anaya and S.J. Fenves, 4/9/91, (PB91-210930, A08, MF-A01).

NCEER-91-0008 "Nonlinear Analysis of Steel Frames with Semi-Rigid Connections Using the Capacity Spectrum Method," by G.G. Deierlein, S-H. Hsieh, Y-J. Shen and J.F. Abel, 7/2/91, (PB92-113828, A05, MF-A01).

NCEER-91-0009 "Earthquake Education Materials for Grades K-12," by K.E.K. Ross, 4/30/91, (PB91-212142, A06, MF-A01). This report has been replaced by NCEER-92-0018.

NCEER-91-0010 "Phase Wave Velocities and Displacement Phase Differences in a Harmonically Oscillating Pile," by N. Makris and G. Gazetas, 7/8/91, (PB92-108356, A04, MF-A01).

NCEER-91-0011 "Dynamic Characteristics of a Full-Size Five-Story Steel Structure and a 2/5 Scale Model," by K.C. Chang, G.C. Yao, G.C. Lee, D.S. Hao and Y.C. Yeh," 7/2/91, (PB93-116648, A06, MF-A02).

NCEER-91-0012 "Seismic Response of a 2/5 Scale Steel Structure with Added Viscoelastic Dampers," by K.C. Chang, T.T. Soong, S-T. Oh and M.L. Lai, 5/17/91, (PB92-110816, A05, MF-A01).

NCEER-91-0013 "Earthquake Response of Retaining Walls; Full-Scale Testing and Computational Modeling," by S. Alampalli and A-W.M. Elgamal, 6/20/91, not available.

NCEER-91-0014 "3D-BASIS-M: Nonlinear Dynamic Analysis of Multiple Building Base Isolated Structures," by P.C. Tsopelas, S. Nagarajaiah, M.C. Constantinou and A.M. Reinhorn, 5/28/91, (PB92-113885, A09, MF-A02).

NCEER-91-0015 "Evaluation of SEAOC Design Requirements for Sliding Isolated Structures," by D. Theodossiou and M.C. Constantinou, 6/10/91, (PB92-114602, A11, MF-A03).

NCEER-91-0016 "Closed-Loop Modal Testing of a 27-Story Reinforced Concrete Flat Plate-Core Building," by H.R. Somaprasad, T. Toksoy, H. Yoshiyuki and A.E. Aktan, 7/15/91, (PB92-129980, A07, MF-A02).

NCEER-91-0017 "Shake Table Test of a 1/6 Scale Two-Story Lightly Reinforced Concrete Building," by A.G. El-Attar, R.N. White and P. Gergely, 2/28/91, (PB92-222447, A06, MF-A02).

NCEER-91-0018 "Shake Table Test of a 1/8 Scale Three-Story Lightly Reinforced Concrete Building," by A.G. El-Attar, R.N. White and P. Gergely, 2/28/91, (PB93-116630, A08, MF-A02).

NCEER-91-0019 "Transfer Functions for Rigid Rectangular Foundations," by A.S. Veletsos, A.M. Prasad and W.H. Wu, 7/31/91, not available.

NCEER-91-0020 "Hybrid Control of Seismic-Excited Nonlinear and Inelastic Structural Systems," by J.N. Yang, Z. Li and A. Danielians, 8/1/91, (PB92-143171, A06, MF-A02).

NCEER-91-0021 "The NCEER-91 Earthquake Catalog: Improved Intensity-Based Magnitudes and Recurrence Relations for U.S. Earthquakes East of New Madrid," by L. Seeber and J.G. Armbruster, 8/28/91, (PB92-176742, A06, MF-A02).

NCEER-91-0022 "Proceedings from the Implementation of Earthquake Planning and Education in Schools: The Need for Change - The Roles of the Changemakers," by K.E.K. Ross and F. Winslow, 7/23/91, (PB92-129998, A12, MF-A03).

NCEER-91-0023 "A Study of Reliability-Based Criteria for Seismic Design of Reinforced Concrete Frame Buildings," by H.H.M. Hwang and H-M. Hsu, 8/10/91, (PB92-140235, A09, MF-A02).

NCEER-91-0024 "Experimental Verification of a Number of Structural System Identification Algorithms," by R.G. Ghanem, H. Gavin and M. Shinozuka, 9/18/91, (PB92-176577, A18, MF-A04).

NCEER-91-0025 "Probabilistic Evaluation of Liquefaction Potential," by H.H.M. Hwang and C.S. Lee," 11/25/91, (PB92-143429, A05, MF-A01).

NCEER-91-0026 "Instantaneous Optimal Control for Linear, Nonlinear and Hysteretic Structures - Stable Controllers," by J.N. Yang and Z. Li, 11/15/91, (PB92-163807, A04, MF-A01).

NCEER-91-0027 "Experimental and Theoretical Study of a Sliding Isolation System for Bridges," by M.C. Constantinou, A. Kartoum, A.M. Reinhorn and P. Bradford, 11/15/91, (PB92-176973, A10, MF-A03).

NCEER-92-0001 "Case Studies of Liquefaction and Lifeline Performance During Past Earthquakes, Volume 1: Japanese Case Studies," Edited by M. Hamada and T. O'Rourke, 2/17/92, (PB92-197243, A18, MF-A04).

NCEER-92-0002 "Case Studies of Liquefaction and Lifeline Performance During Past Earthquakes, Volume 2: United States Case Studies," Edited by T. O'Rourke and M. Hamada, 2/17/92, (PB92-197250, A20, MF-A04).

NCEER-92-0003 "Issues in Earthquake Education," Edited by K. Ross, 2/3/92, (PB92-222389, A07, MF-A02).

NCEER-92-0004 "Proceedings from the First U.S. - Japan Workshop on Earthquake Protective Systems for Bridges," Edited by I.G. Buckle, 2/4/92, (PB94-142239, A99, MF-A06).

NCEER-92-0005 "Seismic Ground Motion from a Haskell-Type Source in a Multiple-Layered Half-Space," A.P. Theoharis, G. Deodatis and M. Shinozuka, 1/2/92, not available.

NCEER-92-0006 "Proceedings from the Site Effects Workshop," Edited by R. Whitman, 2/29/92, (PB92-197201, A04, MF-A01).

NCEER-92-0007 "Engineering Evaluation of Permanent Ground Deformations Due to Seismically-Induced Liquefaction," by M.H. Baziar, R. Dobry and A-W.M. Elgamal, 3/24/92, (PB92-222421, A13, MF-A03).

NCEER-92-0008 "A Procedure for the Seismic Evaluation of Buildings in the Central and Eastern United States," by C.D. Poland and J.O. Malley, 4/2/92, (PB92-222439, A20, MF-A04).

NCEER-92-0009 "Experimental and Analytical Study of a Hybrid Isolation System Using Friction Controllable Sliding Bearings," by M.Q. Feng, S. Fujii and M. Shinozuka, 5/15/92, (PB93-150282, A06, MF-A02).

NCEER-92-0010 "Seismic Resistance of Slab-Column Connections in Existing Non-Ductile Flat-Plate Buildings," by A.J. Durrani and Y. Du, 5/18/92, (PB93-116812, A06, MF-A02).

NCEER-92-0011 "The Hysteretic and Dynamic Behavior of Brick Masonry Walls Upgraded by Ferrocement Coatings Under Cyclic Loading and Strong Simulated Ground Motion," by H. Lee and S.P. Prawel, 5/11/92, not available.

NCEER-92-0012 "Study of Wire Rope Systems for Seismic Protection of Equipment in Buildings," by G.F. Demetriades, M.C. Constantinou and A.M. Reinhorn, 5/20/92, (PB93-116655, A08, MF-A02).

NCEER-92-0013 "Shape Memory Structural Dampers: Material Properties, Design and Seismic Testing," by P.R. Witting and F.A. Cozzarelli, 5/26/92, (PB93-116663, A05, MF-A01).

NCEER-92-0014 "Longitudinal Permanent Ground Deformation Effects on Buried Continuous Pipelines," by M.J. O'Rourke, and C. Nordberg, 6/15/92, (PB93-116671, A08, MF-A02).

NCEER-92-0015 "A Simulation Method for Stationary Gaussian Random Functions Based on the Sampling Theorem," by M. Grigoriu and S. Balopoulou, 6/11/92, (PB93-127496, A05, MF-A01).

NCEER-92-0016 "Gravity-Load-Designed Reinforced Concrete Buildings: Seismic Evaluation of Existing Construction and Detailing Strategies for Improved Seismic Resistance," by G.W. Hoffmann, S.K. Kunnath, A.M. Reinhorn and J.B. Mander, 7/15/92, (PB94-142007, A08, MF-A02).

NCEER-92-0017 "Observations on Water System and Pipeline Performance in the Limón Area of Costa Rica Due to the April 22, 1991 Earthquake," by M. O'Rourke and D. Ballantyne, 6/30/92, (PB93-126811, A06, MF-A02).

NCEER-92-0018 "Fourth Edition of Earthquake Education Materials for Grades K-12," Edited by K.E.K. Ross, 8/10/92, (PB93-114023, A07, MF-A02).

NCEER-92-0019 "Proceedings from the Fourth Japan-U.S. Workshop on Earthquake Resistant Design of Lifeline Facilities and Countermeasures for Soil Liquefaction," Edited by M. Hamada and T.D. O'Rourke, 8/12/92, (PB93-163939, A99, MF-E11).

NCEER-92-0020 "Active Bracing System: A Full Scale Implementation of Active Control," by A.M. Reinhorn, T.T. Soong, R.C. Lin, M.A. Riley, Y.P. Wang, S. Aizawa and M. Higashino, 8/14/92, (PB93-127512, A06, MF-A02).

NCEER-92-0021 "Empirical Analysis of Horizontal Ground Displacement Generated by Liquefaction-Induced Lateral Spreads," by S.F. Bartlett and T.L. Youd, 8/17/92, (PB93-188241, A06, MF-A02).

NCEER-92-0022 "IDARC Version 3.0: Inelastic Damage Analysis of Reinforced Concrete Structures," by S.K. Kunnath, A.M. Reinhorn and R.F. Lobo, 8/31/92, (PB93-227502, A07, MF-A02).

NCEER-92-0023 "A Semi-Empirical Analysis of Strong-Motion Peaks in Terms of Seismic Source, Propagation Path and Local Site Conditions, by M. Kamiyama, M.J. O'Rourke and R. Flores-Berrones, 9/9/92, (PB93-150266, A08, MF-A02).

NCEER-92-0024 "Seismic Behavior of Reinforced Concrete Frame Structures with Nonductile Details, Part I: Summary of Experimental Findings of Full Scale Beam-Column Joint Tests," by A. Beres, R.N. White and P. Gergely, 9/30/92, (PB93-227783, A05, MF-A01).

NCEER-92-0025 "Experimental Results of Repaired and Retrofitted Beam-Column Joint Tests in Lightly Reinforced Concrete Frame Buildings," by A. Beres, S. El-Borgi, R.N. White and P. Gergely, 10/29/92, (PB93-227791, A05, MF-A01).

NCEER-92-0026 "A Generalization of Optimal Control Theory: Linear and Nonlinear Structures," by J.N. Yang, Z. Li and S. Vongchavalitkul, 11/2/92, (PB93-188621, A05, MF-A01).

NCEER-92-0027 "Seismic Resistance of Reinforced Concrete Frame Structures Designed Only for Gravity Loads: Part I - Design and Properties of a One-Third Scale Model Structure," by J.M. Bracci, A.M. Reinhorn and J.B. Mander, 12/1/92, (PB94-104502, A08, MF-A02).

NCEER-92-0028 "Seismic Resistance of Reinforced Concrete Frame Structures Designed Only for Gravity Loads: Part II - Experimental Performance of Subassemblages," by L.E. Aycardi, J.B. Mander and A.M. Reinhorn, 12/1/92, (PB94-104510, A08, MF-A02).

NCEER-92-0029 "Seismic Resistance of Reinforced Concrete Frame Structures Designed Only for Gravity Loads: Part III - Experimental Performance and Analytical Study of a Structural Model," by J.M. Bracci, A.M. Reinhorn and J.B. Mander, 12/1/92, (PB93-227528, A09, MF-A01).

NCEER-92-0030 "Evaluation of Seismic Retrofit of Reinforced Concrete Frame Structures: Part I - Experimental Performance of Retrofitted Subassemblages," by D. Choudhuri, J.B. Mander and A.M. Reinhorn, 12/8/92, (PB93-198307, A07, MF-A02).

NCEER-92-0031 "Evaluation of Seismic Retrofit of Reinforced Concrete Frame Structures: Part II - Experimental Performance and Analytical Study of a Retrofitted Structural Model," by J.M. Bracci, A.M. Reinhorn and J.B. Mander, 12/8/92, (PB93-198315, A09, MF-A03).

NCEER-92-0032 "Experimental and Analytical Investigation of Seismic Response of Structures with Supplemental Fluid Viscous Dampers," by M.C. Constantinou and M.D. Symans, 12/21/92, (PB93-191435, A10, MF-A03). This report is available only through NTIS (see address given above).

NCEER-92-0033 "Reconnaissance Report on the Cairo, Egypt Earthquake of October 12, 1992," by M. Khater, 12/23/92, (PB93-188621, A03, MF-A01).

NCEER-92-0034 "Low-Level Dynamic Characteristics of Four Tall Flat-Plate Buildings in New York City," by H. Gavin, S. Yuan, J. Grossman, E. Pekelis and K. Jacob, 12/28/92, (PB93-188217, A07, MF-A02).

NCEER-93-0001 "An Experimental Study on the Seismic Performance of Brick-Infilled Steel Frames With and Without Retrofit," by J.B. Mander, B. Nair, K. Wojtkowski and J. Ma, 1/29/93, (PB93-227510, A07, MF-A02).

NCEER-93-0002 "Social Accounting for Disaster Preparedness and Recovery Planning," by S. Cole, E. Pantoja and V. Razak, 2/22/93, (PB94-142114, A12, MF-A03).

NCEER-93-0003 "Assessment of 1991 NEHRP Provisions for Nonstructural Components and Recommended Revisions," by T.T. Soong, G. Chen, Z. Wu, R-H. Zhang and M. Grigoriu, 3/1/93, (PB93-188639, A06, MF-A02).

NCEER-93-0004 "Evaluation of Static and Response Spectrum Analysis Procedures of SEAOC/UBC for Seismic Isolated Structures," by C.W. Winters and M.C. Constantinou, 3/23/93, (PB93-198299, A10, MF-A03).

NCEER-93-0005 "Earthquakes in the Northeast - Are We Ignoring the Hazard? A Workshop on Earthquake Science and Safety for Educators," edited by K.E.K. Ross, 4/2/93, (PB94-103066, A09, MF-A02).

NCEER-93-0006 "Inelastic Response of Reinforced Concrete Structures with Viscoelastic Braces," by R.F. Lobo, J.M. Bracci, K.L. Shen, A.M. Reinhorn and T.T. Soong, 4/5/93, (PB93-227486, A05, MF-A02).

NCEER-93-0007 "Seismic Testing of Installation Methods for Computers and Data Processing Equipment," by K. Kosar, T.T. Soong, K.L. Shen, J.A. HoLung and Y.K. Lin, 4/12/93, (PB93-198299, A07, MF-A02).

NCEER-93-0008 "Retrofit of Reinforced Concrete Frames Using Added Dampers," by A. Reinhorn, M. Constantinou and C. Li, not available.

NCEER-93-0009 "Seismic Behavior and Design Guidelines for Steel Frame Structures with Added Viscoelastic Dampers," by K.C. Chang, M.L. Lai, T.T. Soong, D.S. Hao and Y.C. Yeh, 5/1/93, (PB94-141959, A07, MF-A02).

NCEER-93-0010 "Seismic Performance of Shear-Critical Reinforced Concrete Bridge Piers," by J.B. Mander, S.M. Waheed, M.T.A. Chaudhary and S.S. Chen, 5/12/93, (PB93-227494, A08, MF-A02).

NCEER-93-0011 "3D-BASIS-TABS: Computer Program for Nonlinear Dynamic Analysis of Three Dimensional Base Isolated Structures," by S. Nagarajaiah, C. Li, A.M. Reinhorn and M.C. Constantinou, 8/2/93, (PB94-141819, A09, MF-A02).

NCEER-93-0012 "Effects of Hydrocarbon Spills from an Oil Pipeline Break on Ground Water," by O.J. Helweg and H.H.M. Hwang, 8/3/93, (PB94-141942, A06, MF-A02).

NCEER-93-0013 "Simplified Procedures for Seismic Design of Nonstructural Components and Assessment of Current Code Provisions," by M.P. Singh, L.E. Suarez, E.E. Matheu and G.O. Maldonado, 8/4/93, (PB94-141827, A09, MF-A02).

NCEER-93-0014 "An Energy Approach to Seismic Analysis and Design of Secondary Systems," by G. Chen and T.T. Soong, 8/6/93, (PB94-142767, A11, MF-A03).

NCEER-93-0015 "Proceedings from School Sites: Becoming Prepared for Earthquakes - Commemorating the Third Anniversary of the Loma Prieta Earthquake," Edited by F.E. Winslow and K.E.K. Ross, 8/16/93, (PB94-154275, A16, MF-A02).

NCEER-93-0016 "Reconnaissance Report of Damage to Historic Monuments in Cairo, Egypt Following the October 12, 1992 Dahshur Earthquake," by D. Sykora, D. Look, G. Croci, E. Karaesmen and E. Karaesmen, 8/19/93, (PB94-142221, A08, MF-A02).

NCEER-93-0017 "The Island of Guam Earthquake of August 8, 1993," by S.W. Swan and S.K. Harris, 9/30/93, (PB94-141843, A04, MF-A01).

NCEER-93-0018 "Engineering Aspects of the October 12, 1992 Egyptian Earthquake," by A.W. Elgamal, M. Amer, K. Adalier and A. Abul-Fadl, 10/7/93, (PB94-141983, A05, MF-A01).

NCEER-93-0019 "Development of an Earthquake Motion Simulator and its Application in Dynamic Centrifuge Testing," by I. Krstelj, Supervised by J.H. Prevost, 10/23/93, (PB94-181773, A-10, MF-A03).

NCEER-93-0020 "NCEER-Taisei Corporation Research Program on Sliding Seismic Isolation Systems for Bridges: Experimental and Analytical Study of a Friction Pendulum System (FPS)," by M.C. Constantinou, P. Tsopelas, Y-S. Kim and S. Okamoto, 11/1/93, (PB94-142775, A08, MF-A02).

NCEER-93-0021 "Finite Element Modeling of Elastomeric Seismic Isolation Bearings," by L.J. Billings, Supervised by R. Shepherd, 11/8/93, not available.

NCEER-93-0022 "Seismic Vulnerability of Equipment in Critical Facilities: Life-Safety and Operational Consequences," by K. Porter, G.S. Johnson, M.M. Zadeh, C. Scawthorn and S. Eder, 11/24/93, (PB94-181765, A16, MF-A03).

NCEER-93-0023 "Hokkaido Nansei-oki, Japan Earthquake of July 12, 1993, by P.I. Yanev and C.R. Scawthorn, 12/23/93, (PB94-181500, A07, MF-A01).

NCEER-94-0001 "An Evaluation of Seismic Serviceability of Water Supply Networks with Application to the San Francisco Auxiliary Water Supply System," by I. Markov, Supervised by M. Grigoriu and T. O'Rourke, 1/21/94, (PB94-204013, A07, MF-A02).

NCEER-94-0002 "NCEER-Taisei Corporation Research Program on Sliding Seismic Isolation Systems for Bridges: Experimental and Analytical Study of Systems Consisting of Sliding Bearings, Rubber Restoring Force Devices and Fluid Dampers," Volumes I and II, by P. Tsopelas, S. Okamoto, M.C. Constantinou, D. Ozaki and S. Fujii, 2/4/94, (PB94-181740, A09, MF-A02 and PB94-181757, A12, MF-A03).

NCEER-94-0003 "A Markov Model for Local and Global Damage Indices in Seismic Analysis," by S. Rahman and M. Grigoriu, 2/18/94, (PB94-206000, A12, MF-A03).

NCEER-94-0004 "Proceedings from the NCEER Workshop on Seismic Response of Masonry Infills," edited by D.P. Abrams, 3/1/94, (PB94-180783, A07, MF-A02).

NCEER-94-0005 "The Northridge, California Earthquake of January 17, 1994: General Reconnaissance Report," edited by J.D. Goltz, 3/11/94, (PB94-193943, A10, MF-A03).

NCEER-94-0006 "Seismic Energy Based Fatigue Damage Analysis of Bridge Columns: Part I - Evaluation of Seismic Capacity," by G.A. Chang and J.B. Mander, 3/14/94, (PB94-219185, A11, MF-A03).

NCEER-94-0007 "Seismic Isolation of Multi-Story Frame Structures Using Spherical Sliding Isolation Systems," by T.M. Al-Hussaini, V.A. Zayas and M.C. Constantinou, 3/17/94, (PB94-193745, A09, MF-A02).

NCEER-94-0008 "The Northridge, California Earthquake of January 17, 1994: Performance of Highway Bridges," edited by I.G. Buckle, 3/24/94, (PB94-193851, A06, MF-A02).

NCEER-94-0009 "Proceedings of the Third U.S.-Japan Workshop on Earthquake Protective Systems for Bridges," edited by I.G. Buckle and I. Friedland, 3/31/94, (PB94-195815, A99, MF-A06).

NCEER-94-0010 "3D-BASIS-ME: Computer Program for Nonlinear Dynamic Analysis of Seismically Isolated Single and Multiple Structures and Liquid Storage Tanks," by P.C. Tsopelas, M.C. Constantinou and A.M. Reinhorn, 4/12/94, (PB94-204922, A09, MF-A02).

NCEER-94-0011 "The Northridge, California Earthquake of January 17, 1994: Performance of Gas Transmission Pipelines," by T.D. O'Rourke and M.C. Palmer, 5/16/94, (PB94-204989, A05, MF-A01).

NCEER-94-0012 "Feasibility Study of Replacement Procedures and Earthquake Performance Related to Gas Transmission Pipelines," by T.D. O'Rourke and M.C. Palmer, 5/25/94, (PB94-206638, A09, MF-A02).

NCEER-94-0013 "Seismic Energy Based Fatigue Damage Analysis of Bridge Columns: Part II - Evaluation of Seismic Demand," by G.A. Chang and J.B. Mander, 6/1/94, (PB95-18106, A08, MF-A02).

NCEER-94-0014 "NCEER-Taisei Corporation Research Program on Sliding Seismic Isolation Systems for Bridges: Experimental and Analytical Study of a System Consisting of Sliding Bearings and Fluid Restoring Force/Damping Devices," by P. Tsopelas and M.C. Constantinou, 6/13/94, (PB94-219144, A10, MF-A03).

NCEER-94-0015 "Generation of Hazard-Consistent Fragility Curves for Seismic Loss Estimation Studies," by H. Hwang and J-R. Huo, 6/14/94, (PB95-181996, A09, MF-A02).

NCEER-94-0016 "Seismic Study of Building Frames with Added Energy-Absorbing Devices," by W.S. Pong, C.S. Tsai and G.C. Lee, 6/20/94, (PB94-219136, A10, A03).

NCEER-94-0017 "Sliding Mode Control for Seismic-Excited Linear and Nonlinear Civil Engineering Structures," by J. Yang, J. Wu, A. Agrawal and Z. Li, 6/21/94, (PB95-138483, A06, MF-A02).

NCEER-94-0018 "3D-BASIS-TABS Version 2.0: Computer Program for Nonlinear Dynamic Analysis of Three Dimensional Base Isolated Structures," by A.M. Reinhorn, S. Nagarajaiah, M.C. Constantinou, P. Tsopelas and R. Li, 6/22/94, (PB95-182176, A08, MF-A02).

NCEER-94-0019 "Proceedings of the International Workshop on Civil Infrastructure Systems: Application of Intelligent Systems and Advanced Materials on Bridge Systems," Edited by G.C. Lee and K.C. Chang, 7/18/94, (PB95-252474, A20, MF-A04).

NCEER-94-0020 "Study of Seismic Isolation Systems for Computer Floors," by V. Lambrou and M.C. Constantinou, 7/19/94, (PB95-138533, A10, MF-A03).

NCEER-94-0021 "Proceedings of the U.S.-Italian Workshop on Guidelines for Seismic Evaluation and Rehabilitation of Unreinforced Masonry Buildings," Edited by D.P. Abrams and G.M. Calvi, 7/20/94, (PB95-138749, A13, MF-A03).

NCEER-94-0022 "NCEER-Taisei Corporation Research Program on Sliding Seismic Isolation Systems for Bridges: Experimental and Analytical Study of a System Consisting of Lubricated PTFE Sliding Bearings and Mild Steel Dampers," by P. Tsopelas and M.C. Constantinou, 7/22/94, (PB95-182184, A08, MF-A02).

NCEER-94-0023 “Development of Reliability-Based Design Criteria for Buildings Under Seismic Load,” by Y.K. Wen, H. Hwang and M. Shinozuka, 8/1/94, (PB95-211934, A08, MF-A02).

NCEER-94-0024 “Experimental Verification of Acceleration Feedback Control Strategies for an Active Tendon System,” by S.J. Dyke, B.F. Spencer, Jr., P. Quast, M.K. Sain, D.C. Kaspari, Jr. and T.T. Soong, 8/29/94, (PB95-212320, A05, MF-A01).

NCEER-94-0025 “Seismic Retrofitting Manual for Highway Bridges,” Edited by I.G. Buckle and I.F. Friedland, published by the Federal Highway Administration (PB95-212676, A15, MF-A03).

NCEER-94-0026 “Proceedings from the Fifth U.S.-Japan Workshop on Earthquake Resistant Design of Lifeline Facilities and Countermeasures Against Soil Liquefaction,” Edited by T.D. O’Rourke and M. Hamada, 11/7/94, (PB95-220802, A99, MF-E08).

NCEER-95-0001 "Experimental and Analytical Investigation of Seismic Retrofit of Structures with Supplemental Damping: Part 1 - Fluid Viscous Damping Devices," by A.M. Reinhorn, C. Li and M.C. Constantinou, 1/3/95, (PB95-266599, A09, MF-A02).

NCEER-95-0002 "Experimental and Analytical Study of Low-Cycle Fatigue Behavior of Semi-Rigid Top-And-Seat Angle Connections," by G. Pekcan, J.B. Mander and S.S. Chen, 1/5/95, (PB95-220042, A07, MF-A02).

NCEER-95-0003 "NCEER-ATC Joint Study on Fragility of Buildings," by T. Anagnos, C. Rojahn and A.S. Kiremidjian, 1/20/95, (PB95-220026, A06, MF-A02).

NCEER-95-0004 "Nonlinear Control Algorithms for Peak Response Reduction," by Z. Wu, T.T. Soong, V. Gattulli and R.C. Lin, 2/16/95, (PB95-220349, A05, MF-A01).

NCEER-95-0005 "Pipeline Replacement Feasibility Study: A Methodology for Minimizing Seismic and Corrosion Risks to Underground Natural Gas Pipelines," by R.T. Eguchi, H.A. Seligson and D.G. Honegger, 3/2/95, (PB95-252326, A06, MF-A02).

NCEER-95-0006 "Evaluation of Seismic Performance of an 11-Story Frame Building During the 1994 Northridge Earthquake," by F. Naeim, R. DiSulio, K. Benuska, A. Reinhorn and C. Li, not available.

NCEER-95-0007 "Prioritization of Bridges for Seismic Retrofitting," by N. Basöz and A.S. Kiremidjian, 4/24/95, (PB95-252300, A08, MF-A02).

NCEER-95-0008 "Method for Developing Motion Damage Relationships for Reinforced Concrete Frames," by A. Singhal and A.S. Kiremidjian, 5/11/95, (PB95-266607, A06, MF-A02).

NCEER-95-0009 "Experimental and Analytical Investigation of Seismic Retrofit of Structures with Supplemental Damping: Part II - Friction Devices," by C. Li and A.M. Reinhorn, 7/6/95, (PB96-128087, A11, MF-A03).

NCEER-95-0010 "Experimental Performance and Analytical Study of a Non-Ductile Reinforced Concrete Frame Structure Retrofitted with Elastomeric Spring Dampers," by G. Pekcan, J.B. Mander and S.S. Chen, 7/14/95, (PB96-137161, A08, MF-A02).

NCEER-95-0011 "Development and Experimental Study of Semi-Active Fluid Damping Devices for Seismic Protection of Structures," by M.D. Symans and M.C. Constantinou, 8/3/95, (PB96-136940, A23, MF-A04).

NCEER-95-0012 "Real-Time Structural Parameter Modification (RSPM): Development of Innervated Structures," by Z. Liang, M. Tong and G.C. Lee, 4/11/95, (PB96-137153, A06, MF-A01).

NCEER-95-0013 "Experimental and Analytical Investigation of Seismic Retrofit of Structures with Supplemental Damping: Part III - Viscous Damping Walls," by A.M. Reinhorn and C. Li, 10/1/95, (PB96-176409, A11, MF-A03).

NCEER-95-0014 "Seismic Fragility Analysis of Equipment and Structures in a Memphis Electric Substation," by J-R. Huo and H.H.M. Hwang, 8/10/95, (PB96-128087, A09, MF-A02).

NCEER-95-0015 "The Hanshin-Awaji Earthquake of January 17, 1995: Performance of Lifelines," Edited by M. Shinozuka, 11/3/95, (PB96-176383, A15, MF-A03).

NCEER-95-0016 "Highway Culvert Performance During Earthquakes," by T.L. Youd and C.J. Beckman, available as NCEER-96-0015.

NCEER-95-0017 "The Hanshin-Awaji Earthquake of January 17, 1995: Performance of Highway Bridges," Edited by I.G. Buckle, 12/1/95, not available.

NCEER-95-0018 "Modeling of Masonry Infill Panels for Structural Analysis," by A.M. Reinhorn, A. Madan, R.E. Valles, Y. Reichmann and J.B. Mander, 12/8/95, (PB97-110886, MF-A01, A06).

NCEER-95-0019 "Optimal Polynomial Control for Linear and Nonlinear Structures," by A.K. Agrawal and J.N. Yang, 12/11/95, (PB96-168737, A07, MF-A02).

NCEER-95-0020 "Retrofit of Non-Ductile Reinforced Concrete Frames Using Friction Dampers," by R.S. Rao, P. Gergely and R.N. White, 12/22/95, (PB97-133508, A10, MF-A02).

NCEER-95-0021 "Parametric Results for Seismic Response of Pile-Supported Bridge Bents," by G. Mylonakis, A. Nikolaou and G. Gazetas, 12/22/95, (PB97-100242, A12, MF-A03).

NCEER-95-0022 "Kinematic Bending Moments in Seismically Stressed Piles," by A. Nikolaou, G. Mylonakis and G. Gazetas, 12/23/95, (PB97-113914, MF-A03, A13).

NCEER-96-0001 "Dynamic Response of Unreinforced Masonry Buildings with Flexible Diaphragms," by A.C. Costley and D.P. Abrams," 10/10/96, (PB97-133573, MF-A03, A15).

NCEER-96-0002 "State of the Art Review: Foundations and Retaining Structures," by I. Po Lam, not available.

NCEER-96-0003 "Ductility of Rectangular Reinforced Concrete Bridge Columns with Moderate Confinement," by N. Wehbe, M. Saiidi, D. Sanders and B. Douglas, 11/7/96, (PB97-133557, A06, MF-A02).

NCEER-96-0004 "Proceedings of the Long-Span Bridge Seismic Research Workshop," edited by I.G. Buckle and I.M. Friedland, not available.

NCEER-96-0005 "Establish Representative Pier Types for Comprehensive Study: Eastern United States," by J. Kulicki and Z. Prucz, 5/28/96, (PB98-119217, A07, MF-A02).

NCEER-96-0006 "Establish Representative Pier Types for Comprehensive Study: Western United States," by R. Imbsen, R.A. Schamber and T.A. Osterkamp, 5/28/96, (PB98-118607, A07, MF-A02).

NCEER-96-0007 "Nonlinear Control Techniques for Dynamical Systems with Uncertain Parameters," by R.G. Ghanem and M.I. Bujakov, 5/27/96, (PB97-100259, A17, MF-A03).

NCEER-96-0008 "Seismic Evaluation of a 30-Year Old Non-Ductile Highway Bridge Pier and Its Retrofit," by J.B. Mander, B. Mahmoodzadegan, S. Bhadra and S.S. Chen, 5/31/96, (PB97-110902, MF-A03, A10).

NCEER-96-0009 "Seismic Performance of a Model Reinforced Concrete Bridge Pier Before and After Retrofit," by J.B. Mander, J.H. Kim and C.A. Ligozio, 5/31/96, (PB97-110910, MF-A02, A10).

NCEER-96-0010 "IDARC2D Version 4.0: A Computer Program for the Inelastic Damage Analysis of Buildings," by R.E. Valles, A.M. Reinhorn, S.K. Kunnath, C. Li and A. Madan, 6/3/96, (PB97-100234, A17, MF-A03).

NCEER-96-0011 "Estimation of the Economic Impact of Multiple Lifeline Disruption: Memphis Light, Gas and Water Division Case Study," by S.E. Chang, H.A. Seligson and R.T. Eguchi, 8/16/96, (PB97-133490, A11, MF-A03).

NCEER-96-0012 "Proceedings from the Sixth Japan-U.S. Workshop on Earthquake Resistant Design of Lifeline Facilities and Countermeasures Against Soil Liquefaction, Edited by M. Hamada and T. O'Rourke, 9/11/96, (PB97-133581, A99, MF-A06).

NCEER-96-0013 "Chemical Hazards, Mitigation and Preparedness in Areas of High Seismic Risk: A Methodology for Estimating the Risk of Post-Earthquake Hazardous Materials Release," by H.A. Seligson, R.T. Eguchi, K.J. Tierney and K. Richmond, 11/7/96, (PB97-133565, MF-A02, A08).

NCEER-96-0014 "Response of Steel Bridge Bearings to Reversed Cyclic Loading," by J.B. Mander, D-K. Kim, S.S. Chen and G.J. Premus, 11/13/96, (PB97-140735, A12, MF-A03).

NCEER-96-0015 "Highway Culvert Performance During Past Earthquakes," by T.L. Youd and C.J. Beckman, 11/25/96, (PB97-133532, A06, MF-A01).

NCEER-97-0001 "Evaluation, Prevention and Mitigation of Pounding Effects in Building Structures," by R.E. Valles and A.M. Reinhorn, 2/20/97, (PB97-159552, A14, MF-A03).

NCEER-97-0002 "Seismic Design Criteria for Bridges and Other Highway Structures," by C. Rojahn, R. Mayes, D.G. Anderson, J. Clark, J.H. Hom, R.V. Nutt and M.J. O'Rourke, 4/30/97, (PB97-194658, A06, MF-A03).

NCEER-97-0003 "Proceedings of the U.S.-Italian Workshop on Seismic Evaluation and Retrofit," Edited by D.P. Abrams and G.M. Calvi, 3/19/97, (PB97-194666, A13, MF-A03).

NCEER-97-0004 "Investigation of Seismic Response of Buildings with Linear and Nonlinear Fluid Viscous Dampers," by A.A. Seleemah and M.C. Constantinou, 5/21/97, (PB98-109002, A15, MF-A03).

NCEER-97-0005 "Proceedings of the Workshop on Earthquake Engineering Frontiers in Transportation Facilities," edited by G.C. Lee and I.M. Friedland, 8/29/97, (PB98-128911, A25, MR-A04).

NCEER-97-0006 "Cumulative Seismic Damage of Reinforced Concrete Bridge Piers," by S.K. Kunnath, A. El-Bahy, A. Taylor and W. Stone, 9/2/97, (PB98-108814, A11, MF-A03).

NCEER-97-0007 "Structural Details to Accommodate Seismic Movements of Highway Bridges and Retaining Walls," by R.A. Imbsen, R.A. Schamber, E. Thorkildsen, A. Kartoum, B.T. Martin, T.N. Rosser and J.M. Kulicki, 9/3/97, (PB98-108996, A09, MF-A02).

NCEER-97-0008 "A Method for Earthquake Motion-Damage Relationships with Application to Reinforced Concrete Frames," by A. Singhal and A.S. Kiremidjian, 9/10/97, (PB98-108988, A13, MF-A03).

NCEER-97-0009 "Seismic Analysis and Design of Bridge Abutments Considering Sliding and Rotation," by K. Fishman and R. Richards, Jr., 9/15/97, (PB98-108897, A06, MF-A02).

NCEER-97-0010 "Proceedings of the FHWA/NCEER Workshop on the National Representation of Seismic Ground Motion for New and Existing Highway Facilities," edited by I.M. Friedland, M.S. Power and R.L. Mayes, 9/22/97, (PB98-128903, A21, MF-A04).

NCEER-97-0011 "Seismic Analysis for Design or Retrofit of Gravity Bridge Abutments," by K.L. Fishman, R. Richards, Jr. and R.C. Divito, 10/2/97, (PB98-128937, A08, MF-A02).

NCEER-97-0012 "Evaluation of Simplified Methods of Analysis for Yielding Structures," by P. Tsopelas, M.C. Constantinou, C.A. Kircher and A.S. Whittaker, 10/31/97, (PB98-128929, A10, MF-A03).

NCEER-97-0013 "Seismic Design of Bridge Columns Based on Control and Repairability of Damage," by C-T. Cheng and J.B. Mander, 12/8/97, (PB98-144249, A11, MF-A03).

NCEER-97-0014 "Seismic Resistance of Bridge Piers Based on Damage Avoidance Design," by J.B. Mander and C-T. Cheng, 12/10/97, (PB98-144223, A09, MF-A02).

NCEER-97-0015 "Seismic Response of Nominally Symmetric Systems with Strength Uncertainty," by S. Balopoulou and M. Grigoriu, 12/23/97, (PB98-153422, A11, MF-A03).

NCEER-97-0016 "Evaluation of Seismic Retrofit Methods for Reinforced Concrete Bridge Columns," by T.J. Wipf, F.W. Klaiber and F.M. Russo, 12/28/97, (PB98-144215, A12, MF-A03).

NCEER-97-0017 "Seismic Fragility of Existing Conventional Reinforced Concrete Highway Bridges," by C.L. Mullen and A.S. Cakmak, 12/30/97, (PB98-153406, A08, MF-A02).

NCEER-97-0018 "Loss Asssessment of Memphis Buildings," edited by D.P. Abrams and M. Shinozuka, 12/31/97, (PB98-144231, A13, MF-A03).

NCEER-97-0019 "Seismic Evaluation of Frames with Infill Walls Using Quasi-static Experiments," by K.M. Mosalam, R.N. White and P. Gergely, 12/31/97, (PB98-153455, A07, MF-A02).

NCEER-97-0020 "Seismic Evaluation of Frames with Infill Walls Using Pseudo-dynamic Experiments," by K.M. Mosalam, R.N. White and P. Gergely, 12/31/97, (PB98-153430, A07, MF-A02).

NCEER-97-0021 "Computational Strategies for Frames with Infill Walls: Discrete and Smeared Crack Analyses and Seismic Fragility," by K.M. Mosalam, R.N. White and P. Gergely, 12/31/97, (PB98-153414, A10, MF-A02).

NCEER-97-0022 "Proceedings of the NCEER Workshop on Evaluation of Liquefaction Resistance of Soils," edited by T.L. Youd and I.M. Idriss, 12/31/97, (PB98-155617, A15, MF-A03).

MCEER-98-0001 "Extraction of Nonlinear Hysteretic Properties of Seismically Isolated Bridges from Quick-Release Field Tests," by Q. Chen, B.M. Douglas, E.M. Maragakis and I.G. Buckle, 5/26/98, (PB99-118838, A06, MF-A01).

MCEER-98-0002 "Methodologies for Evaluating the Importance of Highway Bridges," by A. Thomas, S. Eshenaur and J. Kulicki, 5/29/98, (PB99-118846, A10, MF-A02).

MCEER-98-0003 "Capacity Design of Bridge Piers and the Analysis of Overstrength," by J.B. Mander, A. Dutta and P. Goel, 6/1/98, (PB99-118853, A09, MF-A02).

MCEER-98-0004 "Evaluation of Bridge Damage Data from the Loma Prieta and Northridge, California Earthquakes," by N. Basoz and A. Kiremidjian, 6/2/98, (PB99-118861, A15, MF-A03).

MCEER-98-0005 "Screening Guide for Rapid Assessment of Liquefaction Hazard at Highway Bridge Sites," by T. L. Youd, 6/16/98, (PB99-118879, A06, not available on microfiche).

MCEER-98-0006 "Structural Steel and Steel/Concrete Interface Details for Bridges," by P. Ritchie, N. Kauhl and J. Kulicki, 7/13/98, (PB99-118945, A06, MF-A01).

MCEER-98-0007 "Capacity Design and Fatigue Analysis of Confined Concrete Columns," by A. Dutta and J.B. Mander, 7/14/98, (PB99-118960, A14, MF-A03).

MCEER-98-0008 "Proceedings of the Workshop on Performance Criteria for Telecommunication Services Under Earthquake Conditions," edited by A.J. Schiff, 7/15/98, (PB99-118952, A08, MF-A02).

MCEER-98-0009 "Fatigue Analysis of Unconfined Concrete Columns," by J.B. Mander, A. Dutta and J.H. Kim, 9/12/98, (PB99-123655, A10, MF-A02).

MCEER-98-0010 "Centrifuge Modeling of Cyclic Lateral Response of Pile-Cap Systems and Seat-Type Abutments in Dry Sands," by A.D. Gadre and R. Dobry, 10/2/98, (PB99-123606, A13, MF-A03).

MCEER-98-0011 "IDARC-BRIDGE: A Computational Platform for Seismic Damage Assessment of Bridge Structures," by A.M. Reinhorn, V. Simeonov, G. Mylonakis and Y. Reichman, 10/2/98, (PB99-162919, A15, MF-A03).

MCEER-98-0012 "Experimental Investigation of the Dynamic Response of Two Bridges Before and After Retrofitting with Elastomeric Bearings," by D.A. Wendichansky, S.S. Chen and J.B. Mander, 10/2/98, (PB99-162927, A15, MF-A03).

MCEER-98-0013 "Design Procedures for Hinge Restrainers and Hinge Sear Width for Multiple-Frame Bridges," by R. Des Roches and G.L. Fenves, 11/3/98, (PB99-140477, A13, MF-A03).

MCEER-98-0014 "Response Modification Factors for Seismically Isolated Bridges," by M.C. Constantinou and J.K. Quarshie, 11/3/98, (PB99-140485, A14, MF-A03).

MCEER-98-0015 "Proceedings of the U.S.-Italy Workshop on Seismic Protective Systems for Bridges," edited by I.M. Friedland and M.C. Constantinou, 11/3/98, (PB2000-101711, A22, MF-A04).

MCEER-98-0016 "Appropriate Seismic Reliability for Critical Equipment Systems: Recommendations Based on Regional Analysis of Financial and Life Loss," by K. Porter, C. Scawthorn, C. Taylor and N. Blais, 11/10/98, (PB99-157265, A08, MF-A02).

MCEER-98-0017 "Proceedings of the U.S. Japan Joint Seminar on Civil Infrastructure Systems Research," edited by M. Shinozuka and A. Rose, 11/12/98, (PB99-156713, A16, MF-A03).

MCEER-98-0018 "Modeling of Pile Footings and Drilled Shafts for Seismic Design," by I. PoLam, M. Kapuskar and D. Chaudhuri, 12/21/98, (PB99-157257, A09, MF-A02).

MCEER-99-0001 "Seismic Evaluation of a Masonry Infilled Reinforced Concrete Frame by Pseudodynamic Testing," by S.G. Buonopane and R.N. White, 2/16/99, (PB99-162851, A09, MF-A02).

MCEER-99-0002 "Response History Analysis of Structures with Seismic Isolation and Energy Dissipation Systems: Verification Examples for Program SAP2000," by J. Scheller and M.C. Constantinou, 2/22/99, (PB99-162869, A08, MF-A02).

MCEER-99-0003 "Experimental Study on the Seismic Design and Retrofit of Bridge Columns Including Axial Load Effects," by A. Dutta, T. Kokorina and J.B. Mander, 2/22/99, (PB99-162877, A09, MF-A02).

MCEER-99-0004 "Experimental Study of Bridge Elastomeric and Other Isolation and Energy Dissipation Systems with Emphasis on Uplift Prevention and High Velocity Near-source Seismic Excitation," by A. Kasalanati and M. C. Constantinou, 2/26/99, (PB99-162885, A12, MF-A03).

MCEER-99-0005 "Truss Modeling of Reinforced Concrete Shear-flexure Behavior," by J.H. Kim and J.B. Mander, 3/8/99, (PB99-163693, A12, MF-A03).

MCEER-99-0006 "Experimental Investigation and Computational Modeling of Seismic Response of a 1:4 Scale Model Steel Structure with a Load Balancing Supplemental Damping System," by G. Pekcan, J.B. Mander and S.S. Chen, 4/2/99, (PB99-162893, A11, MF-A03).

MCEER-99-0007 "Effect of Vertical Ground Motions on the Structural Response of Highway Bridges," by M.R. Button, C.J. Cronin and R.L. Mayes, 4/10/99, (PB2000-101411, A10, MF-A03).

MCEER-99-0008 "Seismic Reliability Assessment of Critical Facilities: A Handbook, Supporting Documentation, and Model Code Provisions," by G.S. Johnson, R.E. Sheppard, M.D. Quilici, S.J. Eder and C.R. Scawthorn, 4/12/99, (PB2000-101701, A18, MF-A04).

MCEER-99-0009 "Impact Assessment of Selected MCEER Highway Project Research on the Seismic Design of Highway Structures," by C. Rojahn, R. Mayes, D.G. Anderson, J.H. Clark, D'Appolonia Engineering, S. Gloyd and R.V. Nutt, 4/14/99, (PB99-162901, A10, MF-A02).

MCEER-99-0010 "Site Factors and Site Categories in Seismic Codes," by R. Dobry, R. Ramos and M.S. Power, 7/19/99, (PB2000-101705, A08, MF-A02).

MCEER-99-0011 "Restrainer Design Procedures for Multi-Span Simply-Supported Bridges," by M.J. Randall, M. Saiidi, E. Maragakis and T. Isakovic, 7/20/99, (PB2000-101702, A10, MF-A02).

MCEER-99-0012 "Property Modification Factors for Seismic Isolation Bearings," by M.C. Constantinou, P. Tsopelas, A. Kasalanati and E. Wolff, 7/20/99, (PB2000-103387, A11, MF-A03).

MCEER-99-0013 "Critical Seismic Issues for Existing Steel Bridges," by P. Ritchie, N. Kauhl and J. Kulicki, 7/20/99, (PB2000-101697, A09, MF-A02).

MCEER-99-0014 "Nonstructural Damage Database," by A. Kao, T.T. Soong and A. Vender, 7/24/99, (PB2000-101407, A06, MF-A01).

MCEER-99-0015 "Guide to Remedial Measures for Liquefaction Mitigation at Existing Highway Bridge Sites," by H.G. Cooke and J. K. Mitchell, 7/26/99, (PB2000-101703, A11, MF-A03).

MCEER-99-0016 "Proceedings of the MCEER Workshop on Ground Motion Methodologies for the Eastern United States," edited by N. Abrahamson and A. Becker, 8/11/99, (PB2000-103385, A07, MF-A02).

MCEER-99-0017 "Quindío, Colombia Earthquake of January 25, 1999: Reconnaissance Report," by A.P. Asfura and P.J. Flores, 10/4/99, (PB2000-106893, A06, MF-A01).

MCEER-99-0018 "Hysteretic Models for Cyclic Behavior of Deteriorating Inelastic Structures," by M.V. Sivaselvan and A.M. Reinhorn, 11/5/99, (PB2000-103386, A08, MF-A02).

MCEER-99-0019 "Proceedings of the 7th U.S.- Japan Workshop on Earthquake Resistant Design of Lifeline Facilities and Countermeasures Against Soil Liquefaction," edited by T.D. O'Rourke, J.P. Bardet and M. Hamada, 11/19/99, (PB2000-103354, A99, MF-A06).

MCEER-99-0020 "Development of Measurement Capability for Micro-Vibration Evaluations with Application to Chip Fabrication Facilities," by G.C. Lee, Z. Liang, J.W. Song, J.D. Shen and W.C. Liu, 12/1/99, (PB2000-105993, A08, MF-A02).

MCEER-99-0021 "Design and Retrofit Methodology for Building Structures with Supplemental Energy Dissipating Systems," by G. Pekcan, J.B. Mander and S.S. Chen, 12/31/99, (PB2000-105994, A11, MF-A03).

MCEER-00-0001 "The Marmara, Turkey Earthquake of August 17, 1999: Reconnaissance Report," edited by C. Scawthorn; with major contributions by M. Bruneau, R. Eguchi, T. Holzer, G. Johnson, J. Mander, J. Mitchell, W. Mitchell, A. Papageorgiou, C. Scaethorn, and G. Webb, 3/23/00, (PB2000-106200, A11, MF-A03).

MCEER-00-0002 "Proceedings of the MCEER Workshop for Seismic Hazard Mitigation of Health Care Facilities," edited by G.C. Lee, M. Ettouney, M. Grigoriu, J. Hauer and J. Nigg, 3/29/00, (PB2000-106892, A08, MF-A02).

MCEER-00-0003 "The Chi-Chi, Taiwan Earthquake of September 21, 1999: Reconnaissance Report," edited by G.C. Lee and C.H. Loh, with major contributions by G.C. Lee, M. Bruneau, I.G. Buckle, S.E. Chang, P.J. Flores, T.D. O'Rourke, M. Shinozuka, T.T. Soong, C-H. Loh, K-C. Chang, Z-J. Chen, J-S. Hwang, M-L. Lin, G-Y. Liu, K-C. Tsai, G.C. Yao and C-L. Yen, 4/30/00, (PB2001-100980, A10, MF-A02).

MCEER-00-0004 "Seismic Retrofit of End-Sway Frames of Steel Deck-Truss Bridges with a Supplemental Tendon System: Experimental and Analytical Investigation," by G. Pekcan, J.B. Mander and S.S. Chen, 7/1/00, (PB2001-100982, A10, MF-A02).

MCEER-00-0005 "Sliding Fragility of Unrestrained Equipment in Critical Facilities," by W.H. Chong and T.T. Soong, 7/5/00, (PB2001-100983, A08, MF-A02).

MCEER-00-0006 "Seismic Response of Reinforced Concrete Bridge Pier Walls in the Weak Direction," by N. Abo-Shadi, M. Saiidi and D. Sanders, 7/17/00, (PB2001-100981, A17, MF-A03).

MCEER-00-0007 "Low-Cycle Fatigue Behavior of Longitudinal Reinforcement in Reinforced Concrete Bridge Columns," by J. Brown and S.K. Kunnath, 7/23/00, (PB2001-104392, A08, MF-A02).

MCEER-00-0008 "Soil Structure Interaction of Bridges for Seismic Analysis," I. PoLam and H. Law, 9/25/00, (PB2001-105397, A08, MF-A02).

MCEER-00-0009 "Proceedings of the First MCEER Workshop on Mitigation of Earthquake Disaster by Advanced Technologies (MEDAT-1), edited by M. Shinozuka, D.J. Inman and T.D. O'Rourke, 11/10/00, (PB2001-105399, A14, MF-A03).

MCEER-00-0010 "Development and Evaluation of Simplified Procedures for Analysis and Design of Buildings with Passive Energy Dissipation Systems, Revision 01," by O.M. Ramirez, M.C. Constantinou, C.A. Kircher, A.S. Whittaker, M.W. Johnson, J.D. Gomez and C. Chrysostomou, 11/16/01, (PB2001-105523, A23, MF-A04).

MCEER-00-0011 "Dynamic Soil-Foundation-Structure Interaction Analyses of Large Caissons," by C-Y. Chang, C-M. Mok, Z-L. Wang, R. Settgast, F. Waggoner, M.A. Ketchum, H.M. Gonnermann and C-C. Chin, 12/30/00, (PB2001-104373, A07, MF-A02).

MCEER-00-0012 "Experimental Evaluation of Seismic Performance of Bridge Restrainers," by A.G. Vlassis, E.M. Maragakis and M. Saiid Saiidi, 12/30/00, (PB2001-104354, A09, MF-A02).

MCEER-00-0013 "Effect of Spatial Variation of Ground Motion on Highway Structures," by M. Shinozuka, V. Saxena and G. Deodatis, 12/31/00, (PB2001-108755, A13, MF-A03).

MCEER-00-0014 "A Risk-Based Methodology for Assessing the Seismic Performance of Highway Systems," by S.D. Werner, C.E. Taylor, J.E. Moore, II, J.S. Walton and S. Cho, 12/31/00, (PB2001-108756, A14, MF-A03).

MCEER-01-0001 "Experimental Investigation of P-Delta Effects to Collapse During Earthquakes," by D. Vian and M. Bruneau, 6/25/01, (PB2002-100534, A17, MF-A03).

MCEER-01-0002 "Proceedings of the Second MCEER Workshop on Mitigation of Earthquake Disaster by Advanced Technologies (MEDAT-2)," edited by M. Bruneau and D.J. Inman, 7/23/01, (PB2002-100434, A16, MF-A03).

MCEER-01-0003 "Sensitivity Analysis of Dynamic Systems Subjected to Seismic Loads," by C. Roth and M. Grigoriu, 9/18/01, (PB2003-100884, A12, MF-A03).

MCEER-01-0004 "Overcoming Obstacles to Implementing Earthquake Hazard Mitigation Policies: Stage 1 Report," by D.J. Alesch and W.J. Petak, 12/17/01, (PB2002-107949, A07, MF-A02).

MCEER-01-0005 "Updating Real-Time Earthquake Loss Estimates: Methods, Problems and Insights," by C.E. Taylor, S.E. Chang and R.T. Eguchi, 12/17/01, (PB2002-107948, A05, MF-A01).

MCEER-01-0006 "Experimental Investigation and Retrofit of Steel Pile Foundations and Pile Bents Under Cyclic Lateral Loadings," by A. Shama, J. Mander, B. Blabac and S. Chen, 12/31/01, (PB2002-107950, A13, MF-A03).

MCEER-02-0001 "Assessment of Performance of Bolu Viaduct in the 1999 Duzce Earthquake in Turkey" by P.C. Roussis, M.C. Constantinou, M. Erdik, E. Durukal and M. Dicleli, 5/8/02, (PB2003-100883, A08, MF-A02).

MCEER-02-0002 "Seismic Behavior of Rail Counterweight Systems of Elevators in Buildings," by M.P. Singh, Rildova and L.E. Suarez, 5/27/02. (PB2003-100882, A11, MF-A03).

MCEER-02-0003 "Development of Analysis and Design Procedures for Spread Footings," by G. Mylonakis, G. Gazetas, S. Nikolaou and A. Chauncey, 10/02/02, (PB2004-101636, A13, MF-A03, CD-A13).

MCEER-02-0004 "Bare-Earth Algorithms for Use with SAR and LIDAR Digital Elevation Models," by C.K. Huyck, R.T. Eguchi and B. Houshmand, 10/16/02, (PB2004-101637, A07, CD-A07).

MCEER-02-0005 "Review of Energy Dissipation of Compression Members in Concentrically Braced Frames," by K.Lee and M. Bruneau, 10/18/02, (PB2004-101638, A10, CD-A10).

MCEER-03-0001 "Experimental Investigation of Light-Gauge Steel Plate Shear Walls for the Seismic Retrofit of Buildings" by J. Berman and M. Bruneau, 5/2/03, (PB2004-101622, A10, MF-A03, CD-A10).

MCEER-03-0002 "Statistical Analysis of Fragility Curves," by M. Shinozuka, M.Q. Feng, H. Kim, T. Uzawa and T. Ueda, 6/16/03, (PB2004-101849, A09, CD-A09).

MCEER-03-0003 "Proceedings of the Eighth U.S.-Japan Workshop on Earthquake Resistant Design f Lifeline Facilities and Countermeasures Against Liquefaction," edited by M. Hamada, J.P. Bardet and T.D. O'Rourke, 6/30/03, (PB2004-104386, A99, CD-A99).

MCEER-03-0004 "Proceedings of the PRC-US Workshop on Seismic Analysis and Design of Special Bridges," edited by L.C. Fan and G.C. Lee, 7/15/03, (PB2004-104387, A14, CD-A14).

MCEER-03-0005 "Urban Disaster Recovery: A Framework and Simulation Model," by S.B. Miles and S.E. Chang, 7/25/03, (PB2004-104388, A07, CD-A07).

MCEER-03-0006 "Behavior of Underground Piping Joints Due to Static and Dynamic Loading," by R.D. Meis, M. Maragakis and R. Siddharthan, 11/17/03, (PB2005-102194, A13, MF-A03, CD-A00).

MCEER-04-0001 "Experimental Study of Seismic Isolation Systems with Emphasis on Secondary System Response and Verification of Accuracy of Dynamic Response History Analysis Methods," by E. Wolff and M. Constantinou, 1/16/04 (PB2005-102195, A99, MF-E08, CD-A00).

MCEER-04-0002 "Tension, Compression and Cyclic Testing of Engineered Cementitious Composite Materials," by K. Kesner and S.L. Billington, 3/1/04, (PB2005-102196, A08, CD-A08).

MCEER-04-0003 "Cyclic Testing of Braces Laterally Restrained by Steel Studs to Enhance Performance During Earthquakes," by O.C. Celik, J.W. Berman and M. Bruneau, 3/16/04, (PB2005-102197, A13, MF-A03, CD-A00).

MCEER-04-0004 "Methodologies for Post Earthquake Building Damage Detection Using SAR and Optical Remote Sensing: Application to the August 17, 1999 Marmara, Turkey Earthquake," by C.K. Huyck, B.J. Adams, S. Cho, R.T. Eguchi, B. Mansouri and B. Houshmand, 6/15/04, (PB2005-104888, A10, CD-A00).

MCEER-04-0005 "Nonlinear Structural Analysis Towards Collapse Simulation: A Dynamical Systems Approach," by M.V. Sivaselvan and A.M. Reinhorn, 6/16/04, (PB2005-104889, A11, MF-A03, CD-A00).

MCEER-04-0006 "Proceedings of the Second PRC-US Workshop on Seismic Analysis and Design of Special Bridges," edited by G.C. Lee and L.C. Fan, 6/25/04, (PB2005-104890, A16, CD-A00).

MCEER-04-0007 "Seismic Vulnerability Evaluation of Axially Loaded Steel Built-up Laced Members," by K. Lee and M. Bruneau, 6/30/04, (PB2005-104891, A16, CD-A00).

MCEER-04-0008 "Evaluation of Accuracy of Simplified Methods of Analysis and Design of Buildings with Damping Systems for Near-Fault and for Soft-Soil Seismic Motions," by E.A. Pavlou and M.C. Constantinou, 8/16/04, (PB2005-104892, A08, MF-A02, CD-A00).

MCEER-04-0009 "Assessment of Geotechnical Issues in Acute Care Facilities in California," by M. Lew, T.D. O'Rourke, R. Dobry and M. Koch, 9/15/04, (PB2005-104893, A08, CD-A00).

MCEER-04-0010 "Scissor-Jack-Damper Energy Dissipation System," by A.N. Sigaher-Boyle and M.C. Constantinou, 12/1/04 (PB2005-108221).

MCEER-04-0011 "Seismic Retrofit of Bridge Steel Truss Piers Using a Controlled Rocking Approach," by M. Pollino and M. Bruneau, 12/20/04 (PB2006-105795).

MCEER-05-0001 "Experimental and Analytical Studies of Structures Seismically Isolated with an Uplift-Restraint Isolation System," by P.C. Roussis and M.C. Constantinou, 1/10/05 (PB2005-108222).

MCEER-05-0002 "A Versatile Experimentation Model for Study of Structures Near Collapse Applied to Seismic Evaluation of Irregular Structures," by D. Kusumastuti, A.M. Reinhorn and A. Rutenberg, 3/31/05 (PB2006-101523).

MCEER-05-0003 "Proceedings of the Third PRC-US Workshop on Seismic Analysis and Design of Special Bridges," edited by L.C. Fan and G.C. Lee, 4/20/05, (PB2006-105796).

MCEER-05-0004 "Approaches for the Seismic Retrofit of Braced Steel Bridge Piers and Proof-of-Concept Testing of an Eccentrically Braced Frame with Tubular Link," by J.W. Berman and M. Bruneau, 4/21/05 (PB2006-101524).

MCEER-05-0005 "Simulation of Strong Ground Motions for Seismic Fragility Evaluation of Nonstructural Components in Hospitals," by A. Wanitkorkul and A. Filiatrault, 5/26/05 (PB2006-500027).

MCEER-05-0006 "Seismic Safety in California Hospitals: Assessing an Attempt to Accelerate the Replacement or Seismic Retrofit of Older Hospital Facilities," by D.J. Alesch, L.A. Arendt and W.J. Petak, 6/6/05 (PB2006-105794).

MCEER-05-0007 "Development of Seismic Strengthening and Retrofit Strategies for Critical Facilities Using Engineered Cementitious Composite Materials," by K. Kesner and S.L. Billington, 8/29/05 (PB2006-111701).

MCEER-05-0008 "Experimental and Analytical Studies of Base Isolation Systems for Seismic Protection of Power Transformers," by N. Murota, M.Q. Feng and G-Y. Liu, 9/30/05 (PB2006-111702).

MCEER-05-0009 "3D-BASIS-ME-MB: Computer Program for Nonlinear Dynamic Analysis of Seismically Isolated Structures," by P.C. Tsopelas, P.C. Roussis, M.C. Constantinou, R. Buchanan and A.M. Reinhorn, 10/3/05 (PB2006-111703).

MCEER-05-0010 "Steel Plate Shear Walls for Seismic Design and Retrofit of Building Structures," by D. Vian and M. Bruneau, 12/15/05 (PB2006-111704).

MCEER-05-0011 "The Performance-Based Design Paradigm," by M.J. Astrella and A. Whittaker, 12/15/05 (PB2006-111705).

MCEER-06-0001 "Seismic Fragility of Suspended Ceiling Systems," H. Badillo-Almaraz, A.S. Whittaker, A.M. Reinhorn and G.P. Cimellaro, 2/4/06 (PB2006-111706).

MCEER-06-0002 "Multi-Dimensional Fragility of Structures," by G.P. Cimellaro, A.M. Reinhorn and M. Bruneau, 3/1/06 (PB2007-106974, A09, MF-A02, CD A00).

MCEER-06-0003 "Built-Up Shear Links as Energy Dissipators for Seismic Protection of Bridges," by P. Dusicka, A.M. Itani and I.G. Buckle, 3/15/06 (PB2006-111708).

MCEER-06-0004 "Analytical Investigation of the Structural Fuse Concept," by R.E. Vargas and M. Bruneau, 3/16/06 (PB2006-111709).

MCEER-06-0005 "Experimental Investigation of the Structural Fuse Concept," by R.E. Vargas and M. Bruneau, 3/17/06 (PB2006-111710).

MCEER-06-0006 "Further Development of Tubular Eccentrically Braced Frame Links for the Seismic Retrofit of Braced Steel Truss Bridge Piers," by J.W. Berman and M. Bruneau, 3/27/06 (PB2007-105147).

MCEER-06-0007 "REDARS Validation Report," by S. Cho, C.K. Huyck, S. Ghosh and R.T. Eguchi, 8/8/06 (PB2007-106983).

MCEER-06-0008 "Review of Current NDE Technologies for Post-Earthquake Assessment of Retrofitted Bridge Columns," by J.W. Song, Z. Liang and G.C. Lee, 8/21/06 (PB2007-106984).

MCEER-06-0009 "Liquefaction Remediation in Silty Soils Using Dynamic Compaction and Stone Columns," by S. Thevanayagam, G.R. Martin, R. Nashed, T. Shenthan, T. Kanagalingam and N. Ecemis, 8/28/06 (PB2007-106985).

MCEER-06-0010 "Conceptual Design and Experimental Investigation of Polymer Matrix Composite Infill Panels for Seismic Retrofitting," by W. Jung, M. Chiewanichakorn and A.J. Aref, 9/21/06 (PB2007-106986).

MCEER-06-0011 "A Study of the Coupled Horizontal-Vertical Behavior of Elastomeric and Lead-Rubber Seismic Isolation Bearings," by G.P. Warn and A.S. Whittaker, 9/22/06 (PB2007-108679).

MCEER-06-0012 "Proceedings of the Fourth PRC-US Workshop on Seismic Analysis and Design of Special Bridges: Advancing Bridge Technologies in Research, Design, Construction and Preservation," Edited by L.C. Fan, G.C. Lee and L. Ziang, 10/12/06 (PB2007-109042).

MCEER-06-0013 "Cyclic Response and Low Cycle Fatigue Characteristics of Plate Steels," by P. Dusicka, A.M. Itani and I.G. Buckle, 11/1/06 06 (PB2007-106987).

MCEER-06-0014 "Proceedings of the Second US-Taiwan Bridge Engineering Workshop," edited by W.P. Yen, J. Shen, J-Y. Chen and M. Wang, 11/15/06 (PB2008-500041).

MCEER-06-0015 "User Manual and Technical Documentation for the REDARS^{TM} Import Wizard," by S. Cho, S. Ghosh, C.K. Huyck and S.D. Werner, 11/30/06 (PB2007-114766).

MCEER-06-0016 "Hazard Mitigation Strategy and Monitoring Technologies for Urban and Infrastructure Public Buildings: Proceedings of the China-US Workshops," edited by X.Y. Zhou, A.L. Zhang, G.C. Lee and M. Tong, 12/12/06 (PB2008-500018).

MCEER-07-0001 "Static and Kinetic Coefficients of Friction for Rigid Blocks," by C. Kafali, S. Fathali, M. Grigoriu and A.S. Whittaker, 3/20/07 (PB2007-114767).

MCEER-07-0002 "Hazard Mitigation Investment Decision Making: Organizational Response to Legislative Mandate," by L.A. Arendt, D.J. Alesch and W.J. Petak, 4/9/07 (PB2007-114768).

MCEER-07-0003 "Seismic Behavior of Bidirectional-Resistant Ductile End Diaphragms with Unbonded Braces in Straight or Skewed Steel Bridges," by O. Celik and M. Bruneau, 4/11/07 (PB2008-105141).

MCEER-07-0004 "Modeling Pile Behavior in Large Pile Groups Under Lateral Loading," by A.M. Dodds and G.R. Martin, 4/16/07(PB2008-105142).

MCEER-07-0005 "Experimental Investigation of Blast Performance of Seismically Resistant Concrete-Filled Steel Tube Bridge Piers," by S. Fujikura, M. Bruneau and D. Lopez-Garcia, 4/20/07 (PB2008-105143).

MCEER-07-0006 "Seismic Analysis of Conventional and Isolated Liquefied Natural Gas Tanks Using Mechanical Analogs," by I.P. Christovasilis and A.S. Whittaker, 5/1/07, not available.

MCEER-07-0007 "Experimental Seismic Performance Evaluation of Isolation/Restraint Systems for Mechanical Equipment – Part 1: Heavy Equipment Study," by S. Fathali and A. Filiatrault, 6/6/07 (PB2008-105144).

MCEER-07-0008 "Seismic Vulnerability of Timber Bridges and Timber Substructures," by A.A. Sharma, J.B. Mander, I.M. Friedland and D.R. Allicock, 6/7/07 (PB2008-105145).

MCEER-07-0009 "Experimental and Analytical Study of the XY-Friction Pendulum (XY-FP) Bearing for Bridge Applications," by C.C. Marin-Artieda, A.S. Whittaker and M.C. Constantinou, 6/7/07 (PB2008-105191).

MCEER-07-0010 "Proceedings of the PRC-US Earthquake Engineering Forum for Young Researchers," Edited by G.C. Lee and X.Z. Qi, 6/8/07 (PB2008-500058).

MCEER-07-0011 "Design Recommendations for Perforated Steel Plate Shear Walls," by R. Purba and M. Bruneau, 6/18/07, (PB2008-105192).

MCEER-07-0012 "Performance of Seismic Isolation Hardware Under Service and Seismic Loading," by M.C. Constantinou, A.S. Whittaker, Y. Kalpakidis, D.M. Fenz and G.P. Warn, 8/27/07, (PB2008-105193).

MCEER-07-0013 "Experimental Evaluation of the Seismic Performance of Hospital Piping Subassemblies," by E.R. Goodwin, E. Maragakis and A.M. Itani, 9/4/07, (PB2008-105194).

MCEER-07-0014 "A Simulation Model of Urban Disaster Recovery and Resilience: Implementation for the 1994 Northridge Earthquake," by S. Miles and S.E. Chang, 9/7/07, (PB2008-106426).

MCEER-07-0015 "Statistical and Mechanistic Fragility Analysis of Concrete Bridges," by M. Shinozuka, S. Banerjee and S-H. Kim, 9/10/07, (PB2008-106427).

MCEER-07-0016 "Three-Dimensional Modeling of Inelastic Buckling in Frame Structures," by M. Schachter and AM. Reinhorn, 9/13/07, (PB2008-108125).

MCEER-07-0017 "Modeling of Seismic Wave Scattering on Pile Groups and Caissons," by I. Po Lam, H. Law and C.T. Yang, 9/17/07 (PB2008-108150).

MCEER-07-0018 "Bridge Foundations: Modeling Large Pile Groups and Caissons for Seismic Design," by I. Po Lam, H. Law and G.R. Martin (Coordinating Author), 12/1/07 (PB2008-111190).

MCEER-07-0019 "Principles and Performance of Roller Seismic Isolation Bearings for Highway Bridges," by G.C. Lee, Y.C. Ou, Z. Liang, T.C. Niu and J. Song, 12/10/07 (PB2009-110466).

MCEER-07-0020 "Centrifuge Modeling of Permeability and Pinning Reinforcement Effects on Pile Response to Lateral Spreading," by L.L Gonzalez-Lagos, T. Abdoun and R. Dobry, 12/10/07 (PB2008-111191).

MCEER-07-0021 "Damage to the Highway System from the Pisco, Perú Earthquake of August 15, 2007," by J.S. O'Connor, L. Mesa and M. Nykamp, 12/10/07, (PB2008-108126).

MCEER-07-0022 "Experimental Seismic Performance Evaluation of Isolation/Restraint Systems for Mechanical Equipment – Part 2: Light Equipment Study," by S. Fathali and A. Filiatrault, 12/13/07 (PB2008-111192).

MCEER-07-0023 "Fragility Considerations in Highway Bridge Design," by M. Shinozuka, S. Banerjee and S.H. Kim, 12/14/07 (PB2008-111193).

MCEER-07-0024 "Performance Estimates for Seismically Isolated Bridges," by G.P. Warn and A.S. Whittaker, 12/30/07 (PB2008-112230).

MCEER-08-0001 "Seismic Performance of Steel Girder Bridge Superstructures with Conventional Cross Frames," by L.P. Carden, A.M. Itani and I.G. Buckle, 1/7/08, (PB2008-112231).

MCEER-08-0002 "Seismic Performance of Steel Girder Bridge Superstructures with Ductile End Cross Frames with Seismic Isolators," by L.P. Carden, A.M. Itani and I.G. Buckle, 1/7/08 (PB2008-112232).

MCEER-08-0003 "Analytical and Experimental Investigation of a Controlled Rocking Approach for Seismic Protection of Bridge Steel Truss Piers," by M. Pollino and M. Bruneau, 1/21/08 (PB2008-112233).

MCEER-08-0004 "Linking Lifeline Infrastructure Performance and Community Disaster Resilience: Models and Multi-Stakeholder Processes," by S.E. Chang, C. Pasion, K. Tatebe and R. Ahmad, 3/3/08 (PB2008-112234).

MCEER-08-0005 "Modal Analysis of Generally Damped Linear Structures Subjected to Seismic Excitations," by J. Song, Y-L. Chu, Z. Liang and G.C. Lee, 3/4/08 (PB2009-102311).

MCEER-08-0006 "System Performance Under Multi-Hazard Environments," by C. Kafali and M. Grigoriu, 3/4/08 (PB2008-112235).

MCEER-08-0007 "Mechanical Behavior of Multi-Spherical Sliding Bearings," by D.M. Fenz and M.C. Constantinou, 3/6/08 (PB2008-112236).

MCEER-08-0008 "Post-Earthquake Restoration of the Los Angeles Water Supply System," by T.H.P. Tabucchi and R.A. Davidson, 3/7/08 (PB2008-112237).

MCEER-08-0009 "Fragility Analysis of Water Supply Systems," by A. Jacobson and M. Grigoriu, 3/10/08 (PB2009-105545).

MCEER-08-0010 "Experimental Investigation of Full-Scale Two-Story Steel Plate Shear Walls with Reduced Beam Section Connections," by B. Qu, M. Bruneau, C-H. Lin and K-C. Tsai, 3/17/08 (PB2009-106368).

MCEER-08-0011 "Seismic Evaluation and Rehabilitation of Critical Components of Electrical Power Systems," S. Ersoy, B. Feizi, A. Ashrafi and M. Ala Saadeghvaziri, 3/17/08 (PB2009-105546).

MCEER-08-0012 "Seismic Behavior and Design of Boundary Frame Members of Steel Plate Shear Walls," by B. Qu and M. Bruneau, 4/26/08 . (PB2009-106744).

MCEER-08-0013 "Development and Appraisal of a Numerical Cyclic Loading Protocol for Quantifying Building System Performance," by A. Filiatrault, A. Wanitkorkul and M. Constantinou, 4/27/08 (PB2009-107906).

MCEER-08-0014 "Structural and Nonstructural Earthquake Design: The Challenge of Integrating Specialty Areas in Designing Complex, Critical Facilities," by W.J. Petak and D.J. Alesch, 4/30/08 (PB2009-107907).

MCEER-08-0015 "Seismic Performance Evaluation of Water Systems," by Y. Wang and T.D. O'Rourke, 5/5/08 (PB2009-107908).

MCEER-08-0016 "Seismic Response Modeling of Water Supply Systems," by P. Shi and T.D. O'Rourke, 5/5/08 (PB2009-107910).

MCEER-08-0017 "Numerical and Experimental Studies of Self-Centering Post-Tensioned Steel Frames," by D. Wang and A. Filiatrault, 5/12/08 (PB2009-110479).

MCEER-08-0018 "Development, Implementation and Verification of Dynamic Analysis Models for Multi-Spherical Sliding Bearings," by D.M. Fenz and M.C. Constantinou, 8/15/08 (PB2009-107911).

MCEER-08-0019 "Performance Assessment of Conventional and Base Isolated Nuclear Power Plants for Earthquake Blast Loadings," by Y.N. Huang, A.S. Whittaker and N. Luco, 10/28/08 (PB2009-107912).

MCEER-08-0020 "Remote Sensing for Resilient Multi-Hazard Disaster Response – Volume I: Introduction to Damage Assessment Methodologies," by B.J. Adams and R.T. Eguchi, 11/17/08 (PB2010-102695).

MCEER-08-0021 "Remote Sensing for Resilient Multi-Hazard Disaster Response – Volume II: Counting the Number of Collapsed Buildings Using an Object-Oriented Analysis: Case Study of the 2003 Bam Earthquake," by L. Gusella, C.K. Huyck and B.J. Adams, 11/17/08 (PB2010-100925).

MCEER-08-0022 "Remote Sensing for Resilient Multi-Hazard Disaster Response – Volume III: Multi-Sensor Image Fusion Techniques for Robust Neighborhood-Scale Urban Damage Assessment," by B.J. Adams and A. McMillan, 11/17/08 (PB2010-100926).

MCEER-08-0023 "Remote Sensing for Resilient Multi-Hazard Disaster Response – Volume IV: A Study of Multi-Temporal and Multi-Resolution SAR Imagery for Post-Katrina Flood Monitoring in New Orleans," by A. McMillan, J.G. Morley, B.J. Adams and S. Chesworth, 11/17/08 (PB2010-100927).

MCEER-08-0024 "Remote Sensing for Resilient Multi-Hazard Disaster Response – Volume V: Integration of Remote Sensing Imagery and VIEWS^{TM} Field Data for Post-Hurricane Charley Building Damage Assessment," by J.A. Womble, K. Mehta and B.J. Adams, 11/17/08 (PB2009-115532).

MCEER-08-0025 "Building Inventory Compilation for Disaster Management: Application of Remote Sensing and Statistical Modeling," by P. Sarabandi, A.S. Kiremidjian, R.T. Eguchi and B. J. Adams, 11/20/08 (PB2009-110484).

MCEER-08-0026 "New Experimental Capabilities and Loading Protocols for Seismic Qualification and Fragility Assessment of Nonstructural Systems," by R. Retamales, G. Mosqueda, A. Filiatrault and A. Reinhorn, 11/24/08 (PB2009-110485).

MCEER-08-0027 "Effects of Heating and Load History on the Behavior of Lead-Rubber Bearings," by I.V. Kalpakidis and M.C. Constantinou, 12/1/08 (PB2009-115533).

MCEER-08-0028 "Experimental and Analytical Investigation of Blast Performance of Seismically Resistant Bridge Piers," by S.Fujikura and M. Bruneau, 12/8/08 (PB2009-115534).

MCEER-08-0029 "Evolutionary Methodology for Aseismic Decision Support," by Y. Hu and G. Dargush, 12/15/08.

MCEER-08-0030 "Development of a Steel Plate Shear Wall Bridge Pier System Conceived from a Multi-Hazard Perspective," by D. Keller and M. Bruneau, 12/19/08 (PB2010-102696).

MCEER-09-0001 "Modal Analysis of Arbitrarily Damped Three-Dimensional Linear Structures Subjected to Seismic Excitations," by Y.L. Chu, J. Song and G.C. Lee, 1/31/09 (PB2010-100922).

MCEER-09-0002 "Air-Blast Effects on Structural Shapes," by G. Ballantyne, A.S. Whittaker, A.J. Aref and G.F. Dargush, 2/2/09 (PB2010-102697).

MCEER-09-0003 "Water Supply Performance During Earthquakes and Extreme Events," by A.L. Bonneau and T.D. O'Rourke, 2/16/09 (PB2010-100923).

MCEER-09-0004 "Generalized Linear (Mixed) Models of Post-Earthquake Ignitions," by R.A. Davidson, 7/20/09 (PB2010-102698).

MCEER-09-0005 "Seismic Testing of a Full-Scale Two-Story Light-Frame Wood Building: NEESWood Benchmark Test," by I.P. Christovasilis, A. Filiatrault and A. Wanitkorkul, 7/22/09 (PB2012-102401).

MCEER-09-0006 "IDARC2D Version 7.0: A Program for the Inelastic Damage Analysis of Structures," by A.M. Reinhorn, H. Roh, M. Sivaselvan, S.K. Kunnath, R.E. Valles, A. Madan, C. Li, R. Lobo and Y.J. Park, 7/28/09 (PB2010-103199).

MCEER-09-0007 "Enhancements to Hospital Resiliency: Improving Emergency Planning for and Response to Hurricanes," by D.B. Hess and L.A. Arendt, 7/30/09 (PB2010-100924).

MCEER-09-0008 “Assessment of Base-Isolated Nuclear Structures for Design and Beyond-Design Basis Earthquake Shaking,” by Y.N. Huang, A.S. Whittaker, R.P. Kennedy and R.L. Mayes, 8/20/09 (PB2010-102699).

MCEER-09-0009 “Quantification of Disaster Resilience of Health Care Facilities,” by G.P. Cimellaro, C. Fumo, A.M Reinhorn and M. Bruneau, 9/14/09 (PB2010-105384).

MCEER-09-0010 “Performance-Based Assessment and Design of Squat Reinforced Concrete Shear Walls,” by C.K. Gulec and A.S. Whittaker, 9/15/09 (PB2010-102700).

MCEER-09-0011 “Proceedings of the Fourth US-Taiwan Bridge Engineering Workshop,” edited by W.P. Yen, J.J. Shen, T.M. Lee and R.B. Zheng, 10/27/09 (PB2010-500009).

MCEER-09-0012 “Proceedings of the Special International Workshop on Seismic Connection Details for Segmental Bridge Construction,” edited by W. Phillip Yen and George C. Lee, 12/21/09 (PB2012-102402).

MCEER-10-0001 “Direct Displacement Procedure for Performance-Based Seismic Design of Multistory Woodframe Structures,” by W. Pang and D. Rosowsky, 4/26/10 (PB2012-102403).

MCEER-10-0002 “Simplified Direct Displacement Design of Six-Story NEESWood Capstone Building and Pre-Test Seismic Performance Assessment,” by W. Pang, D. Rosowsky, J. van de Lindt and S. Pei, 5/28/10 (PB2012-102404).

MCEER-10-0003 “Integration of Seismic Protection Systems in Performance-Based Seismic Design of Woodframed Structures,” by J.K. Shinde and M.D. Symans, 6/18/10 (PB2012-102405).

MCEER-10-0004 “Modeling and Seismic Evaluation of Nonstructural Components: Testing Frame for Experimental Evaluation of Suspended Ceiling Systems,” by A.M. Reinhorn, K.P. Ryu and G. Maddaloni, 6/30/10 (PB2012-102406).

MCEER-10-0005 “Analytical Development and Experimental Validation of a Structural-Fuse Bridge Pier Concept,” by S. El-Bahey and M. Bruneau, 10/1/10 (PB2012-102407).

MCEER-10-0006 “A Framework for Defining and Measuring Resilience at the Community Scale: The PEOPLES Resilience Framework,” by C.S. Renschler, A.E. Frazier, L.A. Arendt, G.P. Cimellaro, A.M. Reinhorn and M. Bruneau, 10/8/10 (PB2012-102408).

MCEER-10-0007 “Impact of Horizontal Boundary Elements Design on Seismic Behavior of Steel Plate Shear Walls,” by R. Purba and M. Bruneau, 11/14/10 (PB2012-102409).

MCEER-10-0008 “Seismic Testing of a Full-Scale Mid-Rise Building: The NEESWood Capstone Test,” by S. Pei, J.W. van de Lindt, S.E. Pryor, H. Shimizu, H. Isoda and D.R. Rammer, 12/1/10 (PB2012-102410).

MCEER-10-0009 “Modeling the Effects of Detonations of High Explosives to Inform Blast-Resistant Design,” by P. Sherkar, A.S. Whittaker and A.J. Aref, 12/1/10 (PB2012-102411).

MCEER-10-0010 “L’Aquila Earthquake of April 6, 2009 in Italy: Rebuilding a Resilient City to Withstand Multiple Hazards,” by G.P. Cimellaro, I.P. Christovasilis, A.M. Reinhorn, A. De Stefano and T. Kirova, 12/29/10.

MCEER-11-0001 “Numerical and Experimental Investigation of the Seismic Response of Light-Frame Wood Structures,” by I.P. Christovasilis and A. Filiatrault, 8/8/11 (PB2012-102412).

MCEER-11-0002 “Seismic Design and Analysis of a Precast Segmental Concrete Bridge Model,” by M. Anagnostopoulou, A. Filiatrault and A. Aref, 9/15/11.

MCEER-11-0003 ‘Proceedings of the Workshop on Improving Earthquake Response of Substation Equipment,” Edited by A.M. Reinhorn, 9/19/11 (PB2012-102413).

MCEER-11-0004 “LRFD-Based Analysis and Design Procedures for Bridge Bearings and Seismic Isolators,” by M.C. Constantinou, I. Kalpakidis, A. Filiatrault and R.A. Ecker Lay, 9/26/11.

MCEER-11-0005 "Experimental Seismic Evaluation, Model Parameterization, and Effects of Cold-Formed Steel-Framed Gypsum Partition Walls on the Seismic Performance of an Essential Facility," by R. Davies, R. Retamales, G. Mosqueda and A. Filiatrault, 10/12/11.

MCEER-11-0006 "Modeling and Seismic Performance Evaluation of High Voltage Transformers and Bushings," by A.M. Reinhorn, K. Oikonomou, H. Roh, A. Schiff and L. Kempner, Jr., 10/3/11.

MCEER-11-0007 "Extreme Load Combinations: A Survey of State Bridge Engineers," by G.C. Lee, Z. Liang, J.J. Shen and J.S. O'Connor, 10/14/11.

MCEER-12-0001 "Simplified Analysis Procedures in Support of Performance Based Seismic Design," by Y.N. Huang and A.S. Whittaker.

MCEER-12-0002 "Seismic Protection of Electrical Transformer Bushing Systems by Stiffening Techniques," by M. Koliou, A. Filiatrault, A.M. Reinhorn and N. Oliveto, 6/1/12.

MCEER-12-0003 "Post-Earthquake Bridge Inspection Guidelines," by J.S. O'Connor and S. Alampalli, 6/8/12.

MCEER-12-0004 "Integrated Design Methodology for Isolated Floor Systems in Single-Degree-of-Freedom Structural Fuse Systems," by S. Cui, M. Bruneau and M.C. Constantinou, 6/13/12.

MCEER-12-0005 "Characterizing the Rotational Components of Earthquake Ground Motion," by D. Basu, A.S. Whittaker and M.C. Constantinou, 6/15/12.

MCEER-12-0006 "Bayesian Fragility for Nonstructural Systems," by C.H. Lee and M.D. Grigoriu, 9/12/12.

MCEER-12-0007 "A Numerical Model for Capturing the In-Plane Seismic Response of Interior Metal Stud Partition Walls," by R.L. Wood and T.C. Hutchinson, 9/12/12.

MCEER-12-0008 "Assessment of Floor Accelerations in Yielding Buildings," by J.D. Wieser, G. Pekcan, A.E. Zaghi, A.M. Itani and E. Maragakis, 10/5/12.

MCEER-13-0001 "Experimental Seismic Study of Pressurized Fire Sprinkler Piping Systems," by Y. Tian, A. Filiatrault and G. Mosqueda, 4/8/13.

MCEER-13-0002 "Enhancing Resource Coordination for Multi-Modal Evacuation Planning," by D.B. Hess, B.W. Conley and C.M. Farrell, 2/8/13.

MCEER-13-0003 "Seismic Response of Base Isolated Buildings Considering Pounding to Moat Walls," by A. Masroor and G. Mosqueda, 2/26/13.

MCEER-13-0004 "Seismic Response Control of Structures Using a Novel Adaptive Passive Negative Stiffness Device," by D.T.R. Pasala, A.A. Sarlis, S. Nagarajaiah, A.M. Reinhorn, M.C. Constantinou and D.P. Taylor, 6/10/13.

MCEER-13-0005 "Negative Stiffness Device for Seismic Protection of Structures," by A.A. Sarlis, D.T.R. Pasala, M.C. Constantinou, A.M. Reinhorn, S. Nagarajaiah and D.P. Taylor, 6/12/13.

MCEER-13-0006 "Emilia Earthquake of May 20, 2012 in Northern Italy: Rebuilding a Resilient Community to Withstand Multiple Hazards," by G.P. Cimellaro, M. Chiriatti, A.M. Reinhorn and L. Tirca, June 30, 2013.

MCEER-13-0007 "Precast Concrete Segmental Components and Systems for Accelerated Bridge Construction in Seismic Regions," by A.J. Aref, G.C. Lee, Y.C. Ou and P. Sideris, with contributions from K.C. Chang, S. Chen, A. Filiatrault and Y. Zhou, June 13, 2013.

MCEER-13-0008 "A Study of U.S. Bridge Failures (1980-2012)," by G.C. Lee, S.B. Mohan, C. Huang and B.N. Fard, June 15, 2013.

MCEER-13-0009 "Development of a Database Framework for Modeling Damaged Bridges," by G.C. Lee, J.C. Qi and C. Huang, June 16, 2013.

MCEER-13-0010 “Model of Triple Friction Pendulum Bearing for General Geometric and Frictional Parameters and for Uplift Conditions,” by A.A. Sarlis and M.C. Constantinou, July 1, 2013.

MCEER-13-0011 “Shake Table Testing of Triple Friction Pendulum Isolators under Extreme Conditions,” by A.A. Sarlis, M.C. Constantinou and A.M. Reinhorn, July 2, 2013.

MCEER-13-0012 “Theoretical Framework for the Development of MH-LRFD,” by G.C. Lee (coordinating author), H.A Capers, Jr., C. Huang, J.M. Kulicki, Z. Liang, T. Murphy, J.J.D. Shen, M. Shinozuka and P.W.H. Yen, July 31, 2013.

MCEER-13-0013 “Seismic Protection of Highway Bridges with Negative Stiffness Devices,” by N.K.A. Attary, M.D. Symans, S. Nagarajaiah, A.M. Reinhorn, M.C. Constantinou, A.A. Sarlis, D.T.R. Pasala, and D.P. Taylor, September 3, 2014.

MCEER-14-0001 “Simplified Seismic Collapse Capacity-Based Evaluation and Design of Frame Buildings with and without Supplemental Damping Systems,” by M. Hamidia, A. Filiatrault, and A. Aref, May 19, 2014.

MCEER-14-0002 “Comprehensive Analytical Seismic Fragility of Fire Sprinkler Piping Systems,” by Siavash Soroushian, Emmanuel “Manos” Maragakis, Arash E. Zaghi, Alicia Echevarria, Yuan Tian and Andre Filiatrault, August 26, 2014.

MCEER-14-0003 “Hybrid Simulation of the Seismic Response of a Steel Moment Frame Building Structure through Collapse,” by M. Del Carpio Ramos, G. Mosqueda and D.G. Lignos, October 30, 2014.

MCEER-14-0004 “Blast and Seismic Resistant Concrete-Filled Double Skin Tubes and Modified Steel Jacketed Bridge Columns,” by P.P. Fouche and M. Bruneau, June 30, 2015.

MCEER-14-0005 “Seismic Performance of Steel Plate Shear Walls Considering Various Design Approaches,” by R. Purba and M. Bruneau, October 31, 2014.

MCEER-14-0006 “Air-Blast Effects on Civil Structures,” by Jinwon Shin, Andrew S. Whittaker, Amjad J. Aref and David Cormie, October 30, 2014.

MCEER-14-0007 “Seismic Performance Evaluation of Precast Girders with Field-Cast Ultra High Performance Concrete (UHPC) Connections,” by G.C. Lee, C. Huang, J. Song, and J. S. O’Connor, July 31, 2014.

MCEER-14-0008 “Post-Earthquake Fire Resistance of Ductile Concrete-Filled Double-Skin Tube Columns,” by Reza Imani, Gilberto Mosqueda and Michel Bruneau, December 1, 2014.

MCEER-14-0009 “Cyclic Inelastic Behavior of Concrete Filled Sandwich Panel Walls Subjected to In-Plane Flexure,” by Y. Alzeni and M. Bruneau, December 19, 2014.

MCEER-14-0010 “Analytical and Experimental Investigation of Self-Centering Steel Plate Shear Walls,” by D.M. Dowden and M. Bruneau, December 19, 2014.

MCEER-15-0001 “Seismic Analysis of Multi-story Unreinforced Masonry Buildings with Flexible Diaphragms,” by J. Aleman, G. Mosqueda and A.S. Whittaker, June 12, 2015.

MCEER-15-0002 “Site Response, Soil-Structure Interaction and Structure-Soil-Structure Interaction for Performance Assessment of Buildings and Nuclear Structures,” by C. Bolisetti and A.S. Whittaker, June 15, 2015.

MCEER-15-0003 “Stress Wave Attenuation in Solids for Mitigating Impulsive Loadings,” by R. Rafiee-Dehkharghani, A.J. Aref and G. Dargush, August 15, 2015.

MCEER-15-0004 “Computational, Analytical, and Experimental Modeling of Masonry Structures,” by K.M. Dolatshahi and A.J. Aref, November 16, 2015.

MCEER-15-0005 “Property Modification Factors for Seismic Isolators: Design Guidance for Buildings,” by W.J. McVitty and M.C. Constantinou, June 30, 2015.

MCEER-15-0006 "Seismic Isolation of Nuclear Power Plants using Sliding Bearings," by Manish Kumar, Andrew S. Whittaker and Michael C. Constantinou, December 27, 2015.

MCEER-15-0007 "Quintuple Friction Pendulum Isolator Behavior, Modeling and Validation," by Donghun Lee and Michael C. Constantinou, December 28, 2015.

MCEER-15-0008 "Seismic Isolation of Nuclear Power Plants using Elastomeric Bearings," by Manish Kumar, Andrew S. Whittaker and Michael C. Constantinou, December 29, 2015.

MCEER-16-0001 "Experimental, Numerical and Analytical Studies on the Seismic Response of Steel-Plate Concrete (SC) Composite Shear Walls," by Siamak Epackachi and Andrew S. Whittaker, June 15, 2016.

MCEER-16-0002 "Seismic Demand in Columns of Steel Frames," by Lisa Shrestha and Michel Bruneau, June 17, 2016.

MCEER-16-0003 "Development and Evaluation of Procedures for Analysis and Design of Buildings with Fluidic Self-Centering Systems" by Shoma Kitayama and Michael C. Constantinou, July 21, 2016.

MCEER-16-0004 "Real Time Control of Shake Tables for Nonlinear Hysteretic Systems," by Ki Pung Ryu and Andrei M. Reinhorn, October 22, 2016.

MCEER
EARTHQUAKE ENGINEERING TO EXTREME EVENTS
University at Buffalo, The State University of New York
133A Ketter Hall ▪ Buffalo, New York 14260-4300
Phone: (716) 645-3391 ▪ Fax: (716) 645-3399
Email: *mceer@buffalo.edu* ▪ Web: *http://mceer.buffalo.edu*
University at Buffalo *The State University of New York*

ISSN 1520-295X